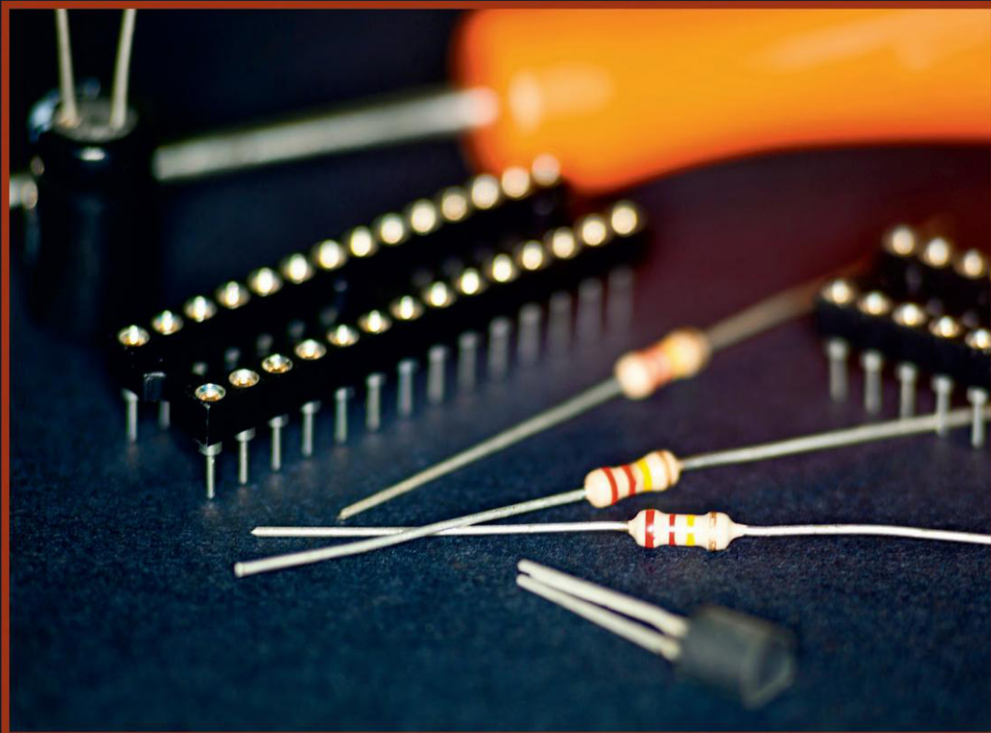


WOODHEAD PUBLISHING SERIES IN ELECTRONIC AND OPTICAL MATERIALS



# FUNCTIONAL DIELECTRICS FOR ELECTRONICS

FUNDAMENTALS OF CONVERSION  
PROPERTIES



YURIY POPLAVKO, YURIY YAKYMENKO

# **Functional Dielectrics for Electronics**

**Woodhead Publishing Series in Electronic and  
Optical Materials**

# **Functional Dielectrics for Electronics**

**Fundamentals of Conversion Properties**

*Yuriy Poplavko*

*Yuriy Yakymenko*



**ELSEVIER**

**WP**

WOODHEAD  
PUBLISHING

An imprint of Elsevier

Woodhead Publishing is an imprint of Elsevier

The Officers' Mess Business Centre, Royston Road, Duxford, CB22 4QH, United Kingdom

50 Hampshire Street, 5th Floor, Cambridge, MA 02139, United States

The Boulevard, Langford Lane, Kidlington, OX5 1GB, United Kingdom

© 2020 Elsevier Ltd. All rights reserved.

No part of this publication may be reproduced or transmitted in any form or by any means, electronic or mechanical, including photocopying, recording, or any information storage and retrieval system, without permission in writing from the publisher. Details on how to seek permission, further information about the Publisher's permissions policies and our arrangements with organizations such as the Copyright Clearance Center and the Copyright Licensing Agency, can be found at our website: [www.elsevier.com/permissions](http://www.elsevier.com/permissions).

This book and the individual contributions contained in it are protected under copyright by the Publisher (other than as may be noted herein).

### Notices

Knowledge and best practice in this field are constantly changing. As new research and experience broaden our understanding, changes in research methods, professional practices, or medical treatment may become necessary.

Practitioners and researchers must always rely on their own experience and knowledge in evaluating and using any information, methods, compounds, or experiments described herein. In using such information or methods they should be mindful of their own safety and the safety of others, including parties for whom they have a professional responsibility.

To the fullest extent of the law, neither the Publisher nor the authors, contributors, or editors, assume any liability for any injury and/or damage to persons or property as a matter of products liability, negligence or otherwise, or from any use or operation of any methods, products, instructions, or ideas contained in the material herein.

### Library of Congress Cataloging-in-Publication Data

A catalog record for this book is available from the Library of Congress

### British Library Cataloging-in-Publication Data

A catalogue record for this book is available from the British Library

ISBN: 978-0-12-818835-4 (print)

ISBN: 978-0-12-818836-1 (online)

For information on all Woodhead publications  
visit our website at <https://www.elsevier.com/books-and-journals>

*Publisher:* Matthew Deans

*Acquisition Editor:* Kayla Dos Santos

*Editorial Project Manager:* Peter Adamson

*Production Project Manager:* Sojan P. Pazhayattil

*Cover Designer:* Victoria Pearson

Typeset by SPi Global, India



# Preface

The authors of this book represent the microelectronics department of National Technical University of Ukraine (Kiev Polytechnic Institute), founded 120 years ago and named after Igor Sikorsky, who trained at this institute. Functional dielectrics have been studied, elaborated, and taught in the microelectronics department for many years, and the authors have published hundreds of articles and several books in this area.

The task of this book is to provide engineers specializing in materials science application and research in electronics and information technology with up-to-date and clear ideas about the nature of electrical polarization, dielectric nonlinearity, electrical charge transfer mechanisms, thermal properties, and the nature of thermal stable permittivity in low-loss microwave dielectrics and other functional dielectrics. The book describes in detail the intrinsic mechanisms of electrical polarization and energy transformations in noncentrosymmetric crystals, which are responsible for converting thermal, mechanical, optical, and other actions into electrical signals. In order to extend the use of functional dielectrics into the field of nanoelectronics, this book contains a versatile and comprehensive presentation of the main physical processes that provide the electrical, mechano-electrical, thermo-electrical, and other conversion phenomena in polar crystals.

More detailed descriptions are given to electrical manifestations of polar sensitivity in crystals; interaction of polarization with conductivity is described, as well as anomalies in thermal expansion coefficient and the main peculiarities of heat transfer in polar-sensitive crystals. Some applications of polarity theory to pyroelectrics and piezoelectrics are described. Microwave dielectrics are also of great importance in modern electronics, because they are widely used in communication devices. In them, small dielectric losses can be achieved in single-phase compositions, based on “hard” paraelectric material that resists polar structure formation. The thermal stability of permittivity can be obtained when paraelectricity is suppressed by paramagnetism. Nonlinear dielectrics provide an important opportunity for rapid control by permittivity, used in microwave phase shifters. Other frequency-agile devices are also described: tunable dielectric resonators and phase shifters consisting of microwave dielectrics coupled with control by a piezoelectric air gap that avoids inserted losses.

The authors express their deep gratitude to their colleagues from “Igor Sikorsky Kiev Polytechnic Institute” for their interest in this work and for their valuable comments. The authors are also grateful to their students who pointed out hard-to-understand concepts and asked us for clarification. The responsibility for any remaining errors or shortcomings is, of course, ours.

We want to give special thanks to Prof. Dr. Sci. Yuriy Prokopenko, Ass. Prof. Dr. Victor Kazmirenko, Ass. Prof. Dr. Dmitriy Tatarchuk, and Dr. Yuriy Didenko for their useful collaboration.

Finally, we are deeply grateful to the staff of Elsevier: to Kayla Dos Santos and Peter Adamson for their patience in eliminating the shortcomings of the manuscript.

*Dr. Phys.-Mat. Sci. Prof. Yuriy Poplavko  
Academician of UAS, First Vice Rector, Dr. Sci. Prof. Yuriy Yakymenko*

# Introduction

The dielectrics intended for use in electrical and electronic devices must have good electrical insulating properties, including very low electrical conductivity and high electrical strength. At the same time, in present-day electronics technology, other properties of dielectrics have gained special importance, namely those that allow for *conversion of energy or information*; these dielectrics may be considered **functional materials**.

The functional (or active, or adaptive, or controlled, or smart) dielectrics actively react to changes of temperature, pressure, mechanical stress, electrical and magnetic fields, light illumination, and even smell. Functional dielectrics can be classified as pyroelectrics, ferroelectrics, piezoelectrics, electrets, quantum-electronics materials, microwave dielectrics with tunable permittivity, etc.

Active dielectrics perform different functions. For example, the *piezoelectrics* convert mechanical energy into electrical energy (and vice versa) that is used in piezoelectric filters, ultrasound emitters, piezoelectric transformers, piezoelectric motors, etc. *Pyroelectrics* convert heat into electricity and are applied as sensitive detectors of radiation, thermal-vision devices, etc. The nonlinear properties of *ferroelectrics* and *paraelectrics* and the constant electrical field produced by *electrets* allow use of these functional dielectrics for modulation, detection, amplification, registering, storing, displaying, and other types of electrical conversion of signals carrying information. It is also necessary to mention the use of functional dielectrics in multifunctional electronic devices, along with the active search for new technological solutions to challenges regarding application of these dielectrics in the field of information technology.

The main property of any dielectric is its electrical *polarization*, i.e., the effect of *separation* of electrical charges that remain bonded in spite of their shifting. As a result, an *electrical moment* appears (as a product of charge magnitude and displacement); the volumetric density of this moment is polarization  $P$ . One unusual feature of functional dielectrics is that their electrical polarization can be induced not only by an electrical field, but also by other causes. A comparison of conventional (nonpolar) dielectrics and two categories of polar dielectrics are shown in [Table I.1](#). The essential distinction between active (functional) dielectrics and ordinary dielectrics is obvious.

In many applications of functional dielectrics (such as sensors, actuators, filters, transformers, motors, etc.), they are subjected to external thermal, electrical, mechanical, and other influences—scalar, vector, or tensor types. [Table I.1](#) shows that a conventional dielectric electrically reacts *only* to electrical field action:  $E \Rightarrow P$ , while polar piezoelectrics and pyroelectrics, besides the  $E \Rightarrow P$  response, are capable of electrical response to other actions: mechanical  $X \Rightarrow P$  and thermal  $dT \Rightarrow dP$ .

**Table I.1** Electrical polarization  $P$  as a response to various actions.

Actions	Nonpolar crystals	Piezoelectrics	Pyroelectrics
<b>Scalar</b> action: Temperature $dT$ Pressure $dp$	– –	– –	Pyroelectric effect: $dP = \gamma dT$ Volume piezoelectric effect: $dP = \zeta dT$
<b>Vector</b> action: Electrical field $E$	$P = \epsilon_0 \epsilon E$	$P = \epsilon_0 \chi E + (e^2/c)E$	$P = \epsilon_0 \chi E + (e^2/c)E + (\gamma^2 T)E/(\epsilon_0 C)$
<b>Tensor</b> action: Mechanical stress $X$	–	$P = dX$	$P = d'X$

Note: Parameter  $\gamma$  is pyroelectric coefficient;  $\zeta$  is volumetric piezoelectric modulus;  $d$  is piezoelectric modulus;  $\epsilon$  is elastic stiffness;  $C$  is specific heat. This table does not take into account:

- (1) *flexoelectricity* possible in all dielectrics under nonhomogeneous mechanical action;
- (2) *actinoelectricity* that occurs in piezoelectrics under the  $\text{grad}T$  action;
- (3) *photopolarization* effect in polar (noncentrosymmetric) dielectrics.

At the same time, piezoelectrics respond to electrical action not by ordinary polarization only, of  $P = \epsilon_0 \chi E$ , but also produce an electromechanical response  $P' = (e^2/c)E$ , while pyroelectrics, in addition, also produce an electrothermal response  $P'' = (\gamma^2 T)E/(\epsilon_0 C)$ .

In view of possible applications of dielectrics as functional (converting) elements in electronics, one should identify and describe their properties not only in terms of their exclusively electrical characteristics but also their capability to manifest various electrical, mechanical, and thermal properties. These materials are important also for miniaturization of microwave and telecommunications equipment. In this case, a decisive role is played by the value of permittivity ( $\epsilon$ ), since the planar dimensions of microwave devices are reduced exactly by the factor  $\epsilon$ . In some functional dielectrics (paraelectrics), a large value of  $\epsilon$  can be obtained together with low dielectric losses, which has important technical application in high-frequency devices. Some functional dielectrics allow *electrical control* by permittivity that can be used for electrically controlled microwave devices.

For all the reasons mentioned, interest in ferroelectrics, paraelectrics, piezoelectrics, and pyroelectrics has recently grown in the field of electronics materials science, precisely because of their new applications in instrumentation engineering and electronics, and also owing to significant progress in modern microelectronic and nanoelectronic technologies.

Functional materials are particularly relevant to modern and future instrumentation based on micromachining. In this trend, microelectronic group technology is used in a variety of technical fields. Using modern equipment, micromachining is organically

connected with microelectronics and nanoelectronics. Among contemporary applications of functional dielectrics, one should note the following main areas of particular relevance: ferroelectric and paraelectric thin films *integrated* with semiconductors; microsystems combining sensors, processors, and actuators; *microwave* microelectronics, based on functional dielectric components; *nanodielectrics*, which are prospective technologies for sensors, computer memories, and electrical power generation.

Engineers specializing in the application of materials science to electronics and information technologies need to access the latest knowledge on the nature of electrical polarization, electrical charge transfer mechanisms, thermal properties of functional dielectrics, mechanisms of dielectric losses, as well as intrinsic mechanisms of polarization in noncentrosymmetric crystals, which are responsible for converting thermal, mechanical, optical, and other actions into electrical signals. In order to extend the use of functional dielectrics into the field of nanoelectronics, it is necessary for designers and technologists to have a thorough and deep understanding of the physical processes that provide electrical, mechano-electrical, thermoelectrical, photoelectrical and other conversion phenomena in polar crystals.

It might be that the most striking features of polar dielectrics are, first, the *mutual influence* of mechanical, electrical, and thermal properties on each other and, second, the dependence of these properties on the *conditions* in which polar crystals are studied or applied. To demonstrate this interdependence, the basic mechanical, electrical, and thermal *linear effects* in the nonpolar and polar dielectrics are symbolically compared in Fig. I.1. It is seen that in the ordinary dielectrics these properties are independent, but in the polar crystals they are connected by quite complex interactions.

Fig. I.1A symbolically shows that the elastic deformation  $x$  (strain) in a solid dielectric is proportional to the applied mechanical stress  $X = sX$ , where  $s$  is elastic compliance. Note that this linear relationship can also be written in the reverse direction,  $X = c \cdot x$ , as Hooke's law, where  $c$  is elastic stiffness. Similarly, in a dielectric, electrically induced polarization  $P$  is proportional to the magnitude of the applied electrical field,  $P = \epsilon_0 \chi \cdot E$ , where  $\chi$  is dielectric susceptibility while  $\epsilon_0$  is the electrical constant in SI units. If electrical polarization is induced *nonelectrically*, then another recording of this linear connection will be more convenient:  $E = \epsilon_0^{-1} \xi \cdot P$  where

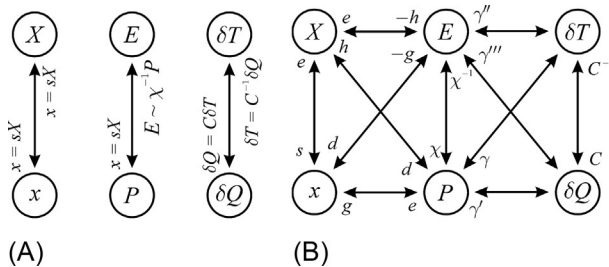


**Fig. I.1** Linking diagram for mechanical, electrical, and thermal effects: (A) In nonpolar dielectric; (B) in polar dielectric.

$\xi = \chi^{-1}$  is dielectric impermeability. Finally, thermal properties are described by the proportionality of the amount of heat  $\delta Q$  in a crystal appearing due to ambient temperature change:  $\delta Q = C \cdot \delta T$  where  $C$  is specific heat.

In polar crystals, the mechanical, electrical, and thermal properties are *interdependent*, so a possible diagram of their interaction looks like two squares connected by one side (Fig. I.1B). This scheme shows how complicated the description of noncentrosymmetric (polar) crystal properties can be.

*Piezoelectricity* is symbolically described by the left square in Fig. I.1B. Two horizontal and two crossed-connecting lines with arrows present eight linear piezoelectric effects that may be observed in polar crystals under different conditions. The number of piezoelectric effects is 8, since this effect can be *direct* or *converse* (2), the crystal can be electrically *open-circuited* or *short-circuited* (2), and the crystal mechanically can be *free* or *clamped* (2), so  $2 \times 2 \times 2 = 8$ . These effects are described by four piezoelectric coefficients-moduli ( $d, e, g, h$ ); further, simplified equations of the direct effects are  $P = d \cdot X, P = e \cdot x, E = -g \cdot x, E_j = -h \cdot X$ , and for the converse effect the equations are  $x = d \cdot E, X = e \cdot E, x = g \cdot P, X = h \cdot P$ . However, all *four* moduli mentioned can be calculated through each other and through known elastic constants, for example, in simplified form:  $d_{in} = \epsilon_0 \epsilon \cdot g = e \cdot s = \epsilon_0 \epsilon \cdot h \cdot s$ , and so on. As can be seen, the description of electromechanical effects in polar crystals (even in the linear case) is not an easy task.

In polar-sensitive crystals, the description of electrothermal effects is also not simple. The *pyroelectric* effect occurs when the disturbance factor is the thermal action on a crystal while the response has an electrical nature. The *electrocaloric* effect is the converse effect: it arises when the electrical field acts on the pyroelectric, while the result is heating or *cooling* of the polar crystal. Both these effects are symbolically presented in the right square in Fig. I.1B.

First, two horizontal lines and two crossed-connected lines with arrows symbolically characterize four options in the pyroelectric effect implementation: the polar crystal can be electrically *open-circuited* or *short-circuited*; in addition, the pyroelectric effect can occur in two different thermal conditions: *adiabatic* with  $\delta Q = 0$  or *isothermal* with  $\delta T = 0$ . So the pyroelectric effect might be described by *four* equations:  $P = \gamma \cdot \delta T, P_i = \gamma' \cdot \delta Q, E = \gamma'' \cdot \delta T, \text{ and } E = \gamma''' \cdot \delta Q$ , in which different pyroelectric coefficients correspond to various boundary conditions.

Second, four lines with arrows, shown in the right part of Fig. I.1B, are used here for symbolic description of the *electrocaloric* effect. As a pyroelectric effect, this effect may be described by *four* different linear relationships (depending on thermal and electrical boundary conditions). However, this effect under normal conditions (at temperature  $\sim 300$  K) is rather weak and is not considered here in more detail. (However, in Chapter 4, a large electrocaloric effect will be discussed, arising when an anti-ferroelectric is switching electrically into a ferroelectric phase, which can be considered as a possible basis for an electrocaloric refrigerator.)

An important consequence of these relationships is the dependence of the crystal *fundamental parameters* on thermal, electrical, or mechanical processes passing in polar crystals at different boundary conditions. For example, dielectric susceptibility of a free crystal  $\chi^X$  (which means the stress  $X = 0$ ) and of a clamped crystal  $\chi^x$  (that

means the strain  $x = 0$ ) can differ, as  $\chi^X > \chi^x$ . Similarly, in polar crystals the elastic stiffness in Hooke's law depends on the electrical conditions: in an open-circuited crystal the elastic stiffness ( $c^P$ ) differs from that in a closed-circuited crystal ( $c^E$ ). Moreover, when Hooke's law is studied in polar crystal, its elastic stiffness depends on isothermal ( $c^T$ ) or adiabatic ( $c^S$ ) conditions. Even the most conservative parameter of a crystal—its heat capacity  $C$  at normal temperatures—turns out to be dependent on the electrical and thermal boundary conditions in which the crystal is studied. For example, in an open-circuited polar crystal the specific heat  $C^E$  differs from the specific heat  $C^P$  of a close-circuited crystal. In the same manner, a difference is seen in the specific heat of mechanically free ( $C^X$ ) and mechanically clamped ( $C^x$ ) polar crystals.

One topic of this book is clarification of *electrical polarization* peculiarities in the polar crystals. A number of electrical, mechanical, and thermal effects in polar crystals are considered and some models of a crystal's internal polarity are discussed. The relationship between pyroelectricity and piezoelectricity is considered on the basis of experimental and theoretical data. At that, instead of the traditional concept of *spontaneous polarization*, outstanding properties of polar crystals (pyro-, piezo-, and ferroelectrics) are explained by other physical causes, namely by the existence in the crystal structure of the *polar-sensitive* interatomic bonds (in other words, to the term "spontaneous polarization" a different meaning is given).

Peculiarities of *covalent-ionic mixed* atomic bonds are, first, the *structural openness* of paired covalent bonds, formed with a minimum number of neighboring atoms (usually *four*), and, second, the *increased polarity* of ionic bonds, if they are hybridized with covalent bonds. Such mixed atomic bonds make possible the origination of an *electrical response to nonelectrical actions* (for instance, when temperature or pressure is changed). Besides, in the ferroelectrics, these peculiar bonds give rise to a *nonlinear* response to external electrical field action with a reversal in the orientation of internal polar sensitivity. Moreover, it is asserted that the main cause of hybridized ionic-covalent bond formation and their existence in some crystals is the distinction in the *electronegativity* of structural ions.

A polar-sensitive structure manifests itself in crystals as an ability to generate electrical (i.e., vector type) response to nonelectrical scalar or more complicated tensor types of actions. For example, the action of mechanical stress  $X$  on a polar crystal-piezoelectric leads to the *direct piezoelectric effect*,  $P = e \cdot X$ , which is an appearance of bound electrical charges of different signs on opposite surfaces of a plane-parallel crystal, the surface density  $q_S$  [C/m<sup>2</sup>] of which corresponds to volumetric density (electrical moment  $P$  [Q/m<sup>2</sup>]), which is *mechanically induced* in a crystal. In the same way, homogeneous (hydrostatic) pressure  $p$  by its action on polar-sensitive pyroelectric crystal leads to the *volumetric piezoelectric effect*  $P = \zeta \cdot p$ , while homogeneous heating (or cooling) of a pyroelectric crystal with temperature increment  $\delta T$  produces a *pyroelectric effect*  $P = \gamma \cdot \delta T$ . All the effects mentioned are possible only in the non-centrosymmetric crystals, because hybridized ionic-covalent atomic bonding causes a *reduction in crystal symmetry*, so polar-sensitive crystals always belong to the non-centrosymmetric classes of crystals.

In this book a novel conception of the physical nature of pyroelectricity and piezoelectricity is used. The proposed models, based on the asymmetry in distribution

of electron density along atomic bonds, are free from any assumptions as to the existence in a crystal of an “internal electrical field,” so there is no need to think about compensation of spontaneous polarization by any “free electrical charges.” Although asymmetric polar-sensitive bonds are not a result of an internal field, nevertheless they can provide a polar response to nonelectrical homogeneous external action (thermal, mechanical, optical, or other) that in principle is impossible in the centrosymmetric crystals.

Some peculiarities of “exclusively” piezoelectric crystals (in other words, *polar-neutral* crystals) can be described as their *ability* to show a polar response to *directional* external influences, defined in the general case by 3D electrical moment  $M_{ijk}$ . In some cases, the moment components obey the critical law  $M \sim (\theta - T)^n$  and vanish at the phase transition temperature  $\theta$ . This dependence can be studied experimentally by partial limitation of deformations in the polar-neutral piezoelectric crystals when their temperature changes. Further, the previously mentioned critical parameter  $n = 1$ , if all components of intrinsic polar sensitivity are oriented in the same plane (two-dimensional case, 2D). For spatial (3D) arrangement of polar-sensitive atomic bonds, the exponent is  $n = 2$ . Both of these laws differ essentially from the linear (1D) directed ferroelectric intrinsic polarization  $M_i(T) = P_i(T)$ , which follows a critical law exponent  $n = 0.5$ .

It can be noted that the proposed method of *partial limitation of strain* opens up the possibility for new applications of *piezoelectrics-semiconductors*: this means that, under technologically created anisotropy in boundary conditions, any crystal of  $A^{III}B^V$  (piezoelectric) type can be transformed into an artificial “pyroelectric” crystal. This property might be used in infrared sensors or in piezoelectric sensors integrated with amplifiers in an  $A^{III}B^V$ -type crystal such as GaAs or GaN.

Some other *indirect evidence* of polar-sensitivity peculiarities of non-centrosymmetric crystals is also discussed in this book:

- structural proximity of the piezoelectrics and the pyroelectrics;
- chemical features of polar crystals, confirming polar-sensitive structure;
- increase in volume at self-ordering of polar-sensitive bonds in crystal;
- influence of intrinsic polarity on permittivity and its frequency dependence;
- high-frequency absorption as a feature of polar-sensitive dielectrics;
- electrically controlled elastic properties of polar crystals;
- heat capacity increase due to different polar-sensitivity orientation in crystals;
- negative thermal expansion coefficient at low temperatures;
- reduced thermal conductivity due to polar-sensitive bonds;
- influence of polar bonds on electrical conductivity;
- influence of polar bonds on dielectric losses in microwave dielectrics;
- suppression of paraelectric  $\epsilon(T)$  instability by paramagnetism; etc.

Thus, in the field of physics, this book examines the nature of intrinsic polarity in the noncentrosymmetric dielectrics and, in particular, why the hybridized ionic-covalent (polar-sensitive) interatomic bond arises and what properties of functional dielectrics it results from. In terms of technical applications of functional dielectrics, the physical and technical basis of their many-sided applications in electronics are considered.

**Chapter 1** is devoted to the general ideology of intrinsic polarity in dielectrics, already partially described; moreover, the general laws of thermodynamics are

explained and applied. For example, if dielectric permittivity increases during heating of a dielectric, i.e., when the temperature coefficient of permittivity is positive ( $TC\epsilon > 0$ ), the change in entropy during polarization must be positive. Thus even without discussing any details of the processes that occur in a dielectric, only using general thermodynamic considerations, it can be concluded that in a dielectric with  $TC\epsilon > 0$  placed in an electrical field, such physical processes occur that reduce the degree of molecular or atomic structure ordering. Conversely, if in a dielectric with  $TC\epsilon < 0$ , i.e., when its permittivity decreases with heating, the change in entropy is negative. This means that the basic mechanisms that determine polarization, when an external electrical field is applied, cause an increase in the ordering of molecules (ions and atoms) in the dielectric. These results are applied later, when discussing the method of thermal stabilization of dielectric permittivity.

In the *polar dielectrics*, the concept of entropy becomes more complex. Recall that usually, for any material, so-called vibrational entropy is considered to be the number of microstates by which thermal energy can be divided between particles. The higher the temperature, the greater the vibrational entropy, but it becomes smaller if the binding energy of particles is greater. That is why, with increasing pressure, vibrational entropy decreases and the thermal expansion coefficient of the dielectric is positive. For polar crystals, a very important concept is configurational entropy, i.e., that part of the system's entropy that is due to the various positions of some parts of a system. This entropy characterizes the number of ways in which groups of atoms are distributed in space. With increasing pressure, partial ordering of dynamic nanoscale clusters collapses and mutual chaos increases. That is why configurational entropy increases with pressure increase, and the thermal expansion coefficient of the polar-sensitive dielectric becomes negative. The negative coefficient of thermal expansion in such crystals shows the importance of configurational entropy for their property descriptions. In turn, it indicates the presence in polar-sensitive crystals of the specific ordering-disordering processes.

In **Chapter 2**, various experimental evidence of the existence of polar sensitivity in crystals is considered, such as the increase in their volume while the self-ordering of polar-sensitive atomic bonds occurs. This also leads to piezoelectric and electrocaloric contributions to *permittivity* of polar crystals, dependence of polar crystal *elastic properties* on various electrical boundary conditions, etc. Some features of charge transfer in the polar-sensitive crystals are also explained, such as the physical nature of the *giant change* of conductivity in the critistors, posistors, and varistors. Moreover, some other field-controllable *switching elements*, particularly those that exhibit *colossal* magnetoresistance, as well as the *high sensibility* of nanostructured sensors based on zinc oxide, are discussed.

The *electrically induced* polar properties are also investigated: electrically induced piezoelectric modulus in paraelectrics and relaxor ferroelectrics, and electrical control by resonant frequency of piezoelectric resonators and filters. *Thermomechanically induced* pyroelectricity is examined as well; the original methods of pyroelectric response and volumetric piezoelectric effect, obtained in the polar-neutral piezoelectrics (nonpyroelectrics), are described. Two- and three-dimensional structural arrangements of polar-sensitive bonds in polar-neutral piezoelectrics are analyzed;

the artificial pyroelectric effects for 10 classes of polar-neutral piezoelectric crystals are calculated and experimentally tested in quartz and gallium arsenide crystals. This effect can be used in single-chip pyroelectric and piezoelectric matrix sensors.

**Chapter 3** is dedicated to the thermal physics of polar crystals. Particularly, the *specific heat* of polar crystals contains an additional contribution from the ordering-disordering process of polar-sensitive atomic bonds. It is explained by the increased number of ways of mutual arranging of the polar bonds; moreover, the change in configurational entropy corresponds to the same change in macroscopic entropy.

Another important parameter, the *thermal expansion coefficient*  $\alpha$ , corresponds to features of interatomic bonds in polar crystals, when the peculiar polar-sensitive structure arises as the compensation of atomic electronegativity. The negative value of  $\alpha$  at low temperatures means that entropy increases with pressure rise, which can occur only in the case of configurational entropy, reflecting processes of structural ordering. At that, some results obtained for polar crystals can be applied to semiconductors as well. The difference in thermal expansion as well as in mismatch between the lattice parameter of film and substrate is used in some modern microelectronics technologies.

*Heat transfer* in polar crystals is also discussed; it is provided mostly by *short* lattice waves having low velocity; moreover, the polar crystal looks like a turbid medium. These waves demonstrate strong scattering on diffuse-type nanosized inhomogeneous structure, in which phonon interaction is determined mostly by the polar-sensitive bonds, because the wavelength of the warmth-carrier phonons is commensurable with the crystal lattice parameter. Polar-sensitive (mixed ionic-covalent) bonds strongly affect the processes of heat transfer in polar crystals: their thermal conductivity is much less than that in pure-ionic or pure-covalent crystals. Different anomalies of thermal diffusion in the vicinity of ferroelectric and antiferroelectric phase transitions are also described: when ordered polar structure spontaneously changes into disordered nonpolar structure. In the ordered phase the thermal diffusion coefficient increases; this indicates that disordering of polar-sensitive bonds hinders diffusion of heat.

**Chapter 4** is the introduction to pyroelectricity and corresponding materials. Pyroelectrics represent one of the important classes of functional dielectrics, because they efficiently react to *changes in temperature* (as well as to pressure and other mechanical actions). These are the polar-sensitive dielectrics, which can be defined also as materials that allow direct energy conversion, represented as the thermoelectric and, vice versa, the electrothermal power converters. The transformative function of polar crystals is due to their peculiar physical structure and chemical composition. Different mechanisms of pyroelectricity and, inverse to it, the electrocaloric effect are reviewed in the aspects of their use in electronic devices at various boundary conditions (adiabatic and isothermal, mechanically free or clamped crystals, short-circuited or open-circuited circumstances). The nature of thermoelectrical coupling in polar-sensitive crystals and its influence on permittivity and thermal properties of crystals are also described using various models and thermodynamic calculations. Some principles of operation of the main types of pyroelectric sensors are considered: motion detection sensors, infrared thermometers for high precision pyrometry, pyroelectric vidicons of both vacuum and microelectronic

design, etc. Physical mechanisms and applications of electrically induced pyroelectric and electrocaloric effects at various conditions are also described. The possibilities of the electrocaloric effect are discussed in connection with possible applications in miniature solid-state refrigeration systems.

**Chapter 5** is devoted to the basic physical mechanisms of the piezoelectric effect. A piezoelectric is a solid-state transducer of mechanical energy into electrical energy (direct effect) or an electromechanical transducer (converse effect). At that, mechanically induced electrical polarization is directly proportional to strain, i.e., this is the odd (linear) effect, possible only in noncentrosymmetric material. The piezoelectric effect is characterized by various piezoelectric moduli (third-rank tensors) depending on the combination of boundary conditions under which piezoelectricity is used or studied. The interrelationship of mechanical and electrical properties of a piezoelectric is characterized by the electromechanical coupling coefficient, the square of which shows how much of the energy applied to the piezoelectric is converted into another kind of energy. Parameters of some piezoelectric materials can be controlled by electrical field as well as characteristics of piezoelectric filters and surface acoustic wave devices.

A model description of piezoelectricity is given for one-directional polar-sensitive bonds, representing the *longitudinal* piezoelectric effect; for polar bonds oriented in-plane corresponding to the *transverse* piezoelectric effect; and, finally, for spatial distribution of polar bonds (the *shear* piezoelectric effect). The *electro-induced* piezoelectric effect and the method of *strain partial limitation* for the volumetric piezoelectric effect are considered. In addition to the linear converse piezoelectric effect, a quadratic *electrostriction effect* is analyzed, when induced strain is proportional to the square of field strength. Naturally, the sign of this deformation does not change when electrical polarity changes. In an electrical bias field the electrostriction looks like a piezoelectric effect. In this case, the magnitude of such electrically induced piezoelectric effect in relaxor ferroelectrics can be very large.

**Chapter 6** concerns microwave dielectrics, which are of great importance for modern electronics because they are widely used in communication devices and military equipment. In particular, microwave electronics needs dielectric materials that combine increased permittivity, small dielectric losses, and high thermal stability. The distinctions of this chapter are the attempts to find physical substantiations of such features of microwave dielectrics as the physical nature of large permittivity compatible with small dielectric loss. Increased permittivity can be obtained in the ionic crystals with sufficiently open structure, which makes it possible to use greater polarizability of semifree electron orbitals. Furthermore, the displacive type paraelectrics can be applied as a basic material, the structure of which is characterized by a low-frequency transverse lattice optical mode. In some cases thermal stability of permittivity can be obtained in such structures where paraelectricity is suppressed by paramagnetism. Small dielectric losses can be reached only in monophasic composition, based on “hard” paraelectric material (which resists polar structure formation). It is argued also that the main reason for microwave absorption in high-permittivity dielectrics is the presence of a polar-sensitive phase in their composition, so recommendations are to avoid any polar materials that lead to an increase in dielectric losses.

However, the *nonlinear dielectrics*, which provide important opportunities for rapid control of their permittivity (needed for microwave phase shifters), obviously include polar phase. Nevertheless, a compromise may be found in how to combine high dielectric nonlinearity with minimal dielectric losses. Another new solution is proposed for frequency-agile microwave devices: piezoelectrically tunable dielectric resonators, filters, and phase shifters. Macrocomposites designed for this purpose consist of microwave dielectrics coupled with a controlled air-gap, which makes it possible to create fast tunable microwave devices without inserted losses (controlling piezoelectric devices are located outside the waveguide path).

# Physical nature of crystal internal polarity



Particular properties of polar crystals (pyro-, piezo-, and ferroelectrics) are explained by the existence in their structure of peculiar *polar-sensitive interatomic bonds*, which gives new meaning to the traditional concept of spontaneous polarization. Hybridized ionic-covalent polar bonds originate mainly due to a distinction in electronegativity of ions forming polar crystals. Polar bonds cause electrical polarization as a response to a nonelectrical homogeneous action (temperature or pressure). If a polar crystal is a ferroelectric, the polar-sensitive bonds cause a nonlinear response to an electrical field with a reversal of orientation.

The polar-sensitive structure manifests itself in crystals as an ability to provide an electrical (vector-type) response to nonelectrical scalar or more complicated tensor types of actions. Hybridized ionic-covalent bonding causes a reduction in crystal symmetry, so polar crystals always belong to the noncentrosymmetric classes. Moreover, it is exactly the presence of such bonds that determines the noncentrosymmetric structure of some crystals. Hybridized ionic-covalent bonding is a main cause of pyroelectric and piezoelectric properties. The model used is based on the asymmetry in electronic density distribution along atomic bonds, which ensures the ability of a crystal to manifest a polar (electrical) response to nonelectrical action; the model is free from any assumption as to the presence of an internal electrical field in the polar crystal.

## 1.1 Basic elementary mechanisms of polarization

A substantially different approach to understanding polar crystal behavior is taken here. As a rule, the unique properties of polar crystals, in particular pyroelectricity, are widely conceptualized as being due to change in spontaneous polarization [1, 2]. A somewhat different implication of this concept is proposed here, and in this regard another physical mechanism is considered: the peculiar capability of a polar crystal to induce electrical polarization under uniform thermal or mechanical action, i.e., to generate an electrical response to nonelectrical influences [3].

Before discussing the nature of the peculiar polarization existing in polar crystals, the general conception of polarization in dielectrics needs to be clarified, since for this defining question it is necessary to take all details into account. The point is that any dielectric can be polarized by an applied electrical field, but only certain dielectrics can be polarized in a nonelectrical manner.

If electrical field  $E$  is applied to a dielectric, then an electrical polarization arises:  $P = \epsilon_0 \chi E$ , where  $\epsilon_0$  is an electrical constant and  $\chi$  is dielectric susceptibility. Electrical polarization means that a *separation of electrical charges* occurs: for example, on the

opposite surfaces of a plane-parallel dielectric sample, electrical charges of different signs appear; note that these charges are not free but closely bound to the dielectric. Traditionally, the polarization process is described by the electrical induction

$$D = \varepsilon_0 \varepsilon E = \varepsilon_0 E + P,$$

which includes induction of a vacuum  $\varepsilon_0 E$  and polarization of the dielectric  $P = \varepsilon_0 \chi E$ ; dielectric permittivity  $\varepsilon = 1 + \chi$  takes both processes into account. At the moment of the electrical voltage switching on, through the dielectric included in the electrical circuit, a reactive current of electrical charge displacement flows; then it terminates, if the remaining voltage is unchanged and the conductivity of the dielectric is insignificant. The voltage switching off is also accompanied by a jump of electrical depolarization current, which has an opposite sign to the charging current; in this way the electrical polarization reacts only to a *change* in electrical voltage. It is appropriate to note here that, if polarization is induced in a nonelectrical manner (mechanical, thermal, optical, irradiation, or other action), then current (or voltage) arises only during the *change* of this influence, and it does not manifest if the exposure remains unchanged.

The low inertia of the polarization processes, the low dielectric losses, and the wide range of operating temperatures are very important for dielectrics used in high-speed electronics equipment. When an electrical field is applied to a dielectric, the associated charges of the structural units are elastically displaced relative to each other, leading to electrical polarization. The mechanism looks as though the electrical field induces in the dielectric a set of elementary electric moments  $p = qx$ , where  $q$  is the charge of bounded units and  $x$  is their mutual displacement. The electrical moment induced by the field can have contributions from electrons, moving from their equilibrium positions in atoms, and from ions, deviating from their equilibrium state in the crystal lattice. The dipoles (polar molecules), which change their orientation in the electrical field, and macrodipoles, which are electrically charged radicals or complexes in the heterogeneous structures, also lead to polarization.

Furthermore, the electrons, ions, and dipoles (including macrodipoles) can acquire an induced electrical moment (i.e., polarized state) by various mechanisms: (1) the elastic reversible displacement of bound electric charges, (2) the displacement of weakly bound charges with participation of their warm motion, and (3) the macroscopic displacement of semifree charges that later localize on the defects in the dielectric. However, only the first of these mechanisms is considered to determine the properties of dielectrics necessary for their functioning in high-speed electronic devices.

If particles are tightly connected in a structure, the external electrical field or any other impact causes only very small deviations (as compared with atomic dimensions) from a nonpolarized equilibrium state. However, since in the process of polarization *all particles* of a dielectric are involved, even these small displacements of charges result in a significant integral effect—the polarization. This is the mechanism of *quasielastic polarization*, and only it can give the needed permittivity with minimal dielectric losses that is necessary for modern applications of dielectrics.

**First, electronic quasielastic** (optical) polarization is briefly considered. In the nonpolarized state ( $E = 0$ ) electron shells of atoms are located symmetrically with respect to their nuclei (Fig. 1.1A), so that the *effective center* of negative charge of the electron shell coincides with the positively charged nucleus (Fig. 1.1A').

Accordingly, when the field is absent, elemental dipole moment is zero ( $p = 0$ ), since it is determined by a product  $qx = p$ , but any relative displacement of charges  $q^+$  and  $q^-$  is absent:  $x = 0$ . If the electrical field acts on the dielectric, electrical force influences each atom, molecule, or ion, and their electron shells displace with respect to the correspondent nucleus (Fig. 1.1B and B'), whereby the center of negative charge shifts relatively to the positively charged nucleus, so that an elementary polar moment appears:  $p = qx > 0$ .

Such is the mechanism of electronic quasielastic polarization, which occurs in *all* dielectrics and semiconductors; it is very important to note that it is a *least inertial* mechanism, which lags only in the ultraviolet optical range (Fig. 1.1C). Practically

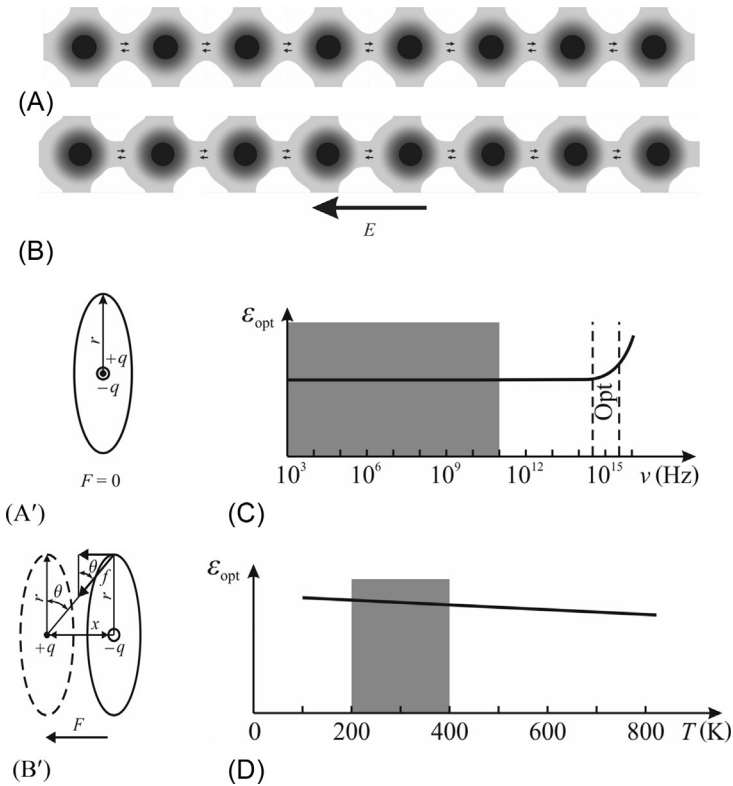


**Fig. 1.1** Simplified model of electronic (optical) polarization: (A) 1D covalent crystal and (A') model consisting of one electron and nucleus; (B) electrical field influence and (B') orbit deformation in local field  $F$ ; (C) frequency dependence of permittivity; (D) temperature dependence of permittivity (*shaded areas* show ranges of technical interest).

speaking, electronic (optical) polarization introduces no dielectric losses over the whole frequency range used in electronics; moreover, electronic permittivity  $\epsilon_e = \epsilon_{\text{opt}}$  is sufficiently thermostable over a wide range of temperatures.

Molecular and covalent crystals have exclusively electronic polarization. Those parts of the electron shells of atoms that can noticeably shift in an electrical field relative to the atomic residue (cores) contribute relatively little to optical permittivity, so usually  $\epsilon_e = \epsilon_{\text{opt}} < 5$ . This is typical for fairly densely packed (“closed”) structures with a coordination number  $\text{CN} = 6\text{--}8$  (the number of nearest neighboring atoms). As a result, electron shells are rigidly connected to their cores and weakly react to external electric fields. It should be noted that permittivity of such materials *decreases* somewhat with rise in temperature, mostly due to the thermal expansion of the dielectric (Fig. 1.1D); respectively, the thermal coefficient of permittivity in these materials is negative:  $TC\epsilon < -10^{-5} \text{ K}^{-1}$  ( $< -10 \text{ ppm/K}$ ).

However, in *covalent semiconductors* (C, Si, Ge, and others) that have looser packed (“open”) structures with  $\text{CN} = 4$ , optical permittivity is elevated:  $\epsilon_e = \epsilon_{\text{opt}} \sim 7\text{--}15$ . This is not surprising, since electron clouds that are more loosely packed to their atomic residues are able to respond more compliant to an applied field and produce greater polarization. In this case temperature dependence of permittivity  $TC\epsilon \sim +10^{-4} \text{ K}^{-1}$ , because in addition to the negative contribution to  $TC\epsilon$  from thermal expansion, there is also another physical mechanism with a *positive* contribution to  $TC\epsilon$  conditioned by the narrowing of the forbidden band of crystal electronic spectrum.

Thus, even in the seemingly simple case of electronic elastic polarization that occurs in crystals with relatively simple structure, the mechanism of polarization is not so simple. It is worth mentioning here that some dielectric crystals that have only electronic polarization can form *polar structures*: in selenium and tellurium a piezoelectric effect is seen, while in one of diamond’s modifications a hexagonal (wurtzite) structure is observed with a pyroelectric symmetry. It is hardly possible in these cases to apply the classic concept of spontaneous polarization.

**Second, the low-inertia mechanism** of polarization, which is very important for dielectric electronics components, is the **quasielastic ionic** polarization, otherwise known as far-infrared polarization, because in this spectrum range it has resonant properties. In a simplified model of an ionic crystal, which is shown in Fig. 1.2A and A’, when the electrical field is absent, the lattice is balanced by cation and anion interaction.

In an ionic crystal, a system of different sign charges is electrically neutral, and it does not show any electrical moment (polarization) of its own in the absence of external influences. But under an applied external electric field, Fig. 1.2B and B’, the cations and anions mutually displace, forming a polarized lattice of  $q^+ - q^-$ , in which the induced elementary electrical moment is  $p = qx > 0$ . In this way a fast ionic polarization arises, and it determines many electrical properties of ionic crystals.

As shown in Fig. 1.2C, a permittivity, conditioned by ionic polarization, does not depend on frequency up to the far-infrared range, where  $\epsilon_{\text{ir}}$  gradually starts to increase (in this frequency range ionic polarization shows resonant dispersion). Dielectric permittivity  $\epsilon_{\text{mw}}$  (measured at microwave frequency,  $\sim 10^{10} \text{ Hz}$ ) includes components of

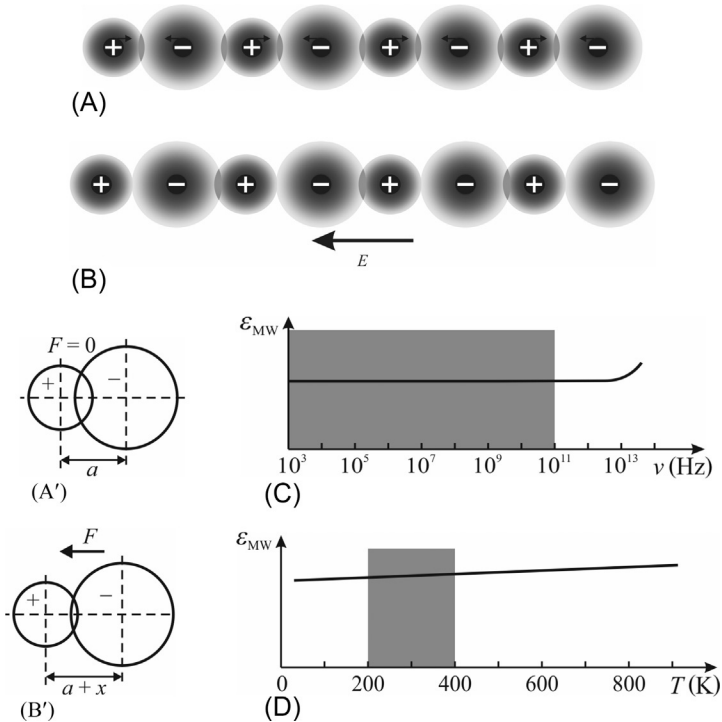


**Fig. 1.2** Ionic polarization: (A) 1D ionic crystal and (A') simplest model, consisting of one positive and one negative ion; (B) electrical field influence and (B') induced deformation  $x$  in local field  $F$ ; (C) frequency dependence of ionic permittivity; (D) ionic permittivity temperature dependence (*shaded areas* show range of technical interest).

optical (electronic) polarization  $\epsilon_{\text{opt}} = \epsilon_e$  and infrared (ionic) polarization  $\epsilon_{\text{ir}} = \epsilon_{\text{ion}}$ . In the majority of ionic dielectrics, their permittivity is not large:  $\epsilon_{\text{mw}} = 8\text{--}12$ . This is due to their dense structure with CN = 6 or 8, creating only small opportunities for elastic displacements of the bound electrical charges. Moreover, as a rule,  $\epsilon_{\text{mw}}$  gradually *grows* with temperature since the ionic contribution to permittivity  $\epsilon_{\text{ir}}$  dominates over  $\epsilon_{\text{opt}}$  and increases with temperature increase (Fig. 1.2D). The reason for the  $\epsilon_{\text{ir}} = \epsilon_{\text{ion}}$  increase is the thermal expansion of crystal: at higher temperatures the distance between ions increases, so the reciprocal shift of ions in the applied electrical field becomes bigger. As a result, the thermal coefficient of permittivity in most of the ionic crystals is positive  $TC\epsilon < +10^{-4} \text{ K}^{-1}$  ( $\sim +100 \text{ ppm/K}$ ).

The model discussed agrees well with experiments for simple ionic crystals of alkali-metal halide types. Correspondingly, the described temperature dependence of permittivity is true in most cases, but not in all dielectrics. In some dielectrics (which are very important for high-frequency electronics) the temperature coefficient of dielectric permittivity can be *negative* and even very large:  $TC\epsilon = -(10^{-3}\text{--}10^{-2}) \text{ K}^{-1}$ . It should be noted that at the same time the permittivity of such ionic crystals can

be large:  $\epsilon = 10^2\text{--}10^4$ . The fact is that the model, described in connection with Fig. 1.2, is too simplified. More in-depth examination confirms that mutual displacement of lattice ions themselves determines only the *inertia* of the far-infrared polarization mechanism. The dielectric contribution of far-infrared polarization depends more on the *electron shells* of ions, which do not move quite synchronously with their cores. These phenomena occur mainly in crystals in which electronic and ionic bonds are mixed.

Therefore, as in the case of electronic polarization, when describing ionic polarization induced by an electrical field, it is the *structure of outer electron shells* that is extremely important. Note that features of polarization described previously may be of particular importance in synthesis and study of nanostructural materials.

**Third**, in addition to quasielastic electronic and ionic polarizations, one more mechanism of low-inertia polarization is possible in the polar dielectrics: it is the **elastic rotation of connected dipoles**. This polarization mechanism is a particular characteristic of polar dielectrics with *hydrogen bonds* and is of academic rather than practical interest. This polarization is possible only in the case when a fairly *rigid ordering* of dipoles exists in a dielectric in the absence of an external electrical field, and that is observed in noncentrosymmetric dielectrics. Parallel or antiparallel ordering of the dipoles in the polar lattices is conditioned by their internal interaction. An externally applied electrical field alters the orientation of the dipole ensemble, thereby induced electrical moment changes and a correspondent polarization occurs. This mechanism of dipole elastic polarization takes place mostly in liquid crystals.

In different dielectrics, there are many **other contributions to permittivity** from various *slower polarization* mechanisms; some of them are denoted in Fig. 1.3:  $\epsilon_{dip}$  is a contribution from weakly bound thermally activated dipoles,  $\epsilon_{EM}$  characterizes the electromechanical reaction of piezoelectric crystals as a whole, while  $\epsilon_{ET}$  is the electrocaloric contribution, seen only in pyroelectric crystals.

Dielectric spectra show that slower mechanisms of polarization do not actually affect the permittivity of dielectrics used in high-frequency electronics. But as will be shown in Section 1.5, they can noticeably increase *dielectric losses*, even in the microwave range of the spectrum. Therefore, it is necessary to describe these polarization mechanisms, at least briefly.

Electrons, ions, and dipoles can also participate in *thermally activated* (relaxation) polarization. In the case when dipoles, ions, or electrons are *weakly connected* in the structure of a dielectric, the thermal motion in a crystal can strongly influence the processes of dielectric polarization. Localized in the nanoscale environment, electrons or ions under the action of thermal motion make thermally activated jumps at distances on the order of atomic dimensions. Relaxation polarization mechanisms are mainly due to structural defects in the dielectrics and lead to dielectric permittivity dispersion and to dielectric losses at relatively low frequencies and radio frequencies.

The Debye polarization mechanism, i.e., activated by thermal motion *dipole polarization*, is a characteristic of some polar crystals and liquid crystals. In the absence of an electrical field ( $E = 0$ ), the dipoles are oriented randomly and equiprobably in all directions; therefore there is no polarization (volumetric density of electrical moment  $P = 0$ ). If an electrical field is applied to such a dielectric ( $E > 0$ ), then some of the

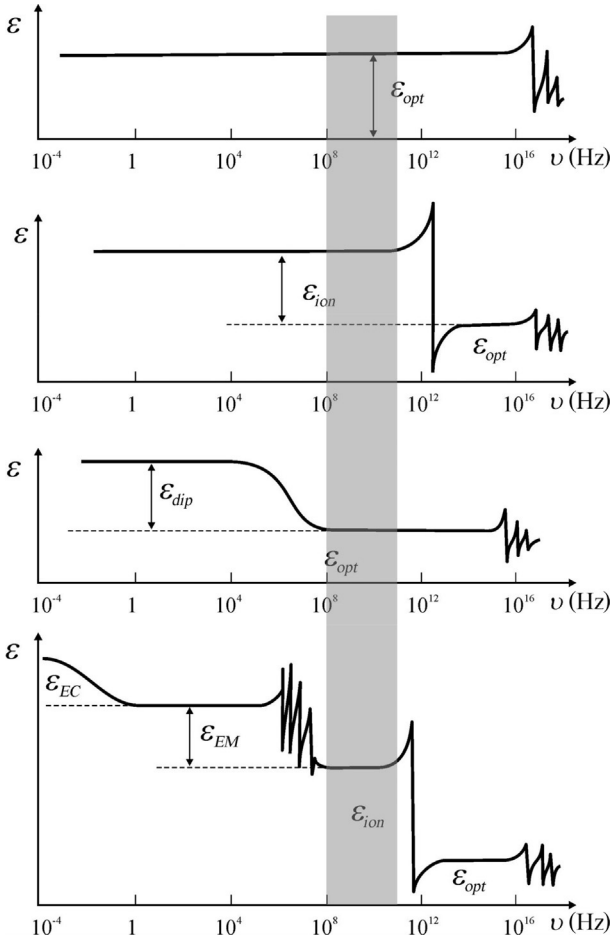


**Fig. 1.3** Dielectric investments to permittivity from different polarization mechanisms:  $\epsilon_{opt}$ —electron displacement;  $\epsilon_{ion}$ —ion displacement;  $\epsilon_{dip}$ —dipole orientation;  $\epsilon_{EM}$ —electromechanical polarization in piezoelectrics;  $\epsilon_{EC}$ —electrocaloric polarization in pyroelectrics (*shaded areas* show the range of technical interest) [4].

dipoles that perform thermal reorientations all the time become predominantly oriented along the applied field, as a result of which a polarized state appears ( $P > 0$ ). It should be borne in mind that only a small portion of the dipoles become oriented, but the higher the electrical field, the greater the number of oriented dipoles. The establishment time of the dipole relaxation polarization is relatively long ( $\tau = 10^{-3} - 10^{-9}$  s) and strongly depends on the temperature.

It should be noted that it would be naive to understand the reorientation of such dipoles as “rotation of some dumbbell-like molecules.” In reality, in the vicinity of asymmetrically located charges that in fact form dipoles, under the action of an electrical field electronic density redistributes, and this process is initiated by the thermal motion. Therefore, the relaxation time of this process depends on temperature exponentially, so at sufficiently low temperature this polarization seems impossible.

The ionic thermal polarization is due to the thermal jumps of weakly bound ions (usually the impurity ions) in the local region of a lattice. It is obvious that such a

polarization occurs in those solid dielectrics that have structural defects. Ions located in the interstitial sites, as well as voids in a regular structure (ionic vacancies), under the action of thermal motion change their location and, being charged particles, change the orientation and magnitude of local electrical polar moments. During chaotic movements (spatially limited by structural defects), the ions overcome potential barriers, creating fluctuating “electrical dipoles.” When an external electrical field is absent, such a motion of charged particles is disordered, random, and not grafted to macroscopic polarization. However, in the electrical field, the distribution of ions changes in the locations of crystal lattice defects, which leads to the induced thermal ionic polarization.

In some solid dielectrics, thermostimulated polarization of the *semifree electrons* (trapped by lattice defects) is observed. Such electrons (or holes) lead to thermal (relaxation) polarization when the ground state of the electrons is degenerate, and the combination of degenerate wave functions creates an electrical dipole moment. When there is no electrical field, thermal fluctuations transfer a localized electron (or hole) from one state to another, but the electrons remain localized: such a chaotic movement of electrons on average does not lead to the polarization of a dielectric. The inclusion of the electrical field leads to the “unipolarity” of electron hops, inducing the electrical moment—polarization. The relaxation time of a thermally activated polarization is rather long:  $10^{-7}$ – $10^{-6}$  s.

Electronic thermal polarization is important in many dielectrics used in technical applications, such as rutile ( $\text{TiO}_2$ ), perovskite ( $\text{CaTiO}_3$ ), and similar complex oxides of titanium, zirconium, niobium, tantalum, lead, cerium, and bismuth. In these substances, especially in their polycrystalline state, a high concentration of defects in crystal structure is observed. During ceramic synthesis from the mixture of oxides (or during crystal growth), a very high temperature is used, and therefore the appearance of oxygen defects—anionic vacancies—is very likely. Electrical compensation for these defects occurs by the *lowering of valence* of cations located near anionic vacancies. Thus, appropriate conditions of electronic exchange between the neighboring cations appear, which lead to the polarization [1].

Not all of the preceding polarization mechanisms occur simultaneously in real dielectrics and play the same role. It should be noted also that different polarization mechanisms may influence each other, so, strictly speaking, these mechanisms cannot be discussed as independent. Nevertheless, the preceding analysis is a fairly accurate approximation.

It is noteworthy also that polarization, induced by the external electrical field, is necessarily accompanied by the mechanical deformation of a dielectric—this is the *electrostriction*, which additionally indicates that a polarized state of dielectrics is a nonequilibrium state, so in the short circuit this polarization usually disappears instantly, when the external electrical field is turned off. It is very important to note here that any dielectric under direct external electrical field influence becomes an artificially polar dielectric and hence acquires piezoelectric and pyroelectric effects. The reason for this is that the center of symmetry (if it existed) in the externally polarized dielectric disappears, while a very important new symmetry element arises—an electrically induced *polar axis*.

This circumstance, which has become a reason for the manifestation of pyroelectric or piezoelectric properties in some dielectrics in the absence of an external electrical field, served as a basis to call these crystals “polar” and to draw subsequent conclusions that in these dielectrics spontaneous polarization exists. However, it is suggested here that the natural polarity of some crystals can be explained in another way, namely not by permanent polarization (spontaneous) but only by the *ability* of some particular structures to induce an electrical response to nonelectrical influences: this is exactly what determines the special properties of polar dielectrics.

## 1.2 Main features of polarization

In any case, whether the “polar dielectric” is induced by the external field or it is a typical polar dielectric, some special behavioral features should be taken into account: as in electrical fields, also under mechanical, thermal, optical, and other influences [4]. These features are: (1) dielectric anisotropy, (2) dielectric nonlinearity, and (3) significant dependence of parameters of a polar dielectric on electrical, mechanical, or thermal conditions.

- **The dielectric anisotropy** often arises in dielectrics under external field influence and always is present in the polar dielectrics. Unlike most dielectrics, which are simple isotropic materials and have identical electrical properties in any direction, in noncentrosymmetric dielectrics their electrical, thermal, and mechanical characteristics show dependence on direction of action and response, i.e., anisotropy. It should be noted that in most of the functional dielectrics their electrical, electromechanical, and electrothermal parameters are quite different in the various directions of crystals or textures.

In the usual *isotropic* dielectrics, vectors  $D$ ,  $E$ , and  $P$  are *collinear*, but in the anisotropic dielectrics these vectors differ in their orientation; however, the vector relation  $D = \epsilon_0 E + P$  always remains true. This vector sum in isotropic dielectrics corresponds to the sum of vector modules, since directions of all three vectors coincide.

The direction of the induced polarization vector in the anisotropic dielectric corresponds not only to the direction of the electrical field applied from outside, but also depends on the orientation of internal elastic bonds of charged crystal particles, so the vector  $P$  is not parallel to the vector  $E$ . Naturally, the electric induction vector  $D$  also has its own direction that differs both from the vector  $E$  and from the vector  $P$ . Therefore, the dielectric constant characterizing the relationship between  $D$  and  $E$  ( $D = \epsilon \epsilon_0 E$ ) is such a parameter that is different in various directions.

Scalar parameters of materials (density, temperature, or specific heat) under specified environmental conditions are described by *one value*. However, the vector, for example, has to be determined by three parameters: namely its projections on the coordinate axes. Therefore, to denote a vector, a subscript is used (for example,  $i, j = 1, 2, 3$ ), and the conversion of one vector to another is more complicated than in the case of a scalar value:  $D_j \sim \epsilon_{ij} E_i$ . In the anisotropic environments, the parameters describing a particular material are recorded with *two indices*: one comes from the vector of “action”  $E_i$ , and the other from the vector of “response”  $D_j$ , whose directions may not correspond to the direction of action.

In the case under consideration, all vectors are considered to be tensors of the first rank, and they are written with the *single* subscript:  $E_i$ ,  $D_j$ , etc. Scalar values, according to this classification, are *zero-rank tensors* that are written with no lower indices and converted using ordinary laws of algebra, for example,  $\delta Q = C \cdot \delta T$ : that is, the change in a heat  $\delta Q$  equals the product of heat capacity  $C$  and temperature change  $\delta T$ . A symbolic image of a scalar quantity in a three-dimensional coordinate system is shown in Fig. 1.4A by a sphere [1].

The permittivity  $\epsilon_{ij}$  and susceptibility  $\chi_{ij} = \epsilon_{ij} - 1$ , as well as the conductivity  $\sigma_{ij}$ , along with some other parameters of anisotropic crystals and textures, are described by *second-rank tensors*. Components of permittivity tensor  $\epsilon_{ij}$  might be presented in the form of a matrix, but in an isotropic dielectric (glass, amber, plastic, etc.), this matrix contains only components of the main (diagonal):  $\epsilon_{ij} = \epsilon$ . However, in polar crystals usually three diagonal components of the  $\epsilon_{ij}$ -matrix ( $\epsilon_{11}$ ,  $\epsilon_{22}$ , and  $\epsilon_{33}$ ) are used to describe permittivity, which in fact is not a fixed number (as in the case of a scalar) but is represented by the surface of an *ellipsoid* of permittivity:  $\frac{x^2}{\epsilon_{11}} + \frac{y^2}{\epsilon_{22}} + \frac{z^2}{\epsilon_{33}} = 1$  shown in Fig. 1.4C. In isotropic dielectrics  $\epsilon_{11} = \epsilon_{22} = \epsilon_{33}$  and the dielectric ellipsoid becomes a *sphere*. In tetragonal, hexagonal, and trigonal crystals (usually determined by a spatial distribution of polar-sensitive bonds) components  $\epsilon_{11} = \epsilon_{22}$ , but they differ from  $\epsilon_{33}$ , so that the dielectric ellipsoid becomes an *ellipsoid of rotation*. This kind

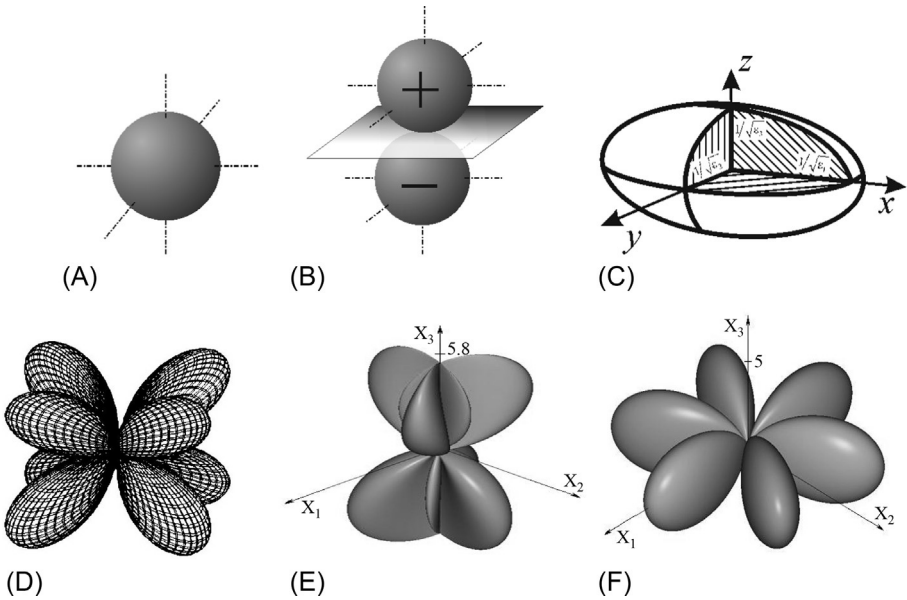


**Fig. 1.4** Images of material tensors of various ranks: (A) Zero-rank tensor (scalar); (B) first-rank tensor (pyroelectric coefficient); (C) second-rank tensor (permittivity); (D–F) third-rank tensors—piezoelectric modulus, correspondingly in GaAs, transverse, and longitudinal in langasite.

of anisotropy can be created artificially by strong electrical or mechanical fields, and is used in optics as electrooptical and piezooptical effects.

In connection with the graphical images shown in Fig. 1.4 for material tensors of different rank, the indicatrix of a first-rank tensor of a pyroelectric coefficient should also be added, which is the characteristic for some polar crystals (Fig. 1.4B), and some characteristic surfaces for the third-rank tensor, which is piezoelectric modulus. These physical quantities are characterized not by single numbers but by full surfaces, demonstrating the value of the given parameter in different directions.

- The **nonlinearity of dielectrics** means the dependence of their permittivity on the intensity of the electrical field. In principle, some dependence  $\epsilon(E)$  should occur in all dielectrics, but usually it becomes noticeable only in a very large electric field:  $10^7$ – $10^{10}$  V/m, i.e., close to the electrical breakdown strength. However, in some dielectrics (ferroelectrics and paraelectrics), the nonlinearity of their permittivity can be significant even in electrical fields on the order of  $10^5$  V/m, much smaller than the breakdown field. It should also be noted that, thanks to new microelectronic technologies, high-quality very thin and nanoscale dielectric layers are obtained, in which the electrical strength is two to three orders of magnitude higher; therefore the electrical breakdown voltage increases significantly, and nonlinearity, even in ordinary dielectrics, becomes important.

Optical nonlinearity is observed not only in films but also in bulk dielectrics: when exposed to a powerful laser beam, nonlinearity is significant in any dielectric, and self-focusing of the laser beam is often observed in them.

- **The boundary conditions** must be considered when the induced electrical moment (polarization) arises in dielectrics, since, due to external electrical field action as well as the change of other external influences, it is especially important to take into account boundary conditions for polar dielectrics. These conditions can be electrical, mechanical, and thermal [5].

Two **electrical** boundary conditions are reduced to the following:

- Electrical field  $E=0$ : i.e., a polar crystal is *electrically free*. This means that the entire surface of a crystal is an equipotential surface, because the dielectric is short-circuited. Since electrical induction is  $D = \epsilon_0 E + P$ , then in an electrically free crystal  $D = P$ , and when induced in a polar crystal polarization generates electrical current:  $j_p = dP/dt$ . In the case of a *static* procedure in a polar crystal study (or application), condition  $E = 0$  can be realized by the entire metallization of a crystal. In practice, this condition is performed by a shorting of electrodes deposited on crystal. Under *dynamic* testing, when mechanically or thermally induced polarization in a polar dielectric is variable in time, the condition  $E = 0$  leads to electrical current, i.e., the crystal is the *source of a current*.
- Electrical induction  $D=0$ : i.e., a polar crystal is *electrically disconnected* and  $D = \epsilon_0 E + P = 0$ ; such a crystal is the *source of a voltage*. In case of static mode of investigation, implementation of this condition requires extremely low crystal conductivity: only in this case is mechanically, thermally or optically induced polarization  $P$  totally compensated by the induced electrical field:  $\epsilon_0 E = -P$ . In the case of dynamic excitation of a polar crystal, condition  $D = 0$  is true, for example, for lattice waves that have longitudinal polarization.

Two **mechanical** boundary conditions are as follows:

- When a crystal is free from any mechanical stresses ( $X = 0$ ): i.e., in a crystal all components of the mechanical stress tensor are zero. This condition can be realized by giving complete

freedom of any deformation of the crystal. In studies of frequency characteristics, this condition is satisfied only at frequencies lower than the first intrinsic mechanical resonances of the crystal.

- When the polar crystal is mechanically clamped ( $\mathbf{x} = \mathbf{0}$ ): i.e., no deformation is possible in it. At low frequencies, these conditions are almost impossible to provide. However, in real experiments, the crystal is clamped by its own inertia, if we conduct the research at frequencies higher than the frequencies of all electromechanical resonances of the crystal.

Two **thermal** boundary conditions are described as follows:

- When the temperature is constant ( $T = \text{const}$ ): this isothermal condition means that the crystal temperature is constant during research or technical application. This case is extremely unlikely for bulk samples, since it is possible only at extremely low frequencies, when there is enough time for the exchange of energy between the crystal and the environment. However, in the thermodynamic theories of polarization, this approximation is usually used. It should be noted that isothermal conditions may be important in the study and application of nanoscale objects.
- When the entropy  $S = \text{const}$ : this *adiabatic condition* means permanent entropy, when there is no energy exchange with the environment during measurements or applications. This is the *usual case* of polar crystal study at comparatively high frequencies.

All the listed conditions of experimental characteristics study are indeed very important for polar-sensitive crystals. In this connection, for example, it is necessary to distinguish  $\epsilon^X$  (permittivity of a free crystal, in which any mechanical stress is absent,  $X = 0$ ), and  $\epsilon^x$  (permittivity of a clamped crystal, in which any electromechanically induced strain is absent,  $x = 0$ ), so only microscopic polarization mechanisms are possible. For most polar crystals the inequality  $\epsilon^X > \epsilon^x$  is always true, because  $\epsilon^X$  contains an additional mechanism of reversible energy storage—elastic displacement of the crystal as a whole.

Electromechanical contributions to permittivity may be quite different. For example, accurate measurements of quartz crystal show  $\epsilon_{11}^X = 4.52$  and  $\epsilon_{11}^x = 4.43$ ,  $\epsilon_{33}^X = 4.70$  and  $\epsilon_{33}^x = 4.64$ ; so that in this crystal the piezoelectric contribution to permittivity is small:  $\epsilon_{11}^X - \epsilon_{11}^x = 0.09$  and  $\epsilon_{33}^X - \epsilon_{33}^x = 0.06$ . However, in barium titanate crystal at 300 K, the components of permittivity are:  $\epsilon_{11}^X = 4000$  and  $\epsilon_{11}^x = 2000$ ,  $\epsilon_{33}^X = 200$  and  $\epsilon_{33}^x = 90$ , so the piezoelectric contribution to permittivity in this crystal is essential:  $\epsilon_{11}^X - \epsilon_{11}^x = 2000$ , while  $\epsilon_{33}^X - \epsilon_{33}^x = 110$ . Moreover, the electromechanical contribution to barium titanate permittivity shows *large anisotropy* and equals approximately half of the total value of permittivity. Similarly, in pyroelectrics, their permittivity measured under adiabatic conditions  $\epsilon^S$  is less than the isothermal permittivity  $\epsilon^D$ ; sometimes the difference reaches 50%.

Another example is the dependence of thermal, electrical, or mechanical processes, occurring in polar crystals, on their boundary conditions. The specific heat  $C^E$  of the open-circuited pyroelectric crystal differs from the specific heat  $C^D$  obtained in a short-circuited crystal. In the same manner, there is a difference in specific heat of mechanically free ( $C^X$ ) and mechanically clamped ( $C^x$ ) crystals. Similarly, elastic stiffness in Hooke's law for polar crystals depends on electrical conditions: open-circuited elastic stiffness ( $c_{klmn}^D$ ) differs from short-circuited ( $c_{klmn}^E$ ). When Hooke's law is studied in the polar crystal, it is necessary to consider that elastic stiffness depends also on isothermal ( $c_{klmn}^T$ ) or adiabatic ( $c_{klmn}^S$ ) conditions [1].

All these features must be taken into account when developing and applying polar crystals in piezoelectronic, acoustoelectric, and pyroelectric devices. However, earlier only the *idealized* boundary conditions were listed; any approach to their implementation can be unique when setting research goals, depending on the electromechanical or electrothermal properties of crystals and films. It is also important to note that in practice polar crystals are used in *intermediate conditions*: they are partially clamped and partially free, not entirely short-circuited nor entirely open-circuited, but are loaded into a certain impedance value. However, the listed idealized boundary conditions should be assumed as a basis for different effects in polar crystal study and applications.

Proceeding from the earlier discussion, one can come to the conclusion that the problem of a complete description of various properties of polar crystals is quite complex. Simplifying this problem, however, it is possible to arrive at the **following conclusions**:

- The ability of *all dielectrics* (and semiconductors) to create induced electrical moment  $P_j = \chi_{ij} E_i$  under electrical field  $E_i$  action. This property is described by symmetric tensor-dielectric susceptibility  $\chi_{ij}$  (or the same dielectric permittivity  $\epsilon_{ij} = 1 + \chi_{ij}$ ), which in isotropic dielectrics looks like scalar quantities:  $\epsilon = 1 + \chi$ . The susceptibility (or permittivity) are *intrinsic properties* inherent in a particular material and can be described by a material second-rank tensor.
- The ability of polar *dielectrics-pyroelectrics* to generate their own thermally induced electrical moment  $P_i = \gamma_i \delta T$  by change of temperature  $\delta T$ . This property is described by a material tensor, the *pyroelectric coefficient*  $\gamma_i$  (this can also be called susceptibility to temperature change). This specific sensitivity to temperature variation (i.e., electrical response to temperature change) is an *intrinsic property*, inherent in a particular pyroelectric and described by a material first-rank tensor (dependent on direction in a crystal and thus quite different from a scalar). It is important to note here that in nonpolar dielectrics an applied electrical field *induces* the ability of a pyroelectric response. Moreover, as shown later, such an *artificial pyroelectric effect* is sometimes more appropriately used in electronics than the thermoelectric response in natural pyroelectrics. There is also one more possibility (described in [Section 1.4](#)) for obtaining an artificial pyroelectric effect; however, this time it is not in any dielectric but in any *piezoelectric* using the technological method of partial mechanical clamping. In this connection, a piezoelectric semiconductor can be used for single-crystal pyrotransistor elaboration.
- The ability of polar *dielectrics-pyroelectrics* to create an induced electrical moment  $P_i = \zeta_i p$  due to a change of hydrostatic (all-around) pressure  $p$ . This is described by a material tensor, the piezoelectric pressure coefficient  $\zeta_i$  (which can also be called susceptibility to alteration of pressure). Such a volumetric piezoelectric effect characterizes sensitivity to change of pressure; this property is inherent only in pyroelectrics and can be described by a material first-rank tensor  $\zeta_i$  (dependent on the direction in the crystal in which this electrical response is studied). In conditions of partial clamping of a crystal, it is possible to obtain a volumetric pyroelectric effect in any piezoelectric; this technology can find some applications in such devices as a single-chip piezotransistor.
- The ability of polar *dielectrics-piezoelectrics* to create an electrical moment (i.e., polarization  $P_i$ ) induced by mechanical stress  $X_{jk}$ :  $P_i = d_{ikl} X_{jk}$ . This property is described by a material tensor, *piezoelectric moduli*  $d_{ikl}$  (which can also be called susceptibility to mechanical stress change). Sensitivity to change in mechanical stress is an *intrinsic property* of the

material, inherent in a particular piezoelectric and described by a third-rank tensor (dependent on stress direction and on the manner of electrical response investigation). Just like the pyroelectric effect, piezoelectric activity can be induced by external fields. In a sufficiently strong bias electrical field, a nonpolar dielectric with high enough permittivity can exhibit an *artificial piezoelectric* effect that is commensurable or even superior to the electromechanical effect of natural piezoelectrics.

These features of polar crystals, including strong anisotropy of properties, perceptible dielectric nonlinearity, dependence of investigated parameters on boundary conditions, etc., can be explained using a simplified model of polar-sensitive bonds characteristic of such crystals.

### 1.3 Peculiarities of polar crystal polarization

In polar crystals under the influence of changing temperature or mechanical factors the separation of bound charges (polarization) arises, which is accompanied by the appearance of a surface charge with density  $q_s = Q_i/S$  (C/m<sup>2</sup>). Moreover, depending on the electrical boundary conditions, in an open-circuited crystal the electrical field can be observed or in the case of a short-circuited crystal the electrical current flows. When temperature changes by  $\delta T$ , the open-circuited mechanically free polar crystal generates a pyroelectric response:  $q_T = \gamma \cdot \delta T$ , while under mechanical stress  $X$  a piezoelectric response occurs:  $q_X = d \cdot X$ . Here  $q_T$  is thermally induced charge,  $\gamma$  is the pyroelectric coefficient measured in [C/(m<sup>2</sup> K)] and  $d$  is piezoelectric modulus measured in [C/N].

Parameters  $\gamma$  and  $d$  characterize the value of crystal electrical responses to temperature change and to mechanical stress, respectively. Both of these effects are linear, so, according to the Curie principle, they must have opposite effects, namely, the *electrocaloric* effect  $\delta T = \eta \cdot (Q_{ap}/S)$  and the *inverse piezoelectric* effect  $X = h \cdot (Q_{ap}/S)$ , where  $\eta$  is the electrocaloric coefficient,  $h$  is the piezoelectric coefficient, and  $Q_{ap}/S = \epsilon_0 \epsilon E$  is density of charge, induced by external field  $E$ . Polarization is traditionally defined as the density of induced electrical moment in a dielectric, but more conveniently can be estimated by the density of bound electric charge induced by various influences on the surface of a dielectric.

It is important to note that none of these responses allows measurement of the value of basic spontaneous polarization. Some doubts about the existence of spontaneous polarization have also been expressed in theoretical works [6]. Because of this, and for some other reasons, the expansion of modeling ideas concerning the nature of polarization of noncentrosymmetric crystals deserves special attention.

Historically, assumptions regarding the existence of spontaneous polarization in some peculiar dielectrics arose in their comparison with ferromagnetics, which have spontaneous magnetization. Similarly to magnetic hysteresis  $B(H)$  in ferromagnetics, the loop of dielectric hysteresis  $P(E)$  was discovered (first in the Rochelle salt crystal, about 100 years earlier). By analogy with nonlinear ferromagnetics, similar substances with dielectric hysteresis acquired the term *ferroelectrics*, while switchable polarization was called “spontaneous” (at present, hundreds of such crystals are known).

However, it should be borne in mind that this supposed similarity of ferromagnetism and ferroelectricity represents only a superficial and formal approach. The point is that in nature there are *no magnetic charges* (as opposed to electrical ones). Moreover, magnetic field  $H$  and magnetization  $B$  are *axial* vectors generated by *closed* microscopic currents, while the electrical field  $E$  and polarization  $P$  are *polar* vectors, generated by electrical charges of different signs and location. Besides, being caused by closed currents, spontaneous magnetization can exist in the equilibrium state for an unlimited time. At the same time, polar vectors of electrical field  $E$  and polarization  $P$  are caused by the presence of *noncompensated* electrical charges: electrical potential starts and ends on electrical charges, while electrical field  $E$  is the gradient of potential. Moreover, in accordance with the Lorentz relation (connecting polarization and electrical field:  $E = \epsilon_0 \chi P$ ), the spontaneous polarization  $P_S$  should be accompanied by the internal electrical field  $F_S$ .

As for ferroelectrics, which are characterized by switchable polarization, the notion “internal electric field  $F_S$ ” can be matched to the notion of “coercive field,” which is experimentally determined from the hysteresis loop in conjunction with the value of polarization. But the concept of spontaneous polarization (which might seem reasonable for ferroelectrics) began to be used without grounded reasons as applied to all pyroelectrics, while ferroelectrics are only a subclass of them. Thereby, a pyroelectric looks like an electrical analog of a permanent magnet; however, if external influences are absent (i.e., in the equilibrium state) neither a pyroelectric crystal nor a ferroelectric crystal is surrounded by an electrical field, while a permanent magnet is surrounded by a magnetic field.

In order to explain the possibility of a stable existence of spontaneous polarization  $P_S$ , it is necessary to accept the idea of the presence in pyroelectrics of some compensating electrical charge of free carriers, needed to screen  $P_S$ . Thus, from the foregoing, it follows that, without the attraction of a notion about such compensating free charge, the concept of spontaneous polarization is not acceptable (at least for such pyroelectrics—insulators not creating electrical fields around themselves). If it is so, then it follows that spontaneously polarized status is a nonequilibrium state: otherwise it should be assumed that in a pyroelectric its  $P_S$  must be compensated by free electrical charges, since without external influence spontaneous polarization cannot manifest itself in any way.

Here it is appropriate to recall *electrets*, which can preserve an electrical field around themselves for a considerable time and obviously have an internal electrical field. However, there is a *fundamental difference* between pyroelectrics and electrets: the polar-sensitive state of pyroelectrics is their basic, equilibrium state, naturally acquired during formation of the crystal and disappearing only when it melts (so that the pyroelectric effect can be manifested in a polar crystal unlimited times). On the contrary, the *residual* polarization of electrets is created artificially by special technology; as a result their polarized state is *temporal* (thermodynamically nonequilibrium). For example, when electrets are heated, depolarizing current is generated by them only once.

Sometimes, those pyroelectrics that retain their own polarity up to crystal destruction or melting are classified as “persistent,” while ferroelectrics with their ability to

change orientation of polarization with a disappearance of this polarization at the Curie point can be referred to as “gentle” pyroelectrics. Further discussion will only be relevant to properties of “persistent” pyroelectrics, i.e., those for which it is assumed “spontaneous polarization” is not switchable. Active electrical properties of such crystals can manifest, first, in the pyroelectric effect and, second, in the volumetric piezoelectric effect. In both effects, under external thermal or hydrostatic influences the *manifestation* of internal polarization can be observed.

As is known, with temperature changes, any pyroelectric demonstrates a correspondent dynamic response in the form of electrical polarization, but its measurement does not allow finding the “quantity of basic polarization,” which varies with temperature. Insofar as the absolute value of “ $P_S$ ” cannot be determined as from pyroelectric so from piezoelectric dynamic experiments, only traditionally these effects are treated as “the change of  $P_S$ .” As already mentioned, this may be in doubt for the spontaneous polarization concept, because experimentally only the *appearance* of a polar response can be measured.

The concept of spontaneous polarization seems much more convincing in the case of “gentle” pyroelectrics-ferroelectrics, in which their polar-sensitive state, first, is switchable and, second, disappears with increasing temperature (usually long before melting of a crystal). However, in this case it is also possible to do without the use of the spontaneous polarization concept—in the external electrical field in ferroelectrics their own polar-sensitive structure is switched, furthermore yielding the possibility of measuring their parameters quantitatively. Therefore, when explaining various properties of polar crystals, there is no need to use the concept of “spontaneous polarization,” i.e., to imagine that in a polar crystal a “permanent polarization” exists. It seems to be a more reasonable assumption that electrical polarization appears as a response to external action (not even electrical) due to the peculiar spatial distribution of polar-sensitive internal bonds of ions that have distinction in ions’ affinity for electrons, i.e., electronegativity [3].

In fact, any investigations of pyroelectric or piezoelectric effects do not allow direct determination of the value of their “spontaneous polarization” but experiments characterize only the magnitude of dynamic response of peculiar polar-sensitive internal crystalline structure. When an electrical field is affected on a “persistent” polar structure, its electrical polarization usually looks like a linear effect (as in ordinary dielectrics). It may seem, however, that the exception is ferroelectrics, in which a switching of their “gentle” polarization is seen: their low-stable enantiomorphic structure changes its polar-sensitive direction. Outwardly this event manifests itself as a dielectric hysteresis loop, which allows measurement of the ability of the polar-sensitive structure to react to external influences that indirectly can characterize its features.

Most of the functional (active) dielectrics belong either to polar *crystals* (pyroelectrics, ferroelectrics, piezoelectrics) or to partially ordered polar *systems* (liquid crystals, electrets, polar polymers, etc.). That is why physical hypotheses relevant to the nature of internal polar-sensitive responses (which are not caused by an external electrical field) deserve particular attention. A “hidden” polar-sensitive quality is exactly that property that can cause electrical (vector) response to nonelectrical action on

matter. Moreover, the external influence can be scalar (i.e., a zero-rank tensor) or it can be a vector (first-rank tensor) or even a second-rank tensor.

Wherein, crystals with “purely ionic” bonds as well as crystals with “purely covalent” bonds are electrically nonsensitive to uniform nonelectrical influence, and these crystals, basically, are characterized by centrosymmetric classes of symmetry. As a rule, in crystals with exclusively ionic bonding, the highest symmetry is observed. In the same way, simple covalent crystals have fully balanced atomic bonds and usually a centrosymmetric structure. That is why such crystalline dielectrics will be considered next, in which polar structures are inherent to the hybridized ionic-covalent bonds. It is exactly this specificity that causes reduction of symmetry in crystals, so most of them belong to noncentrosymmetric classes. Peculiar properties of polar-sensitive crystals are described here by a substantial distinction in their electronegativity (covalent potential) of their atoms, which is balanced by spatial allocation of peculiar internal bonds, sensitive even to nonelectrical external influences on crystals. It is supposed that the primary cause of the existence of internal polar sensitivity is exactly this asymmetry in distribution of electronic density along ionic bonds.

It should be noted that simplified division of a crystal’s atomic electronic structure into *cores* (nuclei with deep electrons) and *shells* (external electrons) is only a first approximation. To explain more complex manifestations of crystal properties, one must take into account the features of cores: total number of electrons in an atom, degree of screening of external electrons from action of the nucleus, etc. It is appropriate to recall that *electronegativity* is a physical property, describing the tendency of an atom to attract electrons; it depends mainly on atomic number as well as on size and structure of the outer electron orbitals. In the internal structure of an atom, the attraction, which the outer electrons feel from the nucleus, depends on the number of protons in the nucleus, on the distance of the outward orbital from the nucleus, and on the degree of screening, which is performed by the inner electrons. The higher the atomic electronegativity, the stronger atoms attract electrons toward themselves.

For the reasons listed, in various atoms the difference in their electronegativity can be very substantial. In the structure of a crystal, the ion with higher electronegativity attracts conjunctive electrons more strongly, and therefore its true charge becomes more negative. Conversely, the ion with lower electronegativity acquires increased positive charge. Together these ions can create a *polar-sensitive bond* and provide needed conditions for noncentrosymmetric structure emerging. In molecules, a perceptible difference in atoms’ electronegativities gives rise to their *interior polarity*: for example, a dipole moment can be created in some molecules (such as in HCl or H<sub>2</sub>O). However, in crystals a significant difference in ions’ electronegativity results in directional polar-sensitive structural motives and, in particular, produces noncentrosymmetric structures.

Accordingly, the noncentrosymmetric structures of polar crystals are a demonstration of mixed ionic-covalent bonds between their ions. These connections are strongly directional and, therefore, such structures lead to different manifestations of asymmetry and complexity of polar crystal structures. The noncentrosymmetric structure is formed owing to the compensation of atomic electronegativity by polar-sensitive bonds in the process of formation of a polar crystal (while it is growing from a liquid

or vapor state of material). At that, depending on the chemical composition of a crystal, a variety of combinations may appear between ions of crystals with two- or three-dimensional polar-active constructions (which, when external actions are exerted on them, can generate electrical responses, describable by tensors of different ranks).

Various models of crystal internal polarity will be considered further. Namely, non-centrosymmetric allocation of electrical charges in polar crystals might be presented by different structural variants, such as one-dimensional dipole-type of polar-sensitive bonds, or two-dimensional formation of asymmetric bonds, or a three-dimensional shape of peculiar atomic bonding. Dipole-type disposition of ions (1D polar-sensitive bonding) corresponds to the classic model of pyroelectric structure that can be described by a vector (first-rank tensor,  $M_i$ ). The 2D polar-sensitive arrangement of ions in-plane can be described by a second-rank tensor,  $M_{ij}$ . The spatial (3D) arrangement of ions joined by polar-sensitive bonds can be described by a third-rank tensor,  $M_{ijk}$ . At that, these models describe both pyroelectrics and piezoelectrics.

## 1.4 Different atomic bonds

As is known, any connections of atoms, molecules, or ions are conditioned by electrical and magnetic interactions. At increased distance between particles the forces of *attraction* dominate, while at short distances, due to overlapping of electron shells, the *repulsion* of particles increases sharply. The energy of repulsion forces can be modeled by a power law  $U_{rep} \sim r^{-8}-r^{-12}$ , while the energy of attractive forces, depending on type of bonds, varies with distance as  $U_{att} \sim r^{-1}-r^{-6}$ . A balance between long-range attraction and short-range repulsion is achieved at the crystal lattice constant:  $r = a$ .

Stable spatial structure of a crystal is formed by restructuring of the atoms' electron arrangement, creating different bonds, which is accompanied by a decrease of total energy. At the formation of chemical bonds, exactly those electrons that belong to valence shells play a major part, since their contribution to solid body formation is much greater than the contribution of the inner electrons of atoms. However, the division into cores and valence electrons is a matter of convention. For this discussion, the most important interatomic links are molecular, ionic, and covalent bonds (Fig. 1.5): it is their combination that makes possible the emergence of stable polar-sensitive bonds, forming noncentrosymmetric crystals.

- In the **molecular crystals**, electrons are completely locked in their molecules (as in atoms of inert gas). Nucleuses of molecules are surrounded by spaces, the shading of which in Fig. 1.5A approximately corresponds to the probability density of finding electrons: in black balls the density of the electron cloud reaches significant value. There are both attraction and repulsion between molecules. The nature of these interactions is as follows: atomic electron shells show strong repulsion only when they very closely approach, but at some distance a weak attraction between electron shells exists due to *quantum fluctuations* of electron density in the shells, described by virtual electrical dipoles or quadrupoles (Fig. 1.5A). This attraction varies with distance approximately as  $U_{att} \sim r^{-6}$ ; such van der Waals bonds are additive and nonsaturated. By the way, this type of bonding *always* exists, and therefore

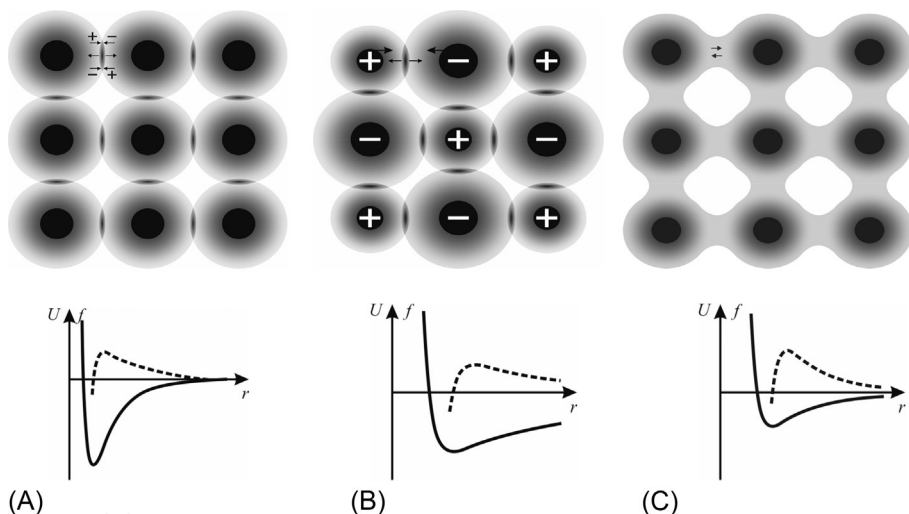


**Fig. 1.5** Two-dimensional image of electrical charge distribution: (A) Molecular crystal, in which quadrupole electronic fluctuation (+ - ... - +) causes attraction of atoms, while partial overlapping of electron shells leads to repulsion ( $\leftarrow \dots \rightarrow$ ) compensating this attraction; (B) ionic crystal where ion attraction is compensated by partial overlapping of electron shells; (C) covalent crystal. In the graphs, the solid curve shows interaction energy while the dotted curve shows interatomic force.

it should be added to all other types of interatomic bonds. Furthermore, in the case of *polar* molecules, *orientation interaction* is also added to the usual intermolecular interaction. In the case of other types of connection, the contribution of molecular bond may be taken into account by the Lennard-Jones potential.

- In **ionic crystals**, interionic bonds are formed between metallic and nonmetallic elements, while the valence electrons move from cations to anions (while in molecular crystals all electrons remain trapped in their own atoms). The attraction energy of dissimilar ions changes with interion relatively slowly:  $U_{att} \sim r^{-1}$ , so that the ionic bonds are the most long-range compared to other types of interatomic bonds. The energy of ion repulsion, as in other crystals, strongly depends on the interatomic distance:  $U_{rep} \sim r^{-8} - r^{-10}$ . Ionic crystals, as well as molecular crystals, are characterized by such a distribution of electronic density, which is almost completely localized near the ions (Fig. 1.5B). In this case, the cations and anions acquire electronic configuration of an inert gas, and therefore the charge distribution in them has almost *spherical symmetry*. Ionic bonds are *saturated*, but they are *not directed*.
- **Covalent crystals** are characterized by such energy of attraction, which varies with the interatomic distance as  $r^{-2} - r^{-4}$  (that is, it is a more short-range bond compared to the ionic bond). In this case, the valence electrons are distributed only between the nearest neighboring atoms (Fig. 1.5C): each covalent bond is formed by a pair of valence electrons that have opposite spin directions. The decrease in the total energy during the formation of covalent bonds is achieved by the quantum effect of exchange interaction. Covalent bonds are *saturated*: only a limited number of bonds can be created by external electron orbitals, and these bonds are also sharply *directed*, which is due to the geometric shape of electron density distribution (a *valence angle* exists between the two bonds).

When the *same atoms* form a covalent bond, each of them gives one of the unpaired electrons per one bond, but the formal charge of atoms remains unchanged, since the atoms that form the bond have an equally socialized electronic pair. If *different atoms* create a covalent bond, it acquires pronounced *polarity* and shows increased *polarizability*, which determines many physical properties of correspondent compounds. The degree of electron density distribution along a covalent bond is determined by the difference in ion electronegativity (as already noted, an ion with greater electronegativity stronger attracts electrons, and its real charge becomes more negative; a lesser electronegative ion acquires, respectively, a positive charge of the same magnitude). Thus, polar sensitivity of a covalent bond is due to uneven distribution of electronic density in it, while its polarizability depends on the binding rigidity of electrons.

- **The effect of structural defects** that violate the strict periodicity of a crystal lattice can lead not only to the *local polar properties* of ionic and covalent crystals, but in rare cases even lead to formation of a *polar-sensitive crystal lattice*.

First, the appearance of a *local polarity* in crystals containing *semifree* (localized) electrons (or electron holes) will be discussed. They are concentrated in the vicinity of structural defects of a dielectric, allowing the localization of electrons (holes) in *two or more equivalent positions*, which are separated by low potential barriers. Thus, structural defect centers are the places of irregularity in the distribution of electric charge in the crystal lattice.

This type of local electron polarization is characteristic of many technically important dielectrics, such as rutile ( $\text{TiO}_2$ ), perovskite ( $\text{CaTiO}_3$ ), and similar complex oxides of titanium, zirconium, niobium, tantalum, lead, cerium, and bismuth. A high concentration of structural defects such as an *anion vacancy* is the structure peculiarity of these substances, especially in their polycrystalline state.

During high-temperature synthesis of ceramics from a mixture of oxides (or during crystal growth) the appearance of anionic vacancies is very likely. Electrical compensation of these defects occurs by the lowering of the valence of cations located near an anion vacancy. Fig. 1.6 shows one of the possible cases of partially bound electron locations near an ionic vacancy in rutile. In the selected part of the  $\text{TiO}_2$  crystal there are three titanium ions as the nearest neighbors to an anion vacancy (in a 3D crystal the number of such neighbors is five). Charge compensation of the oxygen vacancy is carried out by the fact that two of five adjacent to the anion vacancy titanium ions become trivalent: each of them contains in its outer shell one weakly bound electron; at that probability density of these electrons, the wave function is increased in the place of the missing oxygen. Under the influence of chaotic thermal lattice vibrations, these polar centers are oriented randomly, which does not lead to regularly oriented polarization in the crystal: the concentration of anion vacancies in the crystal cannot be very large; so these pseudo-dipoles cannot become self-organized into a polar lattice.

The second example that might have particular interest is that local polarity can be artificially created by *irregular disposition of ions* in a crystal. In a simple case, this can be obtained in the solid solutions of crystals that have *different sizes of ions*: in them, a smaller ion does not occupy its geometrically central position but shifts to one of the nearest ions of opposite polarity. With this, a polar moment is formed,

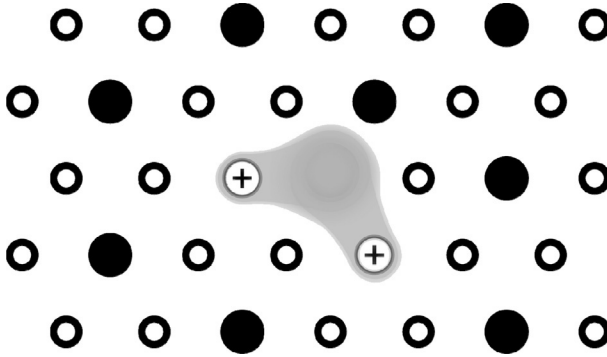


**Fig. 1.6** Local polar centers in rutile: Planar lattice model of titanium dioxide with oxygen anion vacancy located at the intersection of electron clouds;  $\circ$ —oxygen,  $O^{-2}$ ;  $\bullet$ — $Ti^{+4}$ ;  $\oplus$ — $Ti^{+3}$ .

which can change its direction in a lattice, when a small ion jumps closer to another neighboring ion. Fig. 1.7 symbolically shows, for example, a potassium chloride crystal that forms a solid solution with lithium chloride ( $K_{1-x}Li_x$ )Cl, where index  $x$  is  $Li^{+1}$  volumetric concentration.

In a cubic lattice of KCl crystal, a small cation  $Li^{+1}$  jumps closer to one of six neighboring ions  $Cl^{-1}$ , thereby forming a local dipole moment embedded in the lattice. In Fig. 1.7 such equiprobable positions are four, but there are six of them in the volume of a crystal. The solubility of LiCl in the KCl is limited, so that the distance between these dipoles is not enough to create by their interaction a polar lattice able to overcome the energy of thermal vibrations (especially since permittivity in alkali halide crystals is rather small;  $\epsilon < 10$ ). That is why in other similar crystals it is also not possible to obtain any polar lattice in this manner.

However, some experiments with *noncentral cations* imbedding into a crystal matrix with *higher permittivity*, namely, in the nonpolar (paraelectric) crystal  $KNbO_3$  in which  $\epsilon \sim 200$ , turned out to be more successful: the crystal  $(K_{1-x}Li_x)Nb_3$  looks like an *artificial ferroelectric* with a Curie point around 300 K [4]. The interaction of embedded dipoles formed by the noncentral location of  $Li^{+1}$  ions partially replacing  $K^{+1}$  ions in the *highly polarized lattice* opened up a possibility for formation of *self-ordered polarization*.

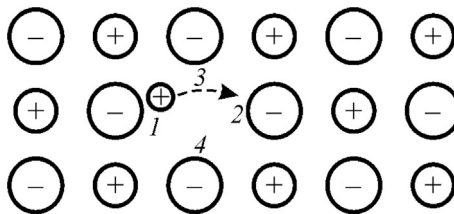


**Fig. 1.7** The ability to create a polar cluster in a simple cubic ionic crystal: Small positive ion localizes nearby one (1) of possible negative ions, having the ability to jump to other position (2).

Another way to obtain *artificially* ordered polarization is the *inhomogeneous deformation* of a highly polarizable dielectric, such as, for example, paraelectric SrTiO<sub>3</sub> that has  $\epsilon \sim 300$  at normal conditions [7]. By creating inhomogeneous deformation, a nonpolar dielectric (but close to polar dielectric by its structure) can be turned into a polar dielectric, if *deformation is nonuniform*. However, such transformation cannot be realized in bulk dielectrics, since they can be destroyed already with strain on the order of fractions of a percent (due to inevitable dislocations and other structural defects). For example, dielectric oxide crystals in their bulk form are *brittle* and will crack even under moderate strains, typically 0.1%. A way around this limitation (peculiar to bulk crystal) is possible by using the earlier described (with the example of (K<sub>1-x</sub>Li<sub>x</sub>)Nb<sub>3</sub>) “chemical pressure” through different size or isovalent cation substitution. However, the disadvantage of such an approach is the introduction of disordering and potentially unwanted local distortions.

However, **thin epitaxial films** of oxide dielectrics, having very perfect structure, are capable of withstanding in-plane deformation of several percent, opening up the possibility to practically obtain new polar materials. Using epitaxial technology and *biaxial misfit* strain, created by underlying substrate, elastically strained thin films of perovskite structure are obtained with *several percents* level of strain [7]. These films acquire various new properties, including properties of *polar dielectrics*, by means of external inhomogeneous influence on their interatomic bonds. For example, *compression in plane* of a cubic lattice that has *m3m* symmetry can transform this structure into a tetragonal lattice of *4m* symmetry with the appearance of polar (including ferroelectric) properties along the axis of fourth order.

Thus, under large strains, physical properties of oxide compositions can be dramatically altered. In Ref. [7] many examples are described regarding transmuting oxides that are neither ferroelectric nor ferromagnetic in their bulk (unstrained) state into ferroelectrics, ferromagnets, or even materials that have both these properties at the same time (multiferroics). It should be noted in passing that epitaxial strain technology provides a potentially unlimited way to provide large biaxial strain (this has been used previously to greatly increase mobility of charge carriers in transistors). As for perovskite dielectrics, the most striking example of strain-induced polarity is shown in epitaxial SrTiO<sub>3</sub> film that demonstrates a gigantic change in electrical properties, with the Curie point increasing more than  $\sim 300$  K, never before seen in any other experiment.

Next, however, the discussion will relate to no-doped and *nonstressed* crystals, the structure of which is shown in Fig. 1.5, where basic types of bonding are listed: all of them have some influence on the peculiar properties of polar crystals. At that, the most significant is the possibility of ionic and covalent bond *hybridization*. This is a feature that leads to manifestation of natural polar sensitivity in crystals.

## 1.5 Polar-sensitive atomic bonds

For further consideration of the nature of internal polarity, we turn to the possibility of creating polar properties in dielectrics *artificially* in uniform impurity-free nonpolar crystal. In fact, in ordinary ionic or covalent crystals, *polar* properties can be obtained

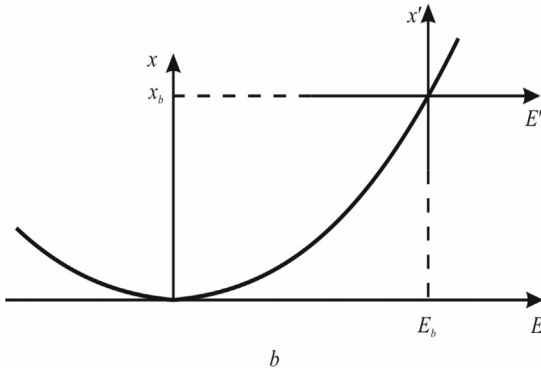


**Fig. 1.8** Representation of piezoelectric effect as linearized electrostriction; in bias field  $E_b$  quasilinear dependence  $x'(E')$  imitates the piezoelectric effect [5].

by applying to an electrical field  $E$  to them. Moreover, the resulting induced polarization  $P = \epsilon_0(\epsilon - 1)E$  is accompanied by *electrostriction*, which is a quadratic effect when relative deformation  $x$  of the crystal increases in the applied field by the *parabolic* law:  $x = R \cdot E^2$  (in contrast to polar crystals, in which field-induced deformation depends on applied field *linearly*, showing a piezoelectric effect:  $x = d \cdot E$ ). It is seen that strain  $x$  in the case of electrostriction does *not change* its sign with change in electrical field sign—unlike the piezoelectric effect.

However, the *linear* electromechanical effect (which is a particular property of polar crystals) can be interpreted as *linearized electrostriction* (Fig. 1.8). Suppose that external constant electrical field (bias field  $E_b$ ) is applied to the usual centrosymmetric crystal which is nonpiezoelectric at  $E_b = 0$ . The applied electrical field changes the original symmetry of a crystal due to its electrical polarization: as seen from Fig. 1.8 strain  $x_b$  increases depending on bias field  $E_b$ . In this way, under fixed external voltage, the structure of the crystal turns into an *artificially created* polar structure (it becomes an “electrically induced noncentrosymmetric” structure).

If that's the case, then the *imitation* of linear electromechanical response (piezoelectricity) can be observed on a wing of an electrostriction parabola: at bias field presence, the alternating electrical field  $E'$  generates a practically linear mechanical response:  $x' \approx d' \cdot E'$  where  $d'$  is an *electrically induced* piezoelectric module. Calculations shows that  $d' \approx 2Q'\epsilon_0^2\epsilon^2E_b$  [5], where  $\epsilon$  is permittivity and  $Q'$  is the electrostriction parameter. It should be noted that in those dielectrics with very large permittivity ( $\epsilon = 10^4$ – $10^5$ ) this effect can be “gigantic” (Fig. 1.9B) and this is now used in electronics.

Similarly, in the presence of an electrical bias field, the *pyroelectric effect* can also be induced in *any* crystal, which also finds some application in modern thermal sensors. In dielectrics with large permittivity, the electrically induced pyroelectric effect can be so great that it exceeds the sensitivity of natural pyroelectricity in polar crystals.

In compliance with such electrically induced piezoelectric and pyroelectric effects (which are possible in any solid dielectric but applicable in dielectrics with large permittivity), one can suppose that the *usual* piezoelectric effect can also be explained as “*linearized electrostriction*” (Fig. 1.8). This assumption might be advanced according

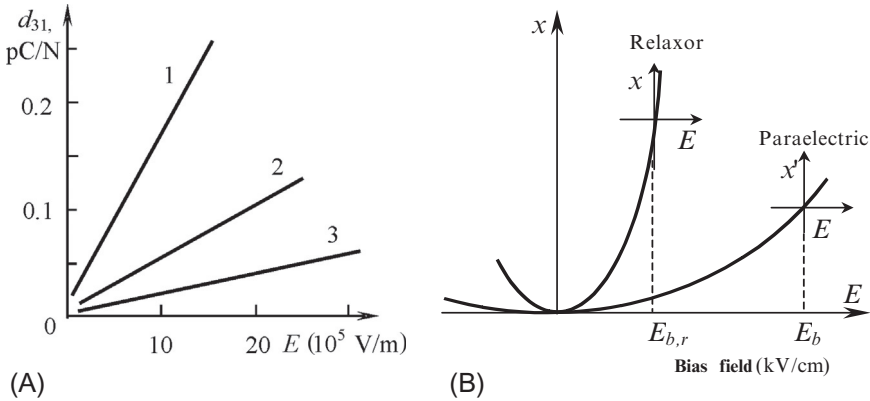


**Fig. 1.9** Electrically induced piezoelectric effect in high- $\epsilon$  dielectrics: (A) Line 1 is SrTiO<sub>3</sub> with  $\epsilon = 300$ ; line 2—CaTiO<sub>3</sub> with  $\epsilon = 150$ ; line 3—TiO<sub>2</sub> with  $\epsilon = 100$ ; (B) comparison of relaxor-ferroelectric and paraelectric [5].

to the concept that the fundamental reason for crystal intrinsic polar-sensitivity is asymmetry in electronic density distribution along polar bonds between ions that have different electronegativity, which *replaces the externally applied field*. In extremely simplified form, three linear models of electron density distribution (covalent, ionic, and mixed bonding) are shown in Fig. 1.10: given in both normal state and under electrical field influence.

In the **covalent crystal**, electrons are equally distributed around their atoms; moreover, electron density between atoms is rather large. The most important property of covalent structure is the openness of the structure, due to the small number of neighboring atoms (four in total) and mutual coupling of electronic pairs having opposite spin. From this follows, by the way, higher electronic polarizability of covalent crystals ( $\epsilon_{opt} = 7\text{--}15$ ) and the highest possible mobility of free electrons in them. For further understanding of the model under discussion, it is important here that the externally applied field *deforms* electron shells of atoms by stretching them, which leads both to electrostriction  $x = \Delta l/l \sim E^2$  and to increased polarization due to relatively free displacement of clots of electron density (Fig. 1.10B).

In **ionic crystals** the mutual attraction of cations and anions is compensated by repulsion of partially overlapping electron shells as well as by essential deformation of electron shells of ions. In contrast to covalent (atomic) crystals, in which magnetic attraction of spins dominates in outer shells, in ionic crystals the outer electron shells are under the action of an electrical field of dissimilar ions (Fig. 1.10C). In an external electrical field, cations and anions are forced to be displaced, which gives such a *deformation* of electron shells of ions so that virtual formations of electron pairs become possible. That is why external field application is accompanied by electrostriction (Fig. 1.10D), the value of which is proportional not only to  $E^2$  but also to  $\epsilon^2$ . If in covalent dielectrics and semiconductors, as a rule  $\epsilon \sim 10$ , then in some highly polarizable nonpolar ionic crystals (paraelectrics) it reaches  $10^2\text{--}10^4$ , which leads to large and even gigantic electrostriction.

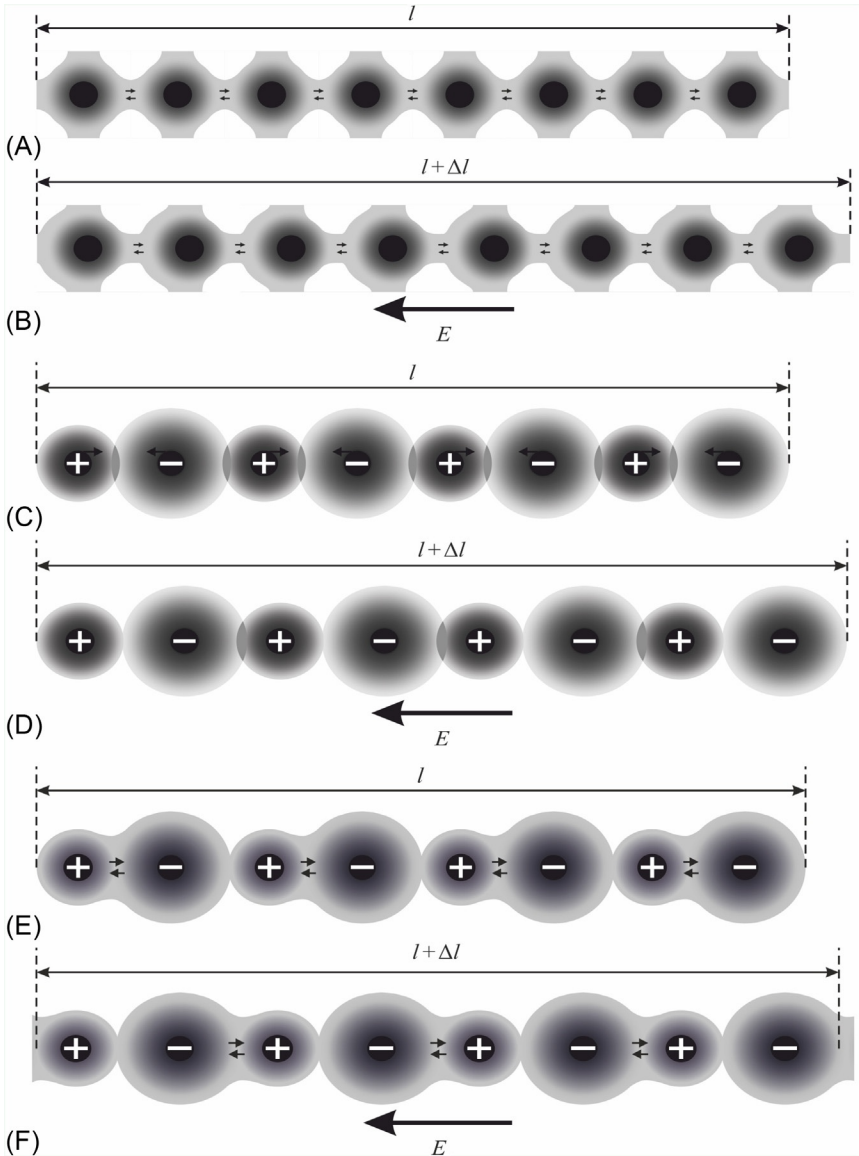


**Fig. 1.10** Simplified model of polarization in different atomic and ionic chains: (A) Symmetric distribution of electron density in covalent lattice (*arrows* symbolize opposite orientation of electron pair spins); (B) polarization of covalent lattice with electrostriction  $\Delta l/l$  in applied electrical field; (C) symmetric ionic lattice where repulsion is due to overlap of electron shells; (D) polarization of ionic lattice and electrostriction  $\Delta l/l$  in applied electrical field; (E) hybridized bond that leads to polar properties of crystals; (F) switching of hybridized bonds in electrical field.

Therefore, being in a *nonequilibrium* polarized state, under the influence of an externally applied field both covalent and especially ionic crystals acquire properties of polar crystals, namely, the ability to demonstrate piezoelectric, pyroelectric, linear electrooptical and other special effects.

The **mixed covalent-ionic bonding**, shown in Fig. 1.10E, is a *distinctive feature* of the model under discussion, as well as a main property of polar crystals that guarantees piezoelectric and pyroelectric effects *without* an external electrical field application. In this way, instead of an external electrical field, which needs to be connected to ionic or covalent crystals and forces them to be in the polarized but nonequilibrium state (as shown in Fig. 1.10B and D), in the case of mixed covalent-ionic crystals their polar-sensitive state is stable without any external field being ensured by one of the fundamental properties of ions—their electronegativity. Therefore, the main point of the model under discussion is that mixed covalent-ionic bonding (Fig. 1.10E), being a feature of polar crystals, guarantees the piezoelectric and pyroelectric properties without external electrical field application to a crystal. In this way, instead of an external electrical field needing to be applied to ionic or covalent crystals and forcing them to be polarized, remaining in a nonequilibrium state (as shown in Fig. 1.10B and D), in the case of mixed covalent-ionic crystals their polar-sensitive state is stable without any external field.

Exactly the distinction in *affinity to electrons* in various ions leads to formation of hybridized polar-sensitive bonds, which determine a crystal's own polarity, replacing in this way the external electrical field, which can polarize any crystal. In a polar crystal its state: "able to polarization in a nonelectrical way" is entirely its equilibrium state at a certain temperature ( $T_1$ ) and pressure ( $p_1$ ), and it is stored in the absence of external influences as much as one wants. If any external influence acting on a polar crystal occurs (change in temperature, mechanical stress, etc.), then a new stable state arises, at  $T_2$  and  $p_2$ . Moreover, a change in state ( $T_1 \rightarrow T_2$  or  $p_1 \rightarrow p_2$ ) is accompanied by the dynamic appearance of surface electrical charges (in other words, thermally or mechanically induced polarization arises), i.e., the pyroelectric or piezoelectric effect becomes apparent.

The simplified model shown in Fig. 1.10E corresponds to a linear pyroelectric crystal, in which internal polar-sensitive bonds are "persistent," but they can be deformed, such as by a temperature change (giving a pyroelectric effect) or by mechanical stress (giving a piezoelectric effect). Such intrinsic polar sensitivity in a linear pyroelectric usually is conserved up to the crystal melting. Under the action of an external *electrical* field, in such a pyroelectric only linear polarization (as in any dielectric) arises with a value of permittivity typical for ordinary ionic crystals.

However, in the case of a *ferroelectric* ("nonlinear" pyroelectric), which can be imagined by the *combined pictures* shown in Fig. 1.10E and F, its intrinsic polar-sensitive bonding is "gentle," i.e., it is not sufficiently stable and can *change its own orientation* to the opposite in an applied electrical field, demonstrating a hysteresis loop and large dielectric permittivity. An increase of temperature can violate a correlation between neighboring polar-sensitive bonds that leads to phase transition into a nonpolar phase at the Curie point. Similarly, increase of hydrostatic pressure in a ferroelectric also destroys its weakly stable ordering of polar-sensitive bonds that leads to transition into a disordered phase.

The concept discussed here of an intermediate type of bond agrees with the assumption of ion deformation due to their polarization that may occur, for example, by distortion of more pliable electron orbitals in anions, thanks to different electronegativity of adjacent ions. Moreover, electron density between ionic residues increases (Fig. 1.10E), i.e., a mixed covalent-ionic bond, possessing a greater degree of charge separation, turns into a polar-sensitive bond. Due to the fact that these bonds are partially covalent, they retain definite orientation, which promotes their strengthening, supporting to withstand chaotic thermal motion in the crystal lattice. Due to fact that these bonds are partially ionic, in them, first, polarizability increases since in addition to electrons the ions are shifted as well, and, second, the rate of reaction upon external action on the crystal is determined by inertia of ion motion (but not by fast electrons), so that they determine the phonon spectrum of the apolar crystal lattice.

Polar-sensitive bonds arise in crystals that have a small coordination number (CN, showing the number of nearest neighbors to a given atom). Thus, an “open” structure corresponds to polar dielectrics and semiconductors: this provides a sufficient space for electron orbits interaction. If in the usual densely packed crystalline structures this number is large (CN = 8–6 for ordinary dielectrics), then, for example, in piezoelectric sphalerite and in pyroelectric wurtzite CN = 4.

The polar-sensitive structure manifests itself in crystals as the ability to provide electrical (vector type) response to a nonelectrical scalar or more complicated tensor type of actions. It is obvious that hybridized ionic-covalent bonding causes reduction in crystal symmetry, so polar crystals always belong to noncentrosymmetric classes of crystals.

The noncentrosymmetric structure of some crystals is caused precisely by the presence of specific interatomic bonds, that is, an ion-covalent (hybridized) bond is the main cause of the pyroelectric, ferroelectric, and piezoelectric properties in the crystals. For example, a piezoelectric effect arises as an electrical response to uniform is *directional* mechanical action on a polar crystal. Its mechanism is that the displacement of ions compresses (or stretches) their *asymmetric* bonds, as a result of which electric charges are induced on the surface of the crystal. On the contrary, if the atomic bonds in a crystal are *centrosymmetric*, no electrical response is possible for any *uniform* mechanical effect: the electrical effects from various charge displacements in this case *compensate* each other.

## 1.6 Modeling of polar-sensitive bonds

From 32 classes of crystals of symmetry, 11 classes are centrosymmetric classes and 21 are noncentrosymmetric classes. Moreover, only in 20 noncentral classes is the odd electromechanical effect (piezoelectricity) possible:  $x = d \cdot E$  (i.e., strain  $x$  in them is proportional to applied electrical field  $E$  while  $d$  is the piezoelectric modulus). Furthermore, from 20 piezoelectric classes of crystals 10 classes belong to pyroelectric classes of symmetry (they have a *special* polar axis), while the other 10 noncentral classes can be referred to as “exclusive” piezoelectrics: they have only *polar-neutral* axes that compensate each other. This means that, taking into account the compensation

effect from all these axes, a polar-neutral crystal does not respond to the *uniform* change of temperature or to hydrostatic pressure influence (as also happens in centrosymmetric crystals).

The deep-laid physical nature of intrinsic polarity in some crystals in many respects remains unclear. It will suffice to mention that occasionally even the homeopolar diamond can have a form of pyroelectric wurtzite (class symmetry  $6mm$ ) in addition to its principal form of  $m3m$  diamond structure. Moreover, among many piezoelectrics, several monatomic crystals exist: Te and Se belong to the piezoelectric structure of quartz-type (32 class of point symmetry) crystals. In the mentioned examples of non-ionic crystals, undoubtedly only the dissymmetry of electron atomic shells can be responsible for the intrinsic polarity of these crystals.

However, in the following discussion only those crystals with *mixed ionic-covalent bonds* will be treated. Moreover, basically the polar-neutral crystals (in other words, “exclusively” piezoelectrics) will be considered, and an original method will be indicated: how to measure any single component of polar sensitivity in polar-neutral crystals. In addition to determining “hidden” polarity, it will be shown that the possibility exists to obtain a pyroelectric response to uniform thermal action from non-pyroelectric crystals, which might have some new applications.

Moreover, the models under discussion, based on asymmetry in electronic density distribution along atomic bonds, are free from any assumptions as to internal electrical field, so their intrinsic polarity does not need to be compensated by free charges. Although asymmetric polar-sensitive bonding is not a result of any internal field, nevertheless it can provide a polar response to nonelectrical homogeneous external impact (thermal, mechanical, or other) that in principle is impossible in centrosymmetric crystals.

The noncentrosymmetric allocation of electrical charges in polar-sensitive structures can be presented by different simplified structural models [4]:

- (1) A quasioone-dimensional structural ordering, which corresponds to the vector (dipole-like) response to external influences; the simplest model uses a linear unidirectional polar bond between two ions (Fig. 1.11A).
- (2) A two-dimensional structural arrangement of polar-sensitive bonds allowing the electrical response to scalar action to be described by the model, which consists of six ions, having asymmetric bonds and located in one plane (Fig. 1.11B).
- (3) A three-dimensional asymmetric polar-sensitive bonding, modeled by eight ions, representing a spatial polar-neutral structure (Fig. 1.11C).

Such modeling of electrical charge allocations looks quite ordinary when describing the dynamic properties of electron shells, for instance, to explain the nature of van der Waals bonding by quantum polar fluctuation in electron shells. Being applied to *polar crystals*, this modeling describes spatial orientation of asymmetric hybridized ionic-covalent bonds. Thus one-, two-, and three-dimensional distributions of polar-sensitive bonds in a space are presented by directionality of structural bonds, which will be used further to describe various properties of functional (polar) dielectrics.

- The simplest case is **dipole-type structural predisposition** (Fig. 1.11A), which corresponds to a quasioone-dimensional disposition of polar-sensitive bonds in a crystal. This is a well-known

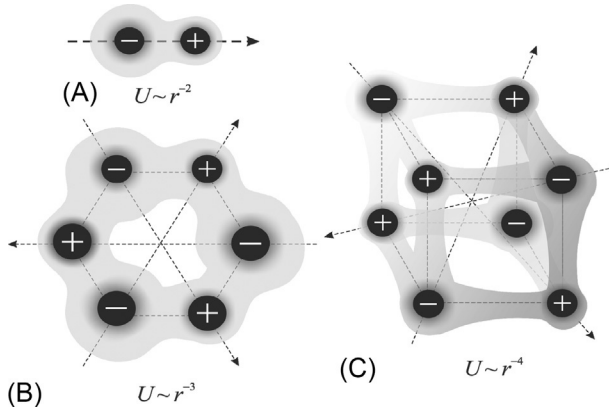


**Fig. 1.11** Simplified representation of polar-sensitive structures in crystals: (A) 1D dipole-like model; (B) 2D polarity modeling; (C) 3D polar construction; polar-sensitive directions are presented by *arrows* while specified rate of energy decrease with distance  $U(r)$  is shown by power function.

concept of pyroelectricity—the *internal ability* of a structure to show *electrical response* (polarization) to nonelectrical action. This case is used here only as a means of describing polar crystal reaction to *homogeneous* dynamic influence: to changing-in-time uniform heating (or cooling) that leads to a pyroelectric effect. The crystal reaction to changing-in-time uniform compression or stretching on crystal can be similarly described, e.g., dynamic hydrostatic influence, which gives a volumetric piezoelectric effect.

Physical properties, which usually are described by a dipole-like model of polar sensitivity, can be described by *material polar vectors*. They might be considered as properties “built into crystal structure.” It is this predisposition of 1D oriented polar-sensitive bonds that results in their vector type reaction to any external scalar influence on pyroelectric crystal. The relevant crystals belong to 10 pyroelectric classes of symmetry (including ferroelectrics as a subclass of pyroelectrics). The ability of such crystals to give an electrical (polar) response  $dM_i$  to homogeneous hydrostatic pressure  $dp$  can be described by a material-type tensor of first rank (vector)  $d_{Vi} = dM_i/dp$ , which characterizes the volumetric piezoelectric effect with module  $dV_i$ . This property is inherent only in crystals of pyroelectric symmetry.

Similarly, the ability of a 1D system of polar-sensitive bonds to have an electrical response to temperature change  $dT$  corresponds to a certain, also “material,” vector  $dM_i/dT$  and can be described by an indicatory surface (indicatrix), “above and below the symmetry plane  $m$  and are characterized by the equation  $\gamma(\varphi) = dM_i/dT = \gamma_{\max} \cdot \cos\varphi$ . It is evident that polar-sensitivity spatial distribution can be described in just the same way. The upper sphere is the indicatory surface for the upper orientation of  $M_i$ , while the bottom sphere means only the change in a sign of pyroelectric coefficient  $\gamma_i$ , if internal polarity has the opposite direction. The material vector  $\gamma_i$  has a maximum in direction, coinciding with the internal polarity direction. So  $\gamma_{\max}$  should be measured in the cut of a crystal made perpendicularly to the polar axis. Angle  $\varphi$  is

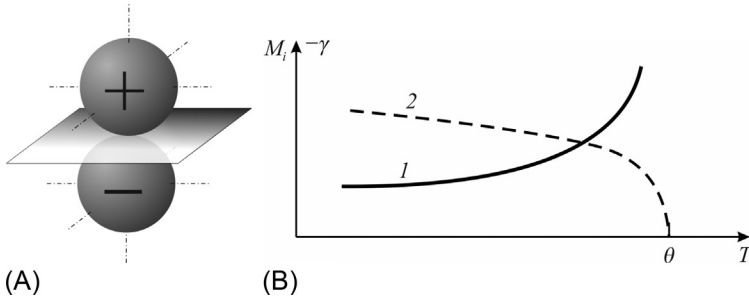


**Fig. 1.12** 1D modeling of polar-sensitive bonding: (A) Indicatory surface of material vector; (B) temperature dependence of pyroelectric coefficient (line 1) and internal polarity (line 2).

the angle between the ordinate and the slanting crystal's cut, in which the pyroelectric effect is studied.

Fig. 1.12B shows an example of a “gentle” (nonlinear) pyroelectric-ferroelectric, in which the polar sensitivity disappears after the phase transition at  $T = \theta$ , and therefore  $M_i(T)$  can be measured quantitatively relative to zero value. In “persistent” (linear) pyroelectrics, the value of  $M_i(T)$  cannot be measured quantitatively (since this dependence is interrupted only at melting of a crystal).

It should be mentioned also that the energy of dipole-to-dipole interaction decreases somewhat slowly with distance: namely, as  $\sim r^{-2}$  (Fig. 1.11A). Such a peculiarity has a significant influence on the *temperature dependence* of intrinsic polar sensitivity, when thermal chaotic movement aspires to destroy internal ordering in structure. It is notable that 1D ordering over the long term looks relatively stable, because it is capable of more strongly withstanding the inescapable disorienting by 3D thermal fluctuations. That is why the usual (linear) pyroelectric can preserve its internal polar sensitivity up to the melting of the crystal. However, if chaotic 3D thermal disordering, nevertheless, can still overcome the steadiness (internal energy) of self-ordering of a polar quasi-1D system (this is the case of ferroelectrics, shown in Fig. 1.12B), then its collapse happens very fast (critically), which leads to a phase transition into the nonpolar phase. Moreover, it is important to note that in a temperature interval of the ordered phase, the dependence of polar sensitivity on temperature is subordinate to Landau's law:  $M_i(T) = M_{max}(\theta - T)^{1/2}$ , i.e., with Landau critical index of 0.5.

There is a further need to consider other, less-studied polar crystals, which are *not pyroelectrics* but belong to the so-called group of “exclusively” piezoelectrics. In this case, more complicated allocation of polar sensitivity needs a different model from the simplest arrangement of dipole-type polar-sensitive bonds. As noted earlier in connection with Fig. 1.11A, the intrinsic polarity of such piezoelectrics can be represented by a plane 2D model (based on the structure of quartz) and by a spatial 3D model (based on sphalerite structure); correspondingly, they can be described by second- and third-rank tensors. As seen in Fig. 1.11B and C, the correspondent intrinsic electrical moments, described by these higher-rank tensors, are totally compensated (in contrast

to the dipole-type structural arrangement). In both these cases any scalar action (e.g., hydrostatic pressure or uniform heating) cannot induce in such crystals any response of a vector character. Only vector or tensor types of outside actions, such as temperature *gradient* (vector  $\text{grad } T$ ) or mechanical stress  $X_{ij}$  (second-rank tensor) are capable of discovering the “hidden” internal polar sensitivity, which awakens its vector-type response, i.e., to induce a voltage on a crystal surface in an open-circuit crystal or generate an electrical current in a short-circuit crystal.

The modeling of internal (or latent, or hidden) polarity discussed in the following text describes an ability of low-symmetric crystals to have an electrical response to a variety of external actions that are *variable in time*. It should be noted that, if the external impact after its switching on (or changing) afterwards remains constant, the polarization does not manifest itself—unlike with electrical conductivity, which exists all the time upon external factor action (fields, illumination, radiation, heat gradient, etc.).

- The **situated in-plane (2D) polar sensitivity** is a typical characteristic of some piezoelectrics that are not pyroelectrics (for instance, quartz). Crystals of a quartz-symmetry are berlinite ( $\text{AlPO}_4$ ), cinnabar ( $\text{HgS}$ ), tellurium ( $\text{Te}$ ), etc. Suppose that these crystals are investigated under *uniform* thermal action, realized under the special condition of *partial limitation of thermally induced strain*. According to the Curie principle, the symmetry of response includes common elements of the action symmetry and symmetry of crystal. In this case, action is scalar but the symmetry of the crystal response is artificially changed by a limitation of its possible deformations (this experimental method is described in more detail in [Chapter 2](#)).

Spatial distribution of internal polar sensitivity in quartz-type crystals can be described in polar coordinates as  $M_{ij}(\theta, \varphi) = M_{\max} \sin^3 \theta \cdot \cos 3\varphi$ , shown in [Fig. 1.13A](#), where  $\theta$  is azimuth angle and  $\varphi$  is plane angle. Using the radius vector directed from the center of this figure, one can determine the magnitude of polar sensitivity in any slanting cut of quartz-type crystals. In particular, the maxims of piezoelectric effect are seen along any one of three polar-neutral axes of X type. In addition, no piezoelectric effect is possible in the directions of the Y and Z axes.

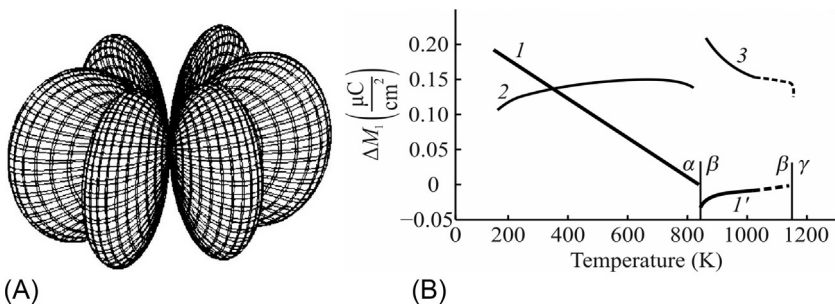


**Fig. 1.13** Internal polar sensitivity in quartz: (A) Indicatory surface; (B) temperature dependence: 1— $M_1$  found in [100]-cut plate in  $\alpha$ -quartz; 1'— $M_1$  found in [110] rod in high-temperature  $\beta$ -quartz; 2—artificial pyroelectric coefficient of [100]-thin cut, 3—piezomodule  $d_{14}$ .

In the case of 2D allocation of polar-sensitive bonds, the energy of their interaction decreases with distance *much faster* than in the case of 1D interaction:  $U \sim r^{-3}$  (Fig. 1.11B). This condition has a significant effect on the interaction of polar-sensitive bonds in their plane. This type of polar sensitivity (described by the *second-rank* tensor  $M_{ij}$ ) can be suppressed by 3D thermal fluctuations more easily than in the case of 1D internal polarity. It is remarkable that correlation between 2D internal polar sensitivity also ceases at a definite critical temperature, so crystals with 2D polarity experience a phase transition into another symmetry state, as is seen in Fig. 1.13B with the example of quartz.

Furthermore, the “effective pyroelectric coefficient  $\gamma_1$ ” vanishes in the vicinity of  $\alpha \rightarrow \beta$  phase transition of quartz at a temperature of  $\theta_1 \approx 850$  K. It is also notable that very special temperature dependence is observed for components of polar sensitivity  $M_{[100]} = \Delta M_1$ . Calculated from  $\gamma_1(T)$ , the  $\Delta M_1 = \int \gamma_1 dT$  decreases with temperature *linearly*:  $\Delta M_1 \sim (\theta - T)$ , that is, with Landau’s *critical index* 1. Previously such linear temperature dependence has been observed for spontaneous polarization of *improper ferroelectrics*. It should be noted that all piezoelectrics of quartz symmetry ( $\text{SiO}_2$ ,  $\text{AlPO}_4$ , and  $\text{HgS}$ ) have an additional  $\alpha \rightarrow \beta$  *high-temperature* transition, namely  $\beta \rightarrow \gamma$ . In their  $\beta$ -phase, quartz and berlinite still remain piezoelectrics, but with intrinsic polar sensitivity described by 3D distribution in a space. Moreover, the highest-temperature  $\gamma$ -phase in these crystals is already nonpolar.

- A **spatially distributed (3D) polar sensitivity** can be seen in some other piezoelectrics (which also are nonpyroelectrics), for instance, in the  $\text{A}^{\text{III}}\text{B}^{\text{V}}$  sphalerite-symmetry semiconductors (like gallium arsenide) or in KDP-type piezoelectrics ( $\text{KH}_2\text{PO}_4$  and many of its analogs in *paraelectric* phase). They are characterized by the third-rank material-type tensor  $M_{ijk} = M_{111}\sin\theta \cdot \sin 2\theta \cdot \cos 2\varphi$  and can be described by the indicatrix shown in Fig. 1.14A.

Well-known ferroelectrics of KDP type (and, close to them, antiferroelectrics of ADP type) at room temperature belong to polar-neutral crystals and are “exclusively” piezoelectrics. Their polar sensitivity is totally compensated and spatially distributed as shown in Fig. 1.14A. In this case, the correlation between polar-sensitive bonds decreases with distance rather fast (as  $r^{-4}$ , Fig. 1.11C), which testifies to the rather weak internal stability of 3D-arranged polar-sensitive bonding, which can be more easily destroyed by the same 3D thermal fluctuations. Fig. 1.14B shows some properties of KDP crystal above its ferroelectric phase transition, where this crystal is piezoelectric of the 422 class of symmetry (only below 150 K does it turn into a ferroelectric). It is seen that internal polar sensitivity very gradually vanishes by the law  $P \sim (\theta - T)^2$ , i.e., with critical index 2.

It was found [8] that crystals of the KDP type in their paraelectric phase, similarly to quartz-type crystals, have a *high-temperature phase transition*, at which symmetry changes from their polar-neutral 422 class to a nonpolar class of symmetry. Measurement of KDP crystal at microwave frequency (at lower frequencies proton conductivity interferes with measurements) shows first the usual slow decrease of permittivity  $\varepsilon_1(T)$ , but then it abruptly decreases at a temperature of  $\theta \approx 480$  K, evidently in connection with the high-temperature phase transition. The presence of this transition is confirmed by measuring the thermal expansion coefficient, which has a deep minimum at the temperature mentioned.

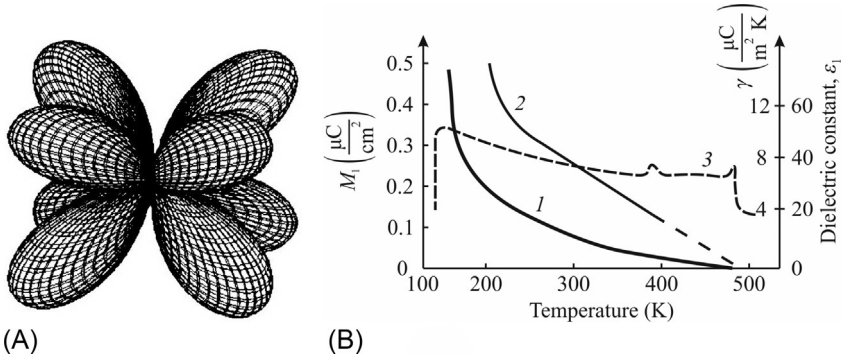


**Fig. 1.14** Intrinsic polarity in paraelectric phase of KDP crystal: (A) Indicatory surface; (B) temperature characteristics of partially clamped crystal: 1—polar sensitivity  $|M| \sim (\theta - T)^2$ ; 2—effective pyroelectric coefficient; 3—permittivity  $\epsilon_1$  at microwaves.

A common feature of all models shown in Figs. 1.12–1.14 is the availability of critical temperature, at which coordination between adjacent polar-sensitive bonds is disrupted with temperature increase. Moreover, in some crystals, the temperature steadiness of polar-sensitive bond allocations can always be described by the critical law  $M(T) \sim (\theta - T)^n$ . This means that a phase transition temperature  $\theta$  really exists, which corresponds to the vanishing of tensor  $M_{ijk}$  with temperature rise. It is established that a critical parameter is  $n = 1$ , if polar-sensitive bonds are arranged in a plane (two-dimensional case, 2D, quartz-type crystals). In the event of a spatial (3D) arrangement of polar-sensitive bonds (KDP and  $A^{III}B^V$  type crystals are examples), the critical exponent is  $n = 2$ . These two cases differ essentially from the 1D dipole-type polar-sensitive bonds in ferroelectrics, which exhibit the well-known critical law  $M_i(T)$  with  $n = 0.5$  (Landau critical index).

In Chapter 2 it will be shown that the described concept of a 3D type arrangement of polar sensitivity can be applied to many other “exclusive” piezoelectrics. For instance, in crystals of  $43m$  and  $23$  of cubic symmetry, polar-sensitive directions also correspond to four threefold axes.

## 1.7 Thermodynamics of polarization processes

A number of physical features of polar crystals can be explained or even predicted by thermodynamics. As mentioned previously, in pyroelectrics a difference exists between the dielectric constant  $\epsilon^T$  measured under *isothermal* conditions ( $dT = \text{const}$ ), or measured during a quarter of alternating voltage period dielectric has quite enough time to exchange by energy with its environment. In the opposite case, permittivity  $\epsilon^S$  is determined in *adiabatic* conditions, i.e., at constant entropy ( $dS = \text{const}$ ), when there is no energy exchange between the studied sample and the environment. In the vast majority of experiments carried out, the polar dielectric is in adiabatic

conditions, while theoretical calculations, in particular the study of phase transitions into polar ferroelectric phase from nonpolar paraelectric phase, presuppose isothermal conditions. Moreover, the difference  $\epsilon^T - \epsilon^S = \Delta\epsilon_{EC}$  (electrocaloric investment in dielectric permittivity) might be significant if permittivity is large and essentially *changes with temperature*, such as near the ferroelectric phase transition.

The isothermal condition seems to be too idealized when studying ordinary bulk samples, but still in this case it is possible to observe a two or more times increase in  $\Delta\epsilon_{EC}$  at infralow frequencies and in thin layers of polar dielectric [5]. However, when nanoscale samples are studied, the isothermal conditions of the experiment become quite realistic at ordinary frequencies and temperatures. So it is not surprising that pyroelectric coefficients and piezoelectric modules of nanoscale materials turn out to be much higher than in the bulk crystals of the same composition.

Before proceeding with thermodynamic analysis of electrical polarization, it is necessary to recall the following. The state of a system or material is characterized by a thermodynamic function called *enthalpy*  $A$  (which means heat content). As tem-

perature increases from  $T_1$  to  $T_2$ , enthalpy increases also:  $A_2 = A_1 + \int_{T_1}^{T_2} C_P \partial T$ , where  $A_1$  is enthalpy at the initial temperature  $T_1$ , and  $A_2$  is enthalpy at the final temperature  $T_2$ ;  $C_P$  is specific heat under constant pressure  $P$ .

As a thermodynamic function, enthalpy can be defined in two ways. The first method is based on values of *internal energy*  $U$  and *work*  $PV$  performed by material relative to the environment:  $A = U + PV$ , where  $P$  is pressure and  $V$  is volume of material. The second method is based on Helmholtz's idea about *free energy*  $F$  (or Gibbs free energy  $G$ ), while the parameter  $TS$  represents energy conditioned by *internal disordering* of a material:  $A = F + TS + PV = G + TS$ , where  $T$  is absolute temperature and  $S$  is *entropy* of the material: a measure of the system's internal disordering (i.e., measure of chaos).

Function  $F = U - TS$  (called the *Helmholtz free energy*) is minimal energy for the equilibrium state of the system, any changes in which occur at *constant volume*.

In solids, when studying thermodynamic processes, it is more expedient to take into account not the pressure but the volume of a system, so another thermodynamic function is used—the Gibbs free energy,  $G = F + PV$ . Its minimum corresponds to the equilibrium of a system, changing at constant temperature and constant volume. At atmospheric pressure the equilibrium conditions of the system are estimated using the *minimum value* of  $F$ .

Enthalpy in all cases increases with temperature, but the contribution of entropy ( $TS$ ) *increases faster*, as seen in Fig. 1.15. Consequently, the Gibbs free energy *decreases* with increasing temperature. Since the thermodynamic function “free energy” is used in many subsequent discussions in this book, it should be noted that at zero absolute temperature the Gibbs free energy is equal to enthalpy:  $G = A$ . At the same time, the free energy decreases with increasing temperature; however, the rate of free energy decreasing with temperature is associated with entropy (Fig. 1.15).

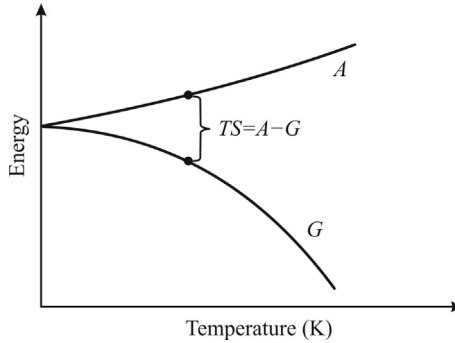


**Fig. 1.15** Temperature dependence of enthalpy and free Gibbs energy  $G$ .

Entropy is defined as a function of the state of a system; the difference of entropy in two equilibrium states 1 and 2 equals to the reduced amount of heat  $\delta Q/T$  the system needs to give in order to transfer it from state 1 to state 2 along any quasistatic path:

$$\Delta S = S_2 - S_1 = \int \delta Q/T.$$

Since entropy is determined up to an arbitrary constant, then in the initial state it is possible to set  $S_1 = 0$ , then  $\Delta S = \int \delta Q/T$ . This integral is taken for an arbitrary quasistatic process. The *differential function* of entropy has a form  $dS = \delta Q/T$ .

Also, since entropy is always positive and always increases with temperature rise, the slope of the free energy plot of temperature continuously increases. When different phases are possible in a dielectric, the value of free energy gives important information about these phase changes, so that the lower the free energy, the more resistant is a phase. In connection with the thermodynamic description of functional dielectric properties, it is necessary to call to mind some basic concepts of thermodynamics: *heat* is energy of thermal motion of particles forming a body; *absolute temperature*  $T$  is a thermodynamic quantity that characterizes the state of a body at its thermodynamic equilibrium, at which absolute temperature is proportional to average kinetic energy of particles; *heat capacity*  $C$  is the ratio of heat that is given to a body from outside to a corresponding increase in temperature. In functional dielectrics heat capacity also depends on mechanical and electrical boundary conditions of a crystal.

Regarding the difference between adiabatic and isothermal permittivity, calculations of  $\Delta \epsilon_{EC}$  can be performed on the basis of a thermodynamic description of the polarization phenomenon. Being a phenomenological theory, thermodynamics allows processes of polarization of dielectrics to be described in terms of their energy. Moreover, a dielectric is regarded as a thermodynamic system, in which the equilibrium state changes, as in an external electric field and as a result of other factors. Methods used in thermodynamics of dielectrics are important, particularly in ferroelectric phase transition descriptions, as well as to explain energetic aspects of piezoelectric

and pyroelectricity, in analyzing thermal expansion of crystals and their thermal conductivity. This section covers, however, only the most general energy relations that characterize the phenomenon of *polarization* in dielectrics.

Recall also that a thermodynamic *process* is a change in state of a system. A thermodynamic *state* is determined by a combination of thermodynamic parameters and characterized by the *internal energy* of a system. Heat is energy that is absorbed by a system with increasing temperature, if it *does not perform work*. To describe the state of a *polarized dielectric*, the following thermodynamic *functions* might be selected: free energy of  $F$ , internal energy  $U$ , and entropy  $S$ . Correspondingly, thermodynamic *parameters* (independent variables) are temperature  $T$  and electrical field  $E$ , which allows the best possible way to characterize permittivity  $\epsilon(T)$ . With this choice of parameters, it is supposed that the *volume* of a dielectric is maintained constant. Therefore, this approach does not include thermal expansion or electrostriction of a dielectric, supposing that these effects are small; however, these restrictions should be considered when using the energy relations obtained in the following paragraphs.

The **first** law of thermodynamics (law of energy conservation) for the dielectric polarization process is:

$$dU = dQ + EdD \quad (1.1)$$

where  $dU$  is change in internal energy per unit volume of dielectric and  $dQ$  is change of a heat. Eq. (1.1) means that increase in energy  $dU$  during a thermodynamic process, in which electrical field  $E$  or temperature  $T$  are changed (or both change simultaneously), equals to the heat  $dQ$  obtained by a dielectric, and work  $EdD$ , which is performed by the electrical field during the polarization process in a dielectric. The free energy that characterizes the maximal work that a system can run at constant temperature is:  $F = U - TS$ .

In compliance with the **second** law of thermodynamics, alteration in entropy:  $dS = dQ/T$ , where  $dS$  can be expressed in terms of parameters  $E$  and  $T$ . However, instead of  $E$ ,  $E^2$  should be selected as independent variable, because energy is a quadratic function of field strength:

$$dS = \frac{\partial S}{\partial T} dT + \frac{\partial S}{\partial(E^2)} d(E^2).$$

It is important to note that the entropy of reversible thermodynamic processes is *total differential*. This means that for a reversible process the value of the integral from  $dS$  does not depend on the path of integration, but it is determined only by the limits of integration, i.e., by the initial and final state of a system in a thermodynamic process. Then to get differential equations for internal energy, this property must be used:

$$dS = M(T, E^2) d(E^2) + N(T, E^2) dT; \quad \frac{\partial N}{\partial(E^2)} = \frac{\partial M}{\partial T}.$$

Now it is possible to calculate thermodynamic functions of a polarized dielectric for three cases:  $\varepsilon = \text{const}$ ,  $\varepsilon = \varepsilon(T)$ , and  $\varepsilon = \varepsilon(T, E)$ .

**First example:  $\varepsilon = \text{const}$ .** In the view  $D = \varepsilon_0 \varepsilon E$ , the change in electrical induction, using the energy conservation law (1.1), is:

$$dD = \varepsilon_0 \varepsilon dE + \varepsilon_0 E d\varepsilon = \varepsilon_0 \varepsilon dE.$$

Turning to variable  $E^2$  and using the relationship  $d(E^2) = 2EdE$ , it is possible to obtain:

$$dD = -\frac{\varepsilon_0 \varepsilon}{2E} d(E^2).$$

Substituting this expression into the preceding equations, and with regard to the dependence of internal energy on selected variables  $T$  and  $E^2$ , it is possible to have:

$$dU = dQ + \frac{1}{2} \varepsilon_0 \varepsilon d(E^2) = \frac{\partial U}{\partial E^2} d(E^2) + \frac{\partial U}{\partial T} dT.$$

From the right side of this equation,  $dQ$  can be determined, to find  $dS$ :

$$dS = \frac{dQ}{T} = \frac{1}{T} \left( \frac{\partial U}{\partial(E^2)} - \frac{1}{2} \varepsilon_0 \varepsilon \right) d(E^2) + \frac{1}{T} \frac{\partial U}{\partial T} dT.$$

According to the property of total differential:

$$\frac{1}{T} \frac{\partial^2 U}{\partial(E^2) \partial T} - \frac{1}{T^2} \left( \frac{\partial U}{\partial(E^2)} - \frac{1}{2} \varepsilon_0 \varepsilon \right) = \frac{1}{T} \frac{\partial^2 U}{\partial T \partial(E^2)}.$$

Now the next differential equation for internal energy can be obtained:

$$\frac{\partial U}{\partial(E^2)} = \frac{1}{2} \varepsilon_0 \varepsilon.$$

After integration, it is possible to obtain an important formula, which expresses the change in internal energy during polarization in the case of constant permittivity:

$$U = U_0(T) + \frac{1}{2} \varepsilon_0 \varepsilon E^2. \quad (1.2)$$

From these expressions it follows that  $\partial S / \partial(E^2) = 0$ . Therefore:

$$\begin{aligned} S &= S_0(T); \\ F &= F_0(T) + \frac{1}{2} \varepsilon_0 \varepsilon E^2. \end{aligned} \quad (1.3)$$

So, while polarization occurs in a dielectric with  $\varepsilon = \text{const}$ , entropy does not change, while the change in internal energy equals the change in free energy.

**Second example:  $\varepsilon = \varepsilon(T)$ .** This case is important for many functional dielectrics used in electronics, because in many dielectrics their permittivity varies with temperature. The change of induction is

$$dD = \varepsilon_0 \varepsilon dE + \varepsilon_0 E \frac{\partial \varepsilon}{\partial T} dT = \frac{\varepsilon_0 \varepsilon}{2E} d(E^2) + \varepsilon_0 E \frac{\partial \varepsilon}{\partial T} dT.$$

Consequently, the change of internal energy is equal to:

$$dU = dQ + \frac{1}{2} \varepsilon_0 \varepsilon d(E^2) + \varepsilon_0 E^2 \frac{\partial \varepsilon}{\partial T} dT = \frac{\partial U}{\partial T} dT + \frac{\partial U}{\partial(E^2)} d(E^2).$$

Defining  $dQ$ , one needs to get

$$dS = \frac{dQ}{T} = \frac{1}{T} \left( \frac{\partial U}{\partial(E^2)} - \frac{1}{2} \varepsilon_0 \varepsilon \right) d(E^2) + \frac{1}{T} \left( \frac{\partial U}{\partial T} - \varepsilon_0 E^2 \frac{\partial \varepsilon}{\partial T} \right) dT.$$

To obtain the differential equation for energy change, the property of total differential  $dS$  is used. After transformations:

$$\frac{\partial U}{\partial(E^2)} = \frac{1}{2} \varepsilon_0 \varepsilon + \frac{1}{2} \varepsilon_0 T \frac{\partial \varepsilon}{\partial T}.$$

Integration of the differential equation leads to an expression for internal energy:

$$U = U_0(T) + \frac{1}{2} \varepsilon_0 \left( \varepsilon + T \frac{\partial \varepsilon}{\partial T} \right) E^2.$$

After integration the following can be obtained:

$$\begin{aligned} \frac{\partial S}{\partial(E^2)} &= \frac{\varepsilon_0}{2T} \left( T \frac{\partial \varepsilon}{\partial T} \right); \\ S &= S_0(T) + \frac{1}{2} \varepsilon_0 \frac{\partial \varepsilon}{\partial T} E^2. \end{aligned}$$

Therefore, free energy is

$$F = F_0(T) + \frac{1}{2} \varepsilon_0 \varepsilon E^2. \quad (1.4)$$

These relations for  $U$ ,  $S$ , and  $F$  are significantly different from expressions that characterize a dielectric with constant permittivity. In particular, from a comparison of these expressions, it is seen that the well-known formula  $\frac{1}{2} \varepsilon_0 \varepsilon E^2$  for polarization

energy characterizes change only of the *free energy*  $F$  of a dielectric in an electrical field, but not change in the internal energy  $U$ .

Turning to the new thermodynamic parameters  $T$  and  $S$  (instead of  $T$  and  $E$ ), it is possible to derive a formula that links  $\epsilon^T$  and  $\epsilon^S$ :

$$\frac{\epsilon^T - \epsilon^S}{(\epsilon^T - 1)(\epsilon^S - 1)} = \frac{\epsilon_0 T}{C_P} \left( \frac{\partial E}{\partial T} \right)_P, \quad (1.5)$$

where  $C$  is specific heat, while index  $P$  means that heat capacity (as well as the derivative  $\partial E/\partial T$ ) is determined for the condition when polarization is constant. As follows from Eq. (1.5), isothermal permittivity is always larger than adiabatic permittivity:  $\epsilon^T > \epsilon^S$ .

The obtained energy relations can be used to analyze many properties of dielectrics associated with the process of polarization. In particular, it is possible to determine whether the type of thermodynamic process used to establish a polarized state has any influence on the magnitude of permittivity.

If the process of polarization is considered to be isothermal ( $dT = 0$ ), the internal energy of polarization equals  $\frac{1}{2}\epsilon_0\epsilon E^2$ , and its temperature dependence is not taken into account during determination of polarization energy. In practice, however, an isothermal process is difficult to implement, since it is possible only at a very slow change of electrical field and having a good heat-conducting contact with the test dielectric and environment (thermostat), which for a bulk sample is possible only in the subsonic frequency range and only for thin-film samples deposited on massive metallic substrates. In other cases, it is impossible for a bulk sample to meet the basic requirement of an isothermal process, which is establishment of thermal equilibrium with the thermostat at all stages of the experiment. Such studies are difficult to achieve in practice. However, as noted earlier, in the case of nanoscale dielectrics, an isothermal process takes place under normal conditions.

Usually most research on dielectrics is carried out under adiabatic conditions ( $dS = 0$ ), that is, during voltage change period any thermal equilibrium between dielectric and environment has no time to install. Even at 50 Hz the electrical field changes 100 times per second; dielectrics, in addition, have low thermal conductivity, which makes heat exchange with the environment difficult. Thus, in most cases, the real energy of dielectric polarization is described by relation (1.4).

From the resulting expressions for  $U$ ,  $F$ , and  $S$ , it follows that change in free energy during polarization does not depend on changes  $\epsilon(T)$ , and always equals  $\frac{1}{2}\epsilon_0\epsilon E^2$ . However, the temperature dependence of permittivity significantly impacts on change in entropy. If permittivity increases during the heating of the dielectric, that is, when the temperature coefficient of permittivity is positive ( $TC\epsilon > 0$ ), the change in entropy  $S - S_0(T)$  during polarization must be positive. Thus, not discussing the details of the processes that occur in the dielectric, just from general thermodynamic considerations it can be concluded that:

*In a dielectric with  $TC\epsilon > 0$  placed in an electrical field, physical processes occur that **reduce** the degree of molecular or atomic structure ordering. Conversely, if in*

a dielectric  $TC\epsilon < 0$ , that is if its permittivity decreases with heating, the change in entropy is negative: basic mechanisms that determine polarization in the case of external electrical field application result in an **increase** in ordering of molecules (ions, atoms) of a dielectric.

**Third example:** entropy in a dielectric in the case of **thermally activated polarization** (these characteristics may affect some polar dielectrics used in electronic technology). In such dielectrics, over a fairly wide range of temperatures and frequencies, a decrease in permittivity with temperature rise is observed [5] in accordance with Curie's law

$$\epsilon = \epsilon_1 + \frac{K}{T}, \quad (1.6)$$

where  $T$  is absolute temperature,  $K$  is the Curie constant, and  $\epsilon_1$  characterizes fast processes of polarization, so it depends only a little on temperature (this dependence is neglected). Calculated from Eq. (1.4), internal energy is:

$$U = U_0(T) + \frac{1}{2}\epsilon_0\epsilon_1 E^2.$$

Therefore, it turns out that a contribution to internal energy is possible only from the temperature-independent part of the polarization.

A change in entropy, on the other hand, is due to a contribution from polarization that varies with temperature:

$$S = S_0(T) - \frac{1}{2}\epsilon_0 \frac{K}{T^2} E^2.$$

Since entropy is a measure of disorder of molecules, which suggests that the specific mechanism of thermal polarization is orientation of dipoles in an electrical field, the obtained expressions can be interpreted as follows: in the absence of an electrical field dipoles are oriented randomly, while electrical field results in partial ordering of dipole orientation, and the greater the field strength, the more dipoles are oriented.

Temperature dependence of permittivity and the main thermodynamic functions of  $\Delta S$ ,  $\Delta U$ , and  $\Delta F$  for a dielectric with thermally activated polarization are shown in Fig. 1.16A. Free energy changes with temperature, because it contains not only a temperature-independent contribution from internal energy, but a contribution from entropy that is dependent on the electrical field:

$$F = F_0(T) + \frac{1}{2}\epsilon_0 \left( \epsilon_1 + \frac{K}{T} \right) E^2. \quad (1.7)$$

From thermodynamic analysis of this example it follows that expression (1.7), which characterizes temperature dependence of permittivity, in principle cannot be true at very low temperatures. This would be contrary to the third law of thermodynamics,

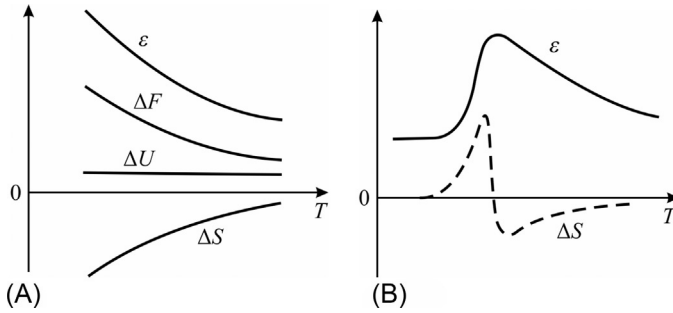


**Fig. 1.16** Temperature dependence of permittivity and main thermodynamic functions for dielectrics with prevailing thermal polarization: (A) Within the limits of Curie law; (B) in wide temperature range.

which states that entropy of any system at absolute zero is a universal constant that can be set equal to zero. From Eq. (1.7) it follows that entropy in the electrical field increases at low temperatures.

Therefore at very low temperatures the Curie formula (1.6) cannot hold true.

Indeed, in the description of thermal polarization, expression (1.6) is a special case of a more general relationship

$$\varepsilon = \varepsilon_1 + \frac{K}{T \left[ 1 + B \exp\left(\frac{b}{T}\right) \right]}, \quad (1.8)$$

which implies that in a broad temperature range, thermally activated polarization is characterized by the *asymmetric maximum* of permittivity (Fig. 1.16B). It is easy to show that change in entropy in this case is different in different parts of the shown temperature dependence of permittivity.

*In that temperature range where permittivity increases with temperature, electrical polarization leads to increase of entropy.*

**Fourth example:**  $\varepsilon = \varepsilon(E, T)$ . As mentioned earlier, dielectric nonlinearity may be of interest for some applications in electronics. It is possible to analyze dielectric nonlinearity at different temperatures, following the same example of thermally activated polarization. From models of polarization (for example, thermal-electronic or thermal-ionic polarization, occurring in solid dielectrics with high concentration of crystal defects), the dependence of permittivity, simultaneously, on temperature and electrical field in simple approximation can be represented as follows:

$$\varepsilon(T, E) \approx \varepsilon_1 + \frac{K \left( 1 - \frac{a}{3} E^2 \right)}{T \left[ 1 + B \exp\left(\frac{b}{T}\right) \right] (1 - aE^2)},$$

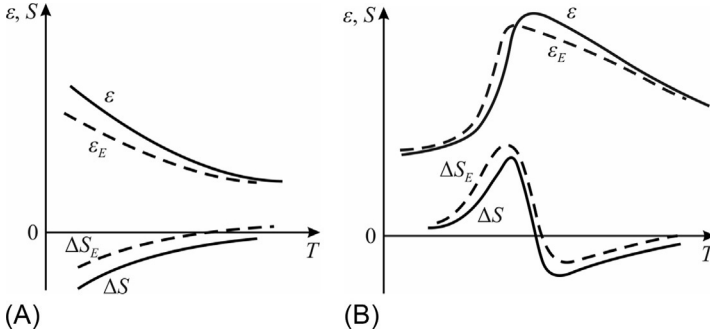


**Fig. 1.17** Temperature dependence of permittivity and entropy for dielectrics with thermally activated polarization in strong electrical field: (A) Within the limits of Curie law; (B) in broad temperature range;  $\epsilon_E$  and  $\Delta S_E$  are determined in strong electrical field.

where  $\epsilon_1$  characterizes fast (elastic types) polarization, which are lightly affected by  $T$  and  $E$ , and  $B$  depends on parameters of molecular models of polarization.

Temperature and field dependence of permittivity and entropy is shown in Fig. 1.17. The  $\epsilon(E)$  dependence in this case has an influence on thermodynamic functions as follows: internal and free energy in a strong electrical field are reduced, while entropy increases. Specific issues related to thermodynamic description of *piezoelectric* and *pyroelectric* effects are discussed further in Chapter 4.

**Fifth example: configurational entropy and thermal expansion of polar crystals.** From the point of view of thermodynamics, the models given in Sections 1.3 and 1.4 need more detailed consideration of the concept of entropy, namely, not only the traditional account of the “vibrational” part of entropy, associated with the dynamics of particles, but also of configurational entropy, since polar-sensitive bonds in their process of ordering-disordering spontaneously form quite various nanoscale configurations. A number of physical phenomena, observed in polar dielectrics, directly indicate a large role for the configuration part of entropy (for example, negative thermal expansion coefficient, maximum of heat capacity during transition from disordered phase to ordered one, increase of volume during this transition, increased phonon scattering during heat transfer, etc.)

Among different features of polar crystals, *thermal expansion* (which will be considered later in Chapter 3) becomes negative in a certain temperature range. It is advisable to start this consideration by discussing the concept of Gibbs function. Gibbs free energy, or thermodynamic potential, is a quantity whose change in course of a thermodynamic process is equal to the change in the internal energy of a system. Gibbs energy shows how much of the total internal energy of a system can be used for transformations or obtained as a result of them under specified conditions, and it allows the fundamental possibility of occurrence of changes in specified conditions to be established. Mathematically, this is the thermodynamic potential of form:

$$G = U + PV - TS,$$

where  $U$  is internal energy,  $P$  is pressure,  $V$  is volume,  $T$  is absolute temperature, and  $S$  is entropy. The minimum of Gibbs potential corresponds to stable equilibrium of a thermodynamic system with fixed temperature, pressure, and number of particles.

For further calculations, it is important to express Gibbs *energy differential* for a system with a constant number of particles:

$$dG = -SdT + VdP \quad (1.9)$$

The *volumetric thermal expansion* coefficient is defined as *relative* change in volume with temperature at constant pressure:  $\alpha = (\partial V/\partial T)_P/V$ . Moreover, the change in volume can be expressed through the Gibbs potential as well as the pressure (1.9) at constant temperature:  $V = (\partial G/\partial P)_T$ , to obtain the following expression:

$$\alpha = \frac{\left( \frac{\partial(\partial G/\partial P)_T}{\partial T} \right)}{V} = \frac{\left( \frac{\partial^2 G}{\partial T \partial P} \right)}{V}$$

By replacing variables in this expression, it is possible to get the final result linking the nature of thermal expansion with entropy and pressure:

$$\alpha = \frac{\left( \frac{\partial(\partial G/\partial T)}{\partial P} \right)}{V} = \frac{\left( \frac{\partial S}{\partial P} \right)_T}{V} \quad (1.10)$$

In almost all solids, as temperature rises, an increase in volume occurs, and parameter  $\alpha > 0$  because repulsive forces of atoms in a crystal lattice act at a short-range distance while attraction forces act at a long-range distance. Expression (1.10) means that the entropy is less the greater the pressure, which corresponds to the normally observed temperature expansion in solids.

On the contrary, in polar crystals in some temperature interval  $\alpha < 0$  that means a rise in entropy with increasing of pressure. Such an unusual phenomenon, which is characteristic of polar crystals, requires a deeper understanding of entropy.

Thus, the traditional understanding of entropy needs to be clarified. Of all properties of thermodynamic systems, the entropy  $S$  (SI unit [J K<sup>-1</sup>]) appears to be a difficult-to-explain property: the point is that temperature  $T$ , pressure  $P$ , and volume  $V$  are easy to measure, while entropy cannot be measured directly. As is known, entropy characterizes the inaccessibility of part of the thermal energy of a system for conversion into mechanical work; in other words, it is a measure of thermal energy of the system per unit temperature that is not available for performing useful work. Often, entropy is interpreted as a degree of disorder or randomness in a system; namely, entropy is due to a number of microscopic configurations that are consistent with the macroscopic quantities ( $P$ ,  $V$ ,  $T$ ) that characterize a system.

As noted, entropy is a function of state, because it does not depend on how a transition from one state of the system to another state is accomplished but is determined only by the initial and final states of a system. Moreover, entropy establishes a connection between macro- and microstates. It is believed that a particular arrangement of particles that is characterized by average quantities is a *macrostate*, while an individual arrangement defining properties of all particles for a given macrostate is a *microstate*. Entropy is related to the number of ways in which a microstate can rearrange itself without affecting the macrostate. Furthermore, for microstates, for example, for a system of  $N$  particles, it is possible to specify coordinates and velocities of particles. It's obvious that the macroscopic state of a system can be described using several macroscopic parameters, for example,  $P$ ,  $T$ ,  $V$ .

Therefore, the peculiarity of entropy is that it is the only function that shows the *direction* of the processes. During an ideal *reversible* process, entropy does not change, while an *irreversible* process always increases total entropy. In connection with the study of polar crystals, the *conditional* separation of entropy into vibrational and configurational becomes important.

The *vibrational entropy* can be considered as the number of microstates by which thermal energy can be divided between particles. The higher the temperature, the greater the vibrational entropy, but it becomes smaller as the binding energy of particles becomes greater. That is why *vibrational entropy decreases with increasing pressure*.

The *configurational entropy* is that part of system entropy that is due to various positions of some parts of a system: this applies to all possible configurations of a system. This entropy characterizes the number of ways in which groups of atoms can be distributed in space. With increasing pressure, the partial ordering of *dynamic nanoscale clusters* collapses and mutual chaos increases. That is why a distinctive feature of *configurational entropy is its growth with increasing pressure*.

With regard to polar crystals, when discussing the relationship of entropy and pressure, Le Chatelier's principle can be applied: the ordering of polar bonds leads to decrease in entropy and increase in volume; therefore, the increase in pressure (which decreases volume) should lead to disordering of the polar bonds and, accordingly, to increase in entropy. Thus, a negative coefficient of thermal expansion proves the importance of configurational entropy accounting for polar crystals properties description. In turn, negative expansion indicates the presence of their own inherent ordering-disordering processes in the polar crystals.

## 1.8 Summary

1. Any dielectric has polarization ability in an external *electrical* field, but only some of the dielectrics—polar types—can be polarized in a *nonelectrical* manner. Unique properties of polar crystals (pyroelectrics, piezoelectrics, etc.) can be described by a peculiar polar-sensitive internal structure, capable of generating electrical response to nonelectrical homogeneous (scalar) actions.

2. Electrical polarization means that electrical charge separations occur (which, however, remain unfree). When electrical voltage switches on, a reactive current flows through a dielectric caused by shifting of electrical charges; next, when voltage switches off, this is also accompanied by flow of depolarization current, inasmuch as electrical polarization is a response only to the *change* in the electrical voltage.
3. Polarization induced by an external electrical field is necessarily accompanied by mechanical deformation of a dielectric—this is the *electrostriction* (electrically induced mechanical strain), which indicates that the polarized state of a dielectric is a nonequilibrium (stressed) state; thus polarization of a dielectric included in a short circuit disappears instantly as soon as the external electrical field is turned off.
4. When an electrical field is applied to a solid dielectric, closely connected charges of structural units are displaced relatively to each other, whereby the dielectric becomes polarized. The electrical moment arising in this manner is conditioned by contributions from: electrons displaced from their equilibrium positions in atoms, ions deviated from their equilibrium state in the crystal lattice, and dipoles that changed their orientation in the external electrical field.
5. Electrons, ions, and dipoles can acquire induced electrical moment (i.e., polarized state) through various mechanisms: (1) elastic reversible displacement of bound electric charges, (2) displacement of weakly bound charges with participation of their thermal motion, and (3) macroscopic displacement of free charges that later localize on defect locations in the dielectric. It should be noted that in polar dielectrics all these processes can occur *without* electrical field application but under the action of varying temperature, uniform pressure, mechanical stress, exposure of sufficiently high energy irradiation, etc.
6. The *dielectric anisotropy* usually arises in dielectrics under external field influence, but it always is present in polar dielectrics. This means that in noncentrosymmetric dielectrics their electrical, thermal, and mechanical characteristics show dependence on the directions of action and response. Any vector is defined by three parameters—projections on coordinate axes. Transformation from one vector to another is described as  $D_i = \epsilon_{0\epsilon_{ij}}E_j$ ; in the anisotropic media, components  $\epsilon_{ij}$  are shown with two indices: one comes from vector  $E_j$  “action,” and the other from “response” vector  $D_i$ , which directions may not correspond to the direction of action.
7. The *dielectric nonlinearity* is associated with permittivity dependence on the electrical field. In principle, an  $\epsilon(E)$  change should be observed in all dielectrics; however, in most of them nonlinearity is small. Nevertheless, in some *polar dielectrics* (ferroelectrics and paraelectrics), dielectric nonlinearity can be essential and has found applications in electronics.
8. The *boundary conditions* are especially important in the case of functional dielectric polarization: these conditions can be electrical, mechanical, and thermal. Two *electrical* boundary conditions are: (1) electrical field  $E = 0$ , which means the polar crystal is electrically free and it is a source of current; (2) electrical induction  $D = 0$ , i.e., the polar crystal is electrically disconnected and it is a source of voltage.
9. Two *mechanical boundary* conditions are: (1) stress  $X = 0$ , which means a mechanically free state of the polar crystal; (2) strain  $x = 0$ , i.e., the polar crystal is mechanically clamped. Two *thermal boundary* conditions are: (1) isothermal condition with invariable temperature ( $\delta T = 0$ ); (2) entropy  $S = \text{const}$ , which corresponds to the adiabatic condition.
10. All dielectrics and semiconductors are able to create an *electrical moment*  $P_i = \chi_{ij} \cdot E_j$  within, induced by an electrical field; this property is described by a second-rank symmetric tensor of dielectric susceptibility  $\chi_{ij}$  (or the same tensor of dielectric permittivity  $\epsilon_{ij} = 1 + \chi_{ij}$ ).

11. Polar *dielectrics-pyroelectrics* have the ability to induce an electrical moment  $P_i = \gamma_i \delta T$  in them by change of temperature  $\delta T$ ; this property is described by a first-rank material tensor: *pyroelectric coefficient*  $\gamma_i$ , i.e., electrical susceptibility to temperature change. Polar dielectrics-pyroelectrics also have the ability to create in them an induced electrical moment  $P_i = \zeta_i p$  due to change of hydrostatic pressure  $p$ , described by a first-rank material tensor: *piezoelectric pressure coefficient*  $\zeta_i$ , i.e., sensitivity to change in pressure.
12. Polar *dielectrics-piezoelectrics* have the ability to create in them an electrical moment induced by mechanical stress:  $P_i = d_{ikl} X_{kl}$ . This property is described by a third-rank material tensor: *piezoelectric modulus*  $d_{ikl}$  (it can also be called susceptibility to mechanical stress).
13. In fact, any experimental investigations of pyroelectric or piezoelectric effects do not allow the value of their “spontaneous polarization” to be directly determined, but experiments characterize only the magnitude of the *dynamic response* of the peculiar polar-sensitive internal crystalline structure.
14. When explaining various properties of polar crystals, you can do without the concept of “spontaneous polarization,” i.e., imagining that in a polar crystal “permanent polarization” *exists*. The assumption also seems reasonable that electrical polarization *appears* as a response to external factors (not even electrical). This is due to the peculiar distribution of polar-sensitive internal bonds having distinction in ion affinity for electrons, i.e., electronegativity.
15. To explain more complex manifestations of crystal properties, a special structure of *cores* needs to be taken into account: the total number of electrons in an atom, degree of screening of external electrons from action of the nucleus, etc. The electronegativity is the property of an atom to attract electrons; it depends on the atomic number (the number of protons in the nucleus), on the degree of screening of internal electrons, and on the structure of external electron orbitals. Atoms with more electronegativity more strongly attract electrons.
16. Noncentrosymmetric structures are formed owing to compensation of atomic electronegativity by polar-sensitive bonding in the process of polar crystal formation (while it is growing from the liquid or steam state of a material). Moreover, dependent on chemical composition of a crystal, a variety of combinations may occur between the ions of crystals having two- or three-dimensional polar-active constructions (which, when external actions are exerted on them, can produce electrical responses, describable by tensors of different ranks). Non-centrosymmetric structures of polar crystals are a demonstration of *mixed ionic-covalent bonds* between their ions. These bonds are strongly directional and, therefore, such structures lead to different manifestations of asymmetry and complexity of polar crystal structures.
17. When an electrical field affects a “persistently arranged” polar structure, its electrical polarization usually looks like a linear effect (as in ordinary dielectrics). It may seem, however, that the exception is ferroelectrics, in which a *switching* of the “gently arranged” polarization is seen: their low-stable enantiomorphic structure can change its polar-sensitive direction. Outwardly this event manifests itself as a dielectric *hysteresis loop*, which allows measurement of the ability of a polar-sensitive structure to react to external actions and indirectly can characterize its features.
18. In ordinary ionic or covalent crystals *specific polar properties* can be obtained by applying to them a direct electrical field  $E$ . Moreover, the resulting induced polarization is accompanied by *electrostriction*, which is a quadratic effect: relative deformation of the crystal increases in the applied field *parabolically*:  $x = R \cdot E^2$  (in contrast to polar crystals, in which field-induced deformation depends on the applied field *linearly* showing a piezoelectric effect:  $x = d \cdot E$ ). Mechanical strain in the case of electrostriction does not change its sign when an electrical field changes sign—unlike in the piezoelectric effect.

19. It can be shown that the linear electromechanical effect (which is a peculiar property of polar crystals) can be interpreted as *linearized electrostriction*. The point is that electrical field changes the original *symmetry* of a crystal due to its electrical polarization. In this way, under fixed external voltage, the structure of a crystal turns into an *artificially created polar* structure (it becomes an electrically induced noncentrosymmetric structure). In dielectrics that have large permittivity, the electrically induced piezoelectric effect can become “gigantic,” and this feature is really used now in electronics. Similarly, in the presence of an electrical bias field in *any* crystal the *pyroelectric* effect can also be induced, which finds application in modern thermal sensors.
20. In compliance with such electrically induced piezoelectric and pyroelectric effects, one can suppose that the *usual* piezoelectric effect can also be explained as “linearized electrostriction.” This assumption might be advanced according to the concept that the fundamental reason for crystal intrinsic polar sensitivity is the asymmetry in electronic density distribution along the polar bonds between ions, which have different electronegativity (this mechanism replaces an externally applied field).
21. *Mixed covalent-ionic bonds*, which in polar crystals are a main property, guarantee piezoelectric and pyroelectric properties without external electrical field application to a crystal. In this way, instead of the external electrical field that must be applied to ionic or covalent crystals in order to force them to have a polarized (although nonequilibrium) state, in the case of mixed covalent-ionic crystals their polar-sensitive state *remains stable* without any external field, being ensured by a fundamental property of ions—their electronegativity.
22. Polar-sensitive bonds arise in such crystals, which have a small coordination number (CN) showing the number of nearest neighbors to a given atom. Thus, polar dielectrics and semiconductors correspond to an “open” structure: they provide sufficient space for electron orbit interaction. In the usual densely packed crystalline structures this number is large (CN = 12 for metals and CN = 8–6 for ordinary dielectrics); for example, in the piezoelectric sphalerite structure and in the pyroelectric wurtzite structure CN = 4.
23. It is exactly the presence of polar-sensitive bonds that determines the noncentrosymmetric structure of some crystals: hybridized ionic-covalent bonds are the main cause of pyroelectric, ferroelectric, and piezoelectric properties. For example, mechanical action on a polar crystal leads to an electrical (piezoelectric) response. Its mechanism lies in the fact that the displacement of ions deforms their *asymmetric bonds* and in this way leads to the appearance of electric charges on the surfaces of a crystal. In the opposite case, when the ionic bonds of the crystal are centrosymmetric, mechanoelectric polarization is impossible because the electrical effects of the displacement of charges compensate each other.
24. Noncentrosymmetric allocation of electrical charges in polar-sensitive structures can be represented by different simplified structural models: (1) quasiohedral structural ordering, which corresponds to a vector (dipole-like) response to external influences; (2) two-dimensional structural arrangement of polar-sensitive bonds allowing electrical response to scalar action to be described by the model, which consists of six ions, having asymmetric bonds and located in one plane; (3) three-dimensional asymmetric polar-sensitive bonding, modeled by eight ions, representing a spatial polar-neutral structure.
25. In some polar crystals a critical temperature can be seen, at which coordination between adjacent polar-sensitive bonds is disrupted by a temperature increase. In these cases temperature steadiness of polar-sensitive bond allocations can be described by the critical law  $M(T) \sim (\theta - T)^n$ . This means that a phase transition temperature  $\theta$  exists, which corresponds to the vanishing of tensor  $M_{ijk}$  with temperature rise. It is established that the critical parameter is  $n = 1$ , if polar-sensitive bonds are arranged in a plane; in the event of a spatial (3D) arrangement of polar-sensitive bonds, the critical exponent is  $n = 2$ . These two cases

differ essentially from the 1D dipole-type polar-sensitive bonds in ferroelectrics that show a well-known critical law  $M_i(T)$  with  $n = 0.5$  (Landau critical index).

26. *Thermal properties* of material are due to the internal energy of molecules, atoms, and electrons. *Potential energy* is a part of the energy of a system or body that depends on the positions of particles in the body in force fields. In solids, the sources of potential energy are Coulomb forces that cause attraction of opposite sign charges and repulsion of same sign charges. *Kinetic energy* (or energy of particle motion in solids) is due to the fact that atoms and ions continuously oscillate because of thermal excitation. A thermodynamic function called *enthalpy* (heat content) characterizes the energy state of a system or material; enthalpy increases with temperature rise. *Entropy* is a measure of internal disordering (chaotic) in a system. The Helmholtz *free energy* has a minimum in the equilibrium state of the system, in which any changes occur at constant volume and temperature.
27. Research and application of dielectrics generally take place under *adiabatic* conditions; during the change of voltage thermal equilibrium between dielectric and surrounding environment cannot be installed in time, so alteration of entropy  $\delta S = 0$ . Therefore, from such experiments an *adiabatic permittivity*  $\epsilon^S$  is generally determined. In those dielectrics in which polarization depends on temperature (paraelectrics, ferroelectrics, pyroelectrics, and others), another—*isothermal*—process of polarization might be important, when  $\delta T = 0$  and permittivity is isothermal:  $\epsilon^T$ . Analytical determination of the relationship between  $\epsilon^T$  and  $\epsilon^S$  may be important both to explain permittivity frequency dependence in a range of subsonic frequencies, and for theoretical calculations. Isothermal dielectric permittivity is always greater than the adiabatic one:  $\epsilon^T > \epsilon^S$ . In most cases this difference is small and can be neglected. However, in pyroelectrics and, especially, in the vicinity of a ferroelectric phase transition, the difference between  $\epsilon^T$  and  $\epsilon^S$  can reach 10%–50%, so it should be taken into account.
28. If dielectric permittivity increases during dielectric heating, i.e., when the temperature coefficient of permittivity is positive ( $TC\epsilon > 0$ ), the change in entropy  $S - S_0(T)$  during polarization must be positive. Thus, not discussing the details of processes that occur in a dielectric but only from general thermodynamic considerations, it can be concluded that in a dielectric with  $TC\epsilon > 0$ , when placed in an electrical field, such physical processes occur that *reduce* the degree of molecular or atomic structure ordering. Conversely, in a dielectric with  $TC\epsilon < 0$ , i.e., when its permittivity decreases with heating, the change in entropy is negative. This means that basic mechanisms that determine polarization in the case of external electrical field application result in an *increase* in ordering of molecules (ions, atoms) in a dielectric.
29. In polar dielectrics, the concept of entropy becomes more complex. As is usual for any material, *vibrational entropy* can be considered as the number of microstates into which thermal energy can be divided between particles. The higher the temperature, the greater the vibrational entropy, but it becomes smaller if the binding energy of particles is greater. That is why, *with increasing pressure vibrational entropy decreases*, and the thermal expansion coefficient is positive.
30. Important for polar crystals, *configurational entropy* is that part of system entropy that is due to various positions of some parts of a system. This entropy characterizes a number of ways in which groups of atoms are distributed in space. With increasing pressure, the partial ordering of dynamic nanoscale clusters collapses and mutual chaos increases. That is why *configurational entropy increases with pressure growth*, and the thermal expansion coefficient is negative.
31. A negative coefficient of thermal expansion in polar crystals proves the importance of configurational entropy for their property descriptions. In turn, this indicates the presence of their own ordering-disordering processes within the polar crystals.

## References

- [1] Y.M. Poplavko, *Electronic Materials. Principles and Applied Science*, Elsevier, 2019.
- [2] J.C. Burfoot, G.W. Taylor, *Polar Dielectrics and Their Application*, Macmillan Press, New Jersey, 1979.
- [3] Y.M. Poplavko, Y.V. Didenko, Spontaneous polarization or manifestation of peculiar internal structure? in: *Third Intern. Conf. on Information and Telecommunication Technologies and Radio Electronics (UkrMiCo'2018)*; Odessa, Ukraine, 2018.
- [4] Y.M. Poplavko, L.P. Pereverzeva, I.P. Raevskiy, *Physics of Active Dielectrics*, South Federal University of Russia, Postov-na-Donu, 2009.
- [5] Y.M. Poplavko, Y.I. Yakymenko, *Piezoelectrics*, Polytechnic Institute, Kiev, 2013.
- [6] K.M. Rabe, C.H. Ahn, J.-M. Triscons (Eds.), *Physics of Ferroelectrics: A Modern Perspectives*, Springer, 2007.
- [7] D.G. Schlom, L.-Q. Chen, C.J. Fennie, et al., Elastic strain engineering of ferroic oxides, *MRS Bull.* 39 (2014) 118.
- [8] L.P. Pereverzeva, Y.M. Poplavko, Pyroelectricity in non-central crystals, *Acta Phys. Pol. A* 84 (2) (1993) 287.

# Manifestations of polar sensitivity in crystals

# 2

Various experimental evidence for the existence of polar sensitivity in some crystals is considered in this chapter: the structural affinity of piezoelectrics and pyroelectrics; chemical features of polar crystals confirming the proximity of their properties; an increase in volume during self-ordering of polar-sensitive bonds; piezoelectric and electrocaloric contributions to polar crystal permittivity; high-frequency dielectric absorption; the dependence of polar crystal elastic properties on various electrical boundary conditions, etc. Some important features of *charge transfer* in polar-sensitive crystals will be explained: the physical nature of the giant change of conductivity in critistors, posistors, and varistors as well as in other field-controllable switching elements, particularly those that exhibit colossal magnetoresistance; the nature of the high sensibility of nanostructured sensors based on zinc oxide is also discussed.

The *electrically induced* polar properties are also discussed in this chapter: electrically induced piezoelectric modulus in paraelectrics and relaxor ferroelectrics, and electrical control by resonant frequency of piezoelectric resonators and filters. *Mechanically induced* pyroelectricity is examined in detail: an original method for obtaining pyroelectric response and volumetric piezoelectric effect in polar-neutral piezoelectrics (nonpyroelectrics) is described. Two- and three-dimensional structural arrangements of polar-sensitive bonds in the polar-neutral piezoelectric are analyzed; artificial pyroelectric effects for 10 classes of polar-neutral piezoelectric crystals are calculated and experimentally tested in the quartz and gallium arsenide type crystals. It is shown that this effect can be used in single-chip pyroelectric and piezoelectric sensors.

## 2.1 Experimental evidence for polar sensitivity

Polar properties of well-known pyroelectrics and ferroelectrics, described by the first-rank tensor (i.e., dipole moment vector  $M_i = P_i$ ), do not need additional evidence [1–3]. However, in the “exclusive” piezoelectrics that are not pyroelectrics, the existence of polar sensitivity, that is, a capability of electrical response to homogeneous nonelectric action, needs some additional experimental grounds [4]. Moreover, all electrical measurements are limited only by vector-type responses—by the detection of voltage or current. That is why it is not surprising that totally compensated internal polar sensitivity is not so easy to be detected in this case. However, there is some other, indirect evidence of polar-sensitivity existence in the noncentral crystals.

(1) The **structural affinity** of *piezoelectrics and pyroelectrics* follows, for example, from the polymorphism of  $\bar{4}3m$  (piezoelectric) and  $6m$  (pyroelectric) structures. Such proximity of piezoelectricity and pyroelectricity is demonstrated in the zinc

sulfide (zinc blende) crystal: interatomic interaction in ZnS provides a configuration of a crystal in which both structures (sphalerite and wurtzite) can coexist.

In the case of sphalerite, the *piezoelectric* internal polar-sensitive structure of ZnS can be described by a 3D spatial distribution: this simulation might be represented by four threefold polar axes of [111]-type, which are crossed at the angle of 109.5 degrees, as shown in Fig. 2.1A. Such an intrinsic 3D polar structure is absolutely *self-compensated* and in this case zinc sulfide should be categorized with the “exclusive” piezoelectrics. However, the second principal structure of ZnS (in which, for simplicity, only positive polar-sensitive directions are shown) is *pyroelectric* wurtzite. This structure includes not only [111]-type polar axes, but in addition the *dipole type* of polar-sensitivity component as well, directed along one of these axes (Fig. 2.1B); this zinc sulfide structure is undoubtedly related to the pyroelectrics.

The difference between the atomic distances of the two main forms of zinc blende is actually so small that these structures with different symmetries can alternate with each other in the same crystal, demonstrating polymorphism. As a result, it turns out that there is no big difference between the pyroelectric and piezoelectric states of this crystal. Accordingly, it seems unconvincing to consider the amplification of polarity in one of the polar-neutral directions in wurtzite as the appearance of a spontaneous polarization.

(2) **Chemical features** of the polar crystals are another important factor, confirming the proximity of different polar-sensitive structure properties.

In the *pyroelectric* crystals, the surfaces of the crystalline plate, which is oriented perpendicularly to the polar axes, have different chemical properties (in particular, different rates of *chemical etching*). As is known, the ferroelectric is a pyroelectric that breaks into domains. Moreover, selective etching is a well-known characteristic of the ferroelectrics, which is used to detect their domain structure: chemical etching occurs with different speeds for “+” and “-” orientation of domains [3].

In the same way, in the *piezoelectric* quartz crystal (which is *not pyroelectric*) the etching occurs much more rapidly on the “positive” side of the polar  $X$ -axis, while the rate of etching is much slower on the “negative” side of the  $X$ -axis. In this way the

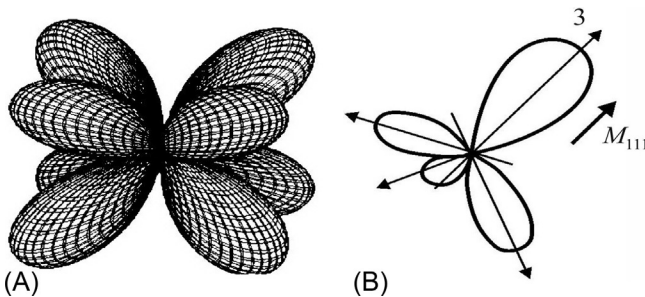


**Fig. 2.1** Spatial distribution of 3D type polar-sensitivity (only the positive directions of polar axes are shown): (A) Total compensation of polar sensitivity in sphalerite; (B) noncompensated “dipole-type” component  $M_{111}$  of polar sensitivity in wurtzite (shown only positive directions).

figures of etching seen on quartz are quite different for “+” and “-” surfaces. The dependence on surface chemical activity of a given piezoelectric indicates, first of all, the directivity of polar-sensitive bonds in it, and, second, the nonsymmetric distribution of binding energy of ions in an electrically positive or negative direction [5]. This phenomenon can also be explained as a “proximity” effect: the propagation of the influence of the polar (noncentrosymmetric) crystal property on its immediate environment<sup>a</sup> that has no relation to “internal field existence” in a crystal.

In contrast to the cubic nonpolar NaCl crystal, the also cubic but polar-sensitive GaAs crystal shows considerable distinction in chemical properties between the two surfaces of the (111)-cut plates. This peculiarity is taken into account during electrode deposition on gallium arsenide: the adhesion of one or another metal on the “positive” and “negative” surfaces of the (111)-cut of GaAs is significantly different, so it is necessary to use different technologies of electrode deposition on them.

Here it is pertinent to mention that direct measurements of the electrical charge density on fresh cleavages of the pyroelectric tourmaline crystal were made: these measurements showed a charge density  $\sim 0.01 \mu\text{C}/\text{cm}^2$  [4].

**(3) Increase in volume** (which means decrease in density) is a characteristic property of the self-ordering of the polar-sensitive bonds in crystal [6]. For instance, in ferroelectric phase transitions into a low-temperature polar phase, the crystal increases its volume as compared with the high-temperature nonpolar phase: this is conditioned by the ordering of previously disordered interatomic bonds. Such expansion of a solid upon cooling is quite an unusual phenomenon, since in the majority of cases the density of solids increases with cooling due to a decrease in the intensity of thermal oscillations of the atoms.

It is noteworthy that, during transition to the antiferroelectric phase from the high-temperature paraelectric phase, the volume of the crystal decreases: i.e., antipolar (counter) ordering is denser than in the polar phase. Moreover, by applying a strong electrical field, the antiferroelectric shows a compelled transition into a ferroelectric phase: furthermore, the jump in volume becomes so significant that it thermodynamically leads to a large electrocaloric effect with a significant cooling by the electrical field (which is interesting for practical use in refrigerators [7]).

The issue of volume increase in ordered structures can also be considered more broadly: for example, ferromagnets also usually expand when cooled from the paramagnetic phase, and this is used in a technique for obtaining alloys with a low coefficient of thermal expansion. In connection with this, it is noteworthy that even during crystallization the density of polar crystals decreases as they grow from their liquid phase (for example, the GaAs crystal can swim on the surface of its melt like ice

<sup>a</sup> Consider, for example, the (111)-cut of a cubic but nonpolar NaCl crystal: then one side of such a plate would be completely covered by the  $\text{Na}^+$  ions and the other by the  $\text{Cl}^-$  ions, creating, it would seem, both an internal and external electric field, and having different chemical activity. But in reality this does not happen: the centrosymmetric NaCl crystal self-neutralizes the surfaces of the (111) slices, so does not create any “proximity” effect and does not become an artificial pyroelectric. So, the peculiarities of polar crystals are explained precisely by the asymmetry in electron density distribution in the elementary unit cell of a crystal, which creates peculiar properties, including the proximity effect.

in water). The point is that in a liquid phase the interatomic polar-sensitive bonds cannot establish their strict orientation due to intensive thermal motion in the disordered liquid structure.

The process of crystal growth from a liquid or vapor phase is undoubtedly influenced by the proximity effect just discussed. During crystallization, a polar crystal spontaneously expands due to establishment of a strong orientation of its polar-sensitive bonds, so the crystal density becomes less than the density of a melt. It is also important to add that crystal growth occurs much more rapidly exactly in the direction of polar (or polar-neutral) bonds: this occurs in pyroelectrics and also in piezoelectrics, and this determines the form of the polar crystal. Moreover, for the manifestation of chemical properties in polar-sensitive crystals, it is not of fundamental importance whether the crystal is pyroelectric or only piezoelectric.

**(4) Dielectric permittivity** frequency dependence of polar-sensitive crystals differs from that of the usual dielectrics. Electrical polarization is the separation of bound electrical charges that is accompanied by deformation of a crystal (strain). Therefore, polarization is not only an electrical but also an electromechanical phenomenon. In the case of a polar-sensitive crystal, electrical energy given to a crystal by an electrical field is stored not only in the microscopic displacements of bound charges, but also in the macroscopic deformation of the crystal as a whole. This deformation is elastically reversible, so it makes an *electromechanical contribution* to the permittivity.

When dielectric properties of polar-sensitive crystals are studied at *lower frequencies* (below the frequency of possible electromechanical resonances), the  $\epsilon^X$  of a *mechanically free* crystal is measured (stress  $X = 0$ ). In this case the crystal's electromechanical reaction  $e^2/\epsilon_0$  contributes to the dielectric constant ( $e$  is the piezoelectric strain modulus). At the same time, at rather high frequencies (above the electromechanical resonances), the  $\epsilon^x$  is determined (crystal is *clamped*, its strain  $x = 0$ ). At high frequencies the own mechanical inertia of the test sample makes its electromechanical reaction impossible.

A comparison of dielectric constants of free and clamped polar crystals is shown in Fig. 2.2 for the most well-known and well-studied polar crystals—ferroelectrics. In Rochelle salt the piezoelectric effect is observed in the entire temperature range,

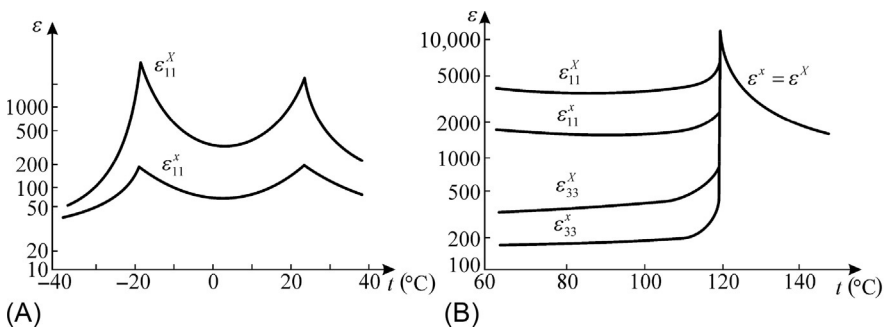


**Fig. 2.2** Temperature dependence of dielectric permittivity in free (at frequency  $10^3$  Hz) and clamped (at frequency  $10^{10}$  Hz) crystals: (A) Rochelle salt, (B) barium titanate.

so everywhere dielectric permittivity of the free and clamped crystal differs greatly (Fig. 2.2A). In the vicinity of ferroelectric Curie points, the effect of clamping is very large:  $\epsilon^X/\epsilon^x \approx 50$ . In another well-known crystal—barium titanate ( $\text{BaTiO}_3$ )—above the Curie point (in the cubic center-symmetric phase) the piezoelectric effect is absent, and  $\epsilon^X = \epsilon^x = \epsilon$ . But below the Curie point in a single-domain  $\text{BaTiO}_3$  crystal near room temperature, the ratio  $\epsilon^X/\epsilon^x$  is about 2 (while in polarized  $\text{BaTiO}_3$  piezoelectric ceramics  $\epsilon^X/\epsilon^x < 2$ ).

A very large dielectric permittivity  $\epsilon^X$  may occur in a mechanically free crystal, but only at low frequencies; in the region of very high frequencies, the dielectric constant  $\epsilon^x$  is significantly reduced. In this case, permittivity's frequency dependence shows a series of electromechanical resonances, as follows from Fig. 2.3, where the study of the  $\text{KH}_2\text{PO}_4$  (KDP crystal) is shown, we note that in this case the ratio  $\epsilon^X/\epsilon^x \approx 100$ , the record high.

The examples in Figs. 2.2 and 2.3 show very large electromechanical contributions to the low-frequency dielectric constant of polar-sensitive crystals. However, in most cases the difference between  $\epsilon^X$  and  $\epsilon^x$  is not so great.

Another possible influence on polar crystal permittivity is the “electrothermal contribution”  $\epsilon_{ET}$ , which is also called the *electrocaloric* contribution. This refers to the difference  $\epsilon^T - \epsilon^S = \epsilon_{ET}$  between the permittivity  $\epsilon^T$  measured under isothermal conditions when  $T = \text{const}$  and the dielectric has enough time to exchange energy with the environment, and the permittivity  $\epsilon^S$  measured in adiabatic conditions, at constant entropy ( $S = \text{const}$ ), when heat exchange with the environment is impossible.

The electrocaloric contribution to permittivity might be essential when  $\epsilon$  is large and its dependence  $\epsilon(T)$  is large, for example, near the ferroelectric phase transition. Sometimes the difference between  $\epsilon^T$  and  $\epsilon^S$  might reach 10%–50% (for example, just below the ferroelectric phase transition).

**(5) High-frequency dielectric absorption** is another remarkable feature of polar-sensitive dielectrics. In polar crystals, there is a fundamental microwave absorption, which greatly exceeds the absorption of centrosymmetric crystals. As a result, the dielectric losses at microwave frequencies are large and have a quasi-Debye character due to the interaction of optical and acoustic phonons [9]. The frequency dependence

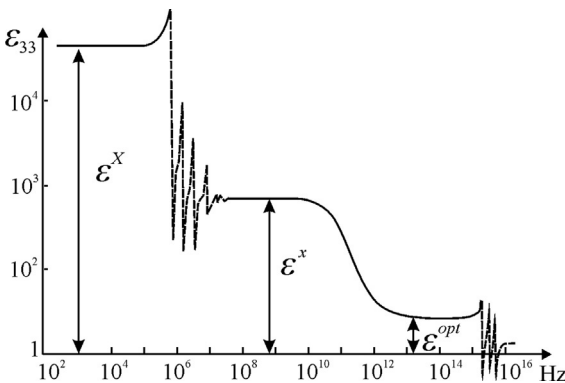


**Fig. 2.3** Dielectric spectrum of KDP crystal near its Curie point: In the frequency range of  $10^5$ – $10^8$  Hz a series of piezoelectric resonances is observed [8].

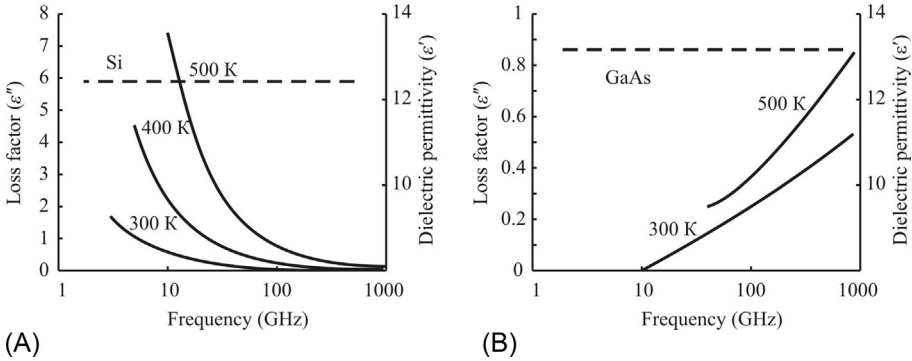


**Fig. 2.4** Frequency dependence of microwave absorption  $\epsilon''$  (solid line) in nonpolar silicon: (A) Polar crystal *s/i*-GaAs; (B) dashed line shows permittivity.

of the dielectric loss is shown in Fig. 2.4 as the imaginary part of the complex dielectric constant  $\epsilon^* = \epsilon' - i\epsilon''$ . In polar-sensitive crystals microwave dielectric losses show an additional maximum of quasi-Debye type absorption due to the interaction between optical and acoustical phonons.

Experimental evidence shown in Fig. 2.4 is a comparison of microwave properties of two semiconductors. One is the nonpolar crystal silicon (Fig. 2.4A), which is characterized only by covalent bonding between atoms; therefore its dielectric losses are caused exclusively by the conductivity ( $\sigma$ ). Correspondingly, in silicon the loss factor decreases with frequency, but increases with temperature:

$$\epsilon''(\omega, T) \approx \sigma_0 \exp[a(T - T_0)] / [\epsilon_0 \omega],$$

where  $\sigma_0$  is conductivity at room temperature  $T_0$ ,  $\epsilon_0$  is the electrical constant, and  $a$  is a parameter that is specific for a given semiconductor.

Another example is gallium arsenide (GaAs), a polar-sensitive crystal semiconductor (Fig. 2.4B) in which conductivity is a thousand times less than in silicon. Since the influence of conductivity on the microwave absorption of this crystal is negligible, it would be expected that in the millimeter wave range the absorption of gallium arsenide given from conductivity should be very small. In fact, however, microwave losses of GaAs are increased and  $\epsilon''(\omega, T)$  increases even more with frequency rise.

The fact is that, in the polar-sensitive crystals, with millimeter waves the losses of polarization are manifested due to the interaction of acoustic and optical phonons. In the nonpolar crystals, optical phonons, which are excited by an ultrahigh frequency electrical field, very weakly dissipate the energy received in acoustic phonons, which are electrically inactive in the nonpiezoelectric crystals and play the role of a “thermal reservoir” of crystal lattice. In polar crystals, on the other hand, due to the absence of a center of symmetry in the elementary cell, acoustic and optical phonons are coupled, so that the superhigh-frequency energy imparted to the crystal is more efficiently converted into heat: this represents the microwave losses.

Loss factor increasing with frequency can be described by the Debye formula:

$$\epsilon''(\omega, T) \approx (\omega/\omega_D) \exp(-U/k_B T),$$

where  $\omega_D$  is the Debye frequency,  $k_B$  is the Boltzmann constant, and  $U$  is the potential barrier of relaxation. As can be seen from the experiments (Fig. 2.4B), in the polar-sensitive crystals the microwave (fundamental) loss factor increases with ascending frequency and with temperature rise.

**(6) Elastic properties** of the polar crystals are also peculiar. In polar crystals, which are similar in chemical composition and crystalline structure, the elastic stiffness ( $c$ ) is usually less than in the nonpolar crystals; correspondingly, their elastic compliance ( $s$ ) is bigger. Both these parameters in the polar crystals essentially depend on the electrical conditions in which the crystal is located: whether it is short-circuited ( $s^D, c^D$ ) or open-circuited ( $s^E, c^E$ ). If the polar crystal is short-circuited, its elastic compliance will be bigger than in the case of the open-circuited crystal ( $s^D > s^E$ ). The reason is that electrical voltage, generated by a strain in the case of the open-circuited crystal, increases its resistance to deformation. An experimental example of this effect is shown in Fig. 2.5.

Experiments show essential differences in the elastic stiffness in the well-known ferroelectric Rochelle salt crystal (Fig. 2.5A),  $c^D > c^E$ . In the entire range of investigation this crystal is polar; moreover, above 24°C it is paraelectric, below -18°C it is antiferroelectric, and between these temperatures Rochelle salt is ferroelectric. The most impressive difference between  $c^D$  and  $c^E$  is seen in the Curie points, where elastic stiffness of the short-circuited crystal decreases by eight times. As known, the elastic stiffness determines the speed of sound in a crystal; it can be seen from Fig. 2.5A that in the short-circuited crystal this speed varies critically at the points of phase transitions. This change in  $c^E$  can be considered the greatest of those known; in fact, in most of the polar crystals, the difference between  $c^D$  and  $c^E$  is not so large but is nevertheless quite noticeable.

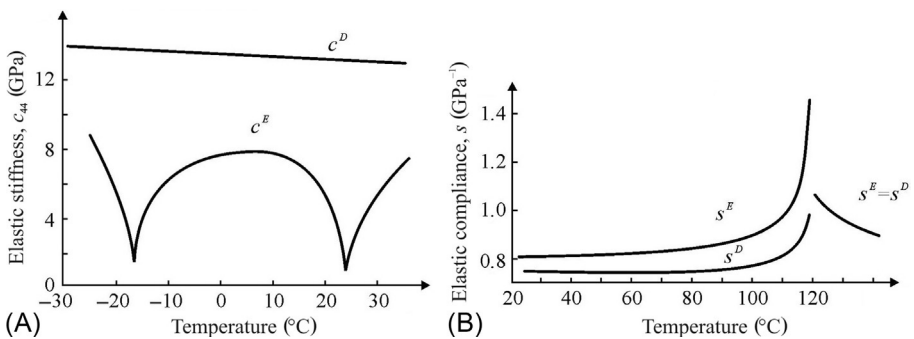


**Fig. 2.5** Effect of electrical conditions on polar crystal elastic properties; (A) Rochelle salt elastic stiffness in its polar direction; (B) barium titanate elastic compliance.

The second example of the influence of *electrical conditions* on the elastic properties of polar-sensitive crystals is shown in Fig. 2.5B. The significant difference between the elastic compliance of an electrically open and a short-circuited crystal can be seen in the polar phase of barium titanate (below its Curie point). In the polar (ordered) phase of barium titanate, the piezoelectric effect is observed, and in the non-polar phase this effect is absent, so  $s^E = s^D$ . Below the temperature of phase transition barium titanate enters a tetragonal polar-sensitive phase that is characterized by the piezoelectric effect, so elastic compliance becomes quite different:  $s^E > s^D$ . The most critical reduction of the compliance  $s^D$  is seen in the Curie point [1].

There are many other examples that show the influence of electrical conditions on polar crystal mechanical and thermal properties. The mechanical boundary conditions may have strong effects on the electrical and also on thermal properties. In that way polar crystals differ from a great number of nonpolar crystals and noncrystalline dielectrics. Further, it will be shown that polar crystals exhibit unusual properties in the field of electrical conductivity as well.

## 2.2 Charge transfer in polar-sensitive crystals

In the study of electrical polarization mechanisms in dielectrics (including piezoelectrics, pyroelectrics, and ferroelectrics), to simplify the task the electrical conductivity of material does not usually need to be taken into account. In turn, when studying the electrical conductivity of semiconductors, as a rule no attention is paid to the phenomenon of their electrical polarization. In most cases, these assumptions are justified; however, there are quite rare but nonetheless important cases when the interdependence of intrinsic polarity and conductivity becomes an essential physical phenomenon. For example, we should not neglect by intrinsic polarity while classification of semiconductors: the nonpolar semiconductors (such as Si or Ge) are characterized by a *nondirect bandgap* electronic energy spectrum, while a main feature of the polar semiconductors, such as  $A^{III}B^V$  crystals (possessing piezoelectric symmetry) and  $A^{II}B^{VI}$  crystals (with pyroelectric symmetry), is the *direct bandgap*.

It will be considered further how a polar-sensitive structure can affect electrical resistance (or conductance) of noncentrosymmetric crystals. It should be noted that this phenomenon manifests itself somewhat *differently* in the ordinary and the elevated electric fields. Moreover, the strong influence of internal polarity is seen both on the *temperature dependence* of resistivity (used in the electronics components *critistors* and *posistors*) and on the *field dependence* of resistivity (which is used in electronics in varistors). It should be noted that understanding the mechanisms of internal polarity action on electrical charge transfer can be important for improving relevant material parameters.

As a first example, the influence of intrinsic polarity on the **temperature behavior of resistivity** is considered. Fig. 2.6 demonstrates different types of thermistors—electronic components that are widely used to measure temperature by means of resistivity alteration. The temperature dependence of electrical resistance in *metals* has been applied for a long time: their resistivity increases with temperature (curve 1)

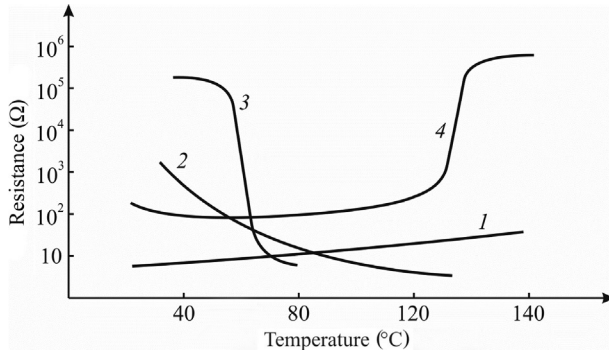


**Fig. 2.6** Temperature dependence of resistance: 1—platinum wire thermistor; 2—negistor utilizing transition-metals oxides; 3—critistor based on vanadium dioxide; 4—posistor utilizing doped barium titanate [10].

thanks to scattering of conduction electrons by lattice vibrations. Although this effect is rather weak, the *positive* temperature coefficient of resistance in metals finds application in sensors. Many wider applications similar to thermistors are also found, in which the *negative* temperature coefficient of resistance is used; these are called *negistors*, seen in curve 2 in Fig. 2.6. Usually they are made of semiconductor oxides, in which resistance decreases noticeably with increasing temperature. The physical nature of the  $R(T)$  decrease in negistors is the increase of free-electron concentration in the semiconductor with temperature rise. Furthermore, the electrical polarity of the material does not have a significant effect on the  $R(T)$  dependence.

As can be seen from Fig. 2.6, there are some materials in which the resistivity is much more sensitive to the change of temperature, and they are, in particular, the polar-sensitive materials called *critistors* (curve 3) and *posistors* (curve 4): they have large negative or positive temperature coefficients of resistance. It is natural to assume that this feature can be explained by the influence of polarity on conductivity. It is important to note that in all temperature characteristics shown in Fig. 2.6 the magnitude of electrical fields and currents practically *does not matter*: in various electrical fields they demonstrate *linear* properties.

However, in some other cases, just the polar sensitivity determines the nonlinear properties in the oxide dielectrics-semiconductors.

Therefore, the second example is related to the effect of intrinsic polarity on the **nonlinear behavior of resistivity**. Fig. 2.7 demonstrates broadly how a strong electrical field can affect the electrical resistance of different materials.

Dielectrics usually retain a very high resistance up to very high field strengths (curve 1), but there is a limit: this is the phenomenon of electrical breakdown due to electronic avalanches, when the resistance of the dielectric drops to zero. Similarly, in semiconductors (curve 2), irreversible breakdown with a decrease in resistance due to generation of new charge carries in an electrical field is also observed. The influence of the polarity of the electrical strength of crystals is not considered here.

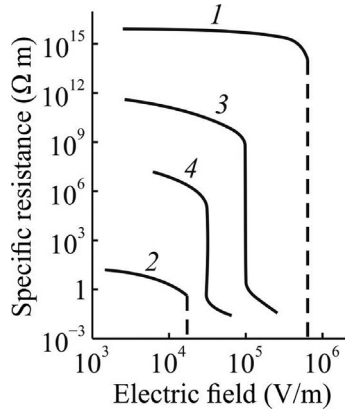


**Fig. 2.7** Field dependence of resistance: 1—typical dielectric; 2—typical; semiconductor; 3—zinc oxide varistor; 4—silicon nitride varistor.

It's quite another matter when the resistance can be changed thousands of times *without electrical breakdown*. This phenomenon might be due to a peculiar electrophysical process (curve 3 in Fig. 2.7); in another case, it might be ascribed to the tunneling effect (curve 4 in Fig. 2.7). Unlike the irreversible effect of electrical breakdown, these  $R(E)$  transfers from the insulating state to the conducting state are reversible, because the dielectric/semiconductor does not undergo any destruction, as happens in the case of electrical breakdown.

Materials in which resistance is characterized by curves 3 and 4 in Fig. 2.7 are dielectrics in a wide range of electrical fields, until anomalous changes in conductivity. In this regard, note that different interatomic bonds of solid dielectrics affect the electrical conductivity in different ways. Ionic bonds promote the transition of electrons to their polaron state, which significantly *reduces conductivity*: the electron mobility in the ionic dielectrics is only  $1\text{--}10\text{ cm}^2\text{ V}^{-1}\text{ s}^{-1}$ . Conversely, in the covalent crystals, their “open” internal structure does not contribute to the formation of small radius and low-mobility polarons but promotes a very high mobility of electrons:  $10^4\text{--}10^5\text{ cm}^2\text{ V}^{-1}\text{ s}^{-1}$ . In both cases, there is a correlation between the mobility and the affinity of atoms to electrons.

At the same time, covalent bonding, in which *two* atoms share two valence electrons, has different extreme cases: first, a covalent bond may approach to metallic bonding, when *all* atoms share between them all valence electrons, and, second, a covalent bond may approach closer to an ionic bond, when one atom completely delegates its valence electrons to another atom.

Two important properties of ionic dielectrics, their increased polarizability and their low conductivity, are *interdependent*. Indeed, the electron (or hole) generated in a dielectric as a result of any activation processes becomes less mobile, since it polarizes the surrounding nanosize region in the crystal by its field. It is obvious that such a charge carrier is forced to move along together with the region polarized by it, forming a *small radius polaron*. The low mobility of such charge carriers makes

possible, in turn, the long existence of the electrostatic field in dielectrics (in the conductors this field is shielded by free charge carriers).

Thus, the relatively stable state in a dielectric with low electronic conductivity is due precisely to the ionic polarization. Heating a crystal or exposing it to a strong electrical field can disrupt this stability, because under external energy exposure electrons can free themselves from their polarized environment: polarons transfer into highly mobile electrons, and the dielectric turns into a more conducting medium.

In some special cases the stable nonconducting state in a dielectric may be compromised, even in a weak electrical field and without essential heating. It is exactly this exceptional case that corresponds to some crystals with polar-sensitive properties. In such polar dielectrics, even a small change in the external conditions (pressure, temperature, mechanical stress, or electrical field) can lead to a huge increase of conductivity (up to  $10^4$ – $10^9$  times), and the dielectric turns into conductive matter but without breakdown. The large jump of conductivity (or resistivity) usually, but not necessarily, is accompanied by a change in the structure of the crystal: that is, it is associated with the peculiar rearrangement of electronic interaction between particles, which can lead to the alteration in crystal symmetry.

Now it would be interesting to find out why this transformation in some crystals is a rare exception. The unusual dependence of resistivity on electrical voltage, i.e., its change by hundreds and thousands of times, takes place in noncentrosymmetric polar crystals with a pyroelectric or piezoelectric structure. In fact, as shown in Fig. 2.7, silicon nitride (SiC) has a pyroelectric wurtzite structure while vanadium dioxide ( $\text{VO}_2$ ) has triclinic piezoelectric symmetry. The unusual dependences  $R(T)$  presented in Fig. 2.6 are a characteristic first for zinc oxide (ZnO) with a polar pyroelectric structure, passing with increasing voltage to another, also polar, sphalerite (piezoelectric) structure, and second for barium titanate ( $\text{BaTiO}_3$ ), which is a ferroelectric with a pyroelectric structure.

Thus, the explanation of an unusual jump-like change in conductivity in some polar crystals reduces to the clarification of the principal physical cause: why the polar sensitivity, leading to the noncentrosymmetry, might have an especially strong influence on the electrical conductivity. An evident reason for the lack of center of symmetry in a crystal is a special kind of atomic bonding: polar-sensitive bonds. This kind of interatomic bonding represents the intermediate case between ionic and covalent bonds: as noted earlier, the pure-ionic, as well as the pure-covalent crystals always demonstrate a centrosymmetric structure, and this means that in such crystals there is no intrinsic (hidden) polarity.

Noncentrosymmetric structures are the result of mixed ionic-covalent bonds between the atoms of a crystal. Like the covalent bond, these mixed bonds are *directional*, which leads to the asymmetry of polar crystal structures. In turn, the non-uniform probability density of the distribution of electrons in the interatomic bonds is due to the difference in the electronegativity of atoms. In addition, this density asymmetry of electronic clouds is the main cause of *internal polarity* in crystals. Electrical conductivity in dielectrics and semiconductors, having an activation character, must depend on the affinity of atoms to electrons: in order to form a free charge carrier, it is necessary to tear an electron from its own atom or ion. At the same time,

the crystals discussed here are not monoatomic, but are chemical compounds. Therefore, the importance is not only due to the electronegativity of individual atoms (measured on the Pauling scale), but the difference of this parameter in neighboring ions.

Consequently, a distinctive feature of polar crystals is a certain system of polar-sensitive bonds. The spatial distribution of polar bonds in a crystal can be complex, but its distinguishing feature is the absence of a center of symmetry. This feature has a decisive influence on the physical characteristics of polar crystals, including their resistivity.

In the case under discussion, the most important influence is that of polar sensitivity on the crystal resistivity. If internal polarity is distributed in a complex manner, then charge carriers are obliged to lead the way through the alternating bipolar nanosize districts that dramatically decrease their mobility—just as an electron in an antiferromagnetic has difficulty finding its way through the antiparallel magnetized lattice. On the contrary, if internal polarity is quite ordered (or becomes ordered by the external field) then charge carrier mobility should be much higher—just like high electroconductivity is peculiar to the ferromagnetic with parallel ordered spins.

In the following paragraphs it will be shown how the model of polar-sensitive bonding can be applied to explain, first, the critical temperature dependence of resistivity and, second, the large jumps of conductivity stimulated by an electrical field in the polar crystals, listed in [Figs. 2.6 and 2.7](#).

First and foremost, the critistor effect in vanadium oxides is considered a phase transition of the insulator-to-metal type. At lower temperature  $\text{VO}_2$  and  $\text{V}_2\text{O}_3$  are wide-gap semiconductors (almost dielectrics), but with temperature increases they exhibit metallic-type behavior: the energy bandgap in these crystals almost disappears. As a result, in a narrow temperature interval their resistivity changes in thousands times; moreover, the critical temperature (within a limited range) can be controlled by the chemical composition. It is natural to assume that this feature is due to the peculiarity of interatomic bonds in vanadium oxides.

As is well known, the covalent bond, in which the adjoining atoms are divided by a pair of valence electrons, on the one hand is close to a metallic bond, in which all valence electrons are generalized in the lattice of a metal. But, on the other hand, the covalent bond is also close to an ionic bond, in which the cation entirely delivers its valence electrons to the anion, and together they constitute the dielectric ionic lattice. It would seem that this feature of a covalent bond could be used to explain the phase transition in vanadium oxide that has been discussed. However, crystals with dielectric-metal type transition having strong  $R(T)$  dependence are extremely rare cases. The point is that a key role in this phenomenon belongs to the hybridized covalent-ionic bonds, which give rise to polar sensitivity and to noncentrosymmetric structure creation.

Indirect confirmation of this mechanism is the dependence of  $\text{VO}_2$  conductivity on pressure, which fairly easily converts this oxide into metal. Upon crystal compression, its atoms become closer to each other and, as a result, there is not enough space for mutual orientation of the hybridized ionic-covalent polar bonds: all valence electrons become generalized in the electronic gas filling a lattice. Now this becomes a metallic

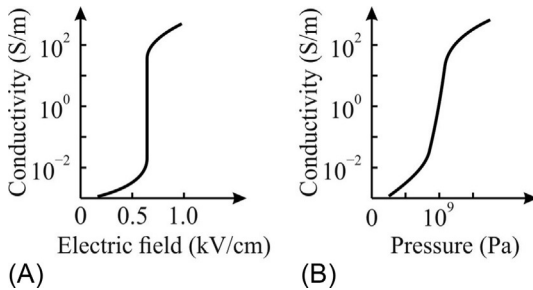


**Fig. 2.8** Changing  $\text{VO}_2$  conductivity in electrical field (A), and with increase of pressure (B) [11].

bond (as was noted, polar bond ordering leads to an increase in crystal volume; respectively, crystal compression destroys the ordering of polar-sensitive bonds).

In Fig. 2.8 temperature dependence of conductivity  $\sigma$  in the  $\text{VO}_2$  crystal is compared with  $\sigma$  dependence on hydrostatic pressure. Experiments show that at very high pressure (as well as in a very large electrical field) a dielectric phase in vanadium dioxide cannot be realized. This means that not only a critical temperature exists (as seen in Fig. 2.6, curve 3), but also critical field and critical pressure exist (when  $\text{VO}_2$  shows a sharp increase of conductivity). As will be shown later, just such dependence on pressure is a characteristic of polar-sensitive coupling in ferroelectrics (their phase transition at higher pressure shifts to low temperatures).

When comparing the characteristics of vanadium oxide in a critistor, it should be noted that, as shown in Fig. 2.6, curve 3 relates to the *ceramic* material, in which  $R(T)$  dependence is somewhat blurred in comparison with a single crystal: its inverse characteristic  $\sigma(T) \sim 1/R(T)$  is shown in Fig. 2.8A. It is seen that in the single crystals this physical phenomenon manifests itself more sharply than in ceramics.

Thus, the mechanism of temperature-induced phase transition in vanadium dioxide looks like this: in the insulating state of  $\text{VO}_2$  a rather complex distribution of polar-sensitive bonds of 3D orientation promotes extremely low mobility of the polaron-type charge carries. The point is that vanadium dioxide in its lower-temperature (dielectric) state has several competing phases dominated by the monoclinic polar-sensitive structure. It is the instability of these phases with their variability and mutual transitions that contributes to formation of charge carriers with bound (polaron) states. Next, when the temperature rises, the growing energy results in rapid liberation of electrons, creating their avalanche with a stepped decrease of resistivity (i.e., with  $\sigma(T)$  spasmodic increase).

An external electrical field also supports the liberation of charge carriers from their bound state, so even at temperatures which are much lower than natural jump of conductivity (in the dielectric phase of  $\text{VO}_2$ ), the electrical field forcedly and rapidly switches  $\text{VO}_2$  into its conducting phase. Moreover, the electrically controlled and rapidly changing “dielectric-to-metallic” reflection of infrared and optical waves from the  $\text{VO}_2$  surface is reached: thus arises an element with electrically guided optical reflection.

In this complicated polar-sensitive structure, a strong coupling of charge carriers with their close neighbors in the lattice is formed. Very low mobility of the formed

polarens stipulates a large resistivity of  $\text{VO}_2$  at lower temperature. Due to the delicate balance of this unstable state, the mechanism of high conductivity appearance resembles a “house-of-cards” destruction or a “domino effect.” When electrons are unfettered, their interaction with the surrounding nano-areas becomes screened; as a result, the avalanche-like increase of free charge carriers occurs. Arising with temperature increase, the high-conductive (quasimetallic) phase of  $\text{VO}_2$  is characterized by a *nonpolar* tetragonal rutile-like structure. It should also be noted that a definite influence on the electrical conductivity is exerted by the magnetic ordering in  $\text{VO}_2$ , which at lowered temperature is antiferromagnetic and at increased temperature is paramagnetic.

It is important to note two features: first, the dielectric-to-metal transition is *very fast* and completely *reversible*. When  $\text{VO}_2$  cools, its dielectric phase instantly returns. Second, the transition from the dielectric phase to the electrically conducting phase can be easily stimulated by an external electrical field, which releases the electrons from their polaron state. During this transition, the electrical resistivity, the opacity, etc., can be changed, up to several orders of magnitude. Due to these properties, vanadium oxide is used as a surface with electrically controlled reflection that can be applied in various sensors and other applications. Fast optical shutters, modulators, cameras, and data storage devices have been developed based on vanadium dioxide.

Thus, vanadium dioxide belongs to the category of **field-controllable switching elements**. The electrical field acts as controlling factor for resistivity, changing resistivity into hundreds of times. As seen in Fig. 2.9A in the *curve*  $E \approx 0$ , below the temperature of  $60^\circ\text{C}$  vanadium dioxide is a dielectric (D), but above  $65^\circ\text{C}$  it exhibits quasimetallic behavior: the bandgap in the electron energy spectrum in vanadium

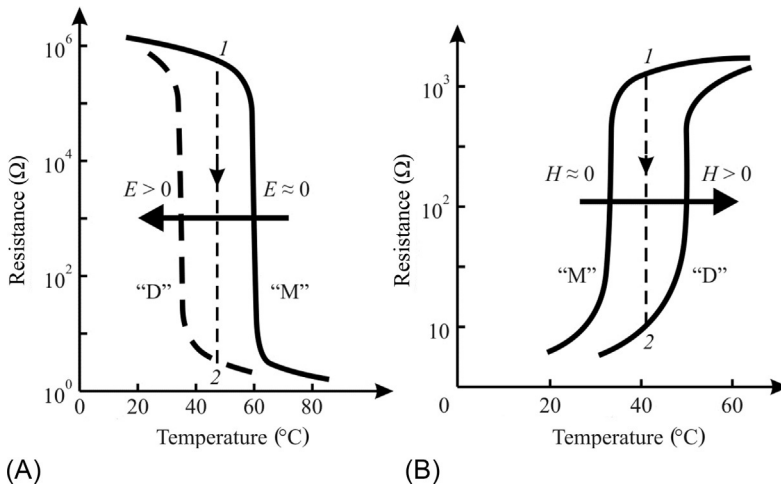


**Fig. 2.9** Resistance control by external fields: (A) Electrical bias field manages  $R$  value in  $\text{VO}_2$ ; (B) magnetic bias field manages  $R$  value in  $(\text{La}_{1-x}\text{Ca}_x)\text{MnO}_3$  (dotted line 1  $\rightarrow$  2 shows large fall in resistance).

oxide almost disappears. As a result, in a narrow temperature interval the resistance of  $\text{VO}_2$  decreases rapidly, passing to the metallic phase (M).

However, if an external *electrical field* is applied to  $\text{VO}_2$  (the usual sample is a thin film with interdigital electrodes), the transition from the D phase into the M phase will start at a much lower temperature, for example at  $\sim 35^\circ\text{C}$ , and the resistance under the controlling field decreases in thousands times, as shown by vertical line  $1 \rightarrow 2$  in Fig. 2.9A. Such a displacement of the phase transition in the electrical field is the physical basis for vanadium oxide applications as switching elements: the externally applied electrical bias field promotes charge carrier liberation from their bound state, so fast switching takes place to the conducting state. As mentioned, the electrically controlled optical reflection from  $\text{VO}_2$  film is used in controlling optical devices.

It should be noted that, in polar-sensitive crystals, a significant control by resistivity is possible not only by using an electrical field but also by applying a *magnetic bias field*. A good example of *magnetic control* using electrical resistance is found in manganites with a perovskite structure, as shown in Fig. 2.9B. These compounds are an important family of oxides with *colossal magnetoresistance*. Among such compounds are interesting polar compounds of the type  $(\text{La}_{1-x}, \text{Ca}_x)\text{MnO}_3$ , where the concentration of Ca may vary within  $0 \leq x \leq 1$ . With this variation, the physical properties of manganites change dramatically; in particular, phase transitions with different types of magnetic and dielectric ordering are seen. In this case, the magnetic ordering is due to double electron transfer through the intermediate oxygen ion  $\text{Mn}^{+3} \leftrightarrow \text{O}^{-2} \leftrightarrow \text{Mn}^{+4}$ . At low temperatures, the magnetically ordered phase  $(\text{La}_{1-x}, \text{Ca}_x)\text{MnO}_3$  has reduced electrical resistance (which is typical for ferromagnetic ordering) while at elevated temperatures, the compound under consideration is a wide-gap semiconductor (almost a dielectric). An application from outside the magnetic field returns this compound to a magnetically ordered phase with low electrical resistance.

Therefore, in addition to the electrical control by resistivity in  $\text{V}_2\text{O}$ , in the case of the  $(\text{La}_{1-x}, \text{Ca}_x)\text{MnO}_3$  compound a magnetic means of resistivity control is applied. Indeed, the parallel ordering of electronic spins in the M phase of the compound corresponds to a low electrical resistance (see Fig. 2.9B, left part at  $H = 0$ ). However, when temperature rises, the growing thermal movement in the manganite lattice destroys the double-exchange mechanism and the ferromagnetic (conducting) phase turns into the nonmagnetic (nearly dielectric, D) phase; correspondingly, a sharp increase of resistance occurs. However, by application of a magnetic bias field in the higher-temperature D phase, the magnetic ordering in the manganite can be forcibly returned (see Fig. 2.9B, curve  $H > 0$ ). Moreover, the resistance falls in hundred times, as is shown by the dotted line  $1 \rightarrow 2$ . Induced by a magnetic field, the “insulator-conductor” transition is referred to as colossal magnetoresistance. This large change in resistivity under the controlling magnetic field can be used in many electronic devices.

Thus, in polar-sensitive material, both electrical and magnetic fields may shift the temperature of “insulator-conductor” type phase transformation, leading to the enormous change in resistivity. Moreover, the phase having reduced resistivity may be located either at elevated temperature or lower temperature.

The list of mechanisms for the strong influence of dielectric polarity on electrical resistivity brings us at last to consider **posistors**, mentioned earlier in connection with Fig. 2.6, curve 4 (note that electronic ceramics with a *positive* temperature coefficient of resistivity are used not only in electronics but in electrical engineering). It is quite unusual for dielectrics and semiconductors to exhibit a temperature range in which their resistivity *increases* with temperature rise (instead of the usual exponential decrease); however, it is observed not only in the manganites of  $(\text{La}_{1-x}\text{Ca}_x)\text{MnO}_3$  type but also in doped ferroelectrics of  $\text{BaTiO}_3$  type.

In ordinary ferroelectrics, the anomaly of electrical resistivity usually is small near their phase transition: the ferroelectric transition in most cases does not significantly change the general activation-type *decrease* of  $R(T)$  with growing temperature, shown by the dotted line in Fig. 2.10A. The electron energy bandgap in most ferroelectrics is large and, therefore, they usually can be considered as dielectrics both above and below their phase transition.

However, using doping, it is possible to significantly reduce electrical resistance in ferroelectrics, as shown by the solid line in Fig. 2.10A. Moreover, near the ferroelectric Curie point ( $\sim 400$  K in  $\text{BaTiO}_3$ ) a sharp increase in  $R(T)$  is seen ( $\sim 10^3$  times increases original value). As already noted, in most cases the posistor effect is used in doped ferroelectric *ceramics* of the barium titanate type, which has a complicated structure (not in crystals). It is important to note that the state with low resistance is peculiar only to the polar-sensitive phase, while at transition to the nonpolar phase the resistance stepwise increases. (It is typical in the more common dielectrics that a decrease in the activation-type resistance is seen only at further heating, significantly higher than the Curie point.)

In the case of ferroelectrics, the strong influence of polar-sensitive ordering on the resistivity is obvious. Experiments show that one-directed polar-sensitive bonds in a

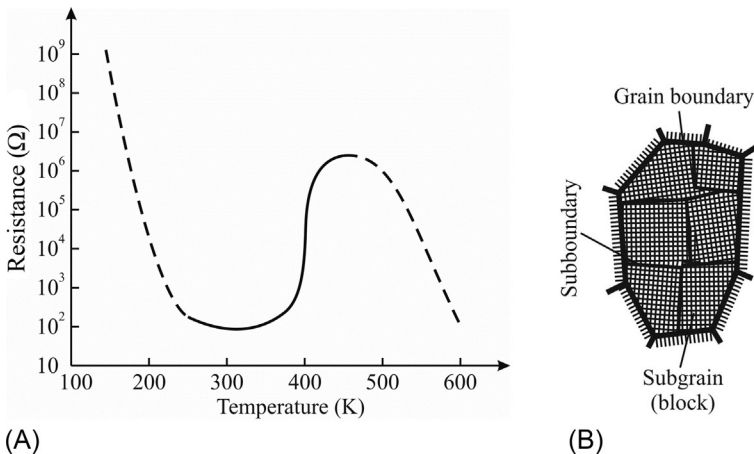


**Fig. 2.10** Resistance temperature dependence in dysprosium doped barium titanate (A) and scheme of crystallite (grain) with (mosaic) structure inside crystallite (B).

structure with tetragonal symmetry of the  $4m$  class do not promote polaron state formation, giving increased conductivity in a doped ferroelectric. When phase transition into the high-temperature nonpolar  $m3m$  phase occurs, the ordering in polar-sensitive bonds disappears and charge carriers transform into polarons with increased effective mass. Here, it is the polycrystalline structure that essentially contributes to the disordering, under which favorable conditions are created for charge-carrier binding and the correspondent increase of electrical resistance. With a further increase in temperature above the limits of the use of a posistor, in the end the polaron states are destroyed by thermal motion and the resistance decreases, as in all semiconductors and dielectrics (see Fig. 2.10A at  $t > 500^\circ\text{C}$ ).

In the posistor effect, a decisive role is seen for the grain boundaries of polycrystalline ferroelectrics: they are relatively “transparent” for charge carrier movement in the ordered polar phase, but become practically “locked” in the nonpolar phase, creating polarons. The scheme of crystallite is shown in Fig. 2.10B: this is a rather complex formation, having both “widened” boundaries and densely located “narrow” dividing walls, which also introduce disorder into the structure. Both grain boundaries and interblock boundaries have a chemical composition similar to a basic ferroelectric, but they have a high concentration of structural defects. The main reason for the low resistance of boundaries in the polar phase is the *proximity effect*<sup>b</sup>, already discussed in connection with chemical peculiarities in the polar crystal surface. As a result, highly ordered interatomic bonds in the polar phase induce polar-type regularity inside the weakly ordered boundaries, which causes lower electrical resistance. When, with temperature increase, thermal motion destroys the ordering of polar-sensitive bonds in the body of crystallite, the ordering is even more disturbed in the numerous wide and narrow boundaries, so the resistance suddenly rises.

The temperature of the sharp increase in posistor resistance could be changed by applying various doped ferroelectric solid solutions. For example, in the composition (Ba, Pb)  $\text{TiO}_3$ , the resistance jump can be increased up to 600 K, while in the composition (Ba, Sr)  $\text{TiO}_3$ , the temperature jump of resistance can be reduced down to 300 K. Thus, ceramic posistors can be designed for applications over a wide range of temperatures. Posistors, which are unusual ceramic elements with low “cold” electrical resistance and high “hot” resistance, are used in thermal control systems, devices that prevent thermal and current overload, engine-start systems, measurement technology, and automatic control systems. Posistors are also used to protect against overvoltage and to avoid high short-circuit current: when the posistor is connected in series with the load, the current in the circuit is limited to a safe level [1].

For the same goal—electrical current limiting in critical situations—other polar conductive materials are used, namely the **varistors**, i.e., ceramic dielectrics-semiconductors, in which the drastic change in conductivity does not indicate a phase transition (as occurs in  $\text{VO}_2$  or in doped  $\text{BaTiO}_3$ ). In the case of varistors, a significant

<sup>b</sup>The proximity effect is well known in magnetism, when a magnet induces magnetization in closely adjacent nonmagnetic material; this effect is also known in superconductivity, when ordinary metal closest to a superconductor also becomes a superconductor; in liquid crystalline substances, ordering peculiar to one phase affects ordering of the neighboring phase, etc.

jump of electronic conductivity (millions of times) is observed, for instance, in carborundum (SiC) or in zinc oxide (ZnO). A comparison of their behavior in strong electrical fields with ordinary dielectrics and semiconductors was shown in Fig. 2.7. Both of these materials mentioned belong to the noncentrosymmetric classes of symmetries with *mutable structure*, which can be changed from the sphalerite (piezoelectric) structure into the wurtzite (pyroelectric) structure.

Varistors are characterized by linear (ohmic) current-voltage dependence, both at a reduced level and an increased level of electrical fields:  $j \sim E$  (Fig. 2.11A). However, it is important that in a low electrical field the varistor has a high electrical resistance: its resistance is close to the dielectric, but in a strong electric field the resistance of the varistor decreases by millions of times and it becomes a typical semiconductor. In this transformation, the electrical breakdown of the varistor does not occur, since the growth of the electrical current in it is limited. The characteristic  $j(E)$  is reversible: the increased current passing through the varistor remains stable. Therefore the physical phenomenon of stepped growth of electrical current in the varistor is essentially different from conventional electrical breakdown.

The features of carborundum varistors and zinc oxide varistors are similar, but the jump of resistance in zinc oxide varistors is much larger. Moreover, the zinc oxide crystal has a large electronic energy bandgap ( $\sim 3.4$  eV). The advantages associated with a large bandgap include higher breakdown voltages and the ability to withstand increased electrical fields, as well as the possibility of applications in higher-temperature and higher-power conditions.

To explain the enormous nonlinearity of electrical conductivity in ZnO, the following should be noted. Zinc oxide crystallizes in two main structures: cubic sphalerite and hexagonal wurtzite, both belonging to the noncentrosymmetric classes of symmetries. In both cases, polar-sensitive bonds are mixed in the complex 3D structure, which corresponds to the structural motifs shown in Fig. 2.11B. The modification of the sphalerite (zinc blende) is a polar-neutral material (of piezoelectric symmetry), while zinc oxide has a 1D-oriented motif of polar wurtzite symmetry (of pyroelectric type).

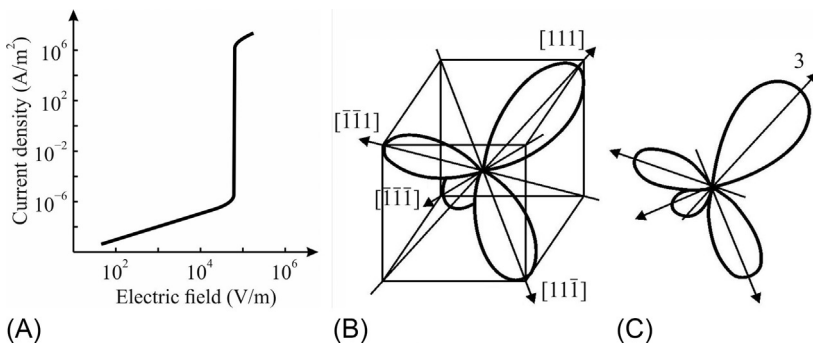


**Fig. 2.11** Zinc oxide nonlinear property: (A) Current-voltage characteristic; (B, C) polarity changing from polar-neutral sphalerite into polar wurtzite (only positive directions of polar axes are shown).

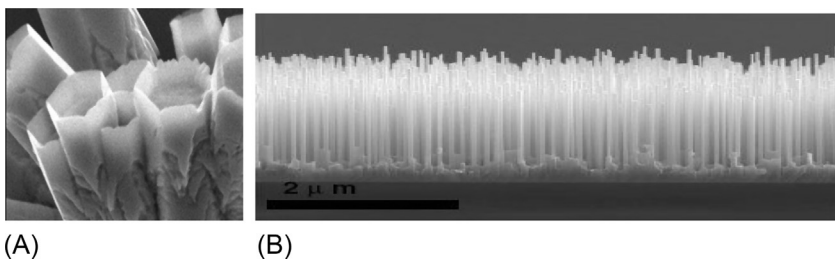
It is important to keep in mind that this material can rather easily *alternate* its structures under the influences of external factors: for example, at high pressure (about 10 GPa) any polar properties in zinc oxide disappear, and the crystal acquires the electrically neutral rock salt structure. This indicates the *high sensitivity* of the ZnO structure to any external impacts, which leads to the importance of this material for applications in electronic devices.

Fig. 2.11B demonstrates a possible physical mechanism to explain how the external electrical field, being applied to zinc oxide in its insulating phase, induces a change in the internal polarity distribution, which in its turn has a strong impact on the electrical conductivity. Of eight possible [111]-type directions of inner polarity (Fig. 2.11B, left), one direction obviously occurs close to the direction of the applied field, which strengthens the polar sensitivity in this direction (following axis 3) at the expense of the other axes (Fig. 2.11B, right) (where, for convenience, only positive directions of polar axes are shown).

Thus, the high-resistance phase of ZnO is the dielectric sphalerite, in which electrical transfer of charge carries occurs in the complex and competing 3D structure: these charge carries are the excitons with large binding energy of  $\sim 60$  meV. The sphalerite phase can be electrically transformed into the low-resistance phase, consisting of mainly 1D-oriented polar wurtzite. As already mentioned (when the posistor effect was discussed in the polar higher-conducting phase of doped barium titanate), 1D polar ordering prevents the binding of charge carriers into the polaron state; moreover, the polarity of wurtzite agrees with this case. On the contrary, very complicated polarity orientations in the sphalerite structure (Fig. 2.11B, left) deepen potential barriers of the polaron state and essentially lower charges mobility. Thus, the mechanism of nonlinearity in ZnO might represent electrically induced switching from the sphalerite structure into the wurtzite structure.

Varistors are widely applied to protect electrical circuits from sudden jumps of voltage: when voltage increases, the current flows through the varistor but not through other elements of the circuit.

The fine balanced polar-sensitive structure of zinc oxide, which is always ready for a strong change of its electrical properties under an external influence, is also used in sensors for various purposes, especially in the nanostructural state (Fig. 2.12). Very thin films of zinc oxide (and, particularly, its nanostructures) are used as components



**Fig. 2.12** Zinc oxide nanostructures used in sensors: (A) Hexagonal nanocrystals; (B) very thin tubular nanocrystals [12].

in solar elements, in piezoelectric nanogenerators, and in luminescent materials such as light-emitting diodes, lasers, etc. Note that superfine ZnO nanocrystals, shown in Fig. 2.12B, are thousands of times thinner than human hair.

Furthermore, the nanoparticles of zinc dioxide demonstrate structures with quite developed surfaces and very delicate forms (Fig. 2.12A), which despite the small size and unusual shape, retain the regularity of the structure inherent in the bulk crystal. As already mentioned, the piezoelectric and pyroelectric properties of polar crystals are strongly influenced by boundary conditions. Apparently for this reason, the piezoelectric module in ZnO nanostructures is larger compared to a conventional bulk crystal.

Internal polar bonds in the ZnO nanostructures are very sensitive to temperature, light, humidity, and even to the composition of surrounding gas. As already discussed in connection with the properties of varistors, the electrical conductivity of zinc oxide varies greatly with structural changes from the sphalerite to the wurtzite. In this case, in the ultrathin nanostructures, the balance of symmetry can be easily broken, as is shown in Fig. 2.12B, which can serve as a physical model for the functioning of ZnO sensors.

### 2.3 Electrically induced polar properties

It was already indicated in Chapter 1 that *polar properties* in the nonpolar dielectrics can be induced by a bias field through electrostriction, which is deformation of a crystal in the electrical field. When this field is small and relative dielectric permittivity  $\epsilon$  is less than 10, the effect of electrostriction is very small and can be neglected. However, in electronics many materials with a large permittivity ( $\epsilon \sim 10^3\text{--}10^4$ ) are applied; in this case the electrostriction (which is proportional to  $\epsilon^2$ ) becomes large.

(1) **Electrostriction** is a quadratic (“even”) effect, and it is different from the inverse piezoelectric effect, which is characterized by a linear (“odd”) dependence of the deformation on the electrical field. In the case of electrostriction, the sign of the deformation  $x(E^2)$  does not depend on the polarity of the electrical field; in most dielectrics, the electrostrictive expansion is observed along the applied field ( $x_3 > 0$ ), while in the transverse direction compression is observed ( $x_1, x_2 < 0$ ). The value of electrostriction is usually small: it is an order of magnitude smaller than the piezoelectric deformation. Only in very large electrical fields can the deformation of electrostriction be compared with the piezoelectric deformation: in quartz, only in a field of 35 kV/cm do these deformations become equal.

In the analytical description of electrostriction, the same boundary conditions are accepted as in the case of the piezoelectric effect. However, usually only electrostriction in *mechanically free* dielectrics ( $X = 0$ ) is considered. Electrostriction dependence of the strain  $x$  on polarization  $P$  or electrical field  $E$  is described by two equations, according to whether the dielectric is electrically clamped or free; in these cases the following equations can be obtained:

$$\begin{aligned} x_{ij} &= Q_{ijkl}P_kP_l + Q'_{ijklgh}P_kP_lP_gP_h + \dots; \\ x_{ij} &= R_{ijkl}E_kE_l + R'_{ijklgh}E_kE_lE_gE_h + \dots; \end{aligned} \quad (2.1)$$

In these series, it is usually sufficient to consider only the first terms of the expansion, since the electrostriction is rather small. However, in the ferroelectric relaxors, the electrostriction can be gigantic; that is why in the preceding series three terms of the expansion in the series are considered:

$$x(E) = RE^2 + R'E^4 + R''E^6 \quad (2.2)$$

It's obvious that coefficients of electrostriction  $Q_{ijkl}$  and  $R_{ijkl}$  ( $i, j, k, l = 1, 2, 3$ ) are four-rank tensors. The electrostriction tensors  $Q_{ijkl}$  and  $R_{ijkl}$ , in principle, have 81 components, but due to the diagonal symmetry of the deformation tensor, only 36 of their components remain as independent. For comparison, other tensors of the fourth rank—elastic constants—are usually represented by components of matrices of the  $c_{mn}$  and  $s_{nm}$  type, where  $m, n = 1, 2, \dots, 6$ . They are symmetrical; therefore even crystals with the lowest symmetry can have a maximum of 21 independent elastic constants. In contrast, the tensors that describe electrostriction,  $Q_{ijkl}$  and  $R_{ijkl}$ , in the limiting case of the smallest symmetry, can have all  $6 \times 6 = 36$  independent components. But in practice, this difficult case does not occur: the majority of these components are usually zero. With increasing crystal symmetry, the number of nonzero components  $Q_{ijkl}$  and  $R_{ijkl}$  decreases significantly, but it never happens (as in the case of the piezoelectric module  $d_{ij}$ ) that *all* components of the electrostriction tensor are zero.

Electrostriction for a highest-symmetry medium (isotropic medium) is described by only two components of the tensor:  $Q_{11}$  and  $Q_{12}$  (respectively,  $R_{11}$  and  $R_{12}$ ), which correspond to the longitudinal expansion and lateral compression of the dielectric in an electric field. Since in practice the giant electrostriction of relaxor ferroelectrics with a diffuse phase transition is usually used, these two parameters turn out to be sufficient.

The so-called “fundamental” electrostriction can be considered as tensor  $Q_{mn}$ , since its components differ only slightly for different solids and weakly depend on changes in external conditions. Even in ferroelectrics, the components  $Q_{mn}$  change little with temperature and frequency and are practically independent of fields. This allows us to consider exactly this tensor as the main characteristic of the electromechanical interaction of atoms, ions, or molecules in a given dielectric.

The components of the tensor  $R_{mn}$ , in contrast to  $Q_{mn}$ , strongly depend on the dielectric permittivity and, therefore, they depend on the temperature and frequency of the applied electrical field. That is why in ferroelectrics with a high permittivity ( $\epsilon \sim 10^4$ ), electrostriction reaches (and may even exceed) the strain that is possible with the piezoelectric effect. Giant electrostriction is important for electronic devices, because it can be used in actuators.

**(2) Electrical control** of the piezoelectric effect is not only of scientific but also of technical interest. A change in the piezoelectric properties of a material upon application of an electrical field finds application in devices based on surface acoustic waves (SAWs), electrically controlled delay lines, and convolvers and electrically tunable piezoelectric filters [6].

The physical mechanisms of electrical control of the piezoelectric effect are different in paraelectrics and piezoelectrics, but in essence they reduce to controlling the speed of sound in a material in which an electric field changes elastic compliance. Typical cases of a change in the speed of sound by a bias electrical field in different dielectrics are shown in Fig. 2.13. The piezoelectric crystal of lithium niobate has a polar-sensitive structure with symmetry of  $3m$ . The speed of sound  $\Delta v/v_0(E)$  in a  $\text{LiNbO}_3$  crystal changes in the electric field by only a fraction of a percent (Fig. 2.13A), which is enough to control SAW devices. The linear dependence  $v(E)$  indicates that the energy of oriented polar-sensitive bonds in a polar  $\text{LiNbO}_3$  crystal significantly exceeds the external control energy.

Another case is shown in Fig. 2.13B, when the piezoelectric effect is *induced* by an external electrical field in a *nonpolar* (centrosymmetric) dielectric. Due to the electrostriction, the bias electrical field transforms the structure of *any* isotropic dielectric into a noncentrosymmetric structure, and induces in it *electromechanical coupling*—i.e., the piezoelectric activity. In Fig. 2.13B the induced piezoelectric effect is so great that for its description it is necessary to use Eq. (2.2).

At the same time, in dielectrics with low permittivity the induced piezoelectric effect is so small that it is difficult to even find it, as the electrostriction is negligible. It is appropriate to remember that in Chapter 1, in Fig. 1.9A, some *intermediate cases* were given: the induced piezoelectric effect in the dielectrics having a permeability of about 100. A comparison of characteristics of ceramics widely used in electronics was given: titanium oxide ( $\text{TiO}_2$ , rutile with  $\epsilon \sim 100$ ), calcium titanate (perovskite,  $\text{CaTiO}_3$  with  $\epsilon \sim 150$ ), and strontium titanate ( $\text{SrTiO}_3$  with  $\epsilon \sim 300$ ) were shown. It is this type of ceramics which is interesting for use in *electrically controlled* piezoelectric resonators and filters: while a bias field is applied the element of the circuit demonstrates piezoelectricity, but once this field is turned off, the piezoelectric effect disappears rapidly. In this case, the resonant frequency of the piezoelectric element can be controlled by the applied electric bias field.

The *piezoelectric modulus* for the *electrically induced piezoelectric effect* can be found from the equation of electrostriction (2.1), omitting, for simplicity, the indices

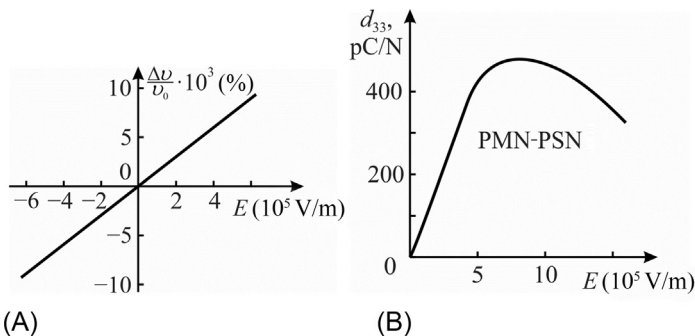


**Fig. 2.13** Electrically tunable and induced piezoelectric effect: (A) Lithium niobate crystal used in controlled delay lines; (B) diffused phase transition ceramics.

of tensor components, as in the case of Eq. (2.2). The deformation is the even function of polarization, which can be described by a rapidly convergent series:

$$x = QP^2 + Q'P^4 + \dots$$

In the case of a rather small alternating electrical field  $E_{\sim}$ , it suffices to restrict it to the first member of the expansion:  $x = QP^2$ . Electrostriction  $x_{\sim}$  in an alternating electrical field is linearized and can be represented as the piezoelectric effect:

$$x_{\sim} = 2QP_y P_{\sim} = d E_{\sim},$$

where parameter  $d$  acts as the piezoelectric modulus, caused by the electrostriction  $Q$ :

$$d \cong 2Q\epsilon_0^2 \epsilon^2 E, \quad (2.3)$$

where  $E = E_{bias}$  is the electrical field that induces the piezoelectric effect.

**(3) Relaxor ferroelectrics peculiarities.** Piezoelectric module induced in a crystal by an electrical field is proportional to the field strength and the *square* of permittivity. Therefore, the field-induced “piezoelectric effect” is higher with a higher dielectric permittivity. As stated earlier in [Chapter 1](#), in the dielectrics with increased dielectric constant ( $\epsilon = 100\text{--}300$ ) the induced piezoelectric module is approximately 0.3 pC/N; however, in a specially developed electrostrictive ceramics  $\text{PbMg}_{1/3}\text{Nb}_{2/3}\text{O}_3\text{-PbSc}_{1/2}\text{Nb}_{1/2}\text{O}_3$  (PSN-PMN) where  $\epsilon = 30,000$ , the piezoelectric module in an electrical field ( $E_{bias} = 10^6$  V/m; see [Fig. 2.13B](#)) is close in magnitude to the piezoelectric materials commonly used in the technique (in PZT ceramics  $d_{31} \cong 500$  pC/N). In this case, the induced piezoelectric effect in crystals of ferroelectric relaxors is even greater.

The comparison of induced polarization in the relaxor ferroelectric PMN with similar polarization of paraelectric material  $\text{Ba}(\text{Ti}_{0.6}\text{Sr}_{0.4})\text{O}_3 = \text{BST}$  (which also has a rather large  $\epsilon \sim 10,000$ ) is shown in [Fig. 2.14](#) (data are obtained by pyroelectric coefficient measurement). The electrically induced polarization  $P_{imd}$  in PMN far exceeds this polarization in BST: the reason is that relaxor ferroelectrics have much greater permittivity ( $\sim 20,000\text{--}40,000$ ). Moreover, in the relaxor ferroelectric polarization  $P_{imd}$  depends on temperature as in the conventional ferroelectrics ([Fig. 2.14B](#)). For technical purposes, it is important that in a field of electrical bias, the relaxor demonstrates not only the piezoelectric effect but also the electrically induced *pyroelectric* effect, the value of which may exceed the pyroelectric coefficient of conventional pyroelectrics. At the same time, compared with the induced pyroelectric effect used in the BST type of paraelectrics, the induced pyroelectric effect in PMN is more thermostable due to the smaller oblique dependence  $P_{imd}(T)$  ([Fig. 2.15](#)).

It was shown that the theoretical calculation for the electrically induced piezoelectric effect gives a value for artificial piezoelectric module of  $d = 2Q\epsilon_0^2 \epsilon^2 E$ . It is obvious that electrically induced piezoelectricity is substantial only in dielectrics with a very high permittivity. However, in the paraelectric materials induced piezoelectricity appears and disappears practically *without inertia*, but in the relaxor ferroelectrics response time is about several microseconds. Nevertheless, in some of the PMN-PSN

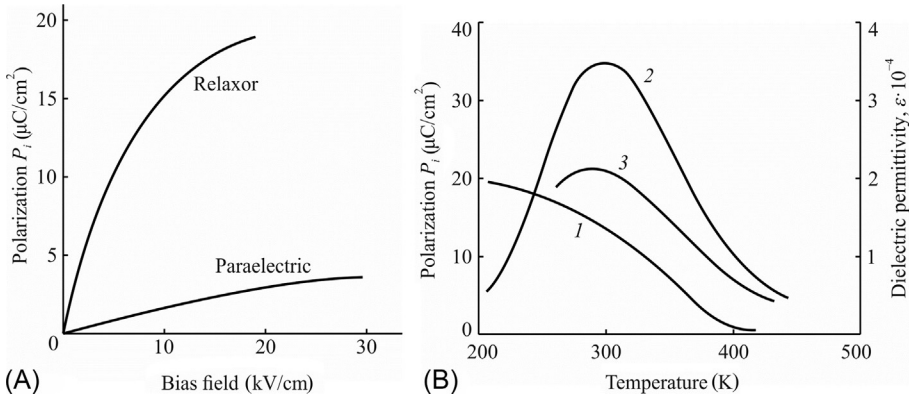
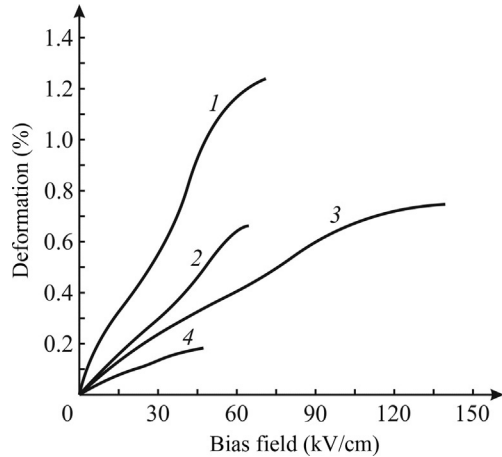


**Fig. 2.14** Relaxor ferroelectric characteristics: (A) Comparison of electrically induced polarization  $P_i$  in PMN with paraelectric BST; (B) PMN properties: 1—induced by 10 kV/cm polarization  $P_i$ ; 2—permittivity at  $E_{bias} = 0$ ; 3—permittivity at  $E_{bias} = 10$  kV/cm.

**Fig. 2.15** Electromechanical effect in relaxors: 1—crystal PZN-4.5%PT; 2—crystal PZN; 3—crystal PMN-24%PT; 4—piezoceramics PZT-8.



relaxor ferroelectrics with  $\epsilon \geq 40,000$  piezoelectric modulus reaches  $d = 2000$  pC/N (more than in the best piezoelectric ceramics of PZT type). For example, high strain in the electrical field is found in the crystals  $\text{PbZn}_{1/3}\text{Nb}_{2/3}\text{O}_3\text{-}4.5\%\text{PbTiO}_3$  (PZN-4.5% PT). Its electrically tunable deformation is 10 times greater than deformation in the widely used piezoelectric ceramics PZT-8 and, unlike piezoelectrics, allows large controllability *without hysteresis*.

Thus, both paraelectrics and relaxor ferroelectrics under a bias electrical field produce an *induced piezoelectric effect*, which immediately disappears after switching off this field. The speed of such control of the piezoelectric effect depends on the inertia of polarization, and its magnitude is limited by the dispersion of permittivity, which

appears at frequencies around hundreds of kilohertz. From the point of view of physics, the electrically induced piezoelectric effect is interesting because it allows an explanation for the microscopic nature of electromechanical coupling in solids (physical models and the thermodynamic theory of this will be discussed further in Chapter 4). From the point of view of technical applications, this effect is important for electromechanical drives and electrically tunable piezoelectric resonators and filters, allowing control of the resonant frequency and bandwidth.

## 2.4 Thermomechanically induced pyroelectricity

Pyroelectricity was briefly discussed in Chapter 1 and will be studied in detail in Chapter 4. In this section, it is important to note the fact that the pyroelectric effect corresponds to the *quasione-dimensional model* of polar-sensitive bond orientation. This means that such an effect is possible in 10 classes of *pyroelectric symmetry* crystals, and one would assume that pyroelectric effect (and volumetric piezoelectric effect as well) is impossible for two-dimensional and three-dimensional models of polar bond arrangements. The main thing shown in this section is that by creating *special boundary conditions* for polar-neutral crystals, the “artificial pyroelectric effect” can be obtained in noncentrosymmetric crystals in all 10 polar-neutral classes of crystals.

(1) First, the **two-dimensional** structural arrangement of the polar-sensitive bonds will be considered (the correspondent simplest model was shown in Figs. 1.11B and 1.13). In the actual (“exclusive”) piezoelectric, the primary pyroelectric effect is always absent ( $\gamma_i^{(1)} = 0$ ) and in mechanically clamped conditions the secondary pyroelectric effect also looks to be impossible ( $\gamma_i^{(2)} = e_{im}\alpha_m = 0$ ). However, in the **partial clamping conditions** any piezoelectric is liable to show a “secondary type” pyroelectric effect, because the sum  $e_{im}\alpha_m \neq 0$ . This is the “artificial pyroelectric effect” [13].

From 10 classes of “exclusive” piezoelectrics, quartz is the simplest example for an explanation of the nature of internal polarity. Trigonal  $\alpha$ -quartz, which belongs to the 32 class of symmetry, is electrically active only in the [100]-type directions that correspond to a (100)-plate of quartz, which is known as a Curie cut. This cut may be prepared perpendicularly to any one of three twofold polar axes:  $I$ ,  $I'$ , or  $I''$  (the distribution of polar activity in quartz crystal was presented in Fig. 1.13A).

Further, it will be shown how it is possible to measure the components of polar sensitivity in the polar-neutral crystal.

In the standard crystallographic setup of quartz crystal, the matrix of piezoelectric coefficients  $e_{im}$  consists of one longitudinal ( $e_{11}$ ), one transverse ( $e_{12}$ ) and three shear components of piezoelectric strain modulus ( $e_{14}$ ,  $e_{25}$ , and  $e_{26}$ ):

$$e_{im} = \begin{bmatrix} e_{11} & e_{12} & 0 & e_{14} & 0 & 0 \\ 0 & 0 & 0 & 0 & e_{25} & e_{26} \\ 0 & 0 & 0 & 0 & 0 & 0 \end{bmatrix}.$$

The transverse component  $e_{12}$  equals the longitudinal one but has the opposite sign:  $e_{12} = -e_{11}$ . Besides, only one of the shear piezoelectric modules ( $e_{14}$ ) is independent;

the other shear components are  $e_{25} = -e_{14}$  and  $e_{26} = 2e_{11}$ . So the only two components of the given matrix are independent.

Before proceeding further, it is necessary to show that *no* homogeneous influence (uniform change of temperature or hydrostatic pressing) can induce an electrical response in a specimen of quartz even being taken from the Curie cut.

First of all, any shear strain cannot be excited in a sample if the external influence is of the scalar type. So only the longitudinal and the transverse electrical response should be taken into account. In the nonclamped quartz sample (i.e., in free-stress state) the longitudinal piezoelectric effect ( $e_{11}x_1$ ) and the transverse effect ( $-e_{12}x_1$ ) *compensate* each other. This is illustrated in Fig. 2.16C, which characterizes uniform thermal influence on a quartz sample: one part of the piezoelectric response ( $e_{11}x_1$ ) induced by thermal deformation  $x_1$  is equals to the other part ( $e_{12}x_1$ ) but with opposite sign.

Since a rather complex phenomenon is discussed here, it makes sense to give the additional proof that any electrical response in an actual piezoelectric really is compensated in the case of scalar influence, as shown in Fig. 2.16C. First of all, note that from the matrix for piezoelectric strain modulus  $e_{im}$  it follows that polarization component  $P_3 = 0$  (in  $Z = 3$  direction, quartz shows no piezoelectric effect) and component  $P_2 = 0$ , because shear strains  $e_{23}$  and  $e_{26}$  cannot be excited by the uniform action. It remains to analyze the polarization component  $P_1$ .

Induced mechanically (by direct piezoelectric effect), this component of electrical polarization can be given by

$$P_1 = e_{1m}x_m = e_{11}x_1 + e_{12}x_2 + e_{13}x_3 + e_{14}x_4 + e_{15}x_5 + e_{16}x_6 = e_{11}x_1 + e_{12}x_2.$$

This sum depends on the mechanical boundary conditions in which the crystal is located:

- (i) In the case when the crystal is totally clamped, any mechanically induced polarization is impossible:  $P_1 = 0$  due to  $x_m = 0$ .
- (ii) It is essential to show that in the case of a free-stress condition (when a quartz crystal can be deformed) any polar response is also absent ( $P_1 = 0$ ).

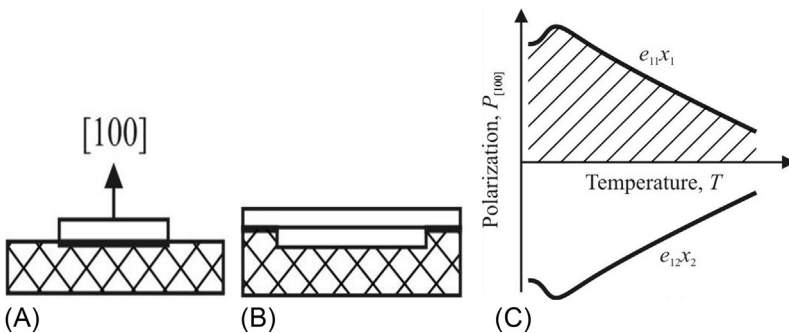


**Fig. 2.16** Partially clamped quartz samples: (A) Tangential strain in thin plate is forbidden by plate soldering to substrate; (B) membrane variant of partial clamping; (C) thermally induced polar response conditioned by piezoelectric effect.

First of all, many components of the piezoelectric strain module of quartz crystal are zero: it is seen from the previous matrix that  $e_{13} = e_{15} = e_{16} = 0$ . Second, in the previous equation the shear strain  $x_4 = 0$  because any shear strain should be absent in the case when external action is uniform.

Third, in free-stress quartz crystal the strains  $x_1$  and  $x_2$  in the (100)-plane are equal:  $x_1 = x_2$ . In fact, in the case of uniform thermal action ( $x_m = \alpha_m dT$ ) these strains are equal due to the parity of the correspondent components of the quartz thermal expansion coefficients:  $\alpha_1 = \alpha_2$  (however,  $\alpha_1 \neq \alpha_3$ ).

Fourth, in the event of uniform stretching (or compression), again the strains  $x_1 = x_2$  due to the equality of the correspondent quartz elastic stiffness components:  $c_{11} = c_{22}$ . Strains could be calculated from the equation  $x_m = c_{mn} X_n$ , where  $X_n$  is the uniform (hydrodynamic) stress. Thus, excitation in the actual piezoelectric of the homogeneous deformation (by thermal or elastic means) does not lead to its polar response, since the piezoelectric contributions from strains  $e_{11}x_1$  and  $e_{12}x_2$  to the polarization  $P_1$  compensate each other (Fig. 2.16C).

(iii) However, in the *partially clamped* quartz crystal the thermally induced polarization will not be zero ( $P_1 \neq 0$ ), and just this circumstance is used here to examine internal compensated (latent) polarity that, in principle, makes possible the use of partially clamped quartz (and other polar-neutral piezoelectrics) in thermal or pressure sensors.

The fundamental idea is that artificial limitation (by mechanical boundary conditions) of any one of the strains ( $x_1$  or  $x_2$ ) should transform the plate of piezoelectric quartz into an artificially created “pyroelectric” crystal [14].

Suppose that one of two types of deformations cannot be realized in the piezoelectric plate. For example, it is possible to suppress the tangential strains ( $x_2 = 0$  and  $x_3 = 0$ ), if the piezoelectric plate is firmly fixed on the massive incompressible substrate with zero coefficient of thermal expansion (in the given case the substrate is fused silica in which  $\alpha \approx 0$  (Fig. 2.16A)). In this case the uniform heating or cooling (as well as hydrostatic compression) will lead to the polar response appearance:  $P_{[100]} = e_{11}x_1$ . Similarly, the prohibition on the normal strain ( $x_1 = 0$ ) with a possibility of tangential strain would cause the response of opposite polarity:  $P_{[100]} = e_{12}x_2$ , but experimental realization of the second case is more difficult.

In practice, it is easier to limit the plane strain  $x_2$ , if the piezoelectric plate is soldered onto fused silica. The only deformation that can be realized in this case is the thickness strain  $x_1$  directed along the polar-neutral axis “1,” which in this manner is turned into the single polar axis. Therefore, substantial reduction of one type of deformation transforms the piezoelectric crystal into an artificial pyroelectric. This effect can also be defined as the polarization of a partially clamped actual piezoelectric by the uniform change of its temperature. Partial clamping is provided by the nonuniform mechanical boundary condition, limiting some of the thermal strains of a crystal, which becomes uniformly but anisotropically stressed.

An artificial thermo-piezoelectric effect can be characterized by the coefficient  $\gamma^*$ , which is equivalent to the pyroelectric coefficient, which depends on electrical, elastic, and thermal properties of the noncentral crystal, as well as on the means of its deformation limitation:

$$\gamma^* = d_{im} \lambda^*_{m}, \quad (2.4)$$

where  $d_{im}$  is piezoelectric modulus and  $\lambda^*_m$  is effective thermoelastic coefficient of partially clamped crystal.

The spatial distribution of the sensitivity of the artificial pyroelectric effect in the crystals of quartz type symmetry (such as berlinite ( $\text{AlPO}_4$ ), cinnabar ( $\text{HgS}$ ), tellurium ( $\text{Te}$ ), etc.) can be found in a similar manner to quartz crystal. It is possible to find “pyroelectric coefficients” in these crystals, even in any slanting plates. The spatial distribution of  $\gamma^*(\theta, \varphi)$  that characterizes the artificial pyroelectric coefficient in the quartz-type crystals can be presented in polar coordinates:  $\gamma^*(\theta, \varphi) = \gamma^*_{max} \sin^3\theta \cdot \cos 3\varphi$ , where  $\theta$  is azimuth angle and  $\varphi$  is plane angle. This spatial pattern is equivalent to the longitudinal piezoelectric modulus distribution that was shown in Fig. 1.13A. Through the radius vector directed from the center of this figure it is possible to determine the size of the artificial effect in any cut of quartz-type crystals. It is obvious that maximums of the effect occur along any of three  $X$ -axes.

In order to get the effective pyroelectric coefficient  $\gamma^* = dP_i/dT$ , the thermodynamic equations for the noncentrosymmetric (but not pyroelectric) crystal should be used. With the assumption that the crystal is short-circuited ( $E = 0$ ), the exact solution is given as:

$$\begin{aligned} dx_n &= s_{nm}dX_m + \alpha_m dT; \\ dP_i &= d_{im}dX_m, \end{aligned} \quad (2.5)$$

where  $s_{nm}$  is components of the elastic compliance tensor. Solving Eq. (2.5) for the trigonal crystal class (which includes quartz crystal) leads to the following expression:

$$\gamma^*_{100} = d_{11}(\alpha_1 s_{33} - \alpha_3 s_{13}) \left[ s_{11} \cdot s_{33} - (s_{13})^2 \right]^{-1}. \quad (2.6)$$

For quartz crystal, one can obtain  $\gamma^*_{100} = 2.6 \mu\text{C m}^{-2} \text{K}^{-1}$ ; in other crystals of the 32 symmetry class this parameter is bigger:  $\gamma^*_{100} = 2.7 \mu\text{C m}^{-2} \text{K}^{-1}$  in berlinite;  $8.7 \mu\text{C m}^{-2} \text{K}^{-1}$  in cinnabar; and  $10 \mu\text{C m}^{-2} \text{K}^{-1}$  for tellurium crystal. This parameter is not very small, because the first known pyroelectric tourmaline has a pyroelectric coefficient  $\gamma = 4 \mu\text{C m}^{-2} \text{K}^{-1}$ , while in wurtzite crystal ( $\text{ZnS}$ ) the usual pyroelectric response is characterized by  $\gamma = 0.3 \mu\text{C m}^{-2} \text{K}^{-1}$ .

In quartz, as in other piezoelectrics the thermomechanically induced pyroelectric effect was studied by a quasistatic method, in which the pyroelectric coefficient is determined by the time during which the pyroelectric current charges the measuring capacitor [12]. Electronic equipment includes the Peltier element used for heating and cooling. Samples having a plate shape about  $100 \mu\text{m}$  thick and an area of  $\sim 1 \text{ cm}^2$  with copper electrodes and soldered onto silica glass substrates were investigated.

The temperature dependence of the artificial pyroelectric response of quartz crystal partially clamped in the (100)-cut is shown in Fig. 2.17 along with the rest of the key parameters. Investigation shows that the artificial pyroelectric coefficient  $\gamma^*_{100}$  changes with temperature very slowly, while the alteration of some other components of tensors might be very complicated. In a wide temperature range, the artificial “pyroelectric” coefficient  $\gamma^*_1$  is almost constant, but it has a tendency to decrease at low temperatures, perhaps due to reduction of the thermal expansion coefficient.

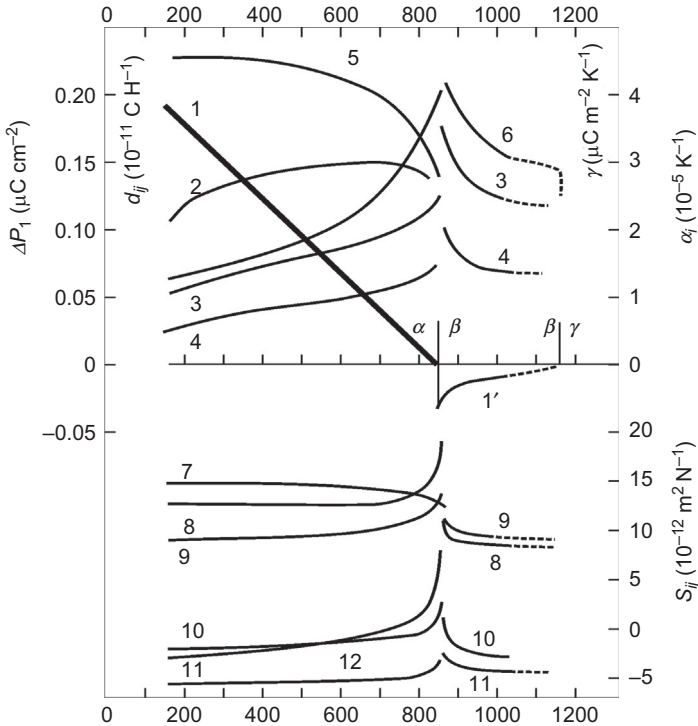


**Fig. 2.17** Latent (hidden) intrinsic polarity temperature dependence for quartz (curve 1) in comparison with dependences of other thermal and elastic parameters of this crystal: 1— $\Delta P_1$  found in [100]-cut thin plate of quartz in  $\alpha$ -phase; 1'— $\Delta P_1$  found in [110] oriented rod in high-temperature  $\beta$ -phase of quartz; 2—artificial pyroelectric coefficient  $\gamma_1^*$  of partially clamped [100]-cut of quartz in  $\alpha$ -phase; 3, 4—thermal expansion coefficients  $\alpha_1$  (3) and  $\alpha_3$  (4) of quartz crystal; 5, 6—piezoelectric modulus  $d_{11}$  (5) and  $d_{14}$  (6) of quartz  $\alpha$ -phase; 7–12—elastic compliance components:  $0.5 \cdot s_{66}$  (7),  $s_{11}$  (8),  $s_{33}$  (9),  $s_{12}$  (10),  $s_{13}$  (11),  $s_{44}$  (12).

In the vicinity of the quartz  $\alpha \rightarrow \beta$  phase transition at temperature  $\theta_1 \approx 850$  K the  $\gamma_1^*$  breaks off. It is remarkable that for thermally induced polarity  $P_{[100]} = \Delta P_1 = \int \gamma_1^* dT$  the simplest linear temperature dependence is observed:  $\Delta P_1 \sim (\theta - T)$  with a critical index  $n = 1$ .

It should be noted that piezoelectrics of quartz symmetry ( $\text{SiO}_2$  and  $\text{AlPO}_4$ ), in addition to  $\alpha \rightarrow \beta$  phase transition, have the second-highest temperature transformation between their  $\beta$  and  $\gamma$  phases. Temperature dependence of the artificial pyroelectric response (Fig. 4.5, curve 1') characterizes quartz in its  $\beta$ -phase with temperature dependence of 3D moment  $M_{ijk}$ . This is described by another equation:  $P_{13} \sim (\theta_2 - T)^2$  with  $\theta_2 = 1140$  K. As seen from Fig. 4.5 (curve 1'), this electrical moment vanishes at the  $\beta \rightarrow \gamma$  phase transition. In the quartz crystal the high-temperature  $\gamma$ -phase is nonpolar. Again, it is necessary to note that the study of volumetric piezoelectric

effect needs a noncompressible substrate, so only theoretical estimation of this effect can be provided [15].

(2) The second factor considered here is the **three-dimensional** structural arrangement of polar-sensitive bonds in the polar-neutral piezoelectric. As in the first example, the well-studied ferroelectric  $\text{KH}_2\text{PO}_4$  (KDP) is described, but in its *paraelectric phase* (above the Curie point). At room temperature and above it, KDP is only a piezoelectric, which belongs to the polar-neutral 422 class of symmetry. In addition to several crystals of KDP type, the antiferroelectrics of ADP ( $\text{NH}_3\text{PO}_4$ ) type have analogous piezoelectric properties. Their polar sensitivity corresponds to the 3D arrangement.

In the standard installation, the piezoelectric module matrix of these crystals shows no longitudinal and no transverse effects:

$$d_{mi} = \begin{pmatrix} 0 & 0 & 0 & d_{14} & 0 & 0 \\ 0 & 0 & 0 & 0 & d_{25} & 0 \\ 0 & 0 & 0 & 0 & 0 & 0 \end{pmatrix}; \quad d_{25} = d_{14}.$$

To find the artificial pyroelectric effect, one needs to *change* the standard setup of a crystal, for example, by turning axes 1 and 2 around the axis 3 at an angle of  $\pi/4$ . In these crystals one needs to select a piezoelectric element not in the form of a thin plate, but as a long rectangular rod, extending along one of the new axes of  $1'$  or  $2'$ , while the electrodes should be deposited on the surface of the piezoelectric element perpendicular to axis  $3' = 4$ .

By limiting the longitudinal deformation of the KDP sample, made in the form of a rectangular rod, it is possible to obtain the artificial pyroelectric effect with coefficient

$$\gamma^*_3 = 2d_{36}\alpha_1(2s_{11} + 2s_{12} + s_{66})^{-1}. \quad (2.7)$$

Fig. 2.18 shows the main properties of KDP crystal *above* its ferroelectric phase transition, where this crystal is only a piezoelectric. Investigations show that in this paraelectric phase, the KDP crystal can be transformed into the artificial pyroelectric with coefficient  $\gamma^*_3 = 6 \mu\text{C m}^{-2} \text{K}^{-1}$ , while in ADP crystal  $\gamma^*_3 = 17 \mu\text{C m}^{-2} \text{K}^{-1}$ . Moreover, it is found that crystals of KDP type in their paraelectric phase also have (like quartz) a high-temperature phase transition, at which this polar-neutral crystal changes its symmetry from the 422 class into the nonpolar class of symmetry. This is confirmed by the measurements of the KDP dielectric constant  $\epsilon_1$ , which at a temperature increase jumps down to a temperature of  $\theta \approx 480 \text{ K}$ , while internal polarity vanishes very gradually by low  $P \sim (\theta - T)^2$  with the same  $\theta$ . To verify the quadraticity of this dependence, the curve 1 in Fig. 2.18 is shown in scale  $P^{1/2}(T)$ , which actually turns out to be linear [15].

Spatial (3D) polar-sensitive bond concepts can be applied for many other polar-neutral piezoelectrics. For instance, in the crystals of the 23 cubic class of symmetry, the polar-neutral directions correspond to four axes of order 3, and it can be shown that an artificial “pyroelectric coefficient” is given by the equation:

$$\gamma^*_{[111]} = 2\sqrt{3}d_{14}\alpha(4s_{11} + 8s_{12} + s_{44})^{-1}. \quad (2.8)$$

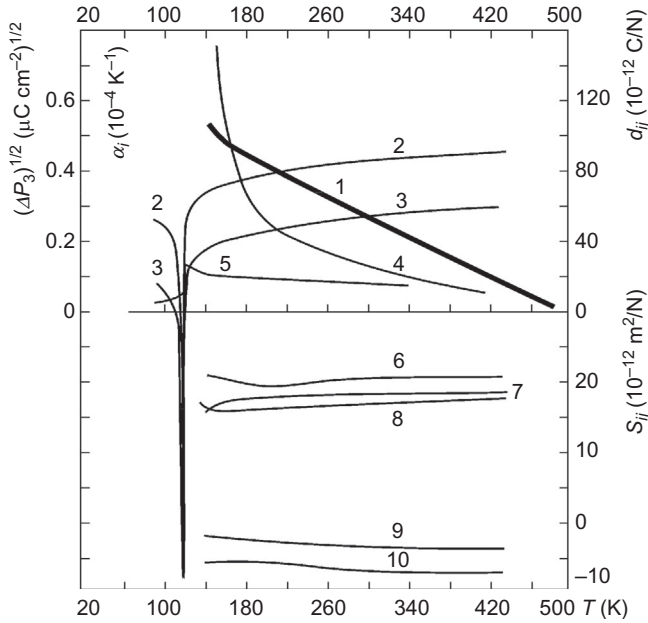


**Fig. 2.18** Latent intrinsic polarity temperature dependence of KDP crystal in comparison with other thermal and elastic parameters of this crystal: 1— $\Delta P_3$  obtained by study of KDP rod oriented in [110] direction; 2, 3—thermal expansion coefficients  $\alpha_3$  (2) and  $\alpha_1$  (3) of KDP crystal; 4, 5—piezoelectric modulus  $d_{36}$  (4) and  $d_{14}$  (5) of KDP crystal; 6–12—elastic compliance:  $0.5 \cdot s_{66}$  (7),  $s_{11}$  (8),  $s_{33}$  (9),  $s_{12}$  (10),  $s_{13}$  (11),  $s_{44}$  (12).

It is interesting to note that parameter  $\gamma^*_{111}$  is rather large in the sillenite type of crystals. Some of them, such as  $\text{Bi}_{12}\text{GeO}_{20}$  and  $\text{Bi}_{12}\text{SiO}_{20}$ , are widely used in electronics. The artificial pyroelectric coefficient in  $\text{Bi}_{12}\text{GeO}_{20}$  is estimated as  $\gamma^* \approx 25 \mu\text{C}/\text{m}^2\text{K}$ ; however, among these classes of piezoelectric crystals, it is possible to find crystals with an artificial “pyroelectric” coefficient up to  $100 \mu\text{C}/\text{m}^2\text{K}$ .

Among possible practical applications of artificial pyroelectricity, the most promising are the semiinsulated (*s/i*) semiconductors of the GaAs group ( $\text{A}^{\text{III}}\text{B}^{\text{V}}$ ). The point is that they might be used as pyroelectric converters in the upper layer of a sandwich composition, which can be integrated with amplifiers (in the bottom layer) using a semiconductor with high-mobility electrons.

These crystals have a sphalerite structure that belongs to the polar-neutral  $\bar{4}3m$  group of symmetry. In the specially oriented plates and by using a restriction of some thermal deformations, the  $\text{A}^{\text{III}}\text{B}^{\text{V}}$  crystal is capable of producing a pyroelectric signal. Moreover, the voltage sensitivity of *s/i*-GaAs, for instance, is close to pyroelectric ceramics: a GaAs plate with a thickness of  $100 \mu\text{m}$  at a temperature change of several degrees shows electrical potential 2 V. This can be of interest for implementation in the multielement planar integral thermal far-infrared detectors. It is assumed that, in a special orientation, semiinsulating layers or microregions embedded in a gallium

arsenide integrated circuit together with amplifiers and switching devices may form a mosaic microstructure of nonselective and highly sensitive infrared detectors.

Polar-sensitive bonds in piezoelectric-active  $A^{III}B^V$  type semiconductors of sphalerite structure are directed along each of threefold axes of cubic crystal. However, polar sensitivity in a crystal is completely compensated; therefore, no scalar influence of it, including uniform temperature change, can produce an electrical response. Nevertheless, this compensation of electrical polarity can be broken in the specially oriented plates (layers), in which thermal deformations are limited. As a result, along one of three-fold polar axes an electrical response appears, and that is the artificial pyroelectric effect.

High-symmetry cubic crystals of class  $\bar{4}3m$  are characterized by the isotropy of thermal expansion coefficient:  $\alpha_m = \alpha$  (in GaAs  $\alpha = 2.8 \cdot 10^{-6} \text{ K}^{-1}$  at 300 K). In these crystals the elastic compliance  $s_{mn}^{E,T}$  tensor is reduced to three independent components (in GaAs  $s_{11}^{E,T} = 12 \cdot 10^{-11}$ ,  $s_{12}^{E,T} = -4.6 \cdot 10^{-11}$ , and  $s_{33}^{E,T} = 17 \cdot 10^{-11} \text{ m}^2/\text{N}$ ). In the main installation of  $A^{III}B^V$  crystal, piezoelectric properties are described by a matrix:

$$d_{im} = \begin{bmatrix} 0 & 0 & 0 & d_{14} & 0 & 0 \\ 0 & 0 & 0 & 0 & d_{25} & 0 \\ 0 & 0 & 0 & 0 & 0 & d_{36} \end{bmatrix}, \quad (2.9)$$

This matrix represents the third-rank tensor of piezoelectric coefficients. In this installation for (100), (010), and (001) crystal plates, all longitudinal ( $d_{11}$ ,  $d_{22}$ ,  $d_{33}$ ) as well as all transverse ( $d_{12}$ ,  $d_{13}$ ,  $d_{21}$ ,  $d_{23}$ ,  $d_{31}$ ,  $d_{32}$ ) modules are zero. Therefore, as usually used in electronics and in most experiments, [100]-oriented plates of  $A^{III}B^V$  semiconductors are *nonsensitive* to any homogeneous mechanical influence, except the shear action (which corresponds to shear modules  $d_{14} = d_{25} = d_{36}$ ). It is obvious from the matrix (2.9) that no response is possible if the external influence on the crystal has a scalar character. In other words, any partial clamping being applied to standard (100)-plates of  $A^{III}B^V$  crystals cannot invoke a polar response. Meanwhile, crystal plates of (100) orientation are conceptually the sole chips used in GaAs type devices. We believe that this is the main reason for mentioned polar effects previously were out of consideration.

Due to the cubic symmetry in standard installations of crystals, the piezoelectric module components are equal:  $d_{14} = d_{25} = d_{36}$  and therefore they might be denoted simply as  $d$ . In gallium arsenide  $d = 2.7 \cdot 10^{-12} \text{ C/N}$ , i.e., it surpasses even the quartz piezoelectric module ( $d_{\text{SiO}_2} = 2.4 \cdot 10^{-12} \text{ C/N}$ ). From Eq. (2.6) one cannot see any opportunity for an artificial pyroelectric effect in GaAs, since the matrix contains only shear piezoelectric components that cannot be excited by homogeneous heat exposure. As shown before, the artificial pyroelectric effect generally occurs due to the decompensation of the contributions from longitudinal and transverse piezoelectric effects, described by the left half of matrix. But in this case (in a *standard installation* of  $A^{III}B^V$  crystals) all components of longitudinal and transverse piezoelectric module are zero.

But in another orientation of crystallographic axes to which the standard matrix (2.9) can be converted, both longitudinal and transverse components of piezoelectric

module appear. These components are maximal in the slice of a crystal, oriented perpendicularly to the axis of the third order (which is the spatial diagonal of a cube), since the greatest polar sensitivity in an  $A^{III}B^V$  crystal coincides with these directions. This polarity is due to mixed ionic-covalent bonding between A and B ions, and anisotropy of electronic density distribution is such that this density is increased in the vicinity of the B-ion. When describing the effect of partial limitation of deformations on piezoelectric properties of a polar crystal, it is more convenient to use not the piezoelectric modulus  $d$  (describing the relationship between mechanical stress  $X$  and the polarization  $P_i = d_{in}X_n$  induced by it) but the piezoelectric constant  $e$ , which relates deformation  $x$  to polarity:  $P_i = e_{in}x_n$ , where  $e_m = d_{in}c_{mn}$  and  $c_{mn}$  is elastic stiffness. The matrix of piezoelectric constants for the main crystal setting corresponds to the piezoelectric modulus (2.9):

$$e_{im} = \begin{pmatrix} 0 & 0 & 0 & e_{14} & 0 & 0 \\ 0 & 0 & 0 & 0 & e_{15} & 0 \\ 0 & 0 & 0 & 0 & 0 & e_{36} \end{pmatrix}$$

This matrix represents the third-rank tensor of piezoelectric coefficients. In this instance, for (100) = (010) = (001) crystal plates as longitudinal ( $e_{11}$ ,  $e_{22}$ ,  $e_{33}$ ) so transverse ( $e_{12}$ ,  $e_{13}$ ,  $e_{21}$ ,  $e_{23}$ ,  $e_{31}$ ,  $e_{23}$ ) modules are zero. That is why the (100) type of GaAs plate is not sensitive to any mechanical strains except the twist ones. The last corresponds to the shear modules  $e_{14} = e_{25} = e_{36}$  but they could not provide any response under *homogeneous* influences. Partial clamping is also useless if it is applied to the standard (100) plates of III–V crystals.

Fig. 2.19A and B shows such an orientation of the  $A^{III}B^V$  crystal, which should be prepared to invoke its polar response. The polar cut of the  $A^{III}B^V$  crystal should be oriented in such a way that the [111]-axis is perpendicular to the studied plane. In the case of a volumetric piezoelectric effect investigation, this (111)-plate has to be fixed onto the “ideally hard” substrate (in trial experiments hard steel might be used,

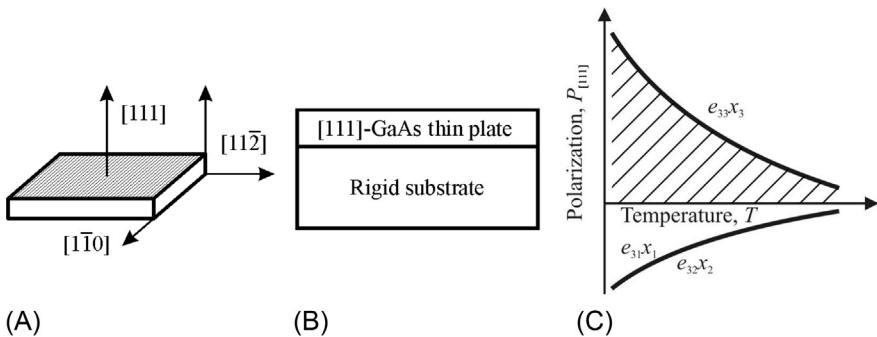


**Fig. 2.19** Partial (in plane) clamping realization: (A) Orientation of  $s/i$ -GaAs [111]-cut; (B) plate soldered to rigid substrate; (C) internal polarity change decompensated by partial clamping.

but in microelectronic piezoelectric sensors it is expedient to use a membrane, clamped along its boundaries). In similar fashion, the *s/i*-GaAs (or GaN) crystalline (111)-plate could be activated for “pyroelectric” response, if a rigid substrate, shown in Fig. 2.19B, had a very small thermal expansion coefficient ( $\alpha \sim 0$ ). In our first experiments the fused silica was used as a substrate, but in microelectronic practical devices the pyro-active *s/i* (dielectric) layer of Ga(AsP) or a (GaAl)As layer can be directly deposited on the substrate, made of GaAs crystal, followed by the etching and forming membrane clamped along the boundaries.

Such partial clamping makes plane strains ( $x_1 = x_2 = 0$ ) impossible, so electrical response from uniform pressure (or thermal deformation) can be realized only perpendicularly to the plane:  $M_3 = e_{33}x_4$ . It is obvious that a composite structure created artificially (Fig. 2.19A) can be used for volumetric piezoelectric effect investigation (or to study the artificial pyroelectric response).

In any form of free-stress sample the longitudinal piezoelectric effect ( $e_{33}$ ) and *two* transverse effects ( $e_{31}$  and  $e_{32}$ ) compensate each other:  $e_{31} + e_{32} = -e_{33}$ . It is illustrated in Fig. 2.19C, which describes thermal investigation of a GaAs (111)-plate: one part of piezoelectric polarization ( $e_{33}x_3$ , induced by thermal deformation  $x_3$ ) equals to other parts ( $e_{31}x_1 + e_{32}x_2$ ) but with opposite sign (in this case, index “3” corresponds to the [111]-axis). Strain components in free-stress cubic crystal are equal:  $x_1 = x_2 = x_3$ , because excitation is homogeneous. That is why, in nonpyroelectric crystal, the sum of piezoelectric coefficients of transverse and longitudinal piezoelectric coefficients is zero:

$$e_{31} + e_{32} + e_{33} = 0 \quad (e_{31} = e_{32} = -1/2e_{33}).$$

As a result, the piezoelectric effect, produced by longitudinal strain component  $x_3 = \alpha dT$  is compensated by the effect of two transverse strain components  $x_1 = x_2 = \alpha dT$ ; therefore no electrical response is possible. Consequently, a free-stress polar (111)-plate of GaAs-type crystals is not sensible to the homogeneous excitations.

However, the artificial limitation of any one of the mentioned strain components ( $x_3$  or  $x_1 + x_2$ ) can transform a piezoelectric (111)-plate of GaAs-type crystal into an artificially created “pyroelectric.” In practice, it is easier to limit the plane strain ( $x_1 + x_2$ ) by a simple mechanical design. In this case, only the thickness strain  $x_3$  can be excited, and just in the direction of polar axis “3” ([111]-direction), which is transformed into a “peculiar” polar axis. This effect is impossible in the free-stress as well as in the free-strain crystals: both artificial effects are the result of nonisotropic partial clamping. Only partially clamped piezoelectric crystal manifests artificial pyroelectricity or a volumetric piezoelectric effect.

Shown in Fig. 2.19, partial clamping violates polar neutrality ( $e_{31}x_1 + e_{32}x_2 = 0$ ) and makes it possible to manifest an artificial pyroelectric effect as  $M_i = e_{33}x_4$ . The greatest effect in crystals of the  $\bar{4}3m$  class of symmetry can be achieved in such a special installation, in which one of the new axis  $3'$  coincides with the polar-neutral axes of [111]. With this new installation, the axis  $l'$  should be directed normally to the

axis passing through the  $3'$  plane of symmetry of a cube, while the orientation of new axis  $2'$  is predetermined by the Descartes coordinate system.

For further calculations, it is expedient to return to the matrix of piezoelectric module. After application of the preceding procedure, the matrix of piezoelectric module for  $\bar{4}3m$  crystal in the new installation is:

$$d_{i'm'} = \begin{bmatrix} 0 & 0 & 0 & 0 & -\frac{d}{\sqrt{3}} & \frac{2d}{\sqrt{6}} \\ \frac{d}{\sqrt{6}} & -\frac{d}{\sqrt{6}} & 0 & -\frac{d}{\sqrt{3}} & 0 & 0 \\ -\frac{d}{2\sqrt{3}} & -\frac{d}{2\sqrt{3}} & \frac{d}{\sqrt{3}} & 0 & 0 & 0 \end{bmatrix}. \quad (2.10)$$

All components of this new matrix are expressed in the terms of shear module  $d$ , taken from the basic installation of the crystal. The third row of the matrix (2.10) characterizes the piezoelectric properties of such a crystal plate, which is cut perpendicularly to axis  $3' = [111]$  and characterized by the longitudinal piezoelectric module  $d_{3'3'} = d/\sqrt{3}$  and by the transverse effect  $d_{3'1'} = d_{3'2'} = -d/2\sqrt{4}$ . The piezoelectric shear components in the third row of this matrix are absent.

Thus, in ideal conditions, the determination of artificial pyroelectric coefficient  $\gamma_{APE} = dM_i/dT$  is possible, when thermoelectrical response from tangential strain is completely suppressed by the rigid substrate:  $dx_1 = dx_2 = 0$ . At uniform change of temperature, the only allowed strain is the  $dx_3$  (hereinafter for simplicity there are no indexes). Since thermal deformation is allowed only in the direction “3,” the corresponding component of mechanical stress tensor  $X_3$  is zero. Another boundary condition is the  $E_3 = 0$ , i.e., the crystal is assumed electrically free (close-circuited), as usually supposed in thermodynamic analysis of piezoelectric and pyroelectric effects. The corresponding equations are presented here:

$$\begin{aligned} dx_n &= s_{mn}^{E,T} dX_m + \alpha_n^E dT, \\ dM_i &= d_{in}^T dX_n. \end{aligned} \quad (2.11)$$

Here  $x_n$  and  $X_m$  are the strain and stress tensor components, parameter  $s_{mn}^{E,T}$  is the elastic compliance,  $d_{in}^T$  is the piezoelectric module and  $\alpha_n^E$  is the thermal expansion; indices  $E$  and  $T$  indicate that the parameters assume constancy of electrical field and temperature. For crystals of the  $\bar{4}3m$  group at chosen boundary conditions, Eq. (2.11) can be specified:

$$\begin{aligned} dx_1 &= s_{11}^{E,T} dX_1 + s_{12}^{E,T} dX_2 + \alpha dT = 0, \\ dx_2 &= s_{12}^{E,T} dX_1 + s_{22}^{E,T} dX_2 + \alpha dT = 0, \\ dx_3 &= s_{31}^{E,T} dX_1 + s_{32}^{E,T} dX_2 + \alpha dT, \\ dM_3 &= d_{31}^T dX_1 + d_{32}^T dX_2. \end{aligned} \quad (2.12)$$

It is necessary to take into account that in the cubic crystals  $s_{11}^{E,T} = s_{22}^{E,T}$  and  $X_1 = X_2$ , for artificial piezoelectric coefficients in a new installation of a crystal (and return back to broken indexes) it is possible to obtain

$$\gamma_{3'} = dM_{3'}/dT = 2 d_{3'1'}\alpha / (s_{1'1'}^{E,T} + s_{1'2'}^{E,T}).$$

After conversion of parameter of above formula, all tensor components should be presented in the standard installation of a crystal (which is usually listed in the reference books):

$$\gamma_{111} = 2\sqrt{3} d_{14}\alpha / (4s_{11}^{E,T} + 8s_{12}^{E,T} + s_{44}^{E,T}). \quad (2.13)$$

For gallium arsenide this coefficient is  $\gamma_{111} = 1.5 \mu\text{C m}^{-2} \text{K}^{-1}$  (estimates show that in gallium nitride this coefficient is much higher). It should be noted that similar calculations of the artificial pyroelectric coefficient for quartz crystal result in  $\gamma_{100} = 2.6 \mu\text{C m}^{-2} \text{K}^{-1}$  and this can be observed along three polar-neutral axes, while the pyroelectric coefficient of the well-known pyroelectric tourmaline is  $4 \mu\text{C m}^{-2} \text{K}^{-1}$  and the maximum effect is possible only along one particular polar axis. In gallium arsenide the artificial pyroelectric effect in the directions of the basic axes [100], [010], and [001] is impossible. The maximum of this effect in the  $A^{\text{III}}B^{\text{V}}$  crystals corresponds to four [111]-type polar-neutral axes.

The indicatory surface of  $\gamma(\theta, \varphi)$  for polar-neutral cubic crystals constitutes of eight identical surfaces that start from the center of a cube to its vertices at the angle of 109.2 degrees. It is possible to find  $\gamma(\theta, \varphi)$  in any direction for a crystal of the gallium arsenide group: the magnitude of the “pyroelectric” coefficient can be determined as a radius-vector emanating from the center of the cube to the intersection with the indicatory surface. As compared with quartz, the indicatory surface of the gallium arsenide crystals group is more complicated, because it characterizes the artificial pyroelectric effect along four polar-neutral axes (and each has two possible directions).

With temperature increase the internal polar sensitivity decreases in all studied piezoelectrics. It should be recalled that in quartz this polarity vanishes at the temperature of  $\alpha \rightarrow \beta$  transition (Fig. 2.17), while in the KDP crystal  $\gamma_{100}$  also vanishes at the high-temperature phase transition (Fig. 2.18). It can be assumed that in piezoelectric crystals of the gallium arsenide group their internal polar sensitivity disappears at the melting point. In Fig. 2.20, the temperature dependence of polar moments  $M_{111}$  of GaAs and GaP crystals and the component  $M_{100}$  of internal polarity of a quartz crystal are compared. In the molten state, any stable polar formations are impossible, but it is noteworthy that the growth of a polar crystal from a melt forms the polar bonds that lead to an increase in the volume of material and, accordingly, a lower crystal density compared to its melt density.

(3) Polar sensitivity can be revealed in **other noncentrosymmetric crystals**. For instance, in trigonal crystals of polar class  $3m$ , in addition to the usual pyroelectric effect, seen along polar axis [001], the artificial pyroelectric response can be observed

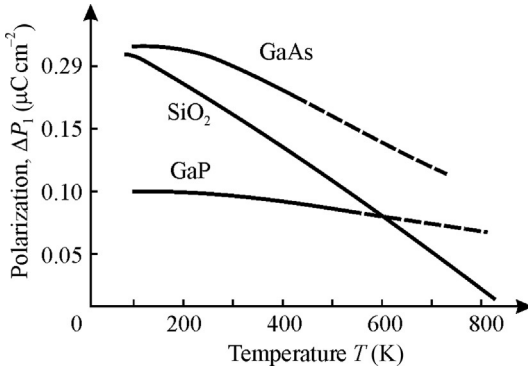


**Fig. 2.20** Temperature dependencies of component  $M_{111}$  for GaAs and GaP crystals in comparison to  $M_{100}$  of  $\text{SiO}_2$  ( $\alpha$ -quartz) crystal.

in the [010]-direction which is perpendicular to the [001] axis. The equation for the artificial pyroelectric effect calculation is (Table 2.1):

$$\gamma^*_2 = dP/dT = d_{22}(\alpha_1 s_{33} - \alpha_3 s_{13})(s_{11} s_{33} - s_{13}^2)^{-1}.$$

In some crystals of polar class  $3m$  it is possible to get such data: in the proustite crystal ( $\text{Ag}_3\text{AsS}_3$ )  $\gamma^*_2 = 10 \mu\text{C m}^{-2} \text{K}^{-1}$ ; in the pyrargyrite crystal ( $\text{Ag}_3\text{SbS}_3$ )  $\gamma^*_2 = 15 \mu\text{C m}^{-2} \text{K}^{-1}$ ; in lithium tantalate ( $\text{LiTaO}_3$ )  $\gamma^*_2 = 20 \mu\text{C m}^{-2} \text{K}^{-1}$ , and in lithium niobate ( $\text{LiNbO}_3$ )  $\gamma^*_2 = 40 \mu\text{C m}^{-2} \text{K}^{-1}$ . Note that the order of magnitude for such polar response is *comparable* to a conventional pyroelectric response: in lithium niobate, for example,  $\gamma_3 = 50 \mu\text{C m}^{-2} \text{K}^{-1}$ .

In the case of anisotropic restriction of thermal deformations, the artificial pyroelectric response can be observed in any piezoelectric, but analysis of this effect very often needs to use nonstandard installation of a crystal. For example, in the cubic piezoelectric class 23, to which the crystal bismuth germanate ( $\text{Bi}_{12}\text{GeO}_{20}$ ) belongs, the polar-sensitive direction is the [111]-type axis, and the maximum effect is observed just in this direction:

$$\gamma^*_{[111]} = 2\sqrt{3}\alpha \cdot d_{14} (4s_{11} + 8s_{12} + s_{44})^{-1},$$

At temperatures near 300 K in piezoelectric  $\text{Bi}_{12}\text{GeO}_{20}$ , this parameter equals  $\gamma^*_{[111]} = 20 \mu\text{C m}^{-2} \text{K}^{-1}$ , which exceeds many times the effects in quartz and GaAs.

The value of the pyroelectric response in partially clamped piezoelectrics depends not only on orientation of the piezoelectric element, but also on its shape. For example, for a long rectangular rod of quartz crystal (symmetry class 32), the artificial pyroelectric coefficient can be determined from the equation:  $\gamma'_1 = d_{11}\alpha_1 s_{11}^{-1}$ . It is assumed that the rod is oriented along axis 2 while electrodes coat the surface perpendicularly to the axis 1; at this orientation and form of sample  $\gamma^*_1 = 2.4 \mu\text{C m}^{-2} \text{K}^{-1}$ . The expressions for the calculation of artificial pyroelectric effect for all 10 classes of actual piezoelectrics (those which do not possess the pyroelectric effect) are shown in Table 4.1. Both in crystals free from any mechanical stresses and in crystals completely clamped, new

**Table 2.1** Artificial pyroelectric effect for 10 classes of actual piezoelectric crystals [15].

Symmetry classes, axes orientation (x,y,z)	Sample and its orientation as to basic axes	Calculation expressions for APE coefficient $\gamma_{NAPE}$	Piezoelectric, $\gamma_{NAPE}$ ( $\mu\text{C}/\text{m}^2\text{K}$ ) found at 300 K
32 (for basic coordinate system)	Rectangular rod with length $l$ along y and thickness along x	$\gamma_1 = \frac{d_{11}^T \cdot \alpha_1^E}{s_{11}^{E,T}}$	SiO <sub>2</sub> , $\gamma_1 = 2.4$
	Disk with normal $d$ directed along x	$\gamma_1 = \frac{d_{11}^T (\alpha_1^E s_{33}^{E,T} - \alpha_3^E s_{13}^{E,T})}{s_{11}^{E,T} \cdot s_{33}^{E,T} - (s_{13}^{E,T})^2}$	SiO <sub>2</sub> , $\gamma_1 = 2.7$
$\bar{4}2m$ (axes x and y are rotated around axis z at the angle of 45 degrees)	Rectangular rod with length $l$ and normal $d$ directed along axis z (a) $l$ is directed on x, (b) $l$ is directed on y.	$\gamma_3 = \frac{\pm 2d_{36}^T \cdot \alpha_1^E}{2 \cdot s_{11}^{E,T} + 2 \cdot s_{12}^{E,T} + s_{66}^{E,T}}$	KDP, (a) $\gamma_3 = -6$ (b) $\gamma_3 = +6$
$\bar{4}3m$ and 23 (axis z is directed on the third fold axis)	Disk, $d$ directed along z	$\gamma_3 = \frac{-2\sqrt{3}d_{14}^T \cdot \alpha^E}{4 \cdot s_{11}^{E,T} + 8 \cdot s_{12}^{E,T} + s_{44}^{E,T}}$	Tl <sub>3</sub> TaSe <sub>4</sub> , $\gamma_3 = -23.5$ ; Bi <sub>12</sub> GeO <sub>20</sub> , $\gamma_3 = -20$
222 (axes x and y are turned around axis z at the angle of 45 degrees)	Rectangular rod with normal $d$ directed along axis z and length $l$ directed (a) $l$ along axis x, (b) $l$ along axis y.	$\gamma_3 = \frac{\pm d_{36}^T (\alpha_1^E + \alpha_2^E)}{s_{11}^{E,T} + s_{22}^{E,T} + 2 \cdot s_{12}^{E,T} + s_{66}^{E,T}}$ (a) corresponds to sign «+» (b) corresponds to sign «-»	
622 and 422 (axes y and z are turned around axis x at the angle of 45 degrees)	Rectangular rod with normal $d$ directed along axis x and length $l$ directed a) $l$ along axis y, b) $l$ along axis z.	$\gamma_3 = \frac{\pm d_{14}^T (\alpha_1^E + \alpha_3^E)}{s_{11}^{E,T} + s_{33}^{E,T} + s_{44}^{E,T} + 2 \cdot s_{13}^{E,T}}$ (a) corresponds to sign «+» (b) corresponds to sign «-»	
$\bar{4}$ (standard)	Rectangular rod with normal $d$ directed along axis z and length $l$ directed (a) $l$ along axis x, (b) $l$ along axis y.	(a) $\gamma_1 = \frac{-d_{31}^T \cdot \alpha_1^E}{s_{11}^{E,T}} = R$ (b) $\gamma_1 = -R$	
$\bar{6}m2$ and $\bar{6}$ (standard)	Disk, normal $d$ is oriented along axis y	$\gamma_1 = \frac{d_{22}^T (\alpha_1^E s_{33}^{E,T} - \alpha_3^E s_{13}^{E,T})}{s_{11}^{E,T} \cdot s_{33}^{E,T} - (s_{13}^{E,T})^2}$	

effects are impossible, because the artificial effects are the result of anisotropic *partial clamping*. Thus, only partially clamped piezoelectrics exhibit artificial pyroelectricity or volumetric piezoelectric effects.

Therefore, in any polar crystals the variations in polar sensitivity under a thermal ( $\delta T$ ) or pressure ( $\delta p$ ) change provide a pyroelectric effect ( $P_i = \gamma_i \delta T$ ) or a volumetric piezoelectric effect ( $P_i = \xi_i \delta p$ ). In this case point,  $P_i$  is the change of vector value. Thus, pyroelectric coefficient  $\gamma_i$  as well as volumetric piezoelectric coefficient  $\xi_i$  are also vectors, and they are inherent to pyroelectrics only. That is why pyroelectrics can transform scalar influences ( $\delta T$  or  $\delta p$ ) into a vector type of response, which can be electrical voltage or electrical current.

## 2.5 Possible applications of artificially formed polarity

It is established, theoretically and experimentally, that in any piezoelectric the volumetric piezoelectric effect and the artificial pyroelectric effect can be realized (note that earlier these effects were considered possible only in crystals and textures of pyroelectric symmetry). The application of partial limitation of the deformations method (partial clamping of crystal) opens new possibilities for the use of piezoelectric (non-pyroelectric) crystals in electronics, because all semiconductors of the  $A^{III}B^{VI}$  group (among which are such promising semiconductors as gallium nitride) are the “exclusive” piezoelectrics: hence, in a single-crystal monolithic device it is possible to combine an acoustic or thermal sensor with a signal amplifier.

From Table 2.2, one can judge the place of the new effects discussed previously among the well-known and well-studied mechanoelectric and thermoelectric effects in the dielectrics and wide energy band semiconductors.

The left side of Table 2.2 lists the possibilities of the *piezoelectric effect* obtained (both conventional and volumetric) in various materials. It is noteworthy that the volumetric piezoelectric effect can be obtained only in 10 classes of crystals of

**Table 2.2** Electrical responses in polar-sensitive dielectrics (classification).

<i>Induced by stress</i>		<i>Induced by temperature</i>
Piezoelectricity	New effects in 20 “piezoelectric” classes of polar crystals	Pyroelectricity
Conventional piezoelectric effect in 20 polar classes (“piezoelectric” classes)	Artificial pyroelectric effect in 20 classes	Conventional pyroelectric effect in 10 polar classes (“pyroelectric” classes)
Volumetric piezoelectric effect in 10 “pyroelectric” classes of polar crystals	Artificial volumetric piezoelectric effect in 20 classes	Tertiary pyroelectric effect in 20 classes of polar crystals
Electric field induced piezoelectricity in all 32 classes		Electric field induced pyroelectricity in all 32 classes

*Note.* The table does not include effects caused by fields (electrical and magnetic), as well as some weak effects, for instance, flexoelectrical effect, which occurs in any crystalline dielectric as thin layers polarized during their bending.

*pyroelectric* symmetry and polar texture ( $\infty:m$  symmetry): only they are suitable for use in acoustic receivers and pressure meters. In the remaining 10 symmetry classes of “exclusive” piezoelectric crystals, hydrostatic pressure does not lead to any electrical response, since it is compensated in their *polar-neutral* structure. Finally, the applied direct electric field induces uniaxial polarity in any solid dielectric and, as a consequence, the manifestation of electrically induced piezoelectric effect (that is linearized electrostriction). In the relaxor ferroelectrics, which have large permittivity, this effect can transcend the ordinary piezoelectric effect.

The right side of Table 2.2 lists the possibilities for obtaining *pyroelectric effects*, which under uniform thermal action are usually manifested in the 10 classes of pyroelectrics and in the polar textures. If, however, thermal action is inhomogeneous—for example, it is characterized by a temperature gradient—then the electrical response appears in *any* noncentrosymmetric crystal, including the “pure-piezoelectric” crystals. This tertiary effect has been known for a long time and is sometimes called actinoelectricity [5]. It is caused by the temperature *gradient* that is due to nonuniform heating. However, this effect is relatively small; in spite of this, it is used sometimes for powerful laser pulse detection, using the highly heat-resistant quartz crystal (other polar crystals could be damaged). Finally, under applied direct electrical field the induced uniaxial polarity appears in any dielectric, with the manifestation of electrically induced pyroelectric effect. In the relaxor ferroelectrics this effect can compete with the pyroelectric effect of the best polar crystals.

In the center of Table 4.2, the effects possible in the crystals of 20 noncentrosymmetric classes under conditions of partial deformation *restriction* are listed. First of all, this is, certainly, the *artificial pyroelectric effect*, obtained not by the application of an external electrical field (when it always arises) but by the artificial restriction of a certain type of deformation. In fact, this is, certainly, a secondary pyroelectric effect, which usually cannot be manifested in the polar-neutral crystals since it is totally compensated. But artificially it is possible to restrict a certain part of the deformations, as a result of which decompensation occurs, i.e., the polar response. In the short-circuited circuit with a polar crystal, under uniform thermal action, a current is generated, while an electrical potential is generated in the open-circuited crystal.

Therefore, in the polar crystals, their internal polar-sensitive structure is noncompensated only in the pyroelectrics, but it is totally self-compensated in the so-called “exclusive” piezoelectrics. Moreover, their self-compensation is total, not being dependent on whether a crystal is in a stress-free state or in a strain-free state. Nevertheless, nonisotropic partial clamping destroys the self-compensation of intrinsic polarity. This decompensation allows the vector response to the scalar influence to be observed in such crystals (Table 2.2).

The effects described here open new possibilities for sensor device development and elaboration. Piezoelectric crystals such as quartz crystals and semiinsulating  $A^{III}B^V$  crystals could find application in these devices (for instance, gallium arsenide or gallium nitride, which are commonly used materials in microelectronics and micro-machining). Technologically, with the use of partial clamping, it is possible to convert the layers of these crystals into the artificial pyroelectrics that, with hybrid or monolithic technology, are comparable to semiconductor devices. A layer with pyroelectric properties could be an acoustic receiver (as part of a piezotransistor) or serve as a

**Table 2.3** Main parameters of artificial pyroelectrics in comparison with usual pyroelectrics.

Crystal	$\gamma$ ( $\mu\text{C m}^{-2} \text{K}^{-1}$ )	$\epsilon$	$F_V$ ( $\text{m}^2 \text{C}^{-1}$ )	$F_D \cdot 10^{-5}$ ( $\text{Pa}^{-1/2}$ )
<i>Artificial pyroelectric effect in partially clamped piezoelectrics</i>				
$\text{Bi}_{12}\text{SiO}_{20}$	27	42	0.08	2.2
$\text{NH}_{14}\text{H}_2\text{PO}_{14}$	17	50	0.02	0.6
<i>s/i</i> -GaAs	1.5	13	0.016	0.1
43 <i>m</i> crystals	0.5–25	7–8	0.01–0.1	0.1–4
$\alpha$ - $\text{SiO}_2$	2.6	4.5	0.033	7
<i>Usual pyroelectric effect in ferroelectrics</i>				
TGS	500	50	0.4	6
PVDF	30	12	0.1	0.9
$\text{LiTaO}_3$	230	48	0.2	5
PZT ceramics	380	300	0.6	6

thermal sensor, as part of a pyrotransistor. Calculated and experimental results needed for pyroelectric sensors are shown in Table 2.3, where  $C_V$  is specific heat,  $F_V = \gamma \cdot (-C_V \epsilon)^{-1}$  is the responsibility, while  $F_D = \gamma \cdot C_V (\epsilon \cdot \tan \delta)^{-1/2}$  characterizes the signal-to-noise ratio of pyroelectric detectors at 300 K and the modulation frequency of 1 kHz.

The polar (piezoelectric and pyroelectric) properties of  $\text{A}^{\text{III}}\text{B}^{\text{V}}$  crystals in electronic devices were apparently not used. However, the polar-sensitive structure of any wide-band gallium arsenide-type crystal can be used to convert mechanical or temperature effects into electrical signals. In this case,  $\text{A}^{\text{III}}\text{B}^{\text{V}}$  semiconductor compounds can be considered as dielectrics, and only the phenomenon of electrical polarization might be taken into account. This assumption is close to reality in *s/i*-GaAs and even more in GaAs solid solutions with AlAs (especially for the GaN crystal). The piezoelectric activity of these semiconductors is usually not taken into account due to their increased conductivity (polarization can be shielded by free charges). But it should be borne in mind that in *s/i*-GaAs the shielding effect becomes insignificant at frequencies above 1 kHz, while the AlGaAs crystal can be used as a piezoelectric and “pyroelectric” sensor even at a frequency of 20 Hz.

Thus, temperature dependence of piezoelectric polar sensitivity can be used in microelectronics for thermal sensors. In a similar way, piezoelectric polar-sensitivity dependence on pressure can be applied in mechanical sensors.

In addition to sensors, as a result of the studies described here, one more important circumstance has been discovered. Significant polar sensitivity in the crystals of the  $\text{A}^{\text{III}}\text{B}^{\text{V}}$  group is observed along any of the [111] directions, whereas in the typically used direction of [100] type these crystals do not respond to vibration and temperature changes. Nevertheless, with planar chip technology, it may turn out that some layers of devices are oriented in the [111] direction. In this case, in such devices electrical noise can occur due to vibrations and, possibly, due to local temperature changes. This feature should be taken into account when designing devices using semiconductors of the  $\text{A}^{\text{III}}\text{B}^{\text{V}}$  group. Eventually, these peculiarities might be used for investigation of noise that arises due to chaotic disturbance of internal polarization.

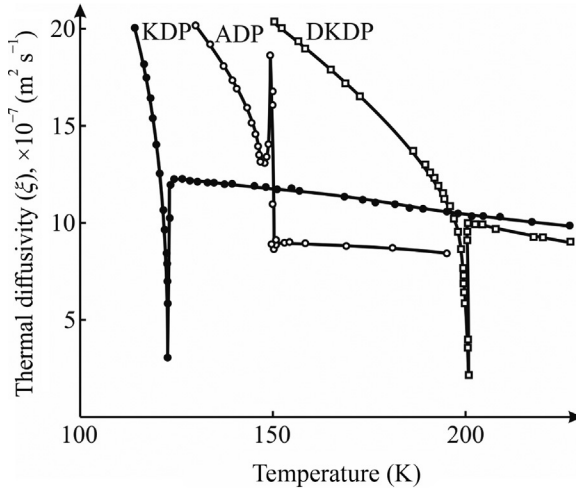
## 2.6 Summary

1. Experimental evidence of the polar sensitivity in crystals includes the *structural affinity* of the piezoelectrics and pyroelectrics, with the example of zinc sulfide uniting in polymorphic structure the regions with sphalerite and wurtzite symmetry, as well as the *chemical features* of polar crystals demonstrating different chemical sensitivity on the surfaces of opposite polarity.
2. Polar-sensitive bond ordering leads to *increased volume* at the transition into the polar phase; such crystals are characterized by the electromechanic and electrocaloric *contributions* to *permittivity* as well as increased high-frequency dielectric *absorption*.
3. Charge transfer in some polar-sensitive crystals may depend on the symmetry of the polar phase: a large *decrease* in resistivity in *critistors* of the vanadium dioxide type occurs from its triclinic (piezoelectric) symmetry, while the large *increase* in resistivity in *posistors* is due to doped barium titanate transition from the polar tetragonal (pyroelectric) structure into the nonpolar cubic phase.
4. Zinc oxide, which is the best material for *varistors* (with its giant change in resistivity), has a polar wurtzite (pyroelectric) structure with possible transformation into another but also polar sphalerite (piezoelectric) state. Other field-controllable switching elements, which exhibit colossal magnetoresistance as well as high sensibility of nanostructured sensors based on zinc oxide, also belong to the polar-sensitive crystals.
5. The *electrically induced* polar properties are caused by *linearized electrostriction*: in dielectrics with high permittivity in a strong electrical field, both the piezoelectric effect and the pyroelectric effect can be induced. They are proportional to the applied field and the square of the dielectric permittivity. In paraelectrics and especially in the relaxor ferroelectrics, electrically induced piezoelectric module can reach and even surpass the piezoelectric module of usual piezoelectrics.
6. The possibility of *electrical control* by piezoelectric effect is interesting for practical application in electronics: using this principle, it is possible to implement tunable piezoelectric resonators and filters and various SAW devices.
7. It is possible to obtain *mechanically induced* pyroelectricity (and the volumetric piezoelectric effect) in any polar-neutral piezoelectric (which is not pyroelectric). For this, the original method of partial limitation of thermal (or elastic) deformations is applied, due to which one of the polar-neutral axes is transformed into the polar axis.
8. Obtaining the artificial pyroelectric effect (or volumetric piezoelectric effect) is achieved in a composite system “nondeformable substrate–oriented plate of polar-neutral crystal.” These studies can be realized in two- and three-dimensional structural arrangements of polar-sensitive bonds; as a result, the artificial pyroelectric effect for 10 classes of polar-neutral piezoelectric crystals is calculated.
9. A main factor is that by creating *special boundary conditions* for piezoelectric crystals the “pyroelectric effect” can be obtained in all 10 polar-neutral classes of crystals. Therefore, in any polar crystals, the changes in polar sensitivity under thermal ( $\delta T$ ) or pressure ( $\delta p$ ) variation provide the pyroelectric effect ( $P_i = \gamma_i \delta T$ ) or the volumetric piezoelectric effect ( $P_i = \zeta_i \delta p$ ). Moreover, pyroelectric coefficient  $\gamma_i$  as well as volumetric piezoelectric coefficient  $\zeta_i$  are the material vectors inherent to the polar crystals only. That is why polar-sensitive crystals can transform scalar influences ( $\delta T$  or  $\delta p$ ) into the vector type of responses, which are electrical voltage or electrical current.

10. Temperature dependence of piezoelectric polar sensitivity can be used in microelectronics for thermal sensors. In a similar way, polar-sensitivity dependence on pressure can be applied in mechanical sensors. Significant polar sensitivity in crystals of the  $A^{III}B^V$  group is observed along any of the [111] directions, whereas in the typically used [100] type direction, these crystals do not respond to mechanical vibrations and temperature changes.
11. In planar chip technology, it may turn out that some layers of devices are oriented in the [111] direction. In this case, in such devices electrical noise can occur due to vibrations and, possibly, due to local temperature changes. This feature should be taken into account when designing devices using semiconductors of the  $A^{III}B^V$  group.

## References

- [1] Y.M. Poplavko, *Electronic Materials. Principles and Applied Science*, Elsevier, 2019.
- [2] K. Uchino, *Ferroelectric Devices*, Marcel Dekker, New York, 2000.
- [3] M.E. Lines, A.M. Glass, *Principles and Application of Ferroelectrics and Related Materials*, Clarendon Press, Oxford, 1977.
- [4] I.S. Jeludev, *Basic of Ferroelectricity*, Atomizdat, Moscow, 1973.
- [5] W.O. Cady, *Piezoelectricity*, Amazon com, New York, 1946.
- [6] Y.M. Poplavko, Y.I. Yakymenko, *Piezoelectrics*, Polytechnic Institute, Kiev, 2013.
- [7] F. Zhuo, Q. Li, H. Qiao, et al., Field-induced phase transitions and enhanced double negative electrocaloric effects in  $(Pb,La)(Zr,Sn,Ti)O_3$  antiferroelectric single crystal, *Appl. Phys. Lett.* 112 (2018) 133901.
- [8] Y.M. Poplavko, L.P. Pereverzeva, A.S. Voronov, Y.I. Yakymenko, *Material Sciences, Part II, dielectrics*, Polytechnik, Kiev, 2007.
- [9] Y.M. Poplavko, Y.V. Didenko, D.D. Tatarчук, Temperature dependences of losses in high frequency dielectrics, *Electron. Commun.* 19 (4) (2014) 9.
- [10] R.E. Newnham, *Properties of Materials: Anisotropy, Symmetry, Structure*, Oxford University Press, Oxford, 2004.
- [11] Y.M. Poplavko, L.P. Pereverzeva, I.P. Raevskiy, *Physics of Active Dielectrics*, South Federal University of Russia, Postov-na-Donu, 2009.
- [12] Y.M. Poplavko, L. Pereverzeva, N.-I. Cho, Y.S. You, Feasibility of microelectronic quartz temperature and pressure sensors, *Jpn. J. Appl. Phys.* 37 (1998) 4041.
- [13] Y.M. Poplavko, L.P. Pereverzeva, *Pyroelectricity of partially clamped piezoelectrics*, *Ferroelectrics* 130 (1992) 361.
- [14] Y.M. Poplavko, N.-I. Cho, Clamping influence on ferroelectric integrated film microwave properties, *Semicond. Sci. Technol.* 14 (1999) 961.
- [15] Y.M. Poplavko, L.P. Pereverzeva, *Termopiezoelectric transducers*, *Ferroelectrics* 131 (1992) 331.



Thermal properties of crystals are due to the internal energy of the *movement* of atoms, ions, or molecules; therefore they are strongly dependent on crystal structure: the stronger the bonds between atoms, the more energy that must be expended for the atoms' thermal vibrations. In other words, more stable interatomic bonds require more energy for their formation. Therefore, the peculiar properties of polar-sensitive bonds should be clearly manifested in the basic thermal properties, which are specific heat, thermal expansion, and thermal conductivity.

It should be recalled that *heat capacity*, denoted  $C$  and measured in J/deg or in cal/(deg mol), is the absorbed (or released) heat when temperature changes. Numerically, specific heat is the energy that must enter into the unit volume of a material to heat it up by 1 deg. Further, in functional dielectrics, heat capacity is dependent on the mechanical and electrical boundary conditions of a crystal. Further, it will be shown that specific heat in polar crystals contains an additional contribution due to the degree of disorder of the polar-sensitive bonds. The statistical possibility of several states being realized increases the total entropy of the system: such *configurational entropy* is a part of total entropy of a system and relates to the *position* of constituent particles rather than to their velocity or momentum. The configurational entropy is physically related to the number of ways of arranging all the **particles** of a system while maintaining some overall set of specified system properties, such as **energy**. The change in configuration entropy corresponds to the same change in macroscopic entropy.

*Heat transfer* can occur in any bodies with nonuniform distribution of temperature, whereby the mechanisms of heat transfer are dependent on the physical state of a crystal. The coefficient of *thermal conductivity*, denoted  $\lambda$  and measured in W/(deg m) (or in the CGS unit system as cal/(deg s cm)), reflects the internal structural peculiarities of a material; numerically it equals to the amount of heat passing through a unit area per unit time at a unit temperature gradient. In the functional dielectrics, heat transfer is significantly smaller than in the conventional dielectrics; moreover, the thermal diffusion may be anisotropic and even dependent on the applied electrical field. Among the many aspects of heat transfer, in this book it is shown that heat transfer in the polar crystals is provided mostly by the short lattice waves having low velocity, so polar crystals looks like a turbid medium. These waves demonstrate strong scattering in the diffuse-type nanosize-inhomogeneous structure, in which phonon interaction is determined mostly by polar-sensitive bonds, because the wavelength of heat-phonons is commensurable with parameters of the crystal lattice. Polar-sensitive (mixed ionic-covalent) bonds strongly affect processes of heat transfer of crystals: their thermal conductivity is much less than that in pure-ionic or pure-covalent crystals. Anomalies of thermal diffusion in the vicinity of ferroelectric and antiferroelectric phase transitions are also described: when the ordered polar structure spontaneously changes to the disordered nonpolar structure. In the ordered phase, the thermal diffusion coefficient increases; this indicates that the disordering of polar-sensitive bonds hinders the diffusion of heat.

The coefficient of *thermal expansion*, which is denoted  $\alpha$  and measured in the units  $\text{deg}^{-1} = \text{K}^{-1}$ , represents the alteration of relative dimensions of a solid body when temperature changes by 1 K. A crystal's thermal deformation is a characteristic feature of *internal connections* of atoms, ions, or molecules; this deformation depends also on the energy of these bonds. In cubic crystals, their thermal expansion is isotropic, but in the functional dielectrics the coefficient of thermal expansion shows a pronounced anisotropic character and can be even *negative* (at low temperatures). It will be shown in the following text that thermal expansion reflects the features of interatomic bonds in crystals; in the polar dielectrics this is a peculiar polar-sensitive structure, arising due to compensation of atoms' electronegativity. The negative value of  $\alpha$  corresponds to the particular case when a crystal's entropy *increases* with pressure rise, which is possible only in the case of *configurational* entropy: a negative expansion region on the  $\alpha(T)$  dependence corresponds to the processes of own structural ordering of polar bonds; moreover, the results obtained for polar crystals can be applied to semiconductors. The difference in thermal expansion as well as the mismatch between lattice parameter of film and substrate is used in modern technologies of microelectronics.

A *convincing example* of internal polarity influence on a crystal's thermophysical properties is the change upon phase transition from the *nonpolar* (high-temperature centrosymmetric) phase into the *polar* (low-temperature pyroelectric) phase in the TGS crystal (triglycinesulfate,  $(\text{NH}_2\text{CH}_2\text{COOH})_3 \cdot \text{H}_2\text{SO}_4$ ).

In connection with the example given in Fig. 3.1, note the following details. In the vicinity of phase transitions, the material first shows anomalies in its main physical properties; second, it allows considerable control of the material parameters by

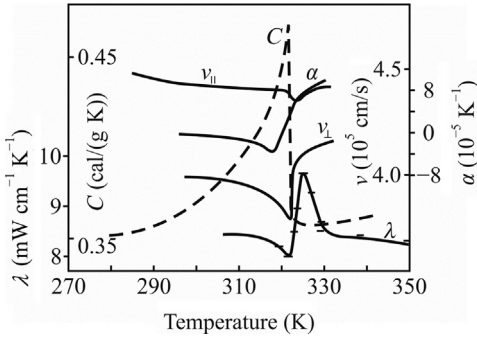


**Fig. 3.1** Temperature dependence of the main TGS parameters: Specific heat  $C$ , ultrasound speeds  $v_1$  in [010] direction and  $v_3$  along [001] direction, linear expansion coefficient  $\alpha$  along [010] direction, and thermal conductivity  $\lambda_1$  along [010] direction (according to Ref. [1]).

external influences that are not very strong, a feature widely used in electrically controlled devices; third, the material is very sensitive to changes in temperature, pressure, humidity, etc. used in various sensory devices.

To understand the physical causes of polar crystal peculiarities, it is necessary to compare the basic energy characteristics of solids with special properties arising due to phase transitions into the phase having internal polarity. In this regard, recall that one of the important crystal physical quantities is the *Debye energy*  $\hbar\omega_D$ . It becomes equal to *thermal energy*  $k_B T$  at a certain temperature, called the *Debye temperature* and denoted by  $\theta_D$ ; therefore  $\hbar\omega_D = k_B \theta_D$  and  $\theta_D = \hbar\omega_D/k_B$ . Thus, the most important characteristics are the facts that Debye frequency  $\omega_D = 2\pi\nu_D$  and Debye temperature are connected with each other by two fundamental constants, the Planck constant  $\hbar$  and the Boltzmann constant  $k_B$ .

The degrees of freedom of atomic particle movement in solids can be divided into two groups. For some degrees of freedom, the interaction energy of particles  $U_{int}$  is small in comparison with thermal motion energy  $k_B T$ . Moreover, when  $U_{int} \ll k_B T$  the appropriate degrees of freedom behave as a *collection* of particles, i.e., as an “almost ideal gas” of phonons, and the applicability of the model of *quasiparticles* is justified. In the discussion here, this term refers to the ordinary nonpolar dielectrics.

In the opposite case, when  $U_{int} \gg k_B T$ , the appropriate degrees of freedom are usually quite ordered, so their movement, too, can be described by the introduction of quasiparticles, in the given case by phonons. The materials in this case include the majority of the functional polar-sensitive dielectrics (piezoelectrics and pyroelectrics), so application of the concept of phonons to them during discussions in various chapters of this book in most cases can be considered justified.

However, in the following discussion a much more complicated case arises: when interaction energy  $U_{int} \sim k_B T$ . In this case, the theoretical description of solids becomes very complicated, especially in the phenomenon of *phase transition* (as in Fig. 3.1, where the nonpolar phase is transitioning into the polar phase). In the vicinity of a *second-order phase transition*, the crystal behaves in such a way when any conventional concept, based on quasiparticles, cannot adequately describe the experimental situation. Normally, the interaction of *closest neighboring* particles in a crystal is considered to be dominant, while the interaction of *distant particles* might be

neglected. However, near a phase transition, in contrast, the interaction of neighboring particles *compensates each another*, and with this background the interaction of those particles located at some distance from one another appears *dominant*. This interaction has a very special character: the probability of *collective movements* is larger than the probability of *individual movements*. This abnormally increased role of collective movements is confirmed by experiments (Fig. 3.1): at temperature  $T = T_C$  a crystal shows a maximum of specific heat, dielectric permittivity in the ferroelectric tends to infinity, with permeability in the ferromagnetic (in superconductors their conductivity actually becomes infinite), and so on.

The crystals with polar-sensitive bonds in certain conditions behave in a complex way: for some phonons—for example, thermal ones—the lifetime is commensurate with inverse frequency of oscillation; that is, the oscillators, which characterize these phonons, turn out to be overdamped. At first glance, an amazing situation arises when a crystal of excellent quality, being ideally transparent in the optical wavelength band and having small attenuation of transmitting acoustic (ultrasonic) waves, turns out to be almost an opaque (turbid) environment for the short waves (heat waves), in which phonons of certain frequency become stuck like feet in a swamp.

Another striking feature of the polar-sensitive crystals is their *compression* when being heated (in contrast to the *extension* of usual crystals), which is observed in low-temperature regions. To explain the physical nature of such negative thermal expansion of polar crystals, a comparison will be carried out of two different scalar influences on polar crystals: the homogeneous change of temperature and the homogeneous (hydrostatic) change of pressure. These actions are united by the fact that, being *scalar*, both these influences lead to the *natural change* (not distorted by the symmetry of external action) in a crystal size, which reflects exactly the peculiarities of crystal internal bonds.

It will be shown that the main thermal effects in crystals are interdependent, and it is expedient to begin our consideration with the specific heat.

### 3.1 Specific heat of polar crystals

It is worth recalling that heat capacity of a body is the physical quantity defined as a ratio of the amount of heat  $dQ$  obtained by a body to correspondingly increase its temperature by  $dT$ :  $C = dQ/dT$ ; the commonly used unit of heat capacity in the SI system is joules/K (J/K). The *specific heat* is heat capacity per given unit of substance measured in kilograms, cubic meters, and moles. Mass specific heat is the amount of heat given to a unit mass of material to heat it up by 1 K and it is measured in  $\text{J kg}^{-1} \text{K}^{-1}$ . Respectively, volumetric specific heat  $C_V$  is the amount of heat necessary to add it to unit volume of material and measured in  $\text{J m}^{-3} \text{K}^{-1}$ . Molar specific heat  $C_\mu$  is measured in  $\text{J}/(\text{mol K})$ , while in the Gauss system specific heat is determined in  $\text{cal}/(\text{g mol K})$ .

As is known, specific heat near 0 K is extremely small, but afterwards  $C(T)$  rapidly increases: below the Debye temperature ( $\theta_D$ ) heat capacity changes as  $C \sim T^3$  due to a fast increase in the number of excited oscillations (phonons). However, in the region

of normal temperatures ( $T > \theta_D$ ) in most crystals, possible lattice vibrations are already excited; therefore, a crystal's energy increases with temperature rise as the average energy  $k_B T$  of normal vibrations; moreover, the specific heat of a crystal lattice should not be dependent on temperature:  $C \approx \text{const}$  (in fact,  $C(T)$  slightly rises due to the anharmonicity of lattice vibrations). Therefore, any significant change or leap in the specific heat is associated with the restructuring of the crystal lattice. However, in most solids, a significant change in heat capacity with temperature is observed only in the low-temperature region and in the vicinity of phase transitions.

Thus, specific heat in solids at normal and elevated temperatures is a rather conservative parameter, as it is determined mostly by the amount of thermally excited phonons. Any excess of heat capacity above its established level (which at normal conditions is almost independent of temperature) would be an unusual property of a crystal. The ferromagnetics are almost the only exception, where in the partially ordered ferromagnetic phase the contribution of the *magnons* to heat capacity is significant (but this disappears above the Curie point). In the polar-sensitive crystals, a similar but much weaker excess in their heat capacity is seen, as compared with the nonpolar crystals. This is clearly expressed near the phase transitions, where a maximum of heat capacity can be more than two times higher than its average value; for example, this is seen at the ferroelectric phase transition in the  $\text{KH}_2\text{PO}_4$  (KDP) crystal.

As an opportune example of specific heat increasing in polar-sensitive crystals, the ferroelectrics can be examined, in which one can compare the heat capacity of the *polar* and *nonpolar* phases (above the phase-transition temperature). As an example, the TGS crystal is elected again; it is nonpolar above its Curie point, and its heat capacity and internal electrical moment  $\Delta M$  are shown in Fig. 3.2.

The fact is that a *gradual increase* and the *maximum* in  $C(T)$  dependence is necessarily manifested in ferroelectric crystals when their phase transition temperature  $T_C$  is approached (Fig. 3.2A). A fundamental part of the heat capacity, which is practically temperature-independent, is shown by the bottom dotted line. Above the upper dotted line, the  $\lambda$ -type maximum of  $C(T)$  is seen, which in this case reaches 50% of the fundamental specific heat (in some ferroelectrics it might be many times greater). This maximum is due to the very nature of the ferroelectric phase transition and corresponds to the latent heat released at the phase transition.

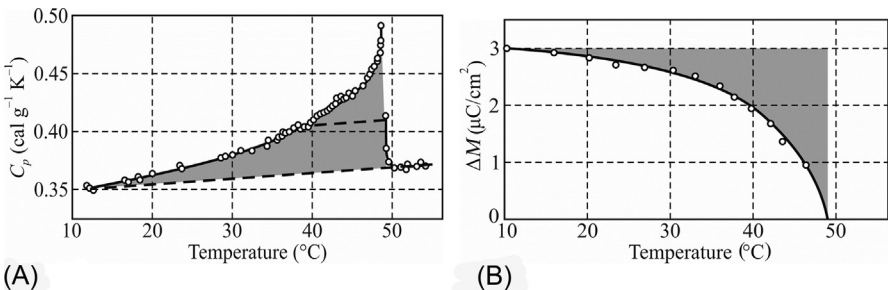


**Fig. 3.2** Temperature dependence of heat capacity (A) following work [2], and averaged electrical moment of polarization fluctuations (B) in TGS =  $(\text{NH}_2\text{CH}_2\text{COOH})_3\text{H}_2\text{SO}_4$ .

However, as discussed here the  $C(T)$  anomaly looks like a rather big region of excess heat capacity. Below the Curie point with decreasing temperature the spontaneous polarization changes very gradually (Fig. 3.2B), because a significant part of the polar sensitive bonds still remains partially disordered—their fraction is shown by a shaded region, which quite corresponds to the temperature region of “increased heat capacity” in Fig. 3.2A. It might be supposed that the contribution to the heat capacity in the gradually ordering phase is due to the configurational entropy. It is pertinent to note that such deviation from the linearity of  $C(T)$  dependence above the Debye temperature occurs very rarely in solids. Concerning this fact, it is appropriate to recall that the analogous case of heat capacity increase is seen in the ferromagnets, in which an additional contribution to  $C(T)$  is due to the collective excitation associated with electronic spin structure in the partially ordered magnetic lattice, i.e., magnons.

The increase of heat capacity peculiar to the polar-sensitive crystals, shown in Fig. 3.2A, requires an explanation. For this purpose, additional experiments were carried out. First, during the measurements, special conditions were created in which the mechanical strain of the crystal was limited; in this case, the maximum in  $C(T)$  dependence was largely suppressed. Second, when measuring heat capacity, the DC electrical bias field was applied to a crystal [3], which also led to a decrease of  $C(T)$  maximum, but at the same time did not shift this blurred maximum on the temperature scale. In addition, a significant *smoothing* of temperature maxima elastic stiffness  $s_{11}$  and  $s_{33}$  in TGS was seen under the influence of a strong CD electric field [1]. Also, the experiment in ultrasound absorption in a TGS crystal near its phase transition shows a decrease in sound absorption in the polar phase and an increase in the nonpolar phase during a DC electrical field application.

All this indicates that a gradual increase in  $C(T)$  and its temperature peak, shown in Fig. 3.2A, is due to the reorganization in the arrangement of polar-sensitive bonds and can be explained by thermal fluctuations of disordered (nonpolar) phase in the depths of the ordered polar phase. Probably, these fluctuations are concentrated inside domain walls, which can dynamically expand and contract. It is possible to offer another explanation for the fact that, below phase transition, the ordering of polarity in the ferroelectrics occurs gradually. The statistical possibility of several states being realized increases the total entropy of a system: such *configurational entropy* is a part of the total entropy of the system, which is related to the position of the constituent particles rather than to their velocity or momentum. It is due to the number of ways of arranging all the particles of a system while maintaining some overall set of specified system properties, such as energy. The change in configuration entropy corresponds to the same change in macroscopic entropy.

From the point of view of macroscopic theory, due to the existing interconnection of electrical, thermal, and mechanical properties of polar crystals, the dependence of their thermal properties on mechanical and electrical boundary conditions of a crystal is not surprising: the heat capacity of a mechanically clamped crystal  $C^x$  differs from the heat capacity of a free crystal  $C^x$ , just as heat capacity of a short-circuited crystal  $C^E$  is not equal to the heat capacity of an electrically free (opened) crystal  $C^D$ . Moreover, the temperature anomaly of TGS heat capacity, shown in Fig. 3.2A, corresponds to the property of an electrically and mechanically free crystal.

Further, it will be shown that specific features of polar-sensitive crystals have a noticeable effect on the heat exchange processes. However, the most impressive difference between polar and nonpolar crystals is their negative thermal deformation at low temperatures when thermal motion in crystals weakens, which allows observation of the details of structural differences.

## 3.2 Polar crystal thermal expansion

The physical phenomenon of thermal expansion of crystals is important for electronic materials applications. Ensuring reliability in microelectronic structures, where the layers of semiconductors, dielectrics, and metals are integrated into a single monolithic structure, needs coordination in the thermal expansion coefficients between components. The point is that these complex structures are synthesized at high temperature but used in normal conditions. Without coordination of thermal expansion coefficients, the obtained structures would be mechanically stressed, which affects their properties and might even lead to local destruction.

However, there are some important cases seen in electronics in which exactly this difference in thermal expansion is applied for managing the combined structure properties. For example, biaxial stressed structures of superconductor films can raise their phase transition temperature; in the same way the mechanical tension of some semiconductor structures can significantly improve the parameters of high-frequency transistors [4].

As for polar dielectrics, a description was given in [Chapter 2](#) of how, using the difference in thermal expansion, it is possible to investigate the components of intrinsic polarity in polar-neutral crystals. To this end, an oriented plate of the piezoelectric being studied should be clamped to the substrate, remaining free in the out-of-plane direction. The substrate must be selected with a low thermal expansion coefficient, so in the piezoelectric plate, when temperature changes, only the normal to a substrate thermal deformation is possible, which produces the secondary piezoelectric effect, imitating pyroelectricity. Using this method, the artificial pyroelectric effect and artificial volumetric piezoelectric effect can be obtained in the noncentrosymmetric semiconductors, which can be used in single-chip piezoelectric and pyroelectric sensors.

Moreover, as was shown in Ref. [5], using the biaxial strain for ferroelectric film, which is clamped to a substrate having a different temperature coefficient of expansion, the phase transition temperature can be altered. Recently, a *mismatch in lattice constant* between the deposited film and the substrate controllable thermal expansion has been applied in a new technological method for producing materials with new properties that are extremely interesting for microelectronics. However, this question deserves more detailed consideration, provided at the end of this section.

**1. Anisotropy of thermal expansion.** The relative deformation of a solid is the dimensionless parameter described by the second-rank tensor  $x_{ij}$ . Deformation of solids can occur not only under the influence of mechanical stress  $X_{kl}$  (second-rank tensor), but also under various other external influences: electrical action described

by the polar vector  $E_k$ , magnetic influence described by the axial vector  $H_k$ , and by scalar (homogeneous) influences, such as the uniform change of temperature  $\delta T$  or the hydrostatic change of pressure  $\delta p$ . In all listed cases, the dimension and the symmetry of parameters that link various actions ( $X_{kl}$ ,  $E_k$ ,  $H_k$ ,  $\delta T$ ,  $\delta p$ ) and linear responses—strain  $x_{ij}$ —induced by these actions are very different:

$$x_{ij} = s_{ijkl}X_{kl}, x_{ij} = d_{ijk}E_k, x_{ij} = \zeta_{ijk}H_k, x_{ij} = \alpha_{ij}\delta T, x_{ij} = \xi_{ij}\delta p,$$

where  $s_{ijkl}$  is elastic compliance (fourth-rank tensor),  $d_{ijk}$  is piezoelectric module (third-rank tensor),  $\zeta_{ijk}$  is piezomagnetic module (third-rank tensor), and  $\alpha_{ij}$  is coefficient of *thermal expansion* (second-rank tensor), exactly the parameter being discussed in this chapter.

It is noteworthy that the first three of these parameters characterize those properties of a crystal that can be obtained by the external action of *fields* of different symmetry, while the symmetry of response (in this case, the strain  $x_{ij}$ ) is composed of symmetry of action and symmetry of a crystal. Therefore, in the case of the multifaceted study of crystal properties, tensors  $s_{ijkl}$ ,  $d_{ijk}$ ,  $\zeta_{ijk}$  can only *indirectly* characterize the nature of internal bonds of atoms (ions) in a crystal. At the same time, the *scalar action* on a crystal (which has the symmetry of a ball) gives such a parameter as  $\alpha_{ij}$ , which reflects the *intrinsic properties* of interatomic bonds, *directly* shown in the response.

Next, only the coefficient of thermal expansion  $\alpha_{ij}$  is considered, since only it describes the anisotropy of polar-sensitive bonds in a crystal. It can be argued that it is the internal polarity, which is one of reasons for both the anisotropy of thermal expansion and the negative deformation as temperature increases in a certain range. This anisotropy is clearly seen from the matrix representation of  $\alpha_{ij}$  in Fig. 3.3, where corresponding matrices for crystals of different symmetry are presented. In the most common *ionic* and *covalent* crystals, the coefficient of thermal expansion is isotropic and can be represented by the scalar value  $\alpha_{ij} = \alpha$ : the components in the main diagonals of the matrix  $\alpha_{ij}$  are the same (Fig. 3.3A). A ball made of such a crystal, as a result of uniform heating or cooling, will change its radius but will not change its shape. It would seem that, in the hexagonal crystals, this ball will turn into the ellipsoid of rotation, and in the rhombic or monoclinic crystals it will be transformed into a general three-axis ellipsoid.

**Fig. 3.3** Matrices of thermal expansion coefficient in crystals of various classes of symmetry: (A) cubic; (B) hexagonal; (C) rhombic; (D) monoclinic; (E) triclinic.

$\alpha_{11}$	0	0	$\alpha_{11}$	0	0	$\alpha_{11}$	0	0
0	$\alpha_{11}$	0	0	$\alpha_{11}$	0	0	$\alpha_{22}$	0
0	0	$\alpha_{11}$	0	0	$\alpha_{33}$	0	0	$\alpha_{33}$
<b>(A)</b>			<b>(B)</b>			<b>(C)</b>		
	$\alpha_{11}$	$\alpha_{12}$	0	$\alpha_{11}$	$\alpha_{12}$	$\alpha_{13}$		
	$\alpha_{12}$	$\alpha_{22}$	0	$\alpha_{12}$	$\alpha_{22}$	$\alpha_{33}$		
	0	0	$\alpha_{33}$	$\alpha_{13}$	$\alpha_{23}$	$\alpha_{33}$		
<b>(D)</b>			<b>(E)</b>					

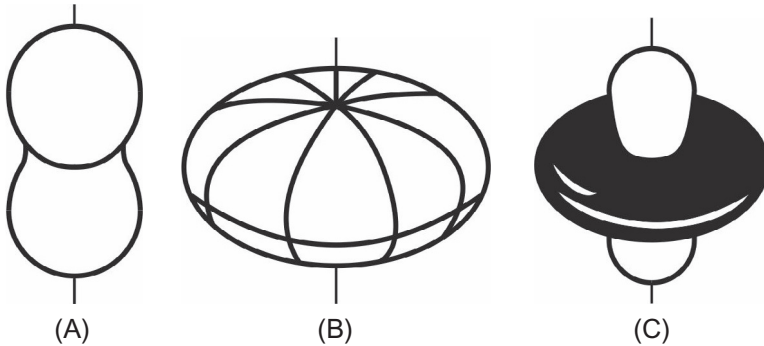


**Fig. 3.4** Different indicatrices for coefficient of thermal expansion when  $\alpha_{11} = \alpha_{22} \neq \alpha_{33}$ : (A)  $\alpha_{33} > \alpha_{11}$ ; (B)  $\alpha_{33} > \alpha_{11}$ ; (C)  $\alpha_{33} > 0$  and  $\alpha_{11} < 0$ ; *black* is negative part of  $\alpha$ .

However, in fact, only in cubic crystals do all diagonal components  $\alpha_{ij}$  have the same sign, while in the low-symmetry crystals the diagonal components  $\alpha_{11}$ ,  $\alpha_{22}$ , and  $\alpha_{33}$  can have not only different values, but also *different signs*. Therefore, instead of surfaces of second rank (ellipsoids), the real indicatrix of the thermal expansion coefficient is characterized by symmetrical but very complex surfaces, examples of which are given in Fig. 3.4. The most complex forms of the indicatrix of thermal expansion can be observed in the triclinic crystals, in which the matrix  $\alpha_{ij}$  cannot be reduced to diagonal form.

Thus, thermal expansion anisotropy reflects the complex distribution of polar-sensitive (i.e., hybridized ionic-covalent) interatomic bonds in the polar crystal, while simple ionic and covalent bonds in a crystal are usually characterized by an isotropic (scalar) thermal expansion coefficient.

**2. Physical nature of thermal expansion.** The change of volume (or dimensions) of a crystal with temperature alteration is a result of the *asymmetry* in the interaction law of neighboring particles. Quantitatively, the degree of volume ( $V$ ) change is characterized by the *volumetric* coefficient of thermal expansion ( $\alpha_V$ ). According to the conventional definition, this coefficient is a relative change of volume when a body is heating/cooling by one degree of temperature at a constant pressure  $p$ , and it can be written as:  $\alpha_V = (1/V) \cdot (\partial V / \partial T)_p$ . As noted, the thermal expansion of polar crystals might be anisotropic and can even be negative. This means that, when temperature increases, the crystal widens (or compresses) differently in various crystallographic directions. Therefore besides the volumetric expansion coefficient, the *linear* thermal expansion coefficient  $\alpha_l$  is widely used:  $\alpha_l = (1/l) \cdot (\partial l / \partial T)_p$ , where  $l$  is the linear dimension of the tested sample. The coefficient of thermal expansion can be presented as a matrix. Moreover, the sum of three diagonal matrix elements approximately equals to the volumetric expansion coefficient:  $\alpha_V \approx \alpha_1 + \alpha_2 + \alpha_3$ .

The investigation of thermal expansion is important in physics, because through this physical phenomenon the nature of interatomic bonds in crystals is manifested. At a temperature round 300 K, the coefficient of thermal expansion in various dielectrics and semiconductors lies in the range  $\alpha = +(1 - 50) \times 10^{-6} \text{ K}^{-1}$ . It has been established that for most crystals this coefficient is *inversely proportional* to the

melting temperature of crystal:  $\alpha \sim T_{\text{melt}}^{-1}$ . This result is quite natural, since the stronger the intermolecular bonds, the more difficult it is to change and wreck them, so the smaller the thermal expansion of crystal, the greater crystal melting point. The binding energy between atoms is characterized by the Debye temperature  $\theta_D$ , and, according to the Lindemann relation, the melting temperature is  $T_m \sim \theta_D^2$ . Hence, the approximate expression follows for the correlation of thermal expansion coefficient with Debye temperature:  $\alpha \sim \theta_D^{-2}$ , from which one can draw the conclusion that the coefficient  $\alpha$  is awaited to be positive quantity.

The change in the size of a crystal during heating or cooling is due to the difference in the laws of atom attraction and repulsion, when neighboring atoms or ions are displaced from their equilibrium position due to atoms' thermal vibrations. An example of  $\alpha(T)$  dependence is shown in Fig. 3.5A for magnesium oxide (MgO) crystal. In this figure, typical for the vast majority of solids, the coefficient  $\alpha$  increases with temperature rise according to the cubic law ( $\alpha \sim T^3$ , like heat capacity  $C$  changes with temperature). An explanation is that the change in volume or in shape of a solid body with temperature alteration is due to the *different nature* of forces acting between atoms.

The energy of atom interactions (Fig. 3.5B) consists of the attraction (negative) and the repulsion (positive) components. When the distance between interacting particles changes, these components vary in different ways. The repulsive force operates at a *very short distance* as the potential energy decreases with distance  $r$  between particles as  $r^{-8}$ – $r^{-12}$ . The nature of these forces is that electronic shells of neighboring atoms or ions can only penetrate each other a little. Conversely, the attraction forces operate at a *rather long distance*, as their energy changes with interatomic distance approximately like  $r^{-1}$ – $r^{-6}$  depending on the nature of attraction (i.e., on the type of atomic bonds: ionic, covalent, or molecular).

The total energy versus distance  $U(r)$  is always characterized by the *asymmetric* minimum (Fig. 3.5B). However, at the lowest temperature the bottom of the potential

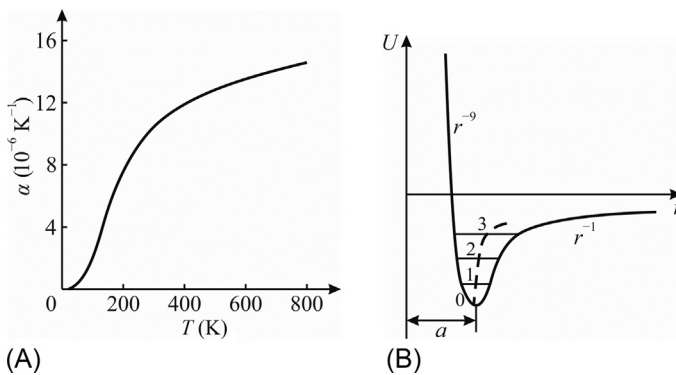


**Fig. 3.5** Typical thermal expansion in crystals: (A) Temperature dependence of expansion coefficient in MgO; (B) thermal expansion approximate explanation: the increase in amplitude of ion oscillations as temperature rise shown by horizontal lines 0-1-2-3 leads to gradual increase of lattice constant  $a$  shown by *dotted* line (in fact, roughly shown situation develops only in a narrow interval of interatomic distance  $r$ , very deep near the bottom of the energy minimum).

can be well approximated by a symmetric parabola, so that when temperature changes near absolute zero, no alteration in crystal size occurs:  $r = a$ . This explains why close to absolute zero the coefficient of thermal expansion for different solids tends to zero (Fig. 3.5A). However, as the amplitude of thermal oscillations increases, the middle distance between atoms (shown by the dotted line) increases: this is exactly the evident cause of thermal expansion.

Different energy levels are depicted in Fig. 3.5B by the horizontal lines 1-2-3, as far as the amplitude of thermal oscillations increases starting from 0; moreover, the displacement of oscillating atoms to the left becomes less than their displacement to the right. As a result, the time-average equilibrium position of the atom ( $a + x$ ) shown by a dotted line in Fig. 3.5B shifts to the right, and this effect becomes stronger the higher the energy of atom oscillation. In this argument, a special moment is the concept of time-average displacement of vibrating atoms  $\langle x \rangle$ , which actually determines the temperature dependence of the expansion coefficient. According to this description, the physical meaning of the thermal expansion coefficient is:

*The reciprocal value of the slope of a curve, which expresses the dependence of bonding energy on interatomic distance ( $a + x$ ) at the point corresponding to the time-average position of the atom:  $dU(a + x)/d(a + x) \sim 1/\alpha$ .*

Below the Debye temperature, the intensity of thermal oscillations increases nonlinearly, and in accordance with the theory discussed here the parameter  $\alpha(T)$  should be proportional to the specific heat  $C(T) \sim T^3$ . This dependence is found in most crystals of chemical elements and in a number of simple compounds, for example, halide salts and oxides. Moreover, the increase of thermal expansion coefficient with temperature rise corresponds to the Grüneisen law, which establishes the same temperature dependence for heat capacity  $C_V$  and the thermal expansion coefficient of solid dielectrics:  $\alpha = \gamma \cdot C_V / 3K$ . Here  $K$  is the modulus of bulk elasticity (all-round compression) and  $\gamma$  is the Grüneisen constant that enters the equation of state of a solid, being a measure of the anharmonicity of interatomic forces acting in a crystal. It is pertinent to note that, in fact, experimental data indicate some deviations from the Grüneisen law: at low temperatures,  $\gamma(T)$  decreases somewhat more rapidly than the cubic law predicts, while at high temperatures, instead of remaining constant value,  $\gamma(T)$  slowly grows.

An important correlation of temperature expansion with crystal's compressibility  $K$  should also be noted, which shows the degree of crystal deformation under *uniform* (hydrostatic) compression. The relationship  $\alpha_V \Leftrightarrow K$  is due to the fact that both the thermal action and the homogeneous compression are the *scalar actions* on a crystal, and therefore the crystal's reaction: its deformation in both cases relates to the crystal elastic properties and reflects the structure of internal atomic bonds. Therefore, it is not surprising that during further discussion as to the nature of *negative* thermal expansion coefficient, this property will be compared with the modulus of crystal bulk elasticity, which characterizes hydrostatic compression.

The point is that the *homogeneous* scalar actions (of temperature or pressure) possessing the highest symmetry of a sphere make it possible to identify experimentally the *intrinsic symmetry* of the internal bonds of a crystal. Moreover, other methods of

research tend to violate the intrinsic symmetry of any object under study. For instance, in the case of *vector* type action on a crystal (using temperature gradient, electrical, or other fields), as well as in the case of action by a second-rank *tensor* (for instance, by directional mechanical stress), the symmetry of these actions is put together with the symmetry of the crystal, so the characteristics of response distort the received information about the peculiarities of the inherent internal properties of a crystal.

For example, in the overwhelming majority of cases, crystals expand when being heated. This means that a crystal's thermal expansion coefficient is *positive* ( $\alpha > 0$ ), and this is thermodynamically connected with the circumstance that a crystal's entropy  $S$  *decreases* with homogeneous *increase* of pressure. However, in the polar crystals at relatively low temperatures a *negative* value of  $\alpha(T)$  may be observed, which thermodynamically corresponds to the peculiar case when the crystal's entropy *increases* with rising pressure (it will be further shown that this is possible only for *configurational* entropy).

Therefore, by investigation of thermal expansion, one can draw a conclusion about the nature of atomic interactions in a crystal. It will be further shown that the temperature region of negative  $\alpha(T)$  corresponds to the processes of structural ordering of the peculiar polar-sensitive bonds in the polar crystals that arise as a result of the compensation of atom electronegativity.

**3. Negative thermal deformation.** As already mentioned (and this is a main subject of this discussion), in the polar crystals in a certain temperature range the parameter  $\alpha(T)$  takes a negative value; moreover, the line  $\alpha(T)$  twice passes through a zero in the temperature interval of 10–100 K before it exhibits the typical growth according to the law  $\alpha \sim T^3$  that is usual for most crystals.

Typical for polar crystals,  $\alpha(T)$  dependence is shown in Fig. 3.6A by the examples of the hexagonal polar crystal ZnO, having a wurtzite structure with  $6m$  symmetry, and the cubic crystal HgTe, which has a polar sphalerite structure of  $43m$  symmetry. It should

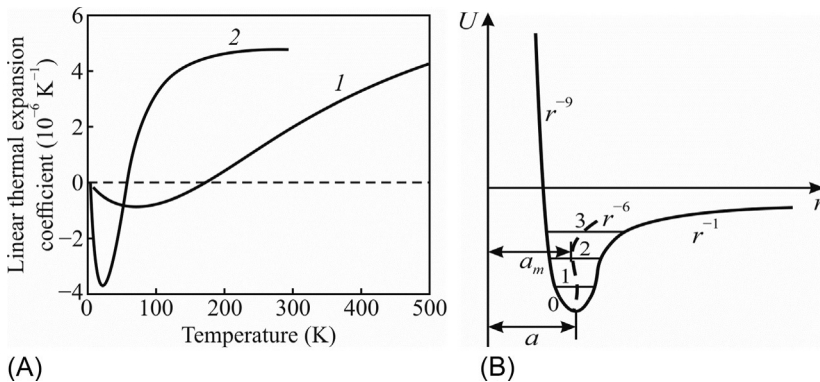


**Fig. 3.6** Thermal expansion in polar crystals: (A)  $\alpha(T)$  dependence in ZnO (1) and in HgTe (2); (B) negative thermal expansion symbolic explanation: in fact, the situation shown develops deeply near the very bottom of the energy minimum.

be noted that, at very low temperatures, their thermal expansion coefficient again becomes positive, so it approaches zero from its *positive* side, although this is invisible in the rough scale of Fig. 3.6A. In this case, the negative contribution to  $\alpha(T)$  disappears: quantum oscillations break any ordering of polar sensitive bonds in the crystal lattice (as in the virtual ferroelectrics  $\text{KTaO}_3$  and  $\text{SrTiO}_3$ ).

The formal explanation of the negative thermal expansion coefficient (which at lower temperatures is typical for any polar crystal) is given in Fig. 3.6B (note that the roughly shown situation develops only in a narrow interval of interatomic distance  $r$ , located very deep near the bottom of the energy minimum). A special characteristic of ion attractions in the polar crystals occurs due to hybridization of ionic-covalent bonds, which becomes so complicated that it leads to a *specific profile* of attraction energy in its dependence on the vicinity of interatomic distance  $r = a \pm x$ . The anharmonic vibrations in the hybridized covalent-ionic bonds become dependent on complex laws of vibration energy; as a result, the ion mutual displacement average over time changes its sign: first it decreases ( $r = a - x$ ), reaching a minimum, but then it increases ( $r = a + x$ ). All this occurs below the Debye temperature, when the lattice vibrations obey the quantum laws. As a result, when temperature increases, the crystal, after initial small growth, next compresses (levels 0-1-2 in Fig. 3.6B) so the lattice parameter reaches the value  $a_m$ . Only then can one see (on levels 2-3 and higher) the temperature coefficient increase:  $\alpha \sim T^3$ , which is usual for temperature expansion coefficient of any solid. The points of the dotted curve in Fig. 3.6B when  $r = a_m$  correspond to a minimum of the  $\alpha(T)$  dependence seen in Fig. 3.6A.

Table 3.1 gives some experimental data regarding the temperature minimum of the thermal expansion coefficient in the polar substances. In most cases,  $\alpha_{min}$  is about 20% of its value in the saturation region of the characteristic  $\alpha(T)$ . The effect of negative expansion is strongly pronounced in the mercury telluride crystal due to its special structure, which also corresponds to the very small sound velocity. As a comparison, in Table 3.1 the low-temperature properties of ice are given, although the polar bond arrangement in the  $\text{H}_2\text{O}$  crystal is substantially different.

**Table 3.1** Minimal value of thermal expansion coefficient ( $\alpha_{min}$ ), its value ( $\alpha_{300}$ ) at temperatures near 300 K, and the temperature  $T_{\alpha_{min}}$  at which  $\alpha_{min}$  is observed in different polar crystals.

Material	$\alpha_{min} \cdot 10^{-6} \text{ (K}^{-1}\text{)}$	$T_{\alpha_{min}} \text{ (K)}$	$\alpha_{300} \cdot 10^{-6} \text{ (K}^{-1}\text{)}$
HgTe	-8	25	8
InSb	-1.4	27	1
ZnO	-1.2	75	5
InAs	-0.9	35	-
InP	-0.5	45	8
$\text{H}_2\text{O}$	-8	40	-
Fused quartz	-9	40	6

It is interesting to note that fused quartz also belongs to the substances with negative values of  $\alpha$  at low temperatures. In this material, pronounced anisotropic polar properties of crystalline quartz are averaged; as a result  $\alpha_{min} = -9 \cdot 10^{-6} \text{ K}^{-1}$  at a temperature of about 40 K, which is 1.5 times higher than  $\alpha_{300} = +6 \cdot 10^{-6} \text{ K}^{-1}$ . After, at higher temperatures, fused quartz  $\alpha$  changes its sign to positive near 190 K. It should be noted that a small minimum at 550–600 K is also seen in the  $\alpha(T)$  characteristic in the region of the  $\alpha$ - $\beta$  quartz transition. It can be concluded that the negative value of  $\alpha$  is a general property of substances with *small coordination number* (with open structure), which are characterized by the tetrahedral arrangement of atoms: in them the ordering of polar-sensitive bonds becomes easier. In contrast, in the structures with a tight packing, the thermal expansion coefficient is always positive.

Since here the properties of polar crystals are discussed, a convincing example that shows the direct relationship of a negative expansion coefficient with structural ordering is given. This is the well-studied barium titanate crystal, passing while cooling from its nonpolar to the polar phase at a temperature of  $\sim 400$  K. During the phase transition from the disordered paraelectric phase into the ordered polar phase, the volume of the  $\text{BaTiO}_3$  crystal *increases* while configurational entropy decreases due to polar fluctuation suppression (which is peculiar to the disordered paraelectric phase). As we have measured, in  $\alpha(T)$  dependence the minimum is observed, i.e., the negative thermal expansion is seen in a certain temperature range, and this is characteristic of many ferroelectrics (Fig. 3.7).

Dynamical structural disordering in  $\text{BaTiO}_3$ , which has a cubic structure, is the internal polarity fluctuations along four symmetry axes of third order [111]-type. The hydrostatic pressure applied to  $\text{BaTiO}_3$  below its Curie point (i.e., in its polar phase) returns this crystal to its paraelectric (nonpolar) phase, in which, naturally, the configurational entropy is larger. Another well-known example of the connection of configurational entropy with pressure is the phase transition in  $\text{H}_2\text{O}$  at 273 K: the freezing of water leads to ice, which has increased volume, but externally applied pressure returns ice into a disordered structure of water with more pronounced configuration entropy due to polar phase fluctuations.

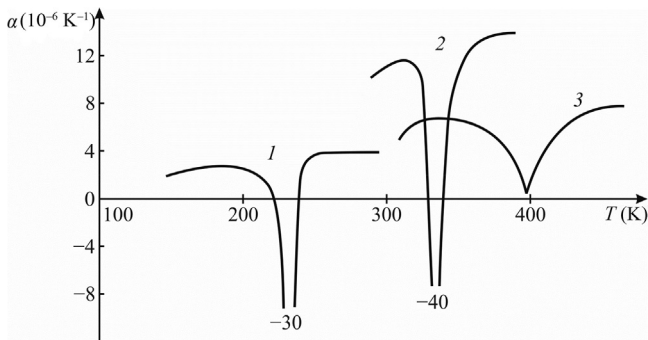


**Fig. 3.7** Thermal expansion coefficient at phase transitions from high-temperature disordered phase into low-temperature ordered phase: 1—KDP; 2—TGS; 3—polycrystalline  $\text{BaTiO}_3$ .

Thus, when discussing negative thermal deformation in the polar crystals, one should pay attention to the fact that  $\alpha(T)$  takes a negative value in the vicinity of ferroelectric phase transitions, since the volume of the low-temperature *ordered* phase becomes greater than the volume of the same crystal but in its *disordered* phase (however, in the case of antiferroelectric phase transitions, the volume of the antipolar phase, on the contrary, decreases; correspondingly, at the phase transition  $\alpha(T)$  shows a maximum).

From the point of crystal lattice dynamics, a negative value of  $\alpha(T)$  corresponds to such features in the polar crystal phonon spectrum that lead to a negative value of the Grüneisen constant. Since this effect is observed at low temperatures, such singularities are due to the *acoustic* vibrational modes; in polar-sensitive crystals the branch of transverse acoustic oscillations bends downward when it approaches the boundary of the Brillouin zone. Therefore this branch can be represented as two parts: the Debye-type mode in the beginning of the spectrum and the Einstein-type mode at its end, exactly the last part of the transverse acoustic branch near the boundary of the Brillouin zone corresponding to negative  $\alpha(T)$ .

In connection with the negative  $\alpha(T)$  that is seen at low temperatures in the polar crystals, it is important to keep in mind other cases of negative thermal expansion coefficient observations. In dielectrics and semiconductors, such cases are known among the crystals that have *layered* and *chain* structures [6].

Typical examples of **chain crystals** are the rhombohedral tellurium and selenium, which, among other things, refer to piezoelectrics of polar-neutral class 32 (the same as quartz). In the Te crystal the transversal thermal expansion coefficient is positive:  $\alpha_1 = \alpha_2 = +27 \cdot 10^{-6} \text{ K}^{-1}$ , while along the chains this coefficient is *negative*:  $\alpha_3 = -1.6 \cdot 10^{-6} \text{ K}^{-1}$ . In Te and Se crystals, the helical chains Te-Te (or Se-Se) are elongated parallel to axis 3. Pronounced anisotropy and a negative value of  $\alpha_3$  are due to the fact that interatomic bonds along the chains are much stronger than the interaction between chains. Therefore, with heating, crystal contracts in the direction 3 but expands in perpendicular directions.

An example of a **layered crystal** is the hexagonal graphite, in which in the direction perpendicular to the plane of layers (where interatomic bonds are weak), a rather big and *positive* thermal displacement of atoms is observed, so in this direction graphite expands with heating:  $\alpha_3 = +30 \cdot 10^{-6} \text{ K}^{-1}$ . However, *along the layers of graphite* (where atomic bonds are very strong) at lower temperatures a *negative* thermal expansion coefficient is seen:  $\alpha_1 = \alpha_2 = -5 \cdot 10^{-6} \text{ K}^{-1}$ , i.e., in this plane, while heating, graphite becomes more compressed. In the graphite layers, the covalent bonds are so strong that at low temperatures thermal vibrations can be excited mostly perpendicularly to the rigid layers (along axis 3). In this case, lateral compression appears, characterized by a negative  $\alpha_1 = \alpha_2$  along the layers. At low temperatures (up to about 300 K), in the graphite layers the transverse acoustic vibrations dominate, being polarized perpendicularly to layers of carbon: this corresponds to negative expansion. Only at a temperature of 650 K, parameters  $\alpha_1(T) = \alpha_2(T)$  acquire positive value—when the intensity of thermal movement becomes significant. Note that a large negative coefficient of thermal expansion is observed also in graphene and nanotubes.

Thus, through temperature dependence on thermal expansion, the features of crystal interatomic bonds are manifested. In the layered crystals positive thermal displacements of atoms are seen perpendicularly to the planes of layers, while in the chain crystals, perpendicularly to the axis of chains. In both cases, in the directions of strong bonds the coefficient of thermal expansion is negative. The conclusion is obvious: *the stronger the interatomic bond, the smaller the thermal expansion coefficient—down to its negative value.*

By comparing these data with polar crystal temperature properties, there is a reason to believe that when temperature decreases below a certain limit, the intensity of thermal oscillations becomes so weak that an inner ordering of polar bonds starts that gradually leads to their strengthening. As a result, the widening of a crystal with temperature decrease results in the negative sign of thermal expansion coefficient. The foregoing makes it possible to affirm that a negative value of thermal expansion coefficient at low temperatures in the polar crystals is due to a partial ordering of polar-sensitive bonds.

These considerations provide a basis for explanation of the negative expansion coefficient in the polar crystals at low temperatures: it is spontaneous ordering of polar-sensitive bonds when thermal oscillations in crystal weaken. In this connection, it is necessary to compare the uniform temperature scalar action (which leads to the crystal widening or compression), and the uniform scalar action of a pressure (hydrostatic action). By different means, both effects give rise to the same result: a change in crystal volume. As is known from thermodynamics, the thermal expansion coefficient is related to the change of entropy  $S$  with pressure:  $\alpha_V = -(dS/dP)_T/V$ . In this way, the *negative* value of  $\alpha(T)$  corresponds to this unusual case when entropy *increases* with increasing pressure. It is unusual in that entropy usually *decreases* with pressure rise, corresponding to the common case of a *positive* thermal expansion coefficient.

Thus, a possible explanation of the negative thermal expansion coefficient is reduced to finding out the reason why entropy can increase with uniform pressure rise. The fact is that entropy depends not only on dynamic characteristics of particles (their **velocity** or **momentum**), but also depends on particles' *equiprobable locations*: It is exactly this factor that determines the *configurational entropy*, i.e., the number of ways of **particles** being arranged, maintaining specific system properties. With increasing pressure *only configurational entropy increases*.

Therefore, comparison of two different scalar influences on thermal and elastic properties of polar crystals shows a compelling correlation: negative thermal expansion is observed, if the increase of homogeneous pressure *increases* configurational entropy (which, in turn, is due to the presence of metastable microscopic states) [7]. It can be argued that it is precisely those states that correspond to the ambiguity in the *orientations* of internal polarity. Indeed, polar bond ordering leads to an increase of crystal volume and to a decrease of configurational entropy. The fact is that hydrostatic compression suppresses the ordering processes and thereby increases entropy.

From the Grüneisen relation ( $\alpha = \gamma C/3K$ ) and taking into account the fact that volumetric compressibility  $K$  only very slightly varies with temperature, while heat capacity temperature dependence is strong:  $C \sim T^3$ , the negative value of  $\alpha$  can be related to temperature variation of  $\gamma$  up to its negative value. Crystal lattice dynamics,

in principle, make it possible to calculate the Grüneisen parameter as a dependence of normal mode frequencies on volume:  $\gamma = -\partial(\ln\omega_D)/\partial(\ln V)$ , where  $\omega_D$  is the Debye frequency [8]. Calculations shows that at low temperatures the Grüneisen parameter  $\gamma$  can decrease and even becomes negative in the case of very small Debye frequency, as for example in the RbI crystal (but this is the only exception [6]).

**4. Negative thermal expansion in semiconductors.** As can be seen from Table 3.1, many polar crystals are semiconductors. In fact, the compounds of the  $A^{III}B^V$  group have a sphalerite structure and they belong to the piezoelectrics, while the semiconductors of the  $A^{II}B^{VI}$  group are pyroelectrics. It is pertinent to note that polar semiconductors are *direct band* semiconductors, while monoatomic semiconductors of diamond symmetry are *nondirect band* semiconductors. By the way, it should be noted that at low temperatures (where *negative*  $\alpha(T)$  is seen) the concentration of free charge carriers in semiconductors is very small and the charge carriers cannot screen possible polar fluctuations in the structure. Therefore, the cause of the negative thermal expansion observed at low temperatures must be sought not in electrical conductivity but in the phenomenon of electrical polarization.

In connection with the foregoing, the presence of a low-temperature minimum in the coefficient of thermal expansion is not surprising. With temperature decrease, the thermal chaotic motion freezes, and existing polar bonds become ordered (configurational entropy decreases), so the crystal occupies a larger volume, demonstrating a negative  $\alpha(T)$ . However, with further cooling to a very low temperature, inescapable quantum oscillations in the crystal lattice prevent further ordering of the fluctuating polarity, so with the approach to 0 K the crystal again compresses a little (in just the same way, the quantum oscillations impede the transition to the ferroelectric phase in the *virtual ferroelectrics*  $KTaO_3$  and  $SrTiO_3$ ).

If in the *polar*  $A^{III}B^V$  and  $A^{II}B^{VI}$  semiconductors, which have noncentrosymmetric structure, the minimum of  $\alpha(T)$  can be considered as explained earlier, then for the *atomic* semiconductors of diamond type, this minimum needs a special explanation. As seen in Fig. 3.8, in germanium a small minimum of  $\alpha(T)$  is observed at a temperature of about 35 K ( $\sim 0.1\theta_D$ ), while in silicon a much deeper minimum  $\alpha(T)$  is seen at a temperature near 60 K ( $\sim 0.1\theta_D$ ).

At first glance, it is difficult to suspect any natural polarity in the semiconductors consisting of only one chemical element and, naturally, possessing only covalent bonds. Nevertheless, the single element polar crystals of tellurium and selenium mentioned earlier even have a pronounced piezoelectric effect and belong to the hexagonal symmetry class 32 (like quartz). The probable reason for this internal polarity lies in significant complications in covalent bond distributions in their structure.

As was shown theoretically [7], the negative coefficient of thermal expansion is due to change in *configurational entropy*. Obviously, it is necessary to indicate which kind of ordering process is possible in crystals of the diamond type. Here it is assumed that the reason for negative  $\alpha(T)$  in germanium and silicon is the fluctuations in partial ordering of the *hexagonal* polar phase when double bonds are mixed with single covalent bonds. This assumption is based on the fact of the existence of the *hexagonal diamond*: initially it was discovered in meteorites but later was synthesized in the laboratory as well [8].

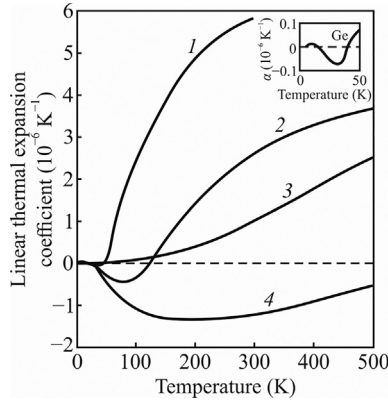


**Fig. 3.8** Thermal expansion coefficient in semiconductors [9]: 1—Ge, 2—Si, 3—C-diamond, 4—C-graphite.

Obtained in special technologic conditions, the hexagonal phase can remain stable only in the super hard and super stable diamond ( $\theta_D \sim 1900$  K and  $T_{melting} \sim 4000$  K), and it can be observed throughout the temperature range due to a very small concentration of charge carriers, which cannot screen any possible polar interactions. However, in silicon ( $\theta_D \sim 600$  K and  $T_{melting} \sim 1700$  K) and in germanium ( $\theta_D \sim 360$  K and  $T_{melting} \sim 1200$  K) the hexagonal phase apparently can exist only in a form of polar fluctuations of [111]-type directions; at that, any polar interactions are screened by the charge carriers. Nevertheless, the direction of natural growth of these crystals from their melt is polar in the [111] direction; moreover, these crystals can float in their own melt (like ice floats in water), which indicates the *decrease* of material density during crystallization. The same property is possessed, for example, by gallium arsenide, which is a polar crystal of sphalerite symmetry. The hexagonal structural feature that accidentally arises in diamond, and probably weakly fluctuating in silicon and germanium, is fully implemented in graphite and graphene, the cellular planes of which are characterized by *negative*  $\alpha_1 = \alpha_2$  with an explicit minimum at a temperature of 180 K ( $\sim 0.1\theta_D$ ; Fig. 3.8). As mentioned earlier, the crosswise direction to the layers of graphite is characterized by a positive  $\alpha_3(T)$ .

It is not by chance that curve 4, as shown in Fig. 3.8, demonstrates the thermal expansion  $\alpha(T)$  in the plane of graphite, in which at a temperature of about 200 K the minima are seen:  $\alpha_{1min} = \alpha_{2min} = -1.5 \times 10^{-6} \text{ K}^{-1}$ . The structural basis in graphite planes is carbon hexagons, in which three single covalent bonds alternate with three double covalent bonds. It should be noted that a stronger C=C double bond is much shorter than a single C—C bond, and it can be assumed that thermal motion in the crystal, arising with increasing temperature from absolute zero, stimulates the formation and hardening of double covalent bonds. In favor of this assumption, it needs to be noted that the temperature minimum of the thermal expansion coefficient in *graphene* is even deeper than in graphite:  $\alpha_{min} = -5.5 \times 10^{-6} \text{ K}^{-1}$  seen at 300 K, and in carbon *nanotubes* at temperature 240 K it reaches  $\alpha_{min} = -9.5 \times 10^{-6} \text{ K}^{-1}$ . One could

assume that, in general, in crystals having negative thermal expansion at low temperatures, a stronger (resulting in compression) covalent bond formation occurs.

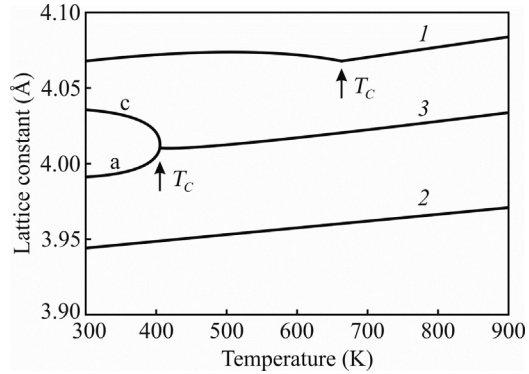
The study of the features of thermal expansion in various crystals has technical and scientific interest. In the vast majority of cases, as temperature rises the solid expands. Therefore, the exceptional case of negative expansion coefficient has a particular interest. The physical nature of negative thermal expansion in polar crystals corresponds to the special case when entropy increases with increasing pressure, which is possible only in the case of configurational entropy. In turn, the presence of this entropy testifies to the processes of structural ordering-disordering in the crystal. The model under discussion, based on the asymmetry in the electronic density distribution along atomic bonds, is free from the assumption of any internal electrical field existence in the crystals. Although polar-sensitive bonding is not a result of an internal field in crystal, it can provide an electrical response to the nonelectrical external action, which is impossible in the centrosymmetric crystals. It is assumed that the physical basis of natural polarity is a distinction in the electronegativity of ions forming a crystal. Since the temperature minimum of the thermal expansion coefficient in the polar crystals is explained by the polar bonds ordering at low temperatures, a proposed concept can be extended to nonpolar semiconductors. In them, too, it can be supposed that the polar tendencies fluctuating in the structure become consolidated at low temperatures.

Thus, in the polar crystals at low temperatures the thermal expansion coefficient  $\alpha$  changes its sign twice, forming a region of  $\alpha$  negative values. The nature of the negative thermal expansion is explained by partial ordering of the polar-sensitive bonds at low temperatures, leading to their long-range interaction and, as a result, to the flattening of the transverse acoustic mode of lattice vibrations near the boundary of the Brillouin zone. The previously described features of thermal expansion in both conventional and polar-sensitive crystals can be used in the development of new technologies for microelectronic materials.

**5. Lattice strain engineering using polar-sensitive films** is based not only on the mismatch of thermal expansion, but to a greater degree on the difference of permanent lattices of the film and the substrate. As known, the occurrence of polarity in a crystal is accompanied by anisotropic change in its size: elongation along the axis of polarization and compression in a perpendicular direction (moreover, the volume of ferroelectrics increases but in the antiferroelectrics it decreases). According to the principle of Le Chatelier, if during formation of the polar phase one of the crystal sizes increases, so a forced change in this size of crystal should lead to a change in its polar state. For example, in the ferroelectrics their phase transition temperature should change [5].

In the functional dielectrics, which possess polar-sensitive properties, the coupling between polarization and mechanical strain is strongly manifested. The external mechanical action not only leads to a piezoelectric effect but can also change the temperature of the ferroelectric phase transition  $T_C$ . For example, hydrostatic pressure can lower the phase transition point by tens of degrees and greatly change the dielectric properties of a bulk ferroelectric. It is important to note that much greater possibilities of mechanical control by polar crystal parameters appear in the epitaxial thin films,

**Fig. 3.9** Temperature dependence of lattice parameters of strained BaTiO<sub>3</sub> film out-of-plane (1) and in-plane (2) in comparison with single crystal BaTiO<sub>3</sub> (3).



which allow *large* biaxial (plane) deformations without film destruction. The highly perfect ferroelectric thin films, which are synthesized on suitable substrates, demonstrate that *strained* ferroelectric thin films can exhibit properties that are greatly superior to the possibilities of their bulk.

This phenomenon may be demonstrated by an example of the most well-studied ferroelectric—barium titanate (Fig. 3.9). The *epitaxial* films of BaTiO<sub>3</sub> were deposited at high temperature on the isomorphic substrate GdScO<sub>3</sub>, which have the same perovskite structure but different lattice parameters. The mismatch in the lattice parameters leads to a forced biaxial compression of the film that leads to increase of its deformation perpendicularly to its plane and contributes to a more stable polarized state of BaTiO<sub>3</sub>, which persists at much higher temperatures.

The biaxial strain can be defined as  $x_s = (a_{||} - a_0)/a_0$ , where  $a_0$  is a lattice parameter of ferroelectric material in its cubic state under stress-free conditions (free-standing) and  $a_{||} = a_{subs}$  is an in-plane lattice parameter of biaxially strained ferroelectric film. The limit of strain can be given by the Griffith criteria for crack formation:  $x_s = (1 - \nu) \cdot (2\gamma / (\pi \cdot E \cdot t))$ , where  $\nu$  is Poisson's ratio,  $\gamma$  is surface energy,  $E$  is Young's modulus, and  $t$  is film thickness (biaxial strain  $x_s$  arises from lattice mismatch with underlying substrate for fully coherent epitaxial growth). With this limit, it is quite possible to largely control the properties of polar-sensitive materials. In addition to the preceding example with the Curie point temperature shift in barium titanate, another impressive example is the conversion of the film virtual ferroelectric strontium titanate into a ferroelectric film, with a sufficiently high Curie temperature (increased from 35 to 300 K). Thus, with biaxial stressed films such materials were obtained that, in the bulk state, are not ferroelectrics at any temperature. Biaxial deformations of films make it possible to increase the Curie point by hundreds of degrees with a simultaneous increase in polarization in the direction perpendicular to the film thickness. Such films have great advantages for use in microwave technology, as will be shown later in Chapter 6.

In a crystal's strain engineering, it is necessary to use only high-quality films, obtained as a rule by molecular-beam epitaxy: the growth of such film on a substrate means the arrangement of the atoms in the film is inherited from the arrangement of

the atoms in the substrate. This technology makes it possible to convert a virtual ferroelectric into a ferroelectric, potential ferromagnetics into ferromagnetics, and even to obtain ferroelectric and ferromagnetic properties together in one film.

Summing up, it should be noted that biaxial deformations, created for controlling the properties of polar-sensitive films, can be obtained by essential mismatch of lattice parameters between the film and the substrate, and their different thermal expansion coefficient. (It should be recalled that bulk crystals usually break down long before the deformation of percentage levels is reached.) Deformations reaching a value of several percent have a great influence on the properties of polar-sensitive thin films and superlattices. Coherent epitaxial films have the advantage that they have very few dislocations (deformation field around the dislocations locally changes the properties of a film). In addition, epitaxial films allow creation of superlattices: both from layers of different polar-sensitive dielectrics, and alternating layers of polar dielectrics and ferromagnetics, thus obtaining films with properties that are not found in natural materials.

### 3.3 Heat transfer in polar-sensitive crystals

Thermal conductivity is a heat transfer by material particles (molecules, atoms, electrons) in the course of their chaotic thermal movement. In a steady state, the flow of thermal energy transferred by heat conduction is proportional to the temperature gradient:  $\Delta Q = -\lambda \text{ grad } T$ . This relation is known as Fourier's heat conduction law, where  $\Delta Q$  is the heat flux vector, the magnitude of which is the amount of energy that passes in a unit time through a unit area, oriented perpendicularly to the direction of heat transfer;  $T$  is temperature and  $\lambda$  is the coefficient of thermal conductivity. In the anisotropic crystals, the thermal conductivity coefficient  $\lambda_{ij}$ , which links the heat flux vector to the temperature gradient vector, is a symmetric material tensor of second rank. Like crystal's permittivity  $\epsilon_{ij}$  or conductivity  $\sigma_{ij}$ , the tensor  $\lambda_{ij}$  can be described by a second-order surface, which usually has the form of an ellipsoid.

Various solids can have quite different thermal conductivities that can vary by thousands of times. Thermal energy can be transferred predominantly by electrons (in metals) and phonons (in dielectrics and semiconductors). In metals, electronic thermal conductivity is large:  $\lambda = 400\text{--}200 \text{ W}/(\text{m K})$  at 300 K. In semiconductors, heat transfer is carried out basically by phonons; it is greatly dependent on temperature: at 300 K usually  $\lambda = 150\text{--}50 \text{ W}/(\text{m K})$ .

In the nonpolar *covalent* dielectrics, thermal conductivity also has a phonon nature with  $\lambda = 80\text{--}30 \text{ W}/(\text{m K})$ ; however, newly developed aluminum nitride AlN shows  $\lambda = 180 \text{ W}/(\text{m K})$  while diamond at 300 K has  $\lambda > 1000 \text{ W}/(\text{m K})$ . All the mentioned dielectrics have a high Debye temperature and, correspondingly, large velocity of sound waves. The relatively high thermal conductivity in covalent crystals is due to the fact that the heat carriers in them (short-wave acoustic phonons located near the boundary of the Brillouin zone) practically do not interact with optical phonons.

In the majority of the *ionic* dielectrics, the phonon type of thermal conductivity at normal temperature is not only significantly less than in metals, but is smaller than in

covalent crystals:  $\lambda = 15\text{--}10\text{ W/(m K)}$ ). It can be assumed that ionic bonding in these crystals contributes to *deceleration* of thermal phonons through the mechanism of their interaction with optical phonons. Such interaction is even more enhanced in the polar-sensitive (noncentrosymmetric) crystals, in which interatomic bonding has a *mixed ionic-covalent* character, so thermal conductivity of these crystals at 300 K usually is less than  $\lambda = 10\text{ W/(m K)}$ .

Heat transfer is phenomenologically described in nonequilibrium thermodynamics, while in the microscopic theory heat transfer in dielectrics is determined mainly by the phonon mutual scattering. At normal temperatures, heat transfer is carried out by *shortwave phonons*, the wavelength of which is commensurable with the parameter of crystal lattices. Therefore, polar-sensitive bonds, which characterize features of noncentrosymmetric crystals, should clearly manifest themselves in their heat transfer.

Indeed, the difference in thermal conductivity  $\lambda$  of polar and nonpolar crystals follows clearly from the comparison with the coefficient of thermal expansion. Fig. 3.10A demonstrates the dependence of  $\lambda$  on  $\alpha^2$  (the causal relationship of these parameters will be explained shortly).

In further discussions of *heat transfer* mechanisms, two parameters are used: *thermal conductivity* ( $\lambda$ ) and *thermal diffusivity* ( $\xi$ ). The first of these parameters is important for assessing *technical properties* of electronics materials: for example, to predict possible overheating of this or that structure. The second parameter is better to use in the *interpretation* of experimental data. Both of these parameters in the polar-sensitive crystals are noticeably less than in common crystalline dielectrics and semiconductors.

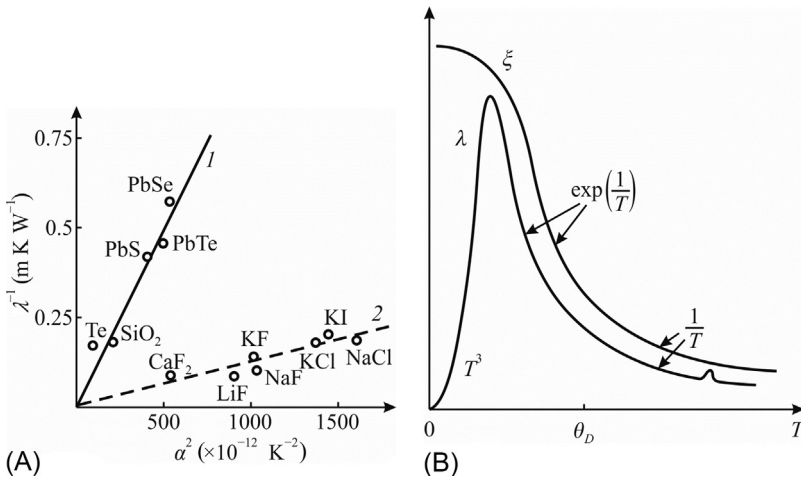


**Fig. 3.10** Main features of heat transfer in crystals: (A) Comparison of thermal resistance in polar and nonpolar crystals at  $\sim 300\text{ K}$ ; (B) comparison of temperature dependence of thermal diffusivity  $\xi$  and thermal conductivity  $\lambda$ .

Comparing the research methods of  $\lambda$  and  $\xi$  investigation, the following should be noted.

**1. Thermal conductivity  $\lambda$ ,** as shown by kinetic theory, depends on crystal specific heat  $C$ , phonon average free path  $\langle l \rangle$  (i.e., between phonon collision with another phonon), and average velocity  $v$  of phonons:  $\lambda = (1/3) \cdot v \cdot l = (1/3) C \cdot v^2 \cdot \tau$ , where  $\tau$  is free path time. It can be shown that the average free path time is determined by the *square* of the anharmonicity coefficient. Therefore, thermal conductivity is related to the thermal expansion coefficient, which also is determined by the coefficient of anharmonicity, but by its *first degree*. Measurements really show that the *inverse* thermal conductivity is proportional to the square of the thermal expansion coefficient:  $1/\lambda \sim \alpha^2$ . Experimental data of different dielectrics and semiconductor comparisons (polar and nonpolar) show that such a relationship really exists (Fig. 3.10A). On line 2, which has smaller slope, the crystals with increased thermal conductivity are grouped: they have predominantly covalent or ionic bonding. The upper curve 1 with larger slope characterizes the crystals with reduced thermal conductivity: they are polar-sensitive crystals, in which mixed ionic-covalent bonds predominate. The ratio  $1/\lambda \sim \alpha^2$  is determined by peculiarities of the interatomic bonds. In this case, it can be considered that crystals with large expansion coefficient have much smaller thermal conductivity.

It is important to note that temperature dependence of thermal conductivity follows rather a complicated law (Fig. 3.10B), since it is determined by the *product* of specific heat  $C$  and phonon average free path  $\langle l \rangle$ . As a result, at low temperatures thermal conductivity *tends to zero* and with rising temperature  $\lambda(T)$  rapidly increases, following the Debye heat capacity law:  $C \sim T^3$ . At that,  $\lambda(T)$  dependence reaches a maximum at temperature  $T \sim 0.1\theta_D$ , and only then decreases in connection with temperature dependence of the average free path of thermal phonons. It should also be noted that when studying anomalies of thermal conductivity (common in polar crystals, especially near phase transitions), the true form of the anomalies  $\lambda(T)$  can be somewhat distorted by an unavoidable *temperature gradient* during measurements. In this respect, other parameter temperature dependence—the thermal diffusivity  $\xi(T)$ —can be studied with greater accuracy.

**2. Thermal diffusivity coefficient  $\xi$**  can be defined as **thermal conductivity** divided by **density**  $\rho$  and by **specific heat** at constant pressure:  $\xi = \lambda/(C_p \cdot \rho)$  ( $\text{m}^2/\text{s}$ ). It measures the rate of heat transfer of a material from its hot side to the cold side. In a sense, thermal diffusivity is a measure of *thermal inertia*; in a substance with high thermal diffusivity, the heat moves rapidly through it, because this substance conducts heat quickly relative to its volumetric heat capacity. At that, thermal diffusivity is determined mainly by the average free path  $\langle l \rangle$  of thermal phonons propagating in the crystal ( $\xi \sim \langle l \rangle$ ). At very low temperatures, the density of phonons is so small that they do not interact, and their free path is large, depending mostly on macroscopic-size defects, including crystal boundaries. Moreover, the parameter  $\xi$  remains nearly constant, keeping its greatest value (Fig. 3.10B). However, it decreases hundreds of times as temperature increases: the point is that the frequency of phonon interactions becomes larger as it is determined by anharmonicity of lattice vibrations, which is measured by the Grüneisen parameter  $\gamma$ .

Thus, average free path of phonons is  $\langle l \rangle \sim a/(\alpha \cdot \gamma \cdot T)$ , where  $a$  is lattice constant and  $\alpha$  is thermal expansion coefficient. As temperature increases, thermal diffusivity falls very fast:  $\xi(T) \sim \langle l \rangle \sim \exp(T^{-1})$ , since the average free path of phonons becomes limited by the interphonon Umklapp processes ( $U$ -processes), which occur with a loss of quasimomentum. Next, with a subsequent increase in temperature (when  $T > \theta_D$ ), in the temperature interval that will be discussed shortly, the lowering of  $\xi(T)$  dependence follows the Aiken law:  $\xi(T) \sim T^{-1}$ .

To identify physical mechanisms of heat transfer, the analysis of *thermal diffusivity* temperature dependence seems much simpler than the analysis of thermal conductivity. For example, in crystals of nonpolar silicon crystal and polar quartz, the speed of sound (determined by long-wave phonons) is about the same:  $\sim 5000$  m/s. However, the speed of *shortwave thermal phonons* differs sharply: at temperature 300 K in silicon  $\xi = 88$  mm<sup>2</sup>/s, while in quartz  $\xi = 1.4$  mm<sup>2</sup>/s. Therefore, the coefficient of thermal diffusion is a stronger criterion for phonon kinetics: it characterizes not a total heat flux but the kinetic characteristics of energy carriers. Its *upper limit* is determined by the so-called Umklapp processes ( $U$ -processes), while the *lower boundary* corresponds to amorphous solids, where energy transfer occurs only between the nearest neighboring cells. It should be noted that such boundaries are difficult to indicate for the thermal conductivity coefficient, since there are no restrictions on the density of energy states.

**3. Thermal transfer features in polar-sensitive crystals.** In any dielectrics and semiconductors, the main contribution to thermal conductivity is given by the acoustic phonons, in which group velocity slows down when the acoustic branch approaches to the boundary of the Brillouin zone. However, the main feature of polar crystals (as all of them are piezoelectrics!) is that the *acoustic phonons are associated with optical phonons*. If optical phonons have large spatial dispersion, they can make a significant *positive* contribution to the heat transfer. But in most cases spatial dispersion is small, so the optical phonons give an additional contribution only in the phonon scattering, which substantially *decreases* thermal conductivity. Exactly this decrease (due to inhibitory interference of optical phonons) explains the difference in thermal conductivity of polar and nonpolar crystals, shown in Fig. 3.10A.

As already indicated, thermal energy in dielectrics is transferred by the short-length lattice waves (“heat waves”), the propagation velocity in crystal of which is significantly less as compared with the long-length “sound waves.” That is why the crystals that are well-transparent for long elastic waves (sound waves) in the case of short elastic waves look like a turbid medium, because short lattice waves are characterized by a strong scattering of the diffuse-type when the wavelength is comparable with the value of interatomic distances. The smaller the wavelength, the stronger the wave scattering by the nano-inhomogeneous structure; therefore, in the polar-sensitive crystals the main interaction of phonons is determined by the polar-sensitive bonds.

The fact that the value of thermal conductivity is dependent on the degree of ordering of polar-sensitive bonds is clearly seen in the example of ferroelectrics (Fig. 3.11). In the polycrystalline barium titanate, the thermal conductivity is 2.5 times less than in a single crystal, both above and below the Curie point (400 K), because ceramics have a macroscopically disordered structure. In BaTiO<sub>3</sub> crystal and in ceramics in the

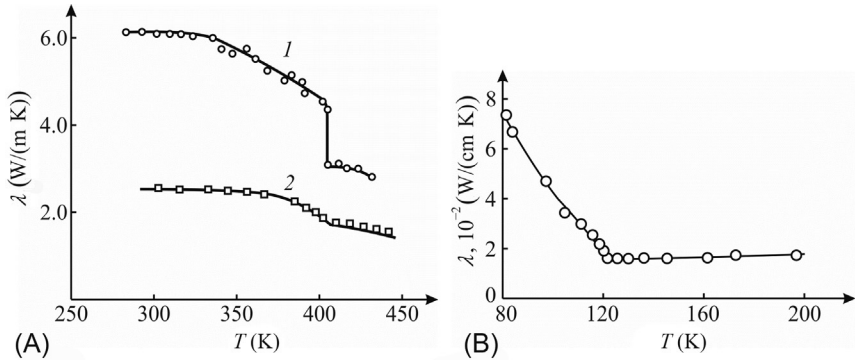


**Fig. 3.11** Thermal conductivity of ferroelectrics near their transition from higher temperature disordered phase into lower temperature ordered phase: (A) Barium titanate crystal (1) and ceramics (2); (B) potassium dihydrogen phosphate ( $\text{KH}_2\text{PO}_4 = \text{KDP}$ ) crystal.

ordered ferroelectric phase, thermal conductivity almost doubles in comparison with the microscopically disordered paraelectric phase. It is also interesting to note that in the  $\text{KH}_2\text{PO}_4$  (KDP) crystal below its Curie point (122K), thermal conductivity increases linearly with cooling, reflecting a gradual process of structural ordering in the ferroelectric phase (however, it also slightly increases when the crystal is heated above the Curie point). In all likelihood, the fluctuations of intrinsic polarity are the main scattering factor for phonons that carry heat.

Significantly decreased thermal conductivity in the polar-sensitive crystals is due to peculiarities of the phonon dissipation process: i.e., by perceptible binding of acoustical and optical phonons. This special feature of crystals with polar-sensitive bonds correlates with their phonon spectrum near the boundary of the Brillouin zone, where the transverse acoustic mode has an anomaly, with an example shown in Fig. 3.12 for GaAs (similar bending in the  $\nu_{\text{TA}}$  mode is seen in quartz). This is the evidence of such interaction between nearest atoms that can be described by the mixing of acoustic and optical phonons.

**4. Thermal conductivity in the vicinity of phase transition** demonstrates peculiarities that are seen when the nonpolar centrosymmetric phase is turning into the polar ferroelectric phase. These crystals include triglycinesulfate (TGS) and its isomorphs, the thermal conductivity of which is shown in Fig. 3.13, together with the reciprocal dielectric permittivity that tends to zero in the phase transition.

In the vicinity of the phase transition the anharmonicity in interatomic interactions sharply manifests itself, so the anomalies in phonon kinetics are expected. The density of elementary excitations increases, so the *heat capacity* (one of the components of thermal conductivity) increases as well. The maximum of specific heat corresponds to the maximum of energy fluctuations; moreover, the relaxation time changes critically. The density of excitations and the growth of anharmonicity lead to a decrease in the *diffusion length* of energy carriers and to a decrease in the intensity of heat transfer.

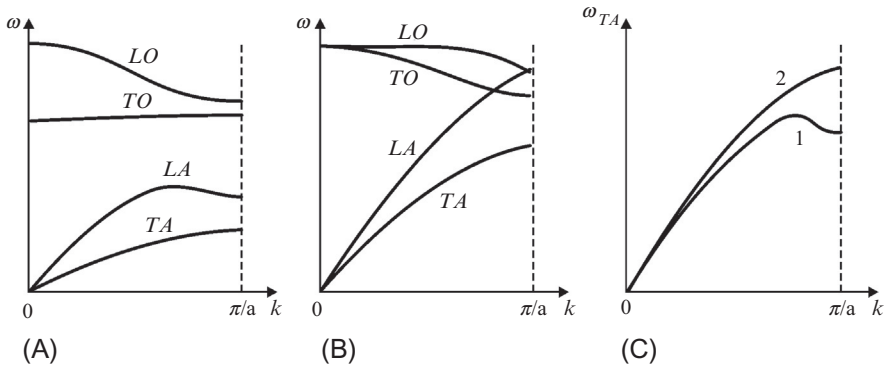


**Fig. 3.12** Phonons spectrum for: (A) Ionic crystal NaI; (B) covalent crystal diamond; (C) TA (transverse acoustic mode) in polar GaAs crystal (1) and in nonpolar NaCl crystal (2).

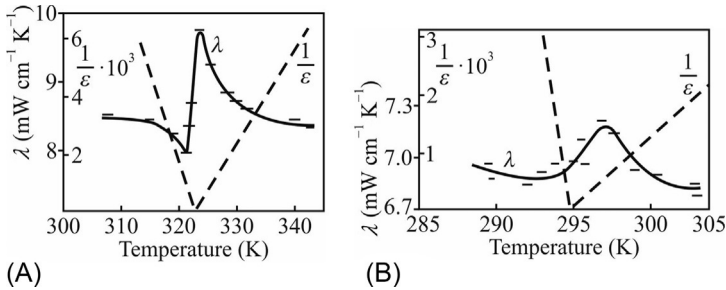


**Fig. 3.13** Thermal conductivity ( $\lambda$ ) temperature dependence and inverse value of permittivity ( $1/\epsilon$ ) along the [010] direction for single crystals TGS (A) and TGSel (B); *small dashed lines* show inevitable temperature gradient at measurements (according to Dimarova and Poplavko [1]).

To explain such an anomaly of thermal conductivity, refer again to Fig. 3.1, where the value of thermal conductivity in the [010] direction in TGS type crystals is compared with other physical parameters, which determine phonon thermal conductivity, namely, with the temperature dependence of specific heat  $C$ , with the speed of acoustic wave propagation in the longitudinal  $v_{lon}$  and transverse  $v_{tr}$  orientation, and with the thermal expansion coefficient  $\alpha$  along [010]. As can be seen, Aiken's law  $\lambda(T) \sim T^{-1}$  for thermal conductivity of TGS in the studied temperature region is not satisfied, which is due to the small average free path of phonons, scattering centers for which are commensurable with the order of the lattice constant. Therefore, temperature variation of thermal conductivity should follow the change in heat capacity. But in this case the minimum of thermal conductivity would not be observed, since the main investment in  $\lambda(T)$  is made by the specific heat change, as can be seen from Fig. 3.1.

It is possible that phonon scattering in the vicinity of phase transition is due not only to the anharmonicity of lattice vibrations, but also to other additional phonon-scattering mechanisms—for example, scattering on the structural heterogeneities. It is possible to reach the conclusion that a thermal conductivity minimum in the phase transition region is due to the mechanism of phonon scattering, considering the interaction of acoustic and optical phonons. It is also possible that near  $T_C$  at temperatures of 40–50°C there is noticeable additional scattering of phonons on the domain walls. In the TGS-family crystals, anomalies of thermal conductivity in the vicinity of phase transition are also observed in the [100] and [001] directions (Fig. 3.13). The absolute values of thermal conductivity of TGS, TGFB, and TGSel, as expected, are on the same order of magnitude. Anisotropy of thermal conductivity is observed in all crystals: the largest value of  $\lambda(T)$  is seen in the [100] direction while the smaller ones are for [010] and [001]. The anisotropy of thermal conductivity in TGS is consistent with the anisotropy of the velocity of ultrasound propagation.

**5. Thermal diffusivity in polar crystals.** As already mentioned, during the study of thermal conductivity anomalies in the polar crystals, two important factors display simultaneously. First is the temperature anomaly of *heat capacity*  $C(T)$  at phase transition (manifestation of latent heat of phase transition). The second is the change in *average free path* of phonons  $\langle l \rangle \sim \xi(T)$  due to ordering of polar-sensitive bonds. As a result, it turns out that heat transfer is determined by a product:  $\lambda(T) = \xi(T) \times C(T)$ . To avoid the influence of heat capacity on heat transfer analysis and to separate out the processes of phonon scattering, another method of measure, namely, the thermal diffusion  $\xi(T)$ , is developed [10], which indicates just the average free path of phonons without taking into account heat capacity  $C(T)$ .

Thermal conductivity temperature dependence can be compared to thermal diffusivity in crystals of the KDP group (Fig. 3.14). These dependences are significantly different. In the  $\lambda(T)$  dependence at the phase transition point, only a bend is seen, followed by a  $\lambda(T)$  rise at low temperature due to the increase of polar-sensitive bond ordering. However, in all studied crystals, on  $\xi(T)$  curves sharp minima are observed,

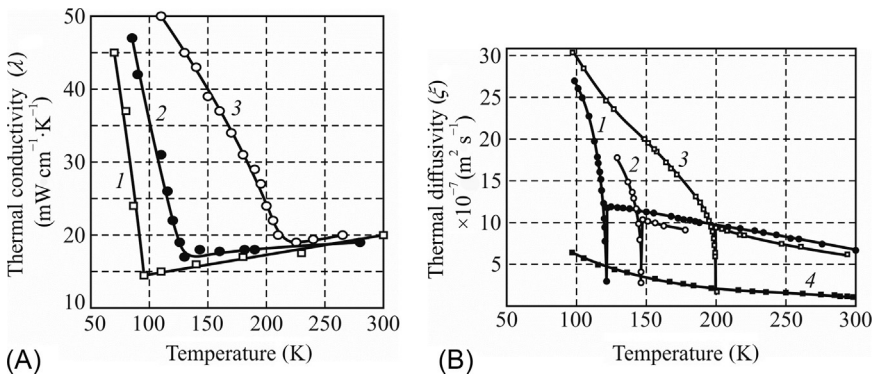


**Fig. 3.14** Thermal conductivity (A) and thermal diffusivity (B) in ferroelectric phosphates: 1— $\text{KH}_2\text{PO}_4$ , 2— $\text{KH}_2\text{AsO}_4$ , 3— $\text{KD}_2\text{PO}_4$ , and 4— $\text{KNaC}_4\text{H}_4\text{O}_6 \cdot 4\text{H}_2\text{O}$  (Rochelle salt).

which indicates rapid shortening in the average wavelength of phonons in the vicinity of the phase transition. Such differences between  $\lambda(T)$  and  $\xi(T)$  dependences are due to fact that in  $\lambda(T)$  a characteristic large decrease in phonon wavelength is compensated by a large maximum of specific heat.

Ferroelectric phosphates, whose investigations are shown in Fig. 3.14, are polar-sensitive piezoelectric crystals in *all* temperature ranges; however, above the Curie point they belong to the *polar-neutral* symmetry class  $42m$  (piezoelectrics), while below the Curie point they belong to the *polar pyroelectric* class  $mm2$ . The thermal diffusion coefficient in phosphates at temperatures close to 300 K equals approximately  $\xi \approx 7 \times 10^{-7} \text{ m}^2/\text{s}$ , which considerably exceeds the value  $\xi \approx 2 \times 10^{-7} \text{ m}^2/\text{s}$  seen in Rochelle salt crystals. The appearance of new collective excitations in the vicinity of phase transition leads to the fact that kinetics of acoustic phonons change: additional scattering and suppression of the heat flux created by it are observed. Exactly this factor is manifested in the form of a heat transfer minimum.

However, sharp anomalies in the  $\xi(T)$  dependence are observed only in the phosphates, in which diffusion coefficient passes through a deep minimum (30%–50% of  $\xi$  value), and its interval of temperature range is 20–30 K. This minimum in the diffusion is due to an increase in the crystal's anharmonicity, which leads to enlargement of interphonon interactions as well as to increase of ultrasound attenuation and increase in the dielectric losses. Increase in the relaxation time of thermal phonons also affects the anomaly of thermal diffusion.

As occurs above the Curie point, so below it the acoustic vibration modes (phonons) in the polar crystals are mixed with optical phonons; therefore optical phonons also participate in heat transfer. The prerequisites for heat transfer are provided by the spatial dispersion of optical modes. In the polar crystals, the process of heat transfer is significantly influenced by optical phonons, since they are associated with acoustic phonons. The interaction of acoustic phonons with soft transverse optical mode (peculiar to ferroelectrics) leads to a significant decrease in the average free path of phonons. It is obvious that, at the point of phase transition, the average free path of thermal phonons is reduced to the possible minimal level. In different crystals and at various temperatures (and even in the case of KDP deuteration, or DKDP) this level remains almost the same (Fig. 3.14B). It was also established that in a wide temperature range just the same very low level of thermal diffusion is seen in the Rochelle salt crystal, so it is not surprising that sharp dips in the  $\xi(T)$  curve are not seen in this crystal.

On the basis of the established lowest limit of the wavelength of thermal phonons (which, apparently, reaches the value of unit cell parameter of a crystal), one can come to the conclusion that, in the disordered phase (above the phase transition temperature), this wavelength still remains an order of magnitude larger and then continues to drop with temperature—as is usual for all crystals. Below the phase transition temperature, the role of structural ordering of polar crystals becomes very noticeable except Rochelle salt, in which a particularly complex structure makes it almost heat-impermeable (resembling glass). As the temperature lowers starting from the Curie point, a very fast increase of thermal phonon wavelengths is observed, which indicates a substantial ordering in the polar-sensitive bonds. Since in this temperature

range there are no noticeable anomalies in the specific heat, so the same dependence is reproduced in the temperature dependence of thermal conductivity.

**6. Electrical field influence on thermal transfer.** The ability to control heat flow by electrical field holds not only scientific but also technical interest. Therefore, in our first experiments this question was studied using the example of a polycrystalline ferroelectric with a diffuse phase transition, in which dielectric permittivity can be changed approximately 10 times by electrical displacement field over a considerable temperature range. These measurements were carried out in the vicinity of the phase transition.

The results of the study of the polycrystalline ferroelectric  $\text{Ba}(\text{Ti},\text{Zr},\text{Sn})\text{O}_3$  are shown in Fig. 3.15. When a constant electrical field is applied, the maximum of thermal conductivity in the region of phase transition remains, but it shifts by 5–8°C toward lower temperatures. This corresponds to a thermal conductivity increase in the ferroelectric phase near the phase transition. The phenomenon of thermal conductivity hysteresis with a change in the magnitude and sign of the electrical field strength is also observed (Fig. 3.15B), which indicates that the scattering of phonons is to some extent due to the domain structure of ferroelectrics. However, for technical applications, the effect of thermal conductivity control seems to be too small.

To study the physical mechanism of field effect on thermal conductivity, single crystals were also studied. A very convenient subject for more detailed studies of thermal diffusion is the TGS crystal, which is a ferroelectric with hydrogen bonds that occupies a middle position in terms of thermal diffusion coefficient: it has no large anomalies near its phase transition at Curie temperature  $T_C = 49^\circ\text{C} \approx 323\text{ K}$  [1]. The peculiarities in the  $\xi(T)$  variations at phase transition from nonpolar (high-temperature) phase to polar (low-temperature) phase are shown in Fig. 3.16. It is found that an electrical bias field significantly changes the anomalies of thermal conductivity and thermal diffusion at phase transition (the electrical field was applied along the polar axis of a crystal, where it shows the greatest impact on the degree of ordering of the polar-sensitive bonds).

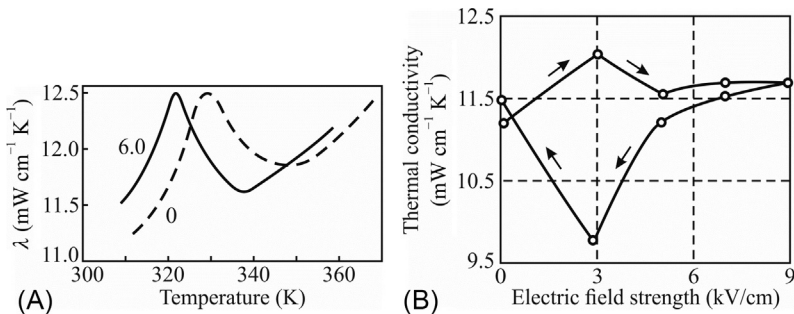


**Fig. 3.15** Influence of bias electrical field on thermal conductivity coefficient ( $\lambda$ ) of nonlinear ferroelectric near phase transition: (A)  $\lambda$  temperature dependence at  $E = 0$  (1) and  $E = 6$  kV/cm (2); (B)  $\lambda$  dependence on electrical field at  $48^\circ\text{C}$  [1].

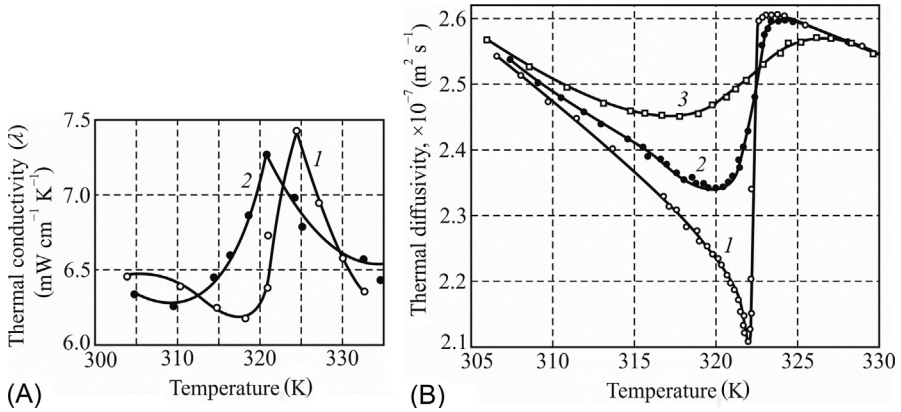


**Fig. 3.16** Thermal conductivity (A) and thermal diffusivity (B) of TGS crystal near phase transition under bias electrical field influence; (A) curve 1— $E = 0$ ; curve 2— $E = 6$  kV/cm; (B) curve 1— $E = 0$ , curve 2— $E = 3.4$  kV/cm, curve 3— $E = 10$  kV/cm.

A phonon's free path in TGS, calculated from the thermal conductivity ( $\lambda \approx 2 \times 10^{-3}$  cal  $\text{cm}^{-1} \text{s}^{-1} \text{deg}^{-1}$ ), specific volumetric heat capacity ( $C \approx 0.6$  cal  $\text{deg}^{-1} \text{cm}^3$ ), and speed of propagation of ultrasound ( $v \approx 4 \times 10^3$  cm  $\text{s}^{-1}$ ), has a value of  $3 \times 10^{-8}$  cm, i.e., has the order of the lattice constant. When an electrical field is applied, the conditions of phonon scattering change, for example, by scattering on domain walls, which in the ferroelectrics have a length on the order of the lattice constant. As noted, thermal conductivity depends not only on the conditions of phonon scattering, but also on the heat capacity and elastic properties of a crystal. As indicated earlier in connection with Fig. 3.2, the heat capacity of the TGS crystal increases as the Curie point approaches and its sharp maximum is observed at the transition point itself. Under the influence of an electrical field “smearing” appears and a decrease in heat capacity jump is seen, but not its temperature shift. The shift of the thermal conductivity maximum in the ferroelectrics, in particular in TGS single crystals, is probably due to a change in not only the conditions of phonon scattering, but also in the elastic properties of the crystal under the influence of a constant electric field in the region of the Curie point.

A big difference is seen in temperature dependences of thermal *conductivity* and temperature dependences of thermal *diffusion*. The influence of applied electrical field on the thermal conductivity can be explained by the shift in frequency of the optical phonon branch. In the absence of a bias field a small minimum accompanied by a maximum of  $\lambda(T)$  is observed, which in the electrical field becomes blurred and shifted to low temperatures (it should be noted also that the magnitude of these anomalies also depends on an unavoidable temperature gradient, of which measurements should be provided). However, any interpretation of changes in  $\lambda(T)$  dependence is also complicated by the fact that thermal conductivity is affected not only by average free path of thermal phonons, but also by the change in specific heat.

As a rule, the group velocity of optical phonons is small and their contribution to heat transfer is small also, so thermal excitation of optical phonons leads only to the additional scattering of thermal phonons. When approaching to the boundary of the Brillouin zone, group velocity of acoustic phonons decreases substantially, and it is this region of the spectrum that is characteristic of thermal phonons. The dispersion of optical phonons, on the other hand, leads to the appearance of a group velocity for them near the Brillouin zone boundary. In the polar crystals, acoustic and optical phonons are connected, so that optical phonons can participate in the heat transfer: this is confirmed by the influence of electrical field on the thermal conductivity and thermal diffusion. The double mechanism of participation of optical phonons can compensate for each other in thermal conductivity, but not in the process of thermal diffusion.

It can be seen that the thermal diffusion coefficient increases substantially in the ordered phase, indicating the degree of disordering of the polar-sensitive bonds, which hinders diffusion of heat: in the electrical displacement field the wavelength of thermal phonons increases. In a certain sense, it is possible to control the heat flux by means of the electrical field, although the practical significance of this effect is insignificant: it occurs in a narrow temperature range and allows heat flux controlling in the range of only 20%.

It is noteworthy that above the Curie temperature (in the disordered phase) the electrical field influence shows the opposite effect: the thermal diffusion coefficient somewhat decreases. Apparently, this is due to the blurring of phase transition and its displacement in an electrical field to higher temperatures.

**7. Thermal diffusion in antiferroelectrics.** The most impressive features of thermal diffusion in polar-sensitive crystals are seen in the antiferroelectrics (Fig. 3.17). Instead of a deep minimum in  $\xi(T)$  dependence, a sharp *maximum* is observed at the Curie point, for example, in ammonium dihydrophosphate (ADP). At first glance, this behavior of  $\xi(T)$  may seem quite unusual. However, the matter is that to heat transfer

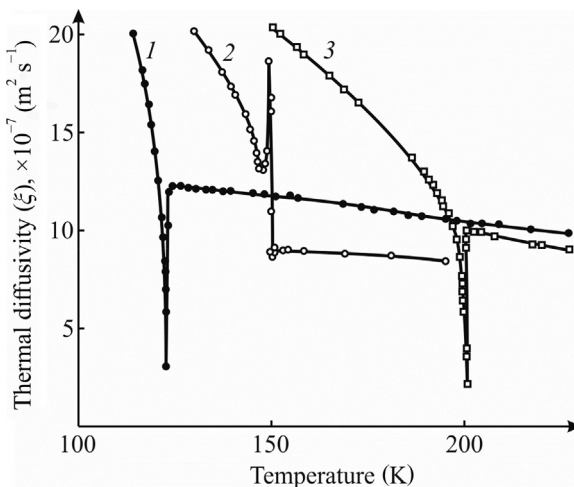


**Fig. 3.17** Thermal diffusion comparison in ferroelectrics KDP (1) and DKDP (3) in comparison with antiferroelectric ADP (2).

in antiferroelectrics the *optical phonons* are substantially added, especially in the vicinity of phase transition. In these crystals the frequency of the lattice optical vibration mode *decreases critically near the boundary of the Brillouin zone*, down to the frequency of the acoustic mode, leading to their mixing. This occurs precisely with the short-wave (thermal) phonons, which ensures the heat transfer. As a result, the coefficient of thermal diffusion *increases* critically precisely at the Curie point, as seen in Fig. 3.17, curve 2.

In contrast, in the *ferroelectric* crystals of KDP and DKDP, the effect of  $\xi(T)$  increase does not exist, because in them the optical lattice mode decreases critically *near the center* of the Brillouin zone, i.e., in the region of long-wavelength phonons. This decrease strongly affects the speed of sound, i.e., long-wavelength phonons, as well as leads to large permittivity at the Curie point: at a frequency of 10 GHz in ferroelectric KDP  $\epsilon_{max} \approx 1000$  while in the antiferroelectric ADP at 10 GHz  $\epsilon_{max} \approx 90$ .

Inasmuch as in ferroelectrics (like KDP) near the center of the Brillouin zone only *long-wave* optical phonons show anomalies of decrease in frequency, so this critical phenomenon has only little effect on the heat transfer realized by short-wave thermal phonons; that is why a *scattering* effect of thermal phonons dominates. It is seen especially in the vicinity of the phase transition when *structural rearrangement* of the crystal occurs: the wavelength of thermal phonons becomes minimal, leading to a deep minimum of  $\xi(T)$  seen in Fig. 3.17, curves 1 and 3. Because of the additional influence of optical phonons, the temperature dependence of thermal conductivity cannot uniquely reflect the change in the kinetics of optical phonons. Such a parameter is the diffusion coefficient, which mainly reflects the dependence of the phonon mean free path on temperature.

An important fact is also that an antiferroelectric type phase transition occurs with the *multiplication* of crystal lattice parameters in the ordered phase, which is accompanied by an *increase* in crystal density. It is quite natural in this case that in the vicinity of the antiferroelectric phase transition, the *maximum* of the thermal expansion coefficient  $\alpha(T)$  is observed (but not the minimum  $\alpha(T)$  usual for ferroelectric phase transitions). The simplest model of this feature is given in Fig. 3.18, where differently located polar-sensitive bonds give an opportunity to explain how the size of a crystal lattice might be changed under different phase transitions.

Therefore, in the antipolar crystals the special arrangement of polar-sensitive bonds can lead not only to an increase in the density of such crystals, but also facilitates the

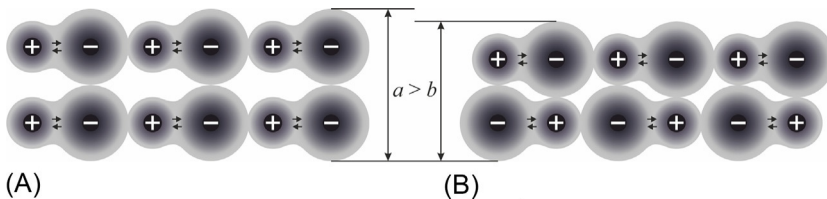


**Fig. 3.18** Comparison of polar ordering (A) lattice with antipolar ordering (B): It is seen that  $a > b$ .

participation of optical phonons in the phenomenon of heat transfer. This becomes especially noticeable near the antiferroelectric phase transition (accompanied by multiplication of crystal lattice parameters), in which the *spatial dispersion* of optical phonons is particularly large exactly at the boundary of the Brillouin zone, since a critical *decrease* in their frequency occurs.

Thus, the mechanism of thermal conductivity of polar-sensitive crystals is predominantly phonons, since the electrical conductivity of these materials is very low and the temperature range is rather small, so it can be assumed that there are no other heat transfer mechanisms (electronic, excitonic, or photonic). Consequently, peculiarities of thermal conductivity discussed here can only be due to a change in phonon scattering conditions. The influence of polar-sensitive (mixed ionic-covalent) bonds greatly affects the phenomenon of heat transfer of crystals: their thermal conductivity is noticeably lower than that in simple covalent or ionic crystals. Studies of the anomalies of *thermal diffusion* in the vicinity of ferroelectric phase transitions, where disordered nonpolar structure changes to an ordered polar structure, make it possible to clarify some features in the behavior of polar-sensitive bonds.

### 3.4 Summary

1. Thermal properties of crystals are due to the internal energy of movement of atoms, ions, or molecules in a lattice that is strongly dependent on crystal structure. Peculiar properties of the polar-sensitive crystals are manifested in their specific heat, thermal expansion, and thermal conductivity.
2. Basic energy characteristics of solids are the *Debye energy*  $\hbar\omega_D$  and the *thermal energy*  $k_B T$ . Debye temperature  $\theta_D = \hbar\omega_D/k_B$  and Debye frequency  $\omega_D = 2\pi\nu_D$  are connected with each other by two fundamental constants: the Planck constant  $\hbar$  and the Boltzmann constant  $k_B$ .
3. The degrees of freedom during atomic particle movement in solids can be divided into two groups. If the interaction energy of particles  $U_{int}$  is small in comparison with thermal motion energy  $k_B T$ , namely  $U_{int} \ll k_B T$ , the appropriate degrees of freedom behave as the *collection* of particles, i.e., as an “almost ideal gas” of phonons; this refers to ordinary nonpolar dielectrics.
4. In the opposite case, when conversely  $U_{int} \gg k_B T$ , then appropriate degrees of freedom are usually quite ordered, but their movement, too, can be described by the introduction of phonons. These substances include a majority of functional polar-sensitive dielectrics (piezoelectrics and pyroelectrics), so the application of the phonons concept to them in most cases can be considered justified.
5. Much more complicated cases arise, if interaction energy  $U_{int} \sim k_B T$ . In this case a theoretical description of solids becomes complicated, especially at the phenomenon of *phase transition*, when the nonpolar phase is turning into the polar phase. So polar-sensitive crystal behaves in such a way that no conventional concept, based on phonons, can adequately describe the experimental situation. This interaction has a special character: the probability of *collective movements* is higher than the probability of *individual movements*. An abnormal increased role of collective movements is confirmed by experiments in the vicinity of phase transition: at temperature  $T = T_C$  a crystal shows a maximum of specific heat, and so on.

6. Crystals with polar-sensitive bonds behave in certain conditions in a complex way: for some phonons, for example, thermal ones, the lifetime of a phonon is commensurate with the inverse frequency of oscillation; that is, the oscillators that characterize them turn out to be overdamped. That is why crystals of excellent optical quality, which are transparent and have small attenuation for transmission of *long* acoustic (ultrasonic) waves, in the case of *short* (heat) waves turn out to be almost an opaque environment, in which phonons of a certain frequency become stuck.
7. *Specific heat* in polar crystals contains an additional contribution due to the degree of disorder of polar-sensitive bonds. The statistical possibility of the realization of several states increases the total entropy of a system: such *configuration entropy* is a part of total entropy of a system, which is related to the position of constituent particles rather than to their velocity or momentum. It is physically related to the number of ways of arranging all the **particles** of a system while maintaining some overall set of specified system properties, such as **energy**. The change in configurational entropy corresponds to the same change in macroscopic entropy.
8. In the polar-sensitive crystals the heat capacity somewhat exceeds this parameter as compared with the nonpolar crystals: this is clearly expressed in the vicinity of phase transitions, where a maximum of heat capacity can be several times higher than its average value. It might be supposed that the additional contribution to heat capacity in the gradually ordering phase is due to the configurational entropy.
9. The statistical possibility of several states being realized increases the total entropy of a system: such *configuration entropy* is related to the position of constituent particles rather than to their velocity or momentum. This is physically related to the number of ways of arranging all the **particles** of a system while maintaining some overall set of specified system properties, such as **energy**. Change in the configuration entropy corresponds to the same change in macroscopic entropy.
10. The thermal expansion reflects the features of interatomic bonds in crystals. Without matching between thermal expansion coefficients, technologically obtained microelectronic structures would be mechanically stressed, which affects their properties and might even lead to local destruction. However, there are some important cases when exactly this difference in thermal expansion is used for managing combined structure properties.
11. In polar dielectrics the peculiar polar-sensitive structures arise due to the compensation of atoms' electronegativity. A negative value of  $\alpha(T)$  corresponds to such a particular case, when a crystal's entropy increases with pressure, an increase that is possible only in the case of configurational entropy: a negative expansion section depending on  $\alpha(T)$  corresponds to the processes of their own structural ordering.
12. A low-temperature minimum of the thermal expansion coefficient can be explained: when temperature decreases, the thermal chaotic motion freezes, and the polar-sensitive bonds existing in crystal become partially ordered (configurational entropy decreases). As a result, the crystal occupies a bigger volume, demonstrating negative  $\alpha(T)$ . With further cooling to very low temperature, the quantum oscillations in the crystal lattice prevent the ordering of fluctuating polarity, so with an approach to 0 K the crystal again compresses a little before  $\alpha(T) \rightarrow 0$  at  $T \rightarrow 0$ .
13. The negative value of  $\alpha(T)$  corresponds to such features in the frequency distribution in the phonon spectrum of polar-sensitive crystal, which simultaneously leads to the negative value of the Grüneisen constant  $\gamma$ . Since this effect is observed at low temperatures, such singularities are due to *acoustic* vibration modes; in polar-sensitive crystals the branch of *transverse acoustic* oscillations curves downward as it approaches to the boundary of the Brillouin zone, and exactly this part of the TA branch near the Brillouin zone boundary corresponds to negative  $\alpha$ .

14. Low-temperature negative thermal expansion in semiconductors of  $A^{III}B^V$  and  $A^{II}B^{VI}$  types is not surprising, as they belong to the polar groups of crystals. However, for atomic semiconductors of diamond type, the  $\alpha(T)$  minimum needs explanation. It might be assumed that the reason for negative  $\alpha(T)$  in germanium and silicon is the fluctuations in partial ordering of the virtual hexagonal polar phase (this assumption is based on the fact of hexagonal diamond existence).
15. *Crystal strain engineering* technology for polar-sensitive films is based not only on the mismatch of thermal expansion, but to a greater degree on the difference in the permanent lattices of film and substrate. According to the principle of Le Chatelier, if during formation of the polar phase one of the crystal sizes increases, the forced change in this size of crystal should lead to a change in crystal polar state.
16. In the biaxial stressed films, such materials are obtained that in the bulk state are not ferroelectrics at any temperature. Biaxial deformations of films make it possible to increase the Curie point by hundreds of degrees with a simultaneous increase in the polarization directed perpendicular to film thickness. Deformations, reaching values of several percents, have a great influence on the properties of polar-sensitive thin films making it possible to obtain films with such properties that are not found in natural materials. Thus, the difference in thermal expansion as well as the mismatch between lattice parameters of film and substrate can be used in modern microelectronics technologies.
17. *The heat transfer* in polar crystals is provided mostly by the short lattice waves having low velocity, so polar crystals look like a turbid medium. These lattice waves demonstrate strong diffuse-type scattering by the nanosize inhomogeneous structure, in which phonon interaction is determined mostly by polar-sensitive bonds, because the wavelength of heat-phonons is commensurable with the parameter of crystal lattice.
18. *The thermal conductivity* depends on crystal specific heat  $C$ , on averaged free path between phonon collisions  $\langle l \rangle$ , and on average velocity  $v$  of phonons:  $\lambda = (1/3) \cdot v \cdot l$ . In the temperature interval discussed here, the dependence of  $\xi(T)$  occurs following the Aiken law:  $\xi(T) \sim T^{-1}$ . Thermal conductivity corresponds to the thermal expansion coefficient:  $1/\lambda \sim \alpha^2$ , which is determined by peculiarities of interatomic bonds. Therefore, crystals with larger expansion coefficient have smaller thermal conductivity.
19. Thermal conductivity in the polar crystals in comparison with the usual crystals is significantly decreased, which is conditioned by peculiarities of the phonon dissipation process: i.e., by perceptible binding of acoustical and optical phonons. This special feature of crystals having polar-sensitive bonds correlates with their phonon spectrum near the boundary of the Brillouin zone, where the transverse acoustic mode is noticeably reduced. This is the evidence of such interaction between nearest atoms that can be described by the mixing of acoustic and optical phonons.
20. *The thermal diffusivity* coefficient  $\xi$  is **thermal conductivity** divided by crystal **density**  $\rho$  and by its **specific heat**  $C$  at constant pressure:  $\xi = \lambda/(C_p \cdot \rho)$ . It measures the rate of heat transfer of a material from the hot side to the cold side. In a sense, thermal diffusivity is the measure of *thermal inertia*; in a substance with higher thermal diffusivity, the heat moves more rapidly through it. At that, thermal diffusivity is determined mainly by the mean free path  $\langle l \rangle$  of thermal phonons propagating in a crystal ( $\xi \sim \langle l \rangle$ ). When  $T > \theta_D$  with increase of temperature  $\xi(T)$  dependence slows down following the Aiken law:  $\xi(T) \sim T^{-1}$ . In all studied ferroelectrics, sharp minima are observed on  $\xi(T)$  curves, which indicate rapid shortening of the average wavelength of phonons in the vicinity of the phase transition.
21. Electrical field influence on thermal transfer has not only scientific but also technical interest. When a constant electric field is applied, the maximum of thermal conductivity in the region of phase transition remains, but it shifts toward lower temperatures. This

corresponds to an increase in thermal conductivity in the ferroelectric phase near the phase transition. A phenomenon of thermal conductivity hysteresis with a change in electrical field strength is also observed, which indicates that the scattering of phonons is to some extent due to the domain structure of the ferroelectric. However, for technical applications, the effect of thermal conductivity control seems to be too small.

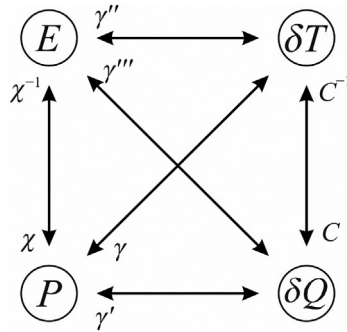
22. Thus, polar-sensitive (mixed ionic-covalent) bonds strongly affect the processes of heat transfer of crystals: their thermal conductivity is much less than that in pure-ionic or pure-covalent crystals. Anomalies of thermal diffusion in the vicinity of ferroelectric and antiferroelectric phase transitions are described by the change of ordered polar structure to a disordered nonpolar structure. In the ordered phase, the thermal diffusion coefficient increases; this indicates that disordering of polar-sensitive bonds hinders the diffusion of heat.

## References

- [1] E.N. Dimarova, Y.M. Poplavko, Electrical bias field influence on ferroelectrics thermal conductivity, *Izv. Akad. Nauk. SSSR Ser. Phys.* 31 (11) (1967) 1842.
- [2] B.A. Strukov, Heat capacity in TGS single crystal, *Solid State Phys.* 6 (9) (1963) 2862.
- [3] B.A. Strukov, K.A. Minaeva, K.A. Taraskin, Electrical field influence on TGS heat capacity, *Izv. Akad. Nauk. SSSR Ser. Phys.* 49 (6) (1985) 982.
- [4] D.G. Schlom, L.-Q. Chen, C.J. Fennie, et al., Elastic strain engineering of ferroic oxides, *MRS Bull.* 39 (2014) 118.
- [5] D.G. Schlom, L.-Q. Chen, C.-B. Eon, et al., Strain tuning of ferroelectric thin films, *Annu. Rev. Mater. Res.* 37 (2007) 589.
- [6] S.I. Novikova, *Thermal Expansion of Solids*, Nauka, Moscow, 1973.
- [7] Z.K. Liu, Y. Wang, S.L. Shang, Origin of negative thermal expansion phenomenon in solids, *Scr. Mater.* 65 (2011) 664.
- [8] C. Kittel, *Introduction to Solid State Physics*, fourth ed., John Wiley, New York, 1976.
- [9] W. Martienssen, H. Warlimont (Eds.), *Springer Handbook of Condensed Matter and Materials Data*, Springer, Berlin, 2005.
- [10] V.F. Zavorotnii, Y.M. Poplavko, Planar temperature waves method for thermoconductivity study, *Pribory Tehnika Exp.* (5) (1984) 189.

## Further reading

- [11] Y.M. Poplavko, *Polar Crystals: Physical Nature and New Effects*, LAMBERT Academic Publishing, Saarbrücken, 2013.
- [12] V.F. Zavorotny, Y.M. Poplavko, L.F. Pasechnik, Diffusion of heat in KDP-type ferro- and antiferroelectrics, *Fiz. Tverd. Tela (St. Petersburg)* 35 (1985) 2832.



Relationship of main parameters describing pyroelectric and electrocaloric effects.

Some extraordinary properties of the natural mineral tourmaline, which when heated attracts small particles, were already known in antiquity (2000 years ago). However, this phenomenon was explained as an *electrical* phenomenon for the first time in the 18th century by Linnaeus and Aepinus, while the term *pyroelectric* arose 200 years ago in the works of D. Brewster (the Greek word “pyro” means “fire”). Pyroelectrics are solid-state *direct converters* of thermal energy into electrical energy<sup>a</sup>. The first theory of pyroelectricity was developed by W. Thomson and W. Voigt at the end of the 19th century.

These relatively rare crystals are found among minerals and also among artificially synthesized crystal pyroelectrics. Mineral pyroelectrics consist mainly of tourmalines (alumina-borosilicate of  $\text{NaMg}\{\text{Al}_3\text{B}_3\cdot\text{Si}_6(\text{OOH})_{30}\}$  with various impurities), while synthetic pyroelectrics are lithium sulfate ( $\text{LiSO}_4 \times \text{H}_2\text{O}$ ), lithium niobate ( $\text{LiNbO}_3$ ), potassium tartaric acid ( $\text{K}_4\text{C}_8\text{O}_{12} \times \text{H}_2\text{O}$ ), and many others [1]. The broadband semiconductors of the  $\text{A}^{\text{II}}\text{B}^{\text{VI}}$  type (CdS, ZnO, etc.) are also pyroelectrics, but their pyroelectricity usually is small. It is interesting to note that crystalline sugar ( $\text{C}_5\text{H}_{10}\text{O}_5$ ) is pyroelectric and for that very reason is used in homeopathic medicines. Recently, significant progress has been made in the use of *artificial* pyroelectric materials in the form of thin films, using gallium nitride (GaN) and cesium nitrate ( $\text{CsNO}_3$ ), as well as some polymers: polyvinyl fluoride and derivatives of cobalt phthalocyanine.

<sup>a</sup> In addition to pyroelectricity, *thermoelectricity* is widely used to refer to solid-state converters of thermal energy into electrical energy. In thermoelectric devices electronic processes in *semiconductors* are used, occurring under conditions of temperature gradient (temperature difference). In this case, the generation of electricity occurs continuously in *stationary* conditions [6]. In pyroelectric devices the electrical *polarization-depolarization* effect is used in nonstationary conditions, when dynamic or periodic temperature changes are obviously required.

Any *ferroelectric* is a potential pyroelectric, but in order to use ferroelectrics as pyroelectric elements they must be monodomainized. Otherwise, the pyroelectric effect is mutually compensated due to the multitude of differently oriented ferroelectric domains [2]. However, it is possible to monodomainize ferroelectrics in various ways, including their polarization by electrical field at increased temperature; moreover, current technologies for producing pyroelectric crystals-ferroelectrics usually use crystal-growing methods that immediately provide their monodomain structure.

Pyroelectrics represent one of the important classes of functional dielectrics, because they efficiently react to *temperature* change (as well as to outside pressure and other mechanical actions). These are polar dielectrics, which can be defined also as materials that allow direct energy conversion, representing mainly thermoelectric and, vice versa, electrothermal power converters. Their transformative function is due to the peculiar physical structure and chemical composition of the polar crystals [12].

The pyroelectric effect and its inverse, the electrocaloric effect, are reviewed in this chapter regarding aspects of their use in electronic devices at various boundary conditions (adiabatic and isothermal development, mechanically free or clamped crystal study, short-circuited or open-circuited conditions). The nature of thermoelectrical coupling in pyroelectrics and its influence on dielectric permittivity and thermal properties of polar crystals are also described by various models and thermodynamic calculations. Physical mechanisms and applications of electrically induced pyroelectric and electrocaloric effects at various conditions are also depicted.

## 4.1 General characteristics of pyroelectrics

In the polar-sensitive dielectric, raising or lowering temperature changes the intensity of particle thermal motion, and therefore changes the orientation of polar-sensitive bonds (or polar molecules) as well as the distance between them, leading to the appearance of *thermally induced polarization*. As a result of such a pyroelectric effect, uncompensated electrical charges appear on the surfaces of polar crystals. Covered by electrodes, the pyroelectric element is usually connected to an amplifier and a pyroelectric *current* flows through the input impedance of the amplifier. In the case of a disconnected (open-circuited) crystal, a pyroelectric *voltage* appears on the crystal surface; however, over time, if the temperature of the crystal remains invariable, this pyroelectric potential gradually decreases to zero.

An *energy* description of this process means that thermal energy is converted by the pyroelectric directly into electrical energy due to its electrically active intrinsic structure; therefore the pyroelectric is a thermoelectric (or, vice versa, electrothermal) power converter. Moreover, its own peculiar internal electrical structure of crystals-pyroelectrics is advantageous from the energy standpoint [3].

The *crystallographic* consideration of this phenomenon comes down to the particular structure of the crystal, which must have the presence of a polar axis, possible only in the polar crystallographic symmetry category. Therefore, according to Neumann's principle, the point symmetry groups of pyroelectric crystals should be the subgroups of the  $\infty\text{-}m$  limit group, which describes the symmetry of a polar vector.

Pyroelectric crystals can have one of the only following symmetry types: a single axis of symmetry of any order and planes of symmetry passing through this axis. Such crystals belong to the 10 polar point symmetry groups shown in Fig. 4.1A. Pyroelectricity does not occur in crystals with a center of symmetry, and there are no pyroelectric crystals among the cubic classes of crystals [2].

As can be seen from the left part of Fig. 4.1A, one of the five types of axes (allowed by the spatial symmetry of crystals) in pyroelectrics should be the *single polar axis*; correspondingly, the five groups of pyroelectric classes of crystals are designated as follows: 1, 2, 3, 4, 6. These numbers indicate the order of polar axis and comply with triclinic, monoclinic, trigonal, tetragonal, and hexagonal classes of symmetry. The five various axes of symmetry listed may *lie in planes* of symmetry (denoted by  $m$ ), forming five more possible classes of pyroelectrics:  $m$ ,  $mm2$ ,  $3m$ ,  $4mm$ , and  $6m$ , as seen in Fig. 4.1A on the right.

Thus, the symmetry of a crystal limits arbitrariness in the orientation of the polar vector, which must either be directed *along* the axis of symmetry or lie in the *plane* of symmetry. When changing external conditions, in particular temperature or pressure, only *limited* measurements of polar response are permissible. If an action exerted is nondirectional, being described by a scalar magnitude (which corresponds to uniform heating or hydrostatic pressure), then changes in the polar response must be consistent with the symmetry of the crystal. In the crystals of eight pyroelectric classes, in which the number indicates the polar axis (Fig. 4.1A), the polar response can vary only by a magnitude, but not in a direction, which must always coincide with the direction of the existing axis of symmetry. However, in crystals with only a *plane* of symmetry (point group  $m$ ), greater freedom is allowed: the polar vector can vary both in magnitude and direction, remaining, nevertheless, invariably in the plane of symmetry. Regarding the crystals included in the triclinic system (group 1), one can say that this symmetry does not impose any restrictions in the orientation of the polar vector, i.e., it is not conditioned by any crystallographic chosen direction. As a result, with temperature or pressure changes, the polar vector can be described in a space by an arbitrary curve.

The pyroelectric effect maximally manifests itself only in one direction of crystal structure, namely along the polar axis, where the maximum of pyroelectric coefficient is seen:  $\gamma_{\max}$  (Fig. 4.1B). In the direction transverse to the polar axis  $\gamma = 0$ ; note that in

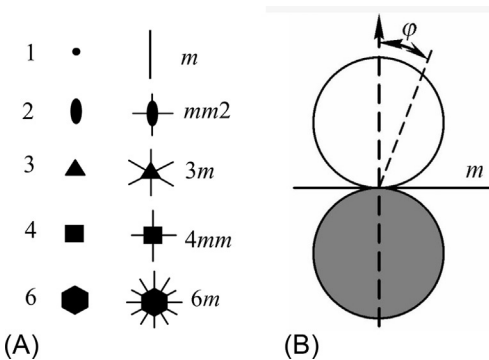


**Fig. 4.1** Pyroelectric crystal formal description: (A) 10 polar symmetry classes, where number indicates the order of symmetry axis, while  $m$  is the plane of symmetry; (B) guide surface (indicatrix) for pyroelectric coefficient  $\gamma(\varphi)$ ; black area shows negative part of pyroelectric coefficient [6].

practice it is sometimes considered more rational to use slanting cuts of pyroelectric crystals where  $\gamma(\varphi) = \gamma_{\max} \cos\varphi$ .

Among the known 32 classes of crystals, 20 classes are piezoelectric ones, and of them 10 classes are pyroelectric (called the “pyroelectric group”; Fig. 4.1A). A common feature of this group of crystals is the lack of certain elements of symmetry: the center of symmetry, the transverse planes of symmetry, and any axes of symmetry of infinite number, perpendicular or oblique with respect to the current axis.

It should be noted that, besides the polar *crystals*, the *polarized ferroelectric ceramics* also have pyroelectric properties (at increased temperature and under an externally applied electrical field most of the ferroelectric domains in ceramics become and then stay oriented). The pyroelectric *texture* formed belongs to the group of polar symmetry  $\infty \cdot m$  ( $\infty$  is the order of symmetry axis). Because of mechanical strength and high chemical resistance, the polarized ferroelectric ceramics very often are used in pyrometry, although usually the pyroelectric sensitivity of the ceramics is less than that of the ferroelectric crystals. In addition to polarized ferroelectric ceramics, some *polymeric films*, for example, polyvinylidene fluoride, have a significant pyroelectric effect. Their advantage is elasticity and their drawback is aging (transformative properties decrease with time).

As is well known, only crystals belonging to noncentrosymmetric classes can have properties described by the odd-rank tensors. Therefore, crystals of all acentric classes exhibit a piezoelectric effect, the quantitative characteristic of which is a third-rank tensor of piezoelectric modulus. An exception among crystallographic classes that do not have a center of symmetry (the total number of which is 21) is the only cubic class with point group 432, which prohibits the appearance of piezoelectric activity by the other elements of symmetry it has. Like all material tensors of odd rank, the tensor of piezoelectric coefficients is impossible in crystals having a center of symmetry.

However, among pyroelectric crystals, there are those in which an external electrical field can change the direction of polarization to its opposite. These are ferroelectrics, and their repolarization occurs due to the fact that their polar structure is only *slightly distorted* in comparison with the nonpolar phase. Therefore, free energy of such a crystal in its polar phase turns out to be comparable with free energy of its nonpolar phase, because the energy barrier separating these modifications has a rather small value. This leads to the fact that the restructuring of the crystal lattice can be done relatively easily by the external field.

**Pyroelectric effect applications** are based mainly on the fact that thermal energy, being radiated in the form of infrared waves, is invisible to human eyes. So, pyroelectric sensors can work as hidden devices, and they are widely used for security and automation applications. The electronics technologies that make use of the pyroelectric effect include mainly *temperature sensors* and *far-infrared (IR) detectors* used in imaging devices. The advantages of pyroelectric sensors as compared to semiconductor-based IR devices consist primarily in the possibility of using them without special cooling—in other words, at normal temperature. In addition, based on the principle of *heating by any radiation*, pyroelectric sensors are nonselective and so are *wide-range* devices, which can register not only thermal but also microwave, X-ray, and optical radiation, including high-power laser radiation. A very

important feature of pyroelectric devices is their much *faster response* than other temperature sensors, as well as their high overload resistance [14].

The basic pyroelectric sensor device is rather simple (Fig. 4.2A): it is a pyroelectric plate supplied with electrodes and irradiated by a studied heat flow. To quickly establish thermal equilibrium, the sensor element should be thin enough (usually tens of micrometers), while for matrix-based IR image devices this element can also have a small area. In the case when the observed object is stationary, the sensor external irradiation should be intermittent, i.e., modulated with a certain frequency (usually several tens of hertz); thus when the irradiation stops for a short time, the pyroelectric element would have enough time to return to its thermal equilibrium (the corresponding chopper can be mechanical or piezoelectric). Electrodes deposited on the element are connected to an amplifier: usually this is a field effect transistor with high input resistance.

The time-dependent pyroelectric response to thermal radiation incident on the sensor element is shown in Fig. 4.2B. As long as irradiation is not present, the pyroelectric is in thermodynamic equilibrium when the energy of ion attraction in the polar-sensitive bonds (governed by the difference in ion electronegativity; see Chapter 1) is completely balanced by the energy of phonons (thermal chaotic motion in a lattice). An increase or decrease in temperature causes a disturbance of this equilibrium, as a result of which the pyroelectric induces electrical polarization, shown in Fig. 4.2A in the form of bound electrical charges on the surface of the pyroelectric element; these charges are compensated by the electrical charges on electrodes.

As seen in Fig. 4.2B, the sensor's temperature approximately reproduces the intensity of the incident energy according to the law  $\delta T(t) \sim [1 - e(-t/\tau_1)]$  with delay time  $\tau_1$ , which depends on the heat capacity and thermal conductivity of the pyroelectric and electrodes. With a small delay, the pyroelectric current  $j_p(t)$  quickly increases to a maximum, but then it gradually drops to almost zero with relaxation time  $\tau_2$

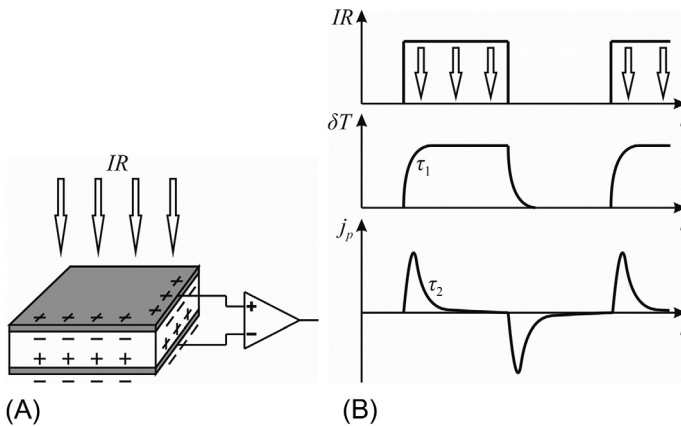


**Fig. 4.2** Principle of pyroelectric sensor operation: (A) Sensor is irradiated by heat flux  $IR$  and signal goes to amplifier; (B) time-dependence of heat flux  $IR$  modulated by square modulator,  $\delta T$  is temperature change of sensor and  $j_p$  is pyroelectric current.

depending on the capacity of the pyroelement and on input resistance of the amplifier. When the pyroelectric element cools and returns to thermal equilibrium with the medium, a new peak of pyroelectric current occurs but of opposite polarity; therefore, the pyroelectric signal repeats the modulation, which has a meandering character.

Among far-infrared pyroelectric devices, there are *motion detector sensors*, which can detect movement of human beings, animals, and anything that radiates thermal infrared radiation [13]. Another class of devices consists of high-precision *infrared thermometers* which require noncontact temperature measurements in the areas where physical contact is not possible, such as moving objects, extremely heated substances, etc. (the sensitivity of pyroelectric thermometers reaches  $10^{-6}$  K). Pyroelectric sensors practically solve the problem of detecting low-power heat energy fluxes, including measurements of the shape and power of short ( $10^{-5}$ – $10^{-9}$  s) *laser radiation pulses*, and can be applied for laser power measurements that have a repetitively pulsed energy up to 25 kHz.

However, the **pyroelectric vidicons** in both vacuum and microelectronic designs can be considered the main applications of pyroelectrics. Pyroelectric transducers of the infrared image (thermal imagers) are intended for the conversion of thermal (or radiation) images into electrical signals or into visible images on a television screen. Infrared vision (“dark vision”) is of great importance in medicine and various other fields and technologies.

Vacuum pyrovidicons make use of the pyroelectric effect to register the spatial distribution of the radiation in infrared imaging systems. To be detected, the thermal image is projected onto a thin plate of pyroelectric—the target. The thermal image creates the electrical relief on this target, which is a distribution of pyroelectric charges; this relief modulates the current in the electronic beam that scans the pyroelectric target. It is important to note that the radiation flux absorbed by a target causes the thermal relief changes over time. As a result of the transformation, “infrared radiation—electrical signal” appears on the screen of the video-controlling device as a visible image formed with a period of the frame of the thermal relief.<sup>b</sup>

Despite the low-energy efficiency of thermoelectric conversion, pyroelectricity should not be considered a weak effect. For example, a 1-mm thick tourmaline plate being heated by 10 K creates a potential of 1.2 kV [2], and this despite the fact that tourmaline has a relatively small pyroelectric coefficient. In the case of a strong pyroelectric—triglycine sulfate (TGS)—its rapid heating may cause electrical breakdown due to the pyroelectric potential arising. Perhaps for this reason, the possibilities

<sup>b</sup> The areas of application of pyroelectric vidicons include, for example, aeroregistration of fires, which allow, on the background of dense smoke, detection of a source of fire and targeting of fire extinguishing agents, to determine the boundaries of underground fires in coal mines, etc. Remote registration of infrared illumination during construction and operation of buildings can reduce the cost of their heating. Pyroelectric vidicons are also used to control various technological processes. For example, they are important for assessing the status of high-voltage transmission lines according to infrared data obtained from vidicons located on helicopters, as well as for checking of isolation of powerful electric machines. They are used also for automated technological control of electronic components that are under electric voltage. Pyroelectric imagers are widely used in medical practice to provide a successful diagnosis of cardiovascular and cancerous diseases [11].

of creating pyroelectric generators, in which the pyroelectric can be repeatedly heated and cooled in order to generate useful electrical energy, have been investigated.

Possible advantages of such pyroelectric generators for power generation (as compared to conventional heat engines and electrical generators) include low operating temperatures, less bulky equipment, and fewer moving parts. Such generators use the principle of multistage devices, optimizing the conditions of energy exchange between successive cascades. To compare the competitiveness of pyroelectrics with other types of similar devices, it is possible to compare data from different types of solid-state energy converters: radioisotope-thermoelectric has a mass of 200 kg/kW and efficiency up to 3%; photovoltaic semiconductors (solar cells) have mass of 10 kg/kW and efficiency up to 40%; a pyroelectric multistage cascade has mass of 4 kg/kW and efficiency up to 10%. Nevertheless, pyroelectric devices are far from being ready for industrial applications.

It is interesting to note that pyroelectrics were used to create large electric fields needed to control deuterium ions in the process of nuclear fusion. For this purpose, a pyroelectric crystal was applied that, under certain conditions, develops pyroelectric voltage that is sufficient for the occurrence of cold-temperature thermonuclear fusion [4]. In this case, a pyroelectric is used to create a high-intensity electrical field in order to accelerate the deuterium ions to bombard a target that also contains deuterium. In this case, two deuterium nuclei can merge into one, forming a nucleus of helium-3 and a high-energy neutron. In one experiment, pyroelectric potassium tantalate was rapidly heated to 40°C and the tungsten needle created a field of 25 GV/m. The device turned out to be a useful neutron generator, but could not be a source of energy since it requires much more energy than it produces.

## 4.2 Pyroelectric effect simulations

As mentioned earlier, the pyroelectric effect can be *naturally* observed in polar crystals (as well as in polarized ferroelectric ceramics and polar polymers). Moreover, this effect can also be *artificially* induced in the nonpolar dielectrics by electrical bias field, as well as by partial restriction of certain types of deformations in polar-neutral piezoelectrics (this latter case was already considered in detail in [Chapter 2](#)). Next, basic models of natural pyroelectricity in polar-sensitive crystals will be considered, followed by the electroinduced pyroelectric effect.

In short, the physical mechanism of the pyroelectric effect is as follows: under constant external conditions (temperature, pressure, etc.), the internal structure of a polar crystal corresponds to its energy minimum. At the same time, polar-sensitive interatomic bonds, striving for mutual ordering, are in *subtle equilibrium* with thermal chaotic motion of atoms of the crystal lattice. When this equilibrium changes, caused for example by a temperature change (i.e., change in thermal energy), the polar crystal immediately reacts to this change by the appearance of electrical polarization—bound charges on the crystal surface.

1. *A simplified model* of the usual pyroelectric effect considers the one-dimensional structural arrangement of polar-sensitive bonds shown previously in

Chapter 1, using the very simple model in Fig. 1.11A, presented in more detail in Fig. 1.14. Traditionally, the pyroelectric effect is explained by two mechanisms: first, by change in the *orientation* of polar-sensitive bonds due to alteration in the intensity of thermal chaotic motion, and, second, due to the piezoelectric effect caused by *thermal deformation* of the polar crystal. Correspondingly, these effects are called the *primary* and the *secondary* effects, which are described by pyroelectric coefficients  $\gamma^{(1)}$  and  $\gamma^{(2)}$ . In the case of a mechanically free crystal, both of these mechanisms contribute to thermally induced electrical response:  $P = \gamma \cdot \Delta T$ , where  $\gamma = \gamma^{(1)} + \gamma^{(2)}$ . The polar-sensitive structure of a pyroelectric (that looks like *hidden* internal polarity) is able to provide an electrical (vector) response to scalar external impacts: in the given case, when temperature changes.

The *primary* mechanism of pyroelectricity, i.e., the change in the orientation of polar-sensitive structural units, manifests itself *regardless* of the mechanical conditions in which the crystal is located (that is, whether it is mechanically free or clamped). It should be noted that the primary effect is most noticeable *above* the Debye temperature ( $T > \theta_D$ ), when thermal fluctuations in the crystal (phonons) become sufficiently active.

The *secondary* mechanism of pyroelectricity, i.e., the piezo-transformation of thermal deformation, is possible in the *mechanically free* crystals only. Usually (but not always) this effect prevails at lower temperatures ( $T < \theta_D$ ).

Both mechanisms are schematically illustrated in Fig. 4.3 by temperature transformations of the one-dimensional model, which is a chain having length  $l$  and made of polar pairs. It is assumed that in the initial state of polar crystal (at very low temperature  $T_1$ ), inevitable quantum oscillations of the crystal lattice prevent the complete ordering of polar-sensitive bonds.<sup>c</sup>

Next, as can be seen from Fig. 4.3, when temperature rises to  $T_2$ , a *partial ordering* of polar-sensitive structure occurs, during which its length decreases on  $-\Delta l_2$ . In Chapter 3 various explanations were given for this compression: the ordering of polar bonds or the establishment of a closer covalent connection.

Further increase of temperature, accompanied by the essential increase of phonon concentration, leads to the thermal expansion of the model chain (the nature of which is also described in Chapter 3). Then this extension continues at  $T_3$  and  $T_4$  in Fig. 4.3.

**2. The secondary pyroelectric effect** can be explained by the one-dimensional model presented earlier as the *piezoelectric* response of a chain. Indeed, any mechanical stretching or compression of a model chain leads to an additional change in specific electrical moment:  $\Delta M_{i2} \sim \Delta l/l$ . Thus, not only from general considerations but also from the given simple model, it follows that *any pyroelectric should have piezoelectric properties* (but the opposite conclusion would be inaccurate in normal conditions).

In the case of a secondary pyroelectric effect, the proportionality of electrical moment  $\Delta M_{i2}$  to temperature increment  $\Delta T$  is a result of *linear* dependence of thermal deformation on temperature:  $\Delta l \sim \alpha \Delta T$ , where  $\alpha$  is the coefficient of thermal

<sup>c</sup> This fact is confirmed by the impossibility of achieving perfect ordering, for example, in the *virtual ferroelectrics*  $\text{KTaO}_3$  and  $\text{SrTiO}_3$ , where polar ordering fails due to quantum oscillations.

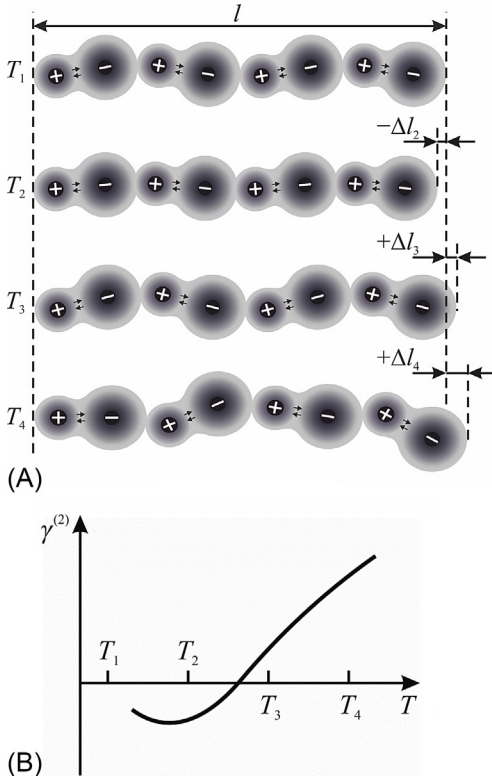


**Fig. 4.3** One-dimensional model of pyroelectricity (A):  $T_1$ —polar-sensitive chain with length  $l$  at very low temperature;  $T_2$ —partial ordering of polar-sensitive bonds accompanied by chain compression on  $-\Delta l_2$ ; while  $T_3$ ,  $T_4$  show thermally activated disordering with chain elongation on  $+\Delta l_3$  and  $+\Delta l_4$ ; (B) secondary pyroelectric coefficient temperature dependence.

expansion, as well as a result also of *linear* dependence of mechanically induced electrical moment  $\Delta M_{i2}$  on relative deformation (strain), which means the direct piezoelectric effect:  $\Delta M_{i2} \sim e\Delta l/l$ , where  $e$  is the piezoelectric strain constant. From these two formulas it is possible to obtain a simple linear equation for the secondary pyroelectric effect:  $\Delta M_i = \gamma^{(2)}\Delta T$ , where  $\gamma^{(2)} = ea$  is the secondary pyroelectric coefficient produced by piezoelectric conversion of thermal strain. Practically, the dependence of  $\gamma^{(2)}(T)$  follows temperature dependence of the thermal expansion coefficient  $\alpha(T)$ , which in polar crystals at low temperatures is negative but then changes following the law  $\gamma^{(2)} \sim \alpha \sim T^3$ .

Some examples of  $\gamma^{(2)}(T)$  dependence in pyroelectric crystals are shown in Fig. 4.4. Usually at low temperatures the pyroelectricity decreases significantly down to negative values. Moreover, the largest secondary pyroelectric coefficient is seen in the lithium sulfate crystal, which at normal temperatures has technical applications as a thermal sensor (due to its low dielectric permittivity and high stability). In the pyroelectrics-semiconductors of the  $A^{II}B^{VI}$  group (CdS is their representative) as well as in other *hexagonal crystals*, whose  $\gamma^{(2)}(T)$  dependence is shown in Fig. 4.4B, the pyroelectric effect is much smaller than in lithium sulfate (note that special characteristics  $\gamma^{(2)}(T)$  of beryllium oxide are due to its very large Debye temperature).

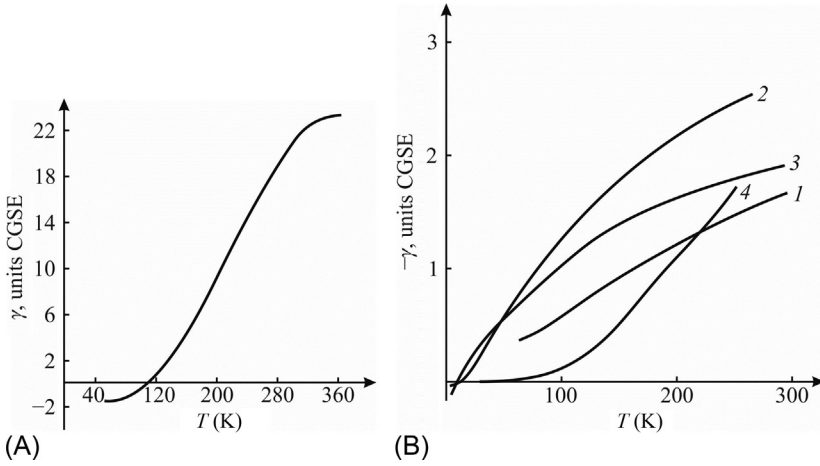


**Fig. 4.4** Secondary pyroelectric coefficient temperature dependence [2]: (A) Lithium sulfate crystal,  $\text{Li}_2\text{SO}_4\text{-H}_2\text{O}$ ; (B) tourmaline,  $\text{NaMg}[\text{Al}_3\text{B}_3\text{-SiO}_2(\text{OOH})_{30}]$  (1), ZnO (2), CdS (3), BeO (4).

It is noteworthy that in most polar crystals, which are discussed in detail in Section 4.3, the thermal expansion coefficient at low temperature becomes negative. Accordingly, their pyroelectric coefficient  $\gamma^{(2)}(T)$  changes its sign, as is seen in Fig. 4.3; moreover, it should be noted that the change in sign of the pyroelectric coefficient could hardly be explained adhering to the model of spontaneous polarization.

Thus the secondary pyroelectric coefficient can be measured as a difference between pyroelectric coefficients of mechanically free and clamped crystals. This coefficient can also be calculated from the equation of piezoelectric response:  $M_i = e_{im}x_m$ , where  $e_{im}$  are components of piezoelectric modulus (third-rank tensor) and  $x_m$  is a component of strain (second-rank tensor). Under thermal influence this effect is excited by thermally induced strains in a crystal:  $x_m = \alpha_m dT$ , where  $\alpha_m$  is a component of the thermal expansion coefficient (which is also a second-rank tensor). It should be noted that, traditionally, components of symmetric second-rank tensors (such as strain  $x_m$ , stress  $X_n$ , and others) are denoted by a single index which, however, has six values:  $m, n = 1, 2, \dots, 6$ , while the components of first-rank tensors (vectors) are usually characterized by an index with three values:  $i = 1, 2, 3$ . As a result, components of the secondary pyroelectric coefficient are written as follows:  $\gamma_i^{(2)} = e_{im}\alpha_m$ .

**3. The primary pyroelectric effect** needs to be discussed in more detail. The bonding energy of polar bonds determines their resilience to chaotic thermal motion, and these bonds react to external action by a change accompanied by the electrical response, i.e., by induced polarization. Weakening or strengthening of polar-sensitive structure steadiness depends on the intensity of thermal motion in the crystal. At that, in the first approximation, thermally induced elementary electrical polar moment  $dm$  can be considered as proportional to the intensity of thermal motion:  $dm \sim k_B T$ . The density of thermally induced electrical moment of 1D polar chain  $M_{i1}$  can be obtained by summing the elementary moments along the chain:  $M_{i1} = \gamma^{(1)}\Delta T$ , where  $\Delta T$  is

some temperature interval and  $\gamma^{(1)}$  is the *primary* pyroelectric coefficient, emergent due to the electrical reaction of the polar-sensitive crystal.

The reaction of “more persistent” polar-sensitive bonds to external influence (in this case, to temperature change) is much weaker than the reaction of “more pliant” polar bonds. Therefore, in “more persistent” pyroelectrics the primary coefficient  $\gamma^{(1)}$  is much less than in the “more pliant” pyroelectrics, which, as a rule, are ferroelectrics. Indeed, in the ferroelectrics, in the end, thermal chaotic motion destroys any correlation of polar-sensitive bond in the Curie point. (In this regard, it should be noted that in ferroelectrics, because of weakness of their polar bonding, the external electrical field is able to reorient the direction of these bonds to the opposite one, forming a dielectric hysteresis loop.)

Currently, dozens of pyroelectric crystals have been investigated and many new compositions have been developed. However, Fig. 4.5 shows only the classic examples: pyroelectric coefficients for two well-studied crystals: Rochelle salt (RS) and triglycine sulfate (TGS). The study of RS is only of academic interest, especially in the sense that two phase transitions are observed in this crystal: a ferroelectric phase transition at  $+24^\circ\text{C}$  and an antiferroelectric phase transition at  $-18^\circ\text{C}$ . In this regard, the pyroelectric coefficient in the RS changes its sign. In the TGS crystal, the primary pyroelectric coefficient reaches a record value among crystalline pyroelectrics ( $\gamma \sim 350 \mu\text{C}/(\text{m}^2\text{K})$ ). In addition, for practical applications, it is very convenient that the maximum of the pyroelectric coefficient  $\gamma^{(1)}(T)$  in TGS crystals is located in the region of normal temperatures.

Summing up this discussion and taking into account both classical mechanisms of pyroelectricity, for thermally induced polarization it is possible to obtain

$$\Delta M_i = (\gamma^{(1)} + \gamma^{(2)}) \Delta T$$

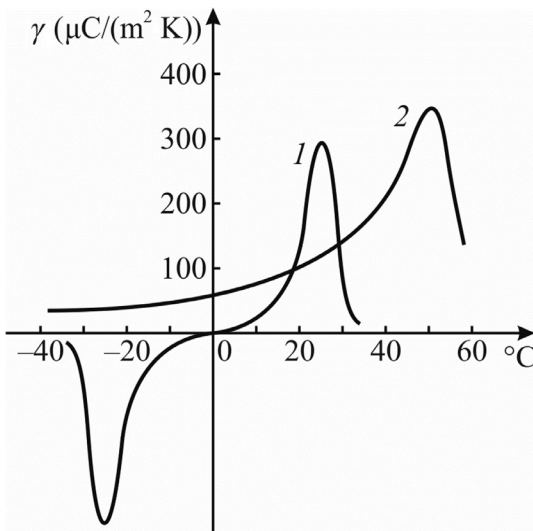


**Fig. 4.5** Pyroelectric coefficient temperature dependence [2]: 1—Rochelle salt ( $\text{KNaC}_4\text{H}_4\text{O}_6 \cdot \text{H}_2\text{O}$ ); 2—triglycine sulfate ( $(\text{NU}_3\text{CH}_2\text{COOH})_3 \cdot \text{H}_2\text{SO}_4$ ).

Electrical moment induced by temperature change in the *linear* (“persistent”) pyroelectrics (such as tourmaline or lithium sulfate crystals) is mostly due to the thermal deformation of a crystal. On the contrary, in the *nonlinear* (“pliant”) pyroelectrics (which include ferroelectrics), temperature-induced electrical moment is caused mainly by the thermal disordering of the dipole-type oriented polar-sensitive structure. At that, a large change of polar-sensitivity with temperature in *ferroelectrics* near their Curie point is described by equation  $\Delta M_i \sim (\theta - T)^{0.5}$ , where  $\theta$  is the Curie-Weiss temperature and power “0.5” is the Landau critical index. In all of these cases, the behavior of pyroelectrics corresponds to the one-dimensional polarity model.

**4. The electrically induced artificial pyroelectric effect** finds application in the infrared image matrix sensors, which use paraelectric ceramics. Such a matrix consists of thousands of identical miniature pyroelectric elements, each of which is connected to its own amplifier (which also has the form of a corresponding matrix). Ceramics are used because in a crystal it is difficult to ensure the uniformity of all the elements due to the inevitable changes in the conditions of crystal growth.

Some designs of IR imagers are known in which the *ferroelectric* ceramics are used below the Curie temperature, in which it is nevertheless necessary to maintain the same polarization of all elements by an electrically bias field. In this case it is advisable to speak of an *electrically supported* pyroelectric effect. Some companies use the lead titanate-based ceramics for such microelectronic imagers, for example,  $\text{Pb}(\text{Ti},\text{Zr})\text{O}_3$ ; such instruments provide infrared observations with a temperature contrast better than 1°C.

For even greater sensitivity, it is possible to choose a dielectric with the highest dependence of permittivity on temperature<sup>d</sup>; such are the ferroelectrics in their *paraelectric phase*, where the dependence of  $\epsilon(T)$  is described by the Curie-Weiss law (Fig. 4.6A). For example, Texas Instruments applied a ceramic solid solution  $\text{Ba}_{0.67}\text{Sr}_{0.33}\text{TiO}_3$  (BST) for this purpose, with a Curie point near 20°C with a permittivity maximum of about 25,000 [14]. However, above the Curie point polar-sensitive bonds in the paraelectric are disordered, so that an external *electrical bias field*  $E_b$  must be applied to induce a pyroelectric effect (in the case of BST, the optimal  $E_b$  is  $\sim 4$  kV/cm).

The dotted line in Fig. 4.6A shows the temperature dependence of polarization *without* external bias field application, while the solid line characterizes the polarization at the bias field. This field shifts the phase transition toward higher temperatures, and such a reduction of  $P(T)$  allows a record temperature change on  $+\delta T$  or  $-\delta T$  by the measuring of pyroelectric current induced by the changing of polarization ( $+\delta P$  or  $-\delta P$ ). At the selected working point (at temperature  $T_b$  and the displacement field  $E_b$ ) the induced polarization equals  $P_b$ , being *nonequilibrium* without external electrical support. The electrical field  $E_b$  that holds the polarization induced by it at a given

<sup>d</sup> Since the pyroelectric coefficient is  $\gamma = dP/dT \approx (\epsilon_0 \cdot d\epsilon/dT)E$ , the external electrical field  $E$ , in principle, always induces pyroelectricity, but this effect is usually imperceptibly small, since typically in the usual crystals  $\epsilon \sim 10$  and permittivity weakly depends on temperature. The exceptions are ferroelectrics, where huge  $\epsilon \sim 10^4$  changes dramatically with temperature according to the Curie-Weiss law. As a result, the induced pyroelectric effect becomes so large that it finds important technical applications.

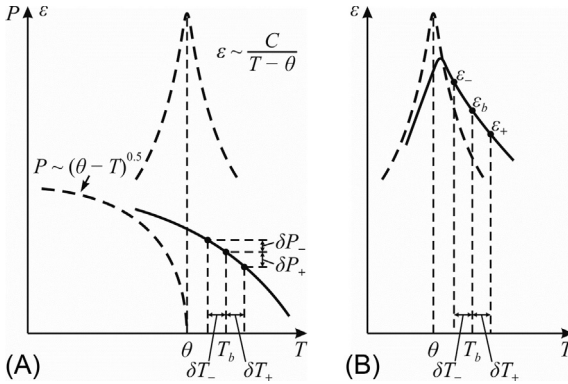


**Fig. 4.6** Electrically induced pyroelectric effect in paraelectric phase of ferroelectric: (A) Dielectric permittivity  $\epsilon$  and reversible polarization  $P$  temperature dependence; (B) dielectric permittivity  $\epsilon$  (dotted line—without bias field, solid line—at bias field).

temperature  $T_b$  resists the polar bonds' natural disordering caused by thermal random motion of the crystal lattice. The change in this temperature on  $\pm \delta T$  due to external heating or cooling disrupts this equilibrium, and when a new equilibrium is established the polarization changes on  $\pm \delta P$ , which leads to registration of a new temperature by the signal current flowing through a corresponding transistor.

It should be noted that the mechanism of electrically induced pyroelectric response can be explained differently (Fig. 4.6B). Peculiar for ferroelectrics, the temperature maximum of permittivity under the action of the electrical displacement field expands and shifts toward high temperatures. At a selected operating point with bias field  $E_b$  and base temperature  $T_b$ , permittivity equals  $\epsilon_b$ , so the sensor element has capacitance  $C_b \sim \epsilon_b$  and contains electrical charge  $Q_b \sim C_b$ . If the sensor's temperature rises by  $+\delta T$ , the capacitance of the element decreases by  $\delta C$ ; moreover, the excess charge  $\delta Q_b$  flows to the input circuit of the amplifier, registering the increase in temperature. Similarly, when temperature decreases by  $-\delta T$ , the capacitance of the pyroelectric element increases, and the bias electrical field additionally infects it with a charge  $+\delta Q_b$ , which is registered by the amplifier in the form of an electrical signal of opposite polarity.

In military technologies, microelectronic matrix pyroelectrics are widely used in vidicons: matrix devices allow the spatial distribution of radiation to be investigated. Such sensitive receivers of radiation can consist of many pyroelectric elements that form the *pyroelectric line* (with several dozen elements) or the pyroelectric matrix ( $10^3$ – $10^5$  elements). In such matrices, thousands of miniature pyroelectric cells are placed on one silicon plate of the processor. Each elementary pyroelement is connected to the input of a corresponding integral transistor so that the square-inch plate is a solid-state IR TV receiver. Such noncooled receivers have very high sensitivity that grows as the square root of the number of elements, and can distinguish between a temperature contrast of 0.1–0.2 degrees.

**5. The thermomechanical induced artificial pyroelectric effect** is described in detail in Chapter 2. Moreover, in any piezoelectric (including nonpyroelectrics) an artificial pyroelectric effect can be obtained, which might have interest for practical applications. The magnitudes of such a mechanically induced pyroelectric effect and

the ordinary pyroelectric effect can be compared by the example of a lithium niobate crystal. In the  $\text{LiNbO}_3$  crystal, in addition to a pyroelectric polar axis, there are also three polar-neutral axes, and in crystal slices made perpendicular to any of these axes with thermal deformation limiting (for example, by sticking such a slice onto silica glass substrate), it is possible to get the artificial pyroelectric effect with artificial pyroelectric coefficient  $\gamma^*_{2} = 40 \mu\text{C m}^{-2} \text{K}^{-1}$ , which is only slightly inferior to the usual pyroelectric coefficient of  $\text{LiNbO}_3$ , equal to  $\gamma_3 = 50 \mu\text{C m}^{-2} \text{K}^{-1}$  [7, 10].

At the same time, the thermomechanically induced pyroelectric effect opens up completely new possibilities for the use of wide-gap semiconductors-piezoelectrics. In them, the artificial pyroelectric effect is not small: the coefficient of gallium arsenide is  $\gamma^*_{111} = 1.5 \mu\text{C m}^{-2} \text{K}^{-1}$  (as compared with the well-known pyroelectric tourmaline with  $\gamma = 4 \mu\text{C m}^{-2} \text{K}^{-1}$ ). In the bismuth germanate ( $\text{Bi}_{12}\text{GeO}_{20}$ ) crystal this parameter equals  $\gamma^*_{[111]} = 20 \mu\text{C m}^{-2} \text{K}^{-1}$ , which exceeds many times the effects in quartz and GaAs. It can be supposed that temperature dependence of piezoelectric polar-sensitivity can be used in microelectronics for thermal sensors [5, 8, 9].

Thus the physical mechanisms of the pyroelectric effect can be varied.

### 4.3 Pyroelectric effect thermodynamic description

The pyroelectric effect is defined as the electrical response of a polar crystal to uniform alteration of crystal temperature. As was shown in the introduction in the discussion of Fig. I.1, the pyroelectric effect can be described by *four* different equations (depending on thermal and electrical conditions). Since the pyroelectric effect can be primary and secondary, mechanical boundary conditions have to be taken into account in these equations. It is advisable to consider thermodynamics of the pyroelectric effect by taking into account those boundary conditions that are used in the most common case of pyroelectrics application, in a thermal sensor.

In a mechanically free crystal (when stress  $X_m = 0$ ) in electrically free conditions (the crystal is situated in a closed circuit when  $E_i = 0$ ), the arising pyroelectric current is defined by the pyroelectric coefficient  $\gamma_i^{X,E}$ , where superscripts indicate the permanency of the electrical field and mechanical stress during thermodynamic processes of pyroelectric response; the subscript means that the pyroelectric coefficient is a vector. In fact, electrical field and mechanical stress are not always zero, but it is assumed that they remain unchanged; for example, a polycrystalline pyroelectric sensor array usually needs an unaltered electrical displacement field to orient ferroelectric domains; moreover, this target is experiencing constant mechanical stress because it is deposited on a substrate.

As follows from the simple model of pyroelectricity shown in Fig. 4.2, traditionally the phenomenological division of pyroelectric effect into primary and secondary effects is accepted, with coefficients  $\gamma^{(1)}$  and  $\gamma^{(2)}$  correspondingly:

$$\begin{aligned} \gamma_i^{X,E} &= \gamma_i^{(1)} + \gamma_i^{(2)} = \gamma_i^x + d_{im}^T \cdot c_{nm}^{X,E} \cdot \alpha_n^{X,E}, \quad i = 1, 2, 3; \quad m, n \\ &= 1, 2, \dots, 6. \end{aligned} \quad (4.1)$$

The contribution of the primary pyroelectric effect can be found during a mechanically clamped crystal study when strain is absent ( $x_n = 0$ ), i.e.,  $\gamma^{(1)} = \gamma_i^x$ . The contribution of the secondary effect can be found experimentally as the difference between pyroelectric coefficients of free and clamped crystals:  $\gamma_i^{(2)} = \gamma_i^{X,E} - \gamma_i^x$ , which can be calculated using Eq. (4.1) with known components of piezoelectric modulus  $d_{im}^T$ , elastic stiffness  $c_{mn}^{X,E}$ , and thermal expansion coefficient  $\alpha_n^{X,E}$  (superscripts correspond to different boundary conditions). Usually in linear (“persistent”) pyroelectrics  $\gamma = 10^{-7}$ – $10^{-5}$  C m<sup>-4</sup> K<sup>-1</sup> while in nonlinear (“pliant”) pyroelectrics-ferroelectrics  $\gamma = 10^{-5}$ – $10^{-3}$  C m<sup>-4</sup> K<sup>-1</sup>.

It should be recalled that symmetry requirements permit both primary and secondary pyroelectric effects only in 10 of 20 piezoelectric classes of crystals. At that, in the pyroelectric crystal a “peculiar polar direction” exists, along which the pyroelectric response shows a maxim (Fig. 4.1B). In the remaining 10 piezoelectric but not pyroelectric classes of crystals, no scalar (homogeneous) influence, including temperature, can result in a vector (electrical) response under *homogeneous* boundary conditions, i.e., if the crystal is mechanically completely free or entirely clamped. In order to excite electrical response in the piezoelectric by thermal influence, the temperature *gradient* or the *inhomogeneous* boundary conditions are needed.

A pyroelectric is a transducer of thermal energy into electrical energy. When using the electrocaloric effect, which is the inverse effect to the pyroelectric effect, electrical energy is converted into a heat. The efficiency of these conversions is characterized by the coefficient of electrothermal bonding  $K_{TE} = K_{ET}$ . The power coefficient of thermoelectric conversion  $K_{TE}^2$  shows what part of thermal energy  $dW_T$  delivered to the reformative element is converted into the electrical energy  $dW_E$ :

$$K_{ET}^2 = dW_E/dW_T. \quad (4.2)$$

In view of some difficulties associated with determination of  $K_{ET}$  in the dynamic regime of work, the efficiency of thermoelectric conversion might be estimated using quasistatic thermodynamic relations derived from Gibbs thermodynamic potential ( $G$ ) or on the basis of electrical potential of Gibbs ( $G_2$ ), which describes equilibrium properties of crystals.

There are eight thermodynamic potentials, corresponding to eight combinations of conjugate thermodynamic variables  $D$  and  $E$ ,  $X$  and  $X$ ,  $S$  and  $T$ ; three of these might be selected as the dependent variables, and the remaining three as the independent variables. For *potential*  $G$  the *independent* variables are stress ( $X$ ), electrical field ( $E$ ), and temperature ( $T$ ), while the *dependent* variables are strain ( $x$ ), electrical displacement ( $D$ ), and entropy ( $S$ ). In the case of *potential*  $G_2$  the *independent* variables are strain ( $x$ ), electrical field ( $E$ ), and temperature ( $T$ ), while the *dependent* variables are stress ( $X$ ), electrical displacement ( $D$ ), and entropy ( $S$ ). The increment of thermodynamic potentials is determined by the work done by the reformative element under certain boundary conditions specific for the functional given element:

$$dG = -x_i dx_i - D_n dE_n - SdT, dG_2 = X_i dx_i - D_m dE_m - SdT,$$

where

$$x_j = -\partial G/\partial X_j; \quad D_m = -\partial G/\partial E_m; \quad S = -\partial G/\partial T,$$

and, correspondingly

$$X_j = -\partial G_2/\partial x_j; \quad D_m = -\partial G_2/\partial E_m; \quad S = -\partial G_2/\partial T;$$

where:  $i, j = 1, 2, 3$ , and  $n, m = 1, 2, \dots, 6$ .

The choice of potentials (of possible eight) to estimate the work carried out by a thermodynamic system is determined by mechanical, electrical, and thermal boundary conditions under which the element of the device works. The change of independent variables ( $X, E, T$ ) that corresponds to the equation of state for the dependent variables ( $x, D, S$ ), where the superscripts  $X, E, T$  denote the so-called boundary conditions, which must be invariable, while crystal parameters are measured:

$$\begin{aligned} dx_n &= s_{nm}^{E,T} dX_m + d_{in}^{X,T} dE_i + \alpha_n^{X,E} dT; \\ dD_n &= d_{nj}^{E,T} dX_j + \varepsilon_{nm}^{X,T} dE_m + \gamma_n^{X,E} dT; \\ dS &= \alpha_j^{X,E} dX_j + \gamma_n^{X,T} dE_n + C^{X,E} dT/T. \end{aligned} \quad (4.3)$$

In the preceding expressions (Eq. 4.3), the following notations are applied:

$$s_{nm}^{E,T} = dx_n/dX_m = -\partial^2 G/\partial X_m \partial X_n$$

– the elastic stiffness, fourth-rank tensor;

$$d_{nj}^{X,T} = d_{nj}^T = dx_n/dE_i = dD_j/dX_n = -\partial^2 G/\partial X_n \partial E_i$$

– the piezoelectric modulus, third-rank tensor;

$$\varepsilon_{ij}^{X,T} = \partial D_i/\partial E_j = -\partial^2 G/\partial E_i \partial E_j$$

– the permittivity tensor, second-rank tensor;

$$\alpha_n^{X,E} = \alpha_n^E = dx_n/dT = -\partial^2 G/\partial T \partial X_n$$

– the thermal expansion tensor of free crystal, second-rank tensor;

$$\gamma_i^{X,E} = \gamma_i^E = dD_i/dT = \partial S/\partial E_i = -\partial^2 G/\partial T \partial E_i$$

– the pyroelectric coefficient, tensor of the first rank;

$$C^{X,E} = T dS/\delta T = -T \partial^2 G/\partial T^2$$

– the specific volumetric heat capacity, scalar (tensor of zero rank).

The transformations of the piezoelectric strain tensor are:  $e_{nj}^{x,T} = e_{nj}^{E,T} = e_{nj}^E$ .

Taking into account that shape and volume of a pyroelectric element do not change ( $x = 0$ , i.e., crystal is mechanically clamped), from the preceding equations in the case of  $E = 0$  it is possible to obtain the contribution to thermally induced polarization  $P_i$  from the *primary* pyroelectric effect:

$$dP_i = \gamma_i^x dT, \quad (4.4)$$

where  $\gamma_i^x = \gamma_i^{(1)}$ .

The preceding equations also allow finding the *piezoelectric contribution* to the pyroelectric coefficient, as well as to the dielectric permittivity and to the volumetric specific heat capacity of a crystal. The measurements of pyroelectric effect are usually carried out at the condition  $E = 0$ . When using Eq. (4.4), it is possible to obtain the following relationship between pyroelectric coefficient of mechanically free ( $X = 0$ ) crystal and mechanically clamped ( $x = 0$ ) crystal:

$$\gamma_i^X = \gamma_i^x + e_{mi}^T \alpha_m^E, \quad (4.5)$$

which means  $\gamma = \gamma^{(1)} + \gamma^{(2)}$ , because the expression  $e_{mj}^T \alpha_m^E = \gamma^{(2)}$  describes the contribution of the *secondary* pyroelectric effect.

At constant temperature, the permittivity of a mechanically free ( $\epsilon_{nm}^{X,T}$ ) crystal and a clamped ( $\epsilon_{nm}^{x,T}$ ) crystal are related as follows:

$$\epsilon_{ij}^{X,T} = \epsilon_{ij}^{x,T} + d_{ni}^T e_{nj}^T, \quad (4.6)$$

where  $d_{ni}^T e_{nj}^T$  is the piezoelectric contribution to permittivity.

For heat capacity of an electrically short-circuited ( $E = 0$ ) and mechanically free ( $X = 0$ ) pyroelectric crystal, the following relation holds:

$$C^{E,X} = C^{E,x} + T \alpha_m^E c_m^{E,T}.$$

Note that the difference between  $C^{E,X}$  and  $C^{E,x}$  is small, so that in the notation of volume specific heat it is possible to keep only one superscript:  $C^E$ .

From the preceding equations it follows that the use of a pyroelectric element in the absence of mechanical stress ( $X = 0$ ) and when an electrical field is absent ( $E = 0$ ), the accumulation of electrical energy in the pyroelectric element  $dW_E$  is described by the potential  $G$ , which in a given boundary condition corresponds to the expression:

$$dW_E = D_i dE_i = (dP_i)^2 / \epsilon_0 \epsilon_{ij}^{X,T} = (\gamma_i^{X,E})^2 (dT)^2 / \epsilon_0 \epsilon_{ij}^{X,T}, \quad (4.7)$$

where  $dP_i = dD_i$  and  $dW_E$  is the quantity of electrical energy obtained in the process of the pyroelectric effect.

The thermal energy  $dW_T$  that is spent on energy storage in a crystal by definition equals to  $dS \cdot dT$ ; under a given boundary condition it corresponds to the expression:

$$dS \cdot dT = (\alpha_m^{X,E} dX_m + \gamma_i^{X,T} dE_i + C^{X,E} dT/T) \cdot dT,$$

where the increments  $dX_m$  and  $dE_i$  respectively represent the appearance of stress and electrical field in the crystal. Estimation of the amount of  $(\alpha_m^{X,E}dX_m + \gamma_i^{X,T}dE_i)$  in different pyroelectric crystals shows that it does not exceed a fraction of a percent of the value  $(C^{X,E}dT/T)$ , so

$$dW_T = C^{X,E}(dT)^2/T_p, \quad (4.8)$$

where  $T_p = T$  is the operating temperature of the element and  $dW_T$  is the obtained quantity of thermal energy.

Thus when the pyroelectric element is mechanically free ( $X = 0$ ), Eq. (4.2) after substitution of Eqs. (4.7), (4.8) can be written as follows:

$$K_{ET}^2 = \left[ (\gamma_i^{X,E})^2 (dT)^2 / \epsilon_0 \epsilon_{ij}^{X,T} \right] / \left[ C^{X,E} (dT)^2 / T_p \right] = (\gamma_i^{X,E})^2 T_p / \epsilon_0 \epsilon_{ij}^{X,T} C^{X,E}.$$

Similarly, the electrothermal conversion factor for a mechanically clamped crystal element is:

$$K_{ET}^2 = \left[ (\gamma_i^{X,E})^2 (dT)^2 / \epsilon_0 \epsilon_{ij}^{X,T} \right] / \left[ C^{X,E} (dT)^2 / T_p \right] = (\gamma_i^{X,E})^2 T_p / \epsilon_0 \epsilon_{ij}^{X,T} C^{X,E}.$$

Calculations show that even in the best pyroelectrics, the electrothermal conversion factor is small: in TGS crystal  $K_{ET}^2 = 4\%$ , in SBN ( $\text{Sr}_{0.5}\text{Ba}_{0.5}\text{Nb}_2\text{O}_6$ )  $K_{ET}^2 = 1.2\%$ , and in  $\text{LiTaO}_3$   $K_{ET}^2 = 1\%$ . In other pyroelectrics this factor is even smaller: in  $\text{BaTiO}_3$   $K_{ET}^2 = 0.25\%$  and in polymer PVDF  $K_{ET}^2 = 0.2\%$ . The relatively low efficiency of thermoelectric conversion is due to the physical nature of this phenomenon in dielectric crystals, which are “electrically persistent” in relation to the external influences. Note in this regard that the efficiency of energy conversion is much higher in the case of the piezoelectric effect. The corresponding electromechanical coupling coefficient  $K_{EM}$  greatly exceeds the pyroelectric coupling coefficient  $K_{ET}$ . The value of  $K_{EM}$  sometimes reaches  $\sim 0.95$ , and in the case of piezoelectric resonance in crystals that have a high electromechanical quality, this coefficient increases to almost 1.

In spite of low efficiency, the pyroelectric effect is used primarily for the detection and measurement of heat flow, and, under certain conditions, for direct transition of thermal energy into electricity. The “direct” conversion of heat into electricity is used in thermal imaging and in highly sensitive temperature sensors. The advantage of pyroelectric sensors is that they use a thermal signal to convert electrical signals to dielectrics, in which electrical conductivity is virtually absent and the “shot noise” produced by the charge carriers is reduced to zero. As is well known, the most important characteristic for the sensor is the signal-to-noise ratio, which in pyroelectrics exceeds this parameter of semiconductor sensors (the latter usually need to be cooled).

The efficiency of pyroelectric sensors that convert infrared radiation into electrical energy is evaluated by special quality parameters commonly called *figures of merit*. In addition to the main parameter (pyroelectric coefficient  $\gamma$ ), the figures of merit used are necessary. For example, for a pyroelectric element under heating conditions, the greater the temperature change, the lower its volumetric specific heat  $C_V$ ; also as the

voltage generated by the element becomes greater, the lower is its permittivity  $\epsilon$ . Depending on where the pyroelectric material is used, the figures of merit are different.

In the case of a *low-impedance* amplifier application, for the efficiency of a sensor the next figure of merit should be used: *current sensitivity*  $S_j = \gamma/C_V$ . However, in the case of a *low-impedance* amplifier another figure of merit is *voltage sensitivity*  $S_V = \gamma/(C_V\epsilon_0\epsilon)$ . For a thermal imaging matrix device, the Landau coefficient  $\alpha_L = (T - \theta)/\epsilon_0 C$  (where  $C$  is the Curie-Weiss constant) is important, as it characterizes the temperature dependence of permittivity, so that the figure of merit is  $\gamma/(C_V\alpha_L\epsilon_0\epsilon)$ . Finally, for a long-distance temperature sensor in which low noise in the pyroelectric is most important, it is recommended to use the following figure of merit:  $\gamma/[C_V(\epsilon_0\epsilon\tan\delta)^{1/2}]$ , where  $\tan\delta$  is the dielectric losses characteristic. Table 4.1 presents a number of options for pyroelectrics with these quality parameters.

The *first group* of pyroelectrics presented in Table 4.1 includes ferroelectrics with *nonlinear* dependence  $P(E)$ : crystals of triglycine sulfate group, lithium niobate and lithium tantalate, potassium nitrate, lead titanate, polarized zirconate-titanate ceramics. In ferroelectrics, the primary pyroelectric effect is mainly used, which is especially large near the Curie point, where the temperature change of polar-sensitive bonds is expressed very strongly and the pyroelectric coefficient reaches a maximum.

The *linear* crystalline pyroelectrics (in which dependence  $P(E)$  is linear) can be attributed to the *second group* of pyroelectrics. In them, the polar-sensitive bonds have the same direction throughout a crystal (unlike ferroelectrics, which are usually divided into domains), and this direction cannot be changed by an external electrical field. The pyroelectric coefficient of linear pyroelectrics varies a little with temperature, never falling to zero as in ferroelectrics. These pyroelectrics include  $A^{II}V^{VI}$  crystals with wurtzite structure (such as CdS) as well as lithium sulfate, lithium tetraborate, and others. In linear pyroelectrics the contribution of secondary pyroelectric effect is relatively large and can exceed the contribution of the primary pyroelectric effect.

Polar polymers (such as PVDF films) and polar composite materials can be placed in the *third group* of pyroelectric materials. They need additional special treatment: stretching the film over several times with subsequent polarization, as a result of which the polymer film acquires pyroelectric properties. The pyroelectric coefficient of polymeric materials is lower than that of polar single crystals and pyroelectric ceramics, but the films have excellent mechanical properties, being flexible materials.

For comparing physical mechanisms of pyroelectricity in different pyroelectric materials, as well as for evaluating the possibilities of their technical application, the temperature dependencies of the current and voltage efficiency of pyroelements are given in Fig. 4.7.

It is noteworthy that crystals with the maximum current sensitivity  $\gamma/C_V = S_j$  do not belong to the thermostable materials. Typically, they are ferroelectrics with a Curie point  $\theta$  of about 300 K. The pyroelectric coefficient is maximal near the  $\theta$ , because in this temperature range the ability of temperature polarization is seen most commonly. The change in specific heat of the material has little effect on the temperature change of quality parameter  $\gamma/C_V$ . Crystals with a maximum of this parameter, the

**Table 4.1** Basic parameters of pyroelectrics used to manufacture sensors:  $\gamma$ —pyroelectric coefficient,  $\epsilon$ —permittivity,  $\lambda$ —thermal conductivity,  $C_V$ —volumetric heat capacity,  $S_j$ —current sensitivity,  $S_V$ —voltage sensitivity (all data given at room temperature).

Pyroelectric	$\gamma$ ( $10^{-5}$ C m $^{-2}$ K $^{-1}$ )	$\epsilon$	$\lambda$ (W/ $\mu$ C)	$C_V$ ( $10^6$ J/(m $^3$ K))	$\gamma/C_V = S_j$ ( $10^{-11}$ A m/W)	$\gamma/(C_V\epsilon) = S_V$ ( $10^{-12}$ A m/W)
TGS $T_C = 49^\circ\text{C}$	40	35	0.4	2.5	16	4.6
DTGS $T_C = 61^\circ\text{C}$	27	18	0.4	2.5	10.8	6.0
LaTGS $T_C = 49.5^\circ\text{C}$	70	35	$\sim 0.4$	2.6	27.5	7.8
DLaTGS $T_C = 49.2^\circ\text{C}$	25	22	$\sim 0.4$	2.6	9.8	4.5
TGFB $T_C = 73.8^\circ\text{C}$	21	15	$\sim 0.4$	1.7	12.5	8.3
TGSe $T_C = 22^\circ\text{C}$	30	400	$\sim 0.4$	1.8	16.8	0.4
LiTaO $_3$ $T_C = 618^\circ\text{C}$	22	52	4.2	3.2	6.9	1.3
LiNbO $_3$ $T_C = 1210^\circ\text{C}$	8	30	$\sim 4.0$	2.8	2.9	0.9
Sr $_{1/2}$ Ba $_{1/2}$ Nb $_2$ O $_6$ $T_C = 116^\circ\text{C}$	60	400	$\sim 2.0$	2.34	25.6	0.6
PLZT (6/80/20) $T_C = 120^\circ\text{C}$	76	1000	1.2	2.6	29	0.3
PLZT (4/65/35) $T_K = 225^\circ\text{C}$	52	680	1.2	2.6	20	0.3
PCD 33/14 $T_K = 420^\circ\text{C}$	17	250	$\sim 2.0$	3.2	5.3	2.0
PVDF	3	11	0.13	2.4	1.3	1.0

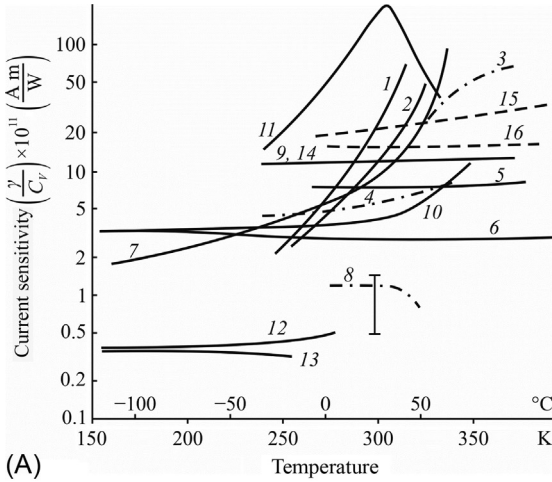
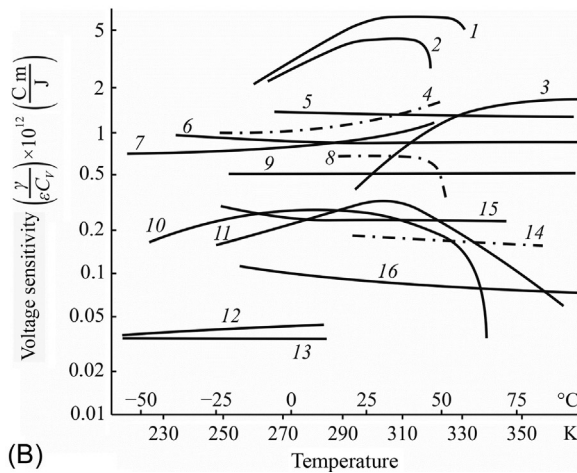


**Fig. 4.7** Temperature dependence of current (A) and voltage (B) sensitivity in different pyroelectrics: 1—DTGS; 2—TGS; 3—BaTiO<sub>3</sub>; 4—Li<sub>2</sub>SO<sub>4</sub>·H<sub>2</sub>O; 5—LiTaO<sub>3</sub>; 6—LiNbO<sub>3</sub>; 7—Pb<sub>5</sub>Ge<sub>3</sub>O<sub>11</sub>; 8—PVDF<sub>2</sub>; 9—SbNbO<sub>4</sub>; 10—Sn<sub>2</sub>P<sub>2</sub>S<sub>6</sub>; 11—Sr<sub>0.75</sub>Ba<sub>0.25</sub>Nb<sub>2</sub>O<sub>6</sub>; 12—CdO; 13—ZnO; 14—PZT-5; 15—PZT-4; 16—PZT-1306.



triglycinsulfate (TGS), deuterated triglycerol sulfate (DTGS), and strontium-barium niobate (SBN), belong to the pyrodetectors. Therefore, in this case the sensitive receivers need some external thermal stabilization. In ferroelectric crystals of barium titanate (BaTiO<sub>3</sub>) and lead germanate (Pb<sub>5</sub>Ge<sub>3</sub>O<sub>11</sub>) with a rather low Curie point (400 and 450 K, respectively), the thermostability of the  $\gamma/C_V$  characteristic is not very good. On the contrary, the thermostatically stable crystals are lithium tantalate (LiTaO<sub>3</sub>) and lithium niobate (LiNbO<sub>3</sub>), as well as lead stibioniate crystals (SbNbO<sub>4</sub>), but the latter are not sufficiently developed technologically.

The current sensitivity of the pyroelectric elements made of tantalate and lithium niobate is on an order of magnitude inferior to the crystals of SBN and TGS. For comparison, in Fig. 4.7 the  $\gamma/C_V$  characteristics of nonferroelectric (but pyroelectric) crystals are shown: cadmium sulfide (CdS) and zincite (ZnS). These pyroelectrics are very

thermostable but have low sensitivity; moreover, with increasing temperature their electrical conductivity increases. However, these pyroelectrics also deserve attention, because they can be relatively easily obtained in the form of thin layers by modern microelectronic technology. Having micron thickness, CdS and ZnS films can be relatively easily integrated into a monolithic structure with silicon.

Other dependencies that are shown in Fig. 4.7B are the temperature variation of the quality parameter of volt-watt sensitivity  $\gamma/(C_V\varepsilon) = S_V$ . In this case, at the temperature peak of parameter  $\gamma$  in the vicinity of the Curie point the ferroelectric is compensated by temperature dependence of its permittivity  $\varepsilon$ . With this parameter, crystals of the TGS type have a clear advantage over other pyroelectrics. However, these crystals are mechanically fragile, water soluble, and, if possible, they should be replaced by the chemically and mechanically durable pyroelectrics such as single crystals LiTaO<sub>3</sub>, SbNbO<sub>4</sub>, and tin thiogipophosphate (Sn<sub>2</sub>P<sub>2</sub>S<sub>6</sub>).

Since most pyroelectrics belong to ferroelectrics, it is advisable to apply the thermodynamic Landau theory developed to describe the properties of the ferroelectrics to analyze, in part, the temperature dependence of figures of merit. Since most of the ferroelectrics used in pyroelectric sensors belong to crystals with a second-order phase transition, then the Landau's proposed expansion of free energy  $F$  in a series on the fluctuations in polarization has the following form:

$$F(P, T) = \frac{1}{2}\alpha_L P^2 + \frac{1}{4}\beta_L P^4, \quad (4.9)$$

where temperature-dependent parameter Landau  $\alpha_L = \alpha_0(T - \theta) = (T - \theta)/\varepsilon_0 C$  ( $\theta$  and  $C$  are temperature and Curie-Weiss constant, respectively);  $\beta_L$  is temperature-dependent parameter Landau. Considering that the electrical field can be defined as the derivative  $\partial F/\partial P$ , Eq. (4.9) can be rewritten as  $E = \alpha_L P + \beta_L P^3$ . For an electrically free crystal ( $E = 0$ ), it is possible to obtain:

$$[(T - \theta)/\varepsilon_0 C]P + \beta_L P^3 = 0. \quad (4.10)$$

Inverse dielectric susceptibility is  $\chi^{-1} = dE/dP = d^2F/dP^2 = \alpha_L + 3\beta_L P^2$  but it is possible to consider that  $\chi \approx \varepsilon$ , since  $\varepsilon = 1 + \chi$  and permittivity of ferroelectrics is very large:  $\varepsilon \gg 1$ . In the polar phase (when  $T < \theta$ ) the condition of minimum free energy follows:  $P = (T - \theta)^{0.5}/\varepsilon_0 C$ . Since dielectric permittivity is defined as

$$\varepsilon \cong (\partial P/\partial E)/\varepsilon_0 = \alpha_L + 3\beta_L P^2,$$

then temperature dependence of the dielectric constant below temperature  $\theta$  is seen to be  $\varepsilon = C/[2(T - \theta)]$ .

According to Debye theory, a heat capacity temperature increase can be given as:  $\Delta C_V = (\partial F/\partial T)$ . Since from the Landau theory it follows that  $P^2 = -\alpha_L/\beta_L$  so equation for free energy will look like

$$F(P, T) = \frac{1}{2}\alpha_L P^2 + \frac{1}{4}\beta_L P^4 = \frac{1}{2}\alpha_L(-\alpha_L/\beta_L) + \frac{1}{4}\beta_L(-\alpha_L/\beta_L)^2 = -\frac{1}{4}\alpha_L^2/\beta_L.$$

As a result of the differentiation of this equation by temperature, we have:

$$\begin{aligned}\Delta C_V &= (\partial F / \partial T) = \frac{1}{2}(\theta - T) / \beta_L (\varepsilon_0 C)^2, \\ C_V &= C_{V0} + \Delta C_V = C_{V0} + \frac{1}{2}(\theta - T) / \beta_L (\varepsilon_0 C)^2.\end{aligned}$$

The substitution of the indicated temperature dependencies  $C_V$ ,  $\varepsilon$ , and  $\gamma = \partial P / \partial T$  in the formula for the basic parameters of the quality of pyroelectrics (see [Table 4.1](#)) allows their temperature dependence to be given in the form:

$$\begin{aligned}\gamma &= \partial P / \partial T = \frac{1}{2}(\beta_L \varepsilon_0 C)^{-1/2} (\theta - T)^{-1/2}, \\ \gamma / C_V &= \frac{1}{2}(\beta_L \varepsilon_0 C)^{-1/2} (\theta - T)^{-1/2} / \left[ C_{V0} + \frac{1}{2}(\theta - T) / \beta_L (\varepsilon_0 C)^2 \right]; \\ \gamma / C_V \varepsilon_0 \varepsilon &= \beta_L^{-1/2} (\varepsilon_0 C)^{-3/2} (\theta - T)^{1/2} / \left[ C_{V0} + \frac{1}{2}(\theta - T) / \beta_L (\varepsilon_0 C)^2 \right].\end{aligned}$$

It is seen that to maximize the efficiency of transformation of the heat signal into an electrical signal, the pyroelectric receiver should have not only high pyroelectric coefficient, but also low heat capacity and low dielectric constant (which determines the capacity of the pyroelectric cell and pyroelectric signal generated on it). Some improvements of the characteristics of the pyroelectric element can be obtained using composite pyroelectric ceramics and polymers. In addition, it should be noted that besides the primary pyroelectric effect ( $\gamma^{(1)}$ ), in mechanically free crystal there is also the secondary pyroelectric effect ( $\gamma^{(2)}$ ) due to the piezoelectric contribution to the pyroelectric coefficient. The contribution to pyroelectricity from secondary pyroelectricity usually is less than the contribution from primary pyroelectricity.

Thus thermodynamic and other calculations and estimates provide the opportunity to explain the features of pyroelectrics, and they also allow engineers to choose pyroelectric materials for certain devices.

## 4.4 Electrocaloric effect

According to the Curie principle, any linear physical effect in crystals must have an opposite effect. For example, opposite to the direct piezoelectric effect is the inverse piezoelectric effect. Similarly, the inverse to the pyroelectric effect is the electrocaloric effect. In this way, pyroelectric not only converts thermal energy into electrical energy, but vice versa.

In short, the physical mechanism of the electrocaloric effect is as follows: a constant electrical field applied from the outside to a polar crystal *violates its equilibrium state* under certain conditions, which is established thermodynamically at a given temperature and pressure and corresponds to the energy minimum. In this case, the mutual ordering of polar-sensitive interatomic bonds, existing in equilibrium structure of a pyroelectric, changes. If an applied field is directed accordingly internal orientation of polar bonds, then it increases total energy of a crystal which heats up. If this field is directed oppositely, then crystal energy decreases, which is expressed in its cooling.

Understanding the physical mechanism and taking into account the influence of this effect is important for describing and predicting some properties of polar crystals, especially in the case of their phase transitions. Controlled by voltage, electrocaloric cooling (or heating) depends on the polarity of the applied electrical field and crystal polarity. Moreover, alternating voltage can generate in a crystal the *temperature wave*. Electrocaloric effect can be used for temperature control by electrical voltage, basically to achieve cooling.

Electrocaloric effect consists of the changing of temperature  $\Delta T$  of pyroelectric crystal when an electrical field  $\Delta E$  is applied to it. In accordance with this, the equation for the electrocaloric effect is

$$\Delta T = \xi \cdot \Delta E, \text{ or in the differential form } \xi = dT/dE,$$

where  $\xi$  is a coefficient of the electrocaloric effect. Electrocaloric (as well as pyroelectric) properties have only crystals of 10 polar classes: 1, 2, 3, 4, 6,  $m$ ,  $2m$ ,  $3m$ ,  $4m$ ,  $6m$ .

It is possible to find the relationship between electrocaloric coefficient ( $\xi$ ) and pyroelectric coefficient ( $\gamma$ ). The possibility of inducing electrical polarization  $P$  in the polar-sensitive crystal reflects the *change* in heat content in a crystal that is described by entropy  $S$ . Moreover, internal energy  $U$  of the crystal remains *unchanged*, which makes it possible to write down the next relationships:

$$dU = 0 = EdP + TdS,$$

from which it follows

$$T = -E \left( \frac{dP}{dS} \right), \text{ and } \frac{\partial T}{\partial E} = -\frac{dP}{dS} = -\left( \frac{\partial P}{\partial T} \right) \cdot \left( \frac{\partial T}{\partial S} \right).$$

Taking into account the fact that  $\partial T/\partial E = \xi$  and  $\partial P/\partial T = \gamma$ , it can be obtained from thermodynamic relations:  $dS = dQ/T$ , where  $dQ$  is the heat increment equals  $\rho \cdot C \cdot J \cdot dT$  ( $\rho$  is crystal density,  $C$  is crystal heat capacity, and  $J$  is the mechanical equivalent of heat). Next it is possible to get

$$\xi = -\gamma \cdot T / (\rho \cdot C \cdot J).$$

It's clear that electrocaloric and pyroelectric coefficients are proportional to each other but have opposite signs. Therefore crystals with a large pyroelectric effect also exhibit increased electrocaloric effect.

Crystal is a single system: if it is *heated* (or cooled), then the change in its internal polarity occurs due to the electrocaloric effect, which leads to *cooling* (or heating) of the crystal, as a result of which it will tend to maintain its temperature (Le Chatelier's principle). Therefore, when an electrical field is applied to a crystal, the electrocaloric effect can lead to both heating and cooling of a pyroelectric, depending on how the ordered polar bonds of a crystal are directed with respect to the applied field. If this field coincides with the orientation of polar-sensitive bonds, the temperature of the

crystal will increase, but if an electrical field is directed oppositely to their direction, the crystal cools. It is natural that only electrocaloric *cooling* may have interest for technical applications; therefore this possibility needs to be evaluated.

In the *linear* (“persistent”) pyroelectrics, in accordance with the smallness of the pyroelectric effect, the electrocaloric effect is also small: calculations show that a pyroelectric even in a very strong electrical field (already close to the electrical breakdown field) can change its temperature only tenths of a degree kelvin, which obviously does not have any technical interest. However, in the *nonlinear* ferroelectrics (and antiferroelectrics), in which the maximum value of permittivity reaches many thousands, the electrocaloric effect is large enough for a serious discussion of its possible use in *technical* cooling devices (a large electrocaloric effect is described, for example, in Ref. [15]). Therefore, it is necessary to dwell in more detail on the electrocaloric effect in ferroelectric materials.

As is known, in the vicinity of phase transitions in ferroelectrics the latent heat of a transition is released or absorbed: it can be considered that this heat is required to compensate the electrocaloric effect. From this point of view, phase transition looks like this: a crystal *heated* from outside loses the ordering of its polar bonds and, therefore, it is cooled due to the electrocaloric effect, as a result of which *heat is consumed without heating the crystal*. When the crystal is *cooled* through a phase transition, the reverse occurs. Since the temperature of the phase transition can be shifted by electric field application, the process of heat release and heat absorption can be controlled electrically.

As noted, in the *nonlinear* (“pliant”) pyroelectrics-ferroelectrics, the electrocaloric effect maximum is observed in the vicinity of the phase transition: it is caused by the appearance (or disappearance) of polar-sensitive bond ordering. Without application of an external electric field, during external cooling from the paraelectric phase into the ferroelectric phase, the crystal heats up by approximately parts of a degree, but it also cools by the same amount during the phase transition from the ordered (ferroelectric) phase into the disordered paraelectric phase. At that, the change in temperature makes it possible to directly estimate (using the knowledge of crystal specific heat) the latent heat of phase transformation.

When an electrical *field is applied* to the crystal near the ferroelectric phase transition, such a heating-cooling effect becomes significant: using available fields, due to the electrocaloric effect in ferroelectrics it is possible to change the temperature by 1–2°C. Such a change is usually called a *shift of Curie point* under an applied electrical field, when the phase transition temperature shifts to higher temperatures. Considering applications using cyclical operations in a cooling device, this shift in temperature is obviously of technical interest.

Low temperatures are needed both for low-temperature electronics and for home appliances. It is important to achieve solid-state coolers that prevent the use of both environmentally harmful freon and the machine equipment of conventional refrigeration units (with compressors). Interest in electrocaloric cooling, i.e., changes in the temperature of a dielectric in adiabatic conditions in the case of an application of or switching off of an electrical field has been noted for a long time, but mostly in the area of comparatively low temperatures.

The temperature change  $dT$  for one cycle of application of electrical field can be described as follows:

$$dT = -(T/C)(dP/dT)dE,$$

where  $P$  is induced polarization and  $C$  is heat capacity of the dielectric used. Early experiments showed that, when applying an electrical field up to 25 kV/cm in most pyroelectrics and ferroelectrics, the electrocaloric lowering of temperature does not exceed 0.5 K, and that only in a narrow range of temperatures near their Curie point. However, calculations show that a value of  $dT$  less than 1 K is not sufficient for commercial applications of pyroelectric materials in the temperature range 290–310 K.

A literature survey [15] provides guidance on obtaining low temperatures in an operationally important temperature range from liquid nitrogen to freon temperatures using ferroelectric materials. Rather large values of electrocaloric effect ( $2.6^\circ\text{C}$ ) near the phase transition were obtained in antiferroelectric ceramics of a  $\text{Pb}(\text{Zr},\text{Sn},\text{Ti})\text{O}_3$  system, as well as in ceramics  $\text{Pb}(\text{Sc},\text{Nb})\text{O}_3$ . For example, a large electrocaloric effect has recently been obtained with a cycle temperature of about  $4^\circ\text{C}$ . This field-induced phase transition from antiferroelectric into the ferroelectric phase with enlarged electrocaloric effect was obtained for  $(\text{Pb},\text{La})(\text{Zr},\text{Sn},\text{Ti})\text{O}_3$ . Technical interest in such effects is due to the fact that solid-state refrigeration systems based on elastocaloric, magnetocaloric, and electrocaloric materials offer potential advantages over conventional vapor-compression cooling technologies. Moreover, the electrocaloric effect (electrical field inducing adiabatic temperature change in dielectric material) has some advantages, such as the high cooling efficiency and easy miniaturization that are needed for portable cooling devices.

Consider the physical basis of this effect. In the vicinity of a phase transition, all thermodynamic functions of a crystal change, but *differently* for ferroelectrics and antiferroelectrics. A convincing example is the *change in volume*: Fig. 4.8A shows

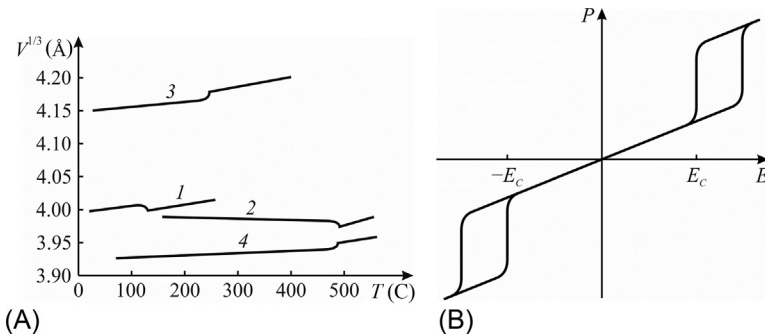


**Fig. 4.8** Explanation of field-induced electrocaloric effect: (A) Temperature dependence of cubic root on unit cell volume in ferroelectrics  $\text{BaTiO}_3$  (1) and  $\text{PbTiO}_3$  (2), and in antiferroelectrics  $\text{PbZrO}_3$  (3) and  $\text{NaNbO}_3$  (4); (B) double hysteresis loop of antiferroelectric.

temperature dependence of the unit cell volume for two ferroelectrics and two antiferroelectrics. It is seen that the volume of ferroelectric polar phase *increases* as compared with the nonpolar phase, while the volume of the antipolar phase *decreases*. Obviously, the greatest change in thermodynamic functions can be expected during the transition from antipolar phase into polar phase and vice versa, which can be realized during the phase transitions antiferroelectric  $\leftrightarrow$  ferroelectric induced by electrical field application. Fig. 4.8B demonstrates the corresponding electrical characteristics in the form of a double dielectric hysteresis loop: in the field interval  $-E$  to  $+E$ , the material is antiferroelectric but it transforms into the ferroelectric polar phases both at positive and negative voltages. Thermodynamically, this corresponds to a large electrocaloric effect,<sup>e</sup> which can be considered as the alternative to other cooling methods (such as a large magnetocaloric effect).

Another interesting physical aspect of the electrocaloric effect is temperature hysteresis in the ferroelectrics, experienced at a phase transition that is close to the first type phase transition [2]. This temperature hysteresis expresses the fact that during heating and cooling the ordering of polar-sensitive bonds occurs at different temperatures. It can be explained by means of the electrocaloric effect, which is rather large in such crystals. Indeed, when the crystal is heated, the transition from ordered (ferroelectric) phase occurs at a temperature slightly higher than the “true” transition temperature, because due to the electrocaloric effect the crystal cools a little and uses its ability to remain ferroelectric at temperatures higher than the “true” temperature of phase transition. On the contrary, when cooling from the paraelectric phase, a ferroelectric crystal tends to remain in its paraelectric phase: whenever the ordering of polar-sensitive bonds occurs in it due to the electrocaloric effect the crystal heats up, which contributes to preserving the paraelectric phase.

In conclusion of the discussion of this topic, is appropriate to recall that, in the polar crystals, the electrocaloric effect influences the value of *permittivity*. When thermal equilibrium is entirely established at the time of electrical field application (at very low frequency), a pyroelectric crystal absorbs applied electrical energy and converts it into thermal energy. This is the *isothermal* means of polarization of a polar crystal, which is characterized by isothermal permittivity  $\epsilon^T$ , detectable at rather low frequency. On the contrary, in the case of somewhat rapid changing of an applied electrical field, the energy process has an adiabatic character (when thermal equilibrium has no time to be set). During measurements, this looks like a decrease of the capacitance of the pyroelectric element, i.e., the decrease of its permittivity. Therefore, adiabatic permittivity  $\epsilon^S$  can be determined at increased frequency, where the difference  $\Delta\epsilon_{EC} = (\epsilon^T - \epsilon^S)$  is the electrocaloric part of low-frequency permittivity; this might be essential only in pyroelectrics, depending on their specific heat and pyroelectric coefficient:  $\Delta\epsilon_{EC} = (\gamma^2 T) / (\epsilon_0 C)$ .

<sup>e</sup> Fig. 4.8A shows different changes in volume  $\delta V$  near the phase of the transitions that are close to first type. The relationship between the change in volume  $\delta V$  and temperature change  $\delta T$  can be qualitatively traced from the thermodynamic equation of state:  $pV = RT$ . Since the pressure  $p$  is constant and the  $R$  is a universal constant,  $\delta V / \delta T = \text{const}$ . It means that increments of  $\delta V$  should result in corresponding change in  $\delta T$ .

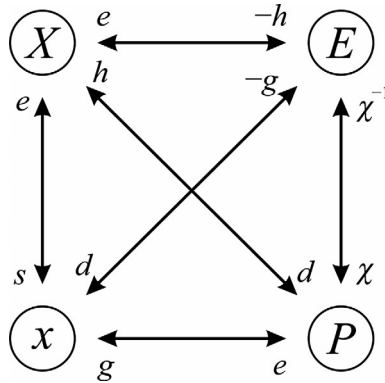
## 4.5 Summary

1. Pyroelectricity is the property of a polar crystal to *produce electrical energy* when it is subjected to a *change* of thermal energy. It is possible also to define the *pyroelectric* effect as the ability of crystals to generate electricity when they are *dynamically* heated or cooled; a pyroelectric becomes polarized positively or negatively in proportional to a *change* in temperature.
2. Pyroelectricity looks like *thermoelectric* power conversion; moreover, this effect is a linear one, so according to the Curie principle, a reversed effect must exist, namely the *electrocaloric* effect, which the *electrothermal* energy conversion characterizes.
3. The physical mechanism of the pyroelectric effect is as follows: under constant external conditions (temperature, pressure, etc.), the structure of a polar crystal corresponds to its energy minimum. At the same time, polar-sensitive interatomic bonds, striving for their mutual ordering, are in *subtle equilibrium* with thermal chaotic motion of atoms in the crystal lattice. When this equilibrium changes, caused for example by change in temperature (i.e., change in thermal energy), the polar crystal immediately reacts by the appearance of electrical polarization—bound charges on the crystal surface.
4. The physical mechanism of the electrocaloric effect is as follows: an electrical field applied from the outside to a polar crystal *violates its equilibrium state* established thermodynamically under certain conditions at given temperature and pressure, which corresponds to the energy minimum. In this case, the mutual ordering of polar-sensitive interatomic bonds, existing in the equilibrium structure, changes. If applied the electrical field is directed accordingly to the internal orientation of the polar bonds, then it increases the total energy of the crystal, which heats up. If this field is directed oppositely, then crystal energy decreases, which is expressed in its cooling.
5. The nature of thermoelectrical coupling in the polar-sensitive crystals and their thermal properties can be described by various models: the *primary* effect, the *secondary* effect, and electrically and mechanically induced *artificial* pyroelectric effects. The hidden intrinsic polarity in pyroelectrics is only their ability to provide an electrical (vector) response to any nonelectrical (scalar) *dynamic* influence (such as uniform change of temperature).
6. The *primary* pyroelectric effect reflects the strength of bonding energy of polar bonds and their resilience to the chaotic thermal motion: these bonds react to external action by such a change, which is accompanied by an electrical response, i.e., by the induced polarization. The *secondary* pyroelectric effect is the piezoelectrically transformed thermal deformation.
7. The *electrically induced* artificial pyroelectric effect exists in all solid dielectrics but has practical meaning only in the dielectrics with very high permittivity ( $10^3$ – $10^4$ ). The electrical field keeps the induced polar state of the dielectric in opposition to thermal motion in crystal; any violation of this equilibrium with temperature changes leads to the electrical response: the artificial pyroelectricity.
8. The *thermomechanically induced* pyroelectric effect manifests itself in any piezoelectric material and arises along the *polar-neutral* axes (in the pyroelectrics, along a special polar axis, being in this case the secondary pyroelectric effect). Partial limitation of thermal deformation turns the polar-neutral axis into a polar one. This effect can be of practical importance in wide-band semiconductors-piezoelectrics of the  $A^{III}B^V$  type, allowing the combination of pyroelectric element with amplifier in monolithic (one-crystal) devices.

9. Very small changes in temperature can produce the perceptible pyroelectric potential: *infrared sensors* are designed from such pyroelectric materials, when heat of a human or animal from several feet away is enough to generate voltage. Among a wide variety of thermal sensors using the pyroelectric effect are included *motion detector* sensors, *infrared thermometers* for high-precision pyrometry, *pyroelectric vidicons* in both vacuum and microelectronic designs, etc.
10. The *electrocaloric* effect has certain prospects for use in miniature solid-state refrigeration systems. Using the electrically induced phase transition from ferroelectric to anti-ferroelectric phase, a cooling of up to 4°C can be obtained in the single transition period.
11. Research and applications of dielectrics is commonly held under *adiabatic* conditions, when entropy does not change:  $\delta S = 0$ . Therefore, from experiments, the adiabatic permittivity  $\epsilon^S$  can be measured. In such dielectrics, in which polarization strongly depends on temperature, another—*isothermal*—process of polarization might be important, when  $\delta T = 0$  and permittivity is isothermal:  $\epsilon^T$ . Isothermal permittivity is always greater than adiabatic:  $\epsilon^T > \epsilon^S$ . In the vicinity of the ferroelectric phase transition the difference between  $\epsilon^T$  and  $\epsilon^S$  can reach 10%–50%, so it should be taken into account.

## References

- [1] J.C. Burfoot, G.W. Taylor, *Polar Dielectrics and Their Application*, Macmillan Press, New Jersey, 1979.
- [2] I.S. Jeludev, *Basics of Ferroelectricity*, Atomizdat, Moscow, 1973.
- [3] M.E. Lines, A.M. Glass, *Principles and Application of Ferroelectrics and Related Materials*, Clarendon Press, Oxford, 1977.
- [4] B. Naranjo, S. Putterman, T. Venhaus, Pyroelectric fusion using a tritiated target, *Nucl. Instrum. Methods Phys. Res. Sect. A Accel. Spectrom. Detect. Assoc. Equip.* 632 (1) (2011) 43–46.
- [5] L.P. Pereverzeva, Y.M. Poplavko, Pyroelectricity in non-central crystals, *Acta Phys. Pol. A* 84 (2) (1993) 287.
- [6] Y.M. Poplavko, *Electronic Materials. Principles and Applied Science*, Elsevier, 2019.
- [7] Y.M. Poplavko, L.P. Pereverzeva, Pyroelectricity of partially clamped piezoelectrics, *Ferroelectrics* 130 (1992) 361.
- [8] Y.M. Poplavko, L.P. Pereverzeva, Pyroelectric response of piezoelectrics, *Ferroelectrics* 134 (1992) 207.
- [9] Y.M. Poplavko, L.P. Pereverzeva, Thermopiezoelectric transducers, *Ferroelectrics* 131 (1992) 331.
- [10] Y.M. Poplavko, L. Pereverzeva, N.-I. Cho, Y.S. You, Feasibility of microelectronic quartz temperature and pressure sensors, *Jpn. J. Appl. Phys.* 37 (1998) 4041.
- [11] Y.M. Poplavko, L.P. Pereverzeva, A.S. Voronov, Y.I. Yakymenko, *Material Sciences, Part II, dielectrics*, Polytechnik, Kiev, 2007.
- [12] I.S. Rez, Y.M. Poplavko, *Dielectrics: Main Properties and Electronics Applications*, Radio e Svyaz, Moscow, 1989.
- [13] C.F. Tsai, M.S. Young, Pyroelectric infrared sensor-based thermometer for monitoring indoor objects, *Rev. Sci. Instrum.* 74 (12) (2003) 5267–5273.
- [14] K. Uchino, *Ferroelectric Devices*, Marcel Dekker, New York, 2000.
- [15] F. Zhuo, Q. Li, H. Qiao, et al., Field-induced phase transitions and enhanced double negative electrocaloric effects in (Pb,La)(Zr,Sn,Ti)O<sub>3</sub> antiferroelectric single crystal, *Appl. Phys. Lett.* 112 (2018) 133901.



Relationship of main parameters describing piezoelectric effects.

The discovery of piezoelectricity dates back to 1880, when Pierre and Jacques Curie discovered this effect in quartz crystals. The technical application of piezoelectrics started in 1920 with the ultrasonic transducer, invented by P. Langevin and applied for transmitting and receiving signals in water, and from Cady’s work on the use of piezoelectric filters in telephony.

Piezoelectricity is a research issue at the intersection of two classical scientific fields: the mechanics of deformed solid bodies, and the electrodynamics of continuous media. Differential equations of electrodynamics establish a link between vectors of electrical field  $E$ , electrical induction  $D$ , magnetic field  $H$ , and magnetic induction  $B$ . Almost all piezoelectrics are dielectrics, and the piezoelectric effect occurs at speeds much slower than the speed of light. In this case, magnetic effects can be ignored, so instead of electrodynamics the electrostatics equations for dielectrics can be applied when  $\text{rot}E = 0$ ,  $\text{div}D = 0$ . With regard to piezoelectrics, the foundations of this theory were laid earlier in [Chapters 1 and 2](#).

The theory of elasticity was elaborated in the 1920–40s with the works of Cauchy, Poisson, and Green. The connection of electrical charges to mechanical pressure in piezoelectric crystals was established in mathematical form by Pockels, while quantitative ratios were given by Voigt in 1910–20; these equations are fundamental for constructing a mathematical model of the piezoelectric effect. It should be noted that in this chapter only homogeneous mechanical deformations and homogeneous electrical fields (identical throughout a crystal) are considered. In the case of heterogeneous deformations, in addition to the piezoelectric effect and electrostriction, other electromechanical phenomena are possible, for example, the *flexoelectrical* effect (which is very important for liquid crystals). In the case of a temperature

gradient in piezoelectrics, the *tertiary* pyroelectric effect occurs (actinoelectricity in Ref. [1]). The theory of flexoelectricity and actinoelectricity are not considered here.

A piezoelectric is the solid-state transducer of mechanical energy into electrical energy (direct effect) or, vice versa, an electromechanical transducer (converse effect). Moreover, mechanically induced electrical polarization is directly proportional to strain; this is the odd (linear) effect, which is possible only in non-centrosymmetric material. The piezoelectric effect is characterized by various piezoelectric moduli—third-rank tensors, depending on the combination of boundary conditions under which piezoelectricity is used or studied [2]. The interrelation of mechanical and electrical properties in piezoelectrics is characterized by the electromechanical coupling coefficient, the square of which shows how much of the energy applied to a piezoelectric is converted into another kind of energy. Parameters of the piezoelectric effect can be controlled by a bias electrical field, which is used in tunable piezoelectric filters and for surface acoustic wave controlling.

Piezoelectricity, together with electrostriction, refers to electromechanical properties of crystals. Electrostriction is the *universal* property of all dielectrics, since deformation in an applied electrical field is partly a manifestation of electrical polarization, when electrically charged particles are forcedly shifted from their initial positions in the process of their separation. Being a quadratic (even) effect, electrostriction does not have any opposite effect. On the other hand, the linear (odd) piezoelectric effect can be either direct or converse. All electromechanical effects substantially depend on electrical and mechanical boundary conditions (described earlier in [Chapter 1](#)).

The model description of piezoelectricity is given here for:

- *longitudinal* piezoelectric effect in the one-directional polar crystal model;
- *transverse* piezoelectric effect in the plane-oriented polar bonds model;
- *shear* piezoelectric effect in spatially distributed polar bonds model;
- *electrically induced* piezoelectric effect in high-permittivity dielectrics;
- *volumetric effect* in polar-neutral crystals under partial limitation of strain.

Thus, in addition to the linear converse piezoelectric effect, electromechanical effects include the quadratic electrostriction effect, in which electrically induced strain is proportional to the square of field strength. Naturally, the sign of this deformation does not change when electrical polarity changes. In a constant electrical bias field, electrostriction looks like a piezoelectric effect. In this case, the magnitude of such an electrically induced piezoelectric effect can be very large in the peculiar case of paraelectrics and relaxor ferroelectrics, with large permittivity [3].

## 5.1 General characteristics of piezoelectricity

As is well known, only the crystals belonging to 21 noncentrosymmetric classes of point symmetry can have properties described by *odd-rank* tensors. Of them, 20 classes exhibit the *piezoelectric effect*, the quantitative characteristic of which is the third-rank tensor  $d_{ijk}$  (piezoelectric coefficient tensor). Like all material tensors of odd ranks, this tensor vanishes in the crystals that have a center of symmetry; therefore, a linear electromechanical effect in centrosymmetric media is impossible.

The fact is that a piezoelectric effect cannot occur in centrosymmetric crystals, since any mechanical action (which *has center of symmetry*) on a centrosymmetric crystal leads to a symmetry group with a center of symmetry (note that stretching, compression, or shear actions are centrosymmetric actions). In other words, after any *uniform* deformation, a centrosymmetric crystal remains centrosymmetric. The presence of a center of symmetry in a deformed crystal means that there is no reason for mechanically induced electrical polarization arising, because there are *no polar directions* in such a crystal.

Manifestation of the piezoelectric effect in *pyroelectrics* is obvious, since they have a *peculiar polar axis*, so any deformation in them leads to electrical polarization. However, in the *polar-neutral* crystals there are also several polar-sensitive directions [4] although they are totally compensated.<sup>a</sup> The piezoelectric effect in these crystals occurs when the *directional* external influence (acting in a certain direction) makes the polar-neutral structure of such a crystal “*uncompensated*”; thus, as a result of directional mechanical influence in the polar-neutral crystal a *special* polar axis arises. Therefore, all polar-neutral crystals should be attributed to the piezoelectrics.

**1. Piezoelectric materials** include the bulk ceramics, ceramic thin films, multi-layer ceramics, single crystals, polymers, and ceramics-polymer composites. In recent years many different piezoelectric film materials have been developed and tested for different microsystems and microelectronic components. For example, film and bulk piezoelectrics can be used in microwave devices, discussed in [Chapter 6](#). Of particular importance are piezoelectric composites of various classes in which far superior parameters can be obtained to those of homogeneous piezoelectric materials [3]. New relaxor-ferroelectric ceramics and crystals exhibit extremely high efficiency in electromechanical energy conversion, which is of particular interest for medical imaging devices and other applications, such as special drives for industrial nondestructive testing.

**2. Practical applications** of instruments and devices that use the piezoelectric effect in their designs are very wide-ranging and constantly expanding [5]. The most important scientific and technical fields of piezoelectric effect use are:

- *piezoelectronics* (piezoelectric technique of the bulk acoustic waves), including development of piezoelectric receivers, piezoelectric transformers, and piezoelectric motors, adaptors, microphones, resonators, and filters;
- *acoustoelectronics* (piezoelectric technique of surface waves), including development of microelectronic data converters: delay lines, filters, sensors of external influences, convolvers, etc.;

<sup>a</sup> An exception among the 21 crystallographic classes that do not have the center of symmetry (as only 20 classes show piezoelectricity) is the cubic class with point group 432, in which the appearance of piezoelectric activity is prohibited by *other elements* of symmetry. Mechanically induced polarization can be obtained in this class only in the case when applied mechanical stress would be *asymmetric*. Moreover, this “mysterious” noncentrosymmetric but nonpiezoelectric class of crystals, in reality, may behave like a piezoelectric in a *strong electrical field*. The description of the converse piezoelectric effect by a simple linear relation  $x = dE$  in the strong electrical fields should be considered only as the first term of the odd series:  $x = dE + d'E^3 + d''E^5 + \dots$ . In reality, in a weak electrical field, for the noncentrosymmetric class 432 the first term of this series is  $d = 0$ , but the *second term* of this series, namely the  $d'$  term, is nonzero.

- *acousto-optics*, which uses the interaction of optical waves with acoustic waves that allows development of deflectors, optical filters, and other optical devices;
- *energy devices* such as piezoelectric power generators, piezoelectric motors, etc.

The main areas of piezoelectric applications in *electronics* are classified in Fig. 5.1, but this is a far-from-complete list. As is known, some products, such as watches, cameras, mobile phones, televisions, computers, and piezoelectric lighters, have become

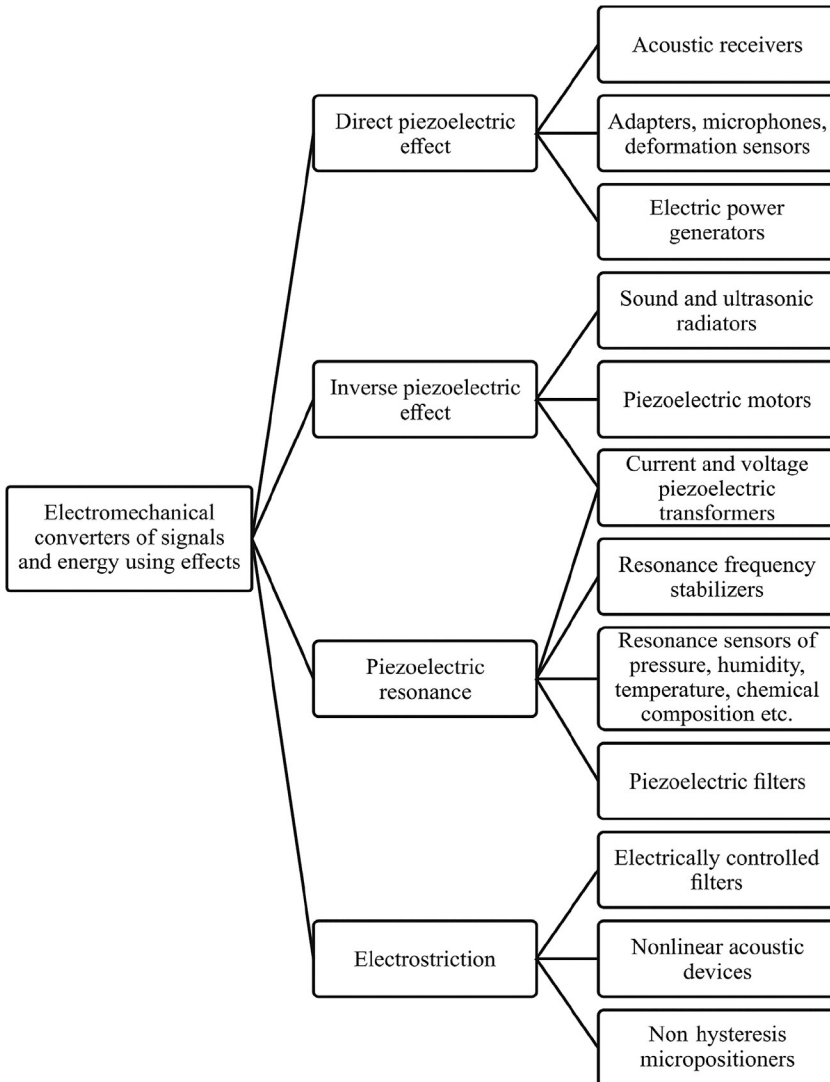


Fig. 5.1 Piezoelectric applications in electronics [6].

the objects of everyday life. Many electronic devices are not possible without the use of piezoelectric elements. These include sonar radiators and antennas, frequency stabilizers in computers, electronic devices and reference timers, power line filters and delay lines in radio and telephone communications, sensors to measure acceleration and vibration, acoustic emission nondestructive testing, piezotransformers and piezomotors, medical ultrasound imaging and medical instruments for various purposes, etc.

Functional assignments of piezoelectric elements found in watches, piezoelectric switches, televisions, and mobile phones are quite diverse, but at the basis of these devices lie the same physical phenomenon: piezoelectricity—that is, the ability of some crystals, ceramics, textures, and composites to produce electricity by changing their shape or size. Conversely, they can change their size or shape under the influence of electrical voltage.

We can mention only some uses of the piezoelectric effect in *microelectronics*:

- Miniature piezoelectric emitters that are effective at high frequencies and have small dimensions (such as those installed in children's toys and music sheets);
- Precision positioning systems, for example, in the needle positioning system in a scanning tunneling microscope or positioners to move hard disk drivers;
- In widescreen printers, printed on solvent ink and inks with ultraviolet hardening;
- Microwave miniature resonant devices based on thin AlN and ZnO films.

A relatively new scientific direction has appeared in *piezoelectronics*. The most important trends among modern applications are:

- Thin piezoelectric films, integrated with semiconductors;
- Microsystems that combine sensors, processors, and actuators;
- Ultrahigh-frequency components based on active dielectrics;
- Nanosized piezoelectrics with various electronic devices being planned.

One of the modern directions of piezoelectronics is converting any motion into electrical current. One example is conversion of human energy into a power supply for various electronic devices: special piezoelectric gear designed for soldiers will allow the use of electric current generated by their movement and thereby eliminate the excessive weight of batteries. Significant advantages can be achieved using nanotechnologies: it is established that as the size of a piezoelectric converter is reduced, its ability to generate energy increases. It has been experimentally shown that nanoparticles of about 20 nm in size produce twice as much current as a monolithic piezoelectric. Dozens of ways of applying nanotechnologies have been proposed, from charging mobile phones using the voice of the consumer to a device that allows reading human thoughts (which is extremely important in neurology).

Some examples of *energy devices* based on piezoelectrics are:

- Vibration dampers for helicopters and airplanes; in particular, a special bearing design has been developed in which the friction is weakened by the vibration, the creation of which does not require special mechanisms (the bearing sleeves are made of piezoelectric material, and electrical voltage makes the piezoelectric shrink and expand, creating a vibration that decreases friction);

- Piezoelectric converters installed in jet aircraft in order to save energy (and, consequently, fuel), in which the vibrations of fuselage and wings are directly transformed into electricity;
- Powered traffic lights have been developed whose batteries are charged from the noise of cars at the street intersections;
- Experiments have been carried out to convert the energy of sea waves into electricity (tidal power plants in the United States). Another example is a piezoelectric system operating experimentally in Japan on the crossroads of railway stations to convert the energy of platform vibrations into electricity [3].

However, this book is not devoted to the consideration of hundreds of piezoelectronic devices; rather, it covers only the *physical bases* of electromechanical transformations in polar crystals and textures.

**3. Piezoelectricity is a linear electromechanical effect** (or *mechano-electrical effect*, which is the same thing) in noncentrosymmetric crystals. In this connection, it is advisable to recall that:

- *Electrical properties* characterize the movement of charged particles in a material caused by an external electrical field. The first property is the electrical polarization, i.e., *charge separation*, representing the *reversible* elastic shift of bound charges. The second electrical property is the electrical conductivity, i.e., *directional movement of free charges*, which is the *irreversible* phenomenon that can be neglected in the context of piezoelectricity.

Moreover, of crystal electrical properties, only dielectric polarization is relevant to the piezoelectric effect. Polarization is described by second-rank tensors of permittivity  $\epsilon_{ij}$  or dielectric susceptibility  $\chi_{ij}$  ( $i, j = 1, 2, 3$ ). When describing electrical polarization as applied to piezoelectricity, only the fast (practically noninertial) mechanisms of elastic displacement of electrons and ions should be taken into account, which makes it possible to disregard fundamental dielectric dispersion  $\epsilon(\omega)$  in almost the entire frequency range of piezoelectric applications (up to 100 GHz).

- *Mechanical properties* are characterized by features of internal bonds between atoms (or between molecules) of a material. Moreover, the *elasticity* should be attributed to the *reversible* mechanical properties, while other mechanical effects, such as fluidity and fracture, are irreversible properties (these last effects are not taken into account when considering piezoelectricity). When describing elastic properties, the discrete structure of crystal is usually ignored, so crystal is considered as a continuous homogeneous medium (*continuum approximation*). This approach is justified up to frequencies near  $10^{12}$  Hz, which is much greater than the usual frequency of operation of conventional piezoelectronics, acoustoelectronics, and acoustooptics (up to 100 GHz).

Therefore when describing piezoelectricity only the reversible (mechanical and electrical) properties of crystals should be taken into account, so the piezoelectric effect is also a *reversible* property (note that reversible electrical properties have already been described in detail in previous chapters).

- *Elastic parameters* of many mechanical properties are most important in describing the piezoelectric effect; they are characterized by material tensors of fourth rank: *elastic stiffness*  $c_{mn}$  and *elastic compliance*  $s_{mn}$  ( $m, n = 1, 2, \dots, 6$ ). It is appropriate to recall that  $c_{mn}$  and  $s_{mn}$  are parameters of Hooke's law, which joins two second-rank tensors: mechanical *stress*  $X_m$  and mechanical *strain*  $x_n$ :  $X_m = c_{mn}x_n$ , or in the converse equation:  $x_n = s_{mn}X_m$ .

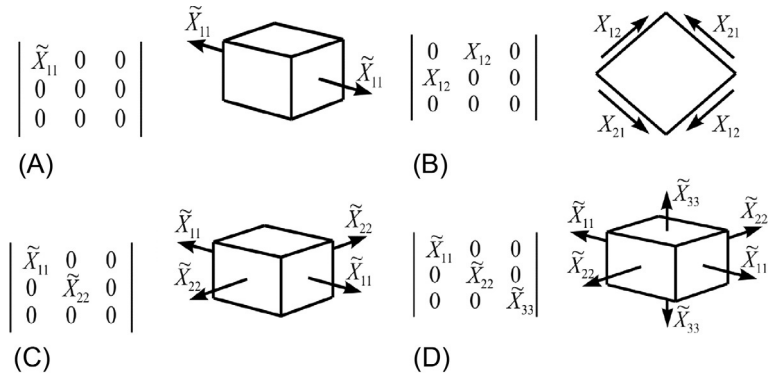


**Fig. 5.2** Matrix representation of stress tensor with geometric explanation of components.

The mechanism of elasticity can be described as follows: deformation of the crystal alters the atomic mutual arrangement and, as a result, forces arise that try to restore the body into its original position. These forces, occurring in a deformed body, are called *internal*, and the magnitude of these forces, being calculated per unit area, is called *stress*.

Homogeneous mechanical stresses, being the second-rank tensor  $X_{ij}$ , can be very diverse, always remaining the *centrosymmetric action* on a piezoelectric.<sup>b</sup> When all components of tensor  $X_{ij}$  are given with regard to the principal axes, some important cases can be shown (Fig. 5.2): (A) line-stressed state (uniaxial stress), such as a uniformly tensile rod; (B) pure shear stress perpendicular to the plane of the figure; (C) plane-stressed state (biaxial stress); (D) volumetric-stressed state (three-axes stress). Hydrostatic action, at which  $X_{11} = X_{22} = X_{33} = -p$  (pressure) is not shown in Fig. 5.2; its matrix is similar to Fig. 5.2D, but the  $X_{ji}$  directions in this case are oriented opposite to what is shown in the figure, and all components have the same magnitude.

*Density of elastic energy*  $W$  of a deformed (or stressed) crystal can be determined from the expression for elementary mechanical work done by forces  $X$  for deformation  $x$ :  $dW = Xdx$ . By integrating this expression,  $W_{elas} = -\frac{1}{2}xX$ , can be obtained. Depending on the task and using Hooke's law in two forms,  $x = sX$  or  $X = cx$ , two equations can be obtained for the density of elastic energy:  $W_{elas} = \frac{1}{2}cx^2 = \frac{1}{2}sX^2$ .

<sup>b</sup> From Ref. [7]. Relative deformation is dimensionless, while the units of stress measurement are  $\text{N/m}^2$  and the same units of measurement are also maintained for elastic rigidity:  $[c] = \text{H/m}^2 = \text{Pa}$  (pascal). Elastic compliance is defined as  $s = \text{Pa}^{-1}$ ; because of the smallness of the pascal unit, the units of gigapascals are often used, equal to  $10^9$  Pa. Knowing all components of one of the elastic tensors, for example, the tensor of elastic stiffness  $c_{mn}$ , it is possible to calculate components of the converse tensor; in the given case, the tensor of elastic compliance:  $s_{mn} = (-1)^{i+j} \Delta c_{mnl} / c_{mn}$ , where  $|c_{mn}|$  is the determinant of the matrix and  $\Delta c_{mnl}$  is the minor of this matrix without the  $m$ -line and  $n$ -column. In addition to tensors of compliance and stiffness, for calculations related to research and practical application of the piezoelectric effect, some other elastic parameters of piezoelectric are significant, which can be calculated with the help of known  $c_{mn}$  or  $s_{mn}$ .

*Volumetric compressibility*  $\langle s \rangle$  is a significant parameter for evaluating the properties of piezoelectrics, for example, for their use as emitters or receivers of elastic waves. This compressibility characterizes the dependence of relative change of the volume  $\Delta V$  of a crystal or texture under the action of hydrostatic pressure  $p$ :  $\Delta V = -ps$ . Volumetric compressibility is formed as an invariant of elastic compliance tensor:  $\langle s \rangle = s_{11} + s_{22} + s_{33} + 2(s_{12} + s_{13} + s_{31})$ . For cubic crystals and isotropic solids, the compressibility looks simpler:  $\langle s \rangle = 3(s_{11} + 2s_{12})$ .

*Volumetric modulus of elasticity*  $K$  is introduced as a parameter converse to compressibility. The parameter  $K$  can also be determined by the tensor of elastic stiffness. For cubic crystals,  $K = (c_{11} + 2c_{12})/3$ . Modulus of elasticity characterizes the ability of material to resist a change in its volume; this parameter is also called volumetric compression modulus. Modulus  $K$  characterizes the ability of an object to resist a change in its volume that is not accompanied by a change in the form of the sample under the influence of normal directional stress that is the same in all directions (this occurs, for example, under hydrostatic pressure conditions). Modulus  $K$  is equal to the ratio of volumetric stress to the value of relative volume compression. It should be noted that volumetric elastic modulus of a nonbinding fluid is different from zero, while for incompressible fluid it is infinite.

*Poisson's coefficient*  $\nu$  is used to characterize elastic properties of a material. As is known, under the action of tensile force the body begins to stretch longitudinally, while (in the vast majority of cases) the cross-section of material decreases. Poisson's coefficient shows how the transverse section of a deformed body changes during its stretching (or compression). Its value is equal to the ratio of relative cross-section of compression  $e'$  (in the case of one-way stretching) to relative longitudinal elongation  $e$ , that is,  $\nu = |e'|/e$ . In the case of an absolutely brittle material, the Poisson's coefficient is 0, and for absolutely elastic material  $\nu = 0.5$ . For most steels this coefficient lies in the region of 0.3; for rubber it is approximately equal to 0.5. Poisson's coefficient is measured in relative units: mm/mm, m/m.

For high-symmetric crystals and isotropic solids, other characteristics of elasticity are used.

The *shear modulus* or rigidity modulus (denoted as  $G$  or  $\mu$ ) characterizes the strained state of pure shear, that is, the ability of a material to resist a shape change while maintaining its volume. The shear modulus is defined as the ratio of shear stress to shear deformation, which is defined as the change in forward angle between the planes in which tensile stresses are applied, to two mutually orthogonal planes. The shear modulus is one of the components of the viscosity phenomenon.

*Young's modulus* ( $E$ ) characterizes the resistance of a material to stretching (or compression) during elastic deformation, or the property of an object to deform along an axis under the action of force along the same axis; it is defined as the ratio of stress to elongation. For cubic crystals,  $E$  equals to each of the first three diagonal components of elastic stiffness, which are the same:  $E = c_{11} = c_{22} = c_{33}$ . Often, Young's modulus, which characterizes the ability to resist tensile deformation, is called simply the *modulus of elasticity*.

In conclusion, it is worth noting that deformation that occurs due to action of an external force *quickly disappears* to zero when this force is removed—this is the case with the so-called “*perfectly elastic solid*.” Only in perfectly elastic materials is Hooke’s law valid: relative deformation (strain) is proportional to mechanical stress, and their behavior during deformation *does not depend on the strain rate*. Exactly this ideal case is implied in the further discussion of the piezoelectric effect.

## 5.2 Model description of piezoelectricity

Manifestations of piezoelectric properties are quite diverse; this is why the electromechanical interaction will first be simulated for the case of *one-directionally* oriented polar-sensitive bonds (*longitudinal* piezoelectric effect); next the model of polar-sensitive bonds *oriented in-plane* (*transverse* piezoelectric effect) will be described, and finally the case of *spatial distribution* of polar-sensitive bonds (*shear* piezoelectric effect) will be considered.

**1. The longitudinal piezoelectric effect** can be explained by the model shown in Fig. 5.3, where a symbolically one-dimensional crystal is presented with length  $l$  and supplied by electrodes (the model represents equally oriented joint polar-sensitive bonds). Under the action of a longitudinal mechanical stress, the  $+X$  crystal lengthens by a value  $\Delta l$  (Fig. 5.3B), creating an electrical moment, which is the mechanically induced electrical polarization  $P$ . It is compensated by the electrical charges of opposite sign that appear on the electrodes.

If in a given model a piezoelectric is investigated or used in a *strain sensor* mode, the induced charges flow into the amplifier input (in this case the crystal is a *current source*). If the studied crystal is electrically open, then an electrical potential occurs and it exists for some time (this is the *voltage-source* mode), but afterwards the induced voltage gradually decreases, being neutralized due to a small but still final electrical conductivity. In any case, polarization dependence on stress is *linear*, as shown in Fig. 5.3D:  $P = d \cdot X$  where  $d$  is the piezoelectric modulus. The change in the sign of mechanical stress seen in Fig. 5.3C leads to the compression of the model crystal and to change in the electrical polarization sign, as well as to the change of sign of the compensating charges. As can be seen from Fig. 5.3D, the dependency  $P(X)$  remains linear.

Since the piezoelectric effect is reversible, the previous test, performed mentally with the model shown in Fig. 5.3, could be carried out in the reverse order, i.e., by applying an electrical field and obtaining longitudinal deformation, which depends on the sign of the field, i.e., to simulate the *converse piezoelectric effect*:  $x = d \cdot E$ , where  $\Delta l/l$  is mechanical strain. It should be noted that the simplest model presented here for the *longitudinal* piezoelectric effect can also describe the *volumetric* piezoelectric effect, since the uniform compression leads, in particular, to a change in the *length* of a chain and produces a corresponding electrical response (moreover, any change in transverse dimensions remains electrically neutral).

As already noted, the piezoelectric effect may not only be longitudinal but can also be transverse and shear effects.

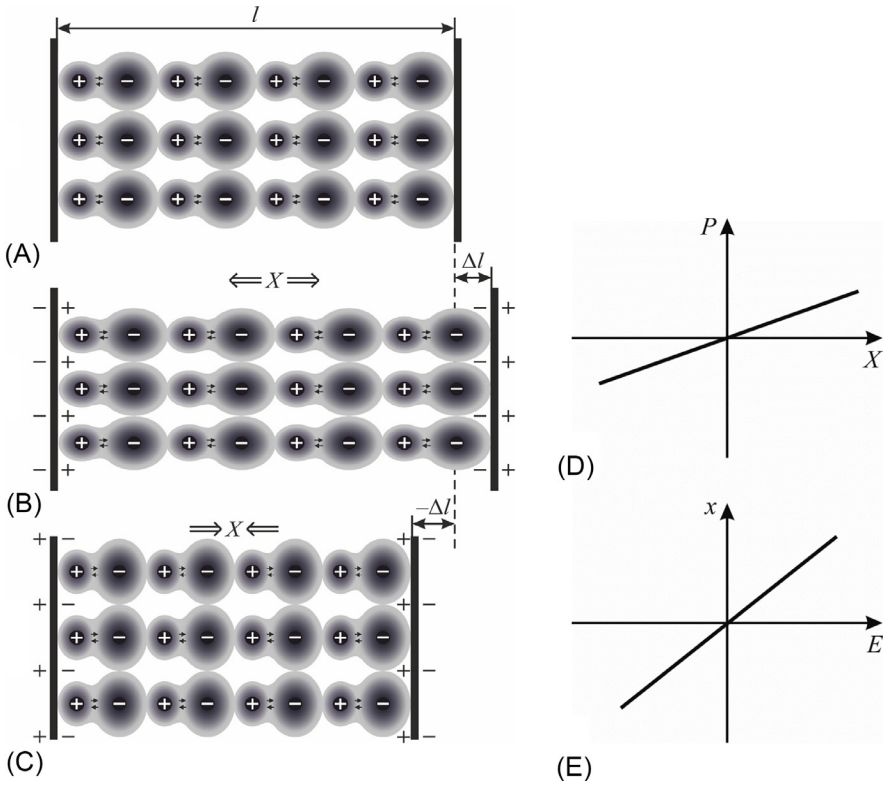


**Fig. 5.3** Simple model of direct longitudinal piezoelectric effect; explanations are given in the text.

**2. The transverse piezoelectric effect** can be explained using a *planar* model resembling the structural features of hexagonal  $\alpha$ -quartz<sup>c</sup>; a simplified explanation of this effect is presented in Fig. 5.4, where the *hexagon* with positive silicon ions and negative ions of oxygen forms a planar *noncentrosymmetric* structure.

Next, a two-dimensional square sample made of piezoelectric-active material is considered (Fig. 5.4B), in which the *inscribed hexagon* symbolically shows a mutual arrangement of electrical charges with three polar-neutral axes  $x'$ ,  $x''$ , and  $x'''$ .

The original structure shown in Fig. 5.4B is *electrically neutral*; moreover, under *uniform* (scalar type) compression or tension, which can change the volume of considered square, it remains totally electrically neutral. Thus, in the model under discussion, the volumetric piezoelectric effect cannot arise (in contrast to the quasione-dimensional structure shown earlier in Fig. 5.3, where *pyroelectric symmetry* is used).

<sup>c</sup> With the piezoelectric effect described in the literature [1–4], it should be noted that usually any microscopic models are avoided, so explanations are limited to piezoelectric symmetry given by formal crystallography. However, currently, when the piezoelectric effect is investigated and used in *nanoscale structures*, microscopic models might be useful.

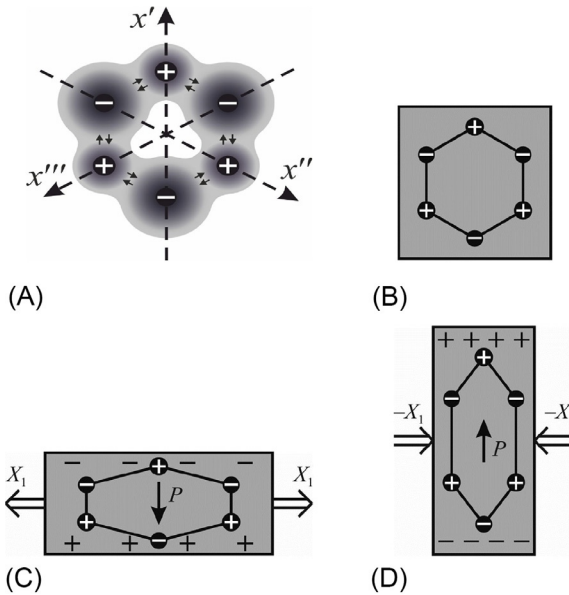


**Fig. 5.4** Simplified model of transverse piezoelectric effect: (A) Model cross-section of quartz perpendicular to six-order axis; (B) "piezoactive square" model; (C and D) longitudinal stress induces transverse polarizations.

At the basis of the structure discussed here is the  $\alpha$ -quartz, which has a rather complex spiral structure, but the main "structural motive" is the hexagon, in which alternating silicon and oxygen ions can be traced: there are two oxygen ions per silicon ion. So in the symbolic projection of two layers of this spiral structure (Fig. 5.4A), the sign "+" should be understood as the ion  $\text{Si}^{+4}$  while the sign "-" means two oxygen ions having the sign "-4".

The directional (tensor type) mechanical action on the piezoelectric-active square sample being considered (Fig. 5.4C) produces a *transverse effect* (not longitudinal). Due to stretching stress applied along the horizontal axis, electrical polarization is induced, not in the same direction, but perpendicularly to it. When the sign of stress changes (Fig. 5.4D), the induced polarity also changes its sign: this is the linear *transverse* piezoelectric effect. A longitudinal piezoelectric effect in this model would also be possible, if mechanical stress were to be applied along the  $x - x'$  axis.

**3. The shear piezoelectric effect** can be explained by the images shown in Fig. 5.5. A piezoelectric-active cube is used now as the model sample, the structure of which has *three polar-neutral axes* (i.e., this cube is a cut made from crystal having quartz symmetry). Moreover, one of the axes of the cube is directed along the  $x$ -direction (i.e., along one of the directions of crystal internal polarity). As in the case of the "piezoelectric square" considered before, this piezoelectric-active cube does not react electrically to any *scalar* action (i.e., neither a pyroelectric nor a volumetric piezoelectric effect are possible in this sample). But the *directional* (tensor) actions in this model allow both the longitudinal and the transverse piezoelectric effects.

However, in the case shown in Fig. 5.5, the piezoelectric-active cube sample is used here only for the explanation of *shear-type* mechanical action. First, such action may be

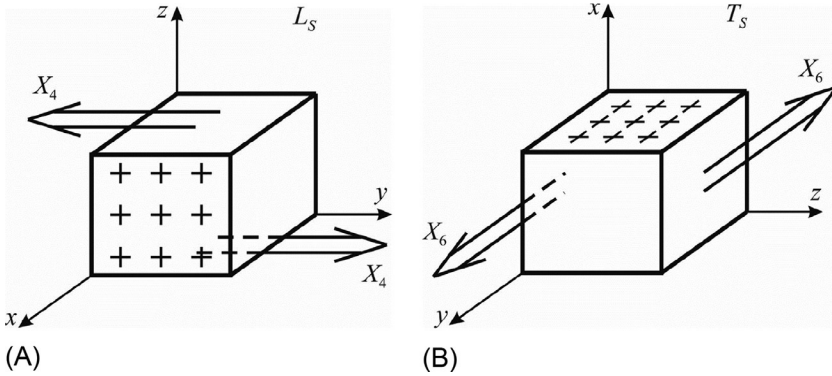


**Fig. 5.5** Model representation of longitudinal (A) and transverse (B) shear piezoelectric effects.

applied *perpendicularly* to the  $x$ -axis of a chosen sample, and along it a mechanically induced electrical polarization occurs. That's why the corresponding piezoelectric effect is called the *longitudinal shear effect*,  $L_S$ . However, another shear piezoelectric effect is also possible, namely the *transverse shear effect*,  $L_T$ , shown in Fig. 5.5B.

In the general case of a low-symmetric crystal, *three* longitudinal  $L$ -effects, *six* transverse  $T$ -effects, *three* longitudinal shear  $L_S$ -effects and *six* transverse shear  $T_S$ -effects can be observed. In crystals of the lowest symmetry and in some slanting cut planes of other polar crystals, the maximum number of piezoelectric moduli can be 18. However, in practically applied piezoelectrics, when the basic installation of crystal is used, this quantity is much smaller, as will be shown shortly.

**4. The piezoelectric effect induced by an electrical field** was already discussed in Chapter 1 in conjunction with Figs. 1.8 and 1.9, and also in Chapter 2 in connection with Figs. 2.13 and 2.14. The piezoelectric effect in an external electrical field manifests essentially in dielectrics with large permittivity (peculiar for paraelectrics and relaxor ferroelectrics) in the form of linearized electrostriction  $Q_e$  [5, 8].

The deformation as an *even* function of polarization can be represented by the fast converging series  $x = Q_e P^2 + Q_e' P^4 + \dots$ . In electrical fields that are not very large, it might be confined to the first member of this series.

When considering possible applications of piezoelectrics, suppose that the polarization contains two components: the first ( $P_b$ ) is induced by a bias (controlling) electrical field, which leads to induced piezoelectricity, and the second component ( $P_{\sim}$ ) is due to a “dynamic field”  $E_{\sim}$  exciting a dynamic piezoelectric response:

$$x = Q_e (P_b + P_{\sim})^2 = Q_e P_b^2 + 2Q_e P_b P_{\sim} + Q_e P_{\sim}^2.$$

If parametric interactions are not taken into account, that is, assuming  $P_b \gg P_{\sim}$ , the last term in the given expression can be neglected. In addition, it can be supposed that polarization  $P_{\sim}$ , which excites the piezoelectric response, is a fast-changing influence compared to  $P_b$  ( $P_{\sim}$  usually changes much faster than the controlling field). In this case, the deformation of paraelectric determined by  $P_b$  can be considered constant

( $x_b = Q_e P_b^2$ ). Thus, electrostriction for a variable field looks linearized and may be perceived as a piezoelectric effect:

$$x = 2Q_e P_b P_{\sim} = d \cdot E_{\sim},$$

where  $d$  plays the role of piezoelectric modulus caused by electrostriction  $Q_e$  and depending on bias electrical field strength. Taking into account that in the paraelectrics  $\epsilon \gg 1$ , it is possible to have

$$P_b = \epsilon_0(\epsilon - 1)E_b \approx \epsilon_0 \epsilon E_b; \quad P_{\sim} = \epsilon_0(\epsilon - 1)E_{\sim} \approx \epsilon_0 \epsilon \cdot E_{\sim}; \quad x_{\sim} = dE_{\sim} \\ \approx 2Q_e \epsilon_0^2 \epsilon^2 E_b E_{\sim}.$$

Denoting further a field that induces the piezoelectric effect through  $E_b = E$ , the artificial piezoelectric modulus is

$$d = 2Q_e \epsilon_0^2 \epsilon^2 E.$$

In cases of electrically induced piezoelectricity and electrical control by parameters of piezoelectric devices, the following physical effects are used:

- *Forced induction of noncentrosymmetric structure* in nonpolar dielectrics by strong electrical field application. As is known, an external field transforms the structure of any dielectric into an artificially polar structure, causing piezoelectric activity. Moreover, an external electrical field by its influence on the speed of sound can change the frequency of a “piezoelectric resonator” (made of a nonpolar dielectric) using the electrically induced piezoelectric effect. Electrostriction of ordinary dielectrics is small, but in some dielectrics, such as rutile ( $\epsilon = 100$ ), calcium titanate ( $\epsilon = 150$ ), or strontium titanate ( $\epsilon = 300$ ), electrically induced piezoelectricity is perceptible [9, 10].
- *Sound velocity change* by an external electrical field in classical piezoelectrics (quartz, langasite, potassium dihydrogen phosphate, niobium lithium, silico sillenite) by means of electrical control of elasticity coefficients (Young’s modulus) of crystal. In normal piezoelectric material, due to large internal bonding, this effect is small but allows, for example, to change the frequency of a piezoelectric resonator a little. Due to the high electromechanical quality factor of these piezoelectrics (such as quartz or lithium niobate), this effect of frequency control becomes technically applicable, for example, in the SAW convectors (processors for pulse convolution).
- *Domains polarization change* in ferroelectrics using electrical field by influencing domain orientation. The controlling field changes both velocity and attenuation of sound, which causes electrical reorganization in piezoelectric devices. However, electrical control of the piezoelectric effect in ferroelectrics is characterized by hysteresis and relatively low operation speed, due to the inertia of domain reorientations.
- *Electroinduced piezoelectric effect in paraelectrics* is a particular but important case of piezoelectric effect induced by electrical field. In this case, the electrical field changes the frequency of the *soft transverse optical mode* of lattice oscillation that strongly affects all properties of paraelectrics. Electrical control of the resonant frequency of piezoelectric resonators made of paraelectrics reaches several percent, which is two orders of magnitude higher than the frequency conversion of resonators made from classical piezoelectric

crystals and an order of magnitude superior to the frequency controlling of resonators made from ferroelectric ceramics.

A distinctive feature of the electrically induced piezoelectric effect is the possibility of piezoelectric activity appearance (in particular, piezoelectric resonance) only at the moment of switching on the electrical control voltage; moreover, the speed of control of resonator parameters can exceed a frequency of 10 kHz.

### 5.3 Direct piezoelectric effect

The piezoelectric effect is always the result of *force action* onto a polar crystal; at that, the force might be mechanical stress or electrical voltage, while the responses of a crystal are electrical polarization or mechanical strain. The *direct* piezoelectric effect is a result of *mechanical action*; to simplify the problem, from this point only the *homogeneous* and *centrosymmetric* actions on the piezoelectric will be considered. As was previously shown in Fig. 5.1, in relation to a particular piezoelectric sample, mechanical stresses might be longitudinal, transverse, shear, or hydrostatic.

The simplest case of *longitudinal* piezoelectric effect is demonstrated in Fig. 5.6: in a sample made of polar crystal, under the action of negative or positive stress electrical polarization appears that shows *linear* dependence on a stress.

In accordance with the first observation of the piezoelectric effect by the Curie brothers, the equations of direct piezoelectrics might have the form:

$$P_i = d_{ijk} \cdot X_{jk}, \quad (5.1)$$

where  $P_i$  are components of polarization vector (tensor of first rank);  $i, j, k = 1, 2, 3$  in accordance with the Cartesian  $x, y,$  and  $z$  axes;  $X_{jk}$  are components of mechanical stress (second-rank tensor); and  $d_{ijk}$  are components of piezoelectric modulus (tensor of third rank). It will be recalled that repeating indices  $j$  and  $k$  in Eq. (5.1) meant summation; thus, presented in shortened form, equations of the direct piezoelectric effect in their expanded form would be seen as three equations, each of them with six terms in their right-hand side. Correspondingly, there must be 27 coefficients, which

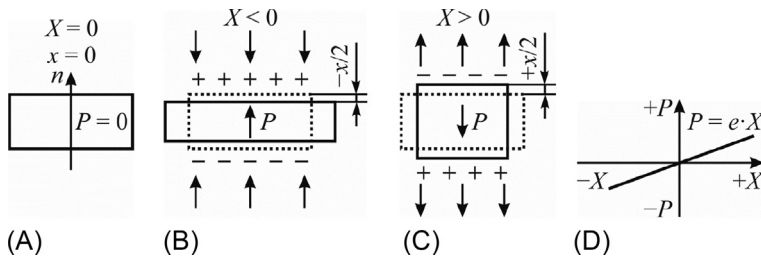


**Fig. 5.6** Direct piezoelectric effect: (A) Plate of polar crystal with vertical directed polar axis in unexcited state; (B) compressive stress  $-X$  is applied to the plate; (C) tensile stress  $+X$  is applied to the plate; (D) linear dependence of induced polarization on applied stress.

connect three components of polarization vector  $P_i$  and nine components of stress tensor  $X_{jk}$ :

	$X_{11}$	$X_{12}$	$X_{13}$	$X_{21}$	$X_{22}$	$X_{23}$	$X_{31}$	$X_{32}$	$X_{33}$
$P_1$	$D_{111}$	$d_{112}$	$D_{113}$	$d_{121}$	$d_{122}$	$d_{123}$	$d_{131}$	$d_{132}$	$d_{133}$
$P_2$	$D_{211}$	$d_{212}$	$d_{213}$	$d_{221}$	$d_{222}$	$d_{223}$	$d_{231}$	$d_{232}$	$d_{233}$
$P_3$	$D_{311}$	$d_{312}$	$d_{313}$	$d_{321}$	$d_{322}$	$d_{323}$	$d_{331}$	$d_{332}$	$d_{333}$

If these 27 components were represented in the form of a matrix, it would be a three-dimensional image, inconvenient for practical use. However, in fact, due to the *symmetry* of the stress tensor,  $X_{jk} = X_{kj}$ , the tensor of piezoelectric moduli is symmetric for the last two indices,  $d_{ijk} = d_{ikj}$ , which decreases the possible number of independent components of the piezoelectric modulus tensor to 18 (all of them really exist in the crystals of lowest symmetry).

In this case, a significantly simplified *matrix representation* of piezoelectric moduli is commonly accepted, as it is more convenient to use a *shortened* matrix record of a third-rank tensor. Moreover, the first index of tensor  $d_{ijk}$  remains unchanged over the value of  $i = 1, 2, 3$ , but the two other indices  $j$  and  $k$ , which also have values 1, 2, and 3, “collapse” into one index  $m = 1, 2, \dots, 6$  according to the rule given in Table 5.1.

In the matrix record, the equation of direct piezoelectric effect takes the form:

$$P_i = d_{im}X_m. \quad (5.2)$$

Now on the right side of these equations there are not nine but six members of the sum. Moreover, it can be seen clearly that, in fact, the number of independent piezoelectric moduli even for the lowest symmetry crystals can be no more than 18. Each of these components is the coefficient of proportionality between corresponding components of electrical polarization  $P_i$  and mechanical stress component  $X_m$ , which generate the polarization  $P_i$ :

	$X_1$	$X_2$	$X_3$	$X_4$	$X_5$	$X_6$
$P_1$	$d_{11}$	$d_{12}$	$D_{13}$	$d_{14}$	$d_{15}$	$d_{16}$
$P_2$	$d_{21}$	$d_{22}$	$D_{23}$	$d_{24}$	$d_{25}$	$d_{26}$
$P_3$	$d_{31}$	$d_{32}$	$D_{33}$	$d_{34}$	$d_{35}$	$d_{36}$

Thus, such an important characteristic of polar crystals as the piezoelectric modulus cannot be described by *one number* (like density or melting point of a crystal), but it is

**Table 5.1** Replacement of tensor indices in matrices.

Tensor indices $i, j, k, l$	11	22	33	23 and 32	31 and 13	12 and 21
Matrices indices $m, n$	1	2	3	4	5	6

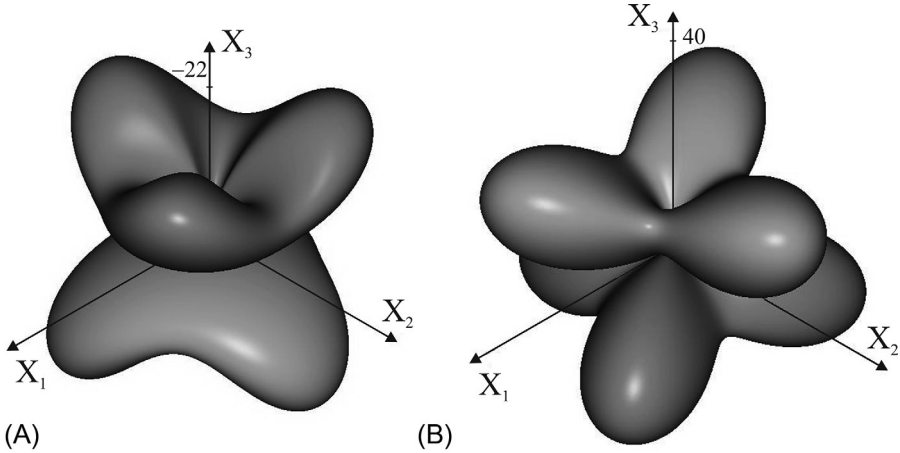


**Fig. 5.7** Indicative surfaces of transverse (A) and longitudinal (B) piezoelectric effects in  $\text{LiNbO}_3$  [5].

a complex characteristic represented by either a matrix or a bulky figure, such as that shown in Fig. 5.7.

In fact, the number of nonzero components of a matrix of piezoelectric moduli can be quite small, if the slant plate of a crystal is not chosen, but its main crystallographic installation. Moreover, the lower the symmetry, the smaller the number of nonzero components in the matrix. As an example, the matrix of piezoelectric moduli of quartz ( $\text{SiO}_2$ ) is shown:

$$d_{im} = \begin{bmatrix} d_{11} & d_{12} & 0 & d_{14} & 0 & 0 \\ 0 & 0 & 0 & 0 & d_{25} & d_{26} \\ 0 & 0 & 0 & 0 & 0 & 0 \end{bmatrix}, \quad \text{where: } \begin{cases} d_{11} = -d_{12} \\ d_{25} = -d_{14} \\ d_{26} = 2d_{11} \end{cases} \quad (5.3)$$

As seen, of 18 possible components of possible piezoelectric modulus in the main installation of quartz crystal, only five positions in matrix (5.3) are nonzero, and at that, only two components of  $d_{im}$  remain independent. A strong anisotropy of the piezoelectric properties of quartz is clearly traceable: along the axis  $Z = 3$  no linear electromechanical reactions are possible while, as with longitudinal effects, so the transverse piezoelectric effects are manifested only along the axis  $X = 1$ .

**1. Figures of merit in piezoelectrics** are quite different parameters.

*Piezoelectric modulus*  $d_{11}$  characterizes the longitudinal piezoelectric effect, i.e., polarization induced along the same direction in which mechanical stress acts. The longitudinal effect is sometimes also called the *L-effect*. The components  $d_{22}$  and  $d_{33}$  have similar physical meaning, characterizing the longitudinal piezoelectric effects along axes, respectively, 2 and 3. Therefore, if indexes in the matrix record of piezoelectric modulus are the same, then these components describe one of three possible longitudinal piezoelectric effects.

*Piezoelectric modulus*  $d_{12}$  characterizes the *transverse* piezoelectric effect or *T-effect*. In this case, elastic stress is applied along axis 2 while the piezoelectric effect is observed along axis 1, perpendicular to axis 2. Other transverse piezoelectric moduli are characterized by coefficients  $d_{13}$ ,  $d_{21}$ ,  $d_{31}$ , and  $d_{32}$ , which are components of the  $d_{im}$  matrix. They express the appearance of polarization along one of the axes 1, 2, or 3 under influence of stretch-compression stresses along one of the axes perpendicular to the response axis.

*Piezoelectric modulus*  $d_{14}$  in Eq. (5.3) characterizes one of the *shear* piezoelectric effects; in quartz, two other shear moduli  $d_{25}$  and  $d_{26}$  do not equal zero; other shear moduli  $d_{13} = d_{15} = d_{24} = d_{26} = d_{34} = d_{35} = d_{36} = 0$ . By this example of shear piezoelectric modulus one can see that piezoelectric polarization may occur not only under compression-stretching stress action, but also under the influence of rotatory shifts. The physical meaning of  $d_{14}$  is as follows: the pair of forces applied along axis 2 induces electrical polarization along axis 1. The shear piezoelectric effect is observed and widely used in many crystals and textures; for instance, the polarized ferroelectric ceramics, widely used in engineering, has two shear moduli  $d_{15}$  and  $d_{24}$  and the matrix of its piezomodulus is the same as in barium titanate crystal ( $\text{BaTiO}_3$ ):

$$d_{im} = \begin{bmatrix} 0 & 0 & 0 & 0 & d_{15} & 0 \\ 0 & 0 & 0 & d_{24} & 0 & 0 \\ d_{31} & d_{32} & d_{33} & 0 & 0 & 0 \end{bmatrix}, \text{ where: } \begin{cases} d_{24} = d_{15} \\ d_{32} = d_{31} \end{cases}$$

In addition to this example, two other matrices of piezoelectric moduli of the most commonly studied piezoelectrics are given here:

For Rochelle salt (RS) in a temperature range of  $t = -18^\circ\text{C}$  to  $+24^\circ\text{C}$ :

$$d_{im} = \begin{pmatrix} d_{11} & d_{12} & d_{13} & d_{14} & 0 & 0 \\ 0 & 0 & 0 & 0 & d_{25} & d_{26} \\ 0 & 0 & 0 & 0 & d_{35} & d_{36} \end{pmatrix};$$

For potassium dihydrogen phosphate crystals (KDP) at any temperature above the Curie point (150 K):

$$d_{im} = \begin{pmatrix} 0 & 0 & 0 & d_{14} & 0 & 0 \\ 0 & 0 & 0 & 0 & d_{25} & 0 \\ 0 & 0 & 0 & 0 & 0 & 0 \end{pmatrix}; \text{ also, } d_{25} = d_{14}.$$

In barium titanate, the shear piezoelectric moduli  $d_{15}$  and  $d_{24}$  are different from zero, while in the piezoelectric phase of KDP crystals (above Curie temperature) only one shear modulus  $d_{36}$  is different from zero. In a general case of study or application of *slanting cuts* of piezoelectric crystals (as well as in crystals of lowest symmetry), there can be *nine* shear moduli: three longitudinal shear moduli ( $L_S$ ) and six transverse shear moduli ( $T_S$ ); Fig. 5.8A shows their difference. Note that the  $L_S$ -effect corresponds to the moduli  $d_{14}$ ,  $d_{25}$ , and  $d_{36}$  and they are characterized by the fact that the induced piezoelectric polarization vector is parallel to the displacement axis and perpendicular

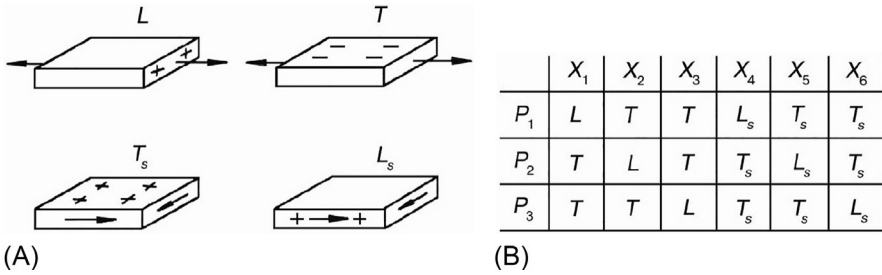


**Fig. 5.8** Different types of piezoelectric moduli: (A) Mutual arrangement of initiating deformation and electrical response; (B) conditional location of longitudinal and transverse piezoelectric moduli in the matrix [7].

to the shear plane. Transverse shear displacement, that is, the  $T_s$ -effect, corresponds to the piezoelectric moduli  $d_{15}$ ,  $d_{16}$ ,  $d_{24}$ ,  $d_{26}$ ,  $d_{34}$ , and  $d_{35}$ . In this case, the vector of polarization is perpendicular to the displacement axis and lies in the displacement plane.

The dimensions of piezoelectric modulus follow from the relation  $d = P/X$ , where  $[P] = \text{C/m}^2$  and  $[X] = \text{N/m}^2$ , so  $[d] = \text{C/N}$ . The piezoelectric modulus of different crystals and textures can be significantly differentiated by magnitude and sign. For example, in ammonium hydrophosphate (ADP) the main piezoelectric modulus  $d_{14} = -1.34 \times 10^{-12} \text{ C/N}$  and  $d_{36} = 20 \times 10^{-12} \text{ C/N}$  (other components of the matrix are zero). From these data, it can be seen that the selected units of measurement of the piezoelectric modulus are too large. Therefore, in practice, it is more convenient to use a unit of pC/N (pico-pendant per newton), where  $1 \text{ pC} = 10^{-12} \text{ C}$ . For example, in barium titanate,  $d_{33} = 150 \text{ pC/N}$ ,  $d_{31} = 70 \text{ pC/N}$ , and  $d_{15} = 250 \text{ pC/N}$ ; moreover,  $d_{24} = d_{25}$  and  $d_{32} = d_{31}$ .

**Expression (5.2)** describes only one of four possible variants of the direct piezoelectric effect characterization, namely for an electrically free ( $E = 0$ ) crystal:  $P_i = d_{im} \cdot X_m$ . Other *idealized* boundary conditions lead to three more equations, also describing the direct piezoelectric effect:

$$\begin{aligned}
 P_i &= e_{in} \cdot x_n; \\
 E_j &= -g_{jm} \cdot E_m; \\
 E_j &= -h_{jn} \cdot x_n.
 \end{aligned}
 \tag{5.4}$$

Here and in future, only the matrix record of the components of third-rank tensors  $e_{in}$ ,  $g_{jm}$ , and  $h_{jn}$  is used. These piezoelectric coefficients, like piezoelectric modulus  $d_{im}$ , characterize the piezoelectric properties of noncentrosymmetric crystals and textures. Units of measurement of all these piezoelectric parameters are:

$d = \text{C/N}$ ,  $g = \text{V m/N}$ ,  $e = \text{C/m}^2$ ;  $h = \text{V/m}$ . In the literature, these moduli are named differently (Uchno), but mostly  $d$  is piezoelectric strain modulus,  $g$  is piezoelectric stress constant,  $e$  is piezoelectric strain constant, and  $h$  is piezoelectric voltage constant. All of these piezoelectric parameters can be independently determined experimentally; the principles of these measurements are shown in **Fig. 5.9**.

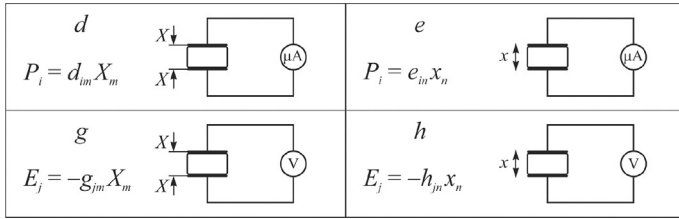


**Fig. 5.9** Experimental determination of various moduli in the case of direct piezoelectric effect [5].

In accordance with boundary conditions considered in [Chapter 1](#),  $d_{im}$ , the component of mechanical stress tensor  $X_m$  acting on a piezoelectric, is determined, as well as  $d$ , the component of the electrical polarization vector  $P_i$  arising from this action ([Fig. 5.9](#)) (moreover, the stress intensity component  $X_m$  is measured as a result of division of force  $F$  acting on area  $S$  of the piezoelectric element). This method of piezoelectric modulus measuring is static; exactly such a method was used when the piezoelectric effect was first detected.

To determine the piezoelectric constant  $e_{in}$  ( $P_i = e_{in} x_n$ ) using the direct piezoelectric effect induced by *strain*  $x_n$ , the crystal must be electrically free ( $E = 0$ ) and mechanically free ( $X = 0$ ). Mechanical deformation<sup>d</sup> can be determined by a dilatometer, while measuring the induced polarization is reduced to the definition of electrical charge  $e$  arising on the piezoelectric surface, whose value is measured by current passing through a microammeter ( $\mu\text{A}$ ) ([Fig. 5.9](#)) (as known, polarization equals the surface charge density on the electrodes). In turn, when coefficients  $g_{im}$  and  $h_{jn}$  are determined, a voltmeter  $V$  can be used, which shows potential  $U = E \cdot t$  induced by crystal deformation or by mechanical stress, accordingly. The larger the thickness of the sample  $t$ , the higher is the potential  $U$ .

In addition to direct measurements, each of the four piezoelectric coefficients can be *calculated* using other coefficients, if elastic parameters ( $c_{mn}$  or  $s_{mn}$ ) and the tensor of permittivity  $\varepsilon_{ij}$  (or the converse tensor  $\beta_{ij} = \varepsilon_{ij}^{-1}$ ) are known. For example, from [Eq. \(5.1\)](#)  $P_i = d_{im} X_m$  and Hooke's law  $X_m = c_{mn} x_n$ , it follows that  $P_i = d_{im} c_{mn} x_n$ . Comparing this expression with [Eq. \(5.4\)](#), it is possible to obtain one of the equations connecting the two piezoelectric coefficients:  $e_{in} = d_{im} c_{mn}$ .

However, in this and other similar relationships, the conditions at which components  $c_{mn}$  and  $s_{mn}$  are defined cannot be ignored: for a short-circuited ( $E = 0$ ) or open-circuited piezoelectric ( $D = 0$ ), therefore  $c_{mn}^E \neq c_{mn}^D$  and  $s_{mn}^E \neq s_{mn}^D$ . Other

<sup>d</sup> A question might arise as to how deformation appears in a piezoelectric, if the vector of electrical field and the tensor of mechanical deformation do not act on the polar crystal. The fact is that homogeneous (scalar) change of temperature leads to crystal thermal expansion-compression, so electrical polarization appears from the secondary pyroelectric effect, as well as hydrostatic (scalar) change of pressure results in strain  $x_n$ —this is the volumetric piezoelectric effect.

relations between piezoelectric coefficients include components of tensors  $\varepsilon_{ij}$  or  $\beta_{ij}$ , which differ for mechanically free ( $\varepsilon_{ij}^X$  or  $\beta_{ij}^X$  when  $X = 0$ ) and mechanically clamped crystals and textures ( $\varepsilon_{ij}^x$  or  $\beta_{ij}^x$ , which means  $x = 0$ ).

In accordance with [relation \(5.2\)](#), which corresponds to the direct piezoelectric effect and taking into account an electrically free crystal, it should be determined that elastic stiffness will be included in this relation with a superscript  $E$ . Consequently, this ratio must be written in the form  $e_{in} = d_{im}c_{nm}^E$ . Similarly, to determine piezoelectric modulus  $d_{im}$  in the direct piezoelectric effect, the piezoelectric also needs to be electrically free ( $E = 0$ ), so the piezoelectric modulus must be determined as follows:  $d_{im} = e_{mj}s_{mn}^E$ .

Other ratios of piezoelectric coefficients are given in more complete equations as follows, which take into account the conditions for determining the dielectric and elastic parameters:

$$d_{mj} = \varepsilon_0 \varepsilon_{ij}^X g_{mi} = e_{nj} s_{mn}^E = \varepsilon_0 \varepsilon_{ij}^x h_{ni} s_{mn}^E;$$

$$e_{mi} = \varepsilon_0 \varepsilon_{ij}^x h_{mj} = d_{ni} c_{mn}^E = \varepsilon_0 \varepsilon_{ij}^X g_{nj} c_{mn}^E;$$

$$g_{mi} = (\beta_{ij}^x / \varepsilon_0) d_{mj} = h_{ni} s_{mn}^D = (\beta_{ij}^X / \varepsilon_0) e_{nj} s_{mn}^D;$$

$$h_{mj} = (\beta_{ij}^X / \varepsilon_0) e_{mi} = g_{ni} c_{mn}^D = (\beta_{ij}^x / \varepsilon_0) d_{ni} c_{mn}^E.$$

**2. The electromechanical coupling factor  $K_{coup}$**  is one of the important figures of merit for piezoelectric materials, and also for elements of piezoelectric devices. It reflects the *interconnection* of electrical and mechanical properties in non-centrosymmetric crystals and textures that demonstrate the piezoelectric effect. Electromechanical coupling can be investigated using various experimental and theoretical methods.

Due to the fact that a piezoelectric is an energy convertor, its electrical and elastic properties need to be considered together. The point is that in a polar-sensitive crystal, any change in its mechanical state leads to a change in its electrical state, and vice versa [7]. The square of the electromechanical coupling factor shows the amount of energy brought to the piezoelectric ( $W_{br}$ ) is converted into another type of energy ( $W_{conv}$ ):

$$K_{coup}^2 = W_{conv} / W_{br}$$

Note that no energy losses (mechanical damping and dielectric losses) are included in this expression, so the  $K_{coup}$  it is not the efficiency coefficient.

In the case of the *direct piezoelectric effect*, the mechanical energy received by the piezoelectric is spent not only on deformation (when elastic energy  $W_{elas}$  is accumulated) but also is spent on electrical polarization, which causes the accumulation of electrical energy  $W_{elec}$ :

$$K_{coup}^2 = \frac{W_{elec}}{W_{br}} = \frac{W_{elec}}{W_{elas} + W_{elec}}. \quad (5.5)$$

The coupling factor  $K_{coup}$  might be different at various boundary conditions when the crystal might be mechanically free or clamped and electrically short-circuited or open-circuited. As with electrical energy, so elastic energy is defined by the quadratic forms. The energy of electrical polarization can be expressed through the electrical field  $E$  and induction  $D$ , using permittivity  $\epsilon$  and inverse permittivity  $\beta$ :

$$W_{elec} = \frac{1}{2}ED = \frac{1}{2}\epsilon_0\epsilon E^2 = \frac{1}{2}\left(\frac{\epsilon_0}{\beta}\right)D^2. \quad (5.6)$$

In the same way, mechanical energy is defined by strain  $x$  or stress  $X$ , as well as by stiffness and compliance characterizing the elastic process:

$$W_{elas} = \frac{1}{2}xX = \frac{1}{2}cx^2 = \frac{1}{2}sX^2, \quad (5.7)$$

In addition to these relations, the electromechanical coupling factor can be defined as the ratio of elastic energy density to the density of elastic and electrical energy:

$$K_{coup}^2 = \frac{W_{EM}^2}{W_{elas}W_{elec}}.$$

where in a mechanically clamped piezoelectric  $W_{EM} = d \cdot X \cdot E$ , while for a mechanically free piezoelectric  $W_{EM} = e \cdot h \cdot E$ , with  $d = P/X$  and  $e = P/x$ .

Although the factor  $K_{coup}$  is a scalar parameter, it depends on the direction of external influences and on other causes. For example, polarized ferroelectric ceramics (a texture of  $\infty m$  symmetry) can be identified by 12 different coupling coefficients, depending on the system of boundary conditions (and possible forms of piezoelectric sample), as well as on the manner of clamping and fixing. Numerical values of  $K_{coup}$  are defined by piezoelectric material properties. Most crystals, ceramics, and textures used in practice have  $K_{coup} = 0.1\text{--}0.5$ , although in some crystals in their particular orientation  $K_{coup}$  reaches a value of 0.8–0.95.

In the case of a *direct* piezoelectric effect, the electromechanical coupling factor can be calculated, if the main parameters of the piezoelectric are known. Taking into account the contribution to polarization from the direct piezoelectric effect  $P_{piezo} = d \cdot X$ , the equation of electrical induction  $D = \epsilon_0 E + P = \epsilon_0 \epsilon E$  takes the form:

$$D = \epsilon_0 \epsilon E + d \cdot X. \quad (5.8)$$

Accordingly, in the equation for linear deformation (Hooke's law  $x = s \cdot X$ ) the piezoelectric contribution to deformation from the converse piezoelectric effect  $x_{ii} = d \cdot E$  should be taken into account:

$$x = s \cdot X + d \cdot E. \quad (5.9)$$

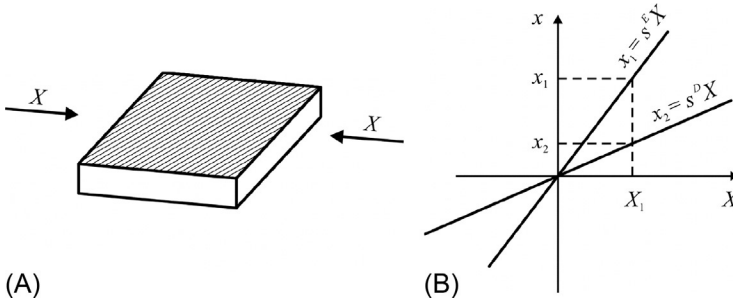


**Fig. 5.10** Difference in elastic compliance in piezoelectric: (A) Mechanical action on piezoelectric plate; (B) Hooke's law in open-circuited ( $s^D$ ) and in short-circuited ( $s^E$ ) polar crystal [5].

Next, the direct piezoelectric effect in a sample plate made of noncentrosymmetric crystal will be considered (Fig. 5.10). Suppose that homogeneous mechanical stress  $X$  acts on the piezoelectric plate, as a result of which it deforms, remaining electrically opened ( $D = 0$ ). Accordingly, from the equation  $D = \epsilon_0 E + P = \epsilon_0 \epsilon E$  it is possible to obtain  $E = -(d/\epsilon_0 \epsilon)X$ . By substituting this in Eq. (5.9), we obtain the next relation:

$$x = (s - d^2/\epsilon_0 \epsilon) \cdot X. \quad (5.10)$$

In the brackets there is a new tensor of elastic compliance, corrected for piezoelectric effect. As can be seen from Eq. (5.10), due to the piezoelectric reaction the compliance of the plate *decreases* (correspondingly, its stiffness increases). Therefore, by applying a mechanical force  $X = X_1$  the plate does not deform to the value of  $x = x_1$  (as if it were in the absence of the piezoelectric effect), but only to the value  $x = x_2 < x_1$ .

The work of external forces brought to a plate ( $W_{br}$ ) is spent not only on the elastic deformation with accumulation of *elastic* energy ( $W_{elas}$ ), but also on creation of *electrical* energy of polarization ( $W_{elec}$ ). Under these conditions, deformation of the piezoelectric plate becomes less ( $x - x_1$ ) as reduced elastic energy compensates the appearance of electrical energy.

Using Eq. (5.10) and the formula for elastic energy  $\frac{1}{2}s \cdot X^2$ , it is possible to determine the mechanoelectric contribution to energy:

$$W_{elas} = W_{br} - W_{elec} = \frac{1}{2}s \cdot X^2 - \frac{1}{2}(d^2/\epsilon_0 \epsilon)X^2.$$

Changed energy in this case, obviously, is electrical energy  $W_{elec}$ . Substituting the obtained expressions into Eq. (5.5), the coupling factor can be found:

$$K_{coup}^2 = W_{elec}/(W_{elas} + W_{elec}) = \frac{1}{2}(d^2/\epsilon_0 \epsilon)X^2 / (\frac{1}{2}sX^2) = d^2/(\epsilon_0 \epsilon \cdot s). \quad (5.11)$$

It should be noted that the ratio of energies in Eq. (5.11) does not depend on the amplitude of fields (mechanical stress  $X$  or electrical field  $E$ ). Thus, the coupling factor  $K_{coup}$  is a parameter *characterizing a given piezoelectric*.

Multiply the numerator and denominator in Eq. (5.11) on  $\frac{1}{4}E^2X^2$ :

$$K_{coup}^2 = (\frac{1}{2}d \cdot E \cdot X)^2 / [(\frac{1}{2}\epsilon_0\epsilon E^2)(\frac{1}{2}s \cdot X^2)] = W_{EM}^2 / (W_{elec} \cdot W_{elas}).$$

The denominator represents a product of energies  $W_{elec} = \frac{1}{2}\epsilon_0\epsilon E^2$  and  $W_{elas} = \frac{1}{2}s \cdot X^2$ , while the numerator corresponds to electromechanical energy  $W_{EM} = \frac{1}{2}d \cdot E \cdot X$ .

**3. Elastic properties dependence on electrical boundary conditions.** While studying mechanical properties of piezoelectrics, a significant difference in the elastic compliance of short-circuited ( $s^E$ ) and open-circuited ( $s^D$ ) polar crystals is observed. Under the influence of outside stress (Fig. 5.10A), strain is linearly increased (Fig. 5.10B) in accordance with Hooke's law. However, if a piezoelectric is electrically short-circuited, its elastic compliance will be bigger than in the case when the crystal is open-circuited. The reason is that the piezoelectric voltage generated by mechanical strain in an open-circuited crystal *increases its harshness* (resistance to deformation).

By comparing of expressions (5.11) and (5.10), it is possible to verify that elastic compliance reduces in  $(1 - K_{coup}^2)$  times:  $d^2/\epsilon_0\epsilon = K_{coup} \cdot s$ . However, in the case of a short-circuited crystal ( $E = 0$ ), piezoelectricity does not affect elastic compliance  $s^E$ . In the same way, for the considered case compliance  $s^D$  of an open-circuited piezoelectric ( $D = 0$ ) is reduced. Expression (5.10) can be rewritten:

$$x = (s^E - d^2/\epsilon_0\epsilon)X = (s^E - K_{coup}^2 s^E)X = s^D X;$$

$$s^D = s^E (1 - K_{coup}^2).$$

From the preceding relations, an important expression follows for electromechanical coupling factor:

$$(s^E - s^D)/s^E = K_{coup}^2. \quad (5.12)$$

Correspondingly, elastic stiffness  $c_{mn}$  (where  $m, n = 1, 2, \dots, 6$ ), which is the tensor converse to the tensor of elastic compliance  $s_{mn}$ , can also be obtained from Eq. (5.12):

$$(c_{mn}^D - c_{mn}^E)/c_{mn}^D = K_{coup}^2. \quad (5.13)$$

In Chapter 2 (Fig. 2.5B) a large difference between elastic stiffness of short-circuited ( $c_{14}^E$ ) and open-circuited ( $c_{14}^D$ ) in a Rochelle salt crystal was shown. In this figure, throughout a given range of temperatures Rochelle salt is a piezoelectric. In the Curie points, elastic stiffness  $c_{14}^E$  of the short-circuited crystal changes very much, being almost an order of magnitude different from  $c_{14}^D$ . Therefore the strong influence of *electrical conditions* on the *mechanical properties* of ferroelectrics is evident.

Since the speed of elastic (sound) waves is determined by elastic stiffness  $c$  and density  $\rho$  of a crystal,

$$v_{\text{sound}} = (c/\rho)^{1/2},$$

then a difference in elastic stiffness  $c^D - c^E$  leads to the differences in speed of sound in the open-circuited and short-circuited crystals. From Fig. 2.5 in Chapter 2 it follows that velocity of sound in the direction corresponding to the stiffness component  $c_{44}$  of Rochelle salt in both Curie points decreases several times as compared with room temperature. This means that elastic stiffness of a piezoelectric due to the piezoelectric effect might vary considerably.

**5. Main applications of direct piezoelectric effect.** There are various engineering approaches for comparing piezoelectric materials [11–14]. For piezoelectrics intended for use as acoustic *signal receivers*, it is necessary to provide high sensitivity at low noise levels. If such piezoelectric receivers are employed in liquid environments, they are called *hydrophones*; if such devices are used in the air, they are called *microphones*. In general, in electronics, instrumentation, and medical technology, such use of piezoelectrics can be generalized by the concept of *piezoelectric sensors*.

In order to assess the suitability of piezoelectric elements, the following quality factor is often used for receiver material:  $d_{ij}/\epsilon_{ij}^{1/2} = K_{res}$ ; this parameter characterizes efficiency in the receiver mode, which is to convert mechanical energy into electrical energy. Taking as example the most famous piezoelectric quartz as the unit of  $K_{res}$ , it can be obtained that this value for piezoelectric ceramic is 4–6 times higher than for quartz: for lithium niobate crystal it is 8 times higher, for a PVDF polymer film 12 times higher, and it is 25 times higher for Rochelle salt. The design and application of piezoelectric receivers or sensors should be guided by these data.

In the piezoelectric sensors the direct piezoelectric effect is used; at that piezoelectric modulus  $g$  and  $h$  should be used as the most convenient parameters for assessing the sensory capability of those or other piezoelectric devices. The direct piezoelectric effect was considered earlier in the idealized boundary conditions, and the following equations for piezoelectric effect were given:  $E_i = -g_{im} \cdot X_m$  and  $E_i = -h_{in} \cdot x_n$ . In this case, the piezoelectric voltage constant  $g_{im}$  is defined as the ratio of piezoelectric modulus  $d_{nj}$  to dielectric constant  $\epsilon_{nj}$ :  $g_{im} = d_{mj}/\epsilon_{ij}$  and characterizes the electrical field  $E$  arising in a piezoelectric under applied stress  $X$ . Therefore, the dimension  $[g]$  is:  $(\text{V/m})/(\text{N/m}) = \text{V m/N}$ . Another piezoelectric constant,  $h$ , can also be defined as the product of the coefficient  $g$  on the corresponding Young's modulus for a certain direction in the crystal, respectively, and the dimension  $h$  equals  $\text{V/m}$ .

Piezoelectric crystals are *direct converters* of mechanical energy into electrical energy. The efficiency of such transformation can be expressed through mechanoelectric coupling coefficient of  $K_{ME}$ , the square of which equates to the product of piezoelectric moduli  $g$  and  $h$ ;  $K_{ME}^2 = d_{nj} \cdot h_{mj}$ . The listed coefficients are important characteristics for such cases when it is necessary to ensure high efficiency of the energy transfer, for example, in the acoustic and ultrasound sensors. For practical devices, the exact charge  $q_x$  generated on the surface of the piezoelectric converter

is important; it is proportional to the force  $F_x$ , which acts along the  $x$ -axis:  $q_x = d \cdot F_x$ . A piezoelectric plate with electrodes deposited on it is the capacitor  $C$ . The voltage  $V$  on this capacitor is determined by the expression  $V = Q/C = d \cdot F/C$ . In turn, capacity can be expressed through dielectric permittivity  $\epsilon$ , surface of electrode  $S$ , and thickness of crystal  $l$  (only the electrode area is taken into account, but not the area of the crystal itself, since piezoelectric induced charge accumulates only on the electrodes):  $C = \epsilon \epsilon_0 S/l$ . Then the expression for electrical voltage on a piezoelectric sensor takes the form  $V = d \cdot F/\epsilon \epsilon_0 S$ .

*Piezoelectric sensory elements* can be used either in a simple lamellar form or in the form of a multilayer structure, in which individual plates are joined together by means of electrodes placed between them. For example, Fig. 5.11A shows a two-layer power sensor. When external force is applied to this sensor, one of its parts is expanded while the other is compressed, which leads to doubling of the output signal (double sensors can be activated in parallel or sequentially). A piezoelectric sensor has a very high output impedance, so to coordinate with subsequent electronic circuits it is necessary to use special interfaces representing voltage converters in current, or voltage amplifiers with high input resistance.

The next example, in Fig. 5.11B, shows a piezoelectric application in *seismic cables*. They are essentially vibration or power sensors implemented as cables, in which an electrical signal appears on the internal conductor (Fig. 5.11B). Piezoelectric cable consists of metal casing covered on the outside by a layer of insulation, and inside it contains the densely pressed piezoelectric ceramic powder enveloping an inner metallic rod. To give such a cable its piezoelectric properties, its sensitive component (ceramic powder) must pass the thermal polarization procedure. The sensor does not register constant (not changing in time) force: only a dynamic change in mechanical force generates an electrical signal. Mechano-electrical sensors are used for a variety of purposes: monitoring vibration of compressors and engines for analysis of traffic flow on motorways, etc.

*Piezoelectric materials* for force sensors need a peculiar combination of properties, namely the large ratio of piezoelectric modulus to permittivity. Such are, for example, lithium sulfate crystals ( $\text{Li}_2\text{SO}_4$ ), which are often used in hydrophones. This piezoelectric is used also for detector heads in ultrasonic defectoscopy. Another example is lithium tetraborate crystals ( $\text{Li}_2\text{B}_4\text{O}_7$ ), which have been developed for use in the receiving mode. This crystal has a small value of permittivity ( $\epsilon_{33} = 10$ ) and relatively small piezoelectric modulus  $d_{33} = 34$  pC, but the parameter  $g_{33} = 0.27$  V/m<sup>2</sup> in

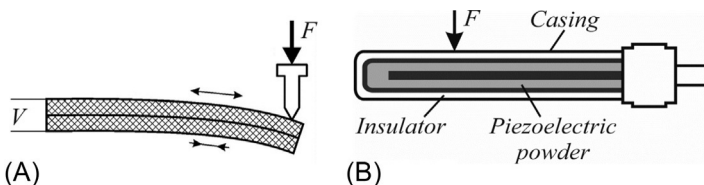


**Fig. 5.11** Piezoelectric sensors: (A) Two-layer (bimorph) piezoelectric force sensor; (B) piezoelectric cable ( $F$  is dynamic mechanical load) [12].

$\text{Li}_2\text{B}_4\text{O}_7$  that is special for hydrophones is greater than for other piezoelectrics. For comparison, the piezoelectric modulus of widely used piezoelectric ceramics ( $d_{33} = 450 \text{ pC/N}$ ) is 13 times larger but the parameter  $g_{33} = 0.03 \text{ V/m}^2$  is 10 times smaller than in lithium tetraborate.

*Vibration sensors* that use the piezoelectric effect are widely applied in airplanes, electric generators, accelerometers, etc. These sensors operate in a frequency range of 2 Hz–5 kHz and are characterized by high attenuation of noise, high linearity, and wide temperature range (especially when quartz crystals are used as sensitive elements). When piezoelectric crystals are applied in the accelerometers, they are located between the casing and *inertial mass*, which makes the acting force proportional to acceleration. Ceramic piezoelectric films are also used in accelerometers: in this case they are the *microsensors* usually deposited on silicon. During formation of integrated silicon microsensors, a thin film of piezoelectric ceramic is usually deposited onto a silicon console. The piezoelectric signal is amplified by a microelectronic circuit embedded in the same microdevice with the piezoelectric sensor.

*Acoustic sensor* applications are much wider than simply detecting vibrations and sound signals. Such include the microscale apparatus and devices based on surface acoustic waves, realized on the principle of detecting mechanical vibrations in solids. Such sensors are used to measure displacements, to determine the concentrations of components, and to measure mechanical stress, force and temperature. Solid-state detectors often form the basis of more complex sensors, such as chemical analyzers, biological research devices, etc. According to the characteristics of surface wave propagation, it is possible to obtain necessary information about biological objects or chemical components on the surface of a film. The use of high-sensitivity piezoelectric devices allows significant success in the visualization of ultrasonic fields, which has resulted in significant increase in resolution, in particular in the case of the use of acoustic holography techniques, for increasing the operating frequency of probing beams.

*In medicine*, progressive development of piezoelectric receivers has greatly facilitated the wide introduction into practice (including medical) of various types of ultrasound flow detection and acoustic emission analysis, as well as cardiography and acoustic visualization of internal organs. This has ensured a sharp increase in the possibilities of medical diagnostics for prevention of complicated cases. Piezoelectric sensors are used in biomedical engineering and “sensorization robots,” which have been developing intensively lately. By introducing a piezoelectric catheter with a shell of polarized polyvinylidene fluoride in the middle of a blood vessel, it was possible to implement a precision diagnosis of valve stenosis, cardiomyopathy, and so on. Using polyvinylidene fluoride, a polyfunctional thermotactile sensor (“artificial skin”) for prosthetics and robots has been developed. Promising results were obtained during the treatment of bone fractures in the case of wrapping fragments of fissile bones using a bimorphic piezoelectric polymeric film; there was a sharp acceleration of the growth of the osteons in the direction of the force lines of the piezoelectric field, which accelerated the recovery of the patient.

*Piezoelectric microphones* work in an acoustic range that is perceived by humans; however, this name can also be used for ultrasonic and infrasound wave detectors.

In essence, the microphone is a pressure sensor adapted to convert sound waves in a wide spectral range. Microphones are characterized by sensitivity, direction, bandwidth, dynamic range, size, cost, etc. An important condition for the use of microphones is the harmonization of acoustic impedances of the medium and device. For sound receivers, the value of the acoustic resistance determines the conditions for reconciliation with the medium.

*Piezoelectric films* made of polyvinylidene fluoride (PVDF) and copolymers have been used for many years to produce pickups for musical instruments. PVDF-based piezoelectric pickups have a very high quality reproduction partly because they have very low  $Q$ -factor: they do not have their own resonance (as in ceramic pickups), and therefore there is virtually no distortion of signals.

*Piezoelectric macrocomposite* materials have high hydrostatic sensitivity, for example, ceramics with a structure of “coral” (macrocomposite), where the ceramic framework is placed in polymer matrix, which reduces the effective permittivity. Others microcomposites are used for hydrophones, created on the basis of thin rods of polarized ceramics, variously bonded and placed in a solid polymer matrix. These materials have significantly superior sensitivity in reception mode to not only the usual piezoceramic, but also lithium tetraborate. *Microcomposite* materials are piezoelectric glass-ceramics: a texture of needle microcrystals of lithium tetraborate or other crystals in a glass-phase matrix obtained by rapid melt-fixing under conditions of a sharp temperature gradient. In piezoelectric glass-ceramics  $\epsilon_{33} = 10$  and  $d_{33} = 20$  pC/N so the important parameter  $g_{33} = 0.1$  V m/N.

*Piezoelectric generators* of high voltage are very simple in their design and can provide both high voltage (for creating, for example, a spark) and significant power that can be used in piezoelectric vibration dampers. Fig. 5.12A shows a principal design of a piezoelectric ignition system: as a rule, two piezoelectric cylinders are designed to work in parallel. Using piezoelectric ceramic cylinders with a diameter

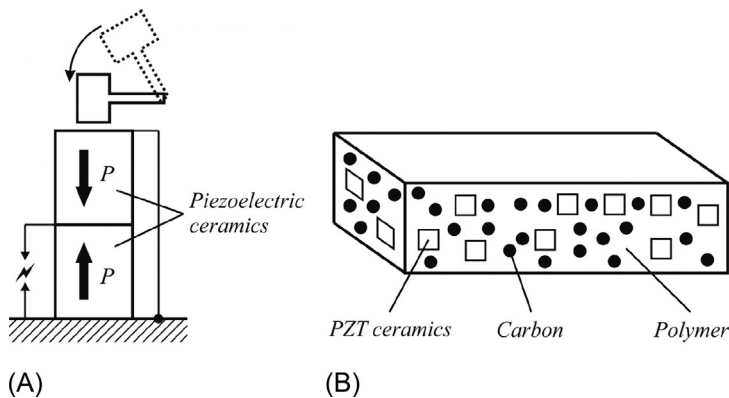


**Fig. 5.12** Application of direct piezoelectric effect at high energies: (A) Piezoelectric lighter, shown direction of ceramics polarization; (B) principal composition of piezoelectric composite for damping of vibrations [3].

of about 10 mm and a length of about 15 mm, it is possible to obtain electrical impulses of 15–25 kV in a time interval near 50 ms.

*Mechanical vibration dampers* are important applications of piezoelectric composites. The vibrational object must be elastically connected with the piezoelectric, forming a single system. The vibration is transmitted to the piezoelectric material and the mechanical vibrational energy is converted into electrical energy due to the direct piezoelectric effect: it is an alternating electrical voltage. To suppress vibrations, a *resistive material* is introduced into the oscillatory system, for example, carbon, as shown in Fig. 5.12B; at that, the flexible polymers are used for composite elasticity. Thus, the energy of mechanical vibrations is quickly transformed by piezoelectric and resistor into heat and the vibrations quickly decay. Piezoelectric dampers are used not only in aviation, particularly in helicopters, but also in industry as well as in household appliances (and for damping vibrations of mountain skis).

*The possible applications* of the direct piezoelectric effect are many and varied. Experiments on generating piezoelectric energy using sea waves have been carried out: a multilayer thin polymer film (PVDF type), with an area of hundreds of square meters, was used as a mechanoelectric energy converter. Experiments were also conducted using a PVDF film for a submerged piezoelectric tidal wave power plant immersed in seawater, with high power. Film converters have been implanted into the human body to convert the mechanical energy of breathing into electrical energy, for example, to power implanted medical devices such as continuously acting insulin pumps.

## 5.4 Converse piezoelectric effect

In the case of the *converse* piezoelectric effect, the driving force mainly is the electrical field  $E$ , while the induced response usually is the mechanical deformation  $x$  (or if the latter is impossible, mechanical stress arises). As already mentioned, when applied to *any dielectric*, electrical voltage causes its deformation, since charged particles of a material are displaced in the process of electrical polarization. Due to this mechanism in all dielectrics, the *quadratic* electromechanical effect occurs (electrostriction) but usually it is very small.

However, in dielectrics with noncentrosymmetric structure, another effect is important, namely the *linear* electromechanical effect. This converse piezoelectric effect was the second observation made by the Curie brothers, and its equation can be written as:

$$x_n = d_{nj}E_j,$$

where  $i = 1, 2, 3$  and  $n = 1, 2, \dots, 6$  accordingly to matrix marks; so in the matrix record the piezoelectric modulus looks like  $d_{nj}$ . It is seen that the component of strain  $x_n$  is directly proportional to the magnitude of the electrical field  $E_j$  applied to a piezoelectric. The simplest model of the converse longitudinal piezoelectric effect is shown in Fig. 5.13.

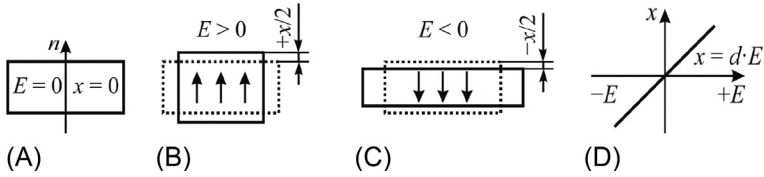


**Fig. 5.13** Converse piezoelectric effect: (A) Polar crystal with vertically directed polar axis  $n$ ; (B) applied electrical field leads to crystal expansion; (C) when sign of electrical field changes, crystal contracts; (D) linear electrical field–strain dependence.

The figure shows symbolically how a piezoelectric sample is expanded or compressed under the action of an electrical field applied along the polar axis  $n$  of a crystal. The sign of deformation changes with a change in electrical polarity (note that in real experiments, even in a strong electrical field the value of relative deformation  $x$  does not exceed 1%).

**1. Fundamentals of converse piezoelectric effect.** Eq. (5.14) corresponds to the piezoelectric effect in a mechanically free ( $X = 0$ ) and open-circuited ( $D = 0$ ) crystal and includes the same piezoelectric modulus  $d$  as in the case of the direct piezoelectric effect. However, this equation represents only one of the possible descriptions of linear electromechanical interaction in noncentrosymmetric crystals and textures. At various boundary conditions, the converse piezoelectric effect can be described by four equations:

$$x_n = d_{nj}E_j; \quad X_m = e_{mj}E_j;$$

$$x_n = g_{ni}P_i; \quad X_m = h_{mi}P_i,$$

where  $d_{nj}$ ,  $g_{ni}$ ,  $e_{mj}$ , and  $h_{mi}$  are the piezoelectric coefficients used in the previous section to describe the direct piezoelectric effect.

The converse piezoelectric effect, as well as the direct one, in principal, allows all piezoelectric coefficients to be determined from experiments (Fig. 5.14).

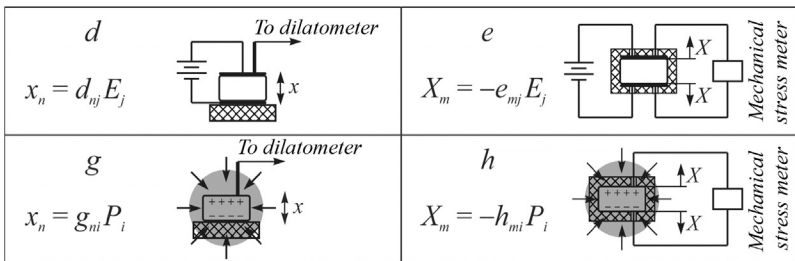


**Fig. 5.14** Experimental methods of piezoelectric coefficient measurement, using converse piezoelectric effect.

For example, to measure piezoelectric modulus  $d$  (Fig. 5.11), it is necessary, first, to know the electrical field applied to the crystal:  $E = U/t$  (where  $U$  is electrical voltage supplied from a low-impedance source,  $t$  is thickness of a sample). Second, mechanical deformation  $\Delta t$  induced by the electrical field should be obtained using a dilatometer that allows the dimensionless relative deformation  $x = \Delta t/t$  to be found.

In the case of the converse piezoelectric effect, the piezoelectric constant  $e_{mj}$  is more difficult to determine (Fig. 5.14, *e*), since the crystal must be mechanically clamped ( $x = 0$ ). Therefore, a measuring element to determine the mechanical force  $F$  created by a piezoelectric of area  $S$  ( $X = F/S$ ) must be mounted in a massive casing to prevent piezoelectric deformation. It is obvious that experimental realization of such a method in the static mode is not reasonable, but the *dynamic* mode of measurement can be successfully carried out at *elevated frequencies*—higher than the frequencies of the inherent mechanical resonances of the piezoelectric sample (when it cannot be deformed).

In principal, it is possible, using the converse piezoelectric effect, to experimentally determine the piezoelectric coefficients  $g_{ni}$  and  $h_{mi}$ . In these experiments, the piezoelectric sample might be polarized by external *scalar action* (uniform variation of hydrostatic pressure). In the case of  $g_{ni}$  measurement, deformation should be found by dilatometer (Fig. 5.14, *g*); while in the second case a pressure needs to be found (Fig. 5.14, *h*).

The use of *four* different piezoelectric coefficients for piezoelectric effect description is justified by various examples of piezoelectric technical application. For example, when choosing a piezoelectric material for ultrasound *emitters*, which are usually used in sonar (and in home appliances, such as washing machines), rather big mechanical deformations must be generated by the converse piezoelectric effect under the influence of electrical voltage. In this case, in order to evaluate the effectiveness of various piezoelectric materials, they must be compared using the magnitude of the piezoelectric modulus  $d$  (according to the equation  $x = d \cdot E$ ).

Piezoelectric cells are also applied as ultrasound *receivers*, but the requirements for these are peculiar: it is necessary to use the direct piezoelectric effect to obtain maximum electrical voltage from the piezoelectric element—the “effort sensor,” which uses the piezoelectric coefficient  $g$ . In this case, the best piezoelectrics are those which have the highest coefficient  $g = d/\epsilon_0\epsilon$ . In other cases, for example, to evaluate the performance of piezoelectric adapters, the coefficients  $h$  and  $e$  might be important.

The previously shown equations of piezoelectric effect (both direct and converse) characterize different connections between mechanical parameters  $X$  and  $x$  and electrical parameters  $P$  and  $E$ . To summarize the problem, these equations can be presented in the form of a diagram—the *piezoelectric square* (Fig. 5.15) in the corners of which the parameters  $x$ ,  $X$ ,  $P$ , and  $E$  are located.

The left vertices of the square show the mechanical stress and strain with their linear relationship, depicted by a straight line, symbolically characterizing a different representation of Hooke’s law:  $x = s \cdot X$  or  $x = c \cdot X$ . The right top of the square pictured in Fig. 5.15 corresponds to electrical field  $E$  and polarization  $P$ , and the connecting line reflects electrical interaction:  $P = \epsilon_0\chi E$  or  $E = (\epsilon_0\chi)^{-1}P$ .

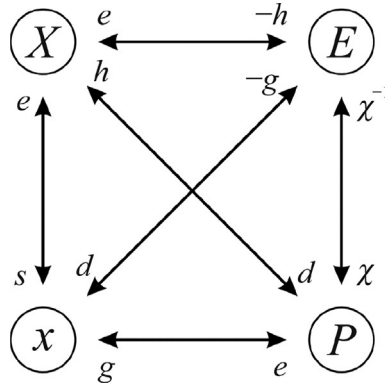


**Fig. 5.15** Relationship of main parameters describing piezoelectric effects [7].

The horizontal lines as well as diagonals of the square in Fig. 5.15 characterize eight linear equations of direct and converse piezoelectric effects. Near the straight lines of these connections, all piezoelectric coefficients are depicted. The piezoelectric coefficient located close to an arrow near the connection line must be multiplied by the parameter nearest to it. For example, the upper part of the piezoelectric square corresponds to two equations of piezoelectric effect  $P = d \cdot E$  and  $X = h \cdot P$ , while the lowest line symbolizes equations  $x = d \cdot E$  and  $E = -h \cdot x$ .

In the previous section, several matrixes of piezoelectric moduli were shown for the *principal installations* of some crystals, and it was seen that most of the 18 possible components in these matrixes are zero. For example, in quartz crystal there are only five nonzero components of piezoelectric modulus (of which two are independent); in barium titanate there are, respectively, five and three; while in KDP crystal only two and one. It is obvious that there is considerable interest in the question: how many of the *nonzero components* of piezoelectric modulus can be seen in all 20 classes of non-centrosymmetric crystals, in which piezoelectricity can be observed?

All these classes are listed in Table 5.2; there notations are given in the international classification, where the main symmetry elements of these classes are listed. Table 5.2 shows the number of nonzero components of *permittivity* tensor for all 20 piezoelectric classes of crystals, as well as for elastic stiffness (or compliance) tensors and the number of nonzero components of piezoelectric coefficient tensors. From Table 5.2 it follows that, with increasing symmetry of crystals, the number of independent components of tensors becomes smaller. The number of nonzero components of piezoelectric modulus reduces to two or three, of which only one component is independent in the last classes of piezoelectric crystals; such piezoelectrics are the easiest objects to study.

The matrix of elastic stiffness  $c_{mn}$  and its converse matrix of elastic compliance  $s_{mn}$ , in principal, would have  $6 \times 6$  components, but these matrixes are symmetric with respect to the main diagonal; therefore, in the general case, the maximum number

**Table 5.2** The number of components of basic “material” tensors of piezoelectric crystal classes [7].

Crystal symmetry	Syngony of lattice	Number of nonzero components $\epsilon_{ij}$	Number of independent components $\epsilon_{ij}$	Number of nonzero components $c_{mn}$	Number of independent components $c_{mn}$	Number of nonzero components $d_{in}$	Number of independent components $d_{in}$
1	Triclinic	9	6	36	21	18	18
2	Monoclinic	5	4	20	13	8	8
<i>M</i>		5	4	20	13	10	10
222	Ortho-rhombic	3	3	12	9	3	3
<i>Mm2</i>		3	3	12	9	5	5
4	Tetragonal	3	2	16	7	7	4
422		3	2	12	6	2	1
$\bar{4}$		3	2	16	7	7	4
4 <i>mm</i>		3	2	12	6	5	3
$\bar{4}2m$		3	2	12	6	3	2
3	Trigonal (rhombohedral)	3	2	24	7	13	6
32		3	2	18	6	5	2
3 <i>m</i>		3	2	18	6	8	4
6	Hexagonal	3	2	12	5	7	4
$\bar{6}$		3	2	12	5	6	2
622		3	2	12	5	2	1
6 <i>mm</i>		3	2	12	5	5	3
$\bar{6}m2$		3	2	12	5	3	1
23	Cubic	3	1	12	3	3	1
$\bar{4}3m$		3	1	12	3	3	1
$\infty \cdot m$	Polarized ceramics	3	2	16	7	5	3

of independent components in them is 21 (which is really seen in triclinic crystals). The increase in the number of symmetry elements in crystals causes an increase in the number of zero components of  $c_{mn}$  or  $s_{mn}$  matrixes and a decrease in the number of independent components. As a result, for most symmetric cubic crystals, in the matrix of elastic stiffness only three independent components of 12 nonzero are counted. In the case of *centrosymmetric* crystals (these symmetry classes are not given in Table 5.2), all 18 components of piezoelectric coefficients are zero; that is, they have no linear electromechanical effect (piezoelectric effect) but they should have the quadratic effect, electrostriction.

Ferroelectric ceramics are considered a major piezoelectric material. Typically, the nonpolarized (isotropic) ferroelectric ceramics after synthesis have “sphere symmetry” (the largest possible symmetry in solids). Technologically, ceramics can be converted into the noncentrosymmetric *texture*  $\infty\text{-}m$  with “cone symmetry,” with an axis of symmetry of infinite order ( $\infty$ ) and symmetry plane  $m$  passing through this axis. In this technology process, a strong electrical field is applied to the ceramics at elevated temperatures. As a result, ferroelectric domains, which initially were oriented chaotically, become reoriented along the applied field, forming a rather stable unipolar texture of domains. After the polarization field is switched off, this structure’s polar properties are stored long term, and it has a set of elastic parameters and piezoelectric coefficients that correspond to tetragonal crystals of class  $4m$ .

**2. Effective permittivity in piezoelectrics.** Different mechanisms of electrical polarization were considered in Section 1.1. However, in the polar-sensitive crystals (piezoelectrics and pyroelectrics), along with “basic permittivity,” due to *microscopic* processes of polarization (ionic, electron, dipole), *macroscopic* polarization is added, which is conditioned by the electromechanical  $\varepsilon_{EM}$  or electrothermal  $\varepsilon_{ET}$  reaction of the polar sample studied as a whole.

Next, only the piezoelectric dielectric contribution  $\varepsilon_{EM}$  will be considered (the electrothermal contribution  $\varepsilon_{ET}$  is discussed in Chapter 4). Electrical induction is characterized by the equation  $D = \varepsilon_0 \varepsilon E$ , where  $\varepsilon_0$  is the electrical constant in SI units and  $\varepsilon$  is permittivity conditioned by some elementary polarization mechanisms. In a piezoelectric that can be freely deformed in an applied electrical field, it is necessary to also take into account the piezoelectric effect  $P = ex$ , where  $e$  is piezoelectric coefficient and  $x$  is mechanical deformation:

$$D = \varepsilon_0 \varepsilon E + ex. \quad (5.14)$$

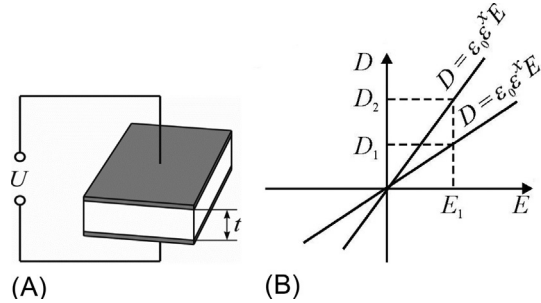
In the same way, the piezoelectric coefficient  $e$  can be found from the electrical contribution to mechanical stress, using the converse piezoelectric effect  $X = -eE$ . As a result, general stress in a piezoelectric is:

$$X = cx - eE.$$

The condition for free deformation of a piezoelectric in an electrical field is the absence of mechanical stress in it ( $X = 0$ ); then it follows that

$$x = eE/c.$$

**Fig. 5.16** Electromechanical contribution to permittivity: electrical induction  $D$  depending on electrical field  $E$  for mechanically free ( $X = 0$ ) and clamped ( $x = 0$ ) piezoelectric. (A) Crystal with electrodes; (B) induction dependence on electrical field.



By substituting this expression into Eq. (5.14), the following can be obtained:

$$D = \epsilon_0 \epsilon E + (e^2/c) = (\epsilon_0 \epsilon + e^2/c) E \quad (5.15)$$

As can be seen from this expression and from Fig. 5.16, the piezoelectric reaction *increases* electrical induction. In the mechanically clamped crystal, when strain is impossible ( $x = 0$ ), electrical field  $E_1$  induces  $D_1 = \epsilon_0 \epsilon E_1^x$ . However, in the mechanically free crystal ( $X = 0$ ) in the same field  $E_1$ , the induction is greater: it is  $D_2 = \epsilon_0 \epsilon E_1^X$ .

The piezoelectric reaction is an additional mechanism to the electrical polarization, because it *imitates* the corresponding contribution to permittivity. If a piezoelectric is mechanically clamped, then  $\epsilon = \epsilon^x$ , but if it is free, then  $\epsilon = \epsilon^X$ . These equations imply the relation between  $\epsilon^x$  and  $\epsilon^X$ :

$$\epsilon^X = \epsilon^x + e^2/\epsilon_0 c \quad (5.16)$$

In practice,  $\epsilon^X$  is measured at low frequency, since the *piezoelectric reaction* of the sample under study is easy to establish, and the electromechanical deformation contributes to permittivity increase. But at sufficiently high frequency (higher than the frequencies of all piezoelectric resonances), when a sample's own mechanical *inertia* does not allow its strain in an external field ( $x = 0$ ), permittivity  $\epsilon^x$  is measured. An experimental comparison of dielectric permittivity of free and clamped piezoelectric crystals was shown in Section 2.1, in Fig. 2.5, on examples of well-known ferroelectrics. At that, in the Rochelle salt crystal the piezoelectric effect is observed throughout the studied temperature range, and everywhere in the research range  $\epsilon^X > \epsilon^x$ . In the vicinity of Curie ferroelectric points, the effect of mechanical clamping is particularly large:  $\epsilon^X/\epsilon^x \approx 50$ . In another studied crystal, barium titanate, above the Curie point in cubic (centrosymmetric) phase,  $\epsilon^X = \epsilon^x = \epsilon$  since there is no piezoelectric effect. But below the Curie point in the single-domain (polarized) BaTiO<sub>3</sub> crystal near room temperature, this ratio is approximately 2. In the polarized ferroelectric ceramics this ratio is  $\epsilon^X/\epsilon^x < 2$ .

**3. Electromechanical interaction at converse piezoelectric effect.** Eqs. (5.5), (5.12) were obtained when considering the direct piezoelectric effect. In a similar way, it is possible to determine the  $K_{coup}$  from the converse piezoelectric effect, when *electrical energy* is applied to a crystal and, in addition, leads to its elastic deformation. Since a piezoelectric is assumed to be mechanically free, the initial equations change in comparison with Eqs. (5.8), (5.9). In the equation of electrical induction  $D = \epsilon_0 \epsilon E$ , the piezoelectric effect of a mechanically free crystal should be taken into account:  $D = \epsilon_0 \epsilon E + ex$  (5.14). Moreover, as shown earlier, the electroelastic contribution to stress  $X_{II} = cx - eE$  needs to be added to the mechanical stress. As a result, the piezoelectric reaction appears as an additional mechanism of electrical polarization, which causes an appropriate contribution to permittivity  $\epsilon^X = \epsilon^x + e^2/\epsilon_0 c$  (5.16). The condition of free deformation of a piezoelectric in an electrical field is the equation  $X = 0$ , so the following was obtained:  $D = \epsilon_0 \epsilon E + (e^2/c)E = (\epsilon_0 \epsilon + e^2/c)E$  (5.15)

Eq. (5.15) allows the electromechanical coupling factor for the converse piezoelectric effect to be determined:

$$W_{br} = W_{elec} + W_{elas} = \frac{1}{2} \epsilon_0 [\epsilon^x + e^2/(\epsilon_0 c)] E^2 = \frac{1}{2} \epsilon_0 \epsilon^X E^2,$$

where  $W_{elec} = \frac{1}{2} \epsilon_0 \epsilon^x E^2$  and  $W_{elas} = \frac{1}{2} (e^2/c) E^2$ .

As a result:

$$K_{coup}^2 = W_{elas} / (W_{elas} + W_{elec}) = e^2 / \{ \epsilon_0 c [\epsilon^x + e^2/(\epsilon_0 c)] \}.$$

The obtained relations make it possible to determine  $K_{coup}$  from the ratio between dielectric constant of free and clamped crystals:

$$\epsilon^X = \epsilon^x + K_{coup}^2 \epsilon^x; \quad \epsilon^X - \epsilon^x / \epsilon^x = K_{coup}^2. \quad (5.17)$$

From the equations obtained, it is possible to find the ratio of mutual energy of electromechanical energy  $W_{EM}$  to the product of mechanical (elastic) energy of electrical energy:

$$W_{EM}^2 / (W_{elas} \cdot W_{EM}) = K_{coup}^2 / (1 - K_{coup}^2).$$

It is seen that in this case the formula differs from the formula obtained during the analysis of the direct piezoelectric effect.

The following is considered the variation of elastic medium with density  $\rho$  under action of stress  $X$ :

$$\rho (d^2x/dt^2) = X, \quad (5.18)$$

similar to the oscillator equation, which describes the variations of mass  $m$  associated with elastic force  $cx$ :  $m(d^2x/dt^2) = -cx$ . The role of mass in Eq. (5.18) is the density  $\rho$ . Substituting expression  $X = cx - eE$  in Eq. (5.18), one can find:

$$\rho(d^2x/dt^2) = cx - eE,$$

and from Eq. (5.15), taking into account the absence of free charges in the elastic medium ( $\text{div}D = 0$ ,  $D = 0$ ), we have:

$$D = \varepsilon_0 \varepsilon E + ex = 0.$$

The latter equations mean that spatially variable electric fields excite acoustic waves in a piezoelectric and, conversely, elastic deformations of a piezoelectric medium are accompanied by waves of electric fields. From the general solution of these equations in the plane wave approach follows the Christoffel equation:

$$(\Gamma - \rho v^2)x = 0, \quad (5.19)$$

where  $\Gamma = c + e/\varepsilon_0 \varepsilon$  is the Christoffel tensor (modified tensor of elastic stiffness).

Although Eq. (5.19) is written for mechanical deformations, electrical potential propagates in a piezoelectric with the same velocity as elastic displacement. From Eq. (5.19) it follows that  $\Gamma = c(1 + K_{coup}^2)$ . Substituting changed speed  $v + \Delta v$  and taking into account that in the absence of the piezoelectric effect and  $\Gamma = c$ , it is possible to obtain the relation:

$$2\Delta v/v_0 + (\Delta v/v_0)^2 = K_{coup}^2.$$

Typically, the change in velocity of elastic waves in piezoelectrics is small. Therefore, in the previous expression one can ignore the term  $(\Delta v/v_0)^2$  and assume that  $K_{coup}^2 \approx 2\Delta v/v_0$ .

**4. Simplest devices consideration.** The electromechanical coupling coefficient in piezoelectric devices characterizes the conversion energy of a piezoelectric better than a set of elastic, dielectric, and piezoelectric constants. For example, the width of the frequency band of an electromechanical filter or converter directly depends on the corresponding coupling factor. Moreover, by means of coupling coefficients it is possible to compare piezoelectric materials that have essentially different permittivity and modulus of elasticity. At that, it should be borne in mind that the coupling coefficient is not a tensor, and formulas for tensor transformation in this case cannot be used.

The influence of boundary conditions on the magnitude of coupling factor is illustrated by consideration of a relatively simple but, from the point of view of technique, the most important case: the characteristics of *polarized ferroelectric ceramics* having symmetry  $\infty \cdot m$ . Depending on the shape of the ceramic piezoelectric element, the direction of its polarization, the location of the electrodes, etc., the coupling coefficient may be longitudinal, transverse, radial, thickness, and so on. Piezoelectric ceramics has 11 different coupling coefficients that describe piezoelectric effects in the case of an electrical field applied *parallel* to polarization axis  $Z$ , and another coupling factor for electrical field directed perpendicular to axis  $Z$ . Each of these coefficients corresponds to a certain system of boundary conditions.

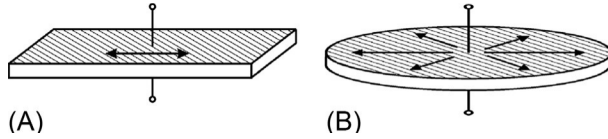


**Fig. 5.17** Piezoelectric oscillations: (A) Ceramic plate polarized in thickness; (B) ceramic disk polarized in thickness (electrodes are shown by shading, deformation is indicated by arrows) [5].

As an example, a rectangular plate with electrodes deposited perpendicularly to the axis of polarization is considered with mechanical stress applied along the plate.

The plate can freely expand in the longitudinal direction, and it is assumed that all other mechanical stresses are zero. The electrical field is applied to the electrodes, and in this case the *transverse* coefficient of electromechanical coupling equals to:

$$K_{31} = d_{31}(\epsilon_{33}s_{11})^{-1/2}. \quad (5.20)$$

Next, the piezoelectric disk is considered, shown in Fig. 5.17B, with a planar system of stresses  $X_1 = X_2$  (and assuming that  $X_3 = 0$ ). In this case, symmetry requires that deformation  $x_1 = x_2$  and deformation  $x_3 = 0$ . For the planar deformation, a radial coupling coefficient should be determined (in the plane perpendicular to polarization axis) in which there is the isotropic mechanical stress:

$$K_{rad} = k_{31} \{2/(1 - \sigma)\}^{1/2} \quad (5.21)$$

where  $\sigma = -s_{12}/s_{11}$  is Poisson's coefficient.

For another stressed system, when  $X_1 = X_2 = 0$  but  $X_3 \neq 0$ , the deformation can be realized in the thickness and all deformations in the plane are absent: ( $x_1 = x_2 = 0$ , but  $x_3 \neq 0$ ). In this case a *thickness coupling coefficient* is determined that characterizes the energy transformation for the case of one-dimensional deformation, and equals to:

$$K_t = h_{33}(\epsilon_{33}/c_{11})^{-1/2}. \quad (5.22)$$

The coupling coefficient in the disk thickness  $K_t$  corresponds to plate vibration on thickness, while the electrodes are deposited onto the largest surfaces, and the plate is polarized between these electrodes. Fig. 5.18A can serve as illustration of this case, provided that piezoelectric oscillations occur on the higher mode (the main, lower mode is the planar mode for which coupling coefficient  $K_{31}$  acts). The mode of oscillation in thickness, corresponding to  $K_t$ , is observed at much higher frequency, when lateral surfaces of the disk can be considered fixed.

Another coupling coefficient for piezoelectric elements that is important in practice can be determined by examining the case of one-dimensional stress oriented parallel to  $Z$  axis; an illustration of this case can be seen in Fig. 5.18B. Characteristic for this case, longitudinal coupling is:

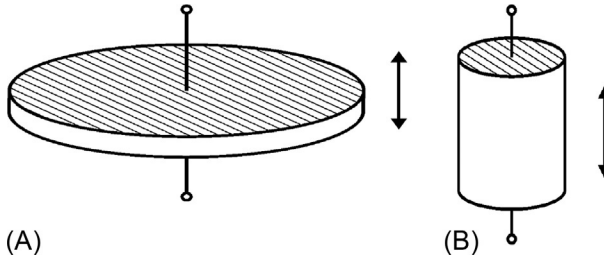


**Fig. 5.18** Examples of piezoelectric oscillations: (A) Disk polarized and deforming in thickness; (B) cylinder polarized in length (electrodes are shown by shading, arrows indicate deformation) [5].

$$K_{33} = d_{33}(\epsilon_{33}/s_{33})^{-1/2}. \quad (5.23)$$

In all the preceding equations, it is assumed that the coupling coefficient has the same sign as the corresponding piezoelectric modulus  $d$ , although, generally speaking, the coupling coefficient has no sign. Since in the *dynamic* conditions of vibrations, due to various types constraints, not all mechanical energy is converted into electrical energy (and vice versa); then dynamical coupling coefficients must be smaller than the corresponding static coefficients. Differences between them depend on values of the coupling coefficients, but usually dynamic coefficients are less than the static ones by 20%–25%.

It is clear from the preceding discussion that there are a large number of coupling factors, and some of them outperform others. In technical applications of piezoelectrics for given electrical and mechanical conditions it is always possible to find a system of mechanical stresses that corresponds to the greatest piezoelectric coupling coefficient.

**5. Applications of converse piezoelectric effect** in electronics are based on electrical energy conversion into mechanical energy, mostly for generating sound and ultrasound in a liquid or air environment [11–14]. Piezoelectrics are also used in contact with a solid, in which ultrasonic or hypersonic waves are excited; in addition, the converse piezoelectric effect has a physical basis of piezoelectric drives and motors. The effectiveness of a piezoelectric transducer in the radiation mode is characterized by the coefficient of quality  $d_{im}/s_{nm} = K_{rad}$ . Comparison of radiating power of different piezoelectrics might be taken with units  $K_{rad} = 1$  for the most famous piezoelectric—quartz. Others piezoelectrics surpass the effectiveness of quartz by 2–20 times; however, newly developed crystals of relaxor ferroelectrics can be more than 50 times more effective than quartz. Nevertheless, the most commonly used material is piezoelectric ceramics. As additional criteria for comparing piezoelectric materials, radiation parameter  $K_{rad}^2/\tan\delta$  can be applied, which characterizes electro-mechanical efficiency of a transducer, as well as mechanical quality factor  $Q_m$ , which determines the acoustomechanical efficiency of an emitter.

*Energy transformers*, depending on frequency range, are subdivided into four types: (1) *sound converters*, i.e., zoomers, vibrators, cellular microphones, high-frequency speakers, sirens, and so on; (2) devices for *ultrasonic technology*, which are used in high-intensity emitters for welding and cutting, washing and cleaning of materials, liquid level sensors, dispersion sprays, fog generators, inhalers, and air humidifiers; (3) *ultrasonic distance meters* in air environment used as distance meters for motor vehicles, sensors of presence and movement in security systems, as a level meter, as devices for remote control, in devices for scaring birds, animals and agricultural pests, etc.; (4) *high-frequency ultrasound* devices applied for equipment for testing materials and nondestructive testing, diagnostics in medicine and industry, delay lines, etc.

*In a liquid medium*, the piezoelectric ceramics are mainly used as ultrasound emitters having high electromechanical coupling coefficient and high mechanical  $Q$ -factor. Such emitters are applied in ultrasonic hydrolocation (sonar) and for distant underwater communication. Ultrasound is widely used also in industry to clean surfaces.

*In a solid environment*, thin films of piezoelectrics-semiconductors (zinc oxide, cadmium sulfide or aluminum nitride) are applied, in most cases for elastic waves operating in the ultrahigh frequency range (microwave), i.e., in the hypersound range. In some cases, very thin plates of lithium niobate, obtained by ionic digestion, are utilized in the microwave range to generate hypersonics in a media. If a sound emitter is a thin film deposited on the surface of a solid medium, then, in addition to piezoelectric ceramics, it is advisable to use vapor-deposited CdSe crystalline films and other piezoelectrics, the sputtering technology of which is well worked out in electronics. Piezoelectric emitters of sound and ultrasound are a part of piezoelectric converters used for radiation of acoustic oscillations, primarily in liquid and solid media.

*Piezoelectric emitters* made from single crystals are used in the higher-frequency range until the strength limit is affected (in frequencies greater than 200 MHz and transmitter-emitter thickness of several micrometers). In the microwave range, piezoelectric emitters are used on the basis of piezoelectrics-semiconductors (with a wide electronic zone). The application of a thin high-strength piezoelectric, working at resonant frequency of longitudinal or transverse oscillations, allows frequencies up to 75 GHz to be reached. Piezoelectric emitters of these types are used mainly in the acoustoelectronics, in devices operating on SAWs.

*Scanning acoustic microscope* with high resolution is one of the most striking achievements of modern piezoelectronics, because the nondestructive control of sub-micron elements up to nanometer sizes becomes possible, which allows investigations without surface damage of scanned crystals chips, which do not withstand the effects of electron microscope bundles, or of X-ray or auger probes.

*Piezoelectric actuators* are solid devices similar to magnetostrictive and thermal expansion actuators. The range of controlled displacement in piezoelectric actuators is similar, but in comparison with magnetic and thermal actuators, the precision of displacement of the piezoelectrics is much better. That is why piezoelectric actuators are used in tunnel and atomic force microscopes, which are well known for their high (atomic) resolution. One more advantage of piezoelectric actuators is their high speed.

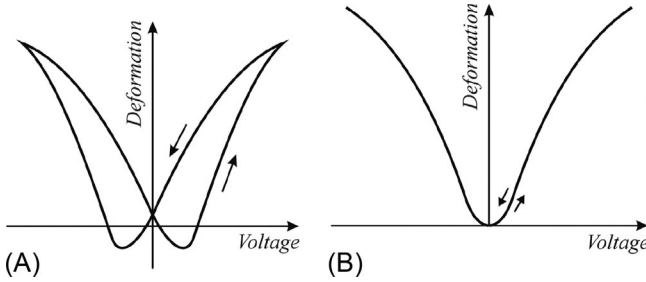


**Fig. 5.19** Comparison of electrically controlled deformation: (A) Usual piezoelectric ceramics; (B) electrostrictive relaxor ferroelectric material of PMN-PT type.

This unique feature, together with multilayer actuator technology, offers important applications for them. The main drawbacks of piezoelectric materials are high electrical voltage, small deformation and hysteresis, i.e., the ambiguous deformation dependence on the control field (Fig. 5.19A). Therefore, considerable efforts of developers are aimed, first, at increasing displacement, and, second, at development of non-hysteresis materials (Fig. 5.19B).

Piezoelectric actuators are divided into three main groups: the *axial* actuators, in which piezoelectric modulus  $d_{33}$  is used; the *transverse* actuators, using  $d_{31}$ ; and the *bending* actuators, also using  $d_{31}$ . Axial and transverse actuators have a common name—multilayer packets—because they are typed in a package of many piezoelectric elements (disks, rods, plates, or bars). The deformation in axial actuators is in the longitudinal direction; batch actuators develop a lot of applied force. In Fig. 5.20A, the principle of construction of an axial packet actuator is shown.

Significantly greater deformation can be obtained in the case of piezoelectric plate *bending*; in this case, a separate piezoelectric plate (monomorph), piezoelectric plate coupled with passive elastic plate (unimorph), two counter-polarized ceramics plates (bimorph), and several polarized piezoelectric plates (multimorph) can be distinguished (Fig. 5.20B). Bending actuators develop smaller force but give considerable displacement (hundreds of microns). In general, bending actuators belong to the

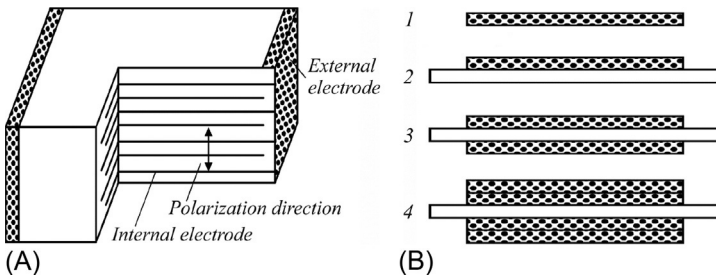


**Fig. 5.20** Piezoelectric actuators: (A) Packet of elements; (B) bending devices (1—monomorph, 2—unimorph, 3—bimorph, 4—multimorph) [3].

low-power group. There are also actuators with a new type of lamellar bimorph, in which the metallic frame prevents lateral deformation and therefore greatly enhances longitudinal deformation (“miniature actuator”) [3].

*Piezoelectric micropositioners* provide the capability of electrically controlled mechanical deformations. Relative deformation in strong electrical fields in piezoelectrics and ceramics can reach  $10^{-3}$ – $10^{-2}$ ; usually electromechanical elements connected to a battery (to reduce control voltage) can develop considerable force. Such micropositioners are used in optical communication systems and optical instrumentation, since electrically controlled mechanical shifts are comparable to or even exceed optical wavelengths. In particular, they are irreplaceable for the development of multi-elemental orbital telescopes with an aperture of tens of meters.

*Piezoelectric motors* utilize piezoelectric plate mechanical oscillations that turn into the circular motion of a rotor: that is, no wire winding or magnetic fields in such engines. The main material for piezomotors is polarized piezoelectric ceramics. The contact point of an oscillating ceramic plate with revolving rotor should be made of sturdy materials (metals or metal cements) resistant to wear: the lifetime of piezomotors depends on the durability of this mechanical contact. The first ultrasonic piezoelectric motors were invented in Igor Sikorsky National Technical University of Ukraine “KPI” by Dr. V.V. Lavrinenko. From that point, a variety of piezoelectric engines have been developed: nonreversible and reversible, with passive rotor and active stator, with active rotor and passive stator, with electrical excitation of oscillations of one and two types, and others.

In piezoelectric engines, quite different oscillations of piezoelectric elements can be used: for example, compression-stretching, bending, shear, torsion, and radial oscillations. The combination of these types of oscillations has made it possible to create a large number of different designs of piezomotors, many of which are currently only undergoing engineering review. It is important to develop more durable materials, which will bring the life of the piezoelectric motor to the necessary level. In electronic devices, piezomotors are used in watches and cameras, tape drives and other mechanical drives, tape recorders, and electrophones; they are also used in robotics. The advantages of piezoengines are the economy and simplicity of construction, high stability, the ability to instantly switch on and stop, and the absence of magnetic fields (which is especially important for electromechanical magnetic recording devices).

## 5.5 Electromechanical resonance

Resonance is a sharp increase in the amplitude of forced oscillations that occurs when the frequency of external influence takes on some particular values (resonance frequencies), which are determined by the properties of the system. The increase in the amplitude of oscillations is only a consequence of resonance, but its cause is coincidence of the external frequency (exciting system) with the internal (own) frequency of the oscillatory system. With the help of the resonance phenomenon, it is possible to amplify even very weak periodic oscillations. While resonance occurs at a certain frequency, an oscillatory system is particularly sensitive to the effect of excitatory force.

The degree of sensitivity in the theory of oscillations is described by the magnitude called the  $Q$ -factor.

Resonance oscillations in a solid elastic body are observed when the frequency of the excitatory force is close to the frequency of its own oscillations. Any mechanical element is characterized by mass, elasticity, and an indicator that characterizes irreversible energy losses, for example, friction or emission radiation to the environment. Each mechanical element (mass, elasticity, friction) has a counteraction (reaction) to the force that affects it, and therefore the oscillatory velocity of their movement depends not only on the magnitude of external force but also on the reaction of a mechanical element. For solids, the mechanical resistance of any element is defined as the ratio of force to the oscillatory velocity.

Since the mass, elasticity, and frictional reactions of mechanical oscillations have different natures, mechanical resonance has a complex nature. In the case of external periodic force, mechanical resistance due to mass increases with frequency and equals the product of mass at a circular frequency. Due to elasticity the mechanical resistance, on the contrary, is conversely proportional to circular frequency and flexibility of an element.

At low frequencies, the reaction of a mass of an element is negligible and may not be taken into account, so the value of the reaction is determined by the elasticity of the element. As the frequency increases, the reaction of elasticity decreases but the mass reaction increases, and finally the moment arrives when, at a certain frequency, the mechanical actions of mass and elasticity are equal and compensate each other. Formally, this compensation is due to a difference in the signs of these resistances. Physically, the compensation is explained by the fact that at low frequencies the external force overcomes only elastic forces and bias coincides with the phase of the external force. When the frequency of the external force becomes large, it has to overcome mainly the inertia of a mass, adding acceleration. In this case, the acceleration phase coincides with the phase of external force, while the phase of displacement becomes the opposite phase of external force (acceleration is the second derivative of displacement in time). Consequently, the directions of mass and elasticity reactions are opposite.

The resonance phenomenon in the electrical circuit of a piezoelectric element is due to the resonance of its mechanical oscillations. In the case of piezoelectric resonance, the amplitude of oscillations at the same value of the exciting electrical field sharply increases, while displacement remains in phase. As a result, the dielectric contribution  $\epsilon_{EM}$  at the resonance frequency  $\omega_r$  rises sharply. With the increase in displacement frequency of the polar bonds, they become antiphase relative to the exciting field, and  $\epsilon_{EM}$  acquires a negative value (antiresonance at frequency  $\omega_a$ ).

The resonance properties of a piezoelectric quasio-one-dimensional rod can be described by a resonant circuit with two capacitors and inductance. Piezoelectric resonances are repeated if the length  $l$  of the piezoelectric rod becomes multiplicative, i.e., if  $l = \lambda, l = 3\lambda/2, l = 2\lambda$ , and so on. This is accompanied by multiple resonance surges for frequency dependence permittivity (see Fig. 2.3 in Chapter 2). Gradually, with increasing frequency, the amplitudes of these bursts become smaller and the electro-mechanical dielectric contribution gradually disappears. It is obvious that the frequency of resonances associated with  $\epsilon_{EM}$  is dependent not only on the properties of a crystal, but also on its geometric dimensions.

**1. The quality factor (or  $Q$ -factor)** of the resonance is an important characteristic of an oscillatory system that determines the resonance band and shows how many times energy reserves in a system are greater than the loss of energy in one period of oscillation. If losses of mechanical or electrical origin in the resonator were absent, then mechanical stresses at the moment of resonance would reach an infinitely great value, and the resonator would be destroyed. However, mechanical and electrical losses are always present, and such a phenomenon is never seen.

Current in the electric circuit of the resonator at resonance always has a finite value and an active character, which is determined by the presence of losses. Quality is conversely proportional to the rate of attenuation of proper oscillations in the system. That is, the higher the  $Q$ -factor of an oscillatory system, the lower the energy loss for each period, and the slower the oscillations die. The general formula for the  $Q$ -factor of any vibration system is:

$$Q = 2\pi \cdot f \cdot W / P_d, \quad (5.24)$$

where  $f$  is frequency of oscillations,  $W$  is energy stored in the oscillatory system, and  $P_d$  is dissipation energy. In an electric resonance circuit, energy dissipates through the final resistance of a circuit; in bulk electromagnetic resonators, energy is lost in the walls of the resonator, in its material, and in contact elements. In piezoelectrics, the oscillation suppression is due to internal friction in a crystal or ceramic.

As is well known, for sequential oscillation circuits in an electrical  $RLC$  circuit, when all three elements are included sequentially:  $Q = R^{-1}(L/C)^{1/2}$  where  $R$ ,  $L$ , and  $C$  are resistance, inductance, and capacitance of the resonance circuit, respectively. For a parallel circuit in which inductance, capacitance, and resistance are included in parallel:  $Q = R(L/C)^{1/2}$ . In the case of an electrical circuit, it is much easier to measure the amplitude (current or voltage) than energy or power. Since power and energy are proportional to the square of amplitude of oscillation, the band of the amplitude-frequency characteristic ( $AFC$ ) will be distanced from a peak at about 3 dB. Therefore, another (equivalent) definition of  $Q$  factor is used, which relates the width of the amplitude resonance curve  $\Delta\omega$  at the level with resonance frequency  $\omega = 2\pi f$ , that is  $Q = \omega/\Delta = \omega/2\delta$ , where  $\delta$  is decay damping.

**2. Resonance in piezoelectrics.** A piezoelectric energy converter usually has pronounced resonance properties near the internal frequency of oscillations of the mechanical system. They are determined by the speed of sound in piezoelectric material and the type of electromechanical oscillations (longitudinal, transverse, radial, bending, etc.).

Experiments show that the generalized conductivity of a piezoelectric element in an alternating current circuit, the frequency of which varies smoothly and widely, linearly *increases* with increasing frequency; that is, conductivity has a *reactive* capacitive character. However, this expected logically capacitive type of conductivity is violated at some frequencies, at which initially a sharp increase in conductivity occurs, followed by a sharp drop (Fig. 5.21). At the moment when conductivity becomes maximal, its character changes—it becomes active. Such an active nature of conductivity is also observed at the time when it is minimal; in the interval between maximum and

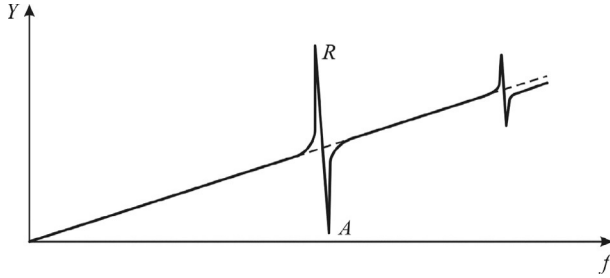


**Fig. 5.21** Frequency dependence of conductivity  $Y$  of piezoelectric element: In points  $R$  (resonance) and  $A$  (antiresonance) conductivity is active, between these points its character is inductive, while at frequencies below point  $R$  and above point  $A$  conductivity is capacitive.

minimum values, conductivity is *inductive*. Therefore, the changes of conduction are typically resonant in nature.

To describe the characteristics of electrical long lines and circuits with distributed parameters, equivalent electrical circuits are widely used, composed of elements with lumped parameters. It is also common to use such equivalent circuits for piezoelectric resonators, considering that the piezoelectric element is usually the mechanical vibration system with distributed parameters such as mass, elasticity, and loss control parameters—for example, friction or acoustic radiation.

In the frequency domain close to resonance, the nature of the piezoelectric resonator conductivity change is similar to that of the conductivity of an electrical sequential oscillation circuit, with a capacitor as a shunt. This can be used as a basis for describing conductivity or resistance in the vicinity of frequencies close to resonance in an equivalent electrical circuit (substitution scheme), composed of elements with lumped parameters (inductance, capacitance, and resistance) whose values are constant and independent of the amplitude of oscillations and frequencies. Such an equivalent circuit in the form of a vibration circuit is depicted in Fig. 5.22A.

At frequency  $f = f_r$ , there is a mechanical resonance, and the current in the electrical circuit of a piezoelectric resonator reaches a maximum value. When the frequency increases up to  $f_a > f_r$ , called the *antiresonance* frequency, impedance of the resonator

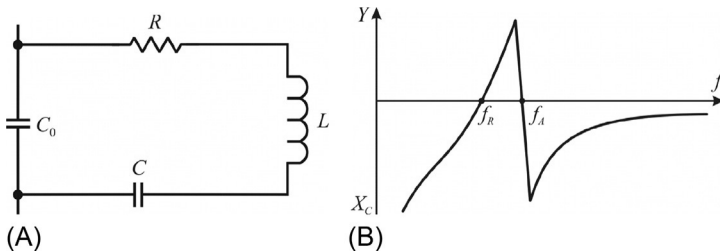


**Fig. 5.22** Piezoelectric resonance: (A) Equivalent electrical circuit; (B) frequency dependence of reactive resistance of piezoelectric resonator.

becomes maximal, and current in the circuit is minimal. Piezoelectric resonance corresponds to two resonant frequencies  $f_r$  and  $f_a$ , at which the resistance of the resonator is active. The first resonance, observed at lower frequency, is characterized by low impedance, and the second—at higher frequency—has high resistance.

In other words, lower-frequency resonance of the equivalent scheme of Fig. 5.22 is caused by the *voltage* resonance (sequential resonance) of the circuit, consisting of a series of inductance  $L$ , capacitance  $C$ , and resistance  $R$ . This branch is called dynamic or piezoelectric; moreover, the listed elements do not exist physically and their parameters can be determined only in conditions of resonance excitation. The second resonance, taking place at higher frequency, is the resonance of *currents* or the parallel resonance, occurring in a parallel circuit, one branch of which contains capacitance  $C_0$  and the other is a consistent connection of the elements  $L$ ,  $C$ , and  $R$ . This resonance is characterized by high resistance.

Elements of an equivalent electrical circuit are called *equivalent* electrical (or dynamic) parameters of the resonator. These are dynamic (equivalent) inductance, dynamic (equivalent) capacity, dynamic (equivalent) resistance, and parallel capacity  $C_0$ . The reactive dynamic parameters  $L$  and  $C$  are determined by the elastic, dielectric, and piezoelectric coefficients, as well as by the density of the piezoelectric. The values of these parameters essentially depend on orientation of a cut of the piezoelectric element, on the type and frequency of the excited mechanical vibrations, and on the size of elements and electrodes. The dynamic resistance of  $R$  depends on internal friction and sources of other mechanical losses. Losses of electrical origin in a piezoelectric resonator are usually small and not taken into account. Only for some types of crystals and piezoelectric ceramics are electrical losses noticeable, and then they should be taken into account.

Dynamic resistance can be measured directly, for example, with a bridge meter of full resistance. Dynamic inductance and capacitance can be measured only by indirect methods. The value  $\Delta f = f_a - f_r$  is called the *resonance interval*. The quality of the piezoelectric resonator is determined by the peculiarity of its frequency characteristic (Fig. 5.17B), and by the value of efficiency. Knowledge of frequencies  $f_a$  and  $f_r$  allows a number of important characteristics of the resonator to be determined, and, in the first place, the coefficient of electromechanical coupling:  $K_{EM} \approx (2\Delta f/f_p)^{1/2}$ . Resonance frequency is calculated from the formula  $f_r = 1/2\pi(L_1C_1)^{1/2}$  while the mechanical  $Q$  factor is defined as  $Q_M = 1/(2\pi f_r C_0 R_1)$ .

Of the four equivalent parameters specified in Fig. 5.22, only the parallel capacity  $C_0$  has concrete physical embodiment: its value is determined by the intermediate capacitance of the piezoelectric and by the capacitance of the housing and mounting. It can be directly measured with some approximation by known methods. In the case of “effective” piezoelectrics, the capacity  $C_0$  varies markedly with frequency: at frequencies below resonance it is larger, and at frequencies above resonance it is smaller. The measurements of parallel capacitance cannot be performed at resonant frequency: it should be measured at frequencies far from resonance. For “effective” piezoelectrics, this capacity must be measured at a frequency higher than resonance, that is, under conditions of a completely clamped piezoelectric.

The equivalent scheme given in Fig. 5.22 is considered to be simplified, but it satisfactorily describes the frequency dependence of the full resistance of resonators near the resonance, and hardware designers in most cases can determine the values of its equivalent parameters. In some cases, an equivalent circuit has to be complicated by introducing into it parameters of other elements, for example inductance of additional circuits (previous and following), and also the capacitance between the full device and the piezoelectric element. In addition, piezoelectric resonators usually have several resonances due to oscillations of various types or overtones of any kind of oscillation. In this case, an equivalent scheme that reflects the presence of several resonances looks like a parallel connection of a number of dynamic branches shunted by a common parallel capacitance.

Experimentally, parameters of a piezoelectric resonator are determined by methods of resonances—antiresonances, changes in electrical load, and the method of circular diagrams, etc.

**3. Applications of piezoelectric resonance**, due to the very high  $Q$ -factor of mechanical vibration systems, are significantly greater than for electrical vibration circuits, because sometimes  $Q$  is characterized by values from thousands to hundreds of thousands [3, 13]. Therefore, amplitudes of mechanical oscillations of a piezoelectric cell at mechanical resonance are  $Q$  times greater than the amplitudes of its oscillations outside of the resonance region. Electrical quantities that characterize oscillations of the piezoelectric element, such as electrical current, are related directly to mechanical stresses and deformations. At the moment of mechanical resonance, the current through the piezoelectric increases and the frequency response of current acquires a resonant character, exactly corresponding to the characteristic of mechanical resonance oscillations. Such is, in general, the picture of resonance phenomena observed in the piezoelectric resonator, which explains the origin of resonance in an electrical circuit.

Piezoelectric resonance is widely used in radio engineering, electronics, electroacoustics, and microelectronics: in filters and resonators, generators and resonant piezoelectric converters, piezoelectric transformers, and even motors. In resonators, mainly crystals are used (quartz, lithium niobate, etc.) or piezoelectric ceramics with small losses. For example, quartz resonators are used as resonant circuits and generators of high-frequency oscillations. The high quality factor ( $10^5$ – $10^6$ ) of a quartz resonator determines the small deviation of generator frequency from its nominal value: ( $10^{-3}\%$ – $10^{-5}\%$ , when ambient temperature, pressure, and humidity change. Widely used miniature quartz resonators with oscillation frequencies of 30 kHz–8 MHz are used in electronic clocks, electronic ignition systems of internal combustion engines, and others. Quartz and other piezoelectric resonators are also used in acoustoelectronic devices for filtration and signal processing: monolithic piezoelectric filters, as well as in filters and resonators on surface acoustic waves (SAWs). The main advantage of resonators on SAWs is the possibility of their use in frequency stabilization devices and narrowband filtering in the frequency range 100–1500 MHz.

*Piezoelectric filters* made of piezoelectric ceramics and manufactured for a frequency range of 1 kHz–10 MHz usually are multilayered. At the same time, at lower frequency bands up to 3.5 kHz, bimorphic elements are used in which the

piezoelectric performs resonant oscillations of a bend-type along its face. In the range of 40–200 kHz, piezoelectric resonators are used with longitudinal oscillations along the length, while at frequencies of 200–800 kHz piezoelectric resonators in the form of disks with radial oscillations are realized. At frequencies above 1 MHz, mainly thickness vibrations of piezoelectric rings are used. The filters being considered differ in simplicity of construction and have small dimensions (in comparison with *LC* filters) and stable working characteristics.

In most cases, piezoelectric elements have only two electrodes, and resonators with such elements are electrical double-pole devices. But in some cases, resonators use piezoelectric elements with a large number of electrodes, having separate leads, for example, with four electrodes. Such resonators with multielement piezoelectrics should be regarded as electrical multipolar devices. Resonators with a four-electrode piezoelectric element are often used in generators and filters, since they allow replacement of two resonators of one frequency with a single four-pole resonator, as well as eliminate unwanted ohmic bonds with a phase shift of 180 degrees between two pairs of terminals, using also voltage transformations and conversion of resistance.

Acoustic resonance, electrically excited at the expense of the piezoelectric effect, is employed in various electronic devices. Piezoelectric resonators have been used in radio engineering for more than 90 years. Their main purpose is to stabilize the frequency of radio generators. Miniature quartz frequency stabilizers are applied in most watches, mobile phones, and computers. The quality and stability of piezoelectric resonators can be very high. This allows them to be utilized as sensors in various devices, in which they measure pressure, acceleration, displacement, temperature and velocity of gases and liquids, determine their chemical composition, etc., since the environmental parameters affect the quality factor and actual frequency of the resonator.

*Precision resonance sensors* also employ resonance. Among them, the resonant precision sensors of *force*, both active and passive, are implemented. As is known, piezoelectric devices cannot measure stationary processes: this means that piezoelectric force sensors can convert only a changing force to a variable electrical signal, but they do not react to a constant magnitude of external force. The range of measurement depends on the frequency of mechanical resonance in the applied piezoelectric crystal, for example, quartz. The principle of such sensors is based on the fact that, upon mechanical loading of quartz crystals, where certain sections are used as resonators in electronic generators, a shift in their resonant frequency occurs. This frequency offset is due to the dependence of some parameters of the crystal on the magnitude of external forces. For example, the coefficient of rigidity depends on the applied load, whereas density and geometric parameters change under these conditions insignificantly. A special direction exists for each cut of crystal, along which the maximum of sensitivity of the piezoelectric resonator is observed.

*Frequency stabilizers* mainly use crystalline quartz. Previously, natural quartz (rock crystal) was used for the manufacture of resonators. Now quartz is artificially hydrothermal. Different designs of quartz resonators can overlap the frequency range  $10^3$ – $10^9$  Hz. They use not only simple oscillations of the “compression-stretching” type of quartz plates in length, width, or thickness, but also bending, twisting, or shear oscillations complicated by the design of the resonators.

The widespread use of quartz is due to its rare combination of unique properties, which ensure the achievement of a mechanical  $Q$ -factor up to  $Q_m \sim 10^7$  and more, with the presence of a number of crystallographic orientations (sections) that change their resonant frequency very little over the operating temperature intervals. Modern quartz resonators provide long-term stability of frequency up to  $10^{-6}$  percent and short-term stability of frequency two to three orders higher. The high level of quartz-growing technology and the production of resonators, including micro-miniaturals (for example, for electronic clocks), make it almost indispensable in frequency stabilization devices and precision narrowband filters. To increase the thermostability of piezoelements, plates of quartz are cut at an angle of 5 degrees to the  $X$ -axis. For special purposes, sections of 18 degrees  $X$  and others are also applied. The most thermostable is the AT-cut of quartz when its plates are cut along the  $X$ -axis at an angle of  $\theta = 35$  degrees to the  $Z$ -axis. Moreover, another double-reversed  $ST$ -section now sees widespread use.

*Piezoelectric transformers* use resonant properties of electromechanical devices. These elements in electronic devices play the role of low-power and small-scale sources of electrical energy. They are distinguished from electromagnetic transformers by their energy conversion scheme: “electrical-acoustical-electrical,” which allows a significant simplification of the design of the piezoelectric transformer (Fig. 5.23B), with none of the wires or windings required in electromagnetic transformers. The piezoelectric voltage and current transformers can be distinguished by peculiarities of application and constructive features. The most common characteristic of piezoelectric transformers is the magnitude of piezoelectric efficiency,  $K_{31}Q_m$ , where  $K_{31}$  is the coefficient of transverse electromechanical coupling and  $Q_m$  is the mechanical  $Q$ -factor for transverse oscillations of the piezoelectric element.

The piezoelectric plate-type transformer in the simplest case has two pairs of electrodes—exciter and generator (Fig. 5.23B). Using the *converse* piezoelectric effect, the exciter creates mechanical deformation in a plate, which covers the entire volume of the piezoelectric element in a form of a resonant wave (piezoelectric

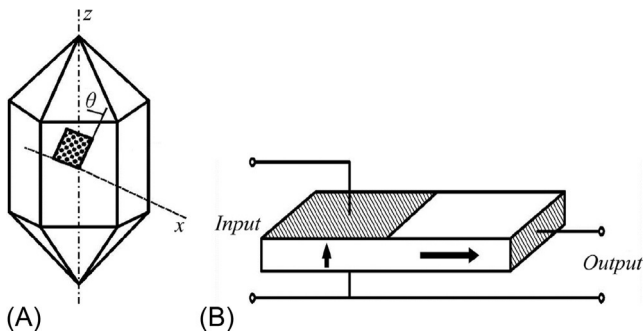


**Fig. 5.23** Piezoelectric resonance: (A) Orientation of thermostable AT-cut in quartz; (B) simplest model of piezoelectric transformer [5].

transformers operate in acoustic resonance mode). In the generator section of a piezoelectric transducer, as a result of the *direct* piezoelectric effect, the alternating signal arises, which is galvanically divided from the input voltage.

The general characteristics of piezoelectric transformers depend on the electric quality factor, which determines their efficiency, and which also depends on the coefficient of electromechanical coupling and mechanical quality of the particular piezoelectric material and on the type of oscillation. Different types of piezoelectric ceramics are applied as a working material in piezoelectric transformers, since ceramics allows both elements of this device—exciter and generator—to be constructively combined in one plate (disk and rod). This is due to the technological possibility of carrying out the multidirectional task of orienting the piezoelectric polarization vector in the process of manufacturing the components of the corresponding monoblock piezoelectric element.

The use of modern piezoelectric ceramics materials allows realization of voltage transformation factor magnitudes of more than 1000, which ensures that output voltage exceeds 10 kV. In addition to the *voltage* transformer mode, these devices are successfully used as transformers of electrical *current*.

The classification of piezoelectric transformers by *working frequency* is as follows:

- Low-frequency transformers, calculated as having resonance frequency below 10 kHz, in particular for industrial frequencies of 1000, 400, and 50 Hz. These very low-frequency piezoelectric elements usually operate in *bending* oscillations. The bimorphic and multilayer devices can be mechanically free or mechanically loaded (to reduce operating frequency).
- Middle-frequency piezoelectric transformers have a frequency range of 10–500 kHz and are constructed with single-layer or multilayer piezoelectric cells, operating on the longitudinal acoustic oscillations of the main mode or in higher modes of oscillation.
- High-frequency piezoelectric transformers, for a frequency range of more than 500 kHz, use thin piezoelectric plates with their higher frequency modes of longitudinal acoustic vibrations in width, or multilayer structures working on oscillations in the thickness of the piezoelectric element.

For the *power transferred* to load, the following designs of piezoelectric transformers can be distinguished:

- Low power (up to 1 W), which usually are made of single-layer piezoelectric elements having a weight less than 1 g;
- Average power (1–50 W) representing the single-cassette piezoelectric transducer containing up to six piezoelectric elements;
- High power (more than 50 W), which are combined multicassette transformers.

The specific transmitted power of piezoelectric transformers is 1–10 W/g or 15–75 W/cm<sup>3</sup>, according to the efficiency value of 90%–95%. Combined piezoelectric transformers that unite both main types of transformers are also known, but they are much more complicated and not well proven in technology. The main application of piezoelectric transformers is secondary sources of electrical power for radio and electronics devices. Piezoelectric transformers are also used in high-voltage generators for gas discharge lamps.

## 5.6 Thermodynamic description of piezoelectric effect

The direct piezoelectric effect is defined as a response of a polar crystal to an external mechanical action, while in the converse piezoelectric effect the electric field produces a deformation that is proportional to it. Moreover, the polar-neutral (“exclusive”) piezoelectrics, which are 10 of 20 classes of polar crystals, do not react to hydrostatic pressure, i.e., to homogeneous (scalar) mechanical action, and therefore they cannot serve as vibration sensors in the air or in a liquid medium. The remaining 10 of the 20 classes of polar crystals are not only piezoelectrics but also pyroelectrics and only they are able to exhibit the volume piezoelectric effect as a response to hydrostatic action, so appropriate sensors are made from them. However, polar-neutral piezoelectrics are also characterized by a set of properties important for electronics applications, which manifest themselves both under directed mechanical action and under the influence of an electrical field.

As shown in the Introduction in connection with Fig. I.1, direct and converse pyroelectric effects, depending on the electrical and mechanical conditions, can be described by *eight* different equations. All of them can be obtained by various thermodynamic potential analyses. As opposed to microscopic theories, the atomic structure of material is not taken into account in thermodynamics, but a material is regarded as a continuum having certain properties. In the case of piezoelectricity, this continuum is anisotropic: its electrical, thermal, and elastic properties depend on the direction of applied forces and fields.

*Thermodynamic potentials.* It is assumed that the thermal, elastic, and electrical properties of piezoelectricity can be described by *six* parameters: two thermal characteristics ( $T$ —temperature,  $S$ —entropy), two mechanical properties ( $X$ —stress,  $x$ —strain), and two electrical properties ( $E$ —electrical field,  $D$ —electrical induction).

If a dielectric receives some amount of heat  $dQ$ , the change in its internal energy  $dU$ , according to the first principle of thermodynamics, is described by the expression:

$$dU = dQ + dW = dQ + Xdx + EdD, \quad (5.25)$$

where  $dW$  is work carried out by electrical ( $EdD$ ) and mechanical ( $Xdx$ ) forces.

As only *reversible* processes are reviewed here (this includes both electrical polarization and mechanical strain), so  $dQ = TdS$  in accordance with the second principle of thermodynamics. As a result, the change in internal energy (5.25) can be represented as a function of the six basic parameters of the dielectric:

$$dU = TdS + Xdx + EdD, \quad (5.26)$$

where the selected basic parameters are  $S$ ,  $x$ , and  $D$ . The remaining parameters ( $T$ ,  $X$ , and  $E$ ) are defined as the derivatives of internal energy  $U$  on entropy  $S$ , strain  $x$ , and electrical induction  $D$ . During differentiation, one parameter is assumed constant and the other two parameters are denoted in the corresponding way:

$$\begin{aligned}
T &= (\partial U / \partial S)_{x,D}; \\
X_n &= (\partial U / \partial x_n)_{S,D}; \\
E_i &= (\partial U / \partial D_i)_{S,x}.
\end{aligned} \tag{5.27}$$

These ratios in a brief form are three equations of state of a polar dielectric: thermal, elastic, and electrical. Earlier, in [Section 1.3](#), the variety of boundary conditions was discussed: electrical, mechanical, and thermal. Correspondingly, of three pairs of related parameters,  $T \Leftrightarrow S$ ,  $X \Leftrightarrow x$ , and  $D \Leftrightarrow E$ ; the three *independent* parameters might be chosen, moreover, in *eight* ways. The objectives of different boundary conditions describing thermal, elastic, and electrical properties of polar crystals determine the choice of eight different thermodynamic functions (potentials), with which one can express the basic equation of state of piezoelectricity. The preceding equation is just one of them:

$$\begin{aligned}
dU &= TdS + Xdx + EdD; & dH &= TdS - xdX - DdE; \\
dH_1 &= TdS - xdX + EdD; & dH_2 &= TdS + Xdx - DdE; \\
dA &= -SdT + Xdx + EdD; & dG &= -SdT - xdX - DdE; \\
dG_1 &= -SdT - xdX + EdD; & dG_2 &= -SdT + Xdx - DdE,
\end{aligned} \tag{5.28}$$

where  $H$ —enthalpy,  $H_1$ —elastic enthalpy,  $H_2$ —electric enthalpy,  $A$ —Helmholtz free energy;  $G$ —Gibbs free energy,  $G_1$ —elastic Gibbs energy,  $G_2$ —electrical Gibbs energy. Indexes of the vector and tensor parameters are omitted for simplicity.

From Eq. (5.10) three equations of state were obtained (5.27). With an increasing number of thermodynamic functions up to eight, the number of equations of state also increases. For example, if the independent variables were to be selected as electrical induction  $D$ , strain  $x$ , and temperature  $T$ , then thermodynamic potential should be nominated the Helmholtz free energy, and the equation of state of a dielectric differs from Eq. (5.27):

$$\begin{aligned}
-S &= (\partial A / \partial T)_{x,D}; \\
X_m &= (\partial A / \partial x_m)_{T,D}; \\
E_i &= (\partial A / \partial D_i)_{T,x}.
\end{aligned}$$

The equation of state can be written as linear differentials of independent variables:

$$\begin{aligned}
dS &= (\partial S / \partial T)_{D,x} dT + (\partial S / \partial x_m)_{D,T} dx_m + (\partial S / \partial D_i)_{x,T} dD_i; \\
dX_n &= (\partial X_n / \partial T)_{D,x} dT + (\partial X_n / \partial x_m)_{D,T} dx_m + (\partial X_n / \partial D_i)_{x,T} dD_i; \\
dE_j &= (dE_j / \partial T)_{D,x} dT + (dE_j / \partial x_m)_{D,T} dx_m + (dE_j / \partial D_i)_{x,T} dD_i.
\end{aligned} \tag{5.29}$$

As the number of potentials is eight, then the full number of such equations is 25. The coefficients in these equations are the generalized state of compliance: they define various fields (electrical, mechanical, and thermal). The most important ones were

mentioned earlier in connection with the description of piezoelectrics: second-rank tensors ( $\epsilon_{ij}$ ,  $\alpha_{ij}$ ), tensors of third rank ( $d_{in}$ ,  $e_{im}$ ,  $h_{jn}$ ,  $g_{jn}$ ), fourth-rank tensors ( $c_{mn}$  and  $s_{mn}$ ). Here the indices are  $i, j, k = 1, 2, 3$ , while  $m, n = 1, 2, \dots, 6$ , and they are used for the matrix presentation of parameters.

As shown earlier, thermodynamic potentials (5.28) with Helmholtz free energy are responsible to describe not only the piezoelectric effect, but the pyroelectric effect, ferroelectric phase transitions, and other phenomena in polar crystals. To describe only the piezoelectric effects, some changes need to be made considering the primary four potentials as adiabatic ones ( $dS = 0$ ) and following four potentials as isothermal ( $dT = 0$ ) ones.

Specifically, in this example—Helmholtz free energy—based on  $dT = 0$ , the piezoelectric effect is described by:

$$\begin{aligned} dX_n &= c^D_{mn} dx_m - h_{in} dD_i; \\ dE_j &= -h_{jm} dx_m + (\beta^x_{ij}/\epsilon_0) dD_i, \end{aligned}$$

in which coefficients of elastic stiffness  $c^D_{mn} = (\partial X_n / \partial x_m)_D = (\partial^2 A / \partial x_n \partial x_m)_D$  that are determined at constant induction, while the parameter  $(\beta^x_{ij}/\epsilon_0) = (\partial E_i / \partial D_j)_x = (\partial^2 A / \partial D_i \partial D_j)_x$  is the *converse permittivity* of clamped crystal. The parameter  $h_{jm}$  is one of four piezoelectric coefficients that also refer to one of the generalized compliances:

$$h_{jm} = -(\partial X_n / \partial D_j)_x = -(\partial E_i / \partial x_n)_D = -(\partial^2 A / \partial x_n \partial D_i).$$

Thus, one of four piezoelectric coefficients ( $d$ ,  $e$ ,  $g$ ,  $h$ ) is discovered. The same pair of equations can be obtained from free energy expression and from other thermodynamic potentials, the number of which in the terms of  $dS = 0$  and  $dT = 0$  is reduced to five. As a result of the thermodynamic relations, four pairs of basic equations of the piezoelectric effect follow as:

$$\begin{aligned} D_i &= d_{in} X_n + \epsilon_0 \epsilon_{ij} E_j; \quad x_m = s^E_{mn} X_n + d_{jm} E_j; \\ D_i &= \epsilon_0 \epsilon^x_{ij} E_j + e_{im} x_m; \quad X_n = c^E_{nm} x_m - e_{jn} E_j; \\ E_j &= (\beta^x_{ji}/\epsilon_0) D_i - h_{jm} x_m; \quad X_n = c^D_{nm} x_m - h_{in} D_i; \\ E_j &= (\beta^x_{ji}/\epsilon_0) D_i - g_{jn} x_n; \quad x_m = s^D_{mn} X_n - g_{im} D_i. \end{aligned}$$

Therefore, all four piezoelectric coefficients are possible to estimate.

Thus, thermodynamic (phenomenological) theory allows all basic equations to be found without clarifying the molecular mechanisms that describe direct and converse piezoelectric effect at the macroscopic level. These equations are used in engineering calculations, and the parameters of these equations can serve as a basis for comparing properties of various piezoelectric materials.

## 5.7 Summary

1. The *piezoelectric effect* occurs in crystals or polarized ceramics for which an electrical voltage appears across the material when pressure is applied. Similar to the pyroelectric effect, this phenomenon is due to asymmetric structure of the material that allows ions to move more easily along one axis than along the others. As pressure is applied, the opposite sides of the piezoelectric acquire the opposite charges, resulting in a voltage appearing across the material.
2. A *piezoelectric* converts mechanical energy into electrical or, conversely, electrical energy into mechanical. The mechanoelectric effect was first observed, which for this reason was called a “direct” piezoelectric effect. The piezoelectric effect is the odd (linear) effect, in which the mechanically induced polarization is directly proportional to the deformation; with the converse piezoelectric effect, the electrically induced deformation is directly proportional to the magnitude of the electrical field. Both piezoelectric effects may happen only in noncentrosymmetric crystals and structures.
3. *Electrostriction* is observed in all dielectrics and it is an even effect, in which deformation of a dielectric caused by an electrical field is quadratically dependent on the magnitude of this field. Thus, the sign of electrostrictive deformation does not change with the change of sign of a field. Electrostriction differs from the piezoelectric effect by the fact that it does not have the converse effect, that is, this effect is exclusively electromechanical, but not “mechanoelectric.”
4. The piezoelectric effect is described by *piezoelectric constants*—tensors of the third rank. Mathematical relations describing piezoelectricity or electrostriction depend on the combination of certain boundary conditions in which the piezoelectric is used or investigated. The main mechanical conditions are reduced either to the possibility of deformation (if the crystal is free) or to their impossibility (when the crystal is clamped). The boundary electrical conditions are that the crystal can be short-circuited or open-circuited.
5. *Piezoelectricity* is the linear electromechanical effect. Moreover, of electrical properties of crystals, only the dielectric polarization (characterized by permittivity) is relevant to the piezoelectric effect. Mechanical properties of piezoelectrics include elasticity, hardness, durability, and others; but for the piezoelectric effect the most important mechanical properties are *elasticity* (which depends on binding forces of atoms in a crystal) and the *velocity* of elastic waves in the piezoelectric (which, in addition to elasticity, depends on specific density).
6. External mechanical influence on a piezoelectric is characterized by the *tensor of mechanical stress*. This symmetric tensor of second rank in its physical nature differs from the symmetric second-rank tensor of permittivity, whose structure is consistent with the *internal symmetry* of a crystal. So the permittivity tensor is the *material* tensor, while the tensor of mechanical stresses is the *field* tensor, characterizing the structure of forces applied to the crystal from outside. From Hooke’s law, which confirms linear proportionality of deformation and mechanical stress, two tensors are very important for piezoelectrics: the tensor of elastic stiffness  $c_{mn}$  (also called Young’s modulus) and the tensor of elastic compliance  $s_{mn}$ . Both of them are symmetric material tensors of the fourth rank. Others special parameters of piezoelectrics important in applications are: *volumetric modulus of elasticity*  $K$ , *volumetric compressibility*  $\langle s \rangle$ , and *Poisson’s coefficient*  $\nu$ , all of them used to characterize the elastic properties of piezoelectric material.
7. In various cases of technical application of piezoelectrics, depending on the symmetry of action of external mechanical forces, five important cases should be distinguished: *linear-stressed* state (uniaxial tension), *plane-stressed* state (two-axis stress), *volume-stressed*

state (three-dimensional stress) and stress of *pure shear*. A separate important case is the *hydrostatic pressure*, in which all components of stress are the same:  $x_{11} = x_{22} = x_{33} = \dots = p$ , where  $p$  is specific pressure. Depending on the symmetry of the mechanical load, as well as symmetry of the piezoelectric, the deformation in it (which is also a symmetric tensor of second rank) can be classified as one-dimensional, two-dimensional, and three-dimensional. Two-dimensional deformation of tensile-compression must be taken into account in modern planar microelectronic technology.

8. The piezoelectric effect can be induced by the electrical field in any solid dielectric as the “*linearized electrostriction*.” In some of the paraelectrics and in the relaxor ferroelectrics the magnitude of the electrically induced piezoelectric effect may outweigh the piezoelectric effect of the best piezoelectric materials. Piezoelectric effect manifestations can be controlled by bias electrical field: for example, the frequency of piezoelectric resonance becomes tunable, or parameters of filters based on SAWs might be controlled. The effectiveness of electrical control of piezoelectric effect is most significant in dielectrics with large permittivity.
9. The mechanical property (elasticity) and electrical property (polarization) of piezoelectric crystals are interrelated, and, therefore, they can be *considered together*. This relationship is characterized by electromechanical coupling coefficient  $K_{EM}$ —one of the most important parameters of piezoelectric materials and devices. In the case of direct piezoelectric effect, the mechanical energy applied to the piezoelectric is spent not only on elastic deformation, but also creates electrical polarization, which causes electrical energy accumulation. Conversely, electrical energy supplied to the piezoelectric (in the case of converse piezoelectric effect) is spent not only for its polarization, but also to its elastic deformation and elastic energy accumulation.
10. The square of electromechanical coupling factor  $K_{EM}^2$  shows what part of energy, attached to a piezoelectric, is converted into the energy of another kind. However, this parameter is not a performance factor: first, because losses of electrical or mechanical power are not considered, and, second, actual conversion efficiency of the piezoelectric depends not only on the  $K_{EM}$ , but largely is due to the shape, orientation, and other peculiarities of the piezoelectric element.
11. *Polar crystals and textures* are distinguished by the fact that their electrical, elastic and thermal characteristics are interdependent. Moreover, during the study (or the use of devices) only the electrical effect (for example, polarization) reveals that the corresponding electrical parameters depend on boundary mechanical and thermal conditions: for example, permittivity of mechanically free crystal ( $\epsilon^X$ ) differs from permeability of clamped piezoelectric crystal  $\epsilon^x$  (which cannot be deformed), and always  $\epsilon^X > \epsilon^x$ . By the same way, elastic stiffness of a piezoelectric (or its elastic compliance) depends on its electrical state (short-circuited or open-circuited) and therefore  $c^E \neq c^D$ ; in some cases they differ by several times.
12. *Thermodynamic* (phenomenological) theory allows, without specifying the molecular mechanisms, all basic equations describing direct and converse piezoelectric effect at the macroscopic level to be obtained. These equations are used in engineering calculations, and parameters of these equations can be the basis for comparing the properties of different piezoelectric materials.
13. For application in electronics and instrumentation, many piezoelectrics of different structures have been developed: crystals, ceramics, polymer materials, films, and composites. One of the most important piezoelectric crystals is quartz, which combines a large mechanical  $Q$ -factor ( $Q_m \sim 10^7$ ) with high thermal stability of resonant frequency in the operating

temperature intervals. In electronics, piezoelectric crystals niobium tantalite, lithium tantalite, and langasite, whose unique characteristics provide a variety of applications in acousto-electronic devices, are widely employed.

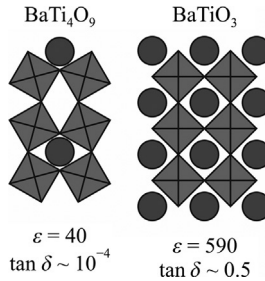
14. *Piezoelectric ceramics* are the most important material for modern piezoelectric devices. In order to meet the needs of technology, dozens of compositions of piezoelectric ceramics have been developed with different sets of parameters, which provide converters of mechanical vibrations from the environment into electrical signals; converters of electrical signals into elastic waves or in mechanical displacements; and devices that use electromechanical resonance.
15. *Polymer piezoelectric films* of PVDF-type (and their corresponding copolymers) are characterized by simple technology and low acoustic impedance, and they are widely applied in piezoelectric polymer sensors and many other devices.
16. *Electrostriction materials* have now acquired great importance, because they differ from piezoelectrics by the absence of hysteresis in deformation-electrical field dependence. They are relaxor ferroelectrics with disordered structure characterized by a blurred temperature maximum  $\epsilon(T)$  in the vicinity of phase transition and record a high electromechanical coupling coefficient.
17. Parameters of piezoelectrics *can be controlled* by a bias electrical field: for example, piezoelectric filter characteristics can be changed as well as surface acoustic wave parameters. Electrical control by piezoelectric properties is manifested most commonly in dielectrics with high permittivity.
18. An external electrical field changing the velocity of elastic wave propagation makes it possible to control resonant frequency or phase of bulk piezoelectric filters or surface acoustic waves. This effect can be used in frequency and phase modulators, and in parametric amplifiers for implementation in new electronic devices. An electro-induced piezoelectric effect can be applied also in parametric devices. Since electromechanical coupling factor depends on permittivity ( $K \sim \epsilon^{3/2}$ ), the most promising dielectrics for parametric devices are those that have  $\epsilon \approx 10^3\text{--}10^4$ .
19. *Piezoelectric sensors* are widely employed in electronics, instrumentation, and medical technology. In these sensors the direct piezoelectric effect is used with the most convenient parameters of piezoelectric modulus  $g$ , which characterizes electrical voltage occurring under applied pressure, and the modulus  $h$  showing voltage per unit strain. Piezoelectric devices employed in liquid media are called *hydrophones*, and piezoelectric devices used in the air are called *microphones*. They are capable of operating in a very wide range of frequencies—from hertz to gigahertz.
20. The *converse piezoelectric effect* is applied, for the most part, to generate sound and ultrasound in a liquid or air environment. As ultrasound emitters, mainly those piezoelectric ceramics with high electromechanical coupling coefficient and large mechanical  $Q$ -factor are employed. Such emitters are used in ultrasonic sonar and in a distant underwater connection.
21. *Piezoelectric actuators* are based on the converse piezoelectric effect and widely applied in electronics and modern instrumentation, as well as in robotics and engineering. Piezoelectric actuators differ in their precision of movement; that is why they are applied in tunnel and atomic force microscopes having high (atomic) resolution.
22. *Piezoelectric motors* have advantages due to the absence of induction windings and magnetic fields. These motors convert high-frequency electric current into mechanical rotation; moreover, the working element is the piezoelectric ceramics, which converts electrical energy into mechanical with high efficiency (90%), exceeding this parameter for many types of engines.

23. *Piezoelectric transformers*, which allow effective replacement of electromagnetic transformers, are used in many cases. These devices operate predominantly in the resonant mode, using the converse piezoelectric effects, as well as the direct.

## References

- [1] W.O. Cady, *Piezoelectricity*, Amazon com, New York, 1946.
- [2] J.C. Burfoot, G.W. Taylor, *Polar Dielectrics and Their Application*, Macmillan Press, New Jersey, 1979.
- [3] K. Uchino, *Ferroelectric Devices*, Marcel Dekker, New York, 2000.
- [4] I.S. Jeludev, *Basics of Ferroelectricity*, Atomizdat, Moscow, 1973.
- [5] Y.M. Poplavko, Y.I. Yakymenko, *Piezoelectrics*, Polytechnic Institute, Kiev, 2013.
- [6] I.S. Rez, Y.M. Poplavko, *Dielectrics: Main Properties and Electronics Applications*, Radio e Svyaz, Moscow, 1989.
- [7] Y.M. Poplavko, *Electronic Materials. Principles and Applied Science*, Elsevier, 2019.
- [8] Y.M. Poplavko, L.P. Pereverzeva, I.P. Raevskiy, *Physics of Active Dielectrics*, South Federal University of Russia, Postov-na-Donu, 2009.
- [9] Y.M. Poplavko, L. Pereverzeva, N.-I. Cho, Y.S. You, Feasibility of microelectronic quartz temperature and pressure sensors, *Jpn. J. Appl. Phys.* 37 (1998) 4041.
- [10] Y.M. Poplavko, L.P. Pereverzeva, Thermopiezoelectric transducers, *Ferroelectrics* 131 (1992) 331.
- [11] Y. Kikuchi, *Ultrasonic Transducers*, Corona Publishing Company, Tokyo, 1969.
- [12] J. Fraden, *AIP Handbook of Modern Sensors: Physics, Designs and Applications*, American Institute of Ohysics, New York, 1993.
- [13] N. Setter, *Piezoelectric Materials in Devices*, EPFL, Swiss Federal Institute of Technology, Lausanne, 2002.
- [14] M.E. Lines, A.M. Glass, *Principles and Application of Ferroelectrics and Related Materials*, Clarendon Press, Oxford, 1977.

# High permittivity microwave dielectrics



Comparison of nonpolar and polar dielectric at frequency of 10 GHz and 300 K.

One important line of electronics development is microwave electronics, where dielectrics are used in technologies mostly as structural and assembly materials, as well as a medium for transmission of microwave signals and their transformation (filtering, modulation, detection, etc.). Microwave dielectrics are basic materials in high-frequency microelectronics; they are widely applied as *passive* microwave components (dielectric resonators, substrates for microstrip lines, electrical capacitors, dielectric resonators, antennae), and as the *functional* elements of microwave technique (tunable filters, phase shifters, modulators, detectors). Thus, microwave dielectrics play an important role in microwave microelectronics, since they are widely used in terrestrial and satellite telecommunications devices (in software radio, the Internet of Things, GPS, environmental monitoring, etc.) [1, 2]. Analysis of modern trends in this field of technical application shows that the main tasks are device integration finding new circuit solutions, new materials, and elaboration of advanced technologies. Moreover, further progress needs new materials with given sets of properties.

Therefore, microwave dielectrics are of great importance in modern electronics. In particular, microwave electronics needs dielectric materials, which combine increased permittivity ( $\epsilon_{mw} \sim 20\text{--}150$ ), small dielectrics losses ( $\tan\delta < 10^{-3}$ ), and high thermal stability of permittivity ( $TC\epsilon = \epsilon^{-1}d\epsilon/dT \rightarrow 0$ ). Such electronic materials are described in hundreds of publications and are generalized in several books, but mainly as empirical development [3]. But it should be noted that further development of new materials depends not only on practical technology, but also on a clear understanding of the characteristics of the properties of these materials and the fundamental science on which these properties are based.

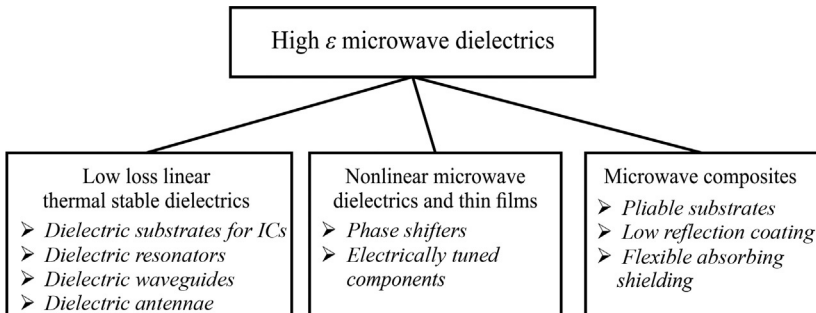
## 6.1 Introduction and classifications

The distinctions of this chapter are the attempts to apply physical substantiations of such features of microwave dielectrics as the large dielectric permittivity and its compatibility with small dielectric loss. Increased permittivity can be obtained in ionic crystals with sufficiently open structure, which makes it possible to use greater polarizability of the semifree electronic orbits. Moreover, as basic material the displacement type of paraelectrics can be applied, the structure of which is characterized by a low-frequency transverse lattice optical mode. In some cases the thermal stability of permittivity can be obtained in such structures where paraelectricity is suppressed by paramagnetism. Small dielectric losses can be reached only in monophasic composition, based on “hard” paraelectric material (which resists polar structure formation). It is argued also that the main reason for microwave absorption in high-permittivity dielectrics is the presence of a *polar-sensitive phase* in their composition, so the recommendation is to avoid any polar materials that lead to an increase in dielectric losses. However, nonlinear dielectrics, which allow the rapid control of their permittivity, used in microwave phase shifters, obviously include a polar phase. Nevertheless, a compromise may be found in how to combine high dielectric nonlinearity with minimal dielectric losses. Another solution is also proposed for the control of frequency-agile devices: tuned resonator filters and phase shifters [4, 5]. The macrocomposites designed for this function consist of microwave dielectrics coupled with a controlled air-gap, which makes it possible to create microwave phase shifters and filters without inserted losses (the controlling piezoelectric device is located outside the waveguide path).

Current and future fields of high-permittivity microwave dielectrics applications are briefly listed in Table 6.1.

- *Linear low-loss thermally stable dielectrics* are the main class of currently used microwave dielectrics with increased value of permittivity  $\epsilon_{mw}$ . At one point, they revolutionized wireless microwave communications, reducing by many times the size and cost of filters, generators, and antennas. They are applied mainly as miniature capacitors, dielectric

**Table 6.1** Main areas of application of microwave high permittivity dielectrics.



resonators, and substrates of microwave circuits, reducing their planar dimensions by  $\epsilon$  times, which is very important for microelectronic devices. Selection of such microwave dielectrics is determined by the frequency range of their use. So, for meter and decimeter waves, the microwave dielectrics with a value of  $\epsilon = 150\text{--}80$  are needed; for centimeter waves, dielectrics with  $\epsilon = 40\text{--}20$  are preferred, while for millimeter waves, a permittivity  $\epsilon = 10\text{--}1.5$  is more common. As indicated in Table 6.1, such dielectrics are mainly used in microwave substrates and waveguides, dielectric resonators, and antennae. Materials for such dielectrics are ceramics, polymers, and composites, including flexible polymer-ceramic composites. Generally, any provision of thermal stabilization from outside is undesirable for microwave devices; that is why parameters of microwave dielectrics should be very stable in the predetermined temperature interval. Usually these dielectrics must have a small temperature coefficient of dielectric constant:  $TC\epsilon = \epsilon^{-1}d\epsilon/dT < 10^{-5} \text{ K}^{-1}$ . This *thermal stability*, as will be shown shortly, is mainly provided due to compensation of the negative contribution to  $TC\epsilon$  occurring due to the electronic polarization mechanism of the positive contribution to  $TC\epsilon$  from the ionic polarization mechanism. The *low dielectric losses* of the dielectrics listed are due to their small electrical conductivity and due to the absence in their composition of any polar-sensitive materials.

- *Nonlinear microwave dielectrics* capable of electrical control by their permittivity  $\epsilon(E)$  are studied in many laboratories around the world, and now they are beginning to be applied in microwave engineering. They use polar-sensitive paraelectrics (which under external influences can go into polar state). Therefore, their nonlinearity is certainly accompanied by increased dielectric losses and significant change in permittivity with temperature (even if they are used as a component of composites); thus it is impossible to guarantee high thermal stability and low microwave losses. However, their applicability is tempting due to the possibility of a fast restructuring of electronic devices up to parametric interaction. Next, the possibility of obtaining a compromise in technology solutions for application of nonlinear dielectrics in microwave electronics will be discussed.
- *Microwave composites* are represented by a wide variety of materials for various purposes, as seen in Table 6.1. The composite is a multicomponent system in which several materials of different structure are combined in order to obtain certain properties of the final material. At the same time, the components of the composite obtained do not enter into chemical reactions, but retain individual properties forming interfacial boundaries; therefore, the properties of a composite material are largely due to the geometrical arrangement of components. Composites are valuable because in them it is possible to obtain *new properties* not available for each component separately. Composite materials allow the developer of electronic materials to solve the necessary technical problems by combining the properties of various materials. The simplest example of a microwave composite material is the matrix mixture based on a polymer with  $\epsilon = 2\text{--}3$  (Teflon or silicon rubber) and ceramic powder filler with  $\epsilon = 100\text{--}140$  (rutile or perovskite). The result will be a low-loss nonfriable composite material with  $\epsilon = 2\text{--}40$  (depending on the percentage of components).

The *pliable microwave substrates* needed for flexible (rubbery) electronics devices that are stretchable, twistable, and deformable seem impossible using rigid microwave substrates. Usually these substrates are dielectric plates with stable permeability ( $\epsilon = 3\text{--}10$ ) and low losses at microwave frequencies ( $\tan\delta \sim 2 \cdot 10^{-3}$ ). In addition, microwave packaging technology requires a low thermal expansion coefficient and high thermal conductivity of substrate materials. All of these properties must be

reproduced in flexible substrates for microwave electronics, given that, from the possible polarization mechanisms, only *nonpolar dielectrics should be used*. Many rubber-ceramics composites have been developed and used whose properties and technology are described in [1].

*Low microwave reflection coatings* are especially important in military electronics and therefore their composition and technology are usually not described in detail. These *absorbent materials* are also a subject of modern research. For them it is necessary to have large dielectric losses, even in thin layers, in order to provide almost complete attenuation of microwave irradiation. Anisotropic crystals with microwave dispersion might be applied in millimeter and submillimeter waves as polarizers, in which strong anisotropy of microwave absorbance of one-axis ferroelectrics is seen. Very close to absorbers due to their mechanisms of physical interaction of components are the metamaterials, which are artificial periodic structures with lattice constants much smaller than the wavelength of incident radiation. These are media consisting of resonance elements, in which negative propagation of electromagnetic waves takes place. Dimensions of “metaatoms” are smaller than the wavelength of radiation interacting with them. They can simulate homogeneous material, the properties of which are absent in natural materials. In some metamaterials a volumetric lattice of microwave dielectric resonators can be used. It can be noted also that electromechanical resonance in very small piezoelectric resonators is also possible to use to get a negative  $\epsilon$ -value. Usually this resonance occurs at frequencies of  $10^5$ – $10^7$  Hz (depending on the size of the piezoelement); to realize this resonance for microwaves, piezoresonators should have a size of only a few microns. It is obvious that microelectronic technology is responsible for bringing this about.

*Flexible absorbing shielding composites* are another important application of microwave electronic materials. Currently, a huge amount of electronic equipment is used at high and ultra-high frequencies, which results in a dense atmosphere of radio waves surrounding us, leading to unwanted electromagnetic interference (EMI). Because of this, there is a real need for shielding materials, absorbing electromagnetic waves; such materials are used in commercial and military equipment, scientific electronic devices, communication devices, and protection for radiation sources. Shielding absorbers of radiation are flexible and light materials necessary to protect electronic equipment from interference and to reduce the risk to human health [2]. Thin layers of metals, various forms of carbon (graphite, graphene, soot, carbide, nanotubes) as well as *conductive polymers* and magnetic materials are good protective materials from EMI. Good electromagnetic absorption is demonstrated by the high conductivity polymers (polyaniline, polypyrrole, polythiophene, etc.), which also show strong environmental resistance. That is why flexible microwave-shielding composites are constructed of these conductive polymers combined with the absorbing solid materials previously listed, which play the role of fillers. Current EMI shielding composites use *magnetic nanoparticles* that provide the best microwave absorption [1].

*Millimeter-wave dielectrics and shielding composites* applied in a frequency range of 30–300 GHz should have special characteristics. Currently, new microwave electronics in this frequency range is being developed: *wireless gigabit* communication

uses a frequency range of 57–66 GHz, *vehicle radar* works in a range of 76–81 GHz, *radio astronomy* and military devices occupy frequencies above 90 GHz, etc. In these cases, the substrates and resonant components must use low-loss dielectrics ( $\epsilon = 6-2$ ,  $\tan\delta = 10^{-3}-10^{-4}$ ). It is obvious that these ceramic and polymeric dielectrics must be nonpolar.

As for *shielding composites* developed for a range of 60–100 GHz, it should be noted that the conductivity contribution to microwave absorption decreases in proportion to frequency increase (dozens of times); similarly decreases in microwave absorption are due to magnetic resonance. Therefore, in the case of absorbent composites intended for millimeter waves, the role of *polar dielectrics* increases: their microwave absorption rises in proportion to frequency increase. In addition, in polar crystals (ferroelectrics of the order-disorder type) absorption in millimeter waves may be extremely *anisotropic*—in one direction these crystals show wave-transparency while in another direction their absorbance is  $\sim 30$  dB/mm [6].

Thus, microwave technologies use a variety of different dielectrics—with low and high dielectric constant, with low and high dielectric losses. In many respects, these properties depend on the polarity of dielectrics: polar-sensitive bonds increase the anharmonicity of lattice vibrations, which leads to dielectric losses in microwaves [5]. These and others features are determined by the diverse mechanisms of electrical polarization.

## 6.2 Polarization mechanisms in microwave dielectrics

Polarization is the main property that determines the peculiarity of a dielectric as a type of material and may occur both under an applied electrical field and other external influences (change of pressure, temperature, or irradiation). In this section, only the polarization that occurs in an externally applied electrical field is considered (a polarization induced by change in temperature or pressure was described in Chapters 4 and 5).

In a dielectric, an electrical field induces the *shift* of associated charges (creating the charge separation = polarization) and the *movement* of free charges (causing the charge transferee = conductivity); both of these phenomena arise simultaneously. At the same time, charge separation (polarization) results in the bias current, which anticipates the applied sinusoidal electrical voltage in phase by  $\pi/2$ , and this current exists as long as the electrical field is applied (this is true both for alternating and direct voltage). In the event when voltage is switched, bias current exists only at that time, when the electrical field is changing, and this current is absent in the case of permanent voltage. Continuing to discuss the differences of these two phenomena, it should be noted that conductivity relates to the *transport phenomena*, while polarization (with rare exceptions) is a *reversible property*. Moreover, the internal structure of dielectrics is unfavorable for free charge carriers moving, so their number is *negligible*; on the contrary, *all particles* of a dielectric participate in polarization.

Microscopic polarization mechanisms have already been considered in Chapter 1, but mainly from the point of view of their *internal polarity*. Moreover, several

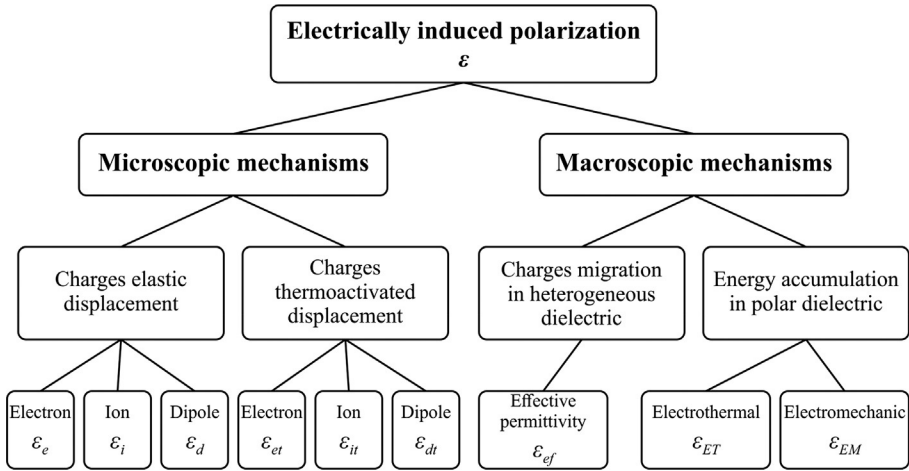


**Fig. 6.1** Dielectric permittivity due to basic mechanisms of electrical polarization.

mechanisms of elastic, thermal, and space-charge polarizations are described, in which locally bound electrons, ions, or dipoles shift in electrical field. For microwave dielectrics, the most important aspect of these mechanisms is their *inertia*. Traditionally, different polarization mechanisms are considered as being “independent,” and this consideration is basically justified. The classification of dielectric contributions of various mechanisms to permittivity is given in Fig. 6.1.

The *quasielastic* (deformation type) induced polarization is the least inertial polarization, being only slightly affected by temperature movement; so dielectrics with this polarization are good materials to use in microwave engineering. Electronic quasielastic polarization (deformation of electron shells of atoms, molecules, or ions in electrical fields), which determines permittivity  $\epsilon_e$ , is a common mechanism for *all dielectrics*. Ionic quasielastic polarization is a characteristic property of such dielectrics and semiconductors in which the ionic type of bonding in the crystal lattice is clearly pronounced; the ionic polarization mechanism is characterized by permittivity  $\epsilon_i$ . Quasielastic dipole polarization with  $\epsilon_d$  is observed in very rare cases: when the external electrical field induces the orientation of closely constrained dipoles.

As already discussed in Chapter 1, only these polarization mechanisms can be fully installed at microwave frequencies, and only they call forth microwave permittivity  $\epsilon_{mw} = \epsilon_e + \epsilon_i$  (Fig. 6.2). However, lower-frequency polarization mechanisms also indirectly affect properties of microwave dielectrics, increasing their *dielectric losses*. The fact is that those microscopic movements of associated electrical charges of dielectrics, which do not have time to be installed during a quarter of an oscillation period of the applied field, cannot accumulate energy during this time for the reversible polarization process. However, they continue to move in-phase with the electrical field like “free” particles, which leads to the irreversible phenomenon of conductivity, i.e., they convert part of the electrical energy they receive into heat—i.e., into the losses.

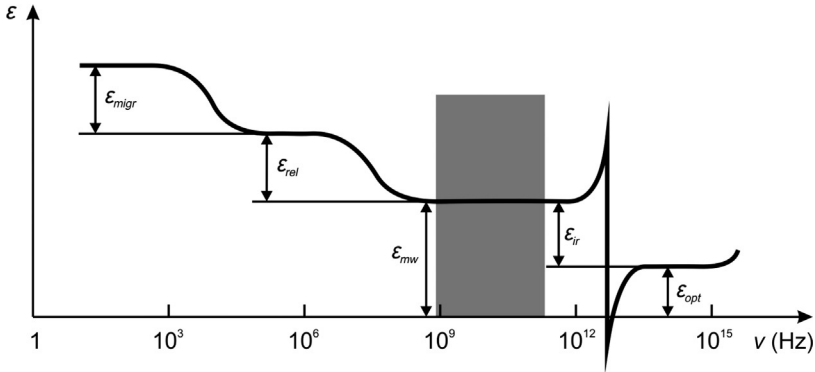


**Fig. 6.2** Generalized frequency dependence of permittivity of nonpolar dielectrics with shown dielectric contributions from different polarization mechanisms; microwave frequency range is darkened; in order to simplify this figure, additional contributions to permittivity from  $\epsilon_{EC}$  and  $\epsilon_{EM}$  peculiar to *polar* dielectrics are not shown.

*Thermally supported* electrically induced polarization (relaxation) in solid dielectrics stipulates the dielectric contribution shown in Fig. 6.2 as  $\epsilon_{rel}$  and designated in Fig. 6.1 as  $\epsilon_{il}$ ,  $\epsilon_{ir}$ , and  $\epsilon_{dr}$ . This polarization, mainly caused by structural defects, is essential if electrons, dipoles, or ions are weakly bound in the structure of the dielectric. Remaining localized in nanoscale areas, these charged particles or dipoles under the influence of thermal motion make thermally activated jumps, moving at distances on the order of atomic dimensions. The electrical field influences the direction of this thermal hopping, which becomes asymmetrical and has sufficient time to generate electrical moment if the frequency is not high. The inertia of thermally activated polarization is much greater in comparison with quasielastic polarization, so that at sufficiently high frequencies this movement of charged particles no longer contributes to polarization but does increase electrical conductivity and losses.

Electrically induced *space-charge polarization* (also called *migration* polarization), for which the dielectric contribution is shown in Fig. 6.2 as  $\epsilon_{migr}$  and designated in Fig. 6.1 as  $\epsilon_{ef}$ , is another additional mechanism of polarization observed in some solids and composite materials with pronounced heterogeneous structure. The cause of this polarization is the presence of layers or regions with different conductivity (for example, electroconductive inclusions in a dielectric). Polarization conditioned by space-charge is the lowest-frequency (highest inertia) mechanism that can have some effect on microwave *absorbing composite* properties.

Thus only some of the polarization mechanisms listed are responsible for  $\epsilon_{mw}$  at microwave frequencies (Fig. 6.2). First is *electronic* elastic polarization, which exists in any material, being the only mechanism that can respond even to optical frequencies; that is why the correspondent permittivity is denoted as  $\epsilon_e = \epsilon_{opr}$ . Second is *ionic* elastic-displacement polarization, which is too slow in the visible optical range but has its own resonance at the far infrared range (that is sufficiently fast for microwaves); so the ionic contribution to permittivity is  $\epsilon_i = \epsilon_{ir}$ . The sum of these polarization

mechanisms determines microwave permittivity  $\epsilon_{mw}$ . As shown in Fig. 6.2, other mechanisms of polarization usually are too slow: migration polarization with permittivity  $\epsilon_{migr}$  is too slow above a frequency of 1 kHz, while relaxation polarization ( $\epsilon_{rel}$ ) cannot contribute to permittivity above a frequency of 100 MHz (nevertheless, there are some polar-sensitive dielectrics—ferroelectrics of the order-disorder type—in which the fundamental polarization occurs exactly in the microwave range, but this feature is not shown in Fig. 6.2).

**1. Key points of microwave dielectric elaboration.** Dielectrics possessing only electronic elastic (optical) polarization have small permittivity  $\epsilon_e = \epsilon_{opt} \leq 6$ , while high-permittivity microwave dielectrics need  $\epsilon_{mw} = 20\text{--}200$ . For this reason, it remains further to consider only dielectrics with a pronounced mechanism of ionic elastic displacement, because this is the only type that allows high-permittivity, low dielectric loss, nonpolar microwave dielectrics. At the same time, ionic bonds of low-loss dielectrics should not be combined with covalent bonds in such a way that polar-sensitive bonds might arise (described in Chapter 1)—they lead to microwave absorption. Thus, with respect to low-loss microwave dielectrics, it is very important that these dielectrics not have any manifestations of polarity in their structure; but in contrast, for absorbing and nonlinear microwave dielectrics, their main characteristics are due precisely to internal polarity [7, 8].

As shown in Chapter 1, in polar dielectrics the lattice optical phonons, which determine the value of permittivity, are associated with acoustic phonons that determine high-frequency absorption; therefore, polar high-permittivity dielectrics are not suitable for use as low-loss microwave dielectrics. It follows that when developing or designing low-loss microwave dielectrics, which usually consist of several components, all possible means should be used to avoid any presence of polar components, which could lead to increase of losses. At that, high permittivity, which is needed for important microwave applications, can be ensured only in crystals having low-frequency transverse lattice optical mode; however, no polar properties should arise in them [9, 10].

Therefore, the first problem is how to obtain *high permittivity* and *low loss* microwave dielectrics; in other words, to find a way to combine high permittivity in the microwave range with no polar phase in a dielectric.

The second, also difficult, problem is to obtain a very high *thermal stability* of permittivity, which has to be greater than the stability of the initial components of the microwave dielectric.

As noted, making further progress in microwave microelectronics requires dielectric materials with a given set of properties; in particular, such dielectrics should combine small losses ( $\tan\delta < 10^{-4}$ ), high dielectric constant ( $\epsilon_{mw} \sim 20\text{--}150$ ) and the greatest possible thermal stability ( $TC\epsilon = \epsilon^{-1}d\epsilon/dT \rightarrow 0$ ). These requirements, on the face of it, seem physically inconsistent: the generally accepted concepts of electronic and ionic polarization mechanisms (described in Chapter 1) do not indicate how it is possible to combine high- $\epsilon$ , low loss, and simultaneously thermostability in a dielectric, especially in the microwave frequency range.

As follows from Fig. 6.2, only *fast electronic and ionic* polarization can be used; moreover, the polar-sensitive dielectrics should be excluded (as sources of undesirable

microwave losses). Within these limits, i.e., without taking into account slower polarization processes, the problem of thermally stable microwave permittivity in dielectrics can be solved only by using electronic ( $\epsilon_e$ ) and ionic ( $\epsilon_i$ ) polarization mechanisms, as illustrated in Fig. 6.2.

**2. Different temperature characteristics need comments.** In the *atomic crystals* and in many *polymeric materials*, only fast electronic (optical) polarization takes place, i.e., the displacement of electron clouds of atoms in the applied electrical field. Due to low inertia, this polarization can provide both very small microwave losses ( $\tan\delta < 10^{-4}$ ) and rather good thermal stability of permittivity:  $TC\epsilon_e < -10$  ppm/K, curve 1 in Fig. 6.3. However, microwave dielectrics possessing only this mechanism of polarization have small permittivity ( $\epsilon_{mw} = \epsilon_e \approx 2-5$ ), which is insufficient for many microwave applications (with the exception of millimeter waves).

In most of the *ionic crystals*, the investment to permittivity  $\epsilon_i$  is also accompanied by low losses ( $\tan\delta < 10^{-3}$ ) and by acceptable thermal stability of  $\epsilon_{mw}$  (curve 2 in Fig. 6.3). In this case, the electronic investment to permittivity  $\epsilon_e$  (which shows negative  $TC\epsilon_e$ ) partially compensates the positive thermal coefficient from ionic polarization:  $TC\epsilon_{mw} < +100$  ppm/K. Since any frequency dispersion of  $\epsilon_i$  at microwaves is absent, losses in ionic crystals are small. However, in most of these crystals permittivity also is not large:  $\epsilon_{mw} = \epsilon_e + \epsilon_i \approx 6-12$ , which is not enough for many important microwave applications (dielectric resonators, antennas, filters, etc.). Nevertheless, high-permittivity ionic nonpolar dielectrics of relatively simple chemical composition and possessing small microwave losses are widely known—some of them are represented in Fig. 6.3 by curves 3–5—but the properties of these dielectrics are due to their fundamental physical nature of polarization and have nonthermostable permittivity.

For example, the *antiferroelectrics* presented in Fig. 6.3 by curve 3 have a permittivity of about 40–60 at 300 K and low losses, but large *positive*  $TC\epsilon_{mw}$ ; however, it should be noted that crystals are too expensive for mass technology, so any microwave technique has to use mostly *ceramic materials*. Curve 4 in Fig. 6.3 demonstrates a *ceramic paraelectric*, namely perovskite  $\text{CaTiO}_3$ , which has  $\epsilon_{mw} = 130$  at 300 K

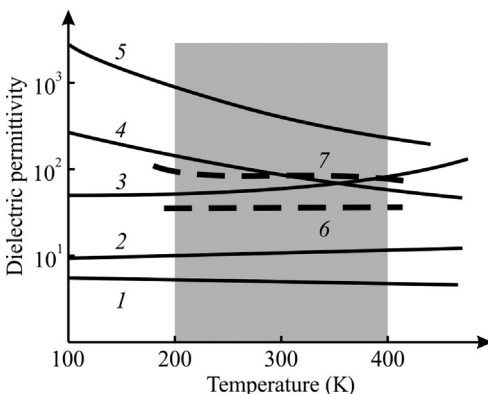


**Fig. 6.3** Typical temperature dependence of  $\epsilon_{mw} = \epsilon_e + \epsilon_i$  in different dielectrics: 1—Atomic and molecular dielectrics with only electronic polarization; 2—ordinary ionic crystals with electronic and ionic polarization; 3—electronic and ionic polarization in antiferroelectrics; 4—“hard” type paraelectric ( $\text{CaTiO}_3$ ); 5—“soft” type paraelectric ( $\text{SrTiO}_3$ ); 6—microwave thermal stable dielectric barium tetratitanate; 7—microwave thermal stable dielectric barium-lanthanide tetratitanate (*darkened area* corresponds to technical applications interval).

and low loss factor but a large negative  $TC\epsilon_{mw}$  corresponding to the fundamental Curie-Weiss dependence  $\epsilon_{mw} \sim C(T - \theta)$  with negative  $\theta$ . It will be shown later that the last fact is important for microwave dielectrics technology, i.e.,  $\text{CaTiO}_3$  is an example of *nonpolar* (“rigid”) paraelectrics, the structure of which is incompatible with polar-sensitive bonds. Curve 5 in Fig. 6.3 refers to  $\text{SrTiO}_3$ , which has  $\epsilon_{mw} = 300$  at normal conditions but a large negative value of  $TC\epsilon$  and represents the group of “soft” paraelectrics (characterized by positive Curie-Weiss temperature  $\theta$ ). They are prone to polar phase formation (leading to increase in microwave losses), but have an important property: the *dielectric nonlinearity* used in electrically controlled microwave devices.

Table 6.2 shows microwave parameters of many ionic crystals (except water-soluble alkali-halides), and some of them have rather large dielectric constants. Among these materials, note that  $\text{Al}_2\text{O}_3$  has  $\epsilon_{mw} \sim 12$  and acceptable thermal stability. Because of very small microwave losses and high thermal conductivity, the polycrystalline  $\text{Al}_2\text{O}_3$  (polycor) and single crystal  $\text{Al}_2\text{O}_3$  (sapphire) are widely used in microwave technology, in spite of their relatively small permittivity  $\epsilon_{mw}$ .

As a rule, the polarization mechanism in most of the ionic crystals provides  $\epsilon_{mw} \sim 10$  with positive  $TC\epsilon > +10^2$  ppm/K. Very seldom in the ionic crystals does  $\epsilon_{mw}$  exceed 20; at that, composite oxide crystals are insulators with increased  $\epsilon_{mw}$  and usually have increased  $TC\epsilon$ . Different microwave permittivity may be observed in chalcogenides, in which  $\epsilon_{mw} = 5\text{--}15$ . It is remarkable that some ionic crystals such as bismuth oxide ( $\text{Bi}_2\text{O}_3$ ) and, close to it, sillenites ( $\text{Bi}_{12}\text{GeO}_{20}$  and others) have  $\epsilon_{mw} \sim 40$ . Used in microwave microelectronics, single crystals of rare earth aluminates ( $\text{LnAlO}_3$  where  $\text{Ln} = \text{La}, \text{Pr}, \text{Nd}, \text{Eu}, \text{Gd}$ ) have  $\epsilon_{mw} = 20\text{--}30$ ; in addition, they are used as substrates for high-temperature superconductive films. Nevertheless, their permittivity still is too small for applications in dielectric resonators, which need a greater permittivity  $\epsilon \sim 40$  at centimeter,  $\epsilon \sim 100$  at decimeter, and  $\epsilon \geq 120$  for meter wave devices (in all cases  $TC\epsilon$  should be close to zero).

Most of the crystals listed in Table 6.2 have a temperature coefficient of permittivity that is too large. An example is titanium dioxide ( $\text{TiO}_2$ ) (however, this crystal served in the first discovery of *dielectric resonators*). Titanium dioxide has three possible structures (brookite, anatase, and rutile), but the most interest is in  $\text{TiO}_2$  with the rutile structure. In all three structures of  $\text{TiO}_2$ , permittivity  $\epsilon_{mw}$  is rather large and microwave losses are small enough, but  $TC\epsilon$  is negative and too large (nevertheless, in many compositions of microwave ceramics rutile-based materials are used). The comparison of many solid crystalline dielectric properties shown in Fig. 6.3 and Table 6.2 does not answer the main question: how to combine in one material high permittivity, small losses, and zero  $TC\epsilon$ , which is very important for application in microwave equipment.

Nevertheless, thermally stable microwave dielectrics are *successfully developed empirically* and widely used in microwave engineering: two of such compositions are shown by curves 6 and 7 in Fig. 6.3. Many more examples of high- $\epsilon$  microwave dielectrics showing  $TC\epsilon < 5$  ppm/K are listed in Table 6.3. Since the loss factor  $\tan\delta$  has a tendency to *rise linearly with frequency*, in order to compare different

**Table 6.2** Some dielectric crystal parameters at 10 GHz and 300 K [5, 7, 11–13].

Crystal	$\epsilon_{mw}$	$TC\epsilon \cdot 10^6 \text{ K}^{-1}$	$\tan\delta \times 10^4$	Crystal	$\epsilon_{mw}$	$TC\epsilon \times 10^6 \text{ K}^{-1}$	$\tan\delta \times 10^3$
SiO <sub>2</sub> , $\epsilon_c$	4.6	40	~1	SmAlO <sub>3</sub>	19	90	–
MgO	9.9	80	1.2	Bi <sub>12</sub> SiO <sub>20</sub>	40	40	6
Al <sub>2</sub> O <sub>3</sub> , $\epsilon_c$	11.6	130	0.7	Bi <sub>12</sub> GeO <sub>20</sub>	43	110	8
GaAs	13	180	20	Bi <sub>12</sub> TiO <sub>20</sub>	44	40	4
Bi <sub>2</sub> GeO <sub>5</sub>	16	180	30	$\beta$ -Nb <sub>2</sub> O <sub>5</sub> , $\epsilon_c$	50	100	10
TeO <sub>2</sub> , $\epsilon_c$	24	50	5	TiO <sub>2</sub> brookite, $\epsilon_c$	66	–50	~1
TiCl	30	–200	5	TiO <sub>2</sub> brookite, $\epsilon_a$	78	–200	~1
LaAlO <sub>3</sub>	27	90	~1	TiO <sub>2</sub> rutile, $\epsilon_c$	170	–1000	~1
PrAlO <sub>3</sub>	25	50	0.8	TiO <sub>2</sub> rutile, $\epsilon_a$	80	–400	0.5
NdAlO <sub>3</sub>	22	70	0.5	BaTiO <sub>3</sub> hexagonal, $\epsilon_a$	300	–600	20
EuAlO <sub>3</sub>	21	200	~1	BaTiO <sub>3</sub> hexagonal, $\epsilon_c$	70	–50	5

**Table 6.3** Permittivity and quality factor  $K$  in the main thermally stable microwave dielectrics [1, 2, 14–16].

Ceramics	$\epsilon_{mw}$	$K \cdot 1000$	Ceramics	$\epsilon_{mic}$	$K \cdot 1000$
(Mg,Ca)TiO <sub>3</sub>	20	50	BaO <sub>4</sub> ·TiO <sub>2</sub>	37	30
Ba(Sn,Mg,Ta)O <sub>3</sub>	40	200	BaO <sub>4,5</sub> ·TiO <sub>2</sub>	40	40
Ba(Zr,Zn,Ta)O <sub>3</sub>	30	150	CaTiO <sub>3</sub> ·LaAlO <sub>3</sub>	40	50
(Zr,Sn)O <sub>2</sub> ·TiO <sub>2</sub>	38	50	BaO·Ln <sub>2</sub> O <sub>3</sub> ·TiO <sub>2</sub>	90–120	3–7

Note. Ln = La, Gd, Nd, Sm, Eu.

microwave dielectrics another quality factor is used, namely, the coefficient  $K = \nu / \tan\delta$ , where  $\nu$  is frequency in gigahertz.

All the microwave dielectrics with increased permittivity mentioned in Table 6.3 are close relatives to perovskite-structure paraelectrics; however, none of the listed microwave dielectrics fits this definition exactly: rather, they can be defined as materials that are “relatives to paraelectrics.” Despite many successful developments, it should be noted that an in-depth study of the physical processes of their polarization is still necessary, since future progress in microwave dielectrics can be expected only through the understanding of the physical mechanisms of their polarization.

Mechanisms of electronic and ionic polarization are considered in general terms in Chapter 1. To understand microwave dielectrics properties, it is necessary to supplement this consideration with *dynamic models*. Moreover, to calculate permittivity using known polarizability it is necessary to express a *local field*  $F$  actually acting between particles, through a macroscopic electrical field  $E$ . This problem was solved by Lorentz:  $F = \frac{\epsilon+2}{3}E$ , and this ratio is very important for high- $\epsilon$  dielectrics because the Lorentz local field exceeds the average macroscopic field by  $(\epsilon + 2)/3$  times, from which follows an expression for permittivity calculation by polarizability:

$\frac{\epsilon+2}{\epsilon-1} = \frac{\sum n_k \alpha_k}{3\epsilon_0}$ . In the case of electronic polarization, this sum contains only one component:  $n_e \alpha_e$ , where  $n_e$  is the volumetric concentration of atoms and  $\alpha_e$  is electronic polarizability, while in the case of ionic polarization this sum has two components, the electronic and ionic terms:  $n_e \alpha_e + n_i \alpha_i$ .

**3. Dynamic properties of electronic (optical) polarization** can be described by a harmonic oscillator model: the particle of mass  $m = m_e$  and charge  $q = e$  is elastically connected with nuclei by the Coulomb force. Any displacement of an electron from its equilibrium position at distance  $+x$  or  $-x$  leads to a returning force  $f$  proportional to the displacement and pointing in the opposite direction:  $f = -cx$ , where  $c$  is coefficient of elasticity of the bond between electron and nuclei. During elastic displacement, force  $f$  is balanced by the force of inertia:  $m \frac{d^2x}{dt^2} = -cx$ . The solution of this equation is harmonic oscillations:  $x = x_0 \cos\omega_0 t$  (or  $x = x_0 \sin\omega_0 t$ ), while the general solution is  $x = x_0 \exp(i\omega_0 t)$ , where  $x_0$  is amplitude and  $\omega_0 = \sqrt{\frac{c}{m}}$  is *proper frequency* of the oscillator. The dielectric constant can be found by examining forced vibrations of the oscillator in a periodic electrical field  $E = E_0 \exp(i\omega t)$ :  $m \frac{d^2x}{dt^2} + cx = qF_0 e^{i\omega t}$ ,

where the right side of the equation represents the force acting on charges inside the dielectric. It is important that in a *polarized environment* the Lorentz local field is different from the applied field:  $F = E + P/(3\epsilon_0)$ , where  $P$  is polarization.

Induced electronic polarization by electrically forced vibrations of  $N$  oscillators per unit volume  $P(t) = Nqx(t)$  is

$$\frac{d^2P}{dt^2} + \left(\frac{c}{m} - \frac{Nq^2}{3\epsilon_0 m}\right)P = \frac{Nq^2}{m}E_0e^{i\omega t};$$

$$P(t) = \frac{Nq^2}{m} \frac{E_0e^{i\omega t}}{\omega_0^2 - \omega^2},$$

$$\epsilon(\omega) = 1 + \frac{\Delta\epsilon}{1 - \left(\frac{\omega}{\omega_0}\right)^2}; \quad \Delta\epsilon = \frac{Nq^2}{\epsilon_0 m \omega_0^2}.$$

(6.1)

where  $\omega_0^2 = \frac{c}{m} - \frac{Nq^2}{3\epsilon_0 m}$  and  $\Delta\epsilon$  is the contribution to permittivity from elastic electronic polarization. This formula explains frequency dependence of electronic (optical) permittivity during its resonant dispersion (Fig. 6.4).

As frequency increases, the dielectric contribution  $\Delta\epsilon$  increases as far as the frequency approaches to the resonant frequency  $\omega_0$ . Above this frequency, the dielectric contribution from polarization becomes negative; later it again increases:  $\epsilon \rightarrow 1$ . In

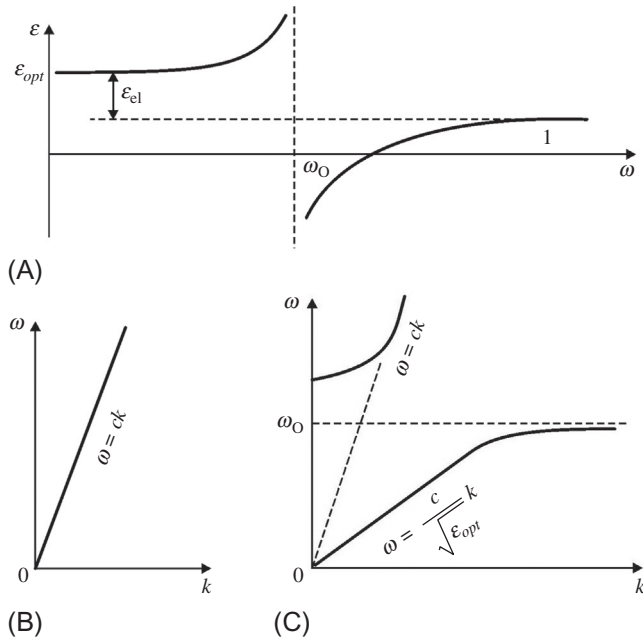


**Fig. 6.4** Electronic (optical) permittivity dispersion: (A) Permittivity frequency dependence; (B) electromagnetic wave dispersion in vacuum; (C) spatial dispersion in dielectric.

experiments, many resonances are observed due to different electrons. The temperature coefficient of electronic permittivity is small and negative ( $TC\varepsilon < 10$  ppm/K).

**4. Dynamical model of ionic (far-infrared) polarization.** Assuming that an oscillator, described by Eq. (6.1), characterizes ionic polarization (which has much lower frequency as compared with electronic polarization),  $\Delta\varepsilon = \varepsilon_{ir}$  needs to be put into Eq. (6.1), as ionic polarization undergoes dispersion in the far-infrared range. In addition, the value of  $\varepsilon(\omega)$  contains contributions from higher frequency electronic permittivity  $\varepsilon_{opt}$ :  $\varepsilon(\omega) = \varepsilon_{opt} + (Nq^2/\varepsilon_0 m\omega_{TO}^2)/(1 - \omega^2/\omega_{TO}^2)$ . Here  $N$  is volumetric concentration of ions,  $q$  is ion charge, and  $m$  is reduced mass. The frequency of the oscillator  $\omega_{TO}$  is one of the proper frequencies of the ionic crystal lattice.

The ionic polarization mechanism to a great extent determines the permittivity of ionic crystals (Table 6.3). Therefore, in order to illustrate this mechanism in detail, the *physical meaning* of  $\omega_{TO}$ —resonant frequency of the oscillator—should be explained. Below this frequency ( $\omega < \omega_{TO}$ ) the dielectric constant is determined by two contributions:  $\varepsilon(0) = \varepsilon_{opt} + \varepsilon_{ir}$ . Above frequency  $\omega_{TO}$  ionic polarization late—there is dispersion of the ionic contribution to permittivity in the frequency range of  $10^{12}$ – $10^{14}$  Hz, and therefore at higher frequency only electronic polarization is possible. The value of frequency  $\omega_{TO}$  has a great influence on ionic crystal permittivity, as shown in Fig. 6.5, where four objects of experimental study have a difference in  $\varepsilon_{ir}$  of about one order of magnitude in value. It is obvious that the smaller the frequency  $\omega_{TO}$ , the larger the permittivity [17–20].

The magnitude and sharpness of the resonance peak of permittivity characterize *damping* of the oscillator, describing  $\varepsilon(\omega)$  dispersion. The more increases in permittivity, the lower the damping of the oscillator and the lower microwave losses of the dielectric, because in this case the maximum of dielectric absorption  $\varepsilon''(\omega)$  is also more acute. The minimum  $\varepsilon'(\omega)$  always takes place in the frequency range of ionic polarization dispersion, but if the maximum of  $\varepsilon'(\omega)$  is no longer observed, it means that the *anharmonicity* of lattice oscillations is large and the oscillator is overdamped; respectively, the maximum of  $\varepsilon''(\omega)$  becomes blurry and microwave losses in such a dielectric are large (an example is polar crystals—ferroelectrics).

Thus, ionic lattice polarization leads to *resonant* frequency dependence of permittivity described by crystal dynamics theory. In a simple model, it is supposed that potential relief of each ion is characterized by the *parabolic* potential well, so the vibrations of ions are characterized by a harmonic oscillator model. In the simplest one-dimensional model, displacement of each ion affects the displacement of neighbor ions, so, waves of *elastic displacement* extend in the entire one-dimensional ionic chain. This spatially periodic process can be described by the equation  $x = x_0 \exp[i(\omega t - kx)]$ , where  $\omega = 2\pi/T$  is the frequency of oscillation, and  $k = 2\pi/\lambda$  is the wave vector modulus. Phase velocity is  $v_{ph} = \lambda/T = \omega/k$  while group velocity is  $v_{gr} = d\omega/dk$  (it exactly characterizes the spreading of the wave's energy and speed of the extending signals).

The medium of the elastic waves is the *discrete chain* of bound ions, so waves with a length less than  $2a$  ( $a$  is the lattice parameter) cannot propagate in this chain. In this model, dependence  $\omega(k)$  shows the frequency and wave number  $k$  connection; in other words, the ratio between elastic vibration energy  $\hat{E} = \hbar\omega$  and momentum  $p = \hbar k$  is

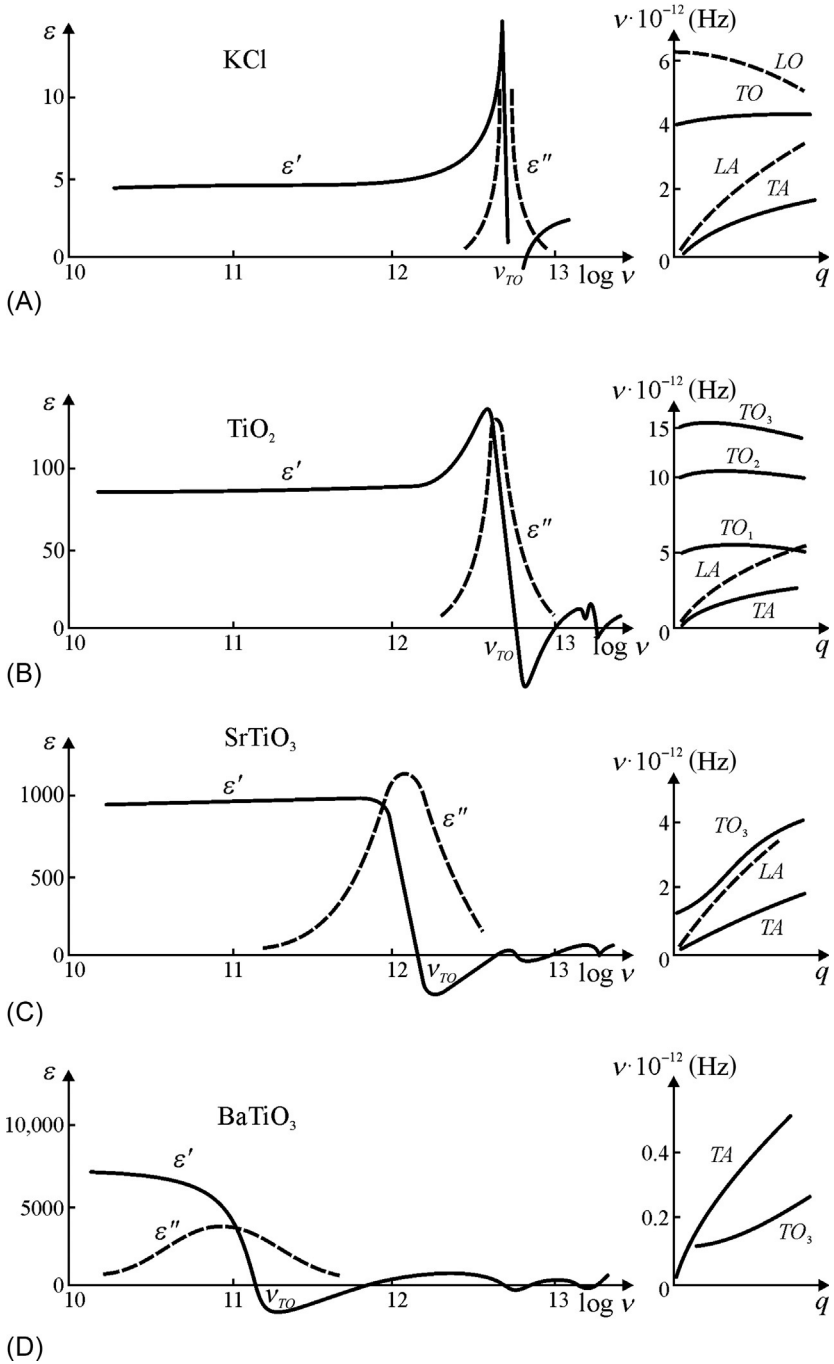


**Fig. 6.5** Dielectric dispersion of far-infrared contribution  $\epsilon_{ir}$  and phonon spectrum of some ionic crystals: (A) Alkali-halide cubic crystal with  $\epsilon_{mw} \approx 5$ ; (B) rutile crystal with  $\epsilon_{mw} \approx 70$ ; (C) strontium titanate with  $\epsilon_{mw} \approx 900$  ( $T = 77$  K); (D) barium titanate crystal with  $\epsilon_{mw} \approx 7000$  ( $T = 410$  K).

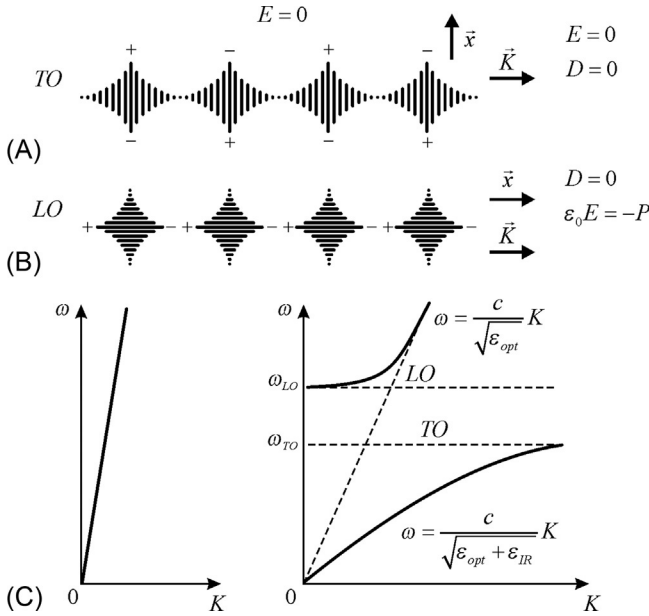


**Fig. 6.6** Lattice elastic waves and dispersion in one-dimensional model of ionic crystal. (A) Transverse waves; (B) longitudinal waves; and (C) dispersion in vacuum and in crystal.

given by equation  $\omega = \pm(c/m)^{1/2}\sin(ka/2)$ . The restriction in space of the wave vector (i.e., interval  $-a$  to  $+\pi/a$ ) is due to the *discreteness* of the oscillating system, while the range of wave vector values is the first Brillouin zone.

The one-dimensional model of an ionic crystal as a chain with alternating cations and anions with lattice parameter  $a$  is shown in Fig. 6.6. Ion displacement in the longitudinal (LO) optical wave is parallel to the direction of wave propagation ( $x \parallel k$ ). If ion displacements are perpendicular to the direction of wave propagation ( $x \perp k$ ), the waves are transverse (TO). They have the same dispersion as longitudinal waves, but their frequencies are lower. In this model, acoustical oscillations LA and TA exist as well, but they are not shown in Fig. 6.6. The frequency of transverse optical phonons  $\omega_{TO}$  is the resonant frequency of the oscillator, which describes permittivity dispersion, while the longitudinal optical frequency  $\omega_{LO}$  corresponds to equality  $\epsilon(\omega) = \epsilon(\omega_{LO}) = 0$ .

To describe lattice vibrations in high-permittivity dielectrics, in the oscillator equation, in addition to strength of inertia  $m(d^2x/dt^2)$  and elastic restoring force  $cx$ , it is necessary to consider the electrical force of vibration interaction  $qF$ , where  $q$  is charge and  $F$  is the microscopic Lorentz field:  $m(d^2x/dt^2) = -cx + qF$ . In a *polarized environment* this field differs from the average macroscopic field:  $F = E + P/(3\epsilon_0)$ . As shown earlier, the vector of elastic displacement in transverse optical vibration mode is perpendicular to the direction of wave propagation ( $x \perp k$ ), so the average macroscopic field  $E = 0$ , since adjacent “clots” of polarization waves are *different in*

*polarity* (Fig. 6.6). Consequently, in the equation shown earlier for transverse electrical field it is necessary to substitute  $F = \frac{1}{3\epsilon_0}P$ . Polarization  $P$  can be expressed in terms of the number of induced dipoles  $N$  per unit volume, while each dipole moment is  $p = qx$ , i.e.,  $P = Nqx$ . As a result, the oscillator equation and its solution take the form

$$m \frac{d^2x}{dt^2} + \left( c - \frac{Nq^2}{3\epsilon_0} \right) x = 0, \quad \omega_{TO}^2 = \frac{1}{m} \left( c - \frac{Nq^2}{3\epsilon_0} \right)$$

where  $\omega_{TO}$  is the proper frequency of such an oscillator, which corresponds to transverse optical phonons. Thus, Lorentz field  $F$  reduces the ion attraction and decreases the oscillator frequency  $\{\omega_0 = (c/m)^{1/2}\}$  to the frequency of transverse optical phonons, i.e., promotes “softening” of the vibrations ( $\omega_{TO} < \omega_0$ ). By the way, this case is associated with polarization of “short-circuited” crystals (Chapter 4) when  $D = P$ , since  $D = \epsilon_0 E + P$  and  $E = 0$ .

For *longitudinal* oscillations, the local Lorentz field has a different effect (Fig. 6.6), since the electrical field  $E$  is directed toward polarization  $P$  and is equal to it:  $\epsilon_0 E = -P$ . In macroscopic theory (Chapter 4), this case corresponds to the “open-circuited” crystal with induction  $D = 0$ . Taking into account the Lorentz field for longitudinal waves, we have:  $D = \epsilon_0 E + P$ , so  $P = -\epsilon_0 E$ ; and  $F = E + \frac{P}{3\epsilon_0} = -\frac{P}{\epsilon_0} + \frac{P}{3\epsilon_0} = -\frac{2P}{3\epsilon_0}$ . Accordingly, the equation of the oscillator, taking into account that  $P = Nqx$ , takes the following form:  $m \frac{d^2x}{dt^2} + \left( c + \frac{2P}{3\epsilon_0} \right) x = 0$ . The proper oscillator frequency that corresponds to longitudinal vibrations is  $\omega_{LO}^2 = \frac{1}{m} \left( c + \frac{2Nq^2}{3\epsilon_0} \right)$ .

Therefore, the oscillator frequency, which characterizes longitudinal optical vibrations in the *polarized medium*, is higher than the frequency of the isolated oscillator  $\{\omega_0 = (c/m)^{1/2}\}$ . The results obtained in the preceding equations explain the location of phonon branches:  $LO$  lies over  $TO$ , and the position of the two characteristic frequencies  $\omega_{LO}$  and  $\omega_{TO}$  (Fig. 6.6). Permittivity of ionic crystals is related to the *difference in frequencies* of the longitudinal and transverse optical vibrations  $\omega_{LO}$  and  $\omega_{TO}$  in the center of the Brillouin zone. In the equation that describes the infrared polarization of ionic crystals only the frequency of transverse optical phonons exists, which describes the dielectric contribution of ionic polarization

$$\epsilon(\omega) = \epsilon(\infty) + \frac{\epsilon(0) - \epsilon(\infty)}{1 - \left( \frac{\omega}{\omega_{TO}} \right)^2}, \quad \epsilon(0) - \epsilon(\infty) = \frac{Nq^2}{\epsilon_0 m \omega_{TO}^2} = \frac{Nq^2}{c - \frac{Nq^2}{3\epsilon_0}} \quad (6.2)$$

This equation implies that the stronger the ionic polarization effects are on dielectric properties of crystals, the higher the ion charge  $q$  and the lower the elastic coupling coefficient of ions  $c$ . Eq. (6.2) allows *quantitative calculation* of the infrared contribution to permittivity. Indeed, ion concentration  $N$  can be found according to the density of crystal,  $m$  is reduced mass of vibrating ions,  $q$  is ionic charge, and  $\omega_{TO}$  is the frequency of “residual” rays, which can be determined experimentally by multiple

reflections of infrared waves from the surface of the crystal being studied. Coefficient  $c$ , describing ion elastic coupling, can be calculated from macroscopic measurements of elastic properties. The greater the density of the crystal, the higher the refractive index  $n^2 = \epsilon_{opt}$  and the higher the polarization of the ionic lattice, which is characterized by the difference of microwave and optical permittivity:  $\epsilon_{mw} - \epsilon_{opt}$ .

Eq. (6.2) allows another way of writing the dispersion equation, describing the frequency dependence of permittivity in the far-infrared region. By eliminating the parameter  $\epsilon_{ir}$ , it is possible to obtain the expression:  $\epsilon(\omega) = \epsilon_{opt} \frac{(\omega_{LO}^2 - \omega^2)}{(\omega_{TO}^2 - \omega^2)}$ , which describes  $\epsilon(\omega)$  in all parts of the spectrum, except for the area of lattice resonance. As follows from previous considerations, the resonant frequency equals the transverse optical frequency  $\omega_{TO}$ , while permittivity *vanishes* at longitudinal frequency:  $\epsilon(\omega_{LO}) = 0$ . With this assumption, analysis of Eq. (6.2) gives:

$$0 = \epsilon(\infty) + \frac{\epsilon(0) - \epsilon(\infty)}{1 - \left(\frac{\omega_{LO}}{\omega_{TO}}\right)^2}, \text{ from which follows } \frac{\epsilon(0)}{\epsilon(\infty)} = \frac{\omega_{LO}^2}{\omega_{TO}^2} \quad (6.3)$$

This last is a very important relationship, which is usually referred to as the Lyddane-Sachs-Teller ratio, describing the connection between total permittivity  $\epsilon(0) = \epsilon_{ir} + \epsilon_{opt}$  and frequencies of longitudinal and transverse modes. As always  $\epsilon(0) > \epsilon(\infty)$ , and the relation of frequencies is  $\omega_{TO} < \omega_{LO}$ . However, in the *covalent crystals* of diamond type, in the center of the Brillouin zone  $\omega_{TO} \approx \omega_{LO}$ , so any far-infrared (ionic) contribution to permittivity is absent (such crystals are diamond, silicon, and germanium).

Electromagnetic waves with frequency  $\omega < \omega_{TO}$  move in ionic crystal with a velocity that is  $(\epsilon_{ir} + \epsilon_{opt})^{1/2}$  times less than in vacuum, where the speed of light  $c = k/\omega$ . Therefore, in ionic crystal, near the frequency  $\omega_{TO}$  (in the initial region of dispersion) the speed of electromagnetic waves is reduced, and this slowing down intensifies because the value of  $\epsilon'(\omega)$  increases with increasing frequency. Next, in the frequency interval between  $\omega_{TO}$  and  $\omega_{LO}$ , an ionic crystal reflects electromagnetic waves; of course, in this frequency range crystal is opaque. Further, with frequency increase ( $\omega > \omega_{LO}$ ), the transparency of ionic crystal is recovered but the speed of electromagnetic waves in the crystal is still less than the velocity of light, because it is delayed by the optical contribution  $(\epsilon_{opt})^{1/2}$  to permittivity.

The previous formulas also allow clarification of the nature of *permittivity temperature dependence* in ionic crystals. Due to thermal expansion, the density of crystal decreases. Thermal expansion affects the value of the electronic part of permittivity  $\epsilon(\infty) = \epsilon_{opt}$  due to its reduction with temperature increase (that is why  $TC\epsilon_{opt}$  is *negative*). In contrast, an *increase* of  $\epsilon_{ir} = \epsilon(0) - \epsilon(\infty) = \epsilon_{mw} - \epsilon(\infty)$  with temperature increase is expected: indeed, due to crystal thermal expansion the distance between ions increases and, therefore, their *interaction weakens*. Consequently, elastic coupling of ions (described by coefficient  $c$ ) decreases; as  $c$  is located in the denominator of Eq. (6.2), then if  $c$  decreases, the dielectric contribution  $\epsilon_{ir}$  increases. In most of the

ionic crystals  $\epsilon_{ir}$  exceeds  $\epsilon_{opt}$ ; therefore, in microwaves,  $\epsilon_{mw} = \epsilon_{ir} + \epsilon_{opt}$  increases with temperature, so  $TC\epsilon_{mw} > 0$ . However, the  $TC\epsilon$  of ionic crystals may also become negative, which is described by the following model.

**5. Electronic shell model of ionic dielectrics polarization.** When dielectric properties of ionic crystals were analyzed previously, the model of a “solid” (i.e., non-polarized) ion is used, supposing that the electrical charge of the ion is located in its center. It is believed that such an ion moves in an electrical field as a whole body, and its electron shell is not deformed. This model is satisfactory to describe the polarization of very simple ionic structures like alkali-halide crystals, especially in cases when the radii of anion and cation are close in their values. However, a noticeable discrepancy occurs when applying the simple dynamic theory, based on the model of a solid ion, to describe, for instance, the properties of thallium haloids. In the case of the TlBr crystal, for example, according to the simple theory,  $\epsilon_{mw} = 11$ , but experimental data gives  $\epsilon_{mw} = 30$ .

There are many other ionic crystals that have *increased* microwave permittivity. In these dielectrics, in addition to ionic bonds, *pliable electronic bonds* between ions have a significant role; as a result, such ionic crystals show negative temperature dependence of permittivity  $TC\epsilon < 0$ . Lattice dynamics theory can explain these peculiar properties of such crystals (as well as the properties of paraelectrics) by the model of polarizing (“soft ion”). Moreover, the main important ratios of the simple dynamic theory of crystals are kept, but in a generalized form.

General principles of molecular physics assume that electron shells of ions *can be deformed*: a partial overlap of electron shells exists between neighboring ions, which creates additional repulsive force. Therefore, if the distance between ions changes (for instance, due to crystal polarization in an external electrical field), the overlap of electron shells results in *redistribution* of electrical charges. This should have an influence on the repulsive force of ions: the frequency of lattice oscillation *decreases*, which ultimately affects the permittivity value. In the model of a *polarized ion*, during electrical polarization, the “*core*” (i.e., the actual nuclei of the atom surrounded by deeper and tougher electron clouds) almost did not change its position. However, the *outer shells* (both for positive and, especially, for negative ions) hold a *relative freedom* while moving in the applied electrical field. Obviously, the shell of a negative ion feels a much larger shift, because the polarizability of a negative ion is larger than the polarizability of a positive ion. Due to the unequal offset of shells, their overlap changes and the electron charges of the ions redistribute.

The main distinction of the “shell model” from the model of a “hard ion” is that, in the case of *transverse optical mode*, the vibrations of the cores of polarized ions do not coincide with the centers of the shells. For this reason, the interaction force acting between ions in the “shell model” is different than in the case of “hard ions”, which significantly affects crystal permittivity. The shell model pays little attention to the optical polarization of crystals, because such polarization is characterized by the *internal shift* between core and shell of each ion. However, ionic (far-infrared) polarization of crystals in this case is described by several mechanisms: the displacement of core and outer electron shell with a certain degree of autonomy. Therefore, during the polarizability calculation, not only the interaction of cores with each other should

be considered, but also the interaction of a core of a given ion with another ion's electron shell, and finally interaction between shells.

When considering the model of a "polarized" ion, it becomes apparent that it would be more correct for elastic polarization arising in ionic crystals to use the term "far infrared polarization" (but not the term "ionic polarization"). Indeed, the mechanism of this polarization consists not only of mutual displacements of ion cores, but also of the shifts of their outer electron shells. The effective mass of electron shells is very small as compared to the masses of ions, so while rapid change occurs in the external electrical field, polarization is formed by the inertia of *core displacements* (electrons always have time to shift following displacements of cores). Therefore, despite the fact that polarization originates largely due to displacement of electrons, the *characteristic frequency* of the far-infrared polarization mechanism is defined by elastic forces and masses of ions, and therefore the corresponding resonant frequency is much less than the optical frequency. Moreover, electron displacement influence leads to *reducing* the far-infrared dispersion frequency. The question is that the short-range repulsion force between ions mainly depends on interaction between adjacent shells of ions, and in the case of "soft shells," repulsive forces are less than for "hard" ions. If the crystal structure is such that elastic repulsive forces are reduced, the contribution of far-infrared polarization might be rather big.

Thus, electronic polarization in ionic crystals affects the frequency of far-infrared vibrations. Accordingly, this effect leads to reduction of transverse optical phonon frequency  $\omega_{TO}$ . Since the frequency of longitudinal oscillations  $\omega_{LO}$  is a very conservative parameter (it practically does not change with temperature), then from the Lyddane-Sachs-Teller relation (Eq. 6.3) it follows that the reduction in  $\omega_{TO}$  leads to an increase in microwave permittivity. From Eq. (6.1) it follows that electronic (optical) polarization affects ionic (far-infrared) polarization, so instead of a simple expression for polarization ( $P = NaF$  where  $a$  is polarizability,  $N$  is ion concentration, and  $F$  is acting electrical Lorentz field), we need to use another relation:

$$P = \left[ a + \frac{nq^2}{m} \frac{1}{(\omega_0^2 - \omega^2)} \right] \left( E + \frac{1}{3\epsilon_0} P \right),$$

where  $1/(3\epsilon_0)$  is the Lorentz coefficient and  $a$  is a parameter that considers optical polarization influence. After some transformation, the following expression for frequency of transverse and longitudinal optical phonons and for dielectric contribution of infrared polarization can be obtained:

$$\begin{aligned} \omega_{TO}^2 &= \frac{c}{m} - \frac{nq^2}{3\epsilon_0 m} \frac{\epsilon(\infty) + 2}{3}; & \omega_{LO}^2 &= \frac{c}{m} + \frac{2nq^2}{3\epsilon_0 m} \frac{\epsilon(\infty) + 2}{3}; \\ \epsilon(0) - \epsilon(\infty) &= \frac{nq^2}{\epsilon_0 m \omega_{TO}^2} \frac{(\epsilon(\infty) + 2)^2}{9} \end{aligned} \quad (6.4)$$

These formulas generalize expressions for frequencies and permittivity obtained in simple models. It should be noted that again the factor  $(\epsilon + 2)/3$  appears, which equals the ratio between the local Lorentz field  $F$  and the average macroscopic field  $E$ .

In these equations, the expression for  $\omega_{LO}$  is the sum. Therefore, the influence of electronic polarization hardly changing the value of longitudinal frequency should be taken into account, as opposed to transverse frequency  $\omega_{TO}$ , which is characterized by the difference. Also, from these equations it follows that the smaller the value of  $\omega_{TO}$ , the greater is the value of  $\varepsilon_{ir} = \varepsilon(0) - \varepsilon(\infty)$ . It should be noted that calculations of  $\varepsilon_{mw}$  by Eq. (6.4) are in good agreement with experimental data for many crystals. In the previously mentioned example of crystal TlBr, which has  $\varepsilon_{opt} = 5.1$  and transverse optical frequency  $\omega_{TO} = 1.1 \cdot 10^{13}$  Hz, calculated by Eq. (6.4), the permittivity  $\varepsilon_{mw} = 30$  matches with experimental values; moreover, the TlBr crystal has *negative* temperature coefficient  $TC\varepsilon = -2 \cdot 10^{-3} \text{ K}^{-1}$ .

The point is that the relations obtained provide opportunities to estimate the temperature coefficient of ionic crystal permittivity:  $TC\varepsilon > 0$  for crystals that have  $\varepsilon = 4-8$ , while in ionic crystals with  $\varepsilon > 10$  the parameter  $TC\varepsilon < 0$ . It is seen from Eq. (6.4) for frequency  $\omega_{TO}$ , the temperature increase due to thermal expansion, on one hand, decreases ratio  $c/m$ , but, on the other hand, the subtrahend  $\varepsilon(\infty)$  also decreases. Thus, the sign of  $\varepsilon_{mw}(T)$  dependence may vary depending on which of these two effects dominates. In the crystals with high electronic polarizability, the effect of frequency  $\omega_{TO}$  increase with temperature rise predominates, which consequently leads to a decrease of  $\varepsilon(T)$ . Even a small increase in  $\omega_{TO}$  with increasing temperature can lead to a noticeable decrease in microwave permittivity, because  $\varepsilon_{mw} \sim 1/\omega_{TO}^2$ . These results are well documented in many studies [21–26].

It should be noted that an important circumstance, namely changing magnitude and sign of  $TC\varepsilon$  in ionic dielectrics that depends on what kind of polarization dominates—electronic or ionic—is used in the art of developing ceramics capacitors. Electronic technique needs electrical capacitors with *different value and sign of  $TC\varepsilon$* . This property is applied in temperature compensating of other elements of the apparatus by electrical capacitors. In many cases it is also desirable to have dielectrics with  $TC\varepsilon = 0$  in a broad temperature range. The importance of this problem is due to the fact that the relative number of ceramic capacitors in modern equipment reaches 80%. By using polycrystalline solid solutions of various oxides with different values and signs of  $TC\varepsilon$ , it is possible to a certain extent to “control” thermal properties of high permittivity dielectrics [27–32].

Since so-called ionic polarization, in fact, is mainly due to deformation and displacement of the outer electron shells of ions, to obtain high permittivity it is important to use as dielectric components those particular ions with more mobile and easily deformable outer electron shells. Their properties can be significantly affected by underlying electron shells (usually  $4f$ -shells), especially if they hold noncompensated magnetic moments (paramagnetic ions of cerium series of lanthanides). That is why, in the synthesis of high- $\varepsilon$  dielectrics the REE oxides are often used. Even the ions having empty  $4f$ -states ( $\text{Ba}^{2+}$  and  $\text{La}^{3+}$ ) are important as components of microwave dielectrics, apparently because of the possibility of the presence of virtual Bohr magnetons in the inner electron shell of these ions.

**6. Paraelectrics of displacement type** belong to dielectrics with the temperature dependence of permittivity described by the Curie-Weiss law:  $\varepsilon(T) = \varepsilon_1 + C/(T - \theta)$ , where  $\theta$  is the Curie-Weiss temperature,  $C$  is the Curie-Weiss constant, and  $\varepsilon_1$  is independent of the temperature part of permittivity. This equation is in good agreement

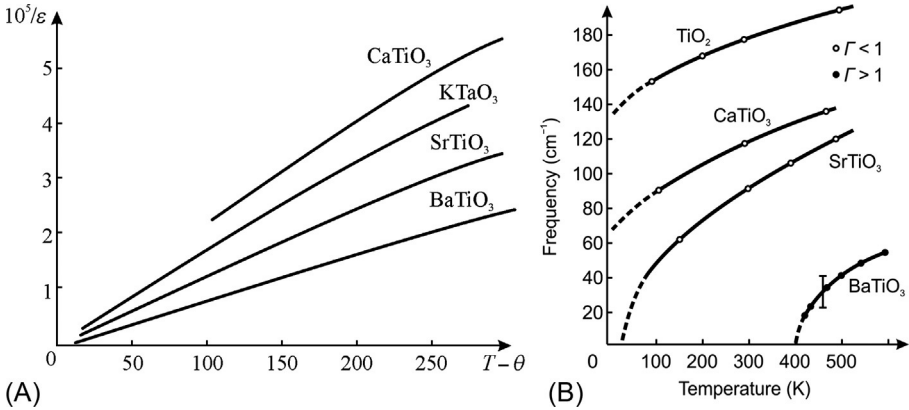


**Fig. 6.7** Temperature dependence of inverse permittivity (A) and frequency  $\omega_{TO}$  (B) for  $\text{TiO}_2$ ,  $\text{CaTiO}_3$ ,  $\text{SrTiO}_3$  and ferroelectric  $\text{BaTiO}_3$  (in its paraelectric phase);  $\Gamma$  is damping factor of oscillator describing permittivity dispersion, frequency  $1 \text{ cm}^{-1} = 30 \text{ GHz}$  [18–23].

with experimental data, as shown in Fig. 6.7A. In most paraelectrics, at Curie temperature  $T_c \approx \theta$  (called the critical temperature) the phase transition occurs in the ferroelectric (or antiferroelectric) state. That is why paraelectricity is usually associated with ferroelectricity [33].

Like ferroelectrics, paraelectrics can be divided into two basic classes.

The *first class* represents the paraelectrics of the “order-disorder” type that are polar (contain dipoles) crystals, in which, as temperature decreases, the dipole-to-dipole interactions give rise to a gradual ordering of dipole orientations, until, finally, when the decreasing temperature reaches  $T_c \approx \theta$ , ferroelectricity arises when most of the dipoles are stably oriented. Such paraelectrics near their second-order phase transition are characterized by a sharp maximum of  $\epsilon(T)$  which later rapidly decreases with temperature rise. A rapid decrease of  $\epsilon(T)$  signifies a rather small Curie-Weiss constant:  $C \approx 10^3 \text{ K}$ .

The *second class* contains the paraelectrics of the *displacive type* that are ionic (not dipole) crystals in which, however, covalent bonds between atoms are also very significant. They usually show the first-order phase transition with relatively slow  $\epsilon(T)$  dependence on paraelectric phase, characterized by a large Curie-Weiss constant:  $C \approx 10^5 \text{ K}$ . These properties of the displacive type paraelectrics can be explained by the dynamic theory of lattice vibrations. In this theory the central idea is that phase transition arises due to *loss of crystal lattice stability* relative to one of transverse optical vibrations. This phenomenon is reflected in the lowering of frequency  $\omega_{TO}$  with decreasing temperature, and it is assumed that while the temperature  $T \rightarrow \theta$  the frequency  $\omega_{TO} \rightarrow 0$ .

Among high-permittivity dielectrics, a special place is occupied by *nonpolar* ionic crystals with permittivity value  $\epsilon \sim 100$  and more. Typical representatives of such dielectrics are rutile ( $\text{TiO}_2$ ) and perovskite ( $\text{CaTiO}_3$ ). It should be noted that these

crystals are characterized also by *increased* optical electronic polarization:  $\epsilon_{opt} > 5$ . Moreover, the far-infrared permittivity of rutile and perovskite is strongly temperature dependent with a large negative coefficient  $T\epsilon < 0$ . These dielectrics are close to paraelectrics: for example,  $\epsilon(T)$  dependence in perovskite in a broad temperature range can be described by the Curie-Weiss law with  $\epsilon_1 = 60$ ,  $C = 4 \cdot 10^4$  K and  $\theta = -90$  K. Calcium titanate can be considered as a material *close to* paraelectrics. However, in the *typical* paraelectrics, which include, for example, SrTiO<sub>3</sub> or KTaO<sub>3</sub>, the Curie-Weiss temperature is *positive* ( $\theta > 0$  K), whereas CaTiO<sub>3</sub> is distinguished by the fact that it has a *negative* characteristic temperature ( $\theta < 0$  K).

From Curie-Weiss law and Eq. (6.3), a relationship follows between frequency and temperature, called the *Cochran law*  $\omega_{TO} = A\sqrt{T - \theta}$ , where  $A$  is temperature coefficient of frequency. This dependence is confirmed by many experiments (Fig. 6.7B). A direct connection between permittivity and temperature dependences of transverse lattice mode frequency is typical for displacive type paraelectrics (tie of  $\epsilon(T)$  and  $\omega_{TO}(T)$  is seen by comparison of the two parts of Fig. 6.7).

A model explanation of the frequency  $\omega_{TO}$  decreasing with temperature decrease and reasons for the consequent high permittivity in certain crystals of perovskite structure may be as follows. Each ion is situated in an equilibrium position under the action of electrostatic (long-range) forces of attraction and short-range forces of repulsion. High polarizability means that application of a rather weak electrical field leads to unusually *large displacements* of ions from their equilibrium position (or, according to the model of a “soft ion,” to large deformation of the electron shells of ions). This also means that the elastic force of repulsion of neighboring ions is rather small, corresponding to lowering of oscillation frequency.

It is logical to assume that, in perovskite-type structures, peculiar conditions are created for some of the ions, namely, substantial compensation of short-range repulsion forces by long-range attraction forces. Thus effects caused by interaction of electron shells of ions lead to a very large value of permittivity with its anomalous temperature dependence as well. The frequency of transverse optical vibration mode in some ionic lattices, which tends to zero when temperature  $T \rightarrow \theta$ , is called the “*soft*” *vibration mode*. Using the Lyddane-Sachs-Teller relation,  $\epsilon(0)/\epsilon(\infty) = [\omega_{LO}/\omega_{TO}]^2$ , it is possible to show that the Cochran law  $\omega_{TO} = A\sqrt{T - \theta}$  actually brings us to the Curie-Weiss law:  $\epsilon(T) \approx C/(T - \theta)$ . To substantiate the possibility of the frequency  $\omega_{TO}$  decreasing in perovskites, one needs to use a *polarized ion* model, in which the interaction of electron shells has a significant effect on the repulsive force of ions. This interaction can cause a condition in which the force generated by polarization of ions is reduced, which allows us to assume  $\omega_{TO}(T) \rightarrow 0$  and, respectively,  $\epsilon(T) \rightarrow \infty$ . In this sense, the expression “loss of crystal stability” might be understood: when small external perturbation (i.e., an external electrical field) leads to a large response—large polarization and large  $\epsilon$ -value.

The last assumption can be illustrated based on the relations in Eq. (6.4). Parameters  $c$  and  $q$ , if one uses the “shell model,” depend on characteristics of crystal structure:  $c$  characterizes a short-range force that returns the displacement of ions, and  $q$  is effective charge. Note that *longitudinal* frequency  $\omega_{LO}$  is *not critical* to any changes in model parameters, as it is determined by the sum of two terms. Conversely, the

frequency  $\omega_{TO}$  is strongly dependent on their difference. In simple crystals (like alkali-haloids) the minuend in Eq. (6.4) is approximately two times greater than the subtrahend, so frequency  $\omega_{TO}$  depends only a little on temperature. However, in perovskite-structured crystals this minuend is very close to the subtrahend, so  $\omega_{TO}$  becomes smaller (much less than  $10^{13}$  Hz). Moreover, even small changes in external conditions such as temperature, pressure, or voltage substantially affect the  $\omega_{TO}$ . As a result, in the vicinity of a “paraelectric-to-ferroelectric” phase transition, not only temperature but also electrical field and pressure greatly change the dielectric properties of such a crystal.

To discuss how it is possible to reduce the temperature dependence of  $\epsilon_{mw}$ , one can express the Curie-Weiss constant through parameters of the model being discussed. The approximate form of the Curie-Weiss law  $\epsilon(T) \approx C/(T - \theta)$  can be obtained if the following formula is put into Eq. (6.1):

$$\frac{m\omega_{TO}^2}{c} = 1 - \frac{nq^2(\epsilon(\infty) + 2)^2}{9c\epsilon_0} = \gamma(T - \theta)$$

Substituting this value in the expression for permittivity in Eq. (6.4), it is possible to obtain

$$\epsilon(0) - \epsilon(\infty) = \frac{nq^2(\epsilon(\infty) + 2)^2}{9c\gamma\epsilon_0} \frac{1}{T - \theta}; \quad A = \sqrt{\frac{c\gamma}{m}}; \quad C = \frac{nq^2(\epsilon(\infty) + 2)^2}{9c\gamma\epsilon_0}.$$

The main obstacle to the use of paraelectrics at microwave frequencies is the temperature instability of  $\epsilon_{mw}$ . Since the nature of this instability is the electronic subsystem of a crystal, the ways to overcome this instability should be sought in the methods of impact on this subsystem. The main contribution to  $\epsilon_{mw}$  gives far-infrared polarization; formally it is called “ionic polarization,” but in fact it is associated with the susceptibility of ion electron orbitals. In the next section it will be described that the greatest part of  $\epsilon_{mw}$  in rutile and perovskite crystals is caused by *highly polarized* oxygen octahedrons  $\text{TiO}_6$  ( $\text{BO}_6$ ) connected at their vertices. In this case, electron clouds that link ions in the system of octahedrons provide enough freedom for easy polarization and leads to  $\epsilon_{mw} > 100$ .

As will be shown later, in the rutile structure there are many possibilities for impacting on crystal properties by the allocation of various ions between oxygen octahedrons. That is why it is possible to govern, by freedom of electron shell interaction and their reciprocal displacement, when different outsider ions are implemented into the structure. In this way, it is possible to significantly weaken the critical  $\epsilon(T)$  dependence (described by the Curie-Weiss law) maintaining high polarizability. The main feature of high permittivity in paraelectrics (or ferroelectrics) is a strong correlation between highly polarized octahedrons. This correlation gives birth to ferroelectricity and almost inevitably results in nonthermostability. In order to avoid strong octahedron correlation, some other kinds of ions should be placed between oxygen octahedrons, and this is the main sense of microwave dielectric compositions.

### 6.3 Some examples of thermally stable microwave dielectrics

Working out new materials is difficult without a fundamental study of their physical properties. Research in this direction occurs in many laboratories, since microwave microelectronics is one of the most up-and-coming subjects of inquiry [1, 3, 34]. At the present moment, there are different models describing properties of high-frequency dielectric materials. However, this area of investigation cannot be considered complete. In connection with this, three assumptions, relating to the improvement of microwave dielectric properties, can be justified. First, high permittivity at microwave frequency can be obtained in crystals with *low-frequency* transverse optical lattice mode in paraelectric-like materials; second, small dielectric losses can be reached only in *monophase compositions* based on “hard-type” paraelectric material, which negates structural internal polarity; third, to achieve thermal stability in dielectrics with  $\epsilon_{mw} \approx 80\text{--}140$ , the “paraelectricity” of the basic material can be suppressed by paramagnetics components.

**1. Thermostable microwave ceramic dielectrics with  $\epsilon_{mw} \sim 40$ .** These important dielectrics are produced for centimeter-wave range and consist of complex compositions in order to achieve very small  $TC\epsilon$  [2, 35]. Moreover, low-loss microwave dielectrics should not be a *mixture* of two or more components, but the structure must be *single phase* (the fact is that borders between different phases are sources of losses). Moreover, in many-component but single-phase dielectrics, the value of  $TC\epsilon$  should be controlled by a change of composition. And of course it is very important to control technological factors in order to improve the achieved parameters.

Many of the microwave high-permittivity dielectrics are based on the structures with  $\text{TiO}_6$ -type *octahedrons*, and in the center of each octahedron an ion  $\text{Ti}^{4+}$  (or other high-valence ion) is located. These octahedrons can be joined one to another by their tops: just this feature provides increased permittivity. This can be confirmed by simple comparison of three forms of  $\text{TiO}_2$ :

- Rutile, in which octahedrons are connected through *one* top, has anisotropic permittivity  $\epsilon_c = 170$ ,  $TC\epsilon_c \approx -1000$  ppm/K,  $\epsilon_a = 80$ ,  $TC\epsilon_a \approx -400$  ppm/K (ceramic form of rutile has  $\epsilon \approx 100$ ,  $TC\epsilon \approx -900$  ppm/K).
- Brookite, where  $\text{TiO}_6$ -octahedrons are connected by *two* tops, has  $\epsilon_c = 66$ ,  $TC\epsilon_c \approx -50$  ppm/K,  $\epsilon_a = 78$ ,  $TC\epsilon_a \approx -200$  ppm/K.
- Anatase, in which  $\text{TiO}_6$  octahedrons are connected by *three* tops, has  $\epsilon \approx 50$  and  $TC\epsilon \approx -70$  ppm/K.

Increased value of  $\epsilon_c$  in rutile is conditioned by *strictly oriented* oxygen octahedrons, which are connected by one top (Fig. 6.8). At that, a strong correlation exists between electron orbitals elongated in the [001] direction. Central four-valence cation  $\text{Ti}^{4+}$  strongly attracts electron orbitals of six surrounding oxygen anions; therefore such an extended electron cloud makes the octahedron a highly polarized structural unit. Comparison of permittivity in anatase, brookite, and rutile demonstrates that the manner of octahedron combination and arrangement is important for electron orbit interference. Interaction of orbitals in the [001] direction *strengthens polarizability* of

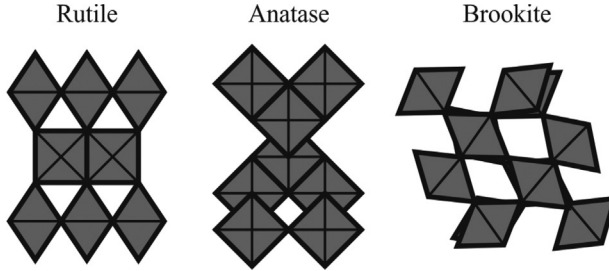


**Fig. 6.8** Comparison of simplified structures of rutile, anatase, and brookite.

rutile, which results in increased  $\epsilon_c$ , while in the perpendicular direction  $\epsilon_a < \epsilon_c$  and  $TC\epsilon_a < TC\epsilon_c$ . These results point out possible ways of controlling  $TC\epsilon$ .

By examining different TiO<sub>2</sub> structures (Fig. 6.8), it is possible to find how to influence the properties of such a crystal by foreign ion placement between octahedrons. In order to suppress the strong correlation between octahedrons, embedded ions should be placed between them, and this might be one of the ideas concerning various compositions of microwave dielectrics with permittivity of 30–50. For example, for the thermal stabilization of rutile permittivity, barium oxide often is used. The outer electron shell of barium ion ( $5s^2p^6$  hybrid) is very remote from the  $Ba^{+2}$ -core due to the empty deep-laid electron orbital  $4f$ ; that is why the  $5s^2p^6$  shell is easily compliant to interaction with its neighborhood. Taking root between the TiO<sub>6</sub> octahedrons, the large ions of  $Ba^{+2}$  show a strong influence on the outer electron shells of the surrounding  $O^{-2}$  ions. In this way it is possible to govern by the peculiarity of interaction of the electron shells, or, in other words, to govern weakly bound electron reciprocal displacement by implementation of different foreign ions into a structure. Using this method, it is possible to significantly weaken the large  $\epsilon(T)$  dependence of rutile, as if it follows the Curie-Weiss law.<sup>a</sup>

The main feature of displacement-type paraelectrics is their strong correlation between highly polarizable octahedrons. Their interaction can result even in the appearance of ferroelectricity (as in the case of BaTiO<sub>3</sub>). With the purpose of finding thermally stable microwave dielectrics, the high sensitivity of octahedrons to embedded ions is used (Fig. 6.9B). It is seen how the fast, large, negative  $TC\epsilon$  of rutile goes to a zero value with the increase of BaO concentration:  $TC\epsilon$  even closely approaches to zero in BaTi<sub>4</sub>O<sub>9</sub> = BaO·4TiO<sub>2</sub> composition. Exactly at this ratio, as follows from Fig. 6.9A, the arrangement of oxygen octahedrons becomes quite different, but it is still regular. This confirms the single-phase structure emergence that provides low losses with sufficient permittivity around  $\epsilon_{mw} \sim 40$ . The  $TC\epsilon$  control is mainly due to the violation in the octahedron orientation in the BaTi<sub>4</sub>O<sub>9</sub> structure (Fig. 6.9B).

<sup>a</sup>Solid solutions with a composition of BaO-TiO<sub>2</sub> have been studied in many works and in great detail [1, 2]. In addition to BaTi<sub>4</sub>O<sub>9</sub>, other single-phase compounds were found that also possess increased thermal stability. Here only a simplified scheme of interactions in these compounds is presented, solely for the purpose of describing the principle of dielectric properties in BaO-TiO<sub>2</sub> system control.

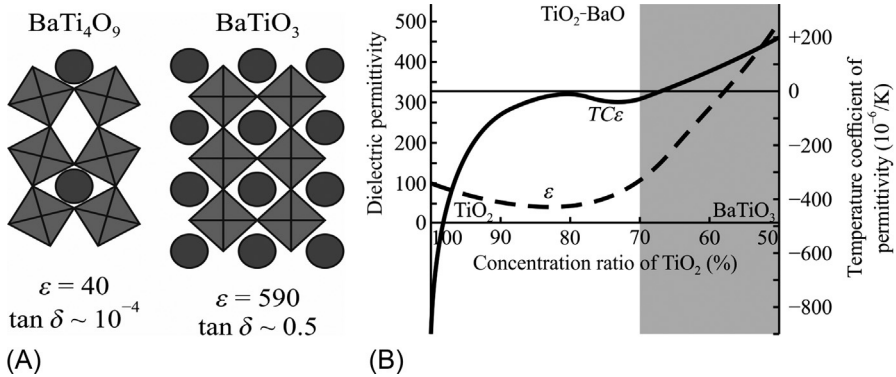


**Fig. 6.9** Mixed oxides  $\text{TiO}_2\text{-BaO}$  with different ratios of  $\text{TiO}_2$  concentration: (A) Reductive structures; (B) permittivity and its temperature coefficient (at 50% ferroelectric  $\text{BaTiO}_3$  arises); shaded area corresponds to mixtures with large microwave losses [62, 63].

Modified by barium, the titanium oxide structure shows a weakening in electron orbital interactions and, thus, less dependence of their permittivity on temperature. At that, in the  $\text{BaTi}_4\text{O}_9$  composition, the parameter  $TC\epsilon$  is still somewhat less than zero; however, the value  $\epsilon_{mw} \approx 37$  is sufficient to use this microwave dielectric in dielectric resonators at centimeter waves. To get  $TC\epsilon \approx 0$ , barium tetratitanate might be additionally doped by  $\sim 1.5\%$  of tungsten oxide. In order to have the possibility of  $TC\epsilon$  control within  $\pm 10$  ppm/K, we use  $\text{BaTi}_4\text{O}_9$  doping by zinc oxide (7%–12%) [36]. Moreover, the single-phase structure and low microwave losses in  $\text{BaTi}_4\text{O}_9\text{:ZnO}_2$  ceramics are preserved, because zinc occupies only a small portion of the central-octahedron positions.

As can be seen from Fig. 6.8, in the composition  $\text{BaO-TiO}_2$  it would be possible to increase permittivity up to 160 at  $TC\epsilon_{mw} \approx 0$ , but subsequent increase of  $\text{BaO}$  concentration gives rise to mixtures containing a polar (ferroelectric) phase, and, as a result, has bigger losses. Finally, when  $\text{BaO}$  concentration reaches 50%, the  $\text{BaO-TiO}_2$  composition corresponds to  $\text{BaTiO}_3$ —a ferroelectric, in which the microwave loss tangent exceeds 0.5 at  $\epsilon_{mw} \approx 600$ . This polar, highly absorbing microwave dielectric could be a component of absorbing microwave composite materials, especially in the millimeter wavelength range.

**2. Thermostable microwave ceramic dielectrics with  $\epsilon_{mw} \sim 100$ .** These dielectrics with a high value of permittivity are used in telecommunication devices of meter and decimeter wave-length ranges and meet the usual requirements of minimal dielectric loss and maximal thermal stability. Displacement-type paraelectrics have relatively low losses with  $\epsilon = 100\text{--}300$  at room temperature. However, as seen from Table 6.4, the temperature coefficient of permittivity in these paraelectrics is too big.

It is vital to note that “soft paraelectrics”  $\text{SrTiO}_3$  and  $\text{KTaO}_3$  have positive Curie-Weiss temperature ( $\theta > 0$  K) and therefore any additives easily activate in them polar phases, which can also be induced by electrical field, mechanical stress, etc. As a result, microwave losses in these materials at 300 K are not small:  $\tan\delta \sim 10^{-2}$  due

**Table 6.4** Permittivity, coefficient of thermal stability, and dielectric losses in ceramic paraelectrics at frequency  $\sim 10$  GHz and temperature 300 K.

Ceramics	$\epsilon_{mw}$	$TC\epsilon_{mw}\cdot 10^6 \text{ K}^{-1}$	$\tan\delta\cdot 10^3$
TiO <sub>2</sub>	100	−900	4
KTaO <sub>3</sub>	110	−600	20
CaTiO <sub>3</sub>	130	−1600	10
SrTiO <sub>3</sub>	300	−3000	25

to possible fluctuations of polar phase in their polycrystalline structure. In contrast, in the “hard paraelectrics” such as TiO<sub>2</sub> or CaTiO<sub>3</sub>, the  $\epsilon(T)$  dependence could be described by the parameter  $\theta < 0$ . Doping or electrical field cannot transform these paraelectrics into polar phase (perhaps they have a tendency to the antiferroelectric ordering). That is why they have lower microwave losses; but the main difficulty of “hard paraelectrics” application at microwave frequency is their  $\epsilon_{mw}$  temperature dependence. Since the physical nature of this dependence lies in the *electronic subsystem* of these crystals, the ways to overcome this instability should be sought in such methods that can impact on this subsystem. Moreover, the main contribution to  $\epsilon_{mw}$  is given by those parts of lattice polarization that are associated with susceptibility of weakly bound electron orbits. Next, a possible explanation will be given of how to suppress Curie-Weiss temperature dependence in such paraelectrics, preserving their low losses and high permittivity.

A high thermal stability of permittivity is reached in BaLn<sub>2</sub>Ti<sub>4</sub>O<sub>12</sub> (BLT)—paraelectric-like compounds with embedded *rare-earth ions* [1, 2]. These polycrystalline dielectrics are stand-outs among many other microwave dielectrics: their permittivity  $\epsilon_{mw}$  is much higher than in other types of microwave ceramics. Later the assumption will be proposed as to the nature of BLT polarization: namely, paramagnetic rare-earth ions can depress thermal nonstability of permittivity in paraelectrics. As noted earlier, increased but nonthermal stable  $\epsilon_{mw}$  in paraelectrics is due to weakly bound electron orbitals with ionic “cores.” In the BLT the *noncompensated* electron spins of paramagnetic ions bind the freedom of these orbitals, increasing their resistance to thermal nonstability. Experimental data on thermal stability and permittivity of BLT are summarized in Table 6.5.

**Table 6.5** Effect of various rare earth oxides on permeability and thermal stability of BLT.

Parameter	Lanthanoid								TiO <sub>2</sub>	CaTiO <sub>3</sub>
	<sup>0</sup> La	<sup>1</sup> Ce	<sup>2</sup> Pr	<sup>3</sup> Nd	<sup>5</sup> Sm	<sup>6</sup> Eu	<sup>7</sup> Gd			
$\epsilon_{mw}$	110	90	85	83	80	75	65	100	150	
$TC\epsilon, 10^{-6} \text{ K}^{-1}$	−700	−400	−250	−80	+60	+100	+160	−900	−1600	

Note. Upper index before RE shows 4f-shell filling; for comparison rutile and perovskite parameters are given as well.

Shown in Table 6.5, compositions look like paraelectrics but some of them are simultaneously paramagnetics as well; at that, in the  $\epsilon(T)$  characteristic the influence of paramagnetism predominates over paraelectric-type thermal nonstability. In  $\text{TiO}_2\text{-Ln}_2\text{O}_3$  compositions the Curie-Weiss law becomes gradually suppressed: as paramagnetism becomes stronger (from Ce to Gd) the parameter  $TC\epsilon$  changes greatly. It is obvious that by using a specially selected solid solution, for example, the (Nd-Sm)  $\text{La}_2\text{TiO}_5$  composition, it is possible to reach a zero thermal coefficient of permittivity.

There is the possibility (with the example of rutile) to influence paraelectric thermal stability by exterior ion allocation between the octahedrons (a similar method was used in  $\text{BaO}\cdot 4\text{TiO}_2$  ceramics). Fig. 6.10 shows one promising way to get thermally stable, high permittivity microwave dielectrics, namely using solid solutions of rutile with the rare-earth oxides:  $\text{Ln}_2\text{TiO}_5$ ,  $\text{Ln}_2\text{Ti}_2\text{O}_7$ , or  $\text{Ln}_2\text{Ti}_3\text{O}_{11}$ , where Ln means the cerium row of lanthanoids: Ce, Pr, Nd, Pm, Sm, Eu, Gd.

The lanthanum ion has similarity to the  $\text{Ba}^{2+}$  ion electron configuration:  $5s^25f^6$ ; this means that the  $\text{La}^{3+}$  ion also has empty  $5f$  energy levels and, therefore, like the  $\text{Ba}^{2+}$  ion, the  $\text{La}^{3+}$  ion is *diamagnetic*. Perhaps for this reason,  $\text{Ln}_2\text{O}_3$  has almost no change from the parameters of rutile; in particular its  $TC\epsilon$ , as before, remains large. At that, the radius of the  $\text{La}^{3+}$  ion ( $r_{\text{La}^{3+}} \sim 0.1$  nm) is much smaller than the barium ion radius ( $r_{\text{Ba}^{2+}} \sim 0.16$  nm). That is why a barium additive reduces the permittivity of rutile more than two times in  $\text{BaTi}_4\text{O}_9$ , while  $\text{TiO}_2\text{-La}_2\text{O}_3$  ceramic has  $\epsilon_{mw} \approx 110$  and  $TC\epsilon \approx -700$  (similar to rutile; Fig. 6.10). Moreover, the somewhat increased  $\epsilon_{mw}$  value in La-BLT is due to a low-energy relaxation process (this will be discussed later).

In  $\text{TiO}_2\text{-Ln}_2\text{O}_3$  compositions, Curie-Weiss type temperature dependence becomes gradually suppressed: from Ce to Gd (as paramagnetism becomes stronger)  $TC\epsilon$  changes greatly (Fig. 6.10). It should be noted that, using solid solutions (for example, the composition (Nd-Sm) $\text{La}_2\text{TiO}_5$ ), it is possible to get a *zero* coefficient  $TC\epsilon_{mw}$ . Indeed, very prospective compositions are elaborated in conditions when both lanthanides and barium are *used together* to obtain thermally stable ceramics (with  $\epsilon \geq 100$  and  $TC\epsilon \approx 0$ ). This is a perovskite-like structure of barium-lanthanum tetratitanates ( $\text{BaLn}_2\text{Ti}_4\text{O}_{12}$ , which is usually called BLT). These monophase structures exist only for the cerium group of the lanthanide row: Ln = La, Ce, Pr, Nd, Sm, Eu.

Other paramagnetic lanthanides of the  $\text{TiO}_2\text{-Ln}_2\text{O}_3$  type, when radius and *magnetic moment* of lanthanide changes, demonstrate a strong influence on microwave

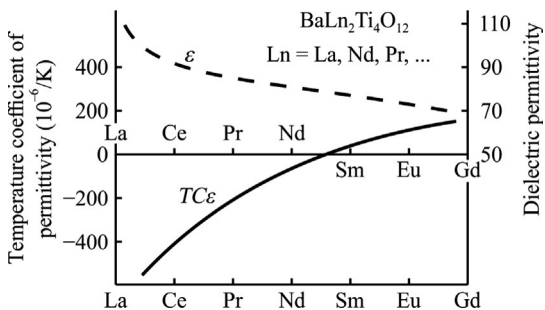


**Fig. 6.10**  $\text{BaLn}_2\text{Ti}_4\text{O}_{12}$  (BLT) permittivity and  $TC\epsilon$  for rare-earth lanthanoids of cerium row.

parameters of this composition, especially on thermal stability. Electron orbital configuration of REE ions is  $4f^{(1...7)}5s^25p^6$ , so they are *paramagnetics* with gradual increase of their magnetic moment: from one to seven Bohr magnetons. Holding rather big dielectric permittivity ( $\epsilon_{mw} \approx 80$ , that exceeds two times the  $\epsilon_{mw}$  of  $n\text{TiO}_2\cdot\text{BaO}$  systems), the compositions  $\text{TiO}_2\cdot\text{Ln}_2\text{O}_3$  can change their  $TC\epsilon$  from negative to positive sign. These compositions, the parameters of which are shown in Fig. 6.11, look like paraelectrics, but they simultaneously are paramagnetics as well; it is obvious that the  $\epsilon(T)$  dependence feels the influence of paramagnetism.

Paramagnetism can be considered a main cause of thermal stability in BLT; Fig. 6.11 shows how gradual increase of paramagnetism (the number of uncompensated spins in the  $f$ -orbital) reduces the temperature coefficient of permittivity in the BLT type solid solutions. At that,  $TC\epsilon$  changes from negative to positive value on a border between neodymium and samarium [37–39].

The most probable mechanism of paramagnetic noncompensated electron spin influence on paraelectric polarization might be *indirect exchange interaction* of the lanthanide ion with the titanium ion through the oxygen ion (Fig. 6.12). Magnetic

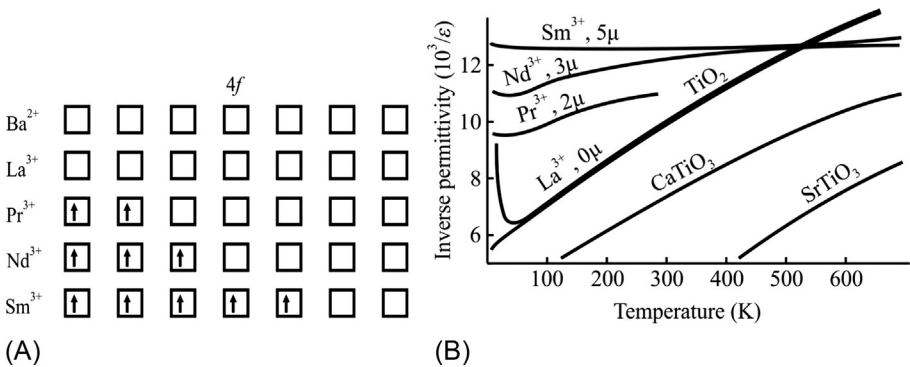


**Fig. 6.11** Suppression of paraelectric  $\epsilon_{mw}$  temperature dependence in BLTs: (A) Location of electronic spins in  $4f$ -orbitals of REE; (B)  $1/\epsilon$  temperature dependence for BLT and in some paraelectrics; number Bohr magnetons in paramagnetic ion (0μ, 2μ, 3μ, 5μ) is shown near curves.

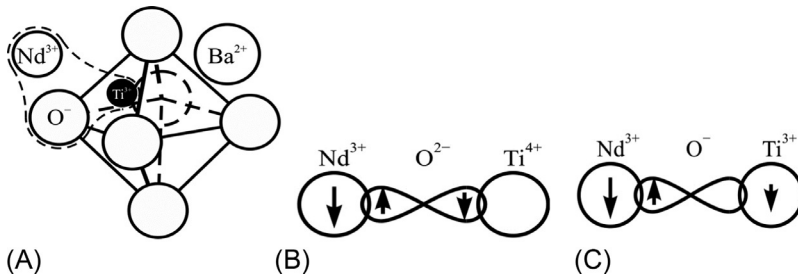


**Fig. 6.12** Indirect exchange interaction in system  $\text{Nd}^{3+}\text{-O}^{2-}\text{-Ti}^{4+}$ : (A) Cell in BLT structure; (B) ground state; (C) excited state.

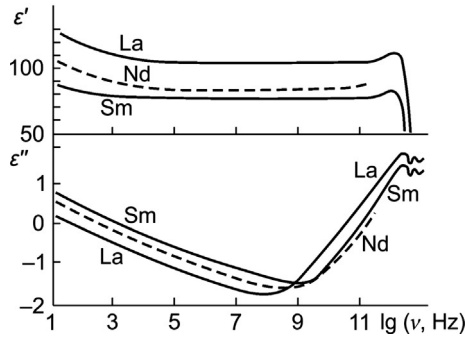


**Fig. 6.13** BLT permittivity  $\epsilon'$  and loss coefficient  $\epsilon''$  frequency dependencies at 300 K.

moments of  $f$ -element ions are not entirely free, even in cases when the ions are separated by diamagnetic ions, and the *overlapping* of  $f$ -wave functions (orbitals) in different sites of the crystal lattice is negligible. This results in *indirect exchange interaction* between localized electrons through perturbation of other electronic sub-systems of diamagnetic ions, surrounding the magnetic ion.

Frequency dependencies of permittivity and loss factor for three typical barium-lanthanide ceramics are shown in Fig. 6.13 [27]. As is seen, in La-BLT a minimum of losses is located near the frequency of 0.1 GHz. More important for applications of Sm-BLT and Nd-BLT (which are components of solid solution with  $TC\epsilon \approx 0$ ), they have a minimum of losses just between the meter and decimeter waves, where these dielectrics have  $\epsilon \geq 100$  and are most promising for applications.

**3. Dielectric losses at very high frequencies**, characterizing transformation of electrical energy into heat energy, are dependent on many physical mechanisms of energy absorption, but in each frequency range a dominating mechanism of losses exists. Various features of polarization mechanisms produce a peculiar dependence of losses on frequency and temperature. In particular, losses are dependent on various types of impurities in a dielectric. Depending on impurities or structural defect concentrations, loss factor  $\epsilon''$  may vary by tens and hundreds of times, while the change of the  $\epsilon'$  value may be relatively small. Therefore dielectric loss looks like the most *sensitive indicator* of structure peculiarities.

There are three main parameters that characterize losses in dielectrics: heat power density  $p$ , loss coefficient  $\epsilon''$ , and loss tangent  $\tan\delta$ . They are depicted as:

$$p = \sigma E^2, \quad \epsilon^* = \epsilon' - i\epsilon'', \quad \epsilon'' = \sigma/(\epsilon_0\omega), \quad \tan\delta = \epsilon''/\epsilon', \quad \tan\delta = \sigma/(\epsilon_0\epsilon'\omega),$$

where  $\epsilon^*$  is complex permittivity, which consists of real ( $\epsilon'$ ) and imaginary ( $\epsilon''$ ) parts, and  $\sigma$  is specific conductivity. The magnitude of losses as well as their dependence on the frequency and temperature indicates certain features of the mechanism of polarization. A microscopic source of losses might be the *conductivity* and the *anharmonicity* of polarization mechanisms. As a rule, the influence of conductivity on microwave losses is minimal, so the main contribution to losses is due to

anharmonicity in crystal lattice vibrations. The primary cause of anharmonicity in crystalline dielectrics is determined by the asymmetry in electronic density distribution along atomic bonds. This is conditioned by a difference in electronegativity of adjacent ions; sometimes the difference in electronegativity of different ions might be significant; this case corresponds to polar materials.

Dielectric losses at microwave frequencies might be the footprints of different processes: (1) conductivity; (2) slow relaxation mechanism described by Debye relaxation (electronic and ionic structural defects, dipoles, etc.); (3) resonant mechanisms of far-infrared polarizations described by the Lorentz oscillator model; (4) fast relaxation (Debye) mechanism of losses peculiar to polar crystals.

**4. Conductivity influence on microwave losses** is possible because free charge carriers, when they acquire energy from an electric field, scatter it on collisions with the crystal lattice. Ionic conductivity is too slow to manifest on microwaves; however, in dielectrics electronic conductivity also exerts a minimal influence upon microwave loss. In semiconductors, conductivity can play a definite role in microwave losses; only high-resistance semiconductors can be like dielectrics as a transparent media for microwaves. Electronic conductivity does not depend on a frequency, including the terahertz range, due to the high mobility of electrons. That is why electronic conductivity might be considered a frequency-independent parameter that is constant in all frequency ranges, including microwaves [37].

As reactive current *increases linearly* with frequency, in the case of *unchanged conductivity* as loss factor  $\epsilon'' = \sigma/(\epsilon_0\omega)$ , so the loss tangent  $\tan\delta = \sigma/(\epsilon_0\epsilon'\omega)$  decreases with frequency rise (therefore at a frequency of 1 GHz the parameter  $\tan\delta$  will be 1000 times less than at a frequency of 1 MHz); at that, permittivity  $\epsilon' = \epsilon$  might be frequency independent. Corresponding experimental data are shown in Fig. 6.14A by the example of the loss factor frequency dependence of silicon crystal. It is obvious that nonpolar, high-resistance silicon crystal can successfully play the role of a dielectric material for microwave substrates at frequencies above 30 GHz.

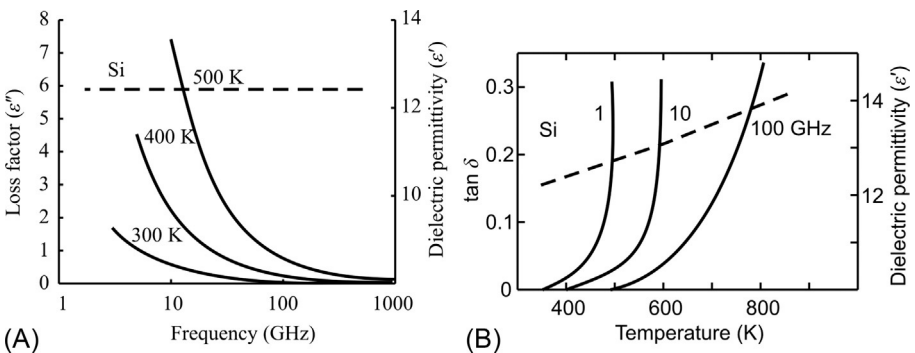


**Fig. 6.14** Frequency (A) and temperature (B) dependencies of microwave losses  $\epsilon''$  and  $\tan\delta$  (solid lines) and permittivity  $\epsilon'$  (dashed lines) for high-resistance silicon in gigahertz range.

Temperature dependence of losses conditional on conductivity shows an exponential increase (Fig. 6.14B). Electrons provoke microwave losses that are strongly dependent on frequency and on temperature:

$$\tan \delta(\omega, T) = \frac{\sigma}{\epsilon_0 \epsilon \omega} \approx \frac{\sigma_0 \exp[a(T - T_0)]}{\epsilon_0 \epsilon \omega}, \quad (6.5)$$

where  $\sigma_0$  is conductivity at certain temperature  $T_0$ ,  $\epsilon_0$  is electrical constant, and  $\epsilon$  is frequency independent permittivity, while  $a$  is a parameter peculiar to the given material. It follows from Fig. 6.14B that at a gigahertz frequency range silicon crystal can play the role of a dielectric up to temperatures of 400–500 K. A small increase of silicon permittivity with temperature (dotted curve in Fig. 6.10) is due to the energy gap decrease in the electronic energy spectrum.

**5. Slow polarization mechanisms (relaxation)**, as usual, do not have much influence on microwave losses, because these mechanisms take place at relatively low frequencies (see Fig. 6.1). Nevertheless, some heterogeneous systems deserve to be mentioned here, since they are used in microwave absorbers and in metamaterials. The migratory polarization arises in dielectrics owing to macroscopic heterogeneity or inclusions. This polarization is delayed at very low frequencies ( $10^{-3}$ – $10^3$  Hz), and this is associated with a significant dispersion of  $\epsilon^*(\omega)$ , which is accompanied by increase of losses at low frequencies. A plausible reason for this polarization is the presence of some particles or layers with different conductivity, as well as the presence of impurities in dielectrics. In some microwave dielectrics (such as metal-polymer composites), effective conductivity becomes essential because the reactive current in the dielectric increases millions of times with frequency rise, so the conductivity of metallic grains (included in the composite material) begins to dominate, and this mechanism becomes significant, if high-loss microwave dielectrics have to be applied in absorbing covers. Another way that losses increase in a composite is in the polar phase, originating in the vicinity of double-charged layers in the metal-dielectric boundaries.

Other possible mechanisms, described well by relaxation polarizations, are the electronic, ionic, or dipole thermally activated polarization [38]. In the case of thermally activated polarization (as well as in migration-type polarization), the dispersion of permittivity usually follows the Debye equation, from which it is possible to obtain frequency dependence of losses:

$$\epsilon^*(\omega) = \epsilon' - i\epsilon'' = \epsilon(\infty) + \frac{\epsilon(0) - \epsilon(\infty)}{1 + i\omega\tau}, \quad \tan \delta = \frac{[\epsilon(0) - \epsilon(\infty)]\omega\tau}{\epsilon(0) + \epsilon(\infty)\omega^2\tau^2}.$$

Here  $\omega = 2\pi\nu$  is electrical field frequency,  $\tau$  is relaxation time,  $\epsilon(0)$  is permittivity taken well below relaxation frequency (when  $\omega\tau \ll 1$ ), and  $\epsilon(\infty)$  is permittivity taken well above relaxation frequency (when  $\omega\tau \gg 1$ ). This formula testifies to a maximum of  $\tan\delta(\omega)$  located near frequency  $\omega = 1/\tau$ . Dielectric permittivity has a relaxation nature, characterized by the gradual decline of  $\epsilon'(\omega)$  and by the broad maximum of  $\epsilon''(\omega)$  (Fig. 6.15).

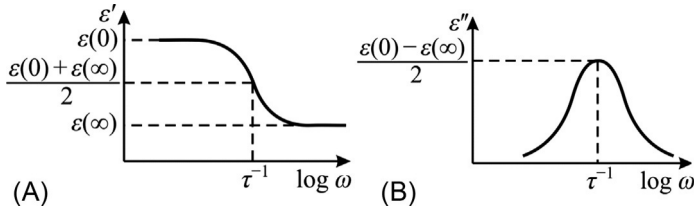


**Fig. 6.15** Dispersion of permittivity (A) and correspondent coefficient of loss maximum (B) in dielectrics with thermally induced (relaxation) mechanisms of polarization.

Setting time  $\tau$  of this kind of polarization is a temperature-dependent parameter that is determined by the structure of the dielectric and by the type of defects (impurities). Generally, at normal temperatures (about 300 K), relaxation time lies in the interval of  $\tau = 10^{-4}$ – $10^{-8}$  s. Any delay of polarization always leads to increased absorption of electrical energy. Therefore thermally induced polarization can be a major cause of dielectric losses at *radio frequencies*. The presence of a loss factor maximum near the frequency of  $10^6$  Hz demonstrates typical relaxation losses. Their contribution to the *microwave* losses can be described by the preceding equation. It is obvious that high-frequency  $\tan\delta$  conditioned by the relaxation process *decreases* proportionally to frequency. At microwaves, such loss factors depend also on the size of the relative contribution from a given relaxation process to dielectric permittivity.

Temperature dependencies of losses are produced by a slow relaxation polarization mechanism (electronic defects, ionic defects, various kinds of dipoles, etc.) and described by the Debye model of relaxation at condition  $\omega\tau > 1$ :

$$\tan\delta = \frac{1}{\omega\tau} \frac{\varepsilon(0) - \varepsilon(\infty)}{(\varepsilon(0)/\omega^2\tau^2) + \varepsilon(\infty)}. \quad (6.6)$$

where  $\tau$  is relaxation time,  $\varepsilon(0)$  is permittivity well below relaxation frequency ( $\omega\tau \ll 1$ ), and  $\varepsilon(\infty)$  is permittivity well above the relaxation frequency ( $\omega\tau \gg 1$ ). This dependence has been repeatedly confirmed experimentally.

**6. Ionic displacive-type polarization** mechanism plays a decisive role in high-frequency losses in those dielectrics with ionic structure. Among these dielectrics there are not only alkali-halide cubic structured crystals but also many simple and complex dielectric oxides, including paraelectrics, piezoelectrics, ferroelectrics, and pyroelectrics, as well as partially ionic polar semiconductors of  $A^{III}B^V$  and  $A^{II}B^{VI}$  groups.

The ionic polarization mechanism is rather fast (install time of  $\sim 10^{-13}$  s); however, it is slower than electronic polarization (install time of  $\sim 10^{-16}$  s). Nevertheless, the ionic mechanism has much less relaxation time than thermally activated relaxation ( $\sim 10^{-6}$  s) and migratory polarization ( $\sim 10^{-1}$  s). Dielectric dispersion for ionic polarization occurs in the far-infrared frequency range, so that in the gigahertz region ionic polarization is completely installed. However, the *low-frequency tail* from a far-infrared maximum of losses is observed at microwaves, especially in the case of

high-permittivity dielectrics, in which the dispersion frequency  $\omega_{TO}$  is much lower than in other ionic crystals. Dispersion of permittivity in ionic crystals is described by the Lorentz equation, which can be used to find the contribution to microwave losses from resonant ionic polarization (i.e., its microwave “tail” below resonant frequency):

$$\begin{aligned}\varepsilon^*(\omega) &= \varepsilon' - i\varepsilon'' = \varepsilon(\infty) + \frac{\varepsilon(0) - \varepsilon(\infty)}{1 - (\omega/\omega_0)^2 + i\Gamma(\omega/\omega_0)}, \\ \tan\delta &= \Gamma \frac{\omega}{\omega_{TO}} \frac{\varepsilon_{mic} - \varepsilon_{opt}}{\varepsilon_{mic}}.\end{aligned}\quad (6.7)$$

Here  $\omega_0$  is the frequency of the oscillator, which equals to  $\omega_{TO}$  (frequency of transverse optical phonon mode);  $\Gamma$  is relative damping coefficient;  $\varepsilon(0)$  is dielectric permittivity taken well below resonant frequency, which is microwave permittivity  $\varepsilon_{mic} = \varepsilon(0)$ ; while  $\varepsilon(\infty)$  is permittivity taken well above resonant frequency, which usually means optical permittivity  $\varepsilon_{opt}$ . Frequency dependence of  $\varepsilon'(\omega)$  demonstrates not only a maximum, but also a minimum, while loss factor  $\varepsilon''(\omega)$  in the vicinity of resonant dispersion shows rather a sharp peak (Fig. 6.16).

Experimental data of  $\tan\delta$  frequency dependence in *nonpolar* crystals usually corresponds to the preceding equation. It is seen that losses increase with frequency increase, and they are as large as frequency  $\omega$  is closer to  $\omega_{TO}$ ; this case is typical for high-permittivity dielectrics. The damping of lattice vibration mode  $\gamma$  is weakly dependent on temperature:  $\gamma(T) = \Gamma\omega_{TO} = \gamma_0 + aT + bT^2$ , where  $\gamma_0$  describes phonon dissipation on impurities and usually dominates, while parameters  $a$  and  $b$  correspond to various many-phonon absorption mechanisms (essential in high-permittivity dielectrics but usually less than  $\gamma_0$ ).

**7. Microwave losses in polar crystals**, among which are ionic compounds (ZnO, Bi<sub>12</sub>SiO<sub>20</sub>, AlN, BN, etc.) in which microwave losses are noticeably bigger than in nonpolar crystals and that cannot be explained by any of the previously listed mechanisms of losses. These dielectrics have small conductivity and very small probability of impurities relaxation, and they also have rather high frequency of their lattice resonance  $\omega_{TO}$ , such that it might have a noticeable effect on microwave losses. For example, semiconductors of A<sup>III</sup>B<sup>V</sup> and A<sup>II</sup>B<sup>VI</sup> groups have essentially increased microwave losses; sillenites (Bi<sub>12</sub>GeO<sub>20</sub> and similar), however, show heightened permittivity ( $\varepsilon \approx 40$ ); at that, increased microwave losses are seen even in very firm

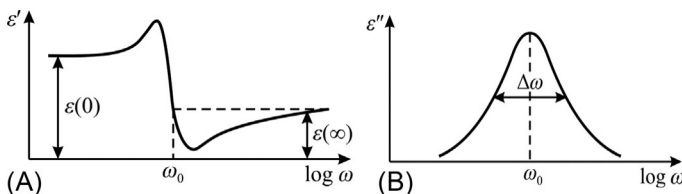


**Fig. 6.16** Frequency dependence of permittivity (A) and loss factor (B) for resonant polarization.

nitrides (AlN, BN, and others), in which permittivity has the usual value for ionic compounds ( $\epsilon < 10$ ).

The characteristic and important example is gallium arsenide, in which the influence on microwave loss from conductivity is very small, but one can see significant growth of losses with frequency. It is supposed that this is a manifestation of the *internal polarity mechanism* on absorption at millimeter and submillimeter waves. Due to the piezoelectric effect, for example, in GaAs, a relaxation process arises conditioned by the interaction of acoustical and optical phonon modes. This electromechanical coupling results in a “leakage” of electric energy from optical phonons excited by the electrical field to the “heat reservoir” of acoustical phonons. This is a reason why gallium arsenide losses increase with increasing frequency. This result is unexpected from the Born crystal dynamics theory of ionic polarization, which predicts only a weak lower-frequency tail from resonance at far-infrared range, when influence on losses should be much less than the losses really observed in the gigahertz range.

Semiconductors of  $A^{III}B^V$  or  $A^{II}B^{VI}$  types represent polar crystals:  $A^{III}B^V$  crystals are piezoelectrics while  $A^{II}B^{VI}$  crystals are pyroelectrics. Peculiarities of frequency and temperature dependencies of losses in GaAs are conditioned by a fast lattice relaxation mechanism (quasi-Debye mechanism). In noncentrosymmetric (polar) materials, microwave loss factor is governed by the previously mentioned mechanism of losses that theoretically is described by the Debye equation [38]. Frequency and temperature dependencies of these losses (Fig. 6.17) are due to fast relaxation polarization mechanism; at condition when  $\omega\tau < 1$ :

$$\tan \delta \approx \frac{\omega}{2\nu_D} \exp \frac{U}{k_B T} \frac{\epsilon(0) - \epsilon(\infty)}{\epsilon(0)}, \quad (6.8)$$

where  $\nu_D$  is Debye frequency,  $k_B$  is Boltzmann constant, and  $U$  is potential barrier. In this case, the loss factor increases with frequency and with temperature. It is seen that losses increase with frequency rise, and they are as big as frequency  $\omega$  is close to  $\omega_{TO}$ .

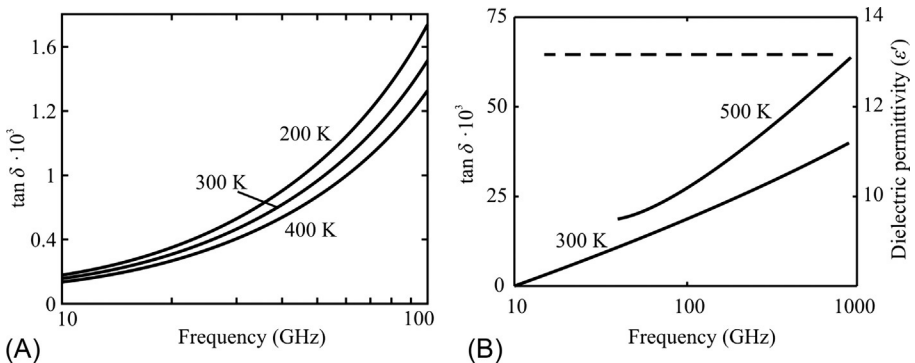


**Fig. 6.17** Loss tangent frequency dependence in GaAs: (A) Low-frequency tail from loss maximum; (B) impact of quasi-Debye mechanism polar crystal (*dashed line* is permittivity).

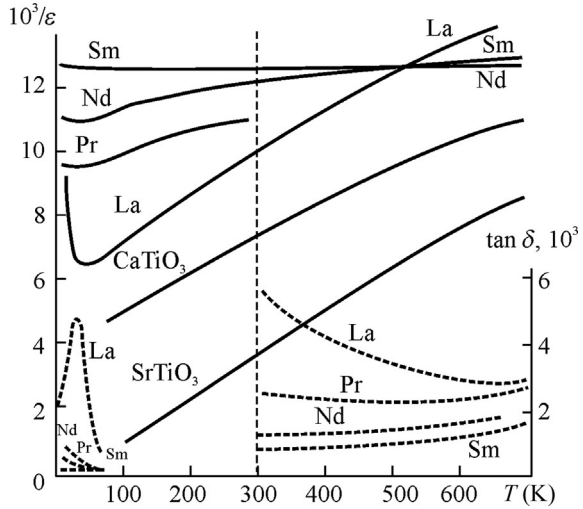
Just this case is typical for higher-permittivity dielectrics. The consequence is that, unlike silicon, wherein the microwave quality factor ( $Q = 1/\tan\delta$ ) of the crystal only increases with frequency so the loss factor decreases with it, in gallium arsenide at millimeter waves the loss factor increases with frequency rise. This should be considered when designing microwave-integrated electronics. Nevertheless, this acoustooptic interaction has almost no effect on the magnitude of microwave permittivity, so practically no dependence of  $\epsilon_{mw}(\omega)$  is observed (Fig. 6.17). Therefore, semiconductors can be used as waveguides and resonant microwave components at centimeter (GaAs) and millimeter (Si) waves.

As already indicated earlier, single-phase perovskite-like structures of BLT-type acceptable for applications can be realized only for the cerium group of the lanthanide row. The main special feature of these structures is  $\text{TiO}_6$  octahedrons linked by tops. It is supposed that, in well-known microwave dielectrics of BLT-types, electron bonds of the  $4f/5d$ -hybrid, caused by rare-earth ions, suppress the interaction of  $\text{TiO}_6$  octahedrons, and this neutralization is highly favorable for thermal stability of permittivity. To check this assumption, in the temperature interval of 10–600 K the *dielectric spectroscopy* method is applied, initiated from low frequencies and extended up to the far-infrared range. The mechanism of anomalously high permittivity  $\epsilon_{mw}$  and low  $TC\epsilon$  in BLTs is that “soft” lattice vibration mode (that usually gives rise to high but thermally unstable permittivity) is “suppressed” by rare-earth ions, violating the long-range correlation connected by oxygen octahedrons  $\text{TiO}_6$ . The main reason for this effect is paramagnetism, which is peculiar to the cerium row of lanthanides. Barium ions play a supporting role for thermal stability and, moreover, support BLT’s manufacturability. The reason for a significant increase in dielectric losses in the BLTs in the range of microwaves and millimeter waves is low-frequency lattice vibrations associated with the low-energy relaxation process. However, this feature of BLTs is not a big disadvantage, when they are used in meter and decimeter waves.

**8. Low-energy relaxation in BLT.** All paraelectrics are characterized by large and negative  $TC\epsilon$ , so it is important to discuss additionally the physical reason why in lanthanides the important parameter  $TC\epsilon$  becomes positive. In this connection it should be noted that, besides lanthanides, this occurs in paramagnetic materials; their ionic radius is 1.5 times smaller than in barium. Moreover, they exhibit the so-called “lanthanide contraction,” which is the smooth decrease of ionic size (from 0.115 nm in cerium down to 0.109 nm for europium). It would be interesting to establish which of these two physical mechanisms appears to be dominant. To clear up this question, the frequency properties of lanthanides are studied over wide frequency and temperature ranges.

The comparison of inverse permittivity for some paraelectrics and some BLTs is shown in Fig. 6.18. Dielectric properties of “basic” composition La-BLT above the temperature of 100 K are very close to  $\text{TiO}_2$  properties, and, at first glance, La-BLT is similar to the paraelectric  $\text{TiO}_2$  in its  $TC\epsilon$  value and sign; the diamagnetic lanthanum ion has a radius  $\sim 0.10$  nm, which is smaller than the ionic radii of paramagnetics praseodymium, neodymium, and samarium. It is important to note that  $\text{TiO}_2 \cdot \text{La}_2\text{O}_3$  composition with diamagnetic  $\text{La}^{+3}$  practically does not change the paraelectric properties of  $\text{TiO}_2$  (at least, above the temperature of 50 K). However, as seen in Fig. 6.18, at low temperatures the  $\epsilon(T)$  dependence even in LaBLT is

**Fig. 6.18** Temperature dependence of  $1/\epsilon$  (solid curves) and  $\tan\delta$  (dashed curves) for BLTs (La, Pr, Nd, Sm) as well as  $\text{TiO}_2$  and  $\text{CaTiO}_3$ ; below 300 K measurement frequency is 1 MHz, and above 300 K it is 10 GHz.



different from  $\epsilon(T)$  for paraelectrics: the  $1/\epsilon(T)$  characteristic shows a minimum, which points to the presence of *relaxation polarization*. While  $\epsilon(T)$  dependence in paraelectrics follows the Curie-Weiss law  $\epsilon = \epsilon_1 + C/(T - \theta)$ , in some of the BLTs the  $\epsilon(T)$  dependence satisfies the Debye relaxation law  $\epsilon(T) = \epsilon_1 + K/T$ .

Temperature anomalies in BLT permittivity are accompanied by dielectric loss maximums (Fig. 6.19), which is typical for relaxation polarization. At temperature

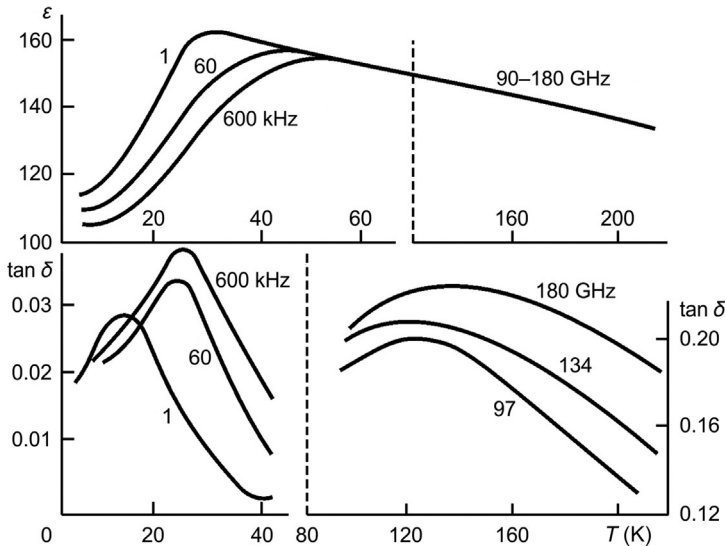


**Fig. 6.19** Low-energy relaxation process in La-BLT: At frequencies of 1–600 kHz anomalies in  $\epsilon$  and  $\tan\delta$  are seen in temperature interval of 4–60 K, and at frequencies of 90–180 GHz.

decreases, maxima of  $\epsilon$  and  $\tan\delta$ , first, decrease along the line La-Pr-Nd (and disappear for Sm), and, second, they shift to lower temperatures. With frequency increase, as it should be for relaxation processes, loss maximums shift to higher frequencies (Fig. 6.19). Very low activation energy results in the fact that, above the temperature of 100 K, the maximums of losses can be observed only in millimeter wavelength range (at 100–200 GHz).

Mechanisms of dielectric losses in the BLTs are associated with a structural mismatch, especially in the case of unwanted polar phase presence. Any boundaries (interfaces) between ceramic grains have disordered structure, and their relaxation frequency may reach the microwave range. It is the polar nanoscale regions that are the main reason for microwave absorption. That is why in BLT ceramic technology, any appearance of a polar phase should be avoided. When used in practice (in the temperature interval of 200–400 K), the relaxation frequency of these processes exceeds the microwave range, so that “relaxation supplement” together with lattice contribution provides the thermal stability of total dielectric permittivity.

Thus, experimental and theoretical investigations show that the dominating mechanism of losses in high-permittivity dielectrics arises from the polar phase existence. In the case of polar-sensitive bonds between atoms, the atomic equilibrium potential manifests a pronounced anharmonicity that is the main microscopic channel to transfer electrical energy into heat (dielectric losses). The anharmonic potential between ions results in a coupling between optical phonons (excited by an electrical field) and acoustical phonons (which represent a “heat reservoir” in crystals). With increasing temperature, and, consequently, with increase in amplitude of the vibration of ions, manifestation of anharmonicity becomes more noticeable and dielectric losses increase. Consequently, with the object of low-loss microwave dielectrics elaboration or application, one needs to avoid or to suppress the dielectric polar (non-centrosymmetric) components, since dielectric losses in them are large because of strong coupling of optical and acoustic phonons.

The high permittivity necessary for microwave technical applications can be obtained in those ionic crystals that have sufficiently open structure to make it possible to use greater polarizability of semifree electron orbits. High permittivity should be obtained using the low-frequency “soft mode” in paraelectric-like material. At that, low dielectric losses can be reached only in the single-phase compositions based on “hard paraelectrics” (which resist any polar structure formation). Finally, thermal stability in high-permittivity dielectrics can be obtained if paraelectric properties are partially suppressed by paramagnetism.

## 6.4 Composite structures with microwave dielectrics

In composite dielectrics, materials with different properties are combined to obtain the necessary technical specifications. Microcomposites are mixtures of crushed materials, and macrocomposites are made up of large parts of various materials; moreover, their location can be organized in a special way [1, 12, 40]. Microwave composites may be divided into the “passive” ones (which do not change their parameters during

operation) and the “functional” composites, with electrically controlled properties that are used for frequency tunable devices. In this section mostly these last types are considered.

Concerning microwave applications, the most widespread microcomposites are the *filled polymers*. For example, the mixture of polymeric Teflon ( $\epsilon = 2$ ,  $\tan\delta \sim 10^{-5}$ ) with finely dispersed rutile ( $\epsilon = 100$ ,  $\tan\delta \sim 10^{-3}$ ) achieves a composite microwave dielectric with  $\epsilon = 2\text{--}40$  and  $\tan\delta \sim 10^{-3}$ . This kind of composite is applied in the decimeter- and centimeter-wave devices, providing a low-loss microwave dielectric with a given effective permittivity. In the same way, a mixture of Teflon with miniature hollow air spheres produces a flexible microwave dielectric with reduced permittivity, within  $\epsilon = 2\text{--}1.3$ , that is important in millimeter-wave techniques. These microwave composite dielectrics are characterized by small dielectric losses, because they use *only nonpolar dielectrics*, such as Teflon or polystyrene (which have only electronic polarization), as well as nonpolar rutile or aluminum oxide with purely ionic polarization.

Another example is matrix mixtures of elastic dielectric (polymer or rubber) with ferrite, carbon, or metallic powders. To use these composites, an opposite problem is posed—ensuring *high losses* to suppress microwave radiation. In this case, the use of *polarity* of the dielectric included in a composite is desirable. These types of composites usually have low microwave reflection with large absorbance, which is important in microwave techniques as microwave-absorbent materials. It should be noted that absorbers of microwave radiation are required not only for military applications (reduction of the radar signature of aircraft, ships, tanks, and other potential targets) but also have important civilian applications (reduction of electromagnetic interference among components and circuits, reduction of back-radiation from microstrip radiators, etc.). At that, the main requirements for absorbers are as follows: (1) the composite should minimize the front-face reflection by impedance matching between air and absorber interface; (2) the composite should actively absorb electromagnetic waves due to conductance, magnetic, or dielectric losses; (3) the composite can be applied in the widest frequency range possible.

A composite absorber that uses metallic, ferrite, or carbonaceous particles in combination with polymer or rubber matrix offers large flexibility for design and properties control, because it can be optimized via changes in both inclusions and embedding matrix. The absorbent properties of such composites can be tailored to a given application through changes in their composition and volume fraction of filler particles. Polymeric and rubber composites filled with ferrite, metallic, or carbonaceous particles provide a versatile system with a wide range of potential applications. Among them are span radar absorbers, electromagnetic protection materials from natural phenomena (lightning), electromagnetic pulse protection, and materials for electromagnetic compatibility for electronic devices and high-intensity radiated field protection.

Another important feature of these composites is that the variations in metallic or ferrite particle content allow independent tuning of the real and imaginary parts of effective permittivity of the composite, in order to match some absorption requirement at a given frequency. One significant advantage of polymeric or rubber composites is

that, depending on the filler particle incorporation-mixing process and the adjustment of the nature and geometry of filler particles, these composites offer multiple degrees of freedom to tune particle aggregation state and overall effective permittivity. There are many electromagnetic properties that need to be studied in filler particles embedded in a polymer matrix, such as the type of interparticle interactions, the long-range dipole-dipole interactions, clustering, the matrix-particle interactions, and multi-contact chain adsorption at the surface of the filler. However, these problems are not discussed in this book in full because there is more extensive literature on these issues [1].

Here it is important to note that microwave absorption mechanisms of most of these composites are based either on electrical conductivity or on ferromagnetic resonance. However, the measure of absorption of both these mechanisms *significantly reduces with increasing frequency*. Therefore, when approaching millimeter waves, other composites may become relevant, in which absorption occurs due to the inclusion of *polar dielectrics* in their composition, in which microwave absorbance, on the contrary, *rises with frequency* (as shown before in Fig. 6.17). The fact is that in a polar dielectric there is a strongly pronounced optical-acoustic interaction, which allows translation of energy obtained by microwave electrical excitation into acoustic oscillations, which in materials are the “thermal reservoir.” At the same time, the effectiveness of such interaction in microwaves *increases with increasing frequency*.

It is necessary to note also that electrical properties (permittivity and losses) in microwave composites containing conductive and magnetic components cannot be electrically controlled. However, if microwave composites involve some of the polar dielectrics (paraelectric or ferroelectric components having electrically tunable permittivity), they might be applied as microwave phase shifters, reconfigurable filters, and other “functional” microwave devices. Further, a sort of dielectric macrocomposite containing *tunable components* with controlled *effective permittivity* by fast electromechanical reconfiguration will also be considered. In this case, uses for controlling polar dielectrics are located *outside the waveguide path* and therefore do not lead to microwave losses.

Next, exclusively the multilayered (not dispersed) microwave composites, which consist of different dielectrics, will be considered, while microwave microcomposites (mixtures) containing different conductive and ferrite components have been extensively studied in other literature [2].

**1. A “passive” dielectric macrocomposite** consisting of several dielectrics represents a nonuniform dielectric structure, manufactured from components of different electrical properties. Used in electronics (and in electrical engineering) macrocomposite materials often are constituted of two or more materials: for example, *layered insulations* made of different polymeric films. Multilayer ceramic elements are also often used in microwave techniques.

Next, a comparison will be made for calculation of parallel and sequential layered dielectrics: in comparatively low-frequency case, and in the high-frequency case (when dielectrics are located in waveguides in which microwave dielectrics can be used or investigated).

At first, the main formulas used for calculation of composite parameters on the basis of a given parameter of components are recalled. In a simplified version of the calculation, the size of components of an inhomogeneous dielectric is considered to be significantly smaller than the length of the electromagnetic wave. In this case, the study of inhomogeneous dielectrics is reduced to calculating the effective permittivity ( $\epsilon_{ef}$ ) and effective dielectric loss tangent ( $\tan\delta_{ef}$ ) of a composite. Thereafter, some examples of a composite's parameters in the case of commensurability of component size with wavelength are also discussed.

- *Two parallel-connected dielectrics* represent one of the simplest cases, wherein it is supposed that  $\epsilon_1, \epsilon_2, \tan\delta_1, \tan\delta_2$  as well as the surfaces  $S_1$  and  $S_2$  are known. Accordingly, effective permittivity and effective dielectric loss tangent are:

$$\epsilon_{ef} = \frac{\epsilon_1 S_1 + \epsilon_2 S_2}{S_1 + S_2}, \quad \tan\delta_{ef} = \frac{C_1 \tan\delta_1 + C_2 \tan\delta_2}{C_1 + C_2}.$$

- *Dielectrics that are randomly distributed but connected in parallel* represent composite dielectrics made of two components with their *arbitrary* distribution; however, location of components is assumed to be parallel. Besides  $\epsilon_1$  and  $\epsilon_2$ , the relative concentration of components  $x_1$  and  $x_2$  should be known. This case generalizes the previous consideration, where effective permittivity and effective dielectric loss tangent are:

$$\epsilon_{ef} = x_1 \epsilon_1 + x_2 \epsilon_2, \quad \tan\delta_{ef} = x_1 \frac{\epsilon_1}{\epsilon_{ef}} \tan\delta_1 + x_2 \frac{\epsilon_2}{\epsilon_{ef}} \tan\delta_2.$$

- *Two series-connected dielectric layers* with known parameters  $\epsilon_1, \epsilon_2, \tan\delta_1$ , and  $\tan\delta_2$ , as well as layer thicknesses  $d_1$  and  $d_2$  (wherein squares of layers are identical:  $S_1 = S_2 = S$  and their capacitances are  $C_1$  and  $C_2$ ). If losses are not too big, effective permittivity and losses are:

$$\epsilon_{ef} = \epsilon_1 \epsilon_2 \frac{d_1 + d_2}{\epsilon_1 d_2 + \epsilon_2 d_1}; \quad \tan\delta_{ef} = \frac{C_2 \tan\delta_1 + C_1 \tan\delta_2}{C_1 + C_2}$$

- *Distributed series-connected layers of two dielectrics* generalize the previous case. Volumetric concentrations of first and second components are  $x_1$  and  $x_2$ ; effective permittivity and loss tangent in the case of small losses are:

$$\epsilon_{ef} = \frac{\epsilon_1 \epsilon_2}{\epsilon_2 x_1 + \epsilon_1 x_2}; \quad \tan\delta_{ef} = \frac{\epsilon_1 x_2 (1 + \tan^2 \delta_1) \tan\delta_2 + \epsilon_2 x_1 (1 + \tan^2 \delta_2) \tan\delta_1}{\epsilon_1 x_2 (1 + \tan^2 \delta_1) + \epsilon_2 x_1 (1 + \tan^2 \delta_2)}$$

However, these relatively simple formulas *are unsuitable* for calculating dielectric macrocomposites located in microwave waveguides.

**2. Microwave composites of air-dielectric type**, which represent analog situations, need much more complicated calculations in order to take into account special allocation of the dielectric sample and the presence of metallic screening (for example, waveguide walls). The simplest but most important case is the examination of

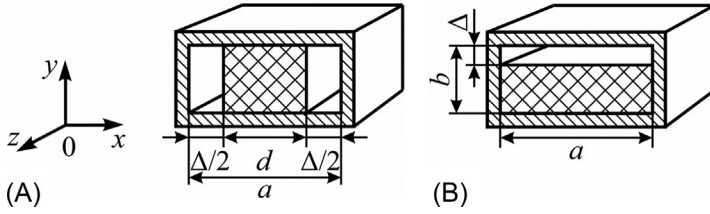


**Fig. 6.20** Upright (A) and horizontal (B) partial filling of waveguide cross-section with dielectric.

two coupled dielectrics, one of which is air with  $\epsilon_1 = 1$  and  $\tan\delta_1 = 0$ , while the other dielectric is crystal or ceramics with arbitrary  $\epsilon_2 = 1-1000$ .

- First, consider a waveguide that is *upright, partially filled with dielectric* in such a way that symmetrical air gaps appear between the sample and narrow walls of a waveguide (Fig. 6.20A). By the way, this situation is important for high- $\epsilon$  material measurement in the waveguides, because ideally dense contact between dielectric and waveguide walls is difficult to provide.

The electromagnetic field distribution problem can be solved utilizing longitudinal wave representation. Boundary conditions in the form of equality of tangential components of the electromagnetic field should be applied at the metal walls and on the air-dielectric boundary. Assuming a symmetrical location of the specimen inside of the waveguide, a magnetic wall condition can be applied at the center of the waveguide in order to reduce the number of unknown variables. Finally, this yields a complex nonlinear equation with respect to complex propagation constant:

$$\beta_{xa} \cot\left(\beta_{xa} \frac{\Delta}{2}\right) - \beta_{xe} \tan\left(\beta_{xe} \frac{a-\Delta}{2}\right) = 0.$$

Here  $\Delta$  is total gap;  $a$  is width of the broad wall of the waveguide;  $\beta_{xa} = \sqrt{k^2 - \gamma^2}$  represents transverse wave number in the air-filled area;  $\beta_{xe} = \sqrt{\epsilon k^2 - \gamma^2}$  corresponds to the transverse wave number in the dielectric specimen;  $\gamma$  is the propagation constant. The result of the calculation is shown in Fig. 6.21 [41–44].

One can note that the higher the permittivity, the less is the gap effect. It is obvious that several tens of micrometers, which usually correspond to the common accuracy of the sample preparation, have no influence on measurement of the final result (Fig. 6.21A) (the same can be said regarding effective loss; see Fig. 6.21B). That makes it possible to study a specimen that covers only the *center part* of the waveguide cross-section: thus, if the specimen covering the whole cross-section is not available, the smaller sample can be used while measuring with corresponding data processing.

- The preceding calculation can be implemented for a more complicated sample: upright located *ferroelectric film* ( $\epsilon_{film} \approx 500-1000$ ) deposited onto a microwave dielectric substrate ( $\epsilon_{subs} \approx 10$ ) and placed in an air-filled waveguide ( $\epsilon = 1$ ); see Fig. 6.22. In this method, a film-on-substrate specimen is centrally situated along the waveguide. At that, electrical field

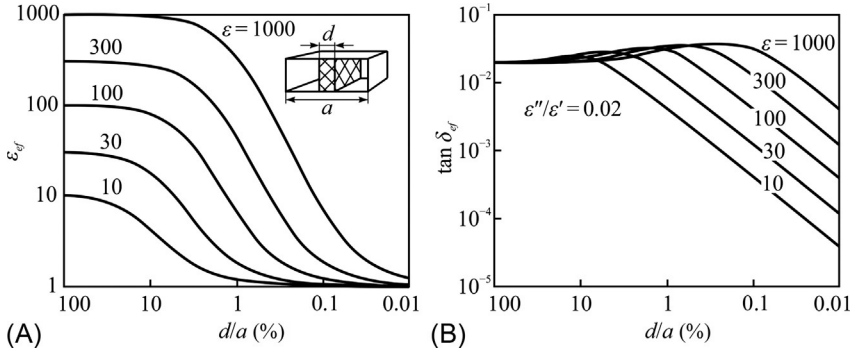


**Fig. 6.21** Effect of upright gaps between specimen and broad walls of waveguide: (A) Effective permittivity; (B) elective loss tangent.

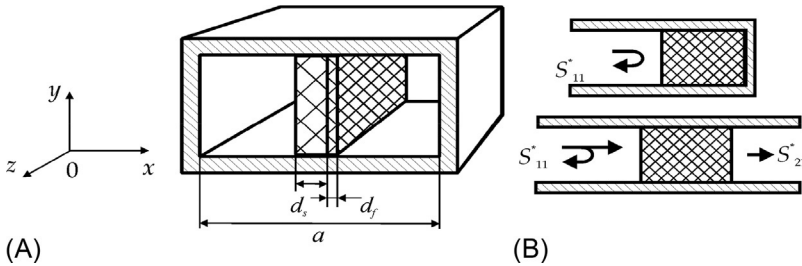


**Fig. 6.22** Schematic representation of experiment for measuring of paraelectric film with  $\epsilon \approx 500$  deposited on a substrate with  $\epsilon = 10$ . (A) Location of the sample in the waveguide. (B) Reflection and transmission coefficient measurement scheme.

intensity is highest in the center of the waveguide, so the highest possible interaction of film with microwave electrical field is provided.

For S-parameter calculations, the electromagnetic field problem can be solved utilizing longitudinal wave representation [44–46]. Applying boundary conditions on media boundaries yields a complex nonlinear equation with respect to complex propagation constant. Numerous experiments with the same samples show reliable repeatability of experiments; the example of measured data is shown in Fig. 6.23, which illustrates fitting data for 0.5-mm thickness MgO substrate and 0.84- $\mu\text{m}$  thick BST film. The average value of substrate permittivity is  $\epsilon_{subs} = 9.9$  while its  $\tan\delta_{subs} = 3 \cdot 10^{-4}$ . As to the film fitting, the calculation exhibits good agreement and yields  $\epsilon_{film} = 450$  and  $\tan\delta_{film} = 0.05$ . Both reflection of a shorted waveguide with a sample and transmission in the two-port system can be used (Fig. 6.22B); however, the first method is preferable because of higher sensitivity.

- The air gap between sample and the broad wall of the waveguide will be the next case, shown in Fig. 6.23. Similarly to the previously discussed situation, the problem of electromagnetic field distribution is solved with a longitudinal wave representation. Applying

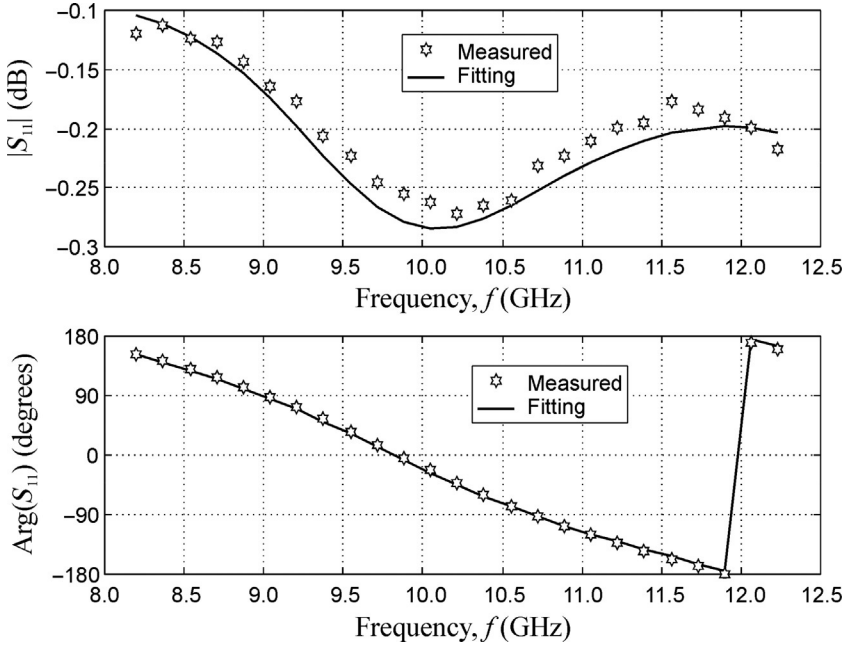


**Fig. 6.23** Measured data and calculation for 0.84  $\mu\text{m}$  BST film on 0.5 mm thickness MgO substrate; specimen length is 2.2 cm.

boundary conditions is studied in the form of equality of tangential components of the electromagnetic field at metallic walls, while the air-dielectric boundary is reduced to a complex nonlinear equation with respect to complex propagation constant:

$$\beta_{ya} \tan(\beta_{ya} - \Delta) + \beta_{ye} \tan(\beta_{ye}(b - \Delta)) = 0,$$

where  $\Delta$  is gap;  $b$  is height of narrow wall of waveguide;  $\beta_{ya} = \sqrt{k^2 - \gamma^2 - \beta_x^2}$  represents the transverse wave number in the air-filled area;  $\beta_{ye} = \sqrt{\epsilon k^2 - \gamma^2 - \beta_x^2}$  is transverse wave number in the dielectric specimen;  $\gamma$  is propagation constant, and  $\beta_x = \pi/a$  is transverse wave number for the basic mode.

Effective permittivity dependence on the air slit is shown in Fig. 6.24A. It is obvious that, if the slot changes, the effective permittivity is modified noticeably, which might be used for a special device, a dielectric phase shifter. An example of an application of this case of a waveguide filling will be considered further in connection with Fig. 6.25.

**3. Tunable dielectric composites with controllable air slit.** One way to achieve controllability of the dielectric characteristics is the *mechanical reconfiguration* of microwave devices. In this case, alteration of microwave device parameters can be attained by the displacement of dielectric or metallic parts of devices. Mechanical

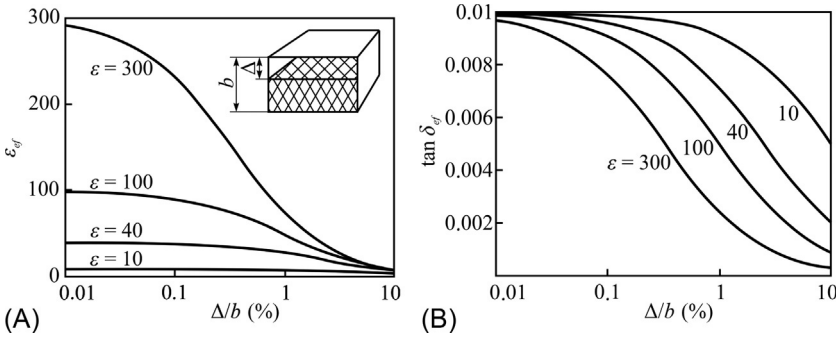


**Fig. 6.24** Effect of horizontal air gap between specimens in waveguide: (A) Effective permittivity; (B) effective loss tangent.

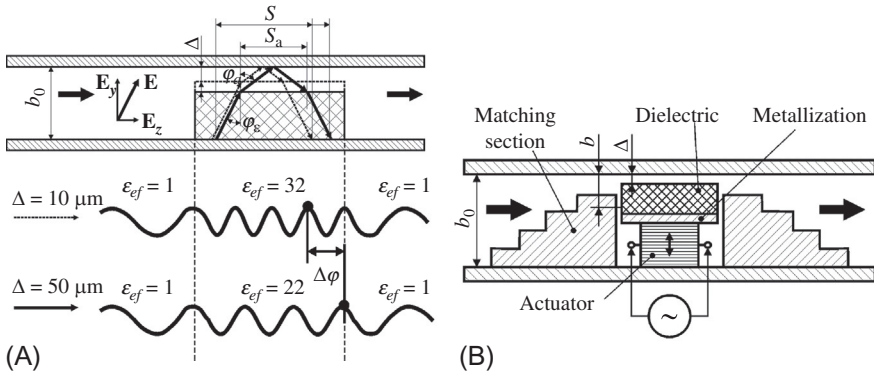


**Fig. 6.25** Waveguide phase shifter: (A) Explanation of phase shift rise at two air slits (10 and 50  $\mu\text{m}$ ); (B) phase shifter design with matching sections and piezoelectric actuator.

tuning is very promising to produce low insertion loss combined with good controllability of microwave subsystems. In the case of ferroelectric permittivity electrical control, microwaves interact with the polar material, which is a part of the microwave line; that is why transmitted energy is partially absorbed in the material. On the other hand, a mechanical control system is located out of the microwave propagation route, so it does not contribute to microwave loss. Moreover, it will be shown that dielectric losses even have a trend to be reduced in such devices. Mechanical control is valid at any frequency range, including millimeter-wave range. The adjustable heterogeneity can be inserted in the part of microwave system in the form of dielectric bodies. The mutual displacement of dielectric bodies in such a system can be used for effective control of electromagnetic characteristics of devices. With the proper design, the displacement of a few tens of micrometers is sufficient for practical applications [47].

One of the trends of modern telecommunication systems development is to use high-tunable components, such as adjustable resonators, phase shifters, etc. These

“active” components can be key elements of smart antennas, phased-array antennas, tunable oscillators, filters, and so on. Many ways are known to design controllable microwave systems, and common physical principles to obtain frequency-agile microwave components can be classified as:

- magnetic means of tuning by permeability of ferrite material,  $\mu(H)$ ;
- electrical means of tuning by permittivity of ferroelectric-type material,  $\epsilon(E)$ ;
- electrical means of tuning by conductivity of semiconductor material,  $\sigma(E)$ ;
- optical means of tuning using conductivity change in semiconductor material,  $\sigma(\Phi)$ ;
- electromechanical reconfiguration of microwave subsystem by displacement  $\Delta$ .

Microwave components using magnetic or electrical tuning, such as  $\mu(H)$ ,  $\sigma(E)$ , and  $\epsilon(E)$ , have a frequency limitation of about 30–40 GHz, because they show increased losses at higher frequencies. Optical tuning that exploits the change in conductivity  $\sigma(\Phi)$  by intensity of the light beam  $\Phi$  also introduces considerable loss in millimeter-wave range. Therefore, the usual tunable microwave components that utilize a material’s intrinsic properties by controlling  $\mu(H)$ ,  $\sigma(E)$ , or  $\epsilon(E)$  have fundamental limitations at millimeter waves. The main reason is that *microwaves interact with functional material* (ferrite, semiconductor, or ferroelectric) which is *part of the microwave line*, so transmitted (or reflected) energy is inevitably partially absorbed in this material.

On the contrary, an *electromechanical system* of control is not a part of the microwave propagation route, so it does not contribute to microwave loss. However, one important disadvantage of mechanical control is the relatively low speed of control. Recent achievements in piezoelectric actuators and MEMS technologies open additional opportunities for combining the advantages of mechanical and electrical tuning techniques. However, for such applications, the tuning system should be highly sensitive to rather small displacements of a device’s components. The key question is how to achieve such *high sensitivity* of a system’s characteristics to *small displacement* of the device parts. This can be realized if partial displacement provides a strong perturbation in the electromagnetic field distribution. For this, a variable dielectric discontinuity (air gap) should be created crossing the path of *electrical field lines*. This tunable air gap should be placed between two dielectric parts or between dielectric and electrode. In this case, alteration of the air gap dimension leads to substantial transformation in the electromagnetic field distribution and changes such characteristics as the resonant frequency, the phase of the propagating wave, and so on [47, 48].

This transformation could be described in terms of a medium’s effective permittivity ( $\epsilon_{ef}$ ). This parameter is very convenient to describe devices with TEM wave propagation, where the propagation constant  $\gamma$  is proportional to  $(\epsilon_{ef})^{1/2}$ ; therefore permittivity can be used to describe tunable devices. For example, effective permittivity of a partially loaded waveguide can be stated as the permittivity of a fully loaded waveguide, which gives numerically the same propagation constant as in a partially loaded waveguide.

**4. Dielectric-air composite phase shifter in a waveguide** uses the basic mode of a rectangular waveguide. To achieve considerable perturbation of an electromagnetic field, the border between dielectric and air is located parallel to the wide wall of

the waveguide, as was shown before in the cross-section in Fig. 6.20B. In the studied example shown in Fig. 6.25, the piezoelectric actuator changes the air slit. When it equals  $\Delta = 10 \mu\text{m}$ , effective permittivity  $\epsilon_{ef} = 32$  and electrical length of the partially filled part of the waveguide contains *four* waves. If the piezoelectric actuator changes the slit to  $\Delta = 50 \mu\text{m}$ , the dielectric-air composite will have  $\epsilon_{ef} = 22$  so the electrical length of the filled waveguide contains *three* waves, and the mechanically controlled phase shift equals  $\Delta\varphi = 2\pi$ .

The permittivity of the movable dielectric is a critical parameter to determine the signal propagation constant: Fig. 6.26 shows an application in this model experiment of various microwave dielectrics that have  $\epsilon = 12\text{--}85$ . There is a refraction caused by the difference in dielectric properties, namely, the traveling wave makes its path in two ways: one is inside the dielectric and the other one is in the air. Moreover, the ratio of the path in the dielectric and in air respectively changes as the air gap varies. Thus, the control over the traveling wave phase shift is obtained by varying that part of the path in which the wave travels in the air slit (outside of the dielectric).

**5. The dielectric-air composite phase shifter with microstrip line** looks more convenient for use in modern microwave systems. Microstrip lines interconnect oscillators, amplifiers, antennas, and so on. Sections of transmission lines are also used as coupling elements for resonators.

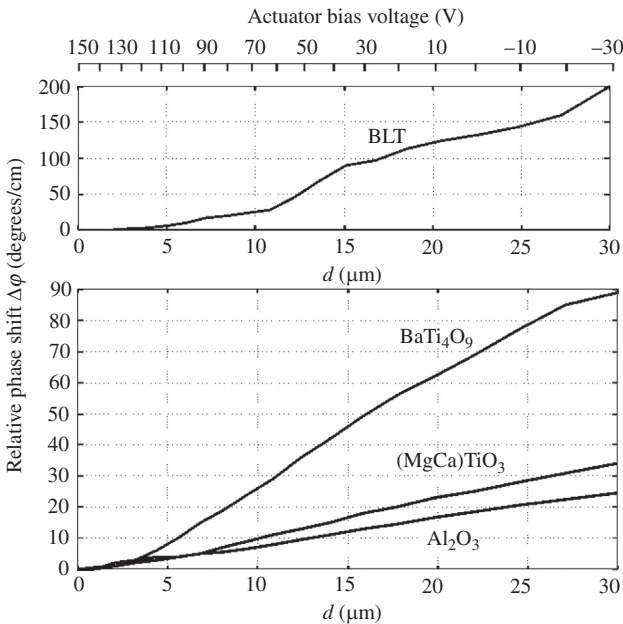


**Fig. 6.26** Measured controlling curves for waveguide phase shifter at frequency of 10.5 GHz with various dielectrics:  $\text{Al}_2\text{O}_3$  ( $\epsilon = 11.6$ ,  $\tan\delta = 0.7 \cdot 10^{-4}$ ),  $(\text{Mg,Ca})\text{TiO}_3$  ( $\epsilon = 21$ ,  $\tan\delta = 2 \cdot 10^{-4}$ ),  $\text{BaTi}_4\text{O}_9$  ( $\epsilon = 37$ ,  $\tan\delta = 3 \cdot 10^{-4}$ ),  $\text{BLT}$  ( $\epsilon = 85$ ,  $\tan\delta = 2 \cdot 10^{-3}$ ).

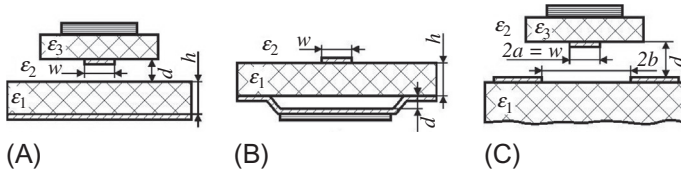


**Fig. 6.27** Profiles of electromechanically controllable microstrip lines (A and B) and coplanar line (C); piezoelectric element is shown by *horizontal touch lines*.

Usually, characteristics of a transmission line are defined at the time of design and remain constant in the fabricated device. However, transmission lines can get some tunability. For example, movement of a dielectric body *above* the microstrip or coplanar line surface results in a propagation constant change. It is possible to show that the most efficient control can be achieved if one of the conductors is detached from the substrate's surface (Fig. 6.27). In this way, a controllable air-dielectric composite is created. Because the tunable discontinuity crosses the electrical field strength lines, it results in high sensitivity.

Principal designs of piezo-driven phase shifters based on microstrip and coplanar lines are shown in Fig. 6.27. Experiments and calculations show that their phase shifting is strongly dependent on the design architecture. It should be noted that designs, shown in Fig. 6.27A and C, need some additional trouble in allocation of the piezoelectric actuator. This problem is much easier in the case of the air slit opened *in the bottom* (ground) electrode, which is partially substituted by the piezoelectric plate (Fig. 6.27B). In all cases, a dielectric discontinuity is created in the plane perpendicular to the electrical field of the microstrip (or coplanar) line.

The propagation constant of the microstrip line at a given frequency  $f$  can be estimated as

$$\gamma = \frac{2\pi f}{c} \sqrt{\epsilon_{ef}},$$

where  $c$  is light velocity. Alteration of the effective permittivity  $\epsilon_{ef}$  due to variation of the air gap having width  $d$  changes the propagation constant, and as a result provides phase shift in a section of the microstrip line. So the main task of device analysis is to determine *effective permittivity* for a prescribed geometrical configuration. This problem was solved numerically using the finite element method. The effectiveness of four different constructions of piezo-tunable phase shifters with microstrip line is verified by simulation and proved experimentally (Fig. 6.28).

As seen, tunability of the microstrip line with a *detached upper electrode* is higher than for the design presented in Fig. 6.28A and B. It is obvious that the designs shown in Fig. 6.28C and D have a higher effect because the dielectric discontinuity is created in the plane perpendicular to the electrical field of the microstrip line. It is necessary to note that tunability of the microstrip line with the disconnected bottom electrode stays between the two discussed designs but closer to the design with the detached upper electrode.

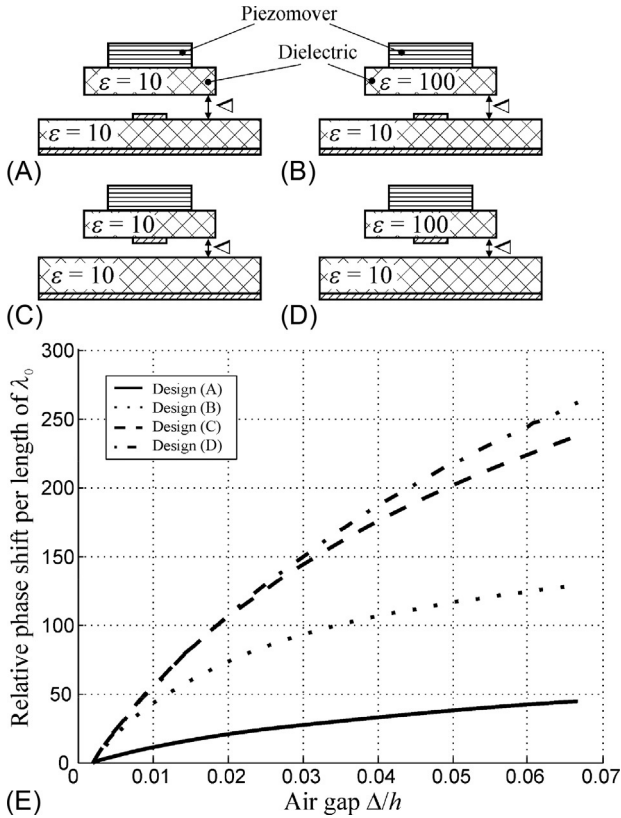


**Fig. 6.28** Tunable microstrip line cross-sections (A–D) and their comparison standardized on wavelength phase shifts (E), shown as function of tunable air gap.

**6. Dielectric-air composite phase shifter with coplanar line** for the most part is more dependent on the substrate than on moving the dielectric above the electrodes. The point is that interelectrode space is the area of highest field concentration. Due to this, the dielectric body, moving up and down above the coplanar line surface (as in Fig. 6.29A), makes only a small perturbation in electromagnetic field distribution.

To increase electromechanical controllability of such a device, it is necessary to arrange tighter dependence of the electromagnetic field on moving dielectric body position. With this purpose, it is proposed to situate a signal strip of coplanar waveguide onto a moving dielectric body and let them lift together (Fig. 6.29B).

Fig. 6.29C shows simulations data for  $50 \Omega$  coplanar lines having Fig. 6.29B design, for the case when dielectric permittivity of both substrate and movable dielectric body is  $\epsilon = 12$ . The qualitative conclusion is that under other same conditions the device with detaching electrode exhibits greater change of effective permittivity, and thus its phase shift more than 1.5 times exceeds that seen in the Fig. 6.29A design. Besides, the curve of phase shift control in the Fig. 6.29B case is less bent.

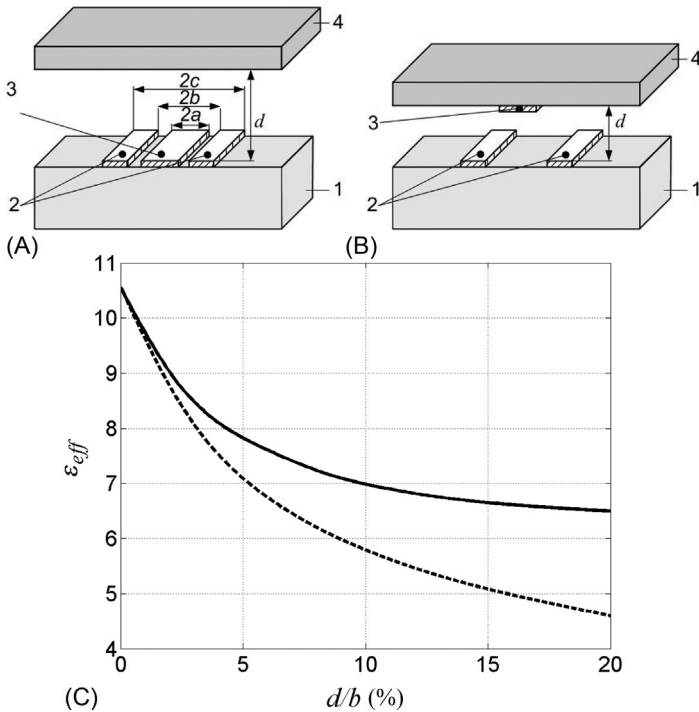


**Fig. 6.29** Coplanar line based phase shifters with signal electrode located on substrate (A) and on moving dielectric body (B): 1—Substrate, 2—ground electrodes, 3—signal electrode, 4—moving dielectric body; (C) effective permittivity of coplanar lines presented in A (solid line) and in B (dashed line) versus normalized air gap.

Obviously, strong perturbation of the electromagnetic field improves controllability of such devices. But quantitatively it depends on the number of design factors, such as line geometry and ratio of substrate and movable dielectric permittivity. As analysis shows, increase of tunable dielectric permittivity leads to an increase of maximum possible relative phase shift for both shown in the Fig. 6.29 designs, though its character is somewhat different. The effect can be explained by the increased role of high-permittivity dielectric, which confines the greater part of the line's electromagnetic field, and thus leads to larger rearrangement of electromagnetic field in the device's cross-section as the dielectric body moves away from the substrate.

The situation becomes different as substrate permittivity is varied. As the substrate's permittivity increases, the smaller is the influence of the moving dielectric. In contrast, with a detached electrode the effect of electromagnetic field redistribution becomes stronger. The absolute values of the latter design exceed their counterparts in times. The presented analysis allows the conclusion that, generally, the low-impedance lines tend to exhibit higher controllability. This can be achieved not only by utilizing high-permittivity material, but with a proper layout as well.

Redistribution of electromagnetic energy to air-filled domains changes also the losses in a system. Because air is almost a lossless medium, a portion of energy confined in air-filled domains experiences practically no dielectric loss. Consequently, more energy reaches the output terminal, resulting in lower effective loss.

**7. A tunable dielectric composite including paraelectric film** is significantly different from previous cases in the method of control used, since it uses not electromechanical but *direct electrical control* by permittivity. At lower frequencies ferroelectrics are well-known tunable dielectric materials; permittivity of these materials can be changed under applied electrical bias field; at microwaves the ability to control permeability in waveguides is also possible. Controllable permittivity leads to alteration of tunable microwave component characteristics, such as propagation constants, resonant frequency, etc. However, dielectric losses in ferroelectric-type tunable components are comparatively high and show substantial increase when approaching to millimeter waves due to fundamental physical reasons [49–52].

A phase shifter based on integrated paraelectric film has advantages in high operation speed, low cost and size, and the possibility of being used in high-frequency microelectronic microwave integrated circuits (MMICs). However, optimal design of such a phase shifter requires simulation; its design should be chosen by comparing various transmission lines used in MMICs. Using simulations of electromagnetic wave transmission in basic MMIC lines (microstrip lines, slotlines, and coplanar lines) a *coplanar line* is chosen as the basic line for a paraelectric film microwave application. The point is that the central electrode of this line is very convenient for applying a controlling (bias) voltage. Microstrip line was rejected because in its planar technology there is a ground electrode problem, while the slotline has the disadvantage of higher radiation loss.

Permittivity control at microwaves by a bias electrical field ( $E_b$ ) is presented in Fig. 6.30B. As shown in the lower insertion, permittivity decreases with the controlling electrical field, and the middle field  $E_m$  corresponds to a middle value of permittivity  $\epsilon_m = (\epsilon_{E=0} + \epsilon_{E_m})/2$ . Permittivity changing  $\Delta\epsilon = \epsilon_{E=0} - \epsilon_{E_m}$  depends on the  $\epsilon$  value. Its relative change of  $\Delta\epsilon/\epsilon_m$  can provide controllable phase-shift runs up to  $2\pi$ .

Field dependence of permittivity is the *dielectric nonlinearity*  $N_\epsilon = \epsilon^{-1}d\epsilon/dE$ , and this parameter increases in a cubic power with  $\epsilon$  value:  $N_\epsilon \sim \epsilon^3$ . So it is obvious that electrical bias field influence is most pronounced near the ferroelectric phase transition, where  $\epsilon$  has a maximum at Curie temperature  $T_C \approx \theta$ . In the vicinity of the temperature maximum, permittivity can be strongly controlled by electrical bias field  $E_b$ , and it is precisely this that is used for microwave-signal phase controlling:  $\epsilon(E_b) = [C/(T - \theta)](1 + aE_b^2)^{-1/3}$ . The bias field at which  $\epsilon$  tunability has a maximum is given by the relation  $E_m = b[(T - \theta)/C]^{3/2}$ . The values of  $a$  and  $b$  are parameters of the material used.

In contrast to ferroelectrics, *paraelectric* material has no domains and no microwave dielectric dispersion. As a result, microwave loss of paraelectric material is not large. A paraelectric is usually considered as a ferroelectric above the Curie temperature  $T_C$ . However, it is more general to define the paraelectric as a dielectric, in which the dielectric constant follows the Curie-Weiss law:  $\epsilon \sim C/(T - \theta)$ , where  $C$  and  $\theta$  are the Curie-Weiss constant and Curie-Weiss temperature, respectively. As pointed out, electrical control by dielectric permittivity is proportional to  $\epsilon^3$ . Because

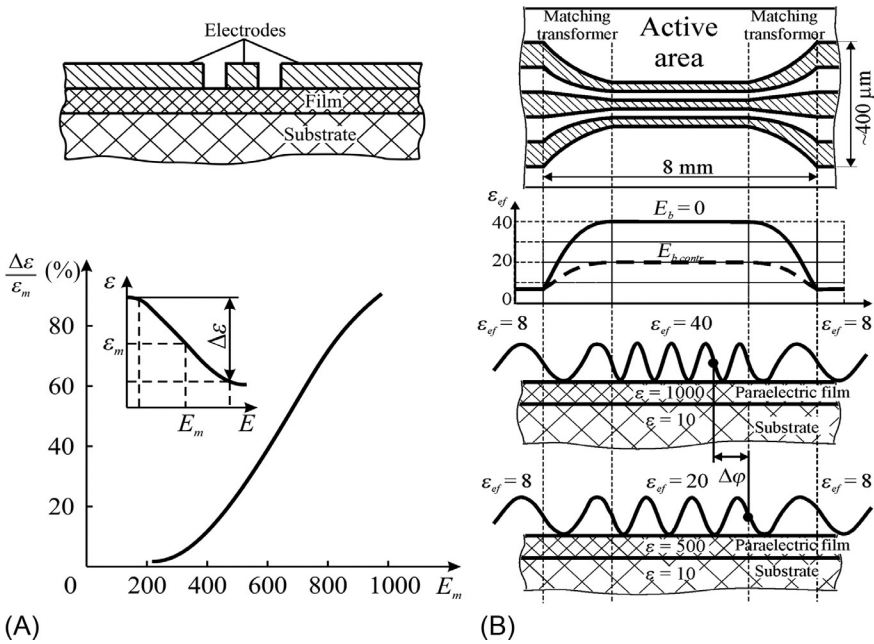


**Fig. 6.30** Coplanar line phase shifter based on paraelectric BST films: (A) (*up*) Cross profile of controllable coplanar line; A (*down*) permittivity handling by electrical field; (B) phase shifter operation.

the  $\epsilon$  value in paraelectric film is lower than in bulk material, this is obviously accompanied by a decrease of  $\epsilon$  tunability. However, a smaller  $\epsilon$  is quite desirable for microwave applications, to increase impedance of the tunable part of the transmission line. Thus, phase shifter elaboration needs to compromise between  $\epsilon$  magnitude and  $\epsilon$  tunability of the chosen paraelectric layer. Additional compromise is needed between film tunability and microwave loss.

Recently, the processing of ferroelectric and paraelectric thin film has become of acceptable quality. As a result, tunable microwave devices based on paraelectric film can be competitive with microwave ferrite and PIN diodes. To compare with microwave ferrite devices ( $\mu$ -controlling) and semiconductors ( $\sigma$ -controlling), the advantages of paraelectrics ( $\epsilon$ -controlling) are: essentially more rapidity, increased microwave power, good matching with semiconductor-based MMIC technology, and the possibility for use of paraelectric devices at much higher frequencies.

The design of a paraelectric phase shifter requires simulation. As shown in Fig. 6.30, a phase shifter consists of five important components: paraelectric thin film, dielectric substrate, electrodes, interfaces film/electrode, and film/substrate. To obtain desirable microwave performance (phase shift  $\Delta\phi$ , insertion loss  $I_L$ , impedance  $Z_0$ , etc.), the design of a paraelectric film phase shifter can be elaborated exceptionally with use of simulation. Exclusively using optimization, the required active and passive dielectric layers as well as metallic guide collocations could be obtained.

A tunable coplanar line is formed by electrodes deposited on a film-on-substrate surface (Fig. 6.30). Electrode collocation has a strong influence on line impedance  $Z_0$  and effective permittivity  $\epsilon_{ef}$ . Simulations show that, for practical purposes, there is no considerable difference in the values of  $Z_0$  and  $\epsilon_{ef}$  for buried electrodes and electrodes deposited onto film. In our experiments, gold electrodes were deposited as chemically inert and high-conductivity material.

The functioning mode of a coplanar line phase shifter is explained in Fig. 6.30. The main principle of phase shifter operation is control over the propagation constant in the microwave line. Toward this end, MMIC substrate with  $\epsilon_s \sim 10$  (silicon, gallium arsenide, magnesium oxide, etc.) is covered by a thin paraelectric film and next by electrodes that actually form the coplanar line. Film permittivity is changed within the limits of  $\epsilon = 1000\text{--}500$  by bias  $E_b$  voltage. As a result, effective permittivity of the composite (film + substrate + air) is controlled in the range of  $\epsilon_{ef} = 40\text{--}20$ . The coplanar design evidently shows the advantage of the composite structure: the pure paraelectric with its middle  $\epsilon \sim 700$  reflects practically 100% of the microwave signal, while the created composite has the middle  $\epsilon \sim 30$ , which is possible to match with the passive part of the coplanar line.

The operation mode of the phase shifter shown in Fig. 6.30 consists of electrical change of the electrical length of the line in its active area. It varies proportional to  $(\epsilon_{ef})^{1/2}$ , which produces the required phase change  $\Delta\varphi$ . If  $E_b = 0$ , the active area of the phase shifter has electrical length equal to four waves; under the bias field it decreases to three waves, which generates a  $2\pi$  phase shift. The matching areas are used to join the low-impedance active area with the other coplanar line (Fig. 6.30), and this is a quite necessary part of the device. Using a network analyzer, a broadband matching of the 5–10  $\Omega$  phase shifter active area with 50- $\Omega$  line should be applied. The novelty of this broadband matching transformer is that it uses the *same film* in which  $\epsilon_{ef}$  is controlled by the same bias voltage. This results in *self-acting trimming*, correspondingly to the actual phase shift. Moreover, the applied transformers are quite long (being broadband) and they represent the exponent taper transformer.

## 6.5 Resonances in dielectric-air slit structures

Microwave dielectric resonators (DR) can be used in a wide variety of microwave devices as an important part of microwave filters, for oscillator frequency control, etc. Dielectric resonators are made from low-loss microwave ceramics ( $\tan\delta \sim 10^{-4}$ ) with high and thermally stable permittivity. In the *decimeter* wave range (cellular phones, ATC transponder space telemetry, airport search radars) the preferred value of DR permittivity is  $\epsilon = 150\text{--}80$ ; in the *centimeter* wave range (military radars, satellite communication down, STL microwave relay, etc.) DR permittivity usually is  $\epsilon = 50\text{--}20$ ; closer to *millimeter* waves (police and car radars, satellite communication up, GPS systems, missile seekers) the permittivity of DRs decreases.

Next, some possibilities of *electrical control* by resonant frequency of a dielectric resonator will be discussed. This control is implemented in tunable macrocomposites of the “dielectric-air slit” type, which can be used in frequency-agile microwave devices.

**1. A frequency tunable DR based on a dielectric-air slit structure** saves a high-quality  $Q$  factor, with the ability to change resonant frequency in a wide range important for microwave subsystems. It is also remarkable that electromechanical control by DR frequency is applicable in *any frequency range*, including millimeter waves. In any other frequency-agile method of tuning, microwaves interact with “active” material (ferrite, semiconductor, or ferroelectric), which is the inside part of the device, so microwave energy is inevitably partially absorbed by this material. However, electromechanical contrivances used for frequency tuning are located *outside* of the microwave path, so this does not lead to microwave losses in tunable devices.

Mechanical rearrangement of a microwave device is based on controlled change of a distance  $\Delta$  between its parts and can be classified as:

- macromechanical reconfiguration in microwave system ( $\Delta \sim \text{cm}$ );
- mechanical reconfiguration by piezoelectric cantilever ( $\Delta \sim \text{mm}$ );
- **mechanical reconfiguration by fast piezo-microactuator** ( $\Delta \sim 50 \mu\text{m}$ );
- microelectromechanical microwave devices, RF MEMS ( $\Delta \sim 5 \mu\text{m}$ ).

*Macromechanical* rearrangement means that microwave device frequency control is based on the displacing of a metallic or dielectric component inside of a waveguide or resonant cavity in order to change microwave device parameters. This is a very slow (quasistatic) mode of controlling. Faster, but also limited in response time ( $10^{-3}$  s), is the use of the *piezoelectric cantilever*, for instance, for electromechanical tuning of a dielectric resonator. On the other hand, *RF MEMS* are the most contemporary devices, but they utilize electrostatic attraction between two microscopic metallic layers; such a peculiar mode of tuning might have problems with outside humidity, vibrations, and designs.

That is why the following discussion focuses only on piezoelectric microactuator applications for controlling by microwave *resonant devices*. Very fast ( $10^{-5}$  s) and miniature piezoelectric actuators are elaborated and tested for dielectric resonator tuning. Modern piezoelectric actuators made of *electrostrictive* materials show no hysteresis. Moreover, they work with relatively small displacement (usually less than  $100 \mu\text{m}$ ) but with high accuracy (about  $0.01 \mu\text{m}$ ). Fortunately, millimeter-wave devices for tuning purposes require a displacement range of only  $10 \mu\text{m}$ ; so microwave tunable devices should be much smaller, and their response will be much faster.

To make use of advanced actuators at microwave frequencies, a new design for some tunable microwave dielectric components is elaborated. The key idea is to provide a *strong perturbation* in the electromagnetic field in the region influenced directly by mechanical control. For that, a tunable discontinuity (air gap) is created perpendicular to the pathway of the electric field lines. This air gap is placed between dielectric plates or between dielectric plate and electrode. In addition, to decrease the air gap thickness required for tuning, dielectrics with higher permittivity should be utilized.

The principle of electromechanical control is shown in Fig. 6.31 with the use of a tunable dielectric composite, in which not an intrinsic property of the material but rather the effective dielectric constant  $\epsilon_{ef}$  of the reconfigured system might be efficiently controlled. By means of a low-voltage piezoelectric mini-actuator, the gap

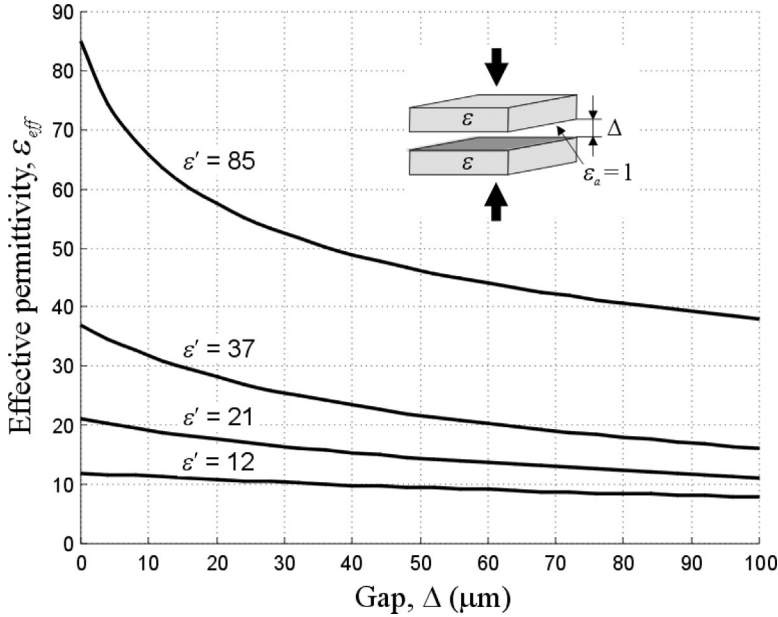


**Fig. 6.31** Effective dielectric constant of dielectric-air composite with dielectric plates with thickness of 1 mm and  $\epsilon = 85, 37, 21, 12$ .

between two dielectric plates is changed. As a result, the effective dielectric constant  $\epsilon_{\text{eff}}$  of the sandwich-type structure strongly varies. The functioning mode of the device shown is similar to the ferroelectric phase shifter, but instead of using ferroelectric having  $\epsilon(E)$  by applying a large voltage, a much lower  $\epsilon_{\text{eff}}$  is governing by low voltage. Moreover, this artificial tunable microwave dielectric (which forms an air-layered composite) has low insertion loss up to millimeter waves, inclusively.

One of the examples is two cylindrical DRs with the  $H_{018}$  mode separated by the air gap  $\Delta$  constituting a *binary DR* [53]. Note that in this binary design, electrical field lines inside the DR are oriented *in parallel* to the air gap. The change of slit  $\Delta$  leads to a not very large alteration of resonant frequency (only several percent; see Fig. 6.32C). The tunability  $\Delta f/f_0$  in this case is much less than the tunability of the slot DR (SDR) shown in Fig. 6.32B, where the electrical field lines are perpendicular to the air gap.

An example of SDR testing is shown in Fig. 6.32D. It is remarkable that no change in quality factor  $Q$  is observed during air gap alteration. Therefore discontinuity in the SDR creates a noticeable perturbation of the electromagnetic field, and, as a result, it significantly shifts resonant frequency Fig. 6.32C. The resonant frequency of basic mode changes up to 10%, while displacement of SDR parts is no more than tens of micrometer depending on wavelength band and permittivity of SDR material. This range of displacement is achievable for modern piezo-actuators and MEMS.

Controllability of the resonant composite SDR can be explained as an alteration of its effective permittivity  $\epsilon_{\text{eff}}$  (Fig. 6.33). In the considered case, the value of  $\epsilon_{\text{eff}}$  decreases two times; correspondingly, the SDR resonant frequency increases up to

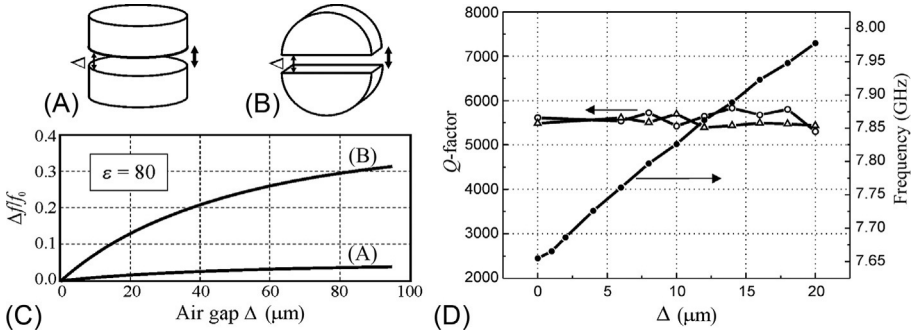


**Fig. 6.32** Dielectric resonator mechanical tuning at 10 GHz: (A) Gap parallel location for binary resonator; (B) gap perpendicular location for slot resonator (SDR); (C) tunability comparison; (D) resonant frequency  $f_0$  and  $Q$ -factor of slot dielectric resonator versus gap thickness.

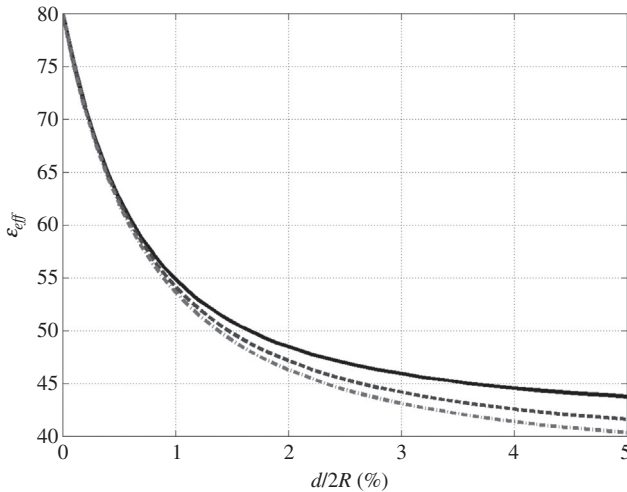


**Fig. 6.33** Effective permittivity versus normalized value of air gap between two parts of disk DR for certain ratios of resonator thickness to its diameter: 0.3 (solid line); 0.5 (dashed line); 0.7 (dash-dot line). Permittivity of dielectric material is equal to 80;  $R$  is DR radius while  $h$  is DR thickness.

30% or higher. At that, controllability slightly rises with the increasing ratio  $h/R$ , where  $R$  is SDR radius and  $h$  is its thickness.

One advantage of such a method of frequency control is the preservation of high  $Q$ -factor. Unloaded quality factor can be expressed as follows:  $Q^{-1} = T \tan \delta$  where  $T$  is energy filling factor, dependent only on permittivity and domain size, and  $\tan \delta$  is the loss tangent of the dielectric material. Factor  $T$  shows a trend to decrease versus gap width increases due to electromagnetic energy accumulation in a gap. As a result, intrinsic  $Q$ -factor of SDR can even rise with resonant frequency increase.

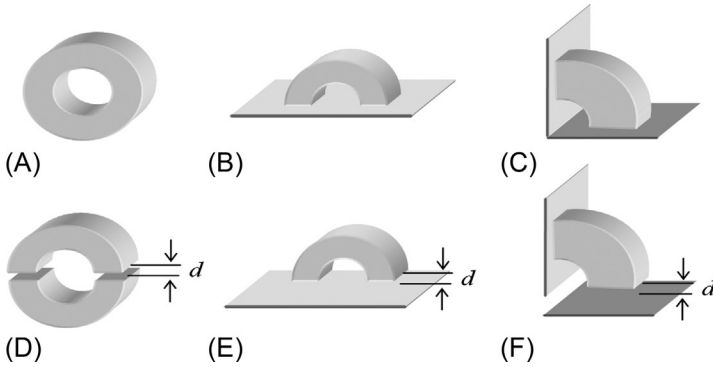


**Fig. 6.34** Passive and tunable ring-type dielectric resonators: (A) Usual DR; (B)  $\frac{1}{2}$  DR reflected in mirror; (C)  $\frac{1}{4}$  DR reflected in two mirrors; (D) tunable ring DR cut on two halves with a controlling slot between them; (E)  $\frac{1}{2}$  DR reflected in a movable mirror; (F)  $\frac{1}{4}$  DR with one movable mirror (moved by actuator).

Some designs of SDRs (and possibilities of their applications) might be diversified by using *reflections* in the metallic mirror (Fig. 6.34). Passive DRs (A, B, C) decrease their size by two times (B) by reflection in one mirror, and by four times (C) by reflection in two mirrors (this is important if one needs to decrease the size of resonant filters based on several DRs).

In the case of frequency-tunable resonators, this method of SDR size decrease can be employed (Fig. 6.34D–F). In this case, it is possible to decrease by two times the thickness of the controllable slot (which might be important for controlling). However, in this case the quality factor of such “imaginary DR” essentially decreases.

In Fig. 6.35 various designs of composite DRs are analyzed to calculate cardinal parameters and to investigate optimal components and materials properties. Among

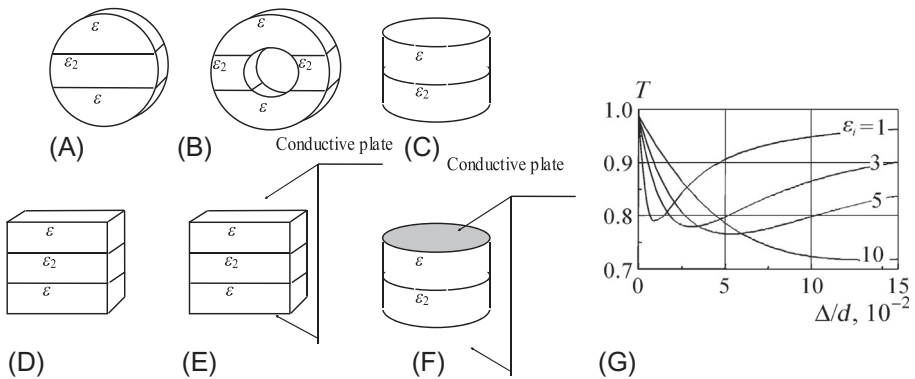


**Fig. 6.35** Different SDRs: (A and C) Disk DR; (B) ring DR; (D and E) rectangular DR; (G) energy filling factor for rectangular split DR:  $\Delta$  is gap thickness,  $d$  is DR thickness; most sensitive change in energy filling with normalized slit  $\Delta/d$  is the case of  $\epsilon_i = 1$ .

them there are *cylindrical* and *ring* resonators as well as *rectangular* resonators. An important parameter is the energy filling factor (Fig. 6.35G). It is obvious that air gap shows its greatest sensitivity in the case of  $\epsilon_i = 1$  (just this circumstance is used in tunable SDR).

**2. Slit DR for measurements and self-stabilization.** Slot dielectric resonator may be applied also to measure loss factor and dielectric constant of thin film materials, including their temperature characteristics. Many kinds of bonding agents, thin polymer packaging, and other thin flexible materials are used in the microwave technique and they need their comparison by properties. Nonorganic film properties are also of interest for microwave applications. Being placed in a gap between two parts of SDR, the film studied changes both DR resonant frequency  $f_0$  and quality factor  $Q$ , which makes it possible to calculate the dielectric parameters of a film.

In the study of SDRs, one very interesting circumstance was discovered: they can provide temperature stabilization of resonant frequency in spite of being made of non-thermostable dielectrics. As was discussed in Section 6.2, the simple microwave dielectrics rutile ( $\text{TiO}_2$ ) and perovskite ( $\text{CaTiO}_3$ ) have  $\epsilon \geq 100$  and a large enough  $Q$ -factor. They would have interest for applications in the decimeter range of microwaves, if they were thermally stable; however, these dielectrics have rather big and *negative* thermal coefficients of permittivity ( $TC\epsilon$ ).

It is shown that even in this case rather good thermal stability of SDR *resonant frequency* can be achieved using special designs of these resonators combined with thin plate silica substrate. The *positive* thermal expansion coefficient  $\alpha_T$  compensates the large negative  $TC\epsilon$ . At that, a high  $Q$  factor is preserved as well as a small size of SDR design. One of the possible designs of “self-stabilized” SDR is shown in Fig. 6.36. Both parts of the SDR are stuck onto a thin silica substrate in such a way that thermal deformation of DR material can decrease or increase the narrow air gap. The extremely high sensitivity of SDR resonant frequency to the size of this gap is used for thermal self-compensation. The resonant frequency temperature coefficient ( $TCf$ ) of SDR is a function not only  $TC\epsilon$  but thermal expansion coefficient  $\alpha_T$  of the material used as well. When temperature changes, the change of SDR

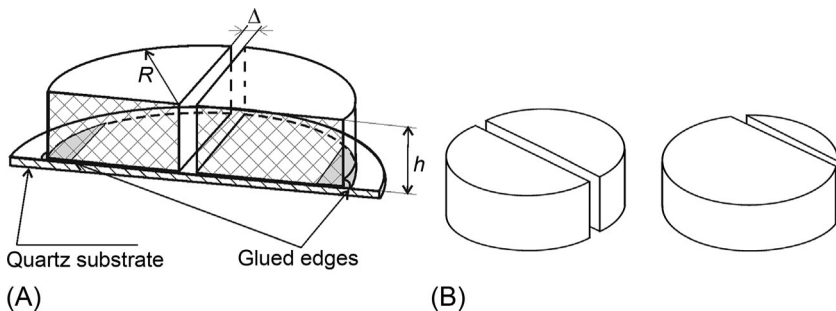


**Fig. 6.36** Cross-section of SDR consisting of two identical parts (A) and nonsymmetric SDR (B).

dimensions compensates  $TC\epsilon$ . As in the calculations, so the experiments show that in special designs it is possible to obtain  $TCf \approx 0$  in spite of big  $TC\epsilon$  of used material.

Experimental verification has been carried out with many designs of SDR. Different ways of fastening the resonator parts, various glues, and the areas covered with glue were tested. It is possible to increase the applicability of the proposed method by using some constructive alterations. For example, the symmetric position of the slit in the resonator was changed to a nonsymmetric one (Fig. 6.36A). It is possible also to modify the method of fastening, using bonding components with various thermal expansion coefficients, etc. A number of other papers have shown wide possibilities for using dielectric resonators for measuring film properties [54–57].

**3. A frequency tunable filter controlled by a “dielectric-air gap” composite** can be realized, as in a waveguide, so with a microstrip line. The SDRs controlled by the piezoelectric actuator provide an opportunity to realize a high-quality frequency tunable microwave filter in which the central frequency and the shape of attenuation-frequency characteristic is controlled electrically with a rather fast response.

Based on these concepts, as with the bandpass, so the bandstop frequency tuned filters were realized (Fig. 6.37). These filters have wide alteration bandwidth (20%–30%) and high quality factor  $Q$  which remains stable while the filter undergoes electromechanical control.

**4. A band-transmitting filter design integrated with stripline** and its characteristics are shown in Fig. 6.38 (experimental data were obtained with a network analyzer). The filter is arranged on a right-angled alumina substrate on which two impedance step resonators are deposited: the length of resonator was 22 mm, ratio between high and low impedance parts  $\sim 10$ , substrate thickness was 0.65 mm, substrate dielectric constant  $\epsilon = 9.2$ .

The technique used for tuning is capable of transforming any microstrip filter into a frequency agile device. With this purpose, the substrate, located under the microstrip device, becomes a “tunable dielectric” (Fig. 6.38). With the purpose of tuning, the substrate located under the filter imitates a “tunable dielectric.” Namely, the part of ground electrode (just under the filter) is removed, and it is replaced by the metallic membrane moved by the piezoelectric actuator, Fig. 6.39A. The thickness of air gap ( $\Delta$ ) is piezoelectrically controlled. During controlling, the scope of the air slit is changed.

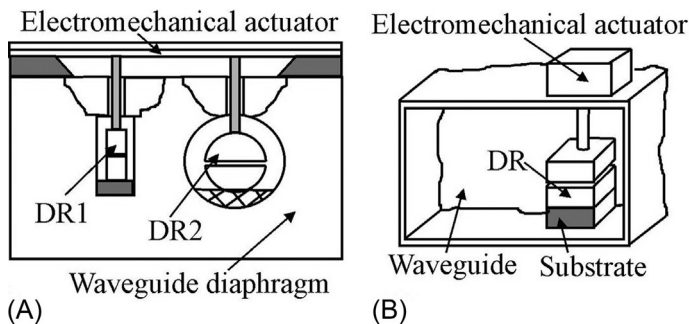


**Fig. 6.37** Tunable SDR filters: (A) With two ring-type DRs; (B) with rectangular SDR.

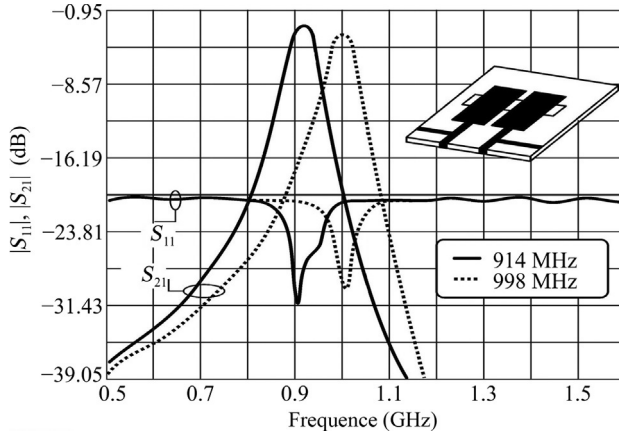


**Fig. 6.38** Two-resonator tunable filter design and characterization.

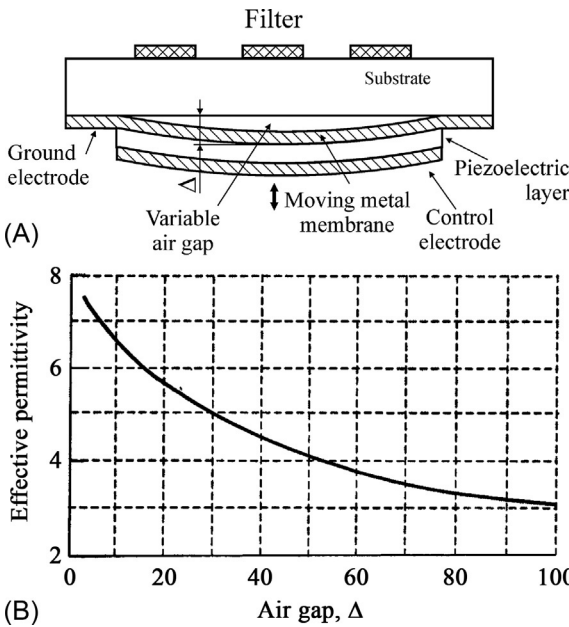


**Fig. 6.39** Principle of effective permittivity tuning by movable substrate: (A) Side view of piezo-moving ground electrode under substrate; (B) changing of substrate  $\epsilon_{ef}$  with air gap thickness in the case of alumina substrate ( $\epsilon_{snb} \approx 10$ ) with thickness  $h = 0.65$  mm.

Such a “tunable substrate” can be described as a dielectric-air composite in which effective permittivity is controlled (Fig. 6.39B). The scope of the  $\epsilon_{ef}$  change depends on substrate permittivity and relationship  $\Delta/h$  where  $\Delta$  is air gap and  $h$  is substrate thickness. In experiments, the effective permittivity of the layered dielectric “alumina-air” decreases from  $\epsilon_{ef} \approx 7$  to  $\epsilon_{ef} \approx 3$ , while the air gap changes from  $\Delta \sim 10 \mu\text{m}$  to  $\Delta \sim 100 \mu\text{m}$  under a controlling voltage of about 300 V.

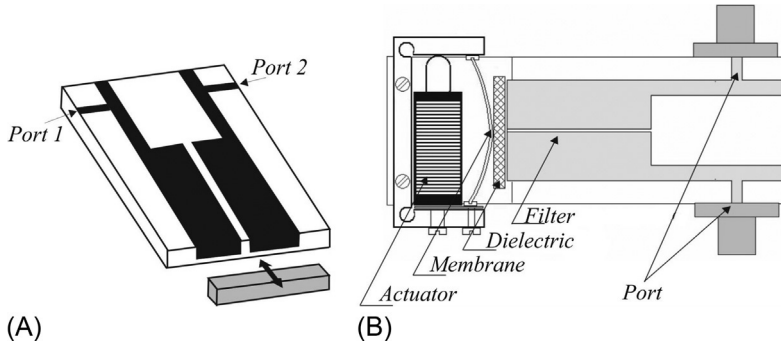


**Fig. 6.40** Frequency tunable microstrip filter: (A) Dielectric bar movement near the end of the resonator; (B) device in assembly with stack actuator.

Therefore, using high-quality microwave dielectrics, it is possible to realize low-loss filters in centimeter and millimeter waves. Tunable dielectric-air structures were studied as in the rectangular waveguide, so in some microstrip and coplanar designs. This way of controlling allows increasing of a device's controllability while maintaining low loss. Simulations were verified and proven by experiment. By scaling and moving to higher frequencies, the required displacements could be reduced to tens of micrometers, thus allowing utilization of small and fast piezo-actuators or MEMS.

**5. A band-transmitting filter controlled from the end** also shows high efficiency of electrical control by resonant frequency. As shown in Fig. 6.40, a dielectric plate with high dielectric permittivity moves near the end part of a filter: this changes the electromagnetic coupling between the resonator and the plate.

The experiment was carried out using a microwave low-loss dielectric with  $\epsilon = 80$ ; to reduce the control voltage, a multilayer stack-actuator was used, the field-controlled deformation of which was amplified by a membrane. The filter can be tuned in the range of 520–580 MHz, while in the bandwidth of the filter the phase of passing signal changes by more than 100 degrees. Many other variants of the piezo-electric control of microwave devices were also proposed and offered [57–61].

From these examples it follows that the methods of piezoelectric control of microwave devices can be quite diverse. Their main difference is the lack of any insertion loss and rather high speed.

## 6.6 Summary

1. Microwave dielectrics are basic materials for microelectronics; they are widely applied as passive microwave components, and as active elements of microwave technique. Of particular importance are microwave dielectrics with *high permittivity*: these nonpolar dielectrics serve as a basis for low-loss materials while polar dielectrics are a basis for microwave-absorbing materials.
2. *Linear thermal stable* dielectrics are the main class of microwave dielectrics applied as miniature capacitors, dielectric resonators, and substrates for microwave circuits, reducing

planar dimensions of devices by  $\epsilon$  times. In their composition any polar-sensitive dielectric should be avoided. *Pliable microwave substrates* are needed for flexible (rubbery) electronics when devices should be stretchable, twistable, and deformable, which looks impossible using rigid microwave substrates.

3. *Nonlinear* microwave dielectrics with electrically controlled permittivity  $\epsilon(E)$  can be used in microwave phase shifters and tunable filters. They use polar-sensitive paraelectrics capable of transitioning to a polar state under external influences; their nonlinearity is accompanied by increased dielectric losses and significant change in permittivity with temperature.
4. For microwave electronics, the first important problem is how to obtain *high permittivity* and *low loss* microwave dielectrics: in other words, finding a way to combine high permittivity in the microwave range with polar phase absence in a dielectric. The second, also difficult, problem is to obtain a very high *thermal stability* of permittivity, which has to be greater than the stability of the initial components of the microwave dielectric.
5. Increased permittivity at microwave frequency can be obtained, using displacive type paraelectrics as basic material, the structure of which is characterized by low-frequency transverse lattice optical mode. At that, only “hard” types of paraelectrics, in which no polar phase (main cause of dielectric losses) can arise, should be applied as components of low-loss dielectrics.
6. Small dielectric losses can be reached only in single-phase compositions; moreover, the composition of low-loss microwave dielectrics must be free from a polar-sensitive phase, which increases dielectric losses.
7. High thermal stability in low-loss microwave dielectrics designed for use in the centimeter-wave range ( $\epsilon = 30 \pm 10$ ) can be obtained in structures where the coordination of highly polarizable structural units (for example, oxygen octahedra) is technologically disrupted by introduction of oxides with large cation size.
8. Microwave dielectrics with increased permittivity ( $\epsilon = 100 \pm 40$ ) can be thermally stabilized when the paraelectricity of the basic material is suppressed by paramagnetism of an introduced component. At that, the composition of low-loss thermal stable microwave dielectrics must be ensured free, using all possible means, from polar-sensitive phases leading to dielectric loss increases.
9. At microwave frequencies, the dominating mechanism of dielectric losses arises from the polar-sensitive phase existence. In the case of mixed covalent-ionic bonds between atoms, atomic equilibrium potential manifests a pronounced anharmonic character, which is a main microscopic channel to transfer microwave energy into heat (dielectric losses).
10. Anharmonic potential between ions results in the coupling between optical phonons (excited by electrical field) and acoustical phonons (which is represented in a crystal “heat reservoir”). With increasing temperature, and, consequently, with increase in the amplitude of ion vibration, the manifestation of anharmonic bonding between atoms becomes more noticeable and dielectric losses increase.
11. *Microwave composites* are represented by a wide variety of materials for various purposes. The composite is a multicomponent system in which several materials of different structure are combined in order to obtain certain properties of the final material. At the same time, components of the obtained composite do not enter into chemical reactions, but retain individual properties, forming interfacial boundaries.
12. *Low microwave reflection coatings* are especially important in military electronics and therefore their composition and technology are usually not described in detail. These *absorbent materials* are also a subject of modern research. For them it is necessary to have large dielectric losses even in thin layers, in order to provide almost complete attenuation of microwave irradiation.

13. *Flexible absorbing shielding composites* have important application in microwave electronic materials. Shielding absorbers of radiation are pliable and light materials necessary to protect electronic equipment from interference and to reduce risks to human health.
14. Composite dielectrics extend the choice of various microwave materials, combining peculiar properties of different components to obtain necessary technical specifications. Microwave composites may be divided into “passive” (which do not change their parameters during operation) and “functional” composites with electrically controlled properties that can be used for frequency tunable devices.
15. A “passive” dielectric macrocomposite consists of several dielectrics representing a non-uniform dielectric structure, manufactured from components having different electrical properties. Their behavior in microwaves differs significantly from the composite’s properties at low frequencies.
16. Functional macrocomposites may include a *paraelectric film* deposited on a substrate with electrically tunable permittivity. This kind of layered composite may be used in various microwave devices, but is most common in the phase shifter, capable of fast handling by a bias electrical field.
17. Tunable dielectric composites with *controllable air slit* permits controllability of dielectric characteristics by *electromechanical reconfiguration* of microwave devices. In this case, the alteration of microwave device parameters can be attained by displacement of dielectric parts of the device.
18. A dielectric-air gap composite makes it possible to realize a *phase shifter* with a microstrip line, which appears to offer more convenience for use in modern microwave systems. Such a composite phase shifter can be obtained also in a coplanar line, with the dielectric body moving up and down above the surface of the coplanar line.
19. A tunable dielectric composite including paraelectric film makes *direct electrical control* of permittivity possible by an applied electrical bias field. Field dependence of permittivity is dielectric nonlinearity:  $N_e = \varepsilon^{-1}d\varepsilon/dE$ ; this parameter increases in cubic power with  $\varepsilon$ -value:  $N_e \sim \varepsilon^3$ .
20. It is possible to electromechanically realize electrical control of the *resonant frequency* of a dielectric resonator (DR) and various filters. This control is implemented in tunable macrocomposites of the dielectric-air gap type, which might be used in frequency-agile microwave devices. The main advantage of such a method of frequency control is preservation of a high  $Q$ -factor.

## References

- [1] M.T. Sebastian, *Dielectric Materials for Wireless Communication*, Elsevier, 2008.
- [2] M.T. Sebastian, R. Uvic, H. Jantunen, *Microwave Materials and Applications*, Wiley, 2017.
- [3] A.G. Belous, *Microwave dielectrics based on complex oxide systems*, in: *Dielectric Materials*, In-Tech. ISBN: 978-953-51-0764-4, 2012, pp. 113–143.
- [4] Y.M. Poplavko, Y.V. Prokopenko, *Ferroelectrics study at microwaves*, in: *Ferroelectrics; Characterization and Modeling*, In-Tech. ISBN: 978-953-307-455-9, 2011, pp. 203–226.
- [5] Y.M. Poplavko, *Dielectric Spectroscopy of Solids; Basic Theory and Method Application*, LAMBERT Academic Publishing, 2013.
- [6] V.V. Meriakri, V.N. Ushatkin, Y.M. Poplavko, *Anisotropic ferroelectrics applications at near-millimetre waverange*, *Radiotekh. Elektron.* 17 (1) (1972) 209.
- [7] Y.M. Poplavko, *Microwave dielectric dispersion mechanisms in ferroelectrics of BaTiO<sub>3</sub> type*, *Izv. Akad. Nauk SSSR Ser. Phys.* 29 (11) (1965) 2020.

- [8] Y.M. Poplavko, V.G. Tzikalov, Ferroelectrics at frequency range of 50–80GHz, *Izv. Akad. Nauk SSSR Ser. Phys.* 33 (7) (1969) 1119.
- [9] Y.M. Poplavko, V.G. Tzikalov, V.I. Molchanov, Microwave dielectric dispersion in paraelectric phase of barium titanate crystals, *Phys. Tverd. Tela* 10 (11) (1968) 3425.
- [10] A.G. Belous, Microwave dielectrics with enhanced permittivity, *J. Eur. Ceram. Soc.* 26 (2006) 1821–1826.
- [11] K. Wakino, K. Minai, H. Tamura, Microwave characteristics of (Zr,Sn)TiO<sub>4</sub> and BaO–PbO–Nd<sub>2</sub>O<sub>3</sub>–TiO<sub>2</sub> dielectric resonator, *J. Am. Ceram. Soc.* 67 (1984) 278–281.
- [12] Y.M. Poplavko, Microwave high dielectric constant ceramics (invited lecture), in: *Proc. Int. Conf. “Electroceramics-V”*, Portugal, vol. 1, 1996, pp. 51–60.
- [13] Y.M. Poplavko, Overview: dielectric permittivity dispersion in ferroelectrics, *Izv. Akad. Nauk SSSR Ser. Phys.* 34 (12) (1970) 2572.
- [14] A. Belous, O. Ovchar, D. Durilin, M. Macek-Krzmanc, M. Valant, D. Suvorov, High-*Q* microwave dielectric materials based on spinel Mg<sub>2</sub>TiO<sub>4</sub>, *J. Am. Ceram. Soc.* 89 (2006) 3441–3445.
- [15] Y.M. Poplavko, Microwave dielectric dispersion in displace type ferroelectrics at the millimetre wavelength, *Ukr. Fiz. Zh.* 14 (12) (1969) 1602.
- [16] Y.M. Poplavko, V.G. Tzikalov, Millimetre wave dielectric dispersion in ferroelectrics and antiferroelectrics above Curie point, *Izv. Akad. Nauk SSSR Ser. Phys.* 34 (12) (1970) 2586.
- [17] A.S. Knjazev, Y.M. Poplavko, A.S. Zakharov, Far infrared spectra of SrTiO<sub>3</sub> crystals and ceramics, *Izv. Akad. Nauk SSSR Ser. Phys.* 35 (9) (1970) 1816.
- [18] A.S. Knjazev, Y.M. Poplavko, A.S. Zakharov, Vibrational spectrum of rutile crystal, *Phys. Tverd. Tela* 15 (8) (1973) 2371.
- [19] Y.M. Poplavko, Temperature dependence of soft mode frequency and damping in various ferroelectrics, *Ferroelectrics* 21 (1–2) (1978) 399.
- [20] Y.M. Poplavko, Dielectric dispersion in barium titanate below and above Curie point, in: *Abstr. Second Intern. Meet. Ferroelectricity*, Kioto, 1970, p. 244.
- [21] Y.M. Poplavko, A.S. Knjazev, Soft mode in vibrational spectrum CaTiO<sub>3</sub>, *Phys. Tverd. Tela* 15 (10) (1973) 3006.
- [22] Y.M. Poplavko, V.V. Meriakri, E.F. Ushatkin, Near-millimetre waverange study of BaTiO<sub>3</sub>, *Phys. Tverd. Tela* 15 (10) (1973) 3082.
- [23] A.S. Knjazev, Y.M. Poplavko, A.S. Zakharov, Dielectric and vibrational spectra of cadmium pyroniobate, *Phys. Tverd. Tela* 16 (3) (1974) 713.
- [24] A.S. Knjazev, Y.M. Poplavko, A.S. Zakharov, Vibrational spectra of rombically distorted perovskites, *Opt. Spektrosk.* 36 (3) (1974) 950.
- [25] A.S. Knjazev, Y.M. Poplavko, A.S. Zakharov, Vibrational and dielectric spectra of anti-ferroelectrics, *Phys. Tverd. Tela* 16 (8) (1974) 2785.
- [26] A.S. Knjazev, Y.M. Poplavko, A.S. Zakharov, Far infrared reflection spectra of bismuth titanate, *Phys. Tverd. Tela* 18 (11) (1976) 3106.
- [27] V.I. Butko, Y.M. Poplavko, Microwave dielectric properties of barium-lanthanide tetratitanates, *Phys. Tverd. Tela* 26 (1984) 2951.
- [28] A.G. Belous, V.I. Butko, Y.M. Poplavko, Dielectric spectra of (La,Me)TiO<sub>3</sub> perovskites, *Phys. Tverd. Tela* 27 (1985) 2013.
- [29] V.I. Butko, Y.M. Poplavko, Dielectric properties of BLT microwave ceramics at low temperatures, *Phys. Tverd. Tela* 28 (1986) 1557.
- [30] V.I. Butko, Y.M. Poplavko, Vibrational spectra of BLT microwave ceramics, *Phys. Tverd. Tela* 28 (1986) 1181.
- [31] Y.M. Poplavko, V.I. Molchanov, V.N. Borisov, Microwave dielectric relaxation in barium lanthanide tetratitanates (BLT), *Ferroelectrics* 156 (1994) 351–356.

- [32] Y.M. Poplavko, M.E. Ilchenko, Nature of thermostability of barium lanthanide tetratitanates, in: Proc. 23-rd Europ. Microwave Conference, Sept. 1993, Madrid, 1993, pp. 600–602.
- [33] M.E. Lines, A.M. Glass, Principles and Application of Ferroelectrics and Related Materials, Clarendon Press, Oxford, 1977.
- [34] R.I. Scott, M. Thomas, C. Hampson, Development of low cost, high performance  $\text{Ba}(\text{Zn}_{1/3}\text{Nb}_{2/3}\text{O}_3)$  based materials for microwave resonator applications, J. Eur. Ceram. Soc. 23 (2003) 2467–2471.
- [35] E.A. Nenashева, L.P. Mudroliuba, N.F. Kartenko, Microwave dielectric properties of ceramics based on  $\text{CaTiO}_3\text{--LnMO}_3$  system (Ln = La, Nd; M = Al, Ga), J. Eur. Ceram. Soc. 23 (2003) 2443–2448.
- [36] Y.M. Poplavko, Nature of dielectrics thermal stability in the microwave waverange (in Russian), Izv. Akad. Nauk Ser. Phys. 60 (10) (1996) 167–172.
- [37] Y.V. Didenko, D.D. Tatarchuk, V.I. Molchanov, Y.M. Poplavko, Effective conductivity of microwave dielectric materials, Electron. Commun. 19 (2(79)) (2014) 23–28.
- [38] Y.V. Didenko, Y.M. Poplavko, High frequency dielectrics: nature of loss, in: Proc. of 34-th Int. Sci. Conf. “Electronics and Nanotechnology”, (ELNANO-2014), Kyiv, 2014, pp. 73–77.
- [39] Y.V. Didenko, Y.M. Poplavko, D.D. Tatarchuk, Temperature dependences of losses in high frequency dielectrics, Electron. Commun. 19 (4(81)) (2014) 28–35.
- [40] L.P. Pereverzeva, Y.M. Poplavko, Ferroelectrics as microwave absorbent packaging, in: Proc. Intern. Symp. Appl. Ferroelectrics, East Brunswick, USA, 1996, pp. 841–845.
- [41] Y.M. Poplavko, V.A. Kazmirenko, M. Kim, S. Baik, Microwave dielectric spectroscopy of ferroelectric thin films, in: MRS Conf., San Francisco, April, 2002, Mat. Res. Soc. Symp. Proc, vol. 720, 2002, pp. H3.2.1–H3.2.6.
- [42] Y.M. Poplavko, V.A. Kazmirenko, Y.V. Prokopenko, Measurement of bulk and film ferroelectric materials properties at microwaves, in: Microwaves, Radar and Wireless Communications, 2002, MIKON-2002. 14th Intern. Conference, vol. 2, 2002, pp. 397–400.
- [43] Y.M. Poplavko, V.A. Kazmirenko, Ferroelectric thin film microwave examination, Ferroelectrics 286 (2003) 353–356.
- [44] Y.M. Poplavko, V.A. Kazmirenko, M. Kim, S. Baik, Electrode-less technique of ferroelectric film study at microwaves, in: 10-th Europ. Meet. on Ferroelectricity, Cambridge, UK, 2003, p. 178.
- [45] Y.M. Poplavko, V.A. Kazmirenko, M. Kim, S. Baik, Contemporary waveguide technique of ferroelectric materials study by vector network analyzer, in: Intern. Microwave Symposium, June 13, 2003, Philadelphia, ARF-61-14, 2003, pp. 437–440.
- [46] Y.M. Poplavko, B. Kim, V. Kazmirenko, Y. Prokopenko, Non-resonant electrode less method for measurement the microwave complex permittivity of ferroelectric films, Meas. Sci. Technol. 16 (2005) 1792–1797.
- [47] E. Furman, M. Lanagan, I. Golubeva, Y. Poplavko, Piezo-controlled microwave frequency agile dielectric devices, in: IEEE International Frequency Control Symposium and Exposition, Montréal, Canada, Aug. 2004, 2004, pp. 266–271.
- [48] Y.V. Prokopenko, Y.M. Poplavko, N. Ruda, Dielectric-air structure as component of electromechanically controlled microwave devices, in: Int. Conf. Mathematical Methods in Electromagnetic Theory, Kiev, 2010, pp. 71–75.
- [49] Y.M. Poplavko, Y.I. Yakymenko, Microwave properties of integrated film in comparison with bulk ferroelectric and paraelectric, in: ISIF 2000 Abstarcts, Aachen, 2000, p. 184.

- [50] B.J. Kim, S. Baik, Y. Poplavko, Y. Prokopenko, Epitaxial BST thin film as microwave phase shifter, in: ISIF 2000 Abstracts, Aachen, 2000, p. 180.
- [51] Y. Poplavko, Y. Prokopenko, S. Baik, B. Kim, Paraelectric film phase shifter, in: Proc. of XIII Int. Conf. on Microwaves, Radar and Wireless Com. MIKON-2000, vol. 2, 2000, pp. 509–512.
- [52] B.J. Kim, S. Baik, Y. Poplavko, Y. Prokopenko, Epitaxial BST thin film as microwave phase shifter, *Integr. Ferroelectr.* 34 (2001) 207–214.
- [53] K. Wakino, T. Nishikawa, S. Tamura, Miniaturised band pass filters using half wave dielectric resonators with improved spurious response, in: Proc. IEEE MTT Symp, 1978, pp. 230–232.
- [54] V. Bovtun, V. Pashkov, Y. Poplavko, S. Kamba, Microwave dielectric properties of high-permittivity thin films studied by thin dielectric resonator method, *J. Appl. Phys.* 109 (2) (2011) 024106.
- [55] V. Bovtun, V. Pashkov, M. Kempa, S. Kamba, Y. Poplavko, Y. Yakymenko, Anisotropic dielectric substrate as thin dielectric resonator, in: *Microwave & Telecommunication Technology (CriMiCo'2012)*, 2012, pp. 573–574.
- [56] V. Bovtun, V. Pashkov, M. Kempa, V. Molchanov, S. Kamba, Y. Poplavko, Y. Yakymenko, Microwave characterization of dielectric substrates for thin films deposition, in: *Int. Conf. Electronics and Nanotechnology, ELNANO-2013*, 2013, pp. 17–20.
- [57] V. Bovtun, V. Pashkov, V. Molchanov, Y. Poplavko, Y. Yakymenko, S. Kamba, Microwave and terahertz dielectric properties of single crystal scandata substrates, in: *Intern. Crimia Conf. "Microwave & Telecommunication Technology" (CriMiCo-2013)*, 2013, pp. 646–648.
- [58] A.A. Voloshin, Y.V. Prokopenko, Y.M. Poplavko, Tunable cylindrical dielectric resonator antenna: design and parameters, in: *Int. Crimia Conf. "Microwave & Telecommunication Technology"*, (CriMiCo-2013), 2013, pp. 620–621.
- [59] K.G. Savin, Y.V. Prokopenko, Y.M. Poplavko, G. Vanderbosh, Mode matching technique solution of eigenproblem for composite metal-dielectric resonator, in: *Intern. Crimia Conf. "Microwave & Telecommunication Technology"*, (CriMiCo-2013), 2013, pp. 644–645.
- [60] V. Kazmirenko, Y. Prokopenko, Y. Poplavko, Tuning range of microwave devices with micro-mechanical control, in: *Proceedings of 2017 XI International Conference on Antenna Theory and Techniques (ICATT)*, April 24–26, 2017, Kyiv, 2017, pp. 34–39.
- [61] K. Savin, V. Kazmirenko, Y. Prokopenko, B. Pratsiuk, G.A. Vandenbosch, Tunable shielded dielectric resonator short-circuited at disk face, in: *Proceedings of 47th European Microwave Conference*, 10–12 Oct. 2017, Nürnberg, 2017, pp. 304–307.
- [62] Y.M. Poplavko, Y.S. You, Future trends in microwave dielectrics, *J. Korean Phys. Soc.* 32 (1998) 1737–1740.
- [63] Y.M. Poplavko, *Thermostable Low Loss Microwave Dielectrics With High Permittivity: Physical Nature of Thermal Stability and Losses*, ISRAMT, Kiev, 1995, pp. 59–62.

## Further reading

- [64] Y.V. Prokopenko, Y.I. Yakymenko, Y.M. Poplavko, Electrostrictive tunable microwave devices, in: *Microwave & Telecommunication Technology (CriMiCo'2012)*, 2012, pp. 509–512.

# Index

Note: Page numbers followed by *f* indicate figures and *t* indicate tables.

## A

- Absorbent materials, 220, 278–280
  - Acoustoelectronics, 163
  - Acousto-optics, 164
  - Adiabatic permittivity, 157, 159
  - AFC. *See* Amplitude-frequency characteristic (AFC)
  - Aiken's law, 120
  - Ammonium hydrophosphate (ADP), 178
  - Amplitude-frequency characteristic (AFC), 203
  - Anharmonicity coefficient, 117
  - Anisotropic crystals, 220
  - Antiferroelectric phase transition, 96, 109, 130, 141
  - Antiferroelectrics, 125–126, 225–226, 225*f*
  - Antiresonance frequency, 204
  - Artificial pyroelectrics, 75, 77–82, 84–91, 88*r*, 158–159
    - electrically induced artificial pyroelectric effect, 142–143, 143*f*, 158
    - thermomechanical induced artificial pyroelectric effect, 143–144, 158
  - Atomic bonds, polar crystals
    - anion vacancy titanium ions, 20
    - bulk dielectrics, 22
    - covalent crystals, 19, 24
    - electrical and magnetic interactions, 18
    - inhomogeneous deformation, 22
    - ionic crystals, 19, 24
    - local electron polarization, 20
    - molecular crystals, 18
    - noncentral cations, 21
    - perovskite dielectrics, 22
    - polar-sensitive atomic bonds, 96, 98
      - coordination number, 27
      - dipole-type structural predisposition, 28
      - electrical charges, noncentrosymmetric allocation, 28
      - electrically induced piezoelectric module, 23, 24*f*
      - electronic density distribution, 28
      - electrical polarization, 23
      - electrostriction, 22–23
      - “exclusive” piezoelectrics, 27–28, 30–31
      - external electrical field, 26
      - ferroelectrics, 26, 32
      - interaction of, 32
      - ionic-covalent bonds, 28
      - KDP crystal, 32
      - Landau's critical index, 32
      - Landau's law, 30
      - linear electromechanical effect, 23
      - linearized electrostriction, 23–24
      - linear pyroelectric crystal, 26
      - low-symmetric crystals, 31
      - material polar vectors, 29
      - mixed covalent-ionic bonding, 26
      - parabolic law, 22–23
      - phase transition, 30
      - polar-neutral crystals, 28
      - situated in-plane (2D) polar sensitivity, 31
      - spatially distributed (3D) polar sensitivity, 32
      - thermal expansion coefficient, 32
      - repulsion forces, 18
      - structural defects, effects of, 20
      - thin epitaxial films, 22
      - valence shells, 18–20
  - Atomic crystals, 225, 225*f*
  - Axial actuators, 200
- ## B
- Ba<sub>0.67</sub>Sr<sub>0.33</sub>TiO<sub>3</sub> (BST), 142
  - BaLn<sub>2</sub>Ti<sub>4</sub>O<sub>12</sub> (BLT), 253
    - indirect exchange interaction, 246–247, 246*f*
    - low-energy relaxation, 253–255, 254*f*
    - paraelectric temperature dependence, 245–246, 246*f*

- BaLn<sub>2</sub>Ti<sub>4</sub>O<sub>12</sub> (BLT) (*Continued*)  
 permittivity and loss coefficient frequency dependencies, 247, 247*f*  
 thermal stability and permittivity, 244–245, 244*t*, 245*f*
- Barium titanate (BaTiO<sub>3</sub>) crystal, 61  
 dielectric permittivity, temperature dependence of, 54–55, 54*f*  
 elastic compliance, 57–58, 57*f*
- Bending actuators, 200–201
- Bismuth germanate (Bi<sub>12</sub>GeO<sub>20</sub>) crystal, 144
- Bismuth oxide (Bi<sub>2</sub>O<sub>3</sub>), 226
- Boltzmann constant, 57, 97, 127–130, 252–253
- C**
- Cadmium sulfide (CdS), 151–152
- Calcium titanate (CaTiO<sub>3</sub>), 72, 225–226, 225*f*, 238–239, 238*f*, 243–244, 254*f*, 275
- Centrosymmetric crystals, 55–56, 113, 163, 191–193
- Chemical etching, 52
- Christoffel equation, 196
- Closed-circuited polar crystal, xii–xiii
- Cochran law, 239
- Colossal magnetoresistance, 65
- Composite material, 218–219, 249
- Composite microwave dielectrics  
 air-dielectric type, 258–261  
 dielectric-air composite phase shifter  
   coplanar line, 266–268, 267*f*  
   microstrip lines, 264–265, 265–266*f*  
 in waveguide, 263–264, 264*f*  
 electrical properties, 257  
 filled polymers, 256  
 microwave absorbance, 257  
 passive dielectric macrocomposite, 257–258  
 polymeric and rubber composites, 256–257  
 tunable dielectric composites  
   with controllable air slit, 261–263, 280  
   ferroelectric and paraelectric film, 268–270, 269*f*, 280
- Composite oxide crystal, 226
- Conductive polymers, 220
- Configurational entropy, xv, 42, 44, 95–96, 108, 110–111
- Converse piezoelectric effect  
 actuators, 199–201  
 effective permittivity, 193–194  
 electrical polarization, 188  
 electromechanical interaction, 195–196  
 emitters, 199  
 energy transformers, 199  
 engines, 201  
 fundamentals of, 189–193  
 linear electromechanical effect, 188  
 liquid medium, 199  
 micropositioners, 201  
 motors, 201  
 scanning acoustic microscope, 199  
 simplest devices, 196–198  
 solid environment, 199
- Coordination number (CN), 4, 27, 47
- Coulomb force, 44–49
- Covalent crystals, 19, 24, 234
- Covalent semiconductors, 4
- Critistors, 59, 59*f*
- Curie point, 15–16, 21–22, 26, 31, 40–41, 114, 123, 125–126
- Curie-Weiss law, 237–240, 242–245, 253–254, 268–269
- D**
- Debye polarization mechanism, 6–7
- Debye temperature, 103–105, 107, 115
- Deuterated triglycerol sulfate (DTGS), 149–151
- Diamagnetic lanthanum ion, 253–254
- Dielectric-air composite phase shifter  
 coplanar line, 266–268, 267*f*  
 microstrip lines, 264–265, 265–266*f*  
 in waveguide, 263–264, 264*f*
- Dielectric constant, 218–219, 224, 226, 228–230, 268–269, 271–272, 272*f*, 275–276
- Dielectric losses, 2–4, 6
- Dielectric permittivity, polar-sensitive crystals  
 electromechanical contribution  
   KDP crystal, 55, 55*f*  
   temperature dependence, in free and clamped crystals, 54–55, 54*f*  
 electrothermal/electrocaloric contribution, 55

- Dielectric resonator (DR), 270–278, 280
- Dielectric spectroscopy method, 253
- Direct converters, 131
- Direct piezoelectric effect
- acoustic sensor, 186
  - crystals, 184–185
  - electrical boundary conditions, elastic properties dependence, 183–184
  - electromechanical coupling factor, 180–183
  - figures of merit, 176–180
  - force action, 174
  - force sensors, 185–186
  - generators, 187–188
  - homogeneous and centrosymmetric actions, 174
  - macrocomposite materials, 187
  - mechanical action, 174
  - mechanical deformation, 179
  - mechanical vibration dampers, 188
  - medicine, 186
  - microphones, 186–187
  - polyvinylidene fluoride (PVDF), 187
  - quartz crystal, 176
  - seismic cables, 185
  - sensors, 184–185, 185*f*
  - vibration sensors, 186
- DTGS. *See* Deuterated triglycerol sulfate (DTGS)
- E**
- Electrical bias field, 23, 44–49
- Elastic electronic polarization, 223–224, 229
- Elastic energy density, 167, 181
- Electrets, ix, 15
- Electrical polarization, ix–xii, 1–2, 16, 23, 34, 163, 188, 221–222, 222*f*
- Electrical polarization-depolarization effect, 131
- Electrical resistivity, 64, 66
- Electrocaloric effect, xii, 145, 153–159
- Electroinduced piezoelectric effect, paraelectrics, 173
- Electromagnetic absorption, 220
- Electromagnetic interference (EMI), 220
- Electromagnetic wave, 220, 234, 256, 258, 268
- Electromechanical coupling, 72
- Electronic polarization, microwave dielectrics, 228
- antiferroelectrics, 225–226, 225*f*
  - atomic and molecular dielectrics, 225, 225*f*
  - dynamic properties, 228–230, 229*f*
  - ionic crystals, 225, 225*f*
- Electronic quasielastic polarization, 3–4, 6, 222
- Electronic shell model, 235–237
- Electronic thermal polarization, 8
- Electron shell, 222, 235–237, 239–240, 242
- Electrostriction, xvii, 8, 70–71, 92, 162
- Energy devices, 164–166
- Epitaxial films, 115
- External electrical field, 166, 172–174, 213–216
- F**
- Far-infrared (IR) detectors, 134–135
- Far-infrared polarization mechanism, 5–6
- Fast relaxation polarization mechanism, 252–253
- Ferroelectricity, ix, 99, 173
- ceramics, 193
  - and paraelectric film, 268–270, 269*f*
  - phase transition, 26, 32–34, 44–49
  - polarization, 15
  - polar-sensitive atomic bonds, 26, 32
  - pyroelectricity, 132
  - thermodynamics, 149
- Ferromagnetism, 15
- Figures of merit, 148–149, 152, 176–180
- Forced induction, noncentrosymmetric structure, 173
- Frequency independent permittivity, 249
- G**
- Gallium arsenide (GaAs), 53–54, 56, 56*f*, 144, 252–253, 252*f*
- Gallium nitride (GaN), 86, 131
- Gibbs free energy, 34, 42–43, 211
- Griffith criteria, 114
- Grüneisen constant, 105, 109–111
- H**
- Harmonic oscillator model, 228–230
- Heat transfer, in polarsensitive crystals, 96

Heat transfer, in polarsensitive crystals

(*Continued*)

antiferroelectrics, thermal diffusion in,

125–127

electrical field, thermal transfer, 123–125

Fourier's heat conduction law, 115

ionic dielectrics, 115–116

noncentrosymmetric crystals, 116

nonequilibrium thermodynamics, 116

nonpolar covalent dielectrics, 115

phase transition, thermal conductivity,

119–121

shortwave phonons, 116

thermal conductivity, 115, 117

thermal diffusivity, 121–123

thermal transfer features, polar-sensitive crystals, 118–119

Helmholtz free energy, 34, 44–49, 211–212

High-frequency microelectronic microwave, 268

High-loss microwave dielectric, 249

High-permittivity microwave dielectrics.

*See* Microwave high permittivity dielectrics

Hooke's law, xi–xiii, 12, 179, 181–183, 190

## I

Induced electrical field, 11

Induced electronic polarization, 229

Induced piezoelectric effect, 72–75, 89–90

Induced space-charge polarization, 223

Industrial nondestructive testing, 163

Infrared sensors, 159

Infrared thermometers, 136, 159

Inverse piezoelectric effect, 153

Ion elastic coupling, 233–234

Ionic displacive-type polarization, 250

Ionic elastic-displacement polarization, 223–224

Ionic polarization, microwave dielectrics,

218, 222, 224, 230, 250–251

antiferroelectrics, 225–226, 225*f*

electronic shell model, 235–237

far infrared polarization, dynamical model, 230–235, 231–232*f*

ionic crystals, permittivity, 225, 225*f*

ionic displacive-type polarization, 250–251, 251*f*

Ionic polar semiconductor, 250

Ionic quasielastic polarization, 222

Isothermal permittivity, 157, 159

## L

Landau critical index, 30, 33, 44–49, 142

Laser radiation pulses, 136

Le Chatelier's principle, 113, 154–155

Linearized electrostriction, 172, 213–216

Linear low-loss thermally stable dielectrics, 218, 278

Lithium niobate (LiNbO<sub>3</sub>) crystal, 143–144

Lithium sulfate crystal, 139, 140*f*, 142

Lorentz coefficient, 236

Lorentz oscillator model, 248

Low dielectric loss, 218–219, 224, 255

Low-energy relaxation process, 245, 253

Lower-frequency polarization mechanism, 222

Low-loss microwave ceramics, 270

Low-loss microwave dielectrics, 224, 255

Low microwave reflection coatings, 220, 279

Lyddane-Sachs-Teller ratio, 234, 236, 239

## M

Macrocomposites, xviii, 187, 218, 257

Magnesium oxide (MgO), 104, 270

Magnetic bias field, 65

Magnetic field, 65

Magnetic nanoparticles, 220

Mechanical sensor, 91–93

Mechanical stress, 12–14, 61, 82–83, 85–89, 167, 174

Meter wave device, 226

MgO. *See* Magnesium oxide (MgO)

Microelectromechanical microwave device, 271

Microelectronic group technology, x–xi

Microelectronic microwave integrated circuits (MMICs), 268

Micromachining, x–xi

Microwave composites, 219, 279–280

Microwave electronics, xvii, 219–220, 279

Microwave electronic material, 220, 278–280

Microwave high permittivity dielectrics, xvii–xviii, 217

applications, 217, 218*t*

composite dielectrics (*see* Composite microwave dielectrics)

- conductivity, 221  
 dielectric-air slit structures, resonances in, 270–278  
 flexible absorbing shielding composites, 220, 280  
 linear low-loss thermally stable dielectrics, 218, 278  
 low microwave reflection coatings, 220, 279  
 microwave composites, 219, 279–280  
 millimeter-wave dielectrics and shielding composites, 220–221  
 nonlinear microwave dielectrics, 218–219, 279  
 pliable microwave substrates, 219–220, 278  
 polarization  
   bias current, 221  
   dielectric crystal parameters, 226, 227*t*  
   electrically induced space-charge polarization, 223–224  
   electrical polarization, 221–222, 222*f*  
   electronic elastic polarization, 223–224  
   electronic polarization (*see* Electronic polarization, microwave dielectrics)  
   inertia, 221–222  
   ionic elastic-displacement polarization, 223–224  
   ionic polarization (*see* Ionic polarization, microwave dielectrics)  
   lower-frequency polarization mechanisms, 222  
   low-loss microwave dielectrics, 224  
   paraelectrics, 237–240, 238*f*  
   quasielastic induced polarization, 222  
   reversible property, 221  
   thermally supported electrically induced polarization, 223, 227*t*  
 polar-sensitive phase, 218  
 thermally stable microwave dielectrics (*see* Thermally stable microwave dielectrics)
- Microwave microelectronics, x–xi, 217, 224  
 Microwave packaging technology, 219–220  
 Millimeter-wave dielectrics, 220–221  
 Motion detector sensors, 136, 159  
 Multicontact chain adsorption, 256–257  
 Multielement planar integral thermal far-infrared detector, 81–82
- N**  
 Nanodielectrics, x–xi  
 Nanoelectronics, xi  
 Negistors, 58–59, 59*f*  
 Neumann's principle, 132–133  
 Noncentrosymmetric crystal, 58, 61, 75, 86–87, 90, 116, 166, 178, 180  
 Nonlinear microwave dielectrics, 219, 224, 279  
 Nonpolar microwave dielectrics, 222, 223*f*, 224  
 Nonpolar dielectrics  
   mechanical, electrical, and thermal effects, xi–xii*f*  
   noncentrosymmetric structure, forced induction of, 173
- O**  
 One-dimensional model  
   ionic crystal, 232, 232*f*  
   pyroelectrics, 138, 139*f*  
 Open-circuited polar crystal, xii–xiii  
 Optical nonlinearity, 11
- P**  
 Paramagnetism, 218, 245–246, 253, 255, 278–280  
 Passive dielectric macrocomposite, 257–258  
 Piezoelectric cantilever, 271  
 Piezoelectricity, ix–xi, xii*t*, xiv*t*, xvii*t*  
   bias electrical field, 162  
   converse piezoelectric effect actuators, 199–201  
   effective permittivity, 193–194  
   electrical polarization, 188  
   electromechanical interaction, 195–196  
   emitters, 199  
   energy transformers, 199  
   engines, 201  
   fundamentals of, 189–193  
   linear electromechanical effect, 188  
   liquid medium, 199  
   micropositioners, 201  
   motors, 201  
   scanning acoustic microscope, 199  
   simplest devices, 196–198  
   solid environment, 199  
   dielectrics, 161

Piezoelectricity (*Continued*)

- direct piezoelectric effect
  - acoustic sensor, 186
  - crystals, 184–185
- electrical boundary conditions, elastic
  - properties dependence, 183–184
- electromechanical coupling factor, 180–183
- figures of merit, 176–180
- force action, 174
- force sensors, 185–186
- generators, 187–188
- homogeneous and centrosymmetric
  - actions, 174
- macrocomposite materials, 187
- mechanical action, 174
- mechanical deformation, 179
- mechanical vibration dampers, 188
- medicine, 186
- microphones, 186–187
- polyvinylidene fluoride (PVDF), 187
- quartz crystal, 176
- seismic cables, 185
- sensors, 184–185, 185*f*
- vibration sensors, 186
- electrical field, 172–174
- electrodynamics, 161
- electromechanical coupling coefficient, 162
- electromechanical resonance
  - mechanical resistance, 202
  - oscillatory velocity, 202
  - quality factor, 165, 203
  - resonance, 201–206
- electrostriction, 162
- flexoelectrical effect, 161–162
- general characteristics of
  - centrosymmetric crystals, 163
  - electrical polarization, 163
  - linear electromechanical effect, 166
  - odd-rank tensors, 162
  - piezoelectric materials, 163
  - polar-neutral crystals, 163
  - practical applications, 163–164
- heterogeneous deformations, 161–162
- longitudinal piezoelectric effect, 169
- elasticity, 161–162
- magnetic effects, 161
- mathematical model, 161–162
- model description of, 162
- piezoelectric resonators, 220
- quartz crystals, 161
- shear piezoelectric effect, 171–172
- structural affinity, 51–52, 52*f*
- technical application, 161
- thermodynamic potential analyses, 210–212
- transformers, 208–209
- transverse piezoelectric effect, 170–171
- Piezo-tunable phase shifters, 265
- Planar lattice model, 21*f*
- Planck constant, 97, 127
- Poisson's coefficient, 168, 197, 213
- Polar crystals
  - atomic bonds (*see* Atomic bonds, polar crystals)
  - basic elementary mechanisms
    - connected dipoles, elastic rotation of, 6
    - in dielectrics, 1
    - dipole relaxation polarization, 6–7
    - electrical induction, 1–2
    - electrical polarization, 1–2
    - electronic quasielastic (optical) polarization, 3–4
    - electronic thermal polarization, 8
    - ionic thermal polarization, 7–8
    - low-inertia mechanism, 4–6
    - permittivity, polarization mechanisms, 6, 7*f*
    - quasielastic polarization, 2
    - relaxation polarization mechanisms, 6
    - semifree electrons, 8
  - chain crystals, 109
  - configurational entropy, 95–96
  - Debye energy, 97
  - ferroelectric (*see* Ferroelectricity)
  - heat transfer, in polar sensitive crystals, 96
    - antiferroelectrics, thermal diffusion in, 125–127
    - electrical field, thermal transfer, 123–125
    - Fourier's heat conduction law, 115
    - ionic dielectrics, 115–116
    - noncentrosymmetric crystals, 116
    - nonequilibrium thermodynamics, 116
    - nonpolar covalent dielectrics, 115
    - phase transition, thermal conductivity, 119–121

- shortwave phonons, 116
- thermal conductivity, 115, 117
- thermal diffusivity, 121–123
- thermal transfer features, polar-sensitive crystals, 118–119
- layered crystal, 109
- phase transition, 97–98
- piezoelectric (*see* Piezoelectricity)
- polarization
  - atomic electronegativity, 17
  - boundary conditions, 11
  - changing temperature/mechanical factors, 14
  - crystalline dielectrics, 17
  - Curie principle, 14
  - dielectric anisotropy, 9
  - elastic stiffness, 12
  - electrets, 15
  - electrical boundary conditions, 11
  - electrical induction, 11
  - electrical polarization, 16
  - electromechanical contributions, permittivity, 12
  - ferroelectrics, 15
  - functional (active) dielectrics, 16–17
  - induced polarization vector, 9
  - intermediate conditions, 13
  - isotropic dielectrics, 9
  - Lorentz relation, 15
  - mechanical boundary conditions, 11–12
  - noncentrosymmetric structures, 17–18
  - noncompensated electrical charges, 15
  - nonlinear ferromagnetics, 14
  - nonlinearity of dielectrics, 11
  - polar dielectric, 9
  - polar-sensitive crystals, 12
  - properties, 13–14
  - scalar values, 10
  - second-rank tensors, 10–11
  - spontaneous magnetization, 15
  - spontaneous polarization, 14–16
  - thermal boundary conditions, 12
  - thermodynamics (*see* Thermodynamics)
  - zero-rank tensors, 10
- pyroelectric (*see* Pyroelectricity)
- specific heat capacity, 98–101
- TGS crystal, 96, 99
- thermal diffusion, 96
- thermal expansion, 96
- anisotropy of, 101–103
- high-frequency transistors, 101
- lattice strain engineering, polar-sensitive films, 113–115
- negative thermal deformation, 106–111
- negative thermal expansion, semiconductors, 111–113
- noncentrosymmetric semiconductors, 101
- phase transition temperature, 101
- physical nature of, 103–106
- physical phenomenon of, 101
- polar dielectrics, 101
- thermal deformation, 101
- Polar dielectrics, 221
  - dielectric anisotropy, 9
  - entropy, xv
  - low-inertia polarization, 6
  - mechanical, electrical, and thermal effects, xi–xii<sup>f</sup>
  - polar-sensitive structures, 128
  - pyroelectrics, 13
- Polarized ferroelectric ceramics, 134
- Polar-neutral piezoelectric crystal, xiv–xvi, 51, 92–93
- Polar-sensitive crystals, xii–xiii, xv
  - charge transfer, 58–70
  - chemical features, 52–53
  - dielectric permittivity
    - electromechanical contribution, 54–55, 54–55<sup>f</sup>
    - electrothermal/electrocaloric contribution, 55
  - elastic properties, 57–58, 57<sup>f</sup>
  - electrically induced polar properties
  - electrostriction, 70–71, 92
  - piezoelectric effect, electrical control of, 71–73, 72<sup>f</sup>
  - relaxor ferroelectric characteristics, 73–75, 74<sup>f</sup>
  - microwave loss factor, 55–57, 56<sup>f</sup>
  - structural affinity, 51–52, 52<sup>f</sup>
  - volume increase in ordered structures, 53–54
- Polyvinylidene fluoride (PVDF), 134, 187
- Posistors, 51, 58–59, 59<sup>f</sup>; 66–67, 92–93
- Potassium dihydrogen phosphate crystals (KDP), 177–178, 191
- Potassium tartaric acid, 131

Precision resonance sensors, 207  
 PVDF. *See* Polyvinylidene fluoride (PVDF)  
 Pyroelectric coefficient measurement, 73  
 Pyroelectric coupling coefficient, 148  
 Pyroelectricity, ix–xi, xii–xiii, xvi–xviii, 28–29, 35–36, 131  
   artificial pyroelectrics, 89–91, 131  
     electrically induced artificial  
       pyroelectric effect, 142–143, 143*f*, 158  
     thermomechanical induced artificial  
       pyroelectric effect, 143–144, 158  
   crystalline sugar, 131  
   crystals, 132–134, 133*f*  
   ferroelectrics, 132  
   high-intensity electrical field, 137  
   infrared thermometers, 136  
   microelectronic matrix pyroelectrics, 143  
   mineral pyroelectrics, 131  
   motion detector sensors, 136, 159  
   one-dimensional model, 138, 139*f*  
   physical mechanism, 158  
   polarized ferroelectric ceramics, 134  
   polymeric films, 134  
   primary pyroelectric coefficient  
     temperature dependence, 138, 140–141, 141*f*, 158  
   pyroelectric generators, 136–137  
   pyroelectric sensors, 134–136, 135*f*, 148–149, 152  
   pyroelectric vidicons, 136, 159  
   secondary pyroelectric coefficient  
     temperature dependence, 137–140, 139–140*f*, 158  
   structural affinity, 51–52, 52*f*  
   synthetic pyroelectrics, 131  
 thermodynamics  
   boundary conditions, 145–147  
   current and voltage sensitivity,  
     temperature dependence of, 149–152, 151*f*  
   dependent variables, 145–146  
   dielectric permittivity, 152  
   elastic stiffness, 146  
   electrical field and mechanical stress,  
     144, 147–148  
   electromechanical coupling coefficient,  
     148  
   electrothermal conversion factor, 148

ferroelectrics, 149  
 Gibbs thermodynamic potential, 145  
 independent variables, 145–146  
 inverse dielectric susceptibility, 152  
 linear pyroelectrics, 149  
 permittivity tensor, 146  
 piezoelectric modulus, 146  
 piezoelectric strain tensor, 147  
 polar composite materials, 149  
 polar polymers, 149  
 primary pyroelectric effect, 144–145, 147  
 pyroelectric coefficient, 144, 146–147  
 pyroelectric sensors, 148–149, 150*r*  
 secondary pyroelectric effects, 144–145, 147, 153  
 thermal expansion tensor, 146  
 thermodynamic Landau theory, 152–153  
 volumetric specific heat capacity,  
   146–147  
 thermomechanically induced  
   pyroelectricity, 75–89

## Q

Quadratic electromechanical effect, 188  
 Quality factor (Q-factor), 187, 199, 201–203, 208, 213–216, 226–228, 228*t*, 252–253, 272–276, 273*f*, 280  
 Quartz crystal, 161, 176, 186, 191, 207  
 Quartz thermal expansion coefficient, 77  
 Quasi-Debye type absorption, 55–56  
 Quasielastic dipole polarization, 222  
 Quasielastic polarization, 2

## R

Radio astronomy, 220–221  
 Rare-earth ions, 244, 253  
 Relaxation polarization mechanism, 6  
 Repulsive force, 43  
 Reversible polarization process, 222  
 Reversible thermodynamic process, 36–37  
 Rochelle salt (RS), 122, 177, 183, 194  
   dielectric permittivity, temperature  
     dependence of, 54–55, 54*f*  
   elastic stiffness, 57, 57*f*  
   pyroelectric coefficient temperature  
     dependence, 141, 141*f*  
 Rubber-ceramics composites, 219–220

## S

- Sapphire ( $\text{Al}_2\text{O}_3$ ), 226
- Satellite telecommunications device, 217
- Shielding composites, 220–221
- Short-range repulsion force, 236, 239
- Silica glass substrate, 78
- Silicon nitride ( $\text{SiC}$ ), 61
- Sinusoidal electrical voltage, 221
- Slot dielectric resonator (SDR), 272–276, 273–276*f*
- Slow relaxation polarization mechanism, 249–250, 250*f*
- Soft transverse optical mode, 173
- Sphalerite, 51–52, 52*f*
- Spontaneous polarization, 1, 4, 14–16
- Strain sensor mode, 169
- Strontium titanate ( $\text{SrTiO}_3$ ), 72, 225–226, 225*f*, 238–239, 238*f*, 243–244
- Structural affinity, 51–52, 92–93
- Surface acoustic waves (SAWs), 71, 206

## T

- Tellurium (Te), 31, 78
- Temperature sensors, 134–135, 148
- TGS. *See* Triglycine sulfate (TGS) crystal
- Thermal expansion, polar crystal, 96
  - anisotropy of, 101–103
  - coefficient, xv–xvi, 219–220
  - ferroelectric film, 101
  - high-frequency transistors, 101
  - lattice strain engineering, polar-sensitive films, 113–115
  - negative thermal deformation, 106–111
  - negative thermal expansion,
    - semiconductors, 111–113
  - noncentrosymmetric semiconductors, 101
  - phase transition temperature, 101
  - physical nature of, 103–106
  - physical phenomenon of, 101
  - polar dielectrics, 101
  - thermal deformation, 101
- Thermally stable microwave dielectrics
  - conductivity influence on microwave losses, 248–249, 248*f*
  - dielectric losses at very high frequencies, 247–248
  - ionic displacive-type polarization, 250–251, 251*f*
  - low-energy relaxation in BLTs, 253–255, 254*f*
  - permittivity and quality factor, 226–228, 228*t*
  - polar crystals, microwave losses in, 251–253, 252*f*
  - slow relaxation polarization mechanism, 249–250, 250*f*
  - thermostable microwave ceramic dielectrics, 241–247, 242–243*f*, 244*t*, 246*f*
- Thermistors, 58–59, 59*f*
- Thermodynamics
  - polarization process
    - adiabatic conditions, 39
    - configurational entropy, 42, 44
    - constant permittivity, 37–39
    - dielectric nonlinearity, 41–42
    - electrical polarization, 34
    - energy conservation law, 37
    - enthalpy, 34
    - entropy, 35
    - ferroelectric phase transition, 35–36
    - first law of, 36
    - functional dielectrics, 35
    - Gibbs free energy, 34
    - isothermal conditions, 33–34
    - isothermal permittivity, 39
    - Le Chatelier's principle, 44
    - polar dielectrics, 33–34
    - pyroelectrics, 33–34
    - reversible process, 44
    - second law of, 36–37
    - theory, 12
    - thermal expansion, 42
    - thermally activated polarization, 40
    - vibrational entropy, 44
    - volumetric thermal expansion coefficient, 43
  - pyroelectricity
    - boundary conditions, 145–147
    - current and voltage sensitivity,
      - temperature dependence of, 149–152, 151*f*
    - dependent variables, 145–146
    - dielectric permittivity, 152
    - elastic stiffness, 146
    - electrical field and mechanical stress, 144, 147–148

- Thermodynamics (*Continued*)
- electromechanical coupling coefficient, 148
  - electrothermal conversion factor, 148
  - ferroelectrics, 149
  - Gibbs thermodynamic potential, 145
  - independent variables, 145–146
  - inverse dielectric susceptibility, 152
  - linear pyroelectrics, 149
  - permittivity tensor, 146
  - piezoelectric modulus, 146
  - piezoelectric strain tensor, 147
  - polar composite materials, 149
  - polar polymers, 149
  - primary pyroelectric effect, 144–145, 147
  - pyroelectric coefficient, 144, 146–147
  - pyroelectric sensors, 148–149, 150*t*
  - secondary pyroelectric effects, 144–145, 147, 153
  - thermal expansion tensor, 146
  - thermodynamic Landau theory, 152–153
  - volumetric specific heat capacity, 146–147
- Thermomechanically induced pyroelectricity, xv–xvi, 75–89
- Titanium dioxide (TiO<sub>2</sub>), 226
- Titanium oxide (TiO<sub>2</sub>), 72, 243
- Tourmalines, 131, 136–137, 140*f*, 144
- Transverse actuators, 200
- Transverse piezoelectric effect, 82
- Triclinic crystals, 103
- Triglycine sulfate (TGS) crystal, 119, 124, 141, 141*f*, 148–149
- Tunable dielectric composites, 261–263, 278–280
- ferroelectric and paraelectric film, 268–270, 269*f*
- with controllable air slit, 261–263
- Tunable piezoelectric filters, 71, 162
- Tunable piezoelectric resonator, 74–75, 92–93
- U**
- Umklapp processes (U-processes), 118
- V**
- Vanadium dioxide (VO<sub>2</sub>), 61–65, 63*f*
- Varistors, 67–70, 92
- Vehicle radar, 220–221
- Vibrational entropy, xv
- Vibration sensors, 186, 210
- Voltage resonance (sequential resonance), 205
- Volumetric expansion coefficient, 103
- Volumetric compressibility, 168, 213–216
- Volumetric modulus of elasticity, 168
- Volumetric piezoelectric coefficient, 89
- Volumetric piezoelectric effect, xv–xvii, 13, 169–170
- W**
- Wurtzite, 51–52, 52*f*
- Y**
- Young's modulus, 114, 168, 173
- Z**
- Zero-rank tensors, 10, 16–17
- Zinc oxide (ZnO) crystal, 60*f*, 61, 67–70, 68*f*, 92
- Zinc sulfide, 51–52, 92–93

Key reference in developing an advanced foundational understanding of the physical mechanisms of dielectric materials and their electronics applications.

*Functional Dielectrics for Electronics* presents an overview of the nature of electrical polarization, dielectric nonlinearity, electrical charge transfer mechanisms, thermal properties, the nature of high permittivity low-loss thermostability, and other functional dielectrics. The book describes in detail the intrinsic mechanisms of electrical polarization and the energy transformations in non-centrosymmetric crystals, which are responsible for converting thermal, mechanical, optical, and other impacts into electrical signals. In order to extend the use of functional dielectrics into the field of nanoelectronics, the book reviews the main physical processes, which provide electrical, mechano-electrical, thermoelectrical, and other conversion phenomena in the polar crystals. Detailed descriptions are given of electrical manifestations of polar sensitivity in the crystals, the interaction of polarization with conductivity, the anomalies in the thermal expansion coefficient, and the main peculiarities of heat transfer in polar-sensitive crystals.

*Functional Dielectrics for Electronics* is a useful reference for materials scientists and engineers working in academia or in R&D in electronics.

### Key Features

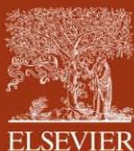
- Provides readers with a fundamental understanding of polar dielectric materials and their physical processes
- Includes different models of polar sensitivity and experimental confirmation of these models
- Discusses thermal expansion, heat transfer, dielectric nonlinearity, and other important aspects for electronics applications

### Author Biographies

**Dr. Yuriy Poplavko** has been teaching electronic materials science topics for the past 40 years in Ukraine, Portugal, and South Korea. During his time at the National Technical University of Ukraine, he has developed several courses in materials science and physics, and has published more than 20 scientific books and manuals (4 books in English, 6 books in Russian, and 10 books in Ukrainian) on dielectrics, polar crystals, ferroelectrics, and many other subjects. Dr. Poplavko is also a renowned expert in the physics of ferroelectrics and dielectrics; he is known primarily for his efforts in discovering the research method of microwave dielectric spectroscopy.

**Dr. Yuriy Yakymenko** is currently the First Vice-Rector of the National Technical University of Ukraine. He has previously served as the Head of the Microelectronics Department and the Dean of the Faculty of Electronics. He is a senior member of the Institute of Electrical and Electronics Engineers, and a member of the National Academy of Science of Ukraine. His scientific activities have been devoted to electronics, information technology, and engineering education. Dr. Yakymenko is the author of more than 250 scientific works, and he has been awarded two state prizes in the field of science and technology.

Cover image: Shutterstock



**WP**  
WOODHEAD  
PUBLISHING

An imprint of Elsevier  
[elsevier.com/books-and-journals](http://elsevier.com/books-and-journals)

ISBN 978-0-12-818835-4



9 780128 188354